

(2)

COMPOSITE MATERIAL AIRCRAFT ELECTROMAGNETIC PROPERTIES AND DESIGN GUIDELINES

ADA 124016



BY

J. A. BIRKEN

W. G. DUFF

D. R. PFLUG

R. A. WALLENBERG

DTIC
FEB 2 1983
A

APPROVED FOR PUBLIC RELEASE
DISTRIBUTION UNLIMITED

DTIC FILE COPY

NAVAL AIR SYSTEM COMMAND
U.S. DEPARTMENT OF THE NAVY

83 02 02 001

UNCLASSIFIED

SECURITY CLASSIFICATION OF THIS PAGE (When Data Entered)

REPORT DOCUMENTATION PAGE		READ INSTRUCTIONS BEFORE COMPLETING FORM
1. REPORT NUMBER AIR-516-5	2. GOVT ACCESSION NO. AD-4124 C16	3. RECIPIENT'S CATALOG NUMBER
4. TITLE (and Subtitle) Composite Material Aircraft Electromagnetic Properties and Design Guidelines		5. TYPE OF REPORT & PERIOD COVERED Jan 1981
7. AUTHOR(s) J. Birken R. Wallenberg W. Duff D. Pflug		6. PERFORMING ORG. REPORT NUMBER 50 - 5779
9. PERFORMING ORGANIZATION NAME AND ADDRESS Atlantic Research Corporation 5390 Cherokee Alexandria, VA 22314		8. CONTRACT OR GRANT NUMBER(s) N00019-79-C-0634
11. CONTROLLING OFFICE NAME AND ADDRESS Naval Air Systems Command ATTN: J. A. Birken (AIR-5161D) Washington, D. C. 20361		10. PROGRAM ELEMENT, PROJECT, TASK AREA & WORK UNIT NUMBERS
14. MONITORING AGENCY NAME & ADDRESS (if different from Controlling Office)		12. REPORT DATE
		13. NUMBER OF PAGES 369
		15. SECURITY CLASS. (of this report) UNCLASSIFIED
		15a. DECLASSIFICATION/DOWNGRADING SCHEDULE N/A
16. DISTRIBUTION STATEMENT (of this Report) Unlimited Distribution		
APPROVED FOR PUBLIC RELEASE DISTRIBUTION UNLIMITED		
17. DISTRIBUTION STATEMENT (of the abstract entered in Block 20, if different from Report)		
18. SUPPLEMENTARY NOTES		
19. KEY WORDS (Continue on reverse side if necessary and identify by block number) Advanced Composite Aircraft Electromagnetic Safety Electromagnetic Pulse (EMP) Composite Material Avionics Lightning Composite Aircraft Safety Solid State Devices Radar Electromagnetic Testing Electromagnetic Compatibility Communication Electronic Warfare Computers		
20. ABSTRACT (Continue on reverse side if necessary and identify by block number) This document collects and primarily summarizes aircraft advanced composite material electromagnetic properties, and secondarily, summarizes composite material mechanical, thermal, environmental, fabrication properties noting their ramifications on electromagnetic performance. It then overview the electromagnetic sub-discipline of threats external to internal aircraft coupling, component and subsystems susceptibility, protective methods as well as test and evaluation of small sample to total aircraft composite material electromagnetic performance. The sub-disciplines constitute a partitioned set of independent variables which allow the reader to locate his area of interest in one section of the book. (see other side)		

DD FORM 1 JAN 73 1473 EDITION OF 1 NOV 65 IS OBSOLETE

UNCLASSIFIED

SECURITY CLASSIFICATION OF THIS PAGE (When Data Entered)

✓
The sub-discipline are then combined to perform total aircraft electromagnetic system performance noting the protective methods, advantages and penalties.
↑

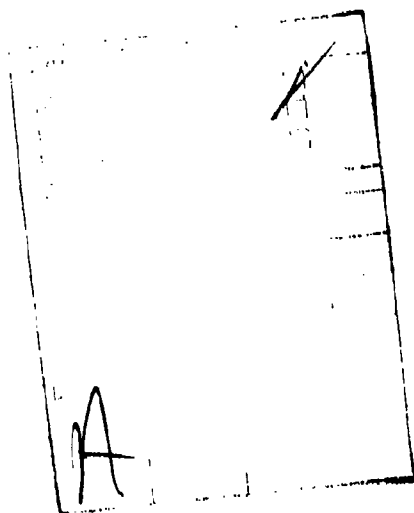


Table of Contents

<u>Section</u>	<u>Page</u>
1.0 Introduction	1-1
2.0 Electromagnetic Threats	2-1
2.1 Natural Threat	2-1
2.1.1 Lightning	2-1
2.1.2 Precipitation Static	2-16
2.2 Friend/Foe Threat	2-19
2.2.1 RF Threat	2-19
2.2.2 EMP Threat	2-26
2.2.3 High Energy Laser, Nuclear Thermal Radiation and Particle Beam Threat	2-28
2.3 References	2-31
3.0 Composition, Fabrication and Mechanical Properties of Composite Materials	3-1
3.1 Composition of Composite Materials	3-1
3.1.1 Fibers	3-1
3.1.2 Matrix Materials	3-3
3.2 Fabrication of Composite Materials	3-5
3.2.1 Tape (Prepreg) and Broad Goods Fabrication	3-5
3.2.2 Layup Process	3-5
3.2.3 Laminate Orientation Code	3-5
3.2.4 Composite Fabrication Processes	3-7
3.3 Mechanical Properties	3-9
3.3.1 Composite Fiber Properties	3-9
3.3.2 Composite Matrix Properties	3-12
3.3.3 Single Laminate Composite Properties	3-12
3.3.4 Crossplied Laminate Composite Properties	3-18
3.4 Environmental Effects on Composite Materials	3-35
3.5 Composite Fatigue	3-35
3.6 References	3-43
4.0 Applications of Composite Materials	4-1
4.1 Early (pre-1973) Aerospace Composite Materials Applications	4-1
4.2 Recent (post-1973) and Current Aerospace Composite Material Applications	4-1
4.2.1 Aircraft Systems	4-1
4.2.2 Propulsion Systems	4-8
4.2.3 Space Systems	4-8
4.2.4 Helicopter Systems	4-9
4.2.5 Other Aerospace Applications	4-9
4.3 Problems in Composite Material Applications	4-10
4.3.1 Graphite Fiber Release	4-10
4.3.2 Galvanic Corrosion	4-11
4.3.3 Fabrication Techniques	4-11
4.4 Future Uses of Composite Materials	4-11
4.4.1 Future Composite Uses in Aerospace Systems	4-11
4.5 References	4-16

Table of Contents (Continued)

<u>Section</u>	<u>Page</u>
5.0 Intrinsic Material Properties	5-1
5.1 Material EM Parameters	5-1
5.1.1 Permeability	5-1
5.1.2 Permittivity	
5.1.3 Conductivity	5-2
5.2 Improvement of Intrinsic Parameters	5-12
5.2.1 Doping	5-12
5.2.2 Intercalation	5-13
5.3 Thermal Modification of EM Intrinsic Parameters	5-19
5.3.1 Conductivity	5-19
5.4 Environmental Modification of EM Intrinsic Parameters	5-19
5.4.1 Moisture	5-19
5.5 Nonlinear Effects	5-22
5.5.1 High-Field Effects	5-22
5.6 References	5-22
6.0 External-to-Internal Coupling	6-1
6.1 Airframe Shielding Effectiveness	6-1
6.1.1 Shielding Effectiveness - Theoretical Considerations	6-1
6.1.2 Measured and Predicted Composite Shielding Effectiveness	6-25
6.1.3 Metallic/Composite Aircraft Weight-Shielding Tradeoffs	6-33
6.2 Composite Joints	6-41
6.2.1 Theory	6-41
6.2.2 Effect on Shielding Effectiveness	6-46
6.3 References	6-51
7.0 Component and Subsystem Susceptibility	7-1
7.1 Component and Circuit Susceptibility	7-1
7.1.1 Analog Circuits	7-1
7.1.2 Digital Circuits	7-2
7.1.3 Semiconductor Devices	7-2
7.1.4 Integrated Circuits	7-9
7.1.5 Electro-Explosive Detonators	7-16
7.2 Subsystem Susceptibility	7-16
7.2.1 Communication and Navigation	7-16
7.2.2 Flight Control Equipment	7-18
7.2.3 Weapons	7-21
7.2.4 Radar	7-21
7.3 References	7-25
8.0 General Analysis and Tradeoff Philosophy	8-1
8.1 Standards and Specifications	8-1
8.2 The System Approach	8-2
8.2.1 Electromagnetic Compatibility (EMC) Program	8-2
8.2.2 Electromagnetic Compatibility (EMC) Plans	8-3
8.2.3 EMC Program Implementation	8-7

Table of Contents (Continued)

<u>Section</u>	<u>Page</u>
8.3 EMC Systems Analysis Procedure Synthesis	8-7
8.3.1 Drivers in Procedure Synthesis	8-7
8.3.2 Guide to EMC Procedure Synthesis	8-15
8.4 Description of Programs and Facilities	8-15
8.4.1 Electromagnetic Compatibility Analysis Center (RADC)	8-16
8.4.2 Intrasytem Analysis Program	8-24
8.4.3 Interference Prediction Process - Number 1 (IIP-1)	8-34
8.4.4 The Cosite Analysis Model (COSAM)	8-35
8.4.5 Specification and Electromagnetic Compatibility Analysis Program (SEMCAP)	8-36
8.4.6 Shipboard Electromagnetic Compatibility Analysis (SEMCA)	8-37
8.5 Data Base Management	8-37
8.5.1 ECAC Data Base Management	8-38
8.5.2 IAP Data Base Management	8-38
8.6 References	8-40
9.0 Measurement Test and Evaluation	9-1
9.1 Techniques for Measuring Intrinsic Parameters	9-1
9.1.1 Permeability	9-1
9.1.2 Permittivity	9-3
9.1.3 Resistivity	9-5
9.1.4 Conductivity	9-7
9.2 EM Shielding Effectiveness Measurement Techniques	9-20
9.2.1 Coupling Between Loops and Probes	9-20
9.2.2 Plane Wave Transmission/Reflection Methods	9-24
9.2.3 Surface Impedance Parameters	9-28
9.2.4 Joint Measurement Techniques	9-32
9.2.5 High Current Injection	9-36
9.2.6 High Voltage Charging-Discharging Phenomena	9-43
9.3 References	9-45
10.0 Protection Methods and Techniques	10-1
10.1 Present Aircraft Protection Systems	10-1
10.1.1 Static Dischargers	10-2
10.1.2 Lightning Arresters	10-2
10.1.3 Radome Strips	10-2
10.1.4 Composite Coating Protection Systems	10-2
10.2 Future Composite Protection-Doping and Intercalation	10-21
10.3 References	10-27
11.0 Design Guidelines	11-1
11.1 Overview	11-1
11.2 Electromagnetic Design Guidelines	11-3
11.2.1 External Electromagnetic Fields	11-5
11.2.2 Electromagnetic Shielding [$T_1(f)$ and $T_2(f)$]	11-5
11.2.3 Joint Leakage [$T_3(f)$]	11-15
11.2.4 Cables [$T_4(f)$]	11-17
11.2.5 Subsystem Susceptibility [$T_5(f)$]	11-21
11.3 Unprotected Aircraft Performance Guidelines	11-23

List of Illustrations

Figure		Page
1.1	Aerospace Avionics Device Technology Trends	1-2
1.2	Electromagnetic System Parameters	1-4
1.3	Peak Open Circuit Voltage Versus Line Length for Three Threats and Four Coupling-Transmission Line Configurations, $X_0 = 0.05m$, $Z_L = 100\Omega$	1-5
1.4	Upper Bounds on Peak Power Versus Line Length for Three Threats and Four Coupling-Transmission Line Configurations $X_0 = 0.5m$, $Z_L = 100\Omega$	1-6
1.5	Wunsch Constant Versus Line Length for Three Threats and Four Coupling-Transmission Line Configurations, X_0	1-7
1.6	Top View of F-14 Using Triangular Patch Data Base of Reference 4	1-8
1.7	Side View of F-14 Using Triangular Patch Data Base of Reference 4	1-9
1.8	Comparison of Surface Current Density with MRC/EMA Code and Surface Patch Model Used in This Report	1-11
1.9	Skin Current Density J_{SC} on Edge No. 29 for Near-Strike Lightning Excitation and Different Rise Times, τ	1-12
1.10	Skin Current Density on Edge No. 29 of Triangular Patch Model of F-14 Aircraft for Various Rise Times τ of Incident NEMP	1-13
1.11	Transfer Impedance Shielding of Structural Materials and Protective Electromagnetic Coatings	1-14
1.12	Improvement Protective Coatings Provided Relative to 8-ply Graphite/Epoxy	1-14
1.13	Weight Penalty Imposed by Protective Coatings	1-15
1.14	Weight/Shielding Figure of Merit of EM Protective Coatings	1-15
2.1	Thundercloud Profile Showing Charge Centers and Temperature and Pressure Gradients (after (1))	2-2
2.2	Current Waveform (not to scale) for a Lightning Flash to Ground	2-5
2.3	Radiated Lightning Spectrum Normalized to 10 km (an EMP spectrum is included for comparison)	2-6
2.4	Radiated Lightning Spectrum Normalized to One Statute Mile	2-6
2.5	Triangular Lightning Current Waveform	2-8
2.6	Space Shuttle Lightning Current Waveform	2-8
2.7	Double Exponential Lightning Current Waveform	2-8
2.8	Triple Exponential Lightning Current Waveform	2-10
2.9	Quadruple Exponential Lightning Current Waveform	2-10
2.10	Spectrum of Space Shuttle Current Lightning Waveform	2-11
2.11	Spectrum of Space Shuttle Current Lightning Waveform	2-12
2.12	Exponential Current Lightning Waveforms	2-12
2.13	Superposition of All Lightning Current Waveforms	2-13
2.14	Lightning Attachment	2-15
2.15	Swept Stroke Phenomenon	2-15
2.16	Aircraft Lightning Strike Zones	2-15
2.17	Lightning Strike Zones	2-15
2.18	Noise Spectrum Properties	2-18
2.19	Noise Spectrum Properties	2-18
2.20	Current Pulses Resulting from Streamers of Several Lengths	2-18

List of Illustrations
(Continued)

<u>Figure</u>		<u>Page</u>
2.21	RF Environment (10 kHz - 100 MHz)	2-20
2.22	RF Environment (100 - 1 GHz)	2-21
2.23	RF Environment (1 - 10 GHz)	2-21
2.24	RF Environment (10 - 100 GHz)	2-21
2.25	EMP Time Domain Waveform	2-27
2.26	EMP in Frequency Domain	2-27
2.27	Back-face Temperature of Graphite/Epoxy Substrate for Several Pulse Fluence Levels	2-30
2.28	Laser Energy Density Necessary to Produce a Level of Stress for Two Failure Modes	2-30
3.1	Fiber-reinforced Composite Material	3-2
3.2	PAN Fiber Graphitization Process	3-4
3.3	Graphite Fiber Tow	3-4
3.4	Boron Fiber Manufacturing Process together with a Boron Cross-section	3-4
3.5	Tape (prepreg) and Broad Goods Fabrication Processes	3-6
3.6	Symmetrical Balanced Layup	3-6
3.7	Composite Fiber Densities Compared to Aircraft Metals	3-10
3.8	Tensile Strength and Modules of Various Composite Fibers and Metals	3-10
3.9	Stress-strain Curves for Composite Fibers	3-11
3.10	Specific Tensile Strength and Modules for Various Composite Fibers and Metals	3-11
3.11	Longitudinal Tensile Strength for Various Single Laminate Composites at Room Temperature (RT) and 350°F	3-13
3.12	Transverse Tensile Strength for Various Single Laminate Composites at Room Temperature (RT) and 350°F	3-13
3.13	Diagonal Tensile/Compressive Strength for Various Single Laminate Composites at Room Temperature (RT) and 350°F	3-13
3.14	Longitudinal Compressional Strength for Various Single Laminate Composites at Room Temperature (RT) and 350°F	3-13
3.15	Transverse Compressive Strength for Various Single Laminate Composites at Room Temperature (RT) and 350°F	3-14
3.16	In-plane Shear Strength for Various Single Laminate Composites at Room Temperature (RT) and 350°F	3-14
3.17	Interlaminar Shear Strength for Various Single Laminate Composites at Room Temperature (RT) and 350°F	3-14
3.18	Diagonal In-plane Shear Strength for Various Single Laminate Composites at Room Temperature (RT) and 350°F	3-14
3.19	Longitudinal Tensile/compression Modulus for Various Single Laminate Composites at Room Temperature (RT) and 350°F	3-15
3.20	Transverse Tension/Compression Modulus for Various Single Laminate Composites at Room Temperature (RT) and 350°F	3-15
3.21	Diagonal Tension/compression modulus for Various Single Laminate Composites at Room Temperature (RT) and 350°F	3-15
3.22	In-plane Shear Modulus for Various Single Laminate Composites at Room Temperature (RT) and 350°F	3-15
3.23	Diagonal In-plane Shear Modulus for Various Single Laminate Composites at Room Temperature (RT) and 350°F	3-16
3.24	Longitudinal Poisson's Ratio for Various Single Laminate Composites at Room Temperature (RT) and 350°F	3-16

Figure	List of Illustrations (Continued)	Page
3.25	Transverse Poisson's Ratio for Various Single Laminate Composites at Room Temperature (RT) and 350°F	3-16
3.26	Diagonal Poisson's Ratio for Various Single Laminate Composites at Room Temperature (RT) and 350°F	3-16
3.27	Longitudinal Thermal Expansion Constant for Various Single Laminate Composites at Room Temperature (RT) and 350°F	3-17
3.28	Transverse Thermal Expansion Constant for Various Single Laminate Composites at Room Temperature (RT) and 350°F	3-17
3.29	Diagonal Thermal Expansion Constant for Various Single Laminate Composites at Room Temperature (RT) and 350°F	3-17
3.30	Single Laminate Composite Densities at Room Temperature (RT) and 350°F	3-18
3.31	Longitudinal Tension Stress-Strain Curve for Various Single Laminate Composites at Room Temperature (solid lines) and 350°F (dotted lines)	3-19
3.32	Transverse Tension Stress-Strain Curve for Various Single Laminate Composites at Room Temperature (solid lines) and 350°F (dotted lines)	3-19
3.33	Diagonal Tension Stress-Strain Curves for Various Single Laminate Composites at Room Temperature (solid lines) and 350°F	3-19
3.34	Bending Stress-Strain Curve for Kevlar 49/Epoxy Compared to Graphite/Epoxy and Aluminum	3-19
3.35	Boron/Epoxy Tensile Strength Curves for the $[0_1/\pm 45_j/90]$ Laminate Family	3-20
3.36	Boron/Epoxy Compressive Strength Curves for the $[0_1/\pm 45_j/90_k]$ Laminate Family	3-20
3.37	Boron/Epoxy In-plane Shear Strength and Modulus Curves $[0_1/\pm 45_j/90_k]$ Laminate Family	3-21
3.38	Boron/Epoxy Extensional Modulus Curves for the $[0_1/\pm 45_j/90_k]$ Laminate Family	3-21
3.39	Boron/Epoxy Poisson's Ratio Curves for the $[0_1/\pm 45_j/90_k]$ Laminate Family	3-22
3.40	Boron/Epoxy Thermal Expansion Coefficient Curves for the $[0_1/\pm 45_j/90_k]$ Laminate Family	3-22
3.41	High-Strength Graphite/Epoxy Tensile Strength Curves for the $[0_1/\pm 45_j/90_k]$ Laminate Family	3-23
3.42	High-Strength Graphite/Epoxy Compressive Strength Curves for the $[0_1/\pm 45_j/90_k]$ Laminate Family	3-23
3.43	Shear Strength Curves for the High-Strength Graphite/Epoxy $[0_1/\pm 45_j/90_k]$ Laminate Family at Room Temperature (RT) and 350°F	3-24
3.44	Extensional Modulus Curves for the High-Strength Graphite/Epoxy $[0_1/\pm 45_j/90_k]$ Laminate Family	3-24
3-45	Shear Modulus Curves for the High-Strength Graphite/Epoxy $[0_1/\pm 45_j/90_k]$ Laminate Family at Room Temperature (RT) and 350°F	3-24
3.46	Poisson's Ratio Curves for the High-Strength Graphite/Epoxy $[0_1/\pm 45_j/90_k]$ Laminate Family	3-25
3.47	Thermal Expansion Coefficient Curves for the High-Strength Graphite/Epoxy $[0_1/\pm 45_j/90_k]$ Laminate Family	3-25
3.48	Tensile Strength Curves for the High-Modulus Graphite/Epoxy $[0_1/\pm 45_j/90_k]$ Laminate Family	3-26
3.49	Compressive Strength Curves for the High-Modulus Graphite/Epoxy $[0_1/\pm 45_j/90_k]$ Laminate Family	3-26
3.50	Shear Strength Curves for the High-Modulus Graphite/Epoxy $[0_1/\pm 45_j/90_k]$ Laminate Family at Room Temperature (RT) and 350°F	3-27

List of Illustrations
(Continued)

<u>Figure</u>	<u>Page</u>
3.51 Extensional Modulus Curves for the High-Modulus Graphite/Epoxy [0 ₁ /+45 _j /90 _k] Laminate Family	3-27
3.52 Shear Modulus Curves for the High-Modulus Graphite/Epoxy [0 ₁ /+45 _j /90 _k] Laminate Family at Room Temperature and 350°F	3-27
3.53 Poisson's Ratio Curves for the High-Modulus Graphite/Epoxy [0 ₁ /+45 _j /90 _k] Laminate Family	3-28
3.54 Thermal Expansion Coefficient Curves for the High-Modulus Graphite Epoxy [0 ₁ /+45 _j /90 _k] Laminate Family	3-28
3.55 Tensile Strength Curves for the Intermediate Strength Graphite Epoxy [0 ₁ /+45 _j /90 _k] Laminate Family	3-29
3.56 Compressive Strength Curves for the Intermediate-Strength Graphite/Epoxy [0 ₁ /+45 _j /90 _k] Laminate Family	3-29
3.57 Shear Strength Curves for the Intermediate-Strength Graphite/Epoxy [0 ₁ /+45 _j /90 _k] Laminate Family	3-30
3.58 Extensional Modulus Curves for the Intermediate Strength Graphite/Epoxy [0 ₁ /+45 _j /90 _k] Laminate Family	3-30
3.59 Shear Modulus Curves for the Graphite/Epoxy [0 ₁ /+45 _j /90 _k] Laminate Family at Room Temperature (RT) and 350°F	3-30
3.60 Poisson's Ratio Curve for the Intermediate-Strength Graphite/Epoxy [0 ₁ /+45 _j /90 _k]	3-31
3.61 Thermal Expansion Coefficient Curves for the Intermediate-Strength Graphite/Epoxy [0 ₁ /+45 _j /90 _k] Laminate Family	3-31
3.62 Longitudinal Tensile Strength for the [0/60] Boron/Epoxy and Graphite/Epoxy Laminate at Room Temperature (RT) and 350°F	3-32
3.63 Transverse Tensile Strength for the [0/60] Boron/Epoxy and Graphite/Epoxy Crossplied Laminates at Room Temperature (RT) and 350°F	3-32
3.64 Longitudinal Compressive Strengths for the [0/60] Boron/Epoxy and Graphite/Epoxy Crossplied Laminates at Room Temperature (RT) and 350°F	3-32
3.65 Transverse Compressive Strengths for the [0/60] Boron/Epoxy and Graphite/Epoxy Crossplied Laminates at Room Temperature (RT) and 350°F	3-32
3.66 In Plan Shear Strengths for the [0/60] Boron/Epoxy and Graphite/Epoxy Crossplied Laminates at Room Temperature (RT) and 350°F	3-33
3.67 Tension/Compression Modulus for the [0/60] Boron/Epoxy and Graphite/Epoxy Crossplied Laminates at Room Temperature (RT) and 350°F	3-33
3.68 In-Plane Shear Modulus for the [0/60] Boron/Epoxy and Graphite/Epoxy Crossplied Laminates at Room Temperature (RT) and 350°F	3-33
3.69 Poisson's Ratio for the [0/60] Boron/Epoxy and Graphite/Epoxy Crossplied Laminates at Room Temperature (RT) and 350°F	3-33
3.70 Thermal Expansion Constants for the [0/60] Boron/Epoxy and Graphite/Epoxy Crossplied Laminates at Room Temperature (RT) and 350°F	3-34
3.71 Denisites for [2/60] Boron/Epoxy and Graphite/Epoxy Crossplied Laminates	3-34

List of Illustrations
(Continued)

<u>Figure</u>		<u>Page</u>
3.72	Laminate Ultimate Tensile and Shear Strength Versus Percent of Laminate, S-GL/T300/S-GL ($0^\circ/\pm 45^\circ/90^\circ$) Family	3-39
3.73	Laminate Ultimate Compression Strength Versus Percent of Laminate, S-GL/T300/S-GL ($0^\circ/\pm 45^\circ/90^\circ$) Family	3-39
3.74	Laminate E_x & G_{xy} Versus Percent Laminate S-GL/T300/S-GL ($0^\circ/\pm 45^\circ/90^\circ$) Family	3-39
3.75	Poisson's Ratio ν_{xy} S-GL/T300/S-GL ($0^\circ/\pm 45^\circ/90^\circ$) Family	3-39
3.76	Longitudinal Coefficient of Thermal Expansion S-GL/T300/S-GL ($0^\circ/\pm 45^\circ/90^\circ$) Family	3-39
3.77	Laminate Ultimate Tensile and Shear Strength Versus Percent of Laminate T300/K-49/T300 ($0^\circ/\pm 45^\circ/90^\circ$) Family	3-39
3.78	Laminate Ultimate Compressive Strength Versus Percent of Laminate T300/K-49/T300 ($0^\circ/\pm 45^\circ/90^\circ$) Family	3-40
3.79	Laminate E_x & G_{xy} Versus Percent of Laminate T300/K-49/T300 ($0^\circ/\pm 45^\circ/90^\circ$) Family	3-40
3.80	Poisson's Ratio ν_{xy} T300/KEV-49-181/T300 ($0^\circ/\pm 45^\circ/90^\circ$) Family	3-40
3.81	Longitudinal Coefficient of Thermal Expansion T300/KEV-49-181/T300 ($0^\circ/\pm 45^\circ/90^\circ$) Family	3-41
3.82	Constant Amplitude Fatigue Data for Unidirectional Boron/Epoxy For $R=0.1$ At Various Temperatures	3-41
3.83	Constant Amplitude Fatigue Data for [0/90] and (0/ ± 45 /90] Cross-plyed Boron/Epoxy Laminates at Room Temperature at $R=0.1$	3-41
3.84	Constant Amplitude Fatigue Data for Unidirectional High-Strength (HS) and High-Modulus (HM) Graphite/Epoxy Laminates at Room Temperature and $R=0.1$	3-42
4.1	Lear Fan 2100, All-Composite Business Aircraft	4-5
4.2	Advanced Composites on the Boeing 767 Transport	4-5
4.3	Navy/McDonnell Douglas AV-8B Advance Harrier Composite Aircraft	4-5
4.4	Use of Composites on the Navy F/A-18	4-7
4.5	Composite Applications on the Dornier Light Transport Aircraft	4-7
4.6	Rolls-Royce RB.211-535 Aircraft Engine	4-7
4.7	Simple Beam Builder Concept for Space Applications Using the Space Shuttle	4-7
4.8	Weight and Cost Savings Possible by Use of Composites for Primary Structures in Transport Aircraft. Chart prepared by NASA	5-13
4.9	Graphite/Epoxy Wing Box	5-13
4.10	Experimental Ford LTD Graphite/Epoxy Automobile	5-15
5.1	Conductivity σ (mhos/m) of Kevlar/Epoxy as a Function of E-Field	5-5
5.2	Conductivity Vs Frequency for Graphite/Epoxy Multi-Ply Samples of Narmco 5208 and Mercurus 3501. The Field is Parallel to 0° Fibers	5-9
5.3	Conductivity Vs Frequency for Unidirectional Samples of Narmco 5208 and Mercurus 3501 Graphite/Epoxy Composite Material. The Field is Parallel to the Fibers	5-9
5.4	Conductivity Vs Frequency for Multi-Ply and Unidirectional Samples of Narmco 5208 and Mercurus 3501 Graphite/Epoxy Composite. The Field is Normal to the 0° Fibers	5-10
5.5	Conductivity Vs Frequency of Samples of Graphite/Epoxy Composite Compared to Samples of Boron/Epoxy and to Aluminum (75MHz-2GHz)	5-10
5.6	Bulk Conductivity Vs Frequency for Samples of 2-Ply and 4-Ply Graphite/Epoxy Composite Material (Mercurus AS3501)	5-11
5.7	Surface Conductivity of Samples of Hercules AS 3501 Graphite/Epoxy Composite Material as a Function of Frequency	5-11

List of Illustrations
(Continued)

<u>Figure</u>		<u>Page</u>
5.8	Conductivity Enhancement for Samples of Hercules AS 3501 Graphite/Epoxy Composite Materials at Two Temperatures	5-14
5.9	Conductivity Enhancement in Samples of Boron Fibers in the Temperature Range 1000°C-1200°C	5-14
5.10	Graphite Crystal Structure	5-15
5.11	Stage Structure for Graphite Interrelated with Potassium	5-17
5.12	Conductivity of Intercalated and Regular Graphite/Epoxy Composite Samples as a Function of Filling Factor	5-17
5.13	Typical Conductivity-Temperature Profile for a Semiconductor	5-20
5.14	Boron Fiber Resistance as a Function of Temperature	5-20
5.15	Transverse Conductivity of Graphite/epoxy (Unidirectional as a Function of Immersion Time in Water at 23°C.	5-20
6.1	Coaxial Loops Separated by An Infinite Plate	6-2
6.3	Normal Incidence Excitation of n Isotropic Composite Layers	6-7
6.4	Oblique Incidence Excitation of n Isotropic Composite Layers	6-7
6.5	Anisotropic Composite Layer Principal Coordinates (Primed) as Related to Global Coordinates (Unprimed)	6-10
6.6	Surface Transfer Impedance as a Function of Frequency	6-26
6.7	Measured Surface Transfer Impedance of 24 Ply T-300 Graphite/Epoxy	6-26
6.8	Magnetic Shielding Effectiveness of a Flat Plate under a Uniform Magnetic Field	6-28
6.9	Magnetic Shielding Effectiveness With a Uniform Incident Magnetic Field	6-28
6.10	Magnetic Shielding Effectiveness of an Enclosure under a Uniform Magnetic Field as a Function of Volume-to-Surface Ratio	6-28
6.11	Magnetic Shielding Effectiveness Breakpoint Behavior for Enclosures	6-28
6.12	Magnetic Shielding of 12 ply (0°, ±45°, 90°) Graphite/Epoxy Bare and with Protection	6-29
6.13	Magnetic Shielding for 24-Ply (0°, ±45°, 90°) Graphite/Epoxy Bare and with Protection	6-29
6.14	Magnetic Shielding Effectiveness for a Mixed-Orientation Graphite/Epoxy Composite Enclosure under a Uniform Field on a Function of Volume-to-Surface. Conductivity = 10^4 . Shield Thickness = 0.003 m	6-30
6.15	Infinite Flat Plate with a Nonuniform Incident Magnetic Field Test Results	6-30
6.16	Magnetic Shielding Effectiveness of a Flat Plate under a Non-uniform Magnetic Field Generated by a Loop Antenna Parallel to the Plate	6-31
6.17	Shielding Effectiveness using Surface Transfer Impedance	6-32
6.18	Electric Shielding Effectiveness of an Enclosure under a Uniform Electric Field	6-34
6.19	Electric Shielding Effectiveness of an Enclosure under a Uniform Electric Field as a Function of Enclosure Volume-to-Surface Ratio	6-34

List of Illustrations
(Continued)

Figure		Page
6.20	E-Field Shielding for 12-ply Graphite/Epoxy Composite Panel	6-35
6.21	E-Field Shielding for 24-ply Graphite/Epoxy Composite Panel	6-35
6.22	Plane-Wave Shielding Effectiveness for 12-ply Graphite/Epoxy Composite Panel	6-36
6.23	Plane-Wave Shielding Effectiveness for 24-ply Graphite/Epoxy	3-36
6.24	High Frequency Graphite/Epoxy Shielding Effectiveness Data	6-37
6.25	Transfer Impedance Shielding of Structural Materials and Protective	6-39
6.26	Improvement Protective Coatings Provide Relative to 8-Ply Graphite/Epoxy (Valid for Frequencies below 10^5 Hz)	6-39
6.27	Forward Fuselage (area = 100 ft ²) Weight Penalty (lbs) Imposed by EM Protective Coatings	6-40
6.28	Weight Shielding Figure of Merit (Shielding Beyond 8-Ply Graphite/Epoxy) of EM Protective Coatings	6-40
6.29	Gain in the Magnetic Shielding Effectiveness of 24-Ply T-300 Graphite Composite Through Applications of Aluminum Foil, Aluminum Screen, and Phosphor Bronze Screen to 24-Ply T-300 Graphite	6-40
6.30	Coating Thickness and Weight Penalty for $Z_{st} = -40$ dB at Low Frequency	6-43
6.31	Coating Thickness and Weight Penalty for $Z_{st} = -60$ dB at Low Frequency	6-43
6.32	Coating Thickness and Weight Penalty for $Z_{st} = -72$ at Low Frequency	6-44
6.33	Joint Coupling	6-44
6.34	Structural Joints	6-45
6.35	Measured Joint Admittance	6-45
6-36	Equivalent Circuit for a Narrow Slot in a Thick Conducting Screen	6-47
6-37	Magnetic Shielding Effectiveness for Tightly Joined Panels	6-48
6-38	Electric Shielding Effectiveness of Tightly Joined Panels	6-48
6-39	Plane-Wave Shielding Effectiveness of Tightly Joined Panels	6-49
6-40	Variation of Magnetic Shielding Effectiveness of 12-Ply Graphite/Epoxy Panels Joined to 24 Ply Graphite/Epoxy Doubler With Hi-Loks	6-49
6.41	Variation of E-Field Shielding Effectiveness of 12-Ply Graphite/Epoxy Joined to 24 Ply Graphite/Epoxy Doubler with Hi-Loks	6-50
6.42	Variation of Plane-Wave Shielding Effectiveness for 12 Ply Graphite/Epoxy Panels Joined to 24 Ply Graphite/Epoxy Doubler With Hi-Loks	6-50
7.1	Amplifier Susceptibility	7-3
7.2	Digital Computer Emission Spectrum	7-3
7.3	Typical Digital Circuit Susceptibility Curves	7-4
7.4	RF Induced Diode Characteristics for IN914 Diode at 220 MHz	7-6
7.5	Characteristics of a 2N2369A Transistor With and Without RF Interference on the Collector Lead	7-6
7.6	Characteristics of a 2N2222A Transistor With and Without RF Interference on the Collector Lead	7-6

List of Illustrations
(Continued)

<u>Figure</u>		<u>Page</u>
7.7	RF Induced Beta Reduction at 220 MHz. RF stimulates the base lead	7-6
7.8	Modified Ebers-Moll NPN Transistor Model Including RF Interference Effects	7-6
7.9	Transistor Characteristics Calculated Using Modified Ebers-Moll Model for the 2N2369A and 2N2222A Transistors	7-6
7.10	Wunsch Constant Range for Representative Transistors	7-8
7.11	Worst Case Susceptibility Values for TTL Devices	7-10
7.12	Worst Case Susceptibility Values for CMOS Devices	7-10
7.13	Worst Case Susceptibility Values for Line Drivers and Receivers	7-11
7.14	Worst Case Susceptibility Values for 0 Amps	7-11
7.15	Worst Case Susceptibility Values for Voltage Regulators	7-11
7.16	Worst Case Susceptibility Values for Comparators	7-12
7.17	Worst Case Susceptibility Values for IC Devices	7-12
7.18	Integrated Circuit Power Density Susceptibility Curves	7-14
7.19	Modified Ebers-Moll Model of 7400 NAND Gate with External Model Configuration used With Computer Circuit Program SPICE	7-14
7.20	Output Voltage for Three 7400 NAND Gate Types Vs Incident RF Power as Simulated by SPICE. Susceptibility Levels of 0.8V for low State and 2.0V for High State Are Shown	7-15
7.21	Values of RF Power Which Cause EM Susceptibility Criteria To Be Exceeded for Three 7400 NAND Gate Types	7-15
7.22	Worst Case IC Failure Levels	7-15
7.23	Range of A for Various Devices	7-15
7.24	Damage Levels for Linear and Digital IC Devices	7-17
7.25	Upset and Burnout Energy of Various Circuit Elements	7-17
7.26	Maximum Field Strength Limits for EEDs	7-17
7.27	Signal-to-Interference Ratio Versus Articulation Score	7-17
7.28	Inertial Navigation System	7-20
7.29	Flight Control System Block Diagram	7-20
7.30	EM Threshold Limits for Various Weapon Systems	7-22
7.31	EM Threshold Limits for Nuclear Weapons	7-22
7.32	Radar Receiver Representation	7-22
7.33	Radar Performance Prediction Flow Chart	7-23
7.34	Radar Range Reduction Due to Radar Desensitization	7-24
8.1	EMC - Cost Effectiveness Tradeoff Model for a System Configuration	8-1
8.2	Driving Elements in EMC Procedure Synthesis	8-11
8.3	IEMCAP Functional Flow	8-13
8.4	TEMACS Structure	8-13
9.1	Permeability Measure Apparatus	9-2
9.2	Permittivity Measurement Apparatus	9-4
9.3	Use of a Guarded Electrode in Composite Sample Capacitors	9-4
9.4	The Two-Point Method for Measurement of Resistivity or Conductivity	9-6
9.5	Four-Point Method for Measurement of Resistivity or Conductivity	9-8

List of Illustrations
(Continued)

Figure	Page
9.6 The Slotted Stripline	9-10
9.7 Low Conductivity Stripline Together with Transmission Line Model	9-12
9.8 Longitudinal Conductivity Model	9-14
9.9 Longitudinal Conductivity Model for Boron/Epoxy	9-16
9.10 Random Fiber Model	9-19
9.11 Two Dipole Method	9-21
9.12 Fully Enclosed System for Measuring Shielding	9-23
9.13 Uniform Plane Wave Shielding Concepts	9-25
9.14 Coaxial System	9-25
9.15 Rectangular Waveguide System	9-25
9.16 Anechoic Chamber System	9-27
9.17 TEM Cell System	9-27
9.18 Near Field Antenna Measurement System	9-27
9.19 Bridge Configuration	9-29
9.20 Equivalent Circuit of Non Ideal Partition	9-29
9.21 Surface Transfer Admittance Measurement With Short Circuit Termination	9-31
9.22 Quadaxial Schematic	9-33
9.23 Schematic of Quadraxial Test Fixture	9-33
9.24 Joint Admittance (different materials joined)	9-35
9.25 Group 1 Standard Lightning Waveform	9-38
9.26 Group 2 Component D Standard Lightning Waveform	9-39
9.27 Basic Circuit For Generating Standard Test Current Waveforms	9-41
9.28 Precipitation Static Test Technique	9-44
10.1 Aircraft Protection Devices	10-3
10.2 Radome Lightning Protection Using Metallic and Segmented Diverters	10-3
10.3 Relative Merit of Lightning Protective Systems	10-7
10.4 Relative Damage Estimates	10-7
10.5 Tension Data on Lightning Protected 10 Ply Graphite/Epoxy Laminates	10-8
10.6 Tension Data for Lightning Protected Graphite-Glass/Epoxy 10 Ply Hybrid Laminates	10-8
10.7 Tension Data for Lightning Protected Graphite-Boron/Epoxy 10 Ply Hybrid Laminates	10-9
10.8 Tension Data for Lightning Protected Graphite-Kevlar/Epoxy	10-11
10.9 Bolted Joint Panel with Protection	10-11
10.10 Bonded Joint Panel with Protection	10-11
10.11 Laminate with Substructure with Protection Isolated and Grounded Fasteners	10-12
10.12 Honeycomb Panel with Bonded Titanium Substructure with Protection	10-12
10.13 Relative Protection Grades of Specimens Exposed to 140°F/100% RH for 1,000 Hours	10-13
10.14 Relative Protection Grades of Specimens Exposed to 1,000 Cycles in the Webber Chamber (-65°F to +250°F)	10-13
10.15 Relative Protection Grades of Environmentally Exposed Specimens Zone 1A Lightning Tests	10-13

List of Illustrations
(Continued)

<u>Section</u>	<u>Page</u>
10.16 Relative Protection Grades of 20 Ply Laminates - Mechanically Damaged and Repaired	10-15
10.17 Relative Protection Grades of Sandwich Panels Mechanically Damaged and Repaired	10-15
10.18 Relative Protection Grades of 20 Ply Laminates Lightning Damaged and Repaired	10-15
10.19 Relative Protection Grades of Sandwich Panels Lightning Damaged and Repaired	10-15
10.20 Spray-and-Bake Coating Selection - Humidity Tests	10-18
10.21 Relative Coating Effectiveness in Moisture Penetration Under Humidity Exposure (6 x 6 in. Panels)	10-18
10.22 Relative Coating Effectiveness in Moisture Penetration Under Thermal Spiking Exposure (6 x 6 in. Panels)	10-19
10.23 Coating Selection - Flexural Stress (260°F) as Percent of Unexposed Strength	10-20
10.24 Coating Selection - Horizontal Shear Strength (260°F) as Percent of Unexposed Strength	10-20
10.25 Effect of Paint Protection on Moisture Pickup of Solid-Foil-Coated Graphite/Epoxy	10-22
10.26 Effect of Paint Protection on Moisture Pickup of Alumazite Z-Coated Graphite/Epoxy	10-22
10.27 Effect of Paint Protection on Moisture Pickup of Thermally Spiked Solid Foil-Coated Graphite/Epoxy	10-22
10.28 Effect of Paint Protection on Moisture Pickup of Thermally Spiked Alumazite Z-Coated Graphite/Epoxy	10-22
10.29 Coating Serviceability Evaluation - Flexural Stress (260°F) as Percent of Unexposed Strength	10-23
10.30 Coating Serviceability Evaluation - Horizontal Shear Strength (260°F) as Percent of Unexposed Strength	10-23
10.31 Magnetic Shielding Effectiveness for 10 Ply Graphite/Epoxy Panel	10-23
10.32 Magnetic Shielding Effectiveness for 24 Ply Graphite/Epoxy Panel	10-23
10.33 Electric Shielding Effectiveness for 12 Ply Graphite/Epoxy Panel	10-24
10.34 Electric Shielding Effectiveness for 24 Ply Graphite/Epoxy Panels	10-24
10.35 Plane Wave Shielding Effectiveness for 12 Ply Graphite/Epoxy Panel	10-24
10.36 Plane Wave Shielding Effectiveness for 24 Ply Graphite/Epoxy Panel	10-24
11.1 Integrated, Multidiscipline Approach to Composite Aircraft Design	11-2
11.2 Composite Aircraft Electromagnetic System Parameters	11-4
11.3 Threat Spectrum	11-6
11.4 RF Signal Threat	11-7
11.5 Transmitter Strengths on Carrier Flightdeck	11-7

List of Illustrations
(Continued)

<u>Figure</u>	<u>Page</u>
11.6 Summary of Composite Material Intrinsic Properties	11-8
11.7 Material Conductivities	11-8
11.8 Published Graphite/Epoxy Shielding Data	11-10
11.9 Composite Material Electromagnetic Shielding for 8-Ply Material (0.00107 m) Thickness	11-11
11.10 Magnetic Shielding Effectiveness for Various Shapes	11-12
11.11 Magnetic Shielding Effectiveness for Various Shapes	11-12
11.12 Surface Transfer Impedances for Different Materials	11-14
11.13 Joint Admittance/Unit Width as a Function of Frequency	11-16
11.14 Two-Wire Line Illuminated by Uniform EM Field	11-18
11.15 Wire Over a Ground Plane	11-20
11.16 Shielded Cable Geometry	11-22
11.17 Aerospace Technology Trends	11-22
11.18 Electronic Component Upset and Burnout Energies	11-24
11.19 Worst Case Absorbed Power Susceptibility	11-24
11.20 Worst Case Power Density Susceptibility Values Assuming $\lambda/2$ Aperature	11-25
11.21 Upper Bounds on Open-Circuit Voltage and Short-Circuit Current Due to Diffusion Through Graphite/Epoxy	11-26
11.22 Upper Bounds on Power Delivered to Transmission Line Termination; Minimum Wunsch Constant of Devices that Will Survive Threat	11-27
11.23 Upper Bounds, Due to Joint Coupling, on Open-Circuit Voltage, Short-Circuit Current, and Power Delivered to Transmission Line Termination; Minimum Wunsch Constant of Devices that Will Survive Threat	11-28
11.24 Voltage, Current, Power and Energies Caused by LEMP, NEMP External Fields in Aluminum and Graphite/Epoxy	11-30
11.25 Transfer Impedance Shielding of Structural Material and Protective EM Coatings	11-31
11.26 Improvement Protective Coatings Provided Relative to 8-Ply Graphite/Epoxy	11-32
11.27 Weight Penalty Imposed by Protective Coatings	11-34
11.28 Weight/Shielding Figure of Merit of EM Protective Coatings	11-35

List of Tables

Table		Page
2.1	Representative Characteristics for Cloud-to-Ground Lightning Flashes	2-5
2.2	Generalized Off-Axis Antenna Data	2-25
2.3	Effect of Variable on CW Laser Response of Graphite/Epoxy	2-29
3.1	Composite Fibers and Vendors	3-2
3.2	Matrix Systems - General Characteristics	3-6
3.3	Mechanical Properties for the Boron:graphite/epoxy Hybrid Laminate Systems [$0_B/\pm 45_{GE}/90_{GE}$]	3-36
3.4	Mechanical Properties of the [S-glass/T-300 graphite/S-glass] Hybrid System	3-36
3.5	Mechanical Properties of the [T-300 graphite/Kevlar 49/T-300 graphite] Hybrid System for Several Test Orientation and Temperatures	3-37
3.6	Data Summary of Environmental Effects on Composite Material Properties	3-38
4.1	Composite Application History (before 1973)	4-2
4.2	Present (post 1973) and Near Future Aerospace Composite Applications	4-3
5.1	Composite Material Relative Permeability	5-4
5.2	Relative Permittivity (Dielectric Constant of Kelvar/Epoxy, Boron/Epoxy, Epoxy Resin, and Graphite/Epoxy in the Frequency Range D.C. - 50 MHz	5-4
5.3	The Conductivity σ (mhos/m) of Kevlar/Epoxy as a Function of Frequency	5-4
5.4	Conductivities of Boron/Epoxy Fibers and Resin in Frequency Range D.C. - 50 MHz	5-4
5.5	Effective Conductivity of Boron/Epoxy as a Function of Number of Plies and Ply Orientation. These results are calculated by Skouby using electromagnetic shielding results	5-4
5.6	Preliminary Conductivities for Multiply Boron/epoxy Composites from Allen (DC to 50 MHz)	5-7
5.7	Final Boron/epoxy Conductivities of Multiply Unidirectional Samples Together with an Average Conductivity from Gajda	5-7
5.8	Maximum, Minimum and Average Conductivities Found in a 60 Fiber Sample of Thornel T300 Fiber-type Taken from Narmco 5209 Pre-ply Types of Graphite/epoxy	5-7
5.9	Edge-to-Edge Resistivity of Graphite/epoxy as a Function of Ply Thickness at 1 kHz	5-7
5.10	Volume Resistivity of Graphite/epoxy as a Function of Ply Thickness at 1 kHz	5-7
5.11	Conductivities of Selected Donor and Acceptor Intercalated Graphite Compounds Compared to Pure Graphite and Common Metals	5-18
5.12	Changes in Mechanical Properties of Thornel 75 Graphite Fibers after Intercalation with HNO_3	5-18
5.13	Nonlinear Thresholds for Unidirectional Uniply Graphite/epoxy	5-21
6.1	High Frequency Graphite/Epoxy Shielding Effectiveness Data	6-37
6.2	Coating Thickness and Weight Penalty for Fixed Shielding	6-42

List of Tables
(Continued)

<u>Table</u>		<u>Page</u>
7.1	Radio Navigation System	7-19
7.2	Interference Effects on Radar Receiver Stages Shown in Figure 7.32	7-23
8.1	Outline of Content of EMC Program Plan	8-4
8.2	Outline of Content of EMC Control Plan	8-4
8.3	Outline of Content of EMC Test Plans	8-6
8.4	Phases of the System Acquisition Life Cycle	8-9
8.5	EMC Decisions Within System Life Cycle	8-9
8.6	EMC Guidance Categories	8-10
8.7	Guidance for EMC Decisions	8-10
8.8	Data Available Versus Phases of Life Cycle	8-13
8.9	Major Parameter Fields Contained in Environmental File (E-File)	8-17
8.10	Description of Environmental Data Subfiles	8-18
8.11	Major Parameter Fields in the Nominal Characteristics Field (NCF)	8-20
8.12	Organization and Platform Allowance Files (OPAF)	8-20
8.13	International Source Documents (SAUF)	8-21
8.14	National Source Documents (SAUF)	8-21
8.15	US Military Source Documents (SAUF)	8-22
8.16	Major Data Fields in the Frequency Allocation Application File (FAAF)	8-23
8.17	Data Fields in the Spectrum Signature File	8-23
8.18	Listing of ECAC Models	8-25
8.19	ECAC Data Base Management Program	8-39
9.1	Lightning Parameters and Lightning Effects	9-37
9.2	Group 1 Lightning Waveform Parameters	9-38
9.3	Group 2 Component D Parameters	9-39
9.4	Current Generator Specifications to Produce Standard Lightning Waveforms	9-41
9.5	Waveform Requirements for Component Testing of Aircraft Zones	9-42
10.1	Possible Lightning Protection Systems	10-5
10.2	Lightning Protection System Ranking	10-6
10.3	Shielding Effectiveness Measurements	10-25

In recent years, with the advent of expensive aviation fuel and the possibility of a cutoff of strategic minerals, composite materials have become more and more attractive as substitutes for metals in aircraft due to their superior strength and weight properties. The use of graphite/epoxy, boron/epoxy and, more recently, Kevlar/epoxy on most modern high performance aircraft is increasing at a steady pace to include much secondary structure. By the 1990 time frame, primary structures such as airframes, fuselages and wings are projected to be wholly composites.

The electromagnetic properties of composite materials differ significantly from those of aircraft metals such as aluminum and titanium. Electrical conductivity may vary from essentially zero (Kevlar/epoxy) to values beginning to approach those of metals (graphite/epoxy). The electrical properties of composites have a large impact on such aircraft characteristics as lightning protection, shielding effectiveness, electrical systems, antenna operation, static electricity buildup and radar cross sections.

Composites vary considerably in their electromagnetic (EM) properties and in their susceptibility to EM hazards. Most interest in composites to date has focused on their mechanical and structural properties; less interest has been placed on their electromagnetic properties. Such EM information is vital in order for aircraft manufacturers to provide adequate EM shielding and grounding in order that the aircraft electronic systems operate acceptably in their expected service environment.

Although several studies have been undertaken to identify and measure all relevant composite EM properties, there exists a need to collect and summarize these studies in a form that will be useful to an EMC engineer working with composite structures. It is the purpose of this handbook to help satisfy that need.

Figure 1-1 depicts a need to know the ramifications on aircraft design when combining the technologies of:

- Low-level avionic devices
- Composite materials
- High-level threats

to assure adequate protection which allows aircraft to survive/operate in the high-level threat environments of nuclear electromagnetic pulse (NEMP), lightning (LEMP), and radar. Metallic aircraft design has had over thirty years to mature. However, these established design philosophies must be carefully reexamined when incorporating the above cited new technologies. Especially critical is flight crew safety and mission effectiveness as fly-by-wire composite aircraft and computer-controlled weapons systems replace traditional human-actuated mechanical systems.






	TUBES	DISCRETE TRANSISTORS	INTEGRATED CIRCUITS (IC)	LARGE SCALE INTEGRATED CIRCUITS (LSI)	VERY LARGE SCALE INTEGRATED CIRCUITS (VLSI)
DEVICE	 250V 1 WATT/DEVICE	 TO-18 12V-24V 10 ⁻¹ -10 ⁻² WATTS/DEVICE	 FLAT PACK 5V-12V 10 ⁻² -10 ⁻³ WATTS/TRANS	 LSI 5V-7V 10 ⁻² -10 ⁻⁴ WATTS/TRANS	 VLSI 1.5V-3V 10 ⁻² -10 ⁻⁵ WATTS/TRANS
CAPSULE	GLASS/ METAL/ CERAMIC	METAL/ CERAMIC	METAL/ CERAMIC/ EPOXY	METAL/ CERAMIC/ EPOXY	CERAMIC/ EPOXY
AIRCRAFT	F-8	F-4	F-14	F-14	V10L
AIRFRAME MATERIAL	ALUMINUM	ALUMINUM	ALUMINUM/TITAN	GRAPHITE-EPOXY ALUMINUM	GRAPHITE-EPOXY ?
TIME	PRE-1960's	1960's	1960's	1970's	1980's

Figure 1.1. Aerospace Avionics Device Technology Trends

Loss of aircraft control or mission effectiveness degradation may be categorized by the following:

Category	Determining Parameter(s)
Device upset	V_{OC} , I_{SC}
Device burnout	Energy into device
Airframe damage	Temperature rise and mechanical displacement

The first category is simply a transient condition on a device not resulting in permanent damage, but which may implant erroneous data resulting in incorrect digital system operation. The second condition permanently destroys electronic devices, rendering portions of the avionic system inoperable until replaced. Electromagnetic effects resulting from nuclear EMP and lightning can cause upset or burnout. In addition, lightning can physically damage airframe sections, which may or may not affect flight safety and mission effectiveness depending on the strike location and aircraft design.

The capability of evaluating the magnitude of these effects during aircraft design or upgrade can

- Realize a 60% electromagnetic "hardening" cost savings
- Shorten the design cycle

- Prevent significant redesign efforts
- Aid contractor in meeting government specifications, thereby reducing government/contractor paperwork efforts in modifying specifications
- Increase government/contractor better insight prior to hardening testing

The electromagnetic effects on aircraft avionics can be evaluated with the knowledge of six basic frequency dependent functions. These are denoted by $D(f)$ and $T_1(f)$ through $T_5(f)$, which are illustrated in Figure 1-2. Combining these functions determines the amount of electromagnetic protection $T_6(f)$ required to bring the avionics box open circuit terminal voltage V_{OC} to levels which will not upset or burn out the avionics components. The open circuit voltage, V_{OC} , which represents an upper bound for the actual voltage, may be calculated from the relation

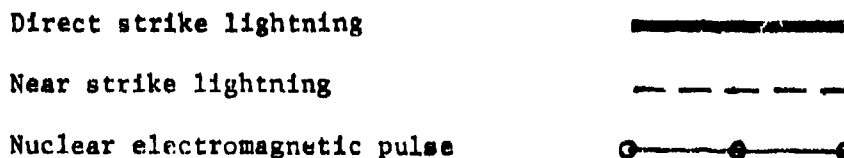
$$V_{OC} = D(f)T_1(f)T_2(f)T_3(f)T_4(f)T_5(f)T_6^{-1}(f)$$

where:

- $D(f)$ - appropriate threat driving function
- $T_1(f)$ - material shielding transfer function
- $T_2(f)$ - current distribution resulting from the aircraft shape and material distribution
- $T_3(f)$ - joint transfer function = $1 + Z_t^{-1} Y_j^{-1}$
- $T_4(f)$ - cable shielding transfer function
- $T_5(f)$ - avionics box terminal penetration characteristic function
- $T_6(f)$ - protective transfer function

This section deals only with the threat $D(f)$, the resulting voltage protection, and the resulting weight penalties imposed by the protection.

Figure 1-3 shows peak avionics box terminal open circuit voltage resulting from the electromagnetic threats of



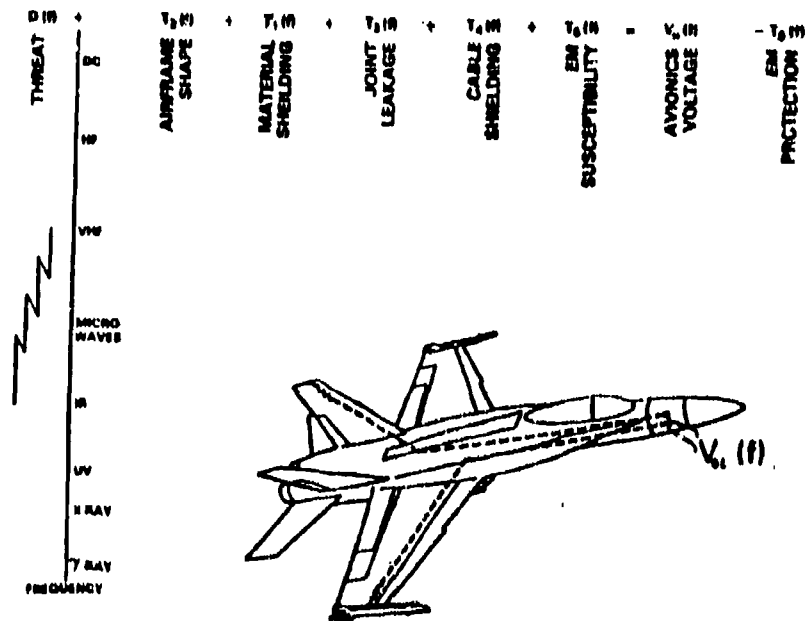


Figure 1.2. Electromagnetic System Parameters

impinging on an F-14 aircraft having an airframe construction of

- All aluminum
- Aluminum and graphite/epoxy

The open circuit voltage V_{OC} is determined by the coupling through composite panels, aluminum panels, and joints which may be summed for total avionics box voltages. An upper bound on the maximum at the box terminal is found by computing the short circuit current at the terminals and multiplying by the open circuit voltage. These results are shown in Figure 1-4. It should be emphasized that these results for peak power represent worst-case values because the open circuit and short circuit conditions cannot occur simultaneously.

Figure 1-5 shows the Wunsch constant results computed for the cases in Figures 1-3 and 1-4. On the right side of Figure 1-5, representative ranges of Wunsch constants for various semiconductor junction devices are given. Thus curves exceeding these Wunsch constant ranges indicate that the device junctions are permanently damaged (burned out) if the avionics box provides no further device protection.

The family of curves in Figures 1-3 through 1-5 were generated from triangular patch surface coupling models of the F-14 similar to those shown in Figures 1-6 and 1-7. These coupling models evaluate the internal electromagnetic fields that result from the aforementioned electromagnetic threats using knowledge of the precise internal electromagnetic flux distribution in the interior of an aircraft under the approximations discussed in Section 6. Coupling models allow accurate calculation of voltages and powers that exist on internal wires of given internal geometric location.

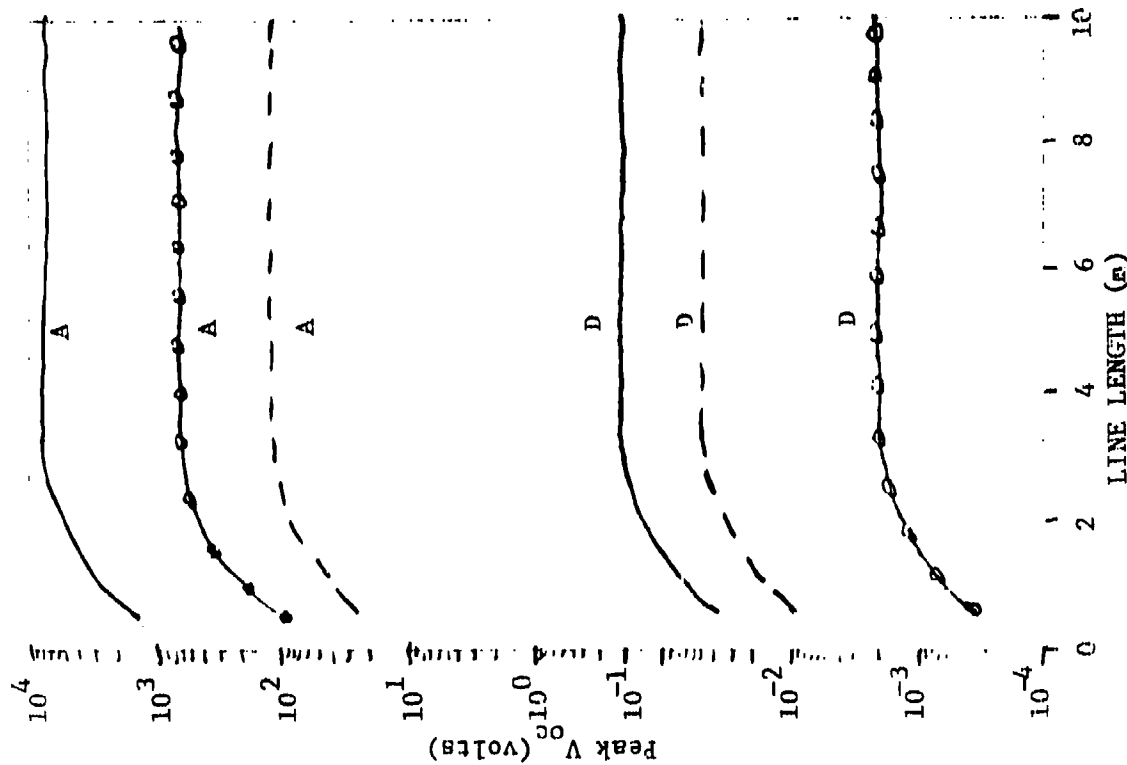
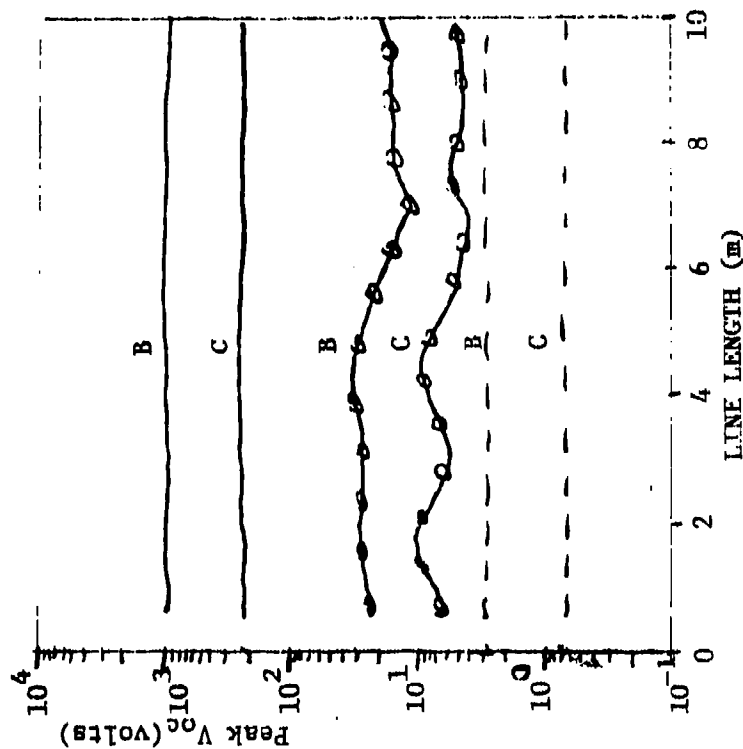


Figure 1.3. Peak Open Circuit Voltage Versus Line Length for Three Threats and Four Coupling-Transmission Line Configurations, $X_o = 0.05m$, $Z_L = 100\Omega$

- A - GRAPHITE EPOXY PANEL COUPLING TO SINGLE WIRE
($\sigma = 2 \times 10^4$ mho/m, THICKNESS = 0 PLY, $L_p = 3m$)
- B - JOINT COUPLING TO SINGLE WIRE ($L_j = 1.79m$)
- C - JOINT COUPLING TO BALANCED TWO-WIRE LINE
($L_j = 1.79m$, $h = 0.5$ in.)
- D - ALUMINUM PANEL COUPLING TO SINGLE-WIRE LINE
($\epsilon = 2.5 \times 10^7$ mho/m, THICKNESS = 1mm, $L_p = 3m$)
- NEP
--- NEAR-STRIKE LIGHTNING
-.- DIRECT-STRIKE LIGHTNING



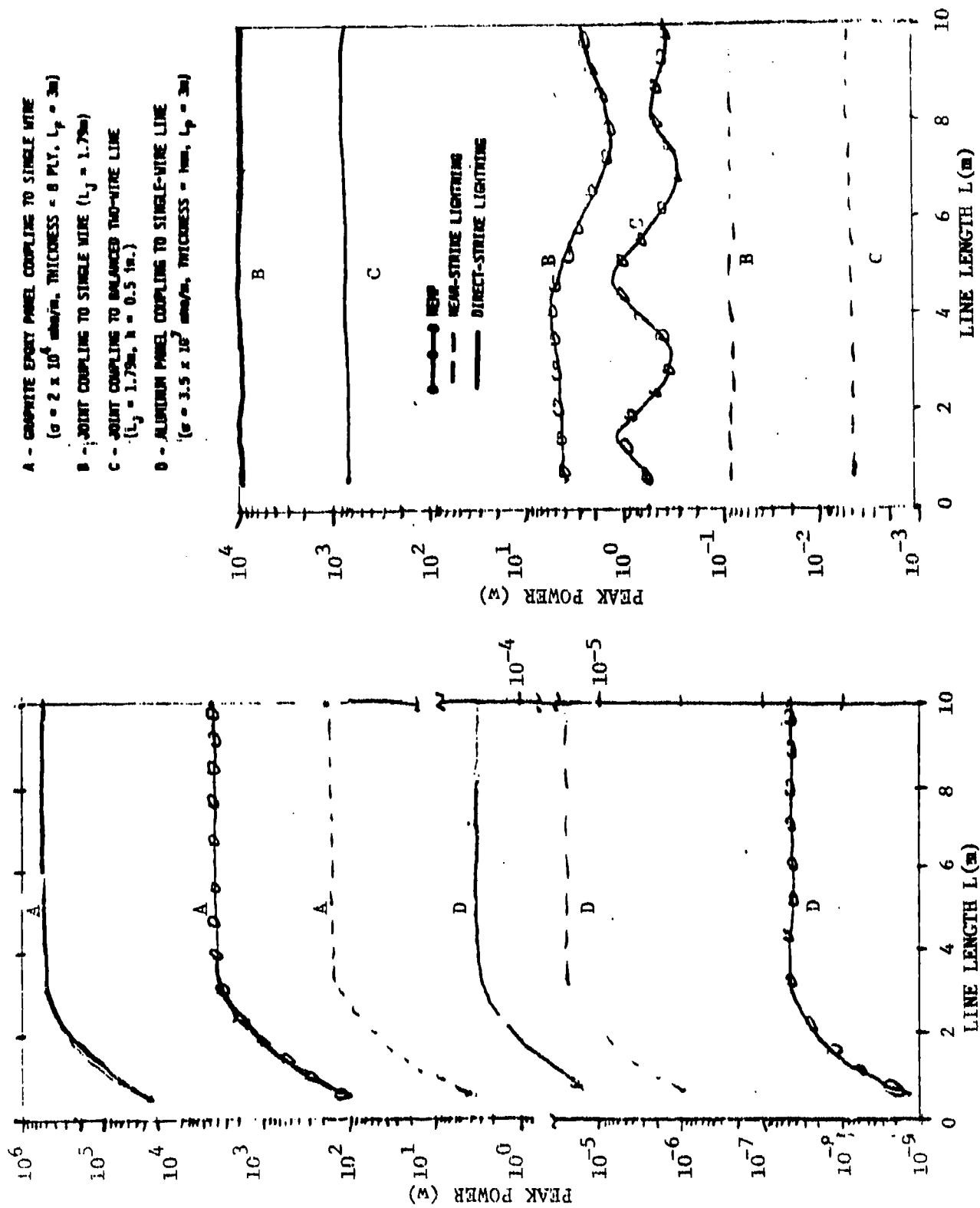


Figure 1.4. Upper Bounds on Peak Power Versus Line Length for Three Threats and Four Coupling-Transmission Line Configurations, $X_0 = 0.5m$, $Z_L = 100\Omega$

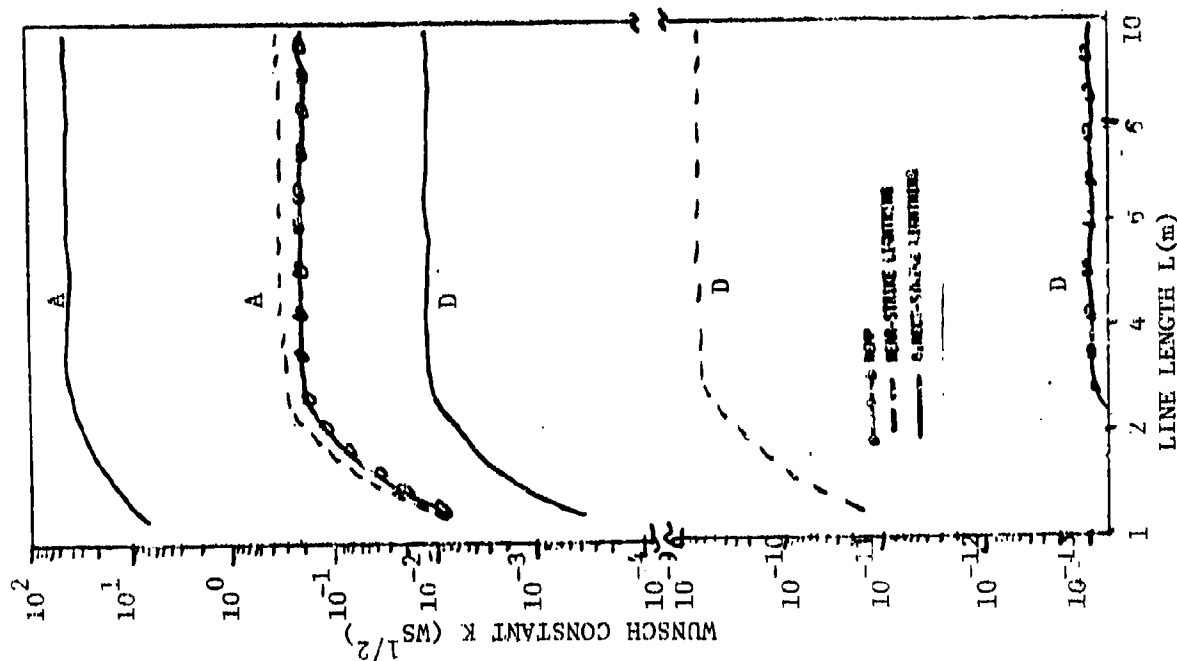
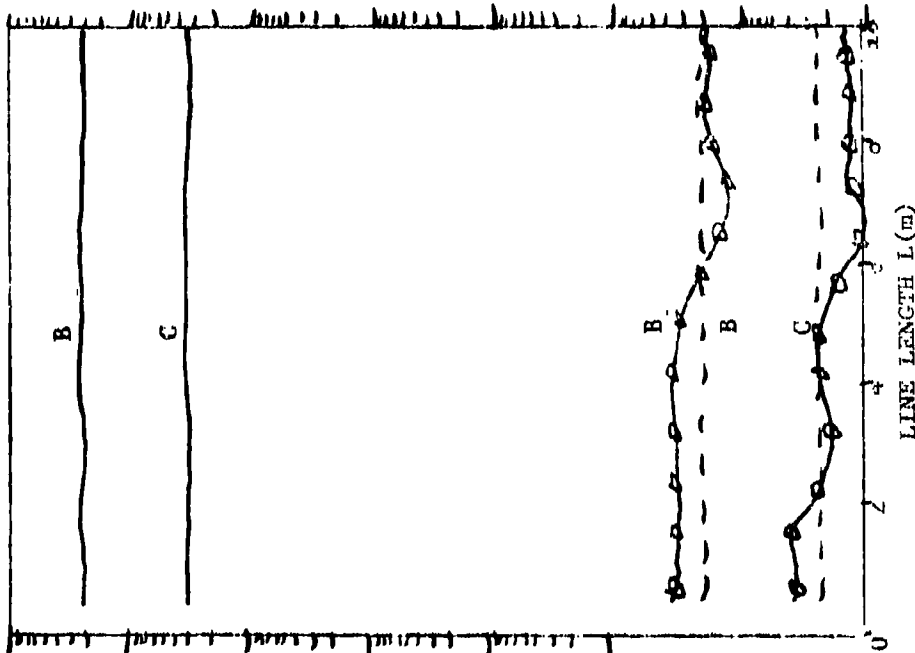
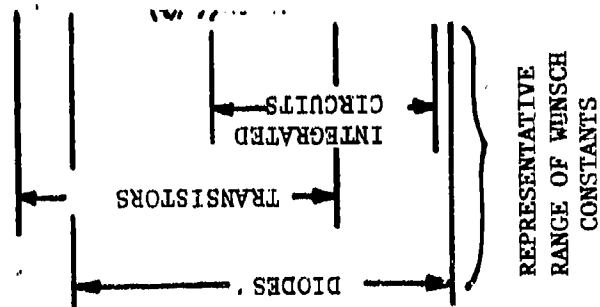


Figure 1.5. Wunsch Constant Versus Line Length for Three Threats and Four Coupling-Transmission Line Configurations, $X_0 = 105m$, $Z_L = 100\Omega$

- A - GRAPHITE EPXY PANEL COUPLING TO SINGLE WIRE
($\sigma = 2 \times 10^4$ ohm/m, THICKNESS = 8 MIL, $L_p = 3m$)
- B - JOINT COUPLING TO SINGLE WIRE ($L_j = 1.75m$)
- C - JOINT COUPLING TO BALANCED TWO-WIRE LINE
($L_j = 1.75m$, $b = 0.5$ in.)
- D - ALUMINUM PANEL COUPLING TO SINGLE-WIRE LINE
($\sigma = 3.5 \times 10^7$ ohm/m, THICKNESS = 1mm, $L_p = 3m$)



WUNSCH CONSTANT K ($WS^{1/2}$)

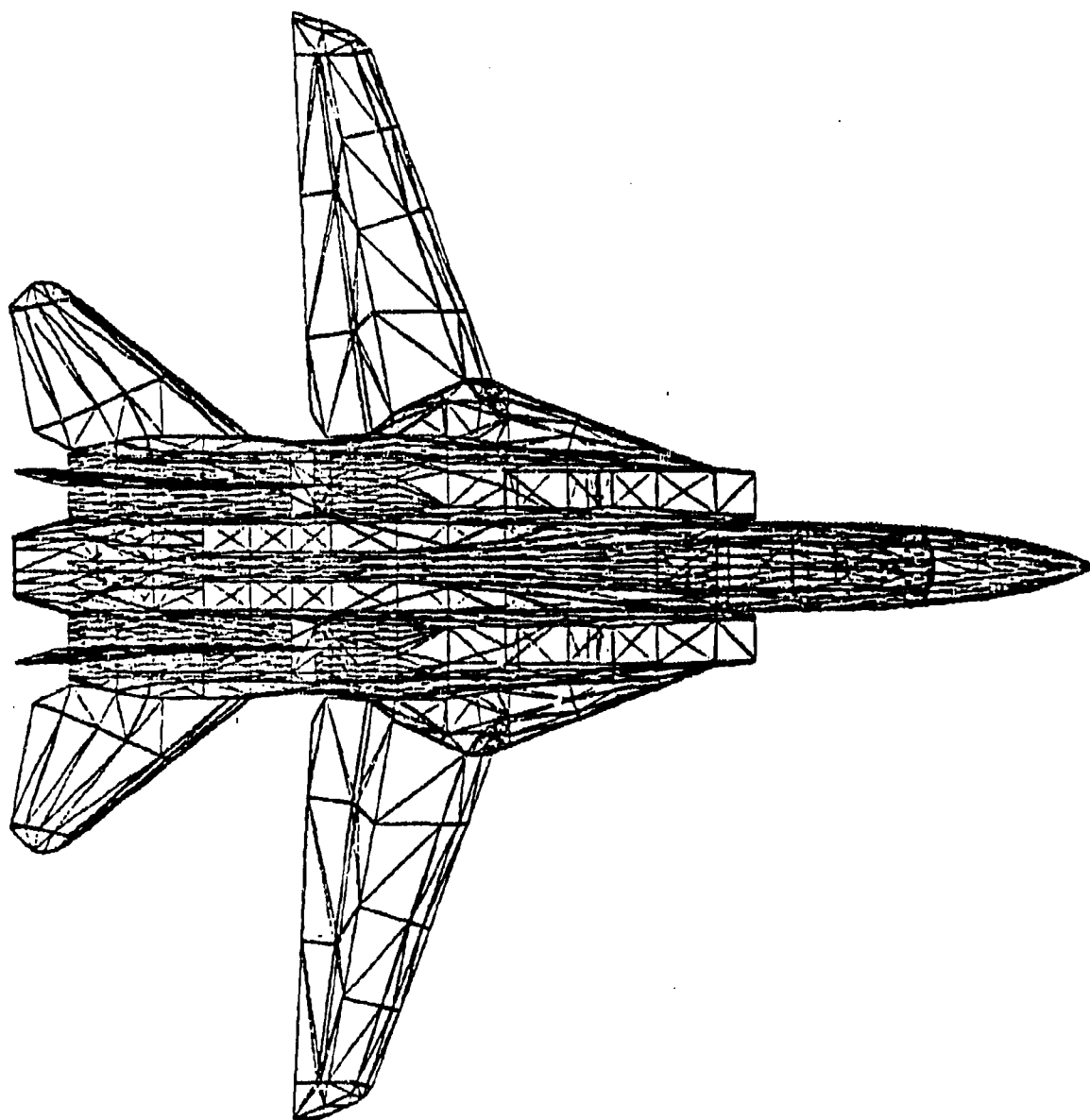


Figure 1.6. Top View of F-14 Using Triangular Patch
Data Base of Reference 4

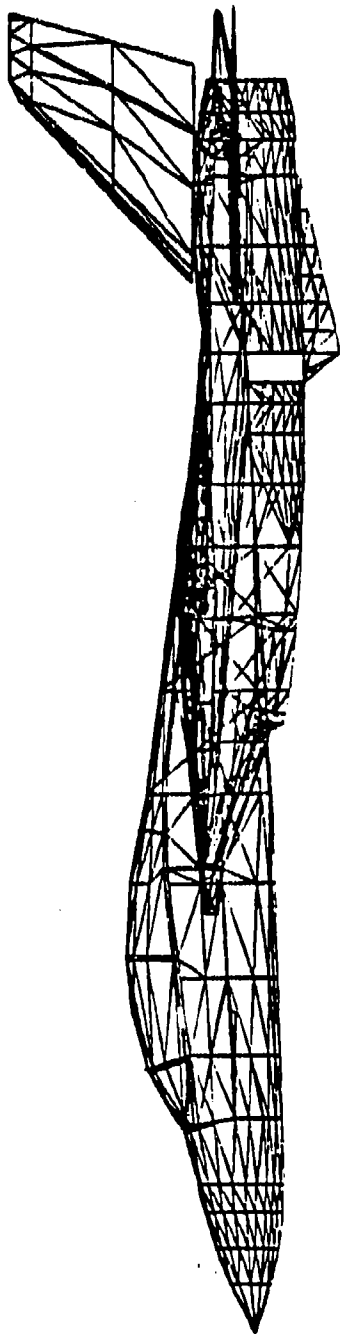


Figure 1.7. Side View of F-14 Using Triangular Patch Data Base
of Reference 4

Figure 1-8 illustrates the outstanding agreement in surface current density J_{sc} , calculated by the well known THREDE code and the triangular patch surface model used in this report. The early time and peak value difference between the codes is being resolved at present in the full-scale F-14 testing currently underway in the Navy's FAANTAEI effort.

The significance of threat rise time, τ , on aircraft vulnerability is examined in Figures 1-9 through 1-12. Figure 1-9 shows an increase in skin current density by a factor of three for a reduction in threat rise times from 0.1 μs to 0.2 μs for near strike lightning. For the NEMP case shown in Figure 1-10, the peak skin current density increased by a factor of 14 for a decrease in rise time from .001 μs to 0.1 μs . These increases in peak surface current due to the higher frequency content in the short rise time threat spectra. However, they have little effect on interior circuit voltages where only joint and panel coupling occurs. This behavior is to be expected in light of the joint admittance and transfer impedance function characteristics.

Figures 1-11 and 1-12 show the transfer impedance shielding capability of coated panels and the improvement obtainable over an 8-ply panel consisting of graphite/epoxy. The weight penalties imposed by the various coating is illustrated in Figure 1-13. Finally, a weight shielding figure of merit is shown in Figure 1-14 using the 8-ply composite panel as a baseline.

The second chapter reviews electromagnetic threats that composite aircraft may expect to experience. The threats will be natural (lightning, precipitation static) and foe (EMP, laser and electronic warfare).

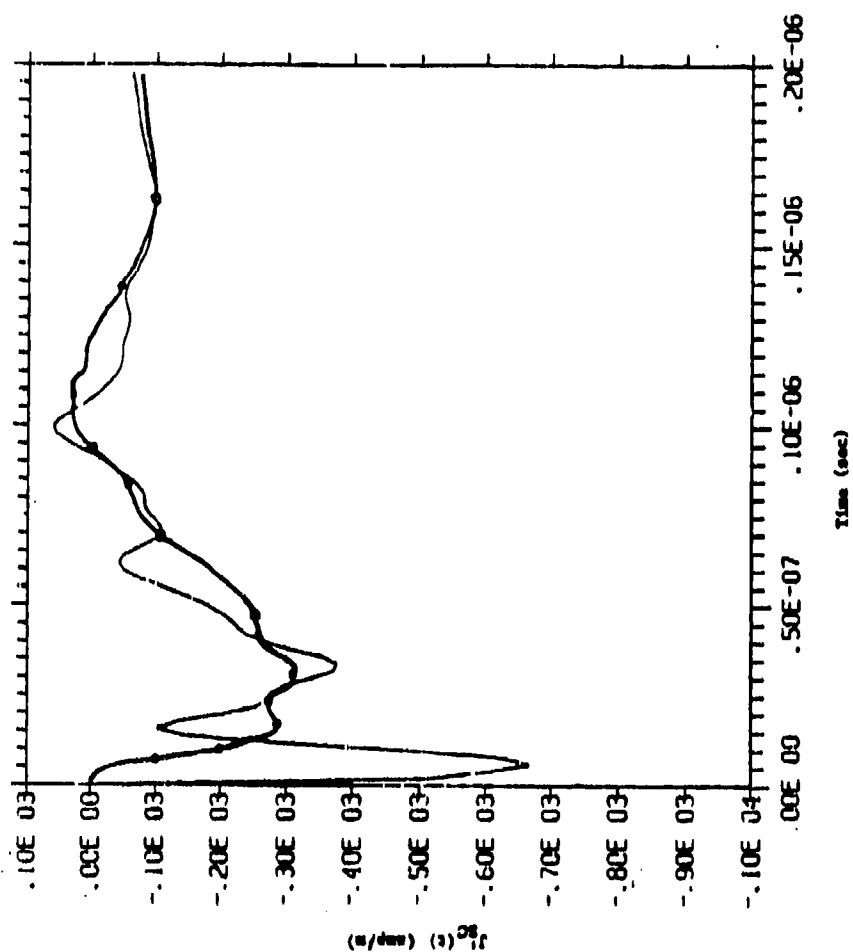
The third chapter describes the composition, fabrication and mechanical properties for composite materials in detail. The effects of modifications, coatings, repairs and environment will be assessed.

The fourth chapter discusses present and future composite material applications. A review of past composite use for aircraft is presented and future uses, including uses outside the aircraft industry, are reviewed.

The fifth chapter investigates and discusses the intrinsic material properties (conductivity, permittivity and permeability) as a function of frequency for graphite/epoxy, boron/epoxy and Kevlar/epoxy. Environmental factor influence is discussed and nonlinear properties investigated.

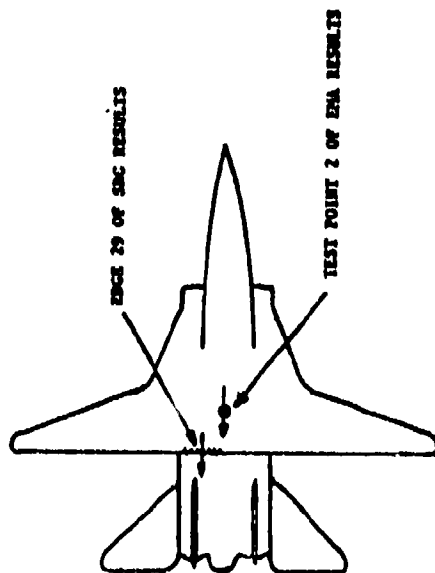
The sixth chapter discusses electromagnetic shielding in detail as it applies to general composite structures. A current list of shielding effectiveness measurements is presented for graphite/epoxy and boron/epoxy. A discussion is given for joint coupling in composite panels.

The seventh chapter surveys the susceptibility of modern digital and integrated circuits to EM energy. Susceptibility curves are presented for a number of modern integrated circuits and the implications for the use of modern digital and integrated circuits on composite aircraft are discussed.



NOTE: Circles denote values abstracted from EMA results.

(b) Plot of $J_s(t)$ for NEMP Excitation



(a) Surface Current Test Point Locations

Figure 1-8. Comparison of Surface Current Density with MRC/EMA Code and Surface Patch Model Used in This Report

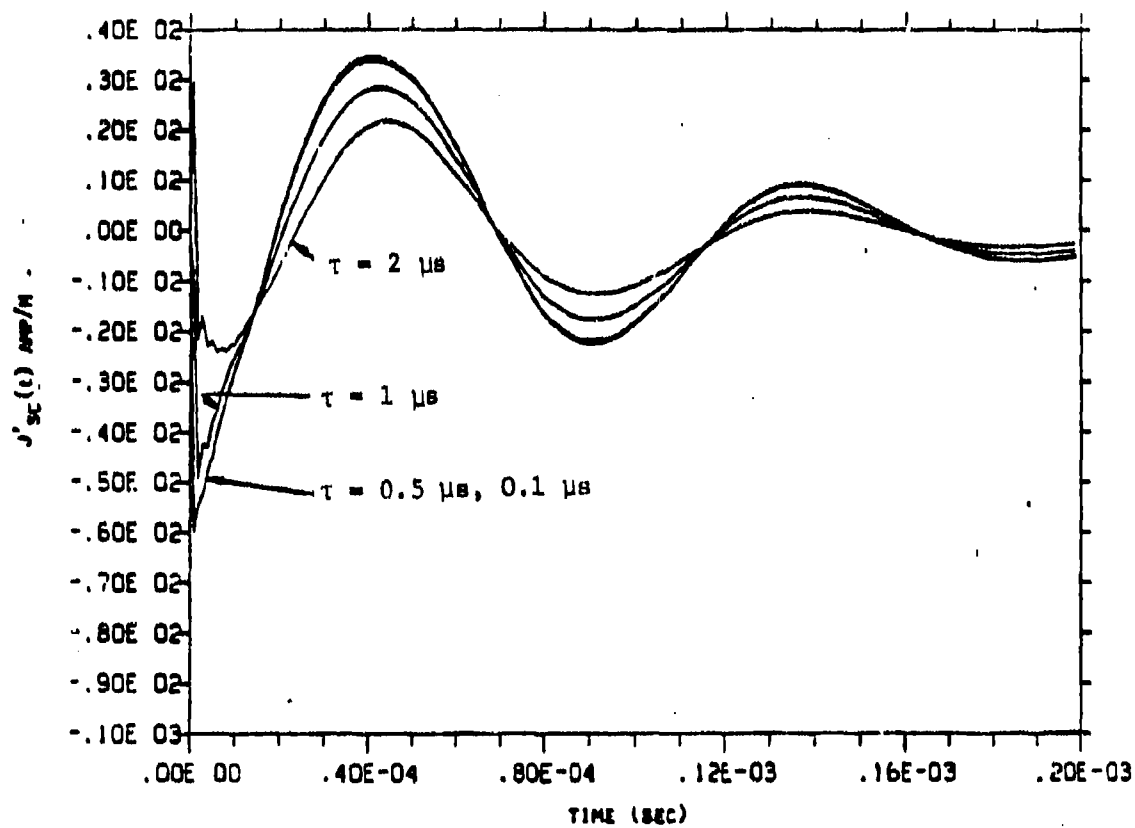


Figure 1.9. Skin Current Density J_{sc} on Edge No. 29 for Near-Strike Lightning Excitation and Different Rise Times, τ

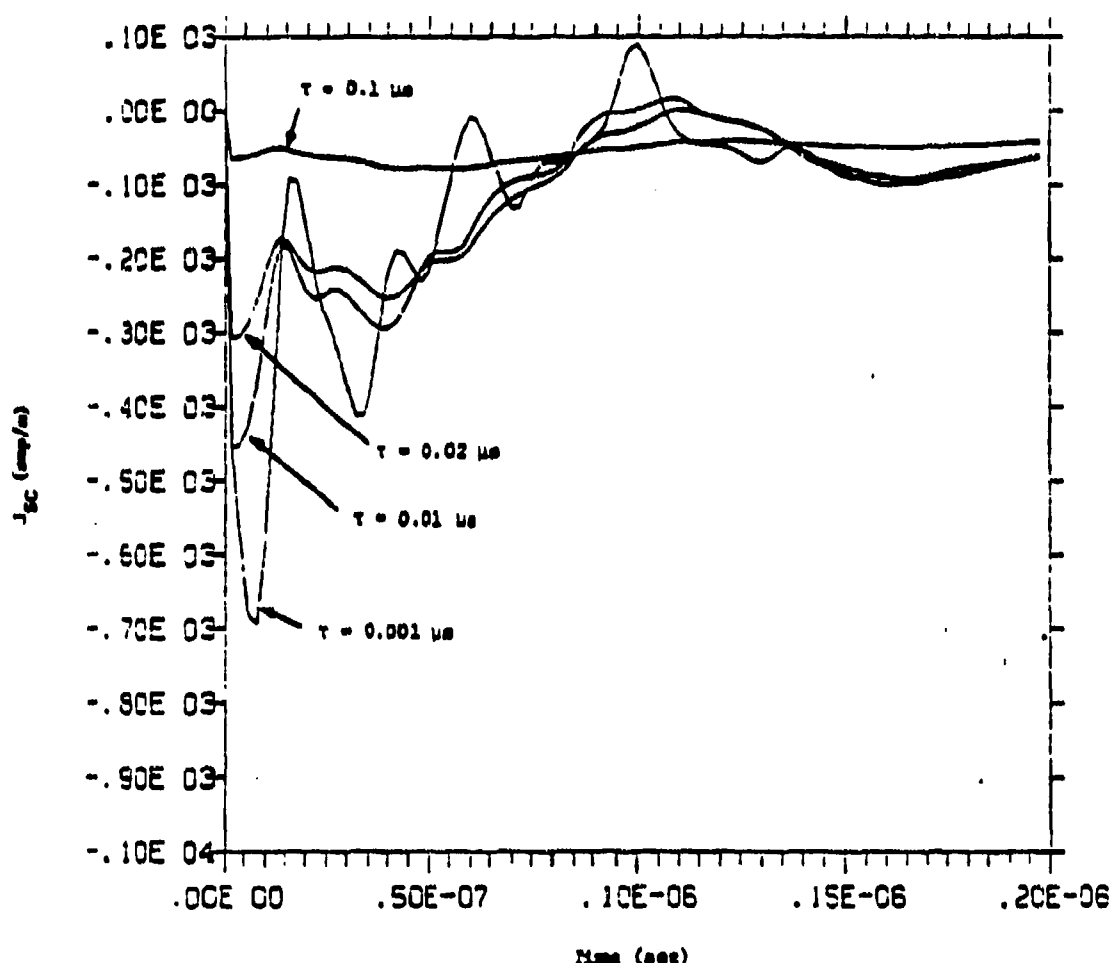


Figure 1.10. Skin Current Density J_{sc} on Edge No. 29 of Triangular Patch Model of F-14 Aircraft for Various Rise Times τ of Incident NEMP

EM PROTECTION OF METALS AND COMPOSITES (T₀)

Transfer Impedance Shielding of Structural Materials and Protective Electromagnetic Coatings

(Valid for Frequencies Below 10⁸ Hz)

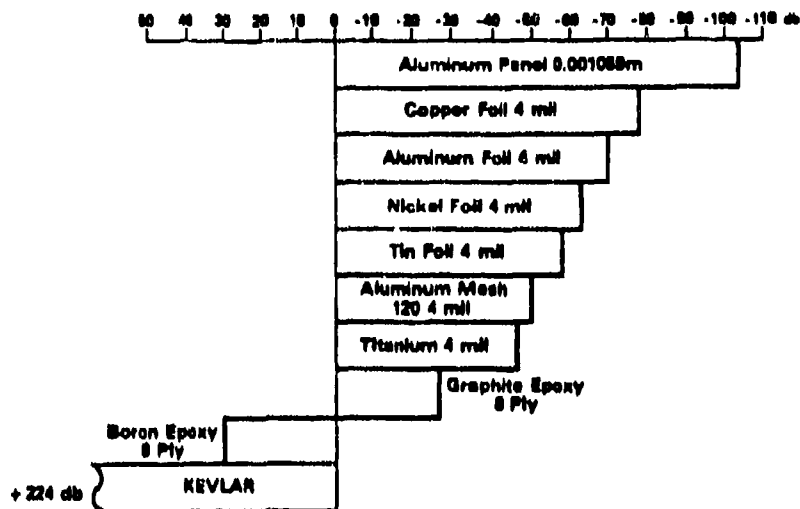


Figure 1.11. Transfer Impedance Shielding of Structural Materials and Protective Electromagnetic Coatings

EM PROTECTION (T₀)

Protective Coatings Improvement Relative to 8-Ply G/E

(Valid for Frequencies Below 10⁸ Hz)

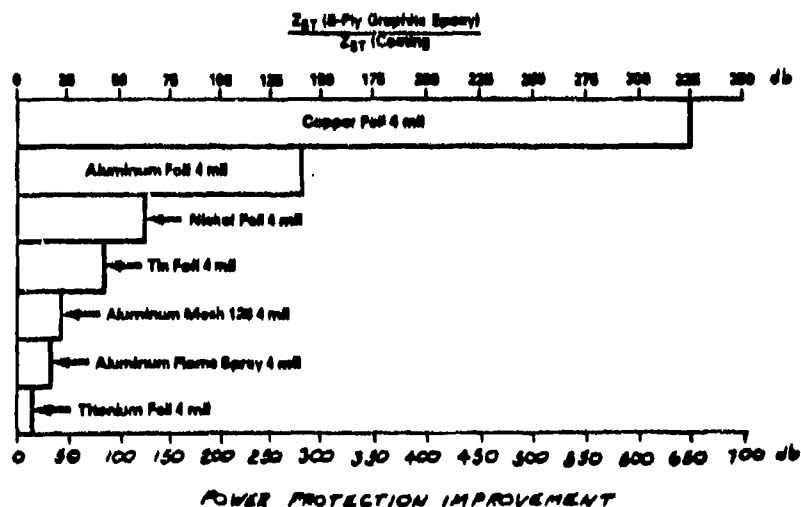


Figure 1.12. Improvement Protective Coatings Provided Relative to 8-Ply Graphite/Epoxy

EM PROTECTION WEIGHT PENALTIES (T₀)

Forward Fuselage AV-8B (Area ~ 100 Ft²) Weight Penalty
(Pounds) Imposed by Electromagnetic Protective Coatings

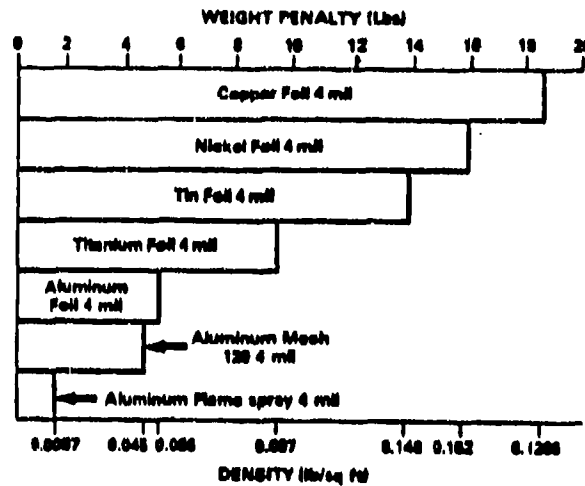


Figure 1.13. Weight Penalty Imposed by Protective Coatings

EM PROTECTION (T₀)

Weight Shielding Figure of Merit

(Protection Beyond 8-Ply G/E Provided by the Weight of 1 Square Foot of Protective Coating)

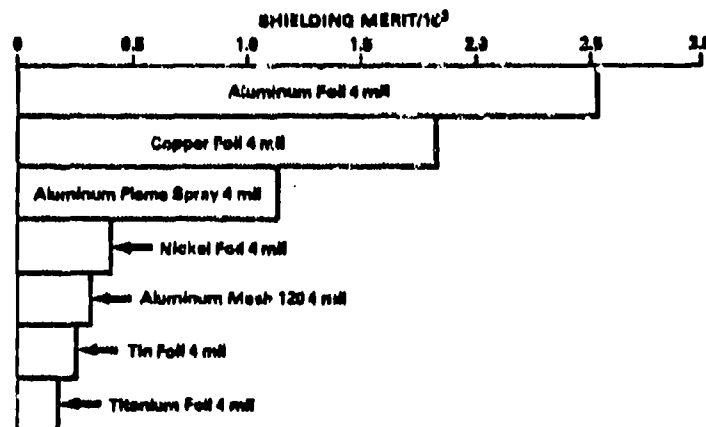


Figure 1.14. Weight/Shielding Figure of Merit of EM Protective Coatings

The eighth chapter discusses the achievement of EMC in a modern electronic system from a systems perspective. The various tools that are used to design and tailor EMC specifications for a given system (in this case, a composite aircraft) are enumerated and described.

The ninth chapter reviews the various methods and techniques for measuring the electromagnetic properties of composite materials.

The tenth chapter reviews the various protection methods that are now being used on composite aircraft. The major task of these methods is to provide lightning and precipitation statics protection. A second task is to provide increased electromagnetic shielding.

The last chapter discusses the various electromagnetic guidelines that are suggested for use in designing electromagnetic compatibility into a composite aircraft system.

The ability to operate successfully under adverse conditions is an extremely important consideration in the design of aircraft using composite material. The adverse conditions discussed in this section are electromagnetic in origin and are termed electromagnetic threats. Some threats, such as lightning and precipitation static, occur naturally in the environment or as a result of normal system operation. Others, such as high powered RF from radars, nuclear electromagnetic pulse, or high energy lasers are man-made and originate from both friendly and hostile sources. Each threat is described in some detail and an assessment made of its possible impact on system performance. Protection methods for aircraft using composites will be discussed in Section 10.0 on Protection Methods and Techniques.

2.1 Natural Threat

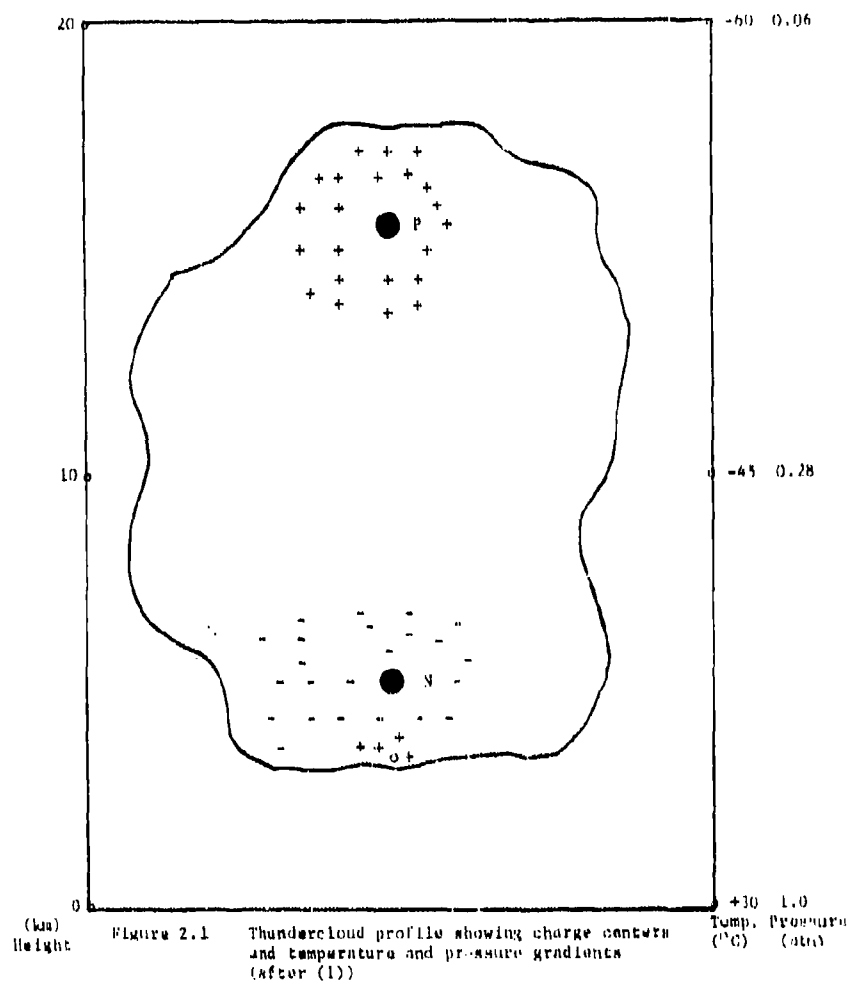
In this section the naturally occurring threats of lightning and precipitation static are discussed. A general description is given for each threat; certain mathematical models are presented that describe the main threat mechanisms, and a brief assessment is made of the impact of the threat on system performance.

2.1.1 Lightning

Lightning may be generally described as a sequence of transient, high current electrical discharges in the atmosphere. The lightning flash that is usually observed is in reality several individual lightning strokes separated by 40 milliseconds or more. Lightning is most commonly associated with thunderstorm activity but may occur in sandstorms, snowstorms, dust clouds from erupting volcanoes, or even in clear air.⁽¹⁾ Only discharges from thunderclouds to ground will be discussed since most available experimental data pertains to this situation.

2.1.1.1 The Lightning Process - Overview(1,4,5,6)

A thundercloud is a dynamic mixture of water droplets, water vapor and ice under the influences of a temperature gradient, a pressure gradient and a gravitational field. The various processes occurring within the cloud cause a separation of electrical charge to occur with large positive charge generally accumulating at the cloud top and large negative charge generally accumulating at the cloud bottom. A cloud profile illustrating charge separation versus the temperature and pressure gradients involved is shown in Figure 2.1. The charge distributions are usually described in terms of major or minor charge centers in the cloud. These centers act as equivalent sources which reproduce the measured E and H fields external to the cloud but do not necessarily coincide with the actual charge distribution. The magnitudes of the charge centers are typically +40 coulombs for major centers and +10 coulombs for minor centers. The detailed mechanism of the charge separation process is not known but is probably similar to the familiar triboelectric or thermoelectric frictional charging processes. The potential difference between major charge centers is on the order of 10^8 volts. This voltage will give a cloud energy of 4×10^9 joules which represents an upper bound on the energy available for the lightning process.



Lightning (cloud-to-ground) will occur whenever the separation of charge in the thundercloud produces an electric field sufficient to cause electrical breakdown of the air gap between cloud and ground. The good weather electric field intensity at the ground is 100 volts/m while the uniform field intensity needed to cause electrical breakdown of dry air at normal atmospheric pressure is 300 kV/m. For non-uniform fields, the field intensity for breakdown will always be less. The electric fields that produce lightning discharges are very non-uniform, being relatively strong at the cloud base and relatively weak at the ground.

There are two mechanisms that are thought to occur in the discharge process. In the first mechanism, which is dominant for uniform fields, the free electrons existing in the air gap are accelerated by the electric field and interact with atoms and molecules in the air to produce additional electrons and ions through electron-impact ionization and photo-ionization. These growths of electron and ion densities are termed avalanches. Numerous avalanches will eventually lead to breakdown of the air gap.

A second mechanism becomes dominant for non-uniform fields. Luminous pulses of ionization, called streamers, propagate out at high velocity from the high field region to the low field region. The streamer head contains an intense electric field capable of producing ionization in the surrounding air allowing the streamer to propagate rapidly. The streamer that initiates the lightning process is unique in that it propagates in a characteristic stepping fashion. This streamer, called the stepped leader, typically propagates at a velocity of 1.5×10^5 m/sec in steps 50m long with a pause of 50 microseconds between steps. About 5 coulombs of charge are deposited along the leader channel, which may be 3 km long and a few meters wide, in about 20 msec. The detailed physics of the stepped leader are not well understood although several theories have been proposed.⁽¹⁾ Many utilize the concept of a non-luminous pilot leader which precedes and guides the luminous stepped leader.

As the stepped leader propagates downward, the high field in the leader head causes upward moving streamers to be launched from ground or a sharp object. Such streamers will be initiated for ground electric field intensities of 10^6 volt/m or greater. When the upward and downward leaders meet, a conducting channel is formed. The leader head is effectively grounded while the leader tail is still at high potential. The result is a very luminous, positive discharge up the leader channel called the first return stroke. Tremendous energy (typically 5×10^8 joules) is delivered to the leader channel in a few microseconds. A large fraction of this energy causes the leader channel to expand and its temperature to rise (up to 30,000°K). This, in turn, produces an explosive cylindrical shock wave which is the main source for thunder. A small fraction (about 1%) of the energy produces the electromagnetic spectrum. The return stroke current is characterized by a rapid rise in current peak value (up to 100 kamps within 10 microseconds) and a propagation velocity of 5×10^7 m/sec. The stroke lasts typically 70 - 100 microseconds.

After the return stroke has traversed the channel, current up to hundreds of amperes will continue to flow for several milliseconds. During this time tens of coulombs of charge may be transferred to the channel. This continuing current is thought to be an important mechanism for maintaining ionization along the conducting channel for subsequent return strokes.

If sufficient charge is made available to the channel from the thundercloud in a time of 100 milliseconds or less, a streamer called a dart leader will traverse the channel. This streamer precedes a subsequent return stroke and is similar to a stepped leader except that the stepping process is usually absent. Subsequent return strokes are usually of less intensity than the first return stroke but otherwise similar in characteristics. The total set of strokes constitutes the lightning flash seen by the eye and is typically a fraction of a second in duration.

Lightning flashes vary widely in their properties depending on lightning type and location on the earth. Table 2.1 lists a range of values for the various components of a lightning flash as found in the literature. The values in this table are meant to give a feeling for the orders of magnitude involved and to serve as a guideline. The total lightning discharge process is illustrated in Figure 2.2 in the time domain. The waveform is not to scale but serves to illustrate the trend of the data given in Table 2.1 and to summarize the preceding discussion.

2.1.1.2 Radiated Lightning Spectrum (Far Field)(4,6,7)

Two measured lightning spectra are shown in Figures 2.3 and 2.4 and include the contributions of many investigators. The measured range is from a few kHz to a few GHz. The spectra are normalized respectively to 10 km and one statute mile and have bandwidths of 1 kHz. The frequency range of maximum signal amplitude is 5-10 kHz and the amplitude decreases roughly as the inverse of the frequency. Beyond a few GHz the spectrum has not been nearly measured.

2.1.1.3 Lightning Near Fields(2,4)

For points reasonably near the discharge channel, the near fields of the lightning are dominant. The near electric field is produced by the charge deposited along the stepped leader channel. An estimate for this field can be given by considering the electric field produced by a uniform line of charge of finite length. Such a field is given by

$$E = \frac{\rho}{2\pi\epsilon_0} \left(\frac{1}{D} - \frac{1}{(L^2 + D^2)^{1/2}} - \frac{L^2}{(L^2 + D^2)^{3/2}} \right) \quad (2.1)$$

Table 2.1 Representative Characteristics for Cloud-to-Ground Lightning Flashes (1)

	Minimum	Average	Maximum
Stepped Leader			
Step Length (m)	3	50	200
Time Between Steps (μsec)	30	50	175
Velocity of Propagation (m/sec)	1×10^8	$1-5 \times 10^8$	2.6×10^8
Charge Deposited on Channel (Coul)	3	5	20
Dart Leader			
Velocity of Propagation (m/sec)	1×10^6	2×10^6	2×10^7
Charge Deposited on Channel (Coul)	0.2	1	6
Return Stroke			
Velocity of Propagation (m/sec)	2×10^7	3×10^7	1.4×10^8
Rate of Current Rise (kA/μsec)	1	10-20	100
Time to Peak Current (μsec)	0.25	2	30
Peak Current (kA)	3	10-20	140
Time to Current Half-Value (μsec)	10	40	150
Charge Transferred (Coul)	0.2	2.5	20
Channel Length (km)	2	5	14
Continuing Current			
Current Duration (msec)	58	160	400
Current Value (A)	30	140	500
Charge Transferred (Coul)	7	26	110
Total Flash			
Strokes per Flash	1	3-4	26
Time Between Strokes (msec)	3	40-80	100
Duration of Flash (sec)	0.01	0.2	2
Charge Transferred (Coul)	3	25	90

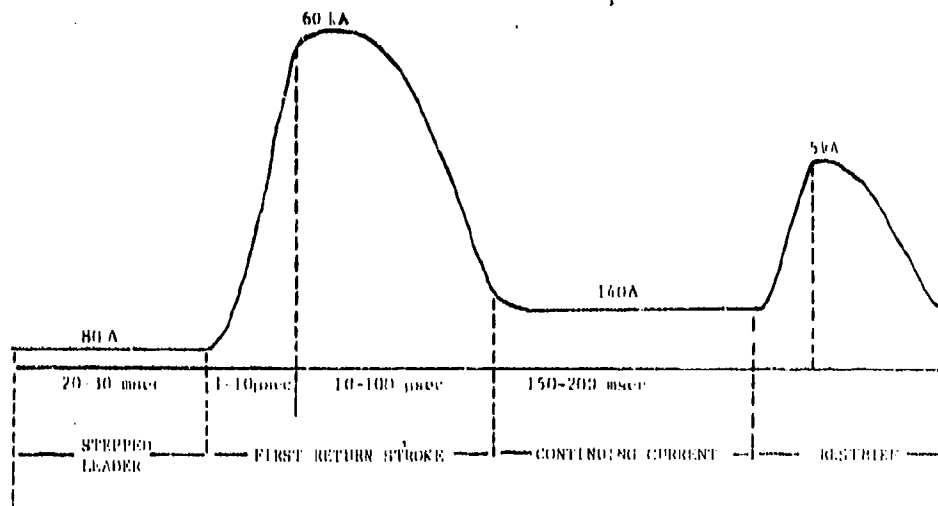


Figure 2.2 Current Waveform (not to scale) for a Lightning Flash to ground (5)

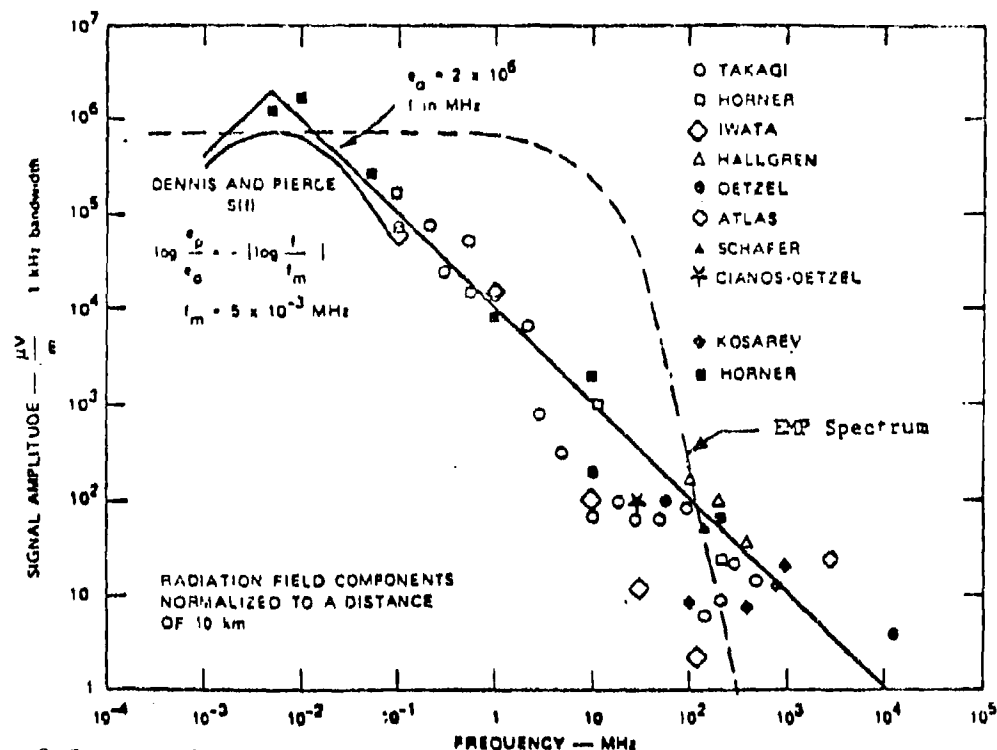


Figure 2.3 Radiated lightning spectrum normalized to 10 km (an EMP spectrum is included for comparison) (4,6)

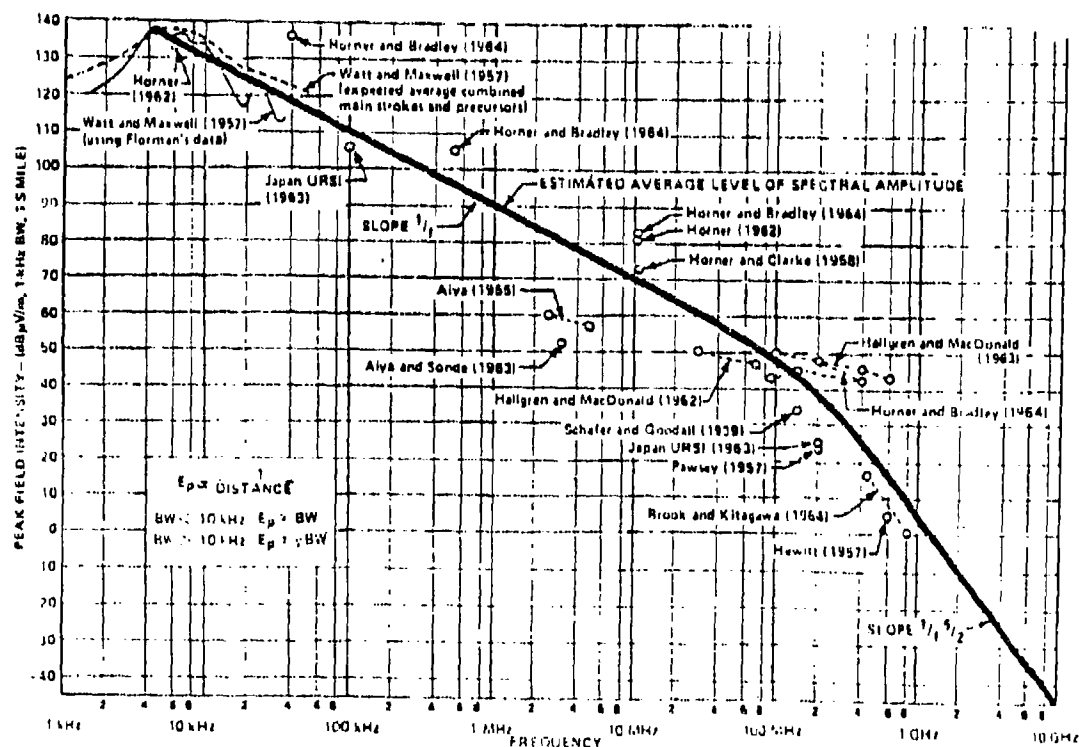


Figure 2.4 Radiated lightning spectrum normalized to one statute mile (6,7)

where ρ is the charge density, L is the length of the leader channel in meters, and D is the distance from the channel in meters. As an order of magnitude estimate, for ρ equal to 1 coulomb per km, L equal to 2.5 km, and D equal to 100m, the field is 200 kV/m which is close to the measured value of 100 kV/m.

The magnetic near field is produced primarily by the large return stroke current which forces the magnetic field to lag behind the electric field. The magnetic near field can be estimated by considering a current moving along a thin cylindrical column. This model for the current gives the magnetic field

$$H = \frac{I}{2\pi D} \left[\frac{L}{(L^2 + D^2)^{1/2}} \right] \quad (2.2)$$

where I is the return stroke current and L and D are as in (2.1).

Several expressions for the current waveform of the return stroke current have been proposed and are in common usage.⁽⁵⁾ One very simple waveform that is often used is the simple triangular function shown in Figure 2.5. This function has a quick rise to a maximum and a slow decay which are the basic requirements for the return stroke current waveform.

The waveform defining the Space Shuttle Lightning Current Waveform is shown in Figure 2.6 and consists of several straight lines bounding the various parts of the actual waveform. The result is a more detailed expression for the current which is still simple.

Analytic expressions commonly used for the waveform are double and quadruple exponentials. A triple exponential is also occasionally used, but this waveform forces the current to jump discontinuously. A typical double exponential function is given by

$$\begin{aligned} I(t) &= I_0(e^{-\alpha t} - e^{-\beta t}) \\ I_0 &= 206 \text{ kA} \\ \alpha &= 1.7 \times 10^4 \text{ Hz} \\ \beta &= 3.5 \times 10^6 \text{ Hz} \end{aligned} \quad (2.3)$$

The waveform for this double exponential is shown in Figure 2.7.

A triple exponential waveform is

$$I(t) = I_0(e^{-\alpha t} - e^{-\beta t}) + I_1 e^{-\gamma t} \quad (2.4)$$

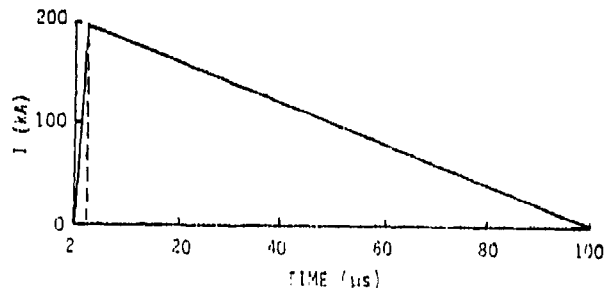


Figure 2.5 Triangular lightning current waveform (5)

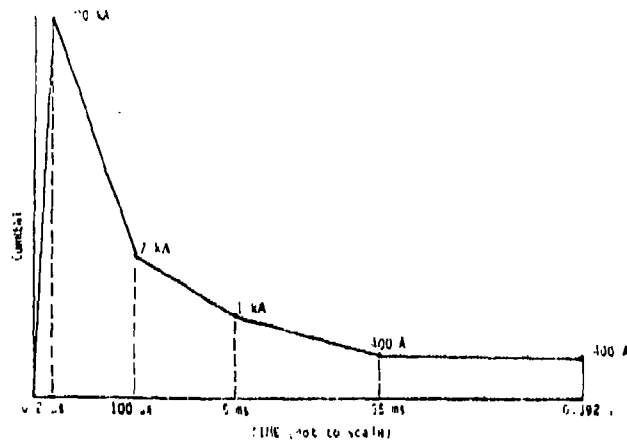


Figure 2.6 Space shuttle lightning current waveform (5)

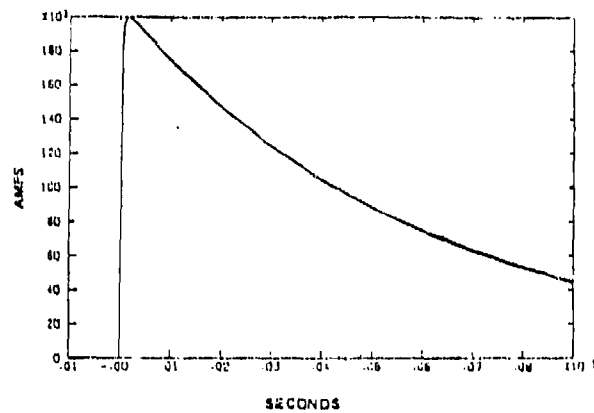


Figure 2.7 Double exponential lightning current waveform (5)

where

$$\begin{aligned}I_0 &= 30 \text{ kA} \\I_1 &= 2.5 \text{ kA} \\ \alpha &= 2 \times 10^4 \text{ Hz} \\ \beta &= 2 \times 10^5 \text{ Hz} \\ \gamma &= 2 \times 10^3 \text{ Hz}\end{aligned}$$

and a quadruple exponential function is

$$I(t) = I_0(e^{-\alpha t} - e^{-\beta t}) + I_1(e^{-\gamma t} - e^{-\delta t}) \quad (2.5)$$

where

$$\begin{aligned}I_0 &= 30 \text{ ka} \\I_1 &= 2.5 \text{ ka} \\ \alpha &= 2 \times 10^4 \text{ Hz} \\ \beta &= 2 \times 10^5 \text{ Hz} \\ \gamma &= 1 \times 10^3 \text{ Hz} \\ \delta &= 2 \times 10^4 \text{ Hz}\end{aligned}$$

The waveform for the triple exponential function is shown in Figure 2.8 and the one for the quadruple exponential function is in Figure 2.9. The double exponential in (2.3) has a maximum current of 206 kA and actually represents a "worst case" situation. The triple and quadruple exponential functions have maximum currents of 30 kA and are more typical of the average current in the return stroke.

The frequency domain representations of these waveforms are interesting and are given in Figures 2.10 - 2.13. The last figure shows the superposition of all the waveforms and indicates general agreement with the overall waveform for a lightning flash given in Figures 2.3 - 2.4.

2.1.1.4 Attachment of Lightning to Aircraft

In addition to the effects of the near and far field RF spectra, there is the effect of the direct attachment of the lightning channel to the aircraft itself. The process of lightning attachment is illustrated in Figure 2.14. As the stepped leader moves downward from the base of the cloud, streamers propagate toward the leader, usually from a sharp point of the aircraft, and away from the aircraft toward another cloud charge center or ground. When the streamers make contact with the stepped leader and

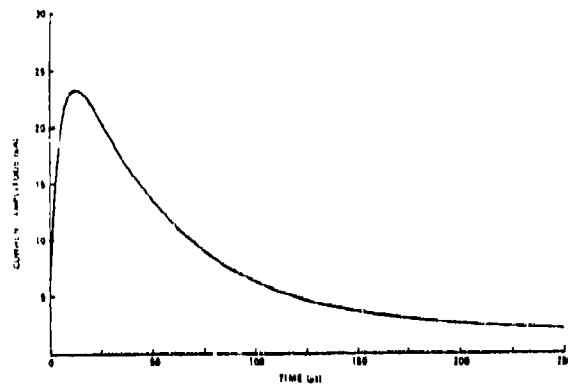


Figure 2.8 Triple exponential lightning current waveform⁽⁵⁾

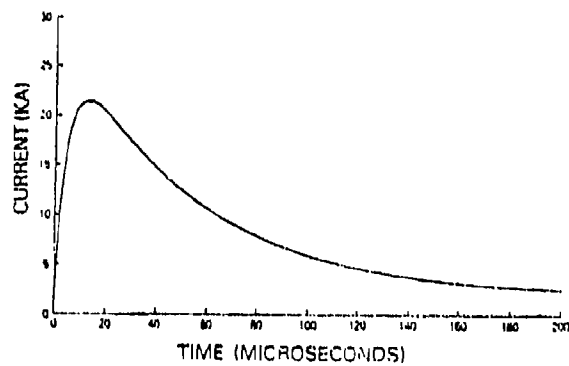


Figure 2.9 Quadruple exponential lightning current waveform⁽⁵⁾

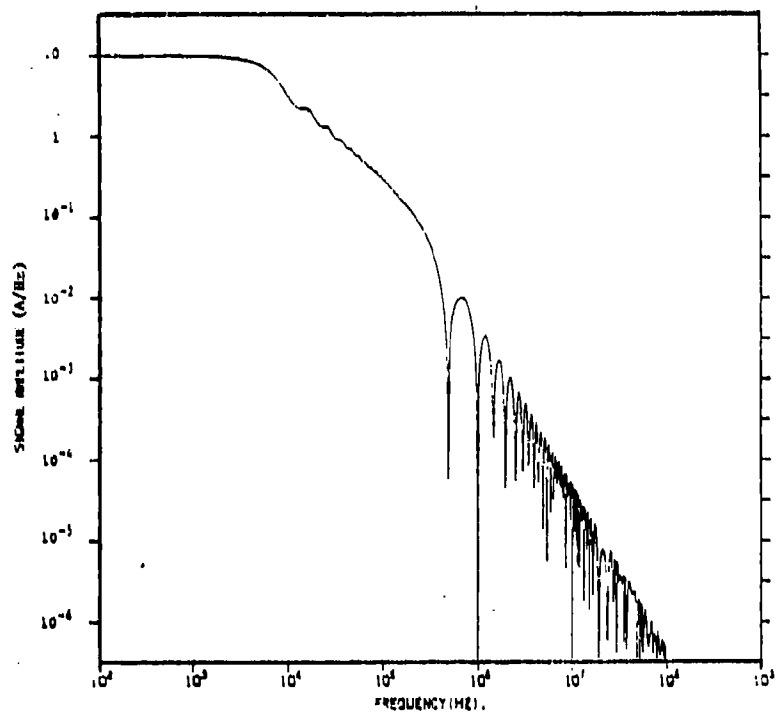


Figure 2.10 Spectrum of triangular current lightning waveform⁽³⁾

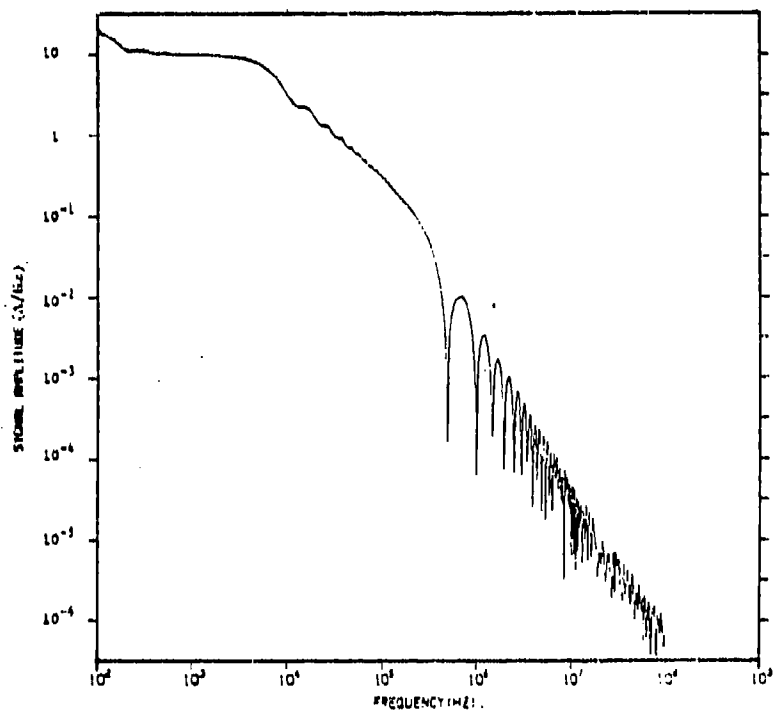


Figure 2.11 Spectrum of Space shuttle current lightning waveform⁽³⁾

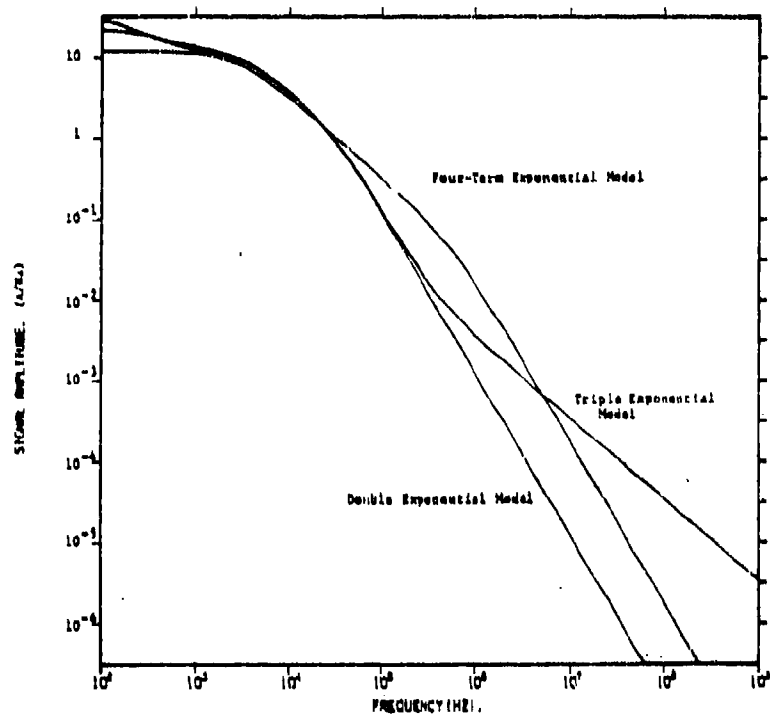


Figure 2.12 Exponential current lightning waveforms⁽⁵⁾

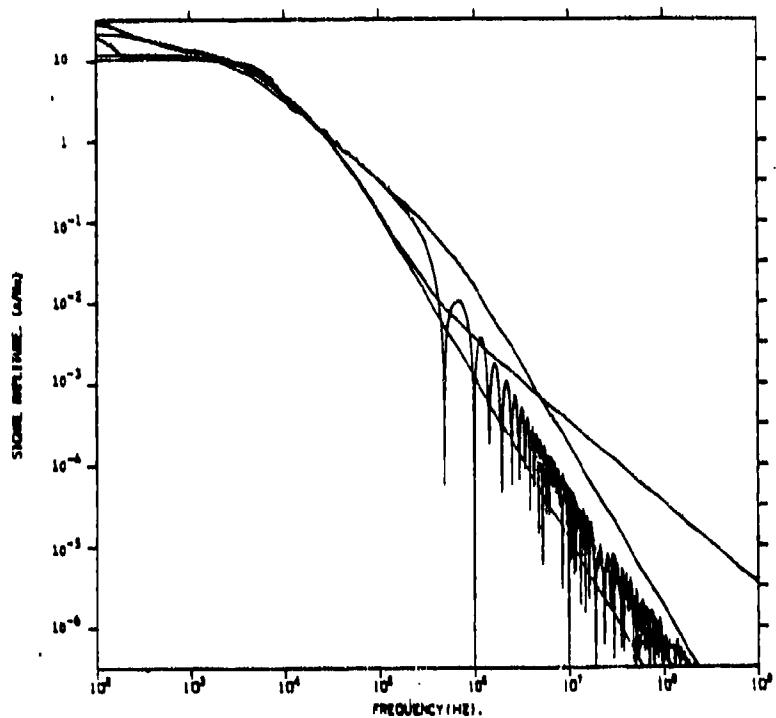


Figure 2.13 Superposition of all lightning current waveforms⁽⁵⁾

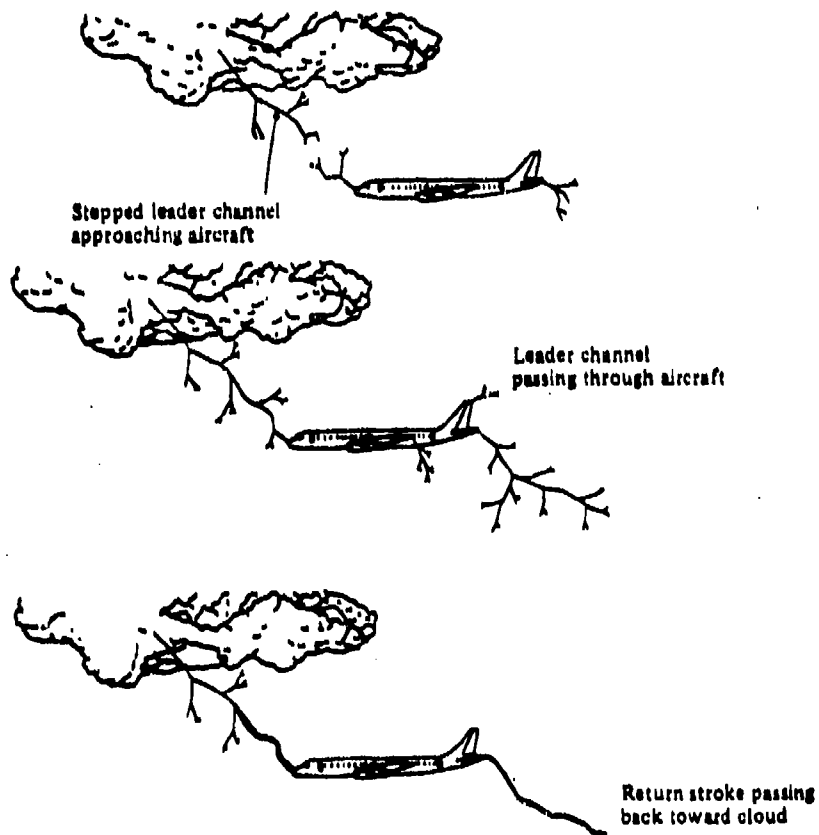


Figure 2.14 Lightning Attachment⁽¹⁰⁾

another cloud charge center or ground, then a conducting lightning channel which includes the aircraft has been established. A return stroke discharge up the channel quickly takes place. There are two initial attachments for the lightning which represent the entry and exit points for the stroke over the aircraft.

Although the motion of the lightning stroke is relatively stationary, the aircraft forward velocity may be quite significant. The result of this velocity differential is that the lightning channel is swept back over the surface of the aircraft from its initial point of attachment to new points of attachment. This process is illustrated in Figure 2.15. The importance of the swept stroke phenomenon is that portions of the aircraft that would not normally be considered likely points of initial lightning attachment may become involved in the lightning process as a result of the backward sweep of the stroke. This swept stroke phenomenon leads to the division of an aircraft into lightning strike zones based on the probability of attachment. These zones are (6,10,11)

- Zone 1: Aircraft surfaces for which there is a high probability of initial lightning attachment (entry or exit).
- Zone 2: Aircraft surfaces across which there is a high probability of a lightning channel being swept from a Zone 1 attachment point.
- Zone 3: All other aircraft surfaces not involved in Zones 1 or 2. There is a low probability of lightning attachment but the surface may carry considerable current.

Zones 1 and 2 may be further subdivided into A and B regions (6,10,11) depending on the probability that the flash will hang on for a period of time. These zones are

- Zone 1A: Initial attachment with low probability of flash hang on, e.g., a leading edge
- Zone 1B: Initial attachment with high probability of flash on, e.g., a trailing edge
- Zone 2A: Swept stroke zone with low probability of flash hang on, e.g., wing mid-cord
- Zone 2B: Swept stroke zone with high probability of flash hang on, e.g., inboard trailing edge.

Two examples of aircraft strike zones are given in Figure 2.16 and Figure 2.17.

2.1.1.5 Lightning Threat Assessment

The threat to composite aircraft from lightning results from either a direct strike or a near miss. Both categories of lightning threat will be discussed separately since different threat mechanisms are involved.

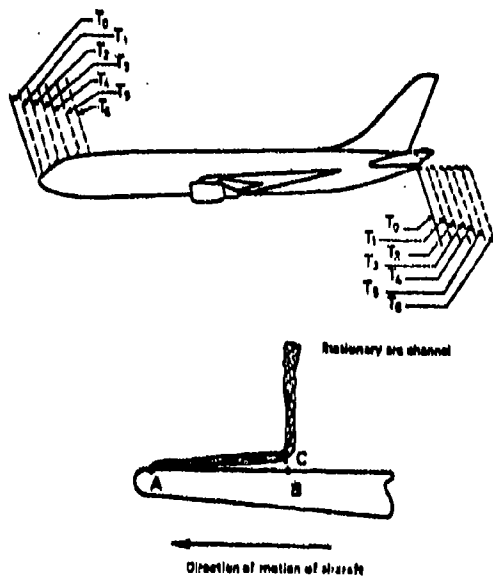


Figure 2.15 Swept Stroke Phenomenon⁽¹⁰⁾

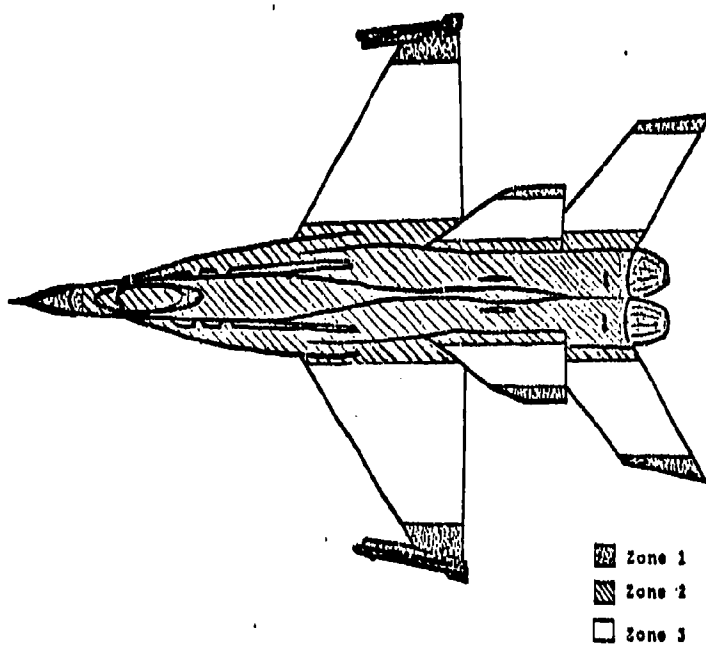


Figure 2.16 Aircraft Lightning Strike Zones⁽⁶⁾

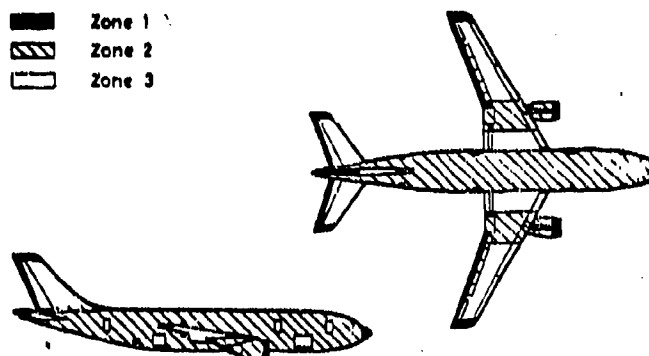


Figure 2.17 Lightning Strike Zones⁽¹⁰⁾

A direct strike on an aircraft takes place when the stepped leader channel becomes attached to the aircraft structure. The aircraft then becomes part of the path traversed by the return stroke. As noted in Section 2.1.1.1 and illustrated in Figure 2.2, the return stroke is characterized by very high currents and explosive shock waves. Tremendous heat will be generated in the aircraft structure due to the finite conductivity of the structure material. Because of their lower conductivity compared to aluminum and other metals, structures made from composites are more susceptible to physical damage (pitting and puncture points) and even complete burnout of the composite structures of the aircraft. Other vulnerable structures include radomes, canopies, external antennas and special composite panels. The shock waves will produce, in addition, extreme mechanical forces and shock wave heating in the aircraft structure.

In addition to physical damage, composite structures are vulnerable to the high electric and particularly magnetic fields that are generated from a near miss or a direct strike. Because unprotected composite structures tend to offer less EM shielding than metal structures, the electromagnetic fields can more easily penetrate and couple to the internal aircraft avionics. Low power integrated circuits on modern aircraft are particularly sensitive to induced transients of this type. The result of such coupling can then be disruption and/or catastrophic failure of the aircraft avionic systems.

Several lightning protection methods do exist for composite aircraft structures to control the lightning threats that have been discussed. These protection methods will be treated in Section 10.0 on Protection Methods and Techniques.

2.1.2 Precipitation Static

2.1.2.1 Overview

The motion of an aircraft or missile through the atmosphere will cause the vehicle to be struck with dust, ice crystals, rain and other material particles. Continuous particle bombardment of the vehicle will cause charges (positive or negative) to separate from the particles. The result is a net charge transfer from the particles to the vehicle creating a possibly large electric potential. The charging rate depends primarily on the vehicle geometry, velocity, and the nature of the colliding particles. Generally, charging is greatest for smaller vehicles with high velocities and for dust and ice crystals. If the surface is sufficiently conducting, the excess charge will move to areas of high field intensity, usually trailing edges or points of the vehicle. For sufficiently high charging rates, corona discharge into the atmosphere will occur. These discharges are in the form of short pulses and are a major source of EM noise in avionic systems. These pulses can be modeled with the waveform⁽⁵⁾

$$f(t) = A_0 e^{-at}$$

(2.6)

Both the amplitude A and the decay constant depend upon the atmospheric pressure ρ , as a function of altitude. The atmospheric pressure ρ is given by

$$\rho = 760 \exp - \frac{h+0.002h^2}{25} \quad (2.7)$$

where h is in kilofeet and ρ is in torrs. The parameters A and α in (2.6) are chosen to be

$$A = 7.90569 \times 10^5 \rho^{0.25} \quad (2.8)$$

$$\alpha = 2.7777 \times 10^{-2} \rho \quad (2.9)$$

to give a good fit to the exponential data for A and α . The noise spectrum is then given by

$$S = A \left(\frac{\gamma}{\pi} \right)^{1/2} (\omega^2 + \alpha^2)^{-1/2} \quad (2.10)$$

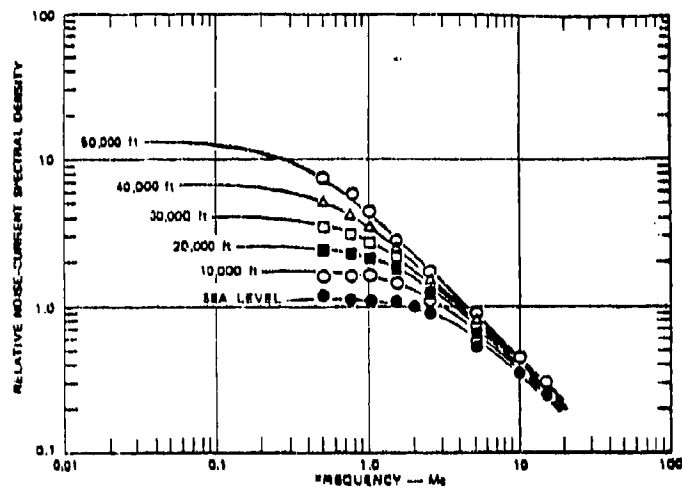
where γ is the number of pulses per minute. This parameter is also a function of atmospheric pressure and good values of γ are given by

$$\gamma = 3.83767 \times 10^3 \rho^{0.48} \quad (2.11)$$

The noise spectrum is shown in Figures 2.18 - 2.19. In Figure 2.18, the impact of altitude on the spectrum is shown for several altitudes. In Figure 2.19, the noise level of the spectrum is shown as a function of discharge current for a fixed altitude (sea level).

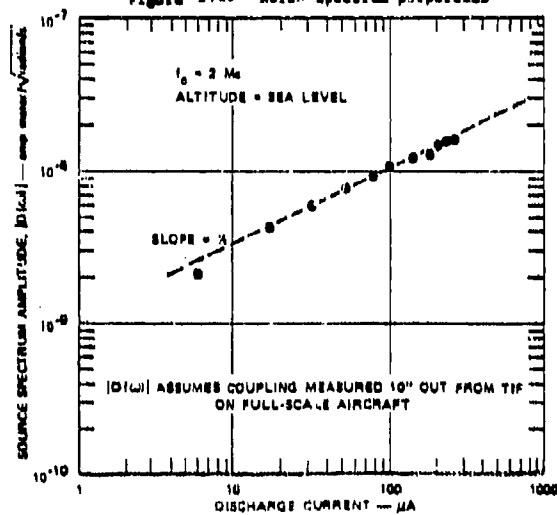
When electric charge is deposited on dielectric media such as radomes, windshields, or structures of intermediate conductivity such as composite structures, the motion of the charge is restricted due to the partial or non-conducting characteristics of these surfaces. For high enough potentials, streamer discharges will occur on the surface. The current for a streamer discharge can be modeled as a double exponential function of the form (5)

$$(2.12)$$



(a) NORMALIZED SPECTRUM SHOWING ALTITUDE EFFECTS

Figure 2.18 Noise spectrum properties (3)



(a) RELATIONSHIP OF ABSOLUTE NOISE LEVEL TO DISCHARGE CURRENT

Figure 2.19 Noise spectrum properties (3)

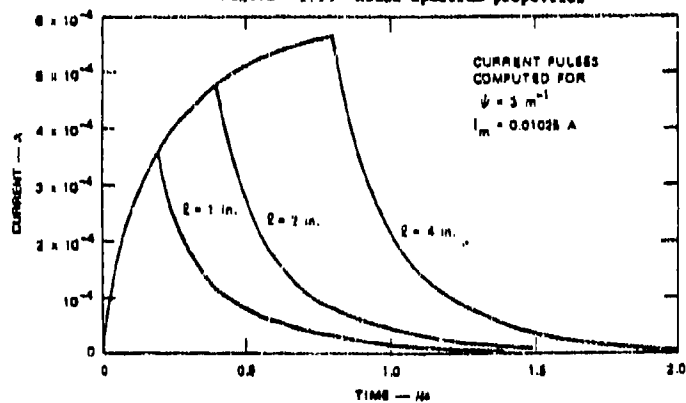


Figure 2.30 Current pulses resulting from streamers of several lengths (3)

where

$$I(t) = I_m(ae^{-\alpha t} + be^{-\beta t})$$

$$I_m = 0.01 \text{ amp}$$

$$a = 0.597$$

$$\alpha = 1.67 \times 10^7 \text{ Hz}$$

$$b = 0.403$$

$$\beta = 3.47 \times 10^6 \text{ Hz}$$

This current discharge is several orders of magnitude smaller than lightning discharges. One effect of such streamer discharges is that the EM fields penetrate the system and couple onto the system avionics. To illustrate the magnitude of this effect, the current induced on a wire located just below the streamer has been calculated for several streamer lengths using a typical coupling factor $\psi = 3\text{m}^{-1}$. The results are shown in Figure 2.20.

2.1.2.2 Precipitation Static Threat Assessment

The threat to composite vehicles from precipitation static results from the broad EM fields radiated during the corona or sparking process. Such fields are a major source of antenna noise. In addition, coupling to avionics can occur by penetration of the fields through composite surfaces (aircraft fuselages) and apertures (joints), such as radomes or canopies.

Specific protection methods exist to minimize precipitation static and are discussed in Section 10.0 on Protection Methods and Techniques.

2.2 Friend/Foe Threat

In this section, the external man-made electromagnetic threats to aircraft composites are described in detail. The threats considered are strong RF sources, nuclear electromagnetic pulse and high energy lasers and particle-beam weapon systems. A general description is given of the electromagnetic field produced by each threat followed by relevant mathematical models and a threat assessment.

2.2.1 RF Threat

In this section, a realistic but unclassified, electromagnetic environment is presented which might be encountered by a composite aerospace vehicle in an operational scenario. This environment is shown in Figures 2.21 - 2.24 and is expressed in terms of an RF power density as a function of frequency from 10 kHz to 100 GHz. The power density levels were computed assuming mainbeam illumination at a distance of 500 meters from the radiating antenna with the target continuously illuminated.

2.2.1.1 RF Environment(8,9)

The power density at a point R meters from the transmitting antenna is expressed by

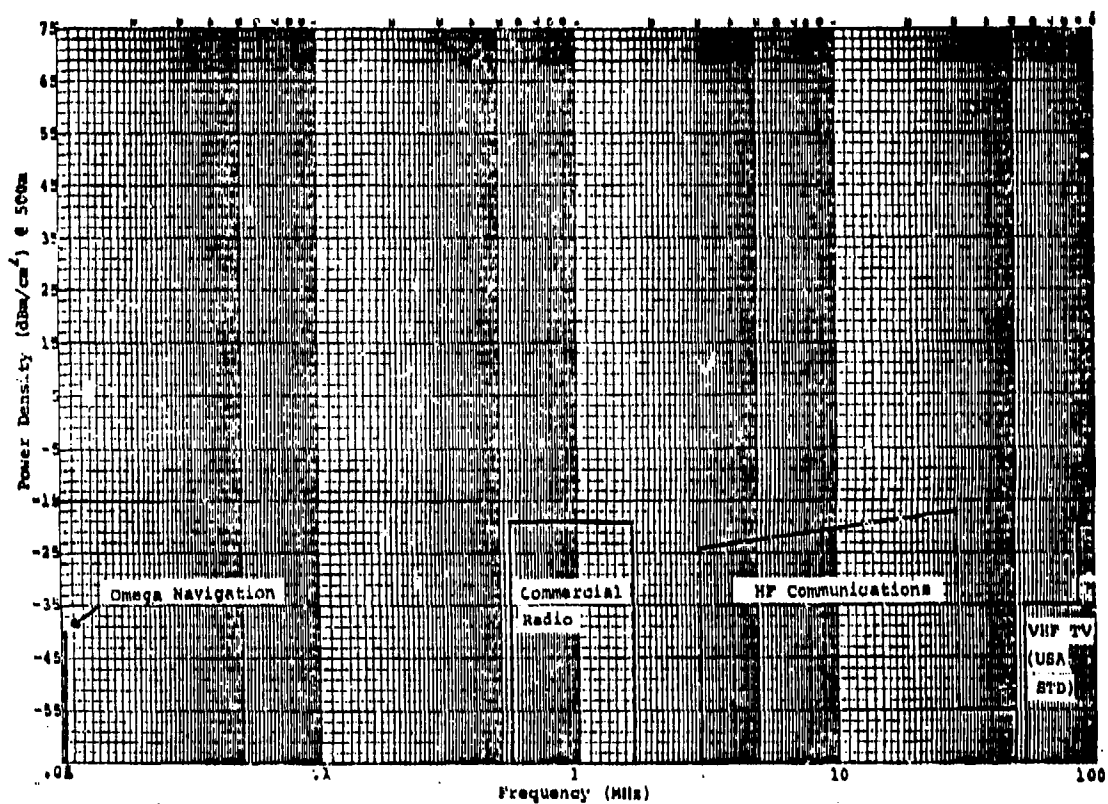


Figure 2.21 RF Environment (10 kHz - 100 MHz)

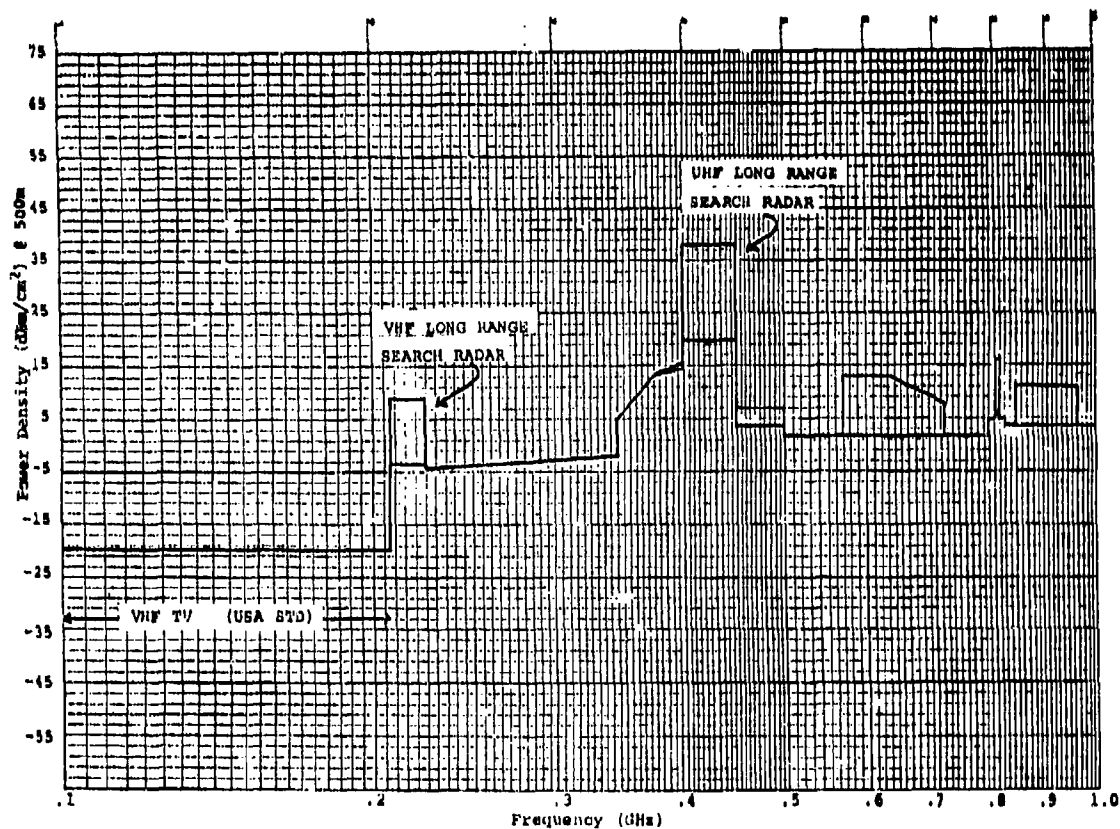


Figure 2.22 RF Environment (100 MHz - 1 GHz)

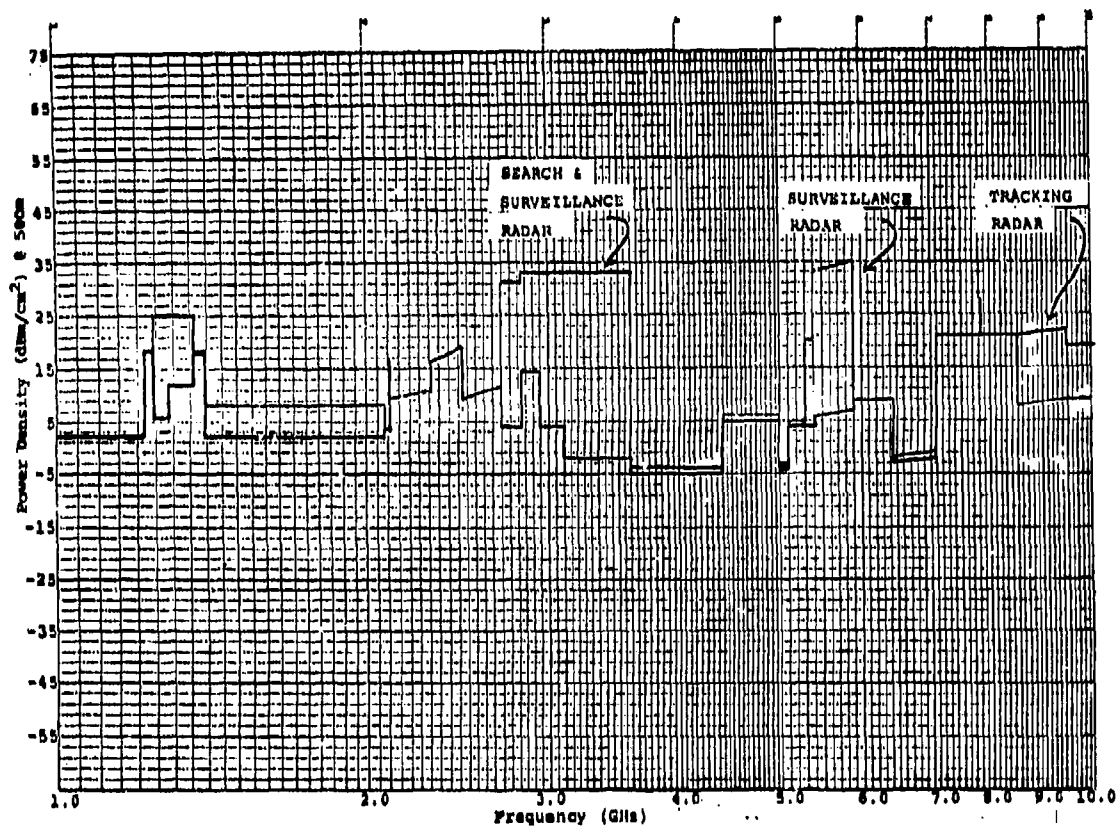


Figure 2.23 RF Environment (1 - 10.0 GHz)

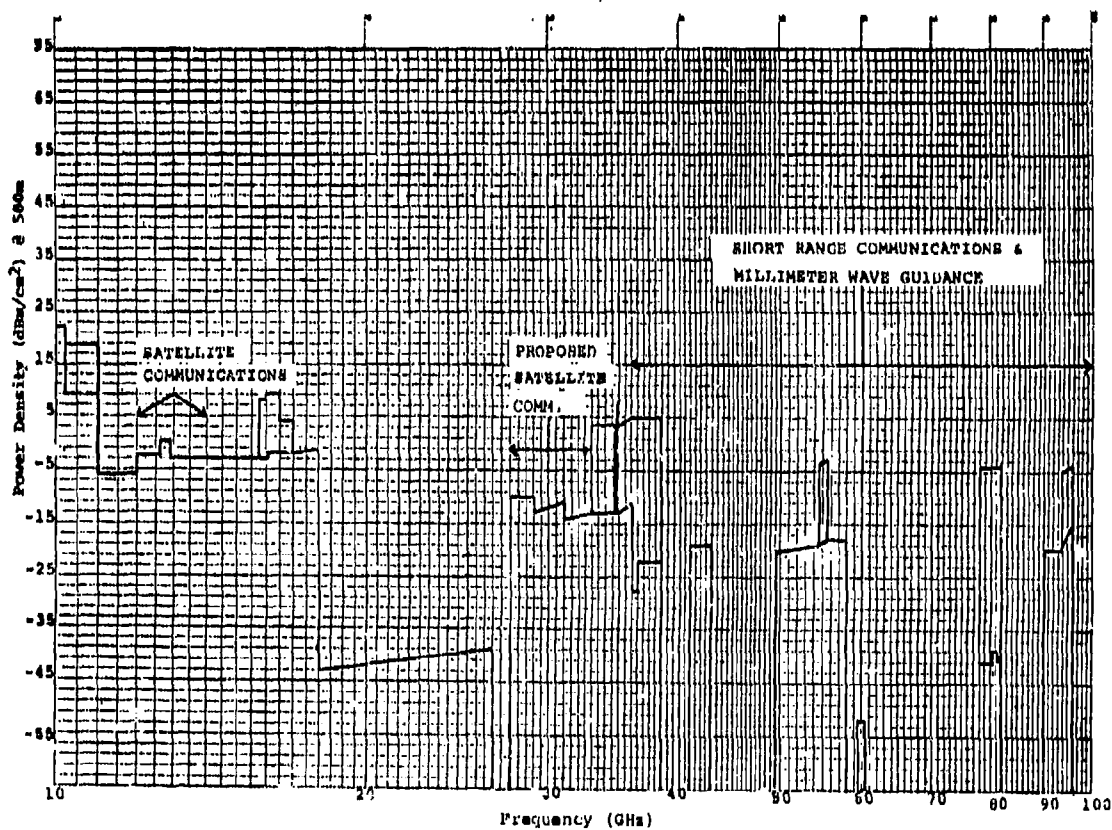


Figure 2.24 RF Environment (10 - 100 GHz)

$$P_d = \frac{P_t G_t}{4\pi R^2} \quad (2.13)$$

where

P_d = antenna power density in watts/m²
 P_t = power transmitted in watts
 G_t = distance from transmitting antenna in meters

The quantity $P_t G_t$ is often referred to as effective radiated power and represents the antenna power available for propagation. Converting (2.13) into logarithmic form with appropriate units conversion yields

$$P_d = P_t + G_t - 10 \log(4\pi R^2) \quad (2.14)$$

where

P_d = antenna power density in dBm/cm²
 P_t = power transmitted in dBm
 G_t = transmitting antenna gain in dB
 R = distance from antenna in centimeters

For a distance of 500 meters (2.14) becomes

$$P_d = P_t + G_t - 105 \quad (2.15)$$

The input data required for (2.15) are transmitter power output P_t and transmitting antenna gain G_t . From (2.14), the power density is inversely proportional to the square of the distance from the source. Doubling the distance from antenna to target results in a 6 dB decrease in power density regardless of whether the target is illuminated by the mainbeam, sidelobes or backlobe of the antenna pattern.

The transmitter power output data was obtained from various manufacturer's published specifications of commercially available power tubes. (8) Several types of tubes were considered and include power triodes, pentodes, traveling wave tubes, crossed field amplifiers, klystrons, magnetrons and gyrotrons. Antenna gains were selected based on typical equipment characteristics in the frequency range of interest.

In the VLF (3-30 kHz) and LF (30-300 kHz) portions of the spectrum relatively few emitters are operational, the most prominent being the Omega Radio Navigation stations. Power density calculated based on these emitters assumed a transmitter output power of 150 kW operating into a 3% efficient antenna system. The MF (300-3000 kHz) portion of the EM spectrum is dedicated primarily to commercial radio broadcasting. Power densities shown in Figure 2.21 are based on an available transmitter output power of 250 kW and an antenna gain of 3 dB.

The HF (3-30 MHz) communications band is used mostly for medium and long range communications. Power density levels in this frequency range were obtained using a nominal 50 kW PEP transmitter output power and antenna gains ranging from 5 to 12 dB. It is possible to achieve transmitter output power of about 250 kW PEP in this frequency range but stations this large are quite few.

In the 30-50 MHz public service band (U.S. allocation) the power density levels were obtained using 50 watt transmitters operating into a collinear antenna array having a gain of approximately 3 dB.

Power densities in the VHF TV band were based on the maximum permissible ERP levels allowed by the U.S. Federal Communications Commission.

Above about 200 MHz output tube powers were obtained from manufacturer's published data contained in commercial catalogs and data sheets. (8) The antenna gain data in the 225-400 MHz range was based on various dipole array configurations. Above 400 MHz, truncated parabolic dishes with a (casecant)² vertical pattern and a narrow horizontal beamwidth (for beam antenna) or full parabolic dishes (pencil beam antenna) were used.

Radar systems usually employ a form of pulse modulation. Thus the output tubes need not be able to operate at full power output continuously (CW) but rather they are turned ON and OFF intermittently (pulsed). The ON/OFF ration is referred to as the duty cycle. In those cases where the nominal tube data specified duty cycle limitation, both the peak and average power levels were recorded. These are shown as double power density lines for given frequency ranges on the graphs of Figures 2.22-2.23. The higher power density value is the peak power density; the lower line is the average power density. If no duty cycle limitations were specified, it was assumed that it could be operated continuously (CW); i.e., the peak and average power outputs are the same.

These are the types of tubes most commonly employed in communications systems. The average power levels are useful in determining component heating produced by the absorbed RF energy. The effects of average power on components are usually frequency independent and will result in thermal damage or burnout. Pulsed RF fields usually cause induced signals in electronic circuits and/or components. Knowledge of the peak power levels to which these circuits/components have been exposed aids in estimating the voltage spikes induced. These spikes may cause erroneous signal levels in analog processing circuits; e.g., if they are sufficient to affect a fast acting AGC circuit, bit errors in digital circuits may occur or, if the induced spikes are large enough, component damage due to short duration voltage or current overload is possible.

In general, communications or navigation system antennas are either omnidirectional, fixed installation arrays, or fixed orientation parabolic dishes which have a fixed area of coverage. If an aircraft is flying a radial course toward or away from one of these antennas it would remain under continuous illumination from the mainlobe if the craft is in the mainbeam pattern or the sidelobe/backlobe if outside of the mainbeam pattern.

Radar antennas are usually designed to scan a volume in space. Fan beam antennas are usually scanned in azimuth only whereas pencil beam antennas are usually scanned in both azimuth and elevation. When used for a search function, pencil beam antennas may be trained on a target during tracking operation. If an antenna is in motion a target may be illuminated only a short time during each antenna scan cycle. In the case of simple fixed elevation, 360° azimuth rotation, the time a given target will be illuminated for each full azimuth scan -- termed dwell time -- is given by

$$T = \frac{B}{6 (\text{SCAN RATE})} \quad (2.16)$$

where

T_D = dwell time in seconds
 B = antenna beamwidth in degrees
 SCAN RATE = antenna rotation rate in revolutions per minute (RPM)

Typical search radar antenna scan rates vary from 1 to 12 RPM. The antenna beamwidths may range from 1.5 to 3°. Using these independent variable ranges, dwell times from 20 to 500 ms may be considered typical. In the case of sector scanning antennas -- either horizontal or vertical scan -- similar relationships can be developed.

The power density levels of Figures 2.22 and 2.23 were calculated assuming mainbeam illumination. This is true when the antenna is omnidirectional or when a target is being tracked by a high gain antenna. Intermittent mainbeam illumination defined by (2.16) will occur when the target is scanned by a search radar. In fixed installations such as landing fields and carrier decks the radar antennas are usually mounted so that the aircraft parking areas, taxiways, and runways will not be illuminated by the mainbeam. In these cases, the aircraft will be subjected to sidelobe and backlobe radiation. For EMI prediction, it is necessary to specify antenna characteristics in the unintentional off-axis radiation region.

A directional antenna has, in addition to a mainbeam or major lobe of radiation, several smaller lobes about the major lobe known as minor lobes of the pattern. In general, an antenna pattern may be subdivided into a mainbeam region, a major sidelobe region and a side- and backlobe region. The mainbeam region is the 10 dB beamwidth of the major lobe of radiation. The major sidelobe region extends to +4 times the 10 dB beamwidth of the major lobe of radiation for high gain antennas ($G > 25$ dB). For medium gain antennas ($10 \text{ dB} < G < 25 \text{ dB}$), the main sidelobe region extends to only + one beamwidth (10 dB). Side- and backlobe regions extend over the remainder of the pattern.

The sidelobe gain in the major sidelobe region of an antenna will vary depending primarily on two factors: (1) the nature of the physical surroundings of the site on which the antenna is located and (2) the mainbeam gain of the antenna. As a general rule the approximate sidelobe gain of an antenna may be determined from the information in Table 2.2. Thus, the more crowded the site, i.e., more electromagnetic reflecting objects and the higher the gain of the transmit antenna, the higher the sidelobe levels. Therefore the power density levels incident on objects outside the antenna mainbeam could be anywhere from 3 dB to 50 dB below the mainbeam gains used to perform the computations required for Figures 2.22 and 2.23.

2.2.1.2 RF Threat Assessment

The primary RF threat to composite aircraft will come from high powered radar systems, particularly for aircraft in low level flight. Average power levels primarily result in local heating effects and are fairly insensitive to frequency. Peak power bursts can be much higher in magnitude and consequently be a threat to devices in avionic systems that are peak power sensitive.

Table 2.2 Generalized Off-Axis Antenna Data

Antenna Type	Siting	Side and Back Lobe Region			Major Side Lobe Region					Mainbeam Region				
		G_B	G_B	G_B	α_S	β_S	G_S	G_S	G_S	α_M	β_M	G_M	G_M	G_M
		$\frac{dB}{iso}$	$\frac{dB}{main beam}$	dB	deg	deg	$\frac{dB}{iso}$	$\frac{dB}{main beam}$	dB	deg	deg	$\frac{dB}{main beam}$	dB	dB
High Gain $G_0 > 25$ dB $f_0 < 1$ GHz	Open	-13	$-(G_0+15)$	8	$8\alpha_0$	$8\beta_0$	G_0-35	-35	8					
	Ave	-10	$-(G_0+10)$	6	$8\alpha_0$	$8\beta_0$	G_0-31	-31	6	α_0	β_0	G_0	0	2
	Crowd	-5	$-(G_0+5)$	4	$8\alpha_0$	$8\beta_0$	G_0-27	-27	4					
Medium Gain $10 \text{ dB} < G_0 < 25 \text{ dB}$ $200 \text{ MHz} \leq f_0 < 1 \text{ GHz}$	Open	-10	$-(G_0+10)$	6	$2\alpha_0$	$2\beta_0$	G_0-20	-20	6					
	Avg	-8	$-(G_0+8)$	5	$2\alpha_0$	$2\beta_0$	G_0-18	-18	5	α_0	β_0	G_0		2
	Crowd	-5	$-(G_0+5)$	4	$2\alpha_0$	$2\beta_0$	G_0-15	-15	4					
Low Gain $G_0 < 10$ dB $f_0 < 200 \text{ MHz}$	Open	-7		4										
	Avg	-5		3						α_0	β_0	G_0		1
	Crowd	-3		2										

α_0 = 10 dB Horizontal Beamwidth

β_0 = 10 dB Vertical Beamwidth

If 10 dB beamwidths cannot be determined, a good approximation is to use twice the 3 dB beamwidth

2.2.2 EMP Threat

The explosion of nuclear weapons in the atmosphere represents a serious electromagnetic threat to composite aircraft. A nuclear explosion produces an EM pulse (EMP) as well as higher frequency components in the visible, x-ray and gamma ray regions of the spectrum. Only the lower frequency EMP will be discussed since this threat is well known.

2.2.2.1 Overview(5)

The EM pulse is assumed to arise from a high altitude air burst of the kind commonly discussed in unclassified literature. The electric field from such a pulse can be modeled by a double exponential waveform which, in the time domain, has the functional form

$$E(t) = E_0(e^{-\alpha t} - e^{-\beta t}) \quad (2.17)$$

where

$$\begin{aligned} E_0 &= 58.15 \text{ kV/m} \\ &= 6.3 \text{ MHz} \\ &= 189 \text{ MHz} \end{aligned}$$

This waveform has a maximum value of 50 kV/m; a rise to peak time of 0.019 microseconds and a time to half peak amplitude of 0.185 microseconds. The magnetic field is assumed to be given by

$$H = \frac{1}{\eta_0} E \quad (2.18)$$

where $\eta_0 = 377$ ohms and is the free space impedance. The EMP waveform is shown in Figure 2.25. This waveform is similar in appearance to the double exponential waveform for lightning in Section 2.1.1.3 but the time scale for EMP is 100 times smaller. This difference in the time scales of the two threats serves to distinguish their impacts on a given aircraft. Because of the time scale difference, there are different frequency components in nuclear EMP than in lightning.

The frequency domain representation of (2.18) is the Fourier Transform given by

$$E(f) = \frac{E_0(\beta - \alpha)}{(\alpha + 2\pi j f)(\beta + 2\pi j f)} \quad (2.19)$$

where f is the frequency. This frequency domain representation of the EMP threat is shown in Figure 2.26. A comparison to the lightning spectrum in Section 2.1.1.3 indicates that EMP has a larger number of high frequency components than does lightning.

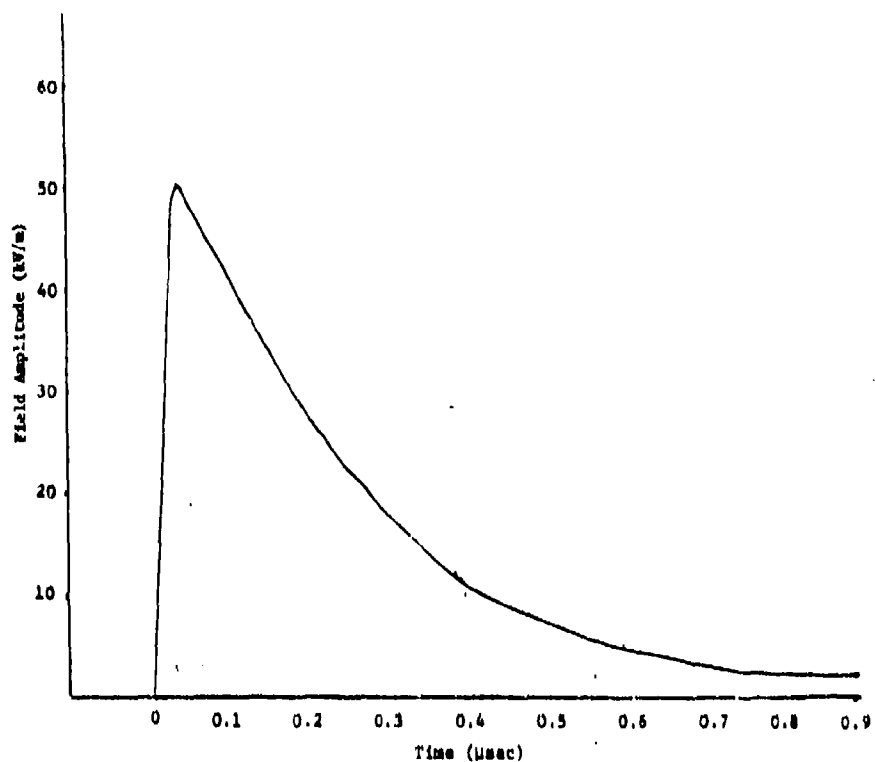


Figure 2.25 EMP Time Domain Waveform (5)

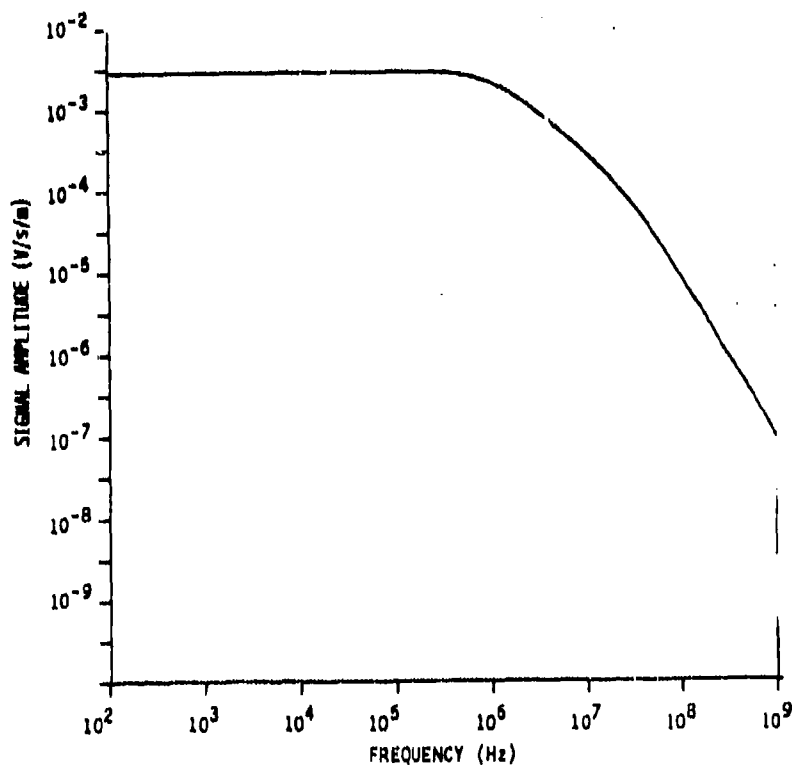


Figure 2.26 EMP in Frequency Domain (5)

2.2.2.2 EMP Threat Assessment

The EMP threat to composite aircraft is primarily EM field penetration through composite structures and is similar in many ways to the lightning threat. The EMP spectrum shown in Figure 2.26 shows the existence of many more high frequency components than in the lightning spectrum (see Figure 2.12). Thus EMP amplitudes will tend to be higher than lightning amplitudes for a given common frequency.

2.2.3 High Energy Laser, Nuclear Thermal Radiation and Particle Beam Threat⁽³⁾

Future electromagnetic environments will probably include laser and particle beam weapons. These devices are presently the subject of intensive classified research and development so only a very general overview will be given here.

A primary candidate for laser weapon systems is the deuterium fluoride laser which operates at 3.8 μ and is capable of several hundred kW (about 500 kW) CW operation. Another prime candidate is the CO₂ laser which operates at 10.6 μ with an output power of 50 - 135 kW. Other chemical lasers are being examined such as the Excimer laser which operates in the V region (0.25 - 0.25 μ) and the Free Electron laser tunable in the vicinity of 3.4 μ at several kW. There are two primary limitations on these laser devices:

1. Thermal blooming which is air heating in the beam that reduces the energy density on the target. The result is an increase in diffraction which defocuses the beam.

2. Aerosol breakdown which is the ionization of particulate matter in the air. A plasma is formed that expands until the entire beam is blocked. This effect occurs at power densities of approximately 10 MW/cm².

Particle beam weapon systems are currently being developed by the U.S. and U.S.S.R. It is expected that the effective ranges of these weapons will be

1. Up to 300 meters - single pulse
2. 4 to 5 km - continuous low PRF
3. Greater than 10 km - continuous pulse propagation

The expected effects on the intended target are

1. Detonation of the high explosive charge in the nuclear warhead carried by the target
2. Disruption of guidance/control/fusing electronics of the target
3. Reduction or voiding of the yield of the nuclear warhead carried by the target.

Energy levels on the order of 100 - 125 joules/gram are required to cause destruction or slumping of nuclear materials, while 210 joules/gram are required to melt lead.

The response of composite structures to thermal pulse heating from a laser, nuclear thermal radiation or a particle beam weapon varies from surface damage to buckling, plastic deformation of the epoxy or complete burn-through with fiber vaporization. This results from the generally (3) low thermal conductivity, high absorptivity, low epoxy combustion temperature and high fiber vaporization temperature of the composite. Figure 2.27 illustrates the backside temperature of a graphite/epoxy substrate as a function of substrate thickness for several energy fluence rates. Drastic strength loss results when steady temperatures reach 400 degrees F.

A summary of the response of a section of graphite/epoxy composite to irradiation by a CW laser is shown in Table 2.3. The composite characteristics most important in determining laser damage are laminate lay-up sequence and preload stress factor. Figure 2.28 illustrates the laser energy density necessary to produce a given level of stress in various composite and metal samples for two kinds of failure modes. The energy density necessary to cause heat-related failure is much smaller than the energy density necessary to produce burn-through failure.

Several methods exist for protection of composite aircraft from thermal radiation threats. These methods are discussed in Section 10.0 on Protection Methods and Techniques.

Table 2.3 Effect of Variable on CW Laser Response of Graphite/epoxy⁽³⁾

Effect of Variables on CW Laser Response of Graphite/Epoxy

Laser/target variable	Effect of laser damage	
	Burn-through mode ^a	Flood loading mode ^b
Lay-up sequence	No effect	Damage significantly greater when O ² load-carrying ply directly irradiated
Preload stress	Little effect below that stress level causing failure during laser irradiation	Damage increases with decreasing energy fluence and increasing preload stress
Airflow velocity	No effect on penetration rate High airflow velocity reduces structural damage	High airflow velocity reduces structural damage
Beam area	Beam areas < 4 cm ² require higher energy levels for penetration	None
Laminate thickness	None	Very little
Fiber/matrix type	None	None
Wavelength	Unknown, all data at 10.6 μ m	Unknown, all data at 10.6 μ m

^aHigh flux, small area irradiation

^bLow flux, large area irradiation

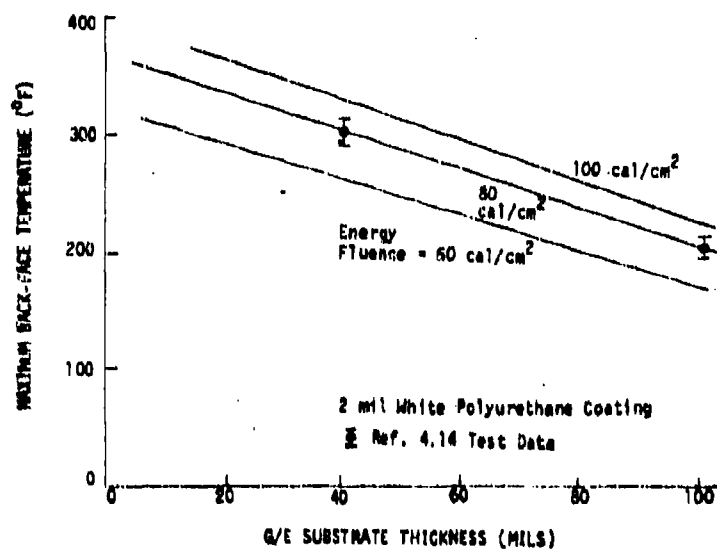


Figure 2.27 Back-face temperature of graphite/epoxy substrate for several thermal pulse fluence levels(3)

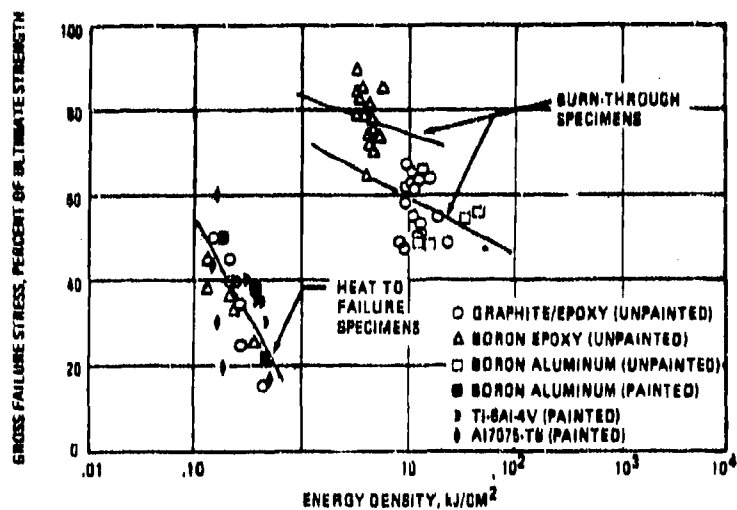


Figure 2.28 Laser energy density necessary to produce a level of stress for two failure modes(3)

2.3 References

1. Ulman, M.A., Lightning, McGraw-Hill, 1969.
2. Strawe, D., Lightning Source Model Development, Lightning Workshop, NOSC, San Diego, California, 1978.
3. Strawe, et. al., Investigation of Effects of Electromagnetic Energy on Advanced Composite Aircraft Structures and their Associated Avionic/Electrical Equipment, Phase II, Volume 1, The Boeing Company, 1977.
4. J. Allen, et. al., A Technology Plan for Electromagnetic Characteristics of Advanced Composites, RADC-TR-76-206, July 1976.
5. Wallenberg, et. al., Advanced Composite Aircraft Electromagnetic Design and Synthesis, Interim Report, Syracuse Research Corp., April 1980.
6. Notebook on Electrical Properties of Composites for Frequencies Above 1 GHz, Atlantic Research Corp., April 1979.
7. Oh, L. L., Measured and Calculated Spectral Amplitude Distribution of Lightning, IEEE Trans. EMC, November 1969.
8. Output Tube Data Sources (Catalogs): Hughes (Electron Dynamics Div); Thompson-CSF; Varian (Palo Alto Tube Division); Hawasaki; Nippon Electric Corp. (NEC); English Electric Valve Co. (EEV), Litton Industries; Continental Electronics Corp.
9. Transmitting Antenna Data Sources are based on general antenna characteristics set forth in: (1) Antenna Engineering Handbook, (Jasik); (2) Reference Data for Radio Engineers, 4th Edition, (ITT Handbook); (3) ARRL Antenna Book, 13th Edition (1977); (4) Antennas, Blake, John Wiley & Sons, 1966; (5) A Handbook Series on Electromagnetic Interference and Compatibility, Vol. 5; (6) Interference Notebook, RADC-TR-66-1 June 1966.
10. J. Phillpott, Recommended Practice for Lightning Simulation and Testing Technique for Aircraft, Culham Laboratory Report CLM-RH3, Abingdon Oxfordshire England, (1977).
11. Schneider, Kendricks and Olson, Vulnerability, Survivability of Composite Structures - Lightning Strike, AFFDL-TR-77-127 Vol. 1 (1978).

3.0 COMPOSITION, FABRICATION AND MECHANICAL PROPERTIES OF COMPOSITE MATERIALS

In the first two parts of this section, a general description is given of the composition and fabrication processes of graphite, boron and Kevlar composite materials. The various fiber and matrix materials for fiber-reinforced materials are discussed as well as the processes by which they are manufactured.

Several procedures in the fabrication process of composites are discussed. The discussion begins with paper tapes and broad goods, continues with layup procedures and ends with an overview of the different kinds of fabrication procedures used to cure the composites.

Mechanical properties are presented in a series of graphs for the fibers, unidirectional laminates, crossplied laminates and hybrid composites. A brief summary is given of composite fatigue data and environmental effects on composites.

3.1 Composition of Composite Materials

The term "composite materials," in principle, may be applied to any material substance composed of heterogeneous parts with distinct interfaces between the parts. For the purposes of this handbook, the term "composite material" will mean fiber-reinforced materials containing high performance fibers and suitable proportions of a bonding or matrix material in order to obtain material properties comparable or superior to metals and fiberglass.⁽¹⁾

The composite fibers determine the overall material strength and stiffness characteristics while the composite matrix determines the transverse mechanical properties (those normal to the fibers), interlaminar shear characteristics and service operating temperatures.⁽¹⁾ Both fiber and matrix are equally important in determining the overall performance characteristics of composite materials. A typical fiber-reinforced composite material schematic is shown in Figure 3.1.

3.1.1 Fibers

A number of different fibers are available commercially for use in composite materials. The most commonly used fibers are graphite, boron, aramid (Kevlar), glass, aluminum and silicon carbide. Only the first three fibers are treated in this handbook. A general list of fiber types and vendors is given in Table 3.1.

3.1.1.1 Graphite Fiber

Most of the commercially used graphite fiber is produced by pyrolyzing precursor polyacrylonitrile (PAN) fibers under tension in furnaces operating between 2500-3000°C.^(1,2) Typically the PAN fiber is pulled through an initial heating stage of 250°C-400°C where it is oxidized to a stable state. The fiber is then pyrolyzed at high temperature varying between 1000°C - 3000°C depending on the amount graphitization required. Both the mechanical and electrical properties of the resulting graphite fibers depend on the degree of graphite crystal structure in

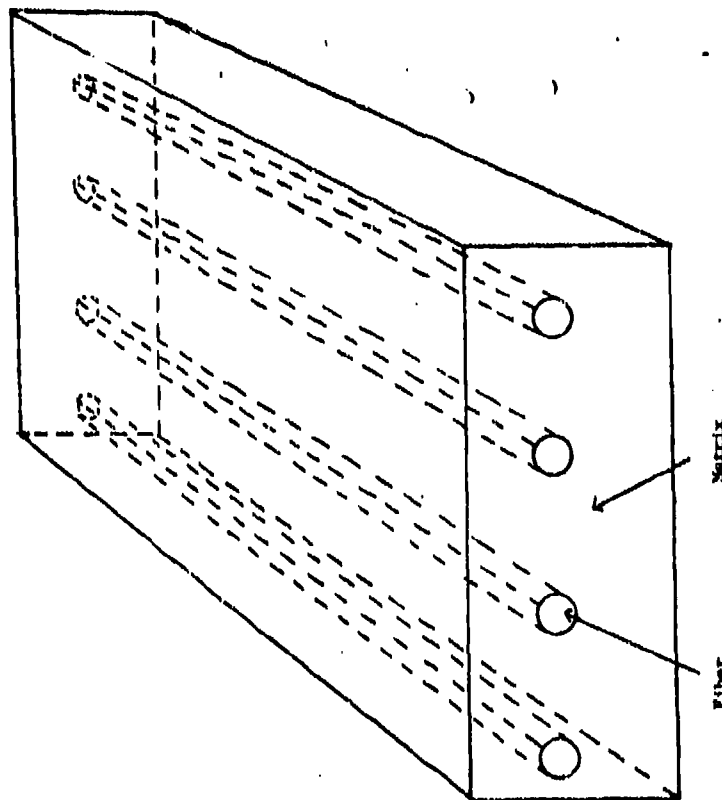


Figure 3.1 Fiber-Reinforced Composite Material

Table 3.1 Composite Fibers and Vendors (1)

Category	Type	(1) Vendor
Polycrystalline Alumina (Al_2O_3)	FR-1	D
	FR-2	D
	SiO ₂ Coated	D
Aramid	KEVLAR 29	D
	KEVLAR 49	D
Carbon (2)	4 MIL/W	CT/A
	5.6 MIL/W	CT/A
	8 MIL/W	CT/A
	4.2 MIL/CC	A
Glass	E*	-
	S*	-
Graphite (Low-Cost High-Strength) (LHS) (PAN)	CELCON (1)	C
	A-5	H
	T-300 (1,2)	U
	TYPE III 3T	M G
Graphite Intermediate Modulus (IM) (PAN)	T-400	U
	TYPE II	M
	HTS	H
	4T	G
Graphite High Modulus (HM) (PAN)	HM	H
	T-50	U
	TYPE I	M
	5T	G
Graphite Ultra-High Modulus (UHM) (PAN)	6T	G
	GY-79	C
Graphite Pitch	TYPE P	U
Silicon (2) Carbide	5.6 MIL/C	A
	5.6 MIL/W	A

(1) A - AVCO
C - Calsonic
CT - Composite Technology
D - DuPont
G - Great Lakes
H - Hercules
M - Morganite
U - Union Carbide

(2) W - Tungsten Core
CC - Carbon Core

the fiber and the degree of crystal orientation along the fiber axes.⁽²⁾ Both of these quantities depend on the fiber tension and temperature used in the graphitization process. A diagram of the PAN fiber conversion process is given in Figure 3.2.

Graphite fiber can also be made by heating and crystallizing pitch.^(1,2) Such pitch fiber has considerably lower strength than PAN fiber. However, pitch fiber process is quicker, cheaper to manufacture, while the high fiber stiffness would allow its use in automotive composites.⁽¹⁾

Once the graphite fibers are produced, approximately 10,000 of the individual fibers are wound together to produce a larger braid called a tow (shown in Figure 3.3). The tows are then combined with the matrix material to form the composite.⁽³⁾

3.1.1.2 Boron Fiber

The production of boron fibers is based on a chemical vapor deposition process.^(1,3) The precursor fiber is tungsten wire preheated to 1200°C to clean the wire surface. Boron is then deposited on the tungsten wire by passing the wire through a heated atmosphere of boron trichloride vapor and hydrogen gas. Various boron-tungsten compounds are formed in the process. The final boron fiber consists of an inner core of unconverted tungsten surrounded by a sheath of boron and boron-tungsten compounds.⁽³⁾ Some attempts have been made to use carbon substrates to replace the tungsten wire, but fiber properties are poorer.⁽¹⁾ The boron fiber manufacturing process and a cross section of a boron fiber are shown in Figure 3.4. The overall boron fiber manufacturing process is quite expensive.^(1,2)

3.1.1.3 Aramid (Kelvar) Fiber

Kelvar aramid fiber is produced from long chain organic polyimide polymers.^(1,4) The polymer is drawn into a fiber under appropriate tension and temperature using standard textile processes. The fiber has low density, high tensile strength, low cost but poor compressive properties. The fiber is then woven into fabrics or, less frequently, used in tapes.⁽¹⁾

3.1.2 Matrix Materials

The most commonly used matrix materials are epoxy resin tapes and chopped fiber-filled thermoplastic injection molding compounds.^(1,2) Other non-metallic matrices such as polyimide, thermoplastics, polyester and vinyl ester compounds, are under development. The most common metallic matrices are aluminum alloys.⁽¹⁾ Choice of a particular matrix depends on the composite properties desired and the service temperature likely to be encountered.

The epoxy resins most often used are the diglycidyl ether of bisphenol A and its dimers, the tetraglycidyl ether of tetraphenolethane, tetraglycidylmethyldianiline, and the epoxies derived from novolacs.⁽²⁾ The curing temperatures are typically 350°F or 260°F for military or commercial aircraft and other high performance applications.⁽¹⁾

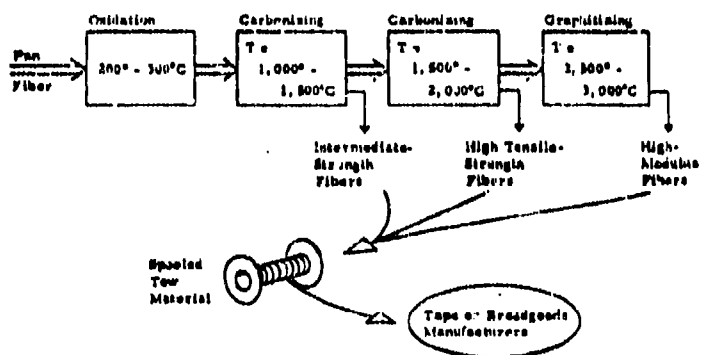


Figure 3.2 PAN Fiber Graphitization Process⁽³⁾

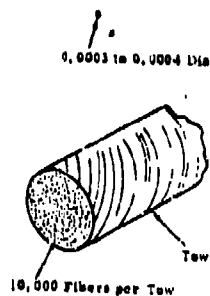


Figure 3.3 Graphite Fiber Tow⁽³⁾

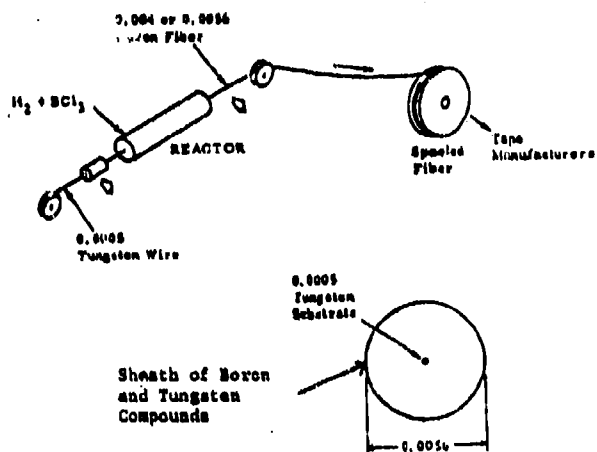


Figure 3.4 Boron Fiber Manufacturing Process Together With a Boron Fiber Cross-section⁽³⁾

Graphite/polyimide materials are being developed for applications on missile and engine components which permit an operating temperature beyond that offered by graphite/epoxy (350°F). Current operating temperature limitations are about 600°F.⁽¹⁾ These matrices, however, require expensive high pressure curing processes (up to 200 psi). A summary of matrix characteristics is given in Table 3.2.

3.2 Fabrication of Composite Materials

This section presents a review of the various fabrication processes that are used to transform a fiber and matrix into a composite material.⁽¹⁾ The fibers are first fabricated into tapes or broad goods when they may be laid up in a crossplied laminate structure of the proper shape. The layup is then cured by a high temperature and/or high pressure process. The total fabrication process has a very large impact upon material properties and total cost of composite materials.

3.2.1 Tape (Prepreg) and Broad Goods Fabrication

As a first step in the manufacture of composites, a set of tapes may be prepared that contain collimated fibers (or tows) preimpregnated with binding resin. Such tapes are called prepregs.⁽¹⁾ Alternatively, a broad sheet of material may be prepared as a woven fabric if it is necessary to produce parts that are difficult to lay up from tape, e.g, flanged rings.⁽¹⁾ The cost of such broad goods is higher than tape⁽¹⁾ and is justifiable only by lower labor costs or by being able to make the part at all. A schematic illustrating the prepreg and broad good position in the total fabrication process is shown in Figure 3.5.

3.2.2 Layup Process

The prepreg or broad goods usually must be laid in a part mold or on a tool.⁽¹⁾ The original process involved manual layups. Such a process is extremely costly because it is very labor intensive. More recent approaches have stressed automated tape layup procedures.⁽¹⁾

A basic decision that must be made at this point is which tape layup method is to be used. One method, the ply-on-ply layup system,⁽¹⁾ is a single step process in which the plies are laid on top of each other to form a simple shape. A drawback is that inspection of the total layup is difficult and repair of defects very costly.⁽¹⁾ A solution to this problem is provided by another method the ply-on-film process,⁽¹⁾ however a second operation is needed to stack the plies on the tool.

The individual plies may be laid up in a variety of styles depending on the desired properties and shape of the part being manufactured. A symmetric balanced layup is shown in Figure 3.6.

3.2.3 Laminate Orientation Code

Because of the numerous multi-ply laminates that are possible for composites with tailored or "engineered" properties, some systematic method is required for describing the orientations of the fibers in a general composite laminate structure.

Table 3.2 Matrix Systems - General Characteristics (1,3)

Matrix Material	Maximum Service Temperature**	General Characteristics
Modified epoxy	350°F continuous*** 400°F intermittent	Thermosetting resin used for low-pressure (up to 100 psi) laminating requiring a minimum of 350°F cure for 350°F service applications.
Polyimide	550°F continuous 700°F intermittent	Thermosetting resin used for low-pressure (up to 100 psi) laminating requiring 350° to 400°F cure plus an extended post-cure. The polyimide resin family is characterized by high cost, difficult processing, good dielectric properties, and non-cured laminate outgassing.
Aluminum	600°F continuous	6061 and 2024 alloys generally require pre-stress diffusion bonding under vacuum and at about 550°F under 3,000 to 1,000 psi pressure to consolidate the composite. 713 aluminum brass alloy requires 1,050°F under vacuum and about 100 psi pressure to consolidate (used with Borec Resin only).

**Minimum service temperature is 40°F

***Even though modified epoxies are generally considered capable of continuous service up to 350°F, most experience with composites has limited only intermittent service as high as 350°F, and there is some question as to degradation of properties after long-term, humidity exposure which limit the service temperature to 275°F.

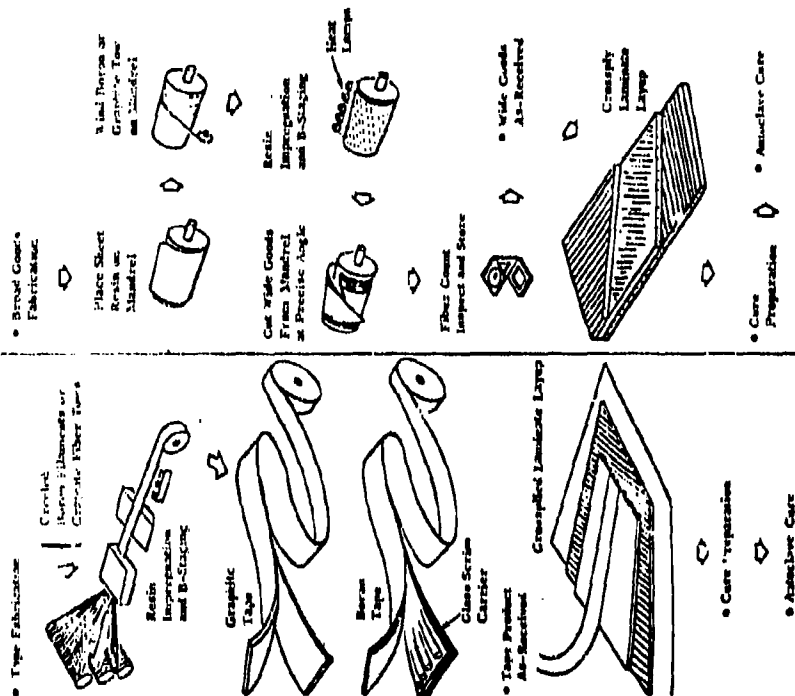


Figure 3.5 Tape (Prepreg) and Broad Goods Fabrication Processes (1)

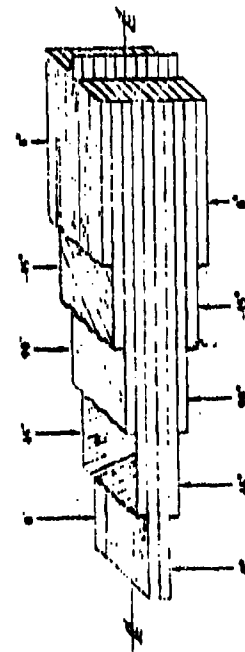


Figure 3.6 Symmetrical Balanced Layer (3)

The most common procedure defines a laminate structure by specifying the orientation angles (in degrees) of the various lamina with respect to a reference direction (which is arbitrary). The orientation angle of lamina with fibers parallel to the orientation direction is 0° . Other orientation angles (including negative angles) are specified similarly. The complete set of periodic lamina angles are listed in stacking order, separated by slashes (or commas), with the complete set enclosed within brackets. For example, the orientation code for the layup shown in Figure 3.6 is

$(0^\circ/-45^\circ/90^\circ/45^\circ/0^\circ/0^\circ/45^\circ/90^\circ/-45^\circ/0^\circ)$

A simplification is commonly made for orientation codes of this type. The center 0° laminates act as a mirror for the other lamina. Consequently, the code can be simplified to

$(0^\circ/-45^\circ/90^\circ/45^\circ/0^\circ)s$

where the "s" indicates a minor reflection at the right-handed 0° laminate is required for the remaining laminate structure.

Another common code⁽³⁾ lists all the laminate orientation angles as before but not in stacking order. Again, referring to Figure 3.6, this orientation code would be

$(0_4/+45_2/90_2)$

indicating four 0° plies, four $+45^\circ$ plies (two of each sign) and two 90° plies. In using ply orientation codes, care is required to determine if ply stacking order is considered.

3.2.4 Composite Fabrication Processes

In this section a brief description is given of the major manufacturing processes that are used for making composite materials. The processes are of two kinds: direct and indirect.⁽²⁾ In direct processes, the fiber is combined with the matrix and the composite formed in one process. The advantages to this method are that the method is simple and cost-effective. A disadvantage is that the types of geometric shapes that can be fabricated are usually restricted. Indirect processes first combine the matrix and fiber in a separate intermediate stage. The stage is then finished in a second procedure. More general shapes are possible with indirect processes but the total processing time is slow and costly. Examples of both procedures will be discussed in this section.

3.2.4.1 Filament Winding

Filament winding is a high-speed process wherein fibers or tapes are wound onto a rotating mandrel with a certain tension and at carefully controlled angles.^(1,2) It is an important direct process for manufacturing composite tubes, motor cases and pressure vessels.⁽¹⁾

3.2.4.2 Pultrusion

This indirect process consists of pulling a bundle of fibers through a resin bath and then through a hot die to form the part shape and cure the composite. Pultrusion is a low-cost method for producing straight or slightly curved shapes with constant cross-section.(1,2)

3.2.4.3 Braiding

In the braiding process, a mandrel is fed through the center of the machine at a fixed rate while fibers wind around the mandrel at a controlled angle. The machine works like a maypole and the process applies to channel sections and webs.(1)

3.2.4.4 Injection Molding

This high-volume direct process involves softening a plastic material (with fibers or fillers) by heat, forcing the material into a mold under high pressure, cooling the material and then ejecting the part from the mold. The process is very fast, inexpensive and applicable to many different kinds of composite parts.(1,2)

3.2.4.5 Compression Molding

In this indirect process, the intermediate material is pressed into the final shape in the mold. The mold is then heated to the cure temperature to bring about a permanent "set" of the material.(1) Curing time is typically 2 to 3 minutes.

3.2.4.6 Thermal Expansion Molding

Prepreg layers are wrapped around blocks of rubber and the blocks placed in a metal cavity. At high temperatures, the blocks expand more than the metal restraining cavity resulting in high curing pressures. This method eliminates the need for a separate autoclave.(1)

3.2.4.7 Vacuum - Bag Molding

In this method, the prepregs are laid onto a mold one ply at a time. The prepregs are then "sucked" against the mold by evacuation of a plastic bag around the mold. A bleeder system is used to remove excess resin and maintain the correct fiber-volume ratio for the composite. The bagged mold is then cured in an autoclave under full vacuum. The cycle is quite slow and is usually restricted to low-volume applications or long cure-time composites.(1,2)

3.2.4.8 Autoclave Molding

This process is similar to the vacuum-bag process except that greater pressures are applied to the layup and denser parts are produced.(1)

3.2.4.9 Honeycomb Sandwich Fabrication

Two methods exist for bonding composite to core materials in making sandwich structures. The first process involves curing the composite facings separately and then bonding to the core. The second method cures and bonds the entire sandwich structure in one process.(1)

3.3. Mechanical Properties

In this section a survey of the more common mechanical properties is given for graphite/epoxy, boron/epoxy and Kevlar. Because of the enormous number of individual laminate structures, a complete survey is out of the question. Measured values of the parameters are restricted to unidirectional laminates and the (0,60) crossplied laminate. More general crossplied lamina, including hybrid structures, are estimated using structural analysis techniques and presented as carpet plots.

3.3.1 Composite Fiber Properties

A very large number of different fiber types are available commercially for the manufacture of composite materials. Such fibers may be continuous or chopped and range from the aramid fibers used in Kevlar and other organic composites, to the graphite and boron-tungsten fibers used in graphite and boron composites. Only continuous fibers will be discussed in this report because of their overwhelming use in aircraft applications.

The key to successful design of composite materials which tailor-made mechanical properties has been the development of good fiber technology.⁽²⁾ Such a technology can endow a fiber with a unique and outstanding set of mechanical properties that cannot be duplicated in the bulk material from which the fiber is made. The anisotropic fiber composite may then be "engineered" to have special properties in selected directions by just picking the required fiber and matrix.

A list of fiber mechanical properties is given in Figures 3.7 to 3.10. The properties are those at room temperature. A comparison is made between several fiber types and between the fibers and metals commonly used in aircraft manufacture. Specific comparisons vary somewhat from figure to figure depending on the data available.

Figure 3.7 shows the density of various composite fibers compared to the density of steel, titanium and aluminum. The graphite fibers are typically 30% less dense than aluminum while Kevlar is almost 45% less dense. Boron fibers have about the same density as aluminum.

Figure 3.8 is a plot of tensile strength and tensile modulus for various composite fibers and aluminum and stainless steel. Kevlar, S-glass and E-glass tend to have high tensile strength while boron and graphite fibers have moderate to high tensile strength and high modulus. Stainless steel has moderate tensile strength and fairly high tensile modulus while aluminum has low tensile properties. As a further illustration of composite fiber tensile properties, stress-strain curves are plotted in Figure 3.9 for selected composite fibers.

The most important information concerning composite fiber mechanical properties is shown in Figure 3.10. In this figure, the specific tensile strength and specific tensile modulus are plotted for various composite fibers, stainless steel and aluminum. By specific tensile strength or modulus is meant the strength or modulus normalized to the fiber density. These data form the basis for marketing decisions of the fibers for aircraft applications because they represent the ratio of strength or stiffness to weight. An examination of Figure 3.10 shows Kevlar having the highest

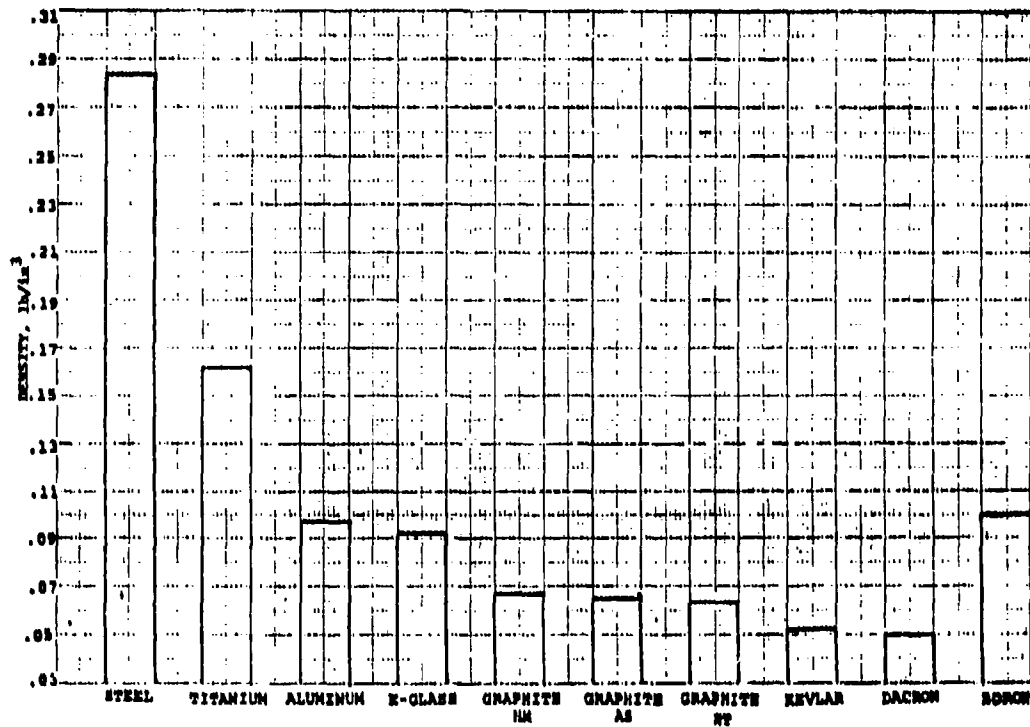


Figure 3.7 Composite Fiber Densities Compared to Aircraft Metals (1-5)

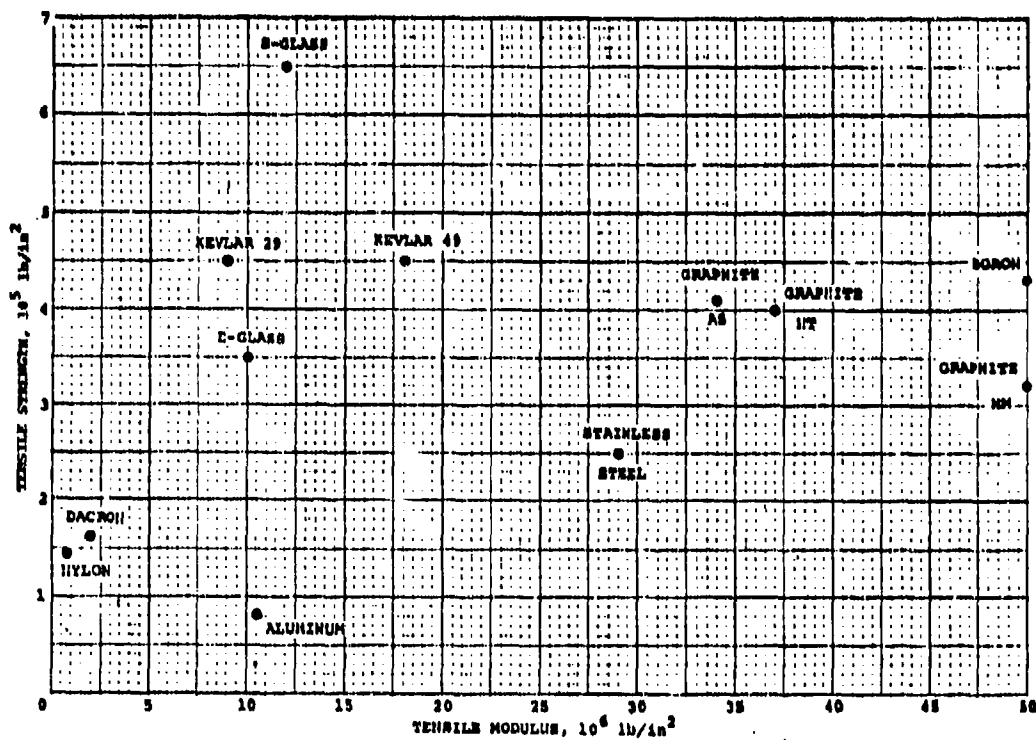


Figure 3.8 Tensile Strength and Modulus of Various Composite Fibers and Metals (1-5)

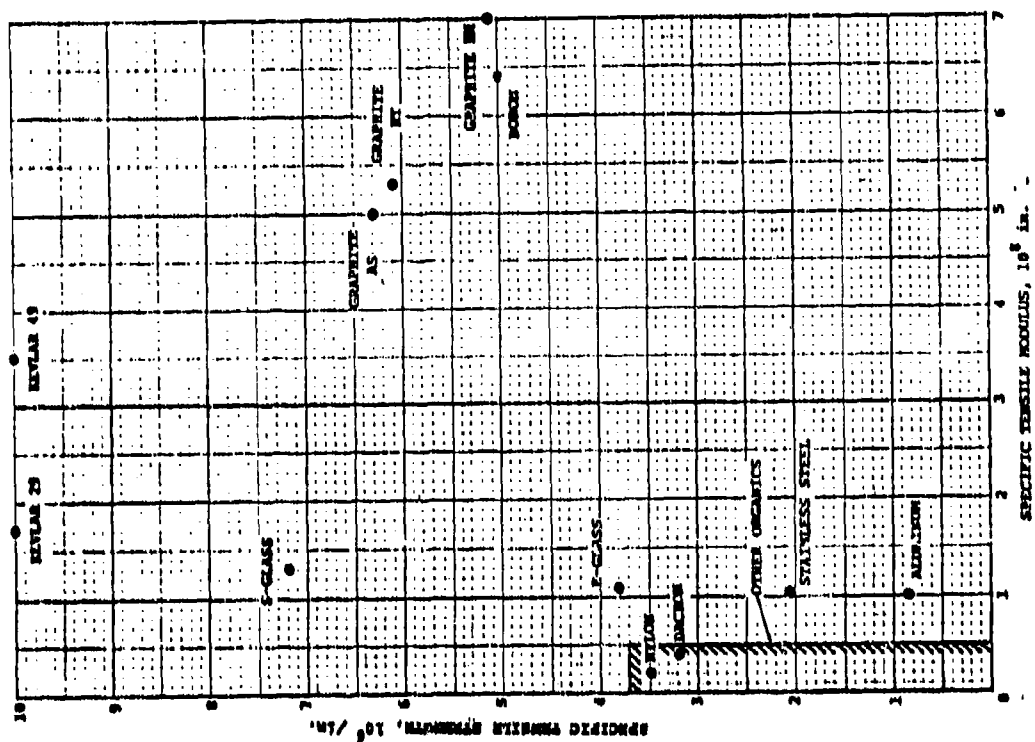


Figure 3.10 Specific Tensile Strength and Modulus for Various Composite Fibers and Metals (4)

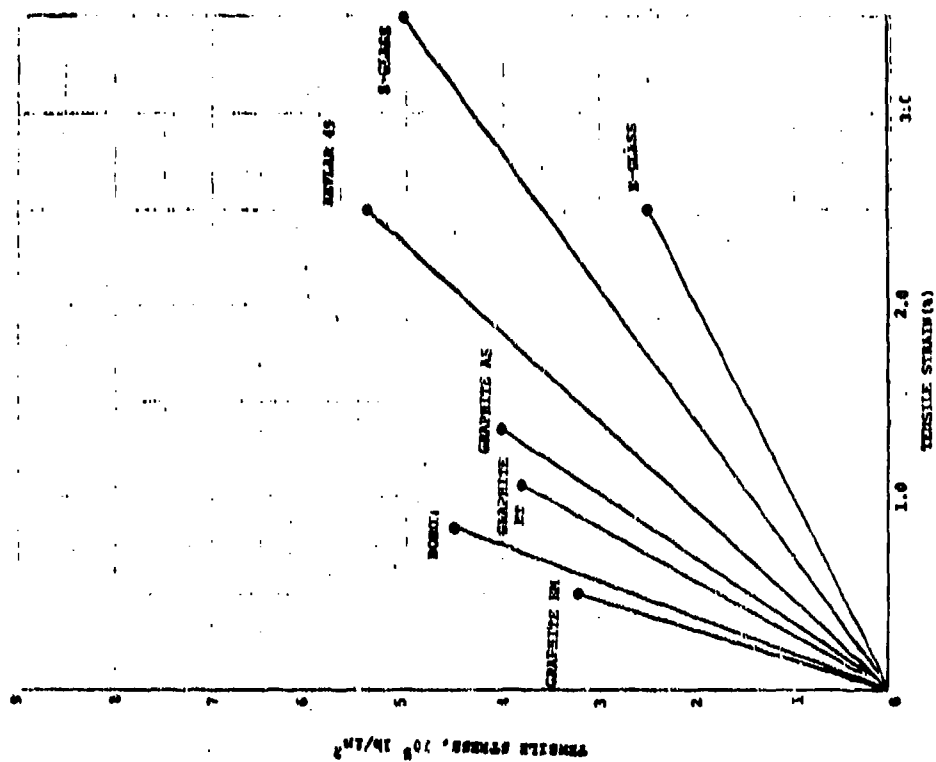


Figure 3.9 Stress-Strain Curves for Composite Fibers (4)

specific strength and high modulus (HM) graphite having the best specific tensile modulus. Both stainless steel and aluminum are poor by comparison; steel because of its high density and aluminum, because of its relatively low tensile strength and modulus.

3.3.2 Composite Matrix Properties

The resin matrix in which the fibers of the composite are immersed performs two important tasks.⁽²⁾ First, the matrix separates the fibers to maximize their contributions to composite strength and minimize the possibility of microcracks and buckling developing in the material because of fibers touching. Second, the matrix binds to the fibers sufficiently to enable the material to bear and transfer stresses safely throughout the material.

The stresses to which the matrix is most sensitive are those transverse to the fiber direction.⁽²⁾ Longitudinal stresses are transmitted mostly by the fibers. In order for the matrix to safely bear and transfer stresses, it is necessary that the matrix precursor liquid wet the fiber surfaces.⁽²⁾ The wetting process brings matrix material close enough to fiber material to allow chemical bonds to be formed. If R is the rate of wetting of the composite fibers by the matrix resin, then ⁽²⁾

$$R = \frac{r \cos \theta}{\eta}$$

where r is the surface tension of the matrix precursor liquid, θ is the contact angle of the liquid on the fiber surface, and η is the liquid viscosity. In general, $r \cos \theta$ is small which implies that reasonable wetting rates are obtainable only with low viscosity precursor liquids.⁽²⁾

A number of different matrix resins are in common commercial use. The resins may be thermosetting or thermoplastic.⁽²⁾ The more common thermosetting resins are polyesters, vinyl esters, epoxy and polyimide and have use temperatures from 200°F to 600°F. Thermoplastic resins include nylon 66, polybutylene, polysulfone, and polyamide with use temperatures from 280°F to 500°F.

The composites giving the best mechanical behavior are made from epoxy resins and are the ones normally used in aerospace applications.⁽²⁾ The epoxy resins commonly used include the diglycidyl ether of bisphenol A and its dimers; the tetraglycidyl ether of tetraphenolethane, tetraglycidyl methyldianiline and epoxies derived from novolacs.⁽¹⁾

3.3.3 Single Laminate Composite Properties

In this section, typical measured values for certain key mechanical and physical properties are given for single laminate graphite/epoxy, boron/epoxy and Kevlar/epoxy composites.^(2,5) The mechanical properties considered are tensile, compressional and shear strengths and the tension, compression and shear moduli elastic constants (including Poisson's ratios). The physical constants considered are density and thermal expansion constants. Numerical data is given for each property (except density) measured longitudinally, transverse and diagonally with respect to the fibers (0°, 90° and +45° with respect to the fiber axes) at both room temperature and 350°F. (Kevlar data is given at room temperature.) All data is shown graphically in Figures 3.11 - 3.30.

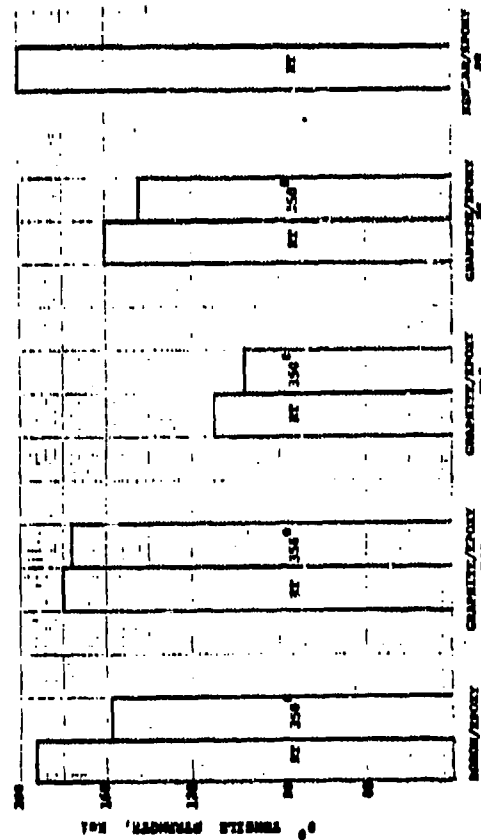


Figure 3.11 Longitudinal Tensile Strength For Various Single Laminate Composites At Room Temperature (RT) and 350°F (Z-5)

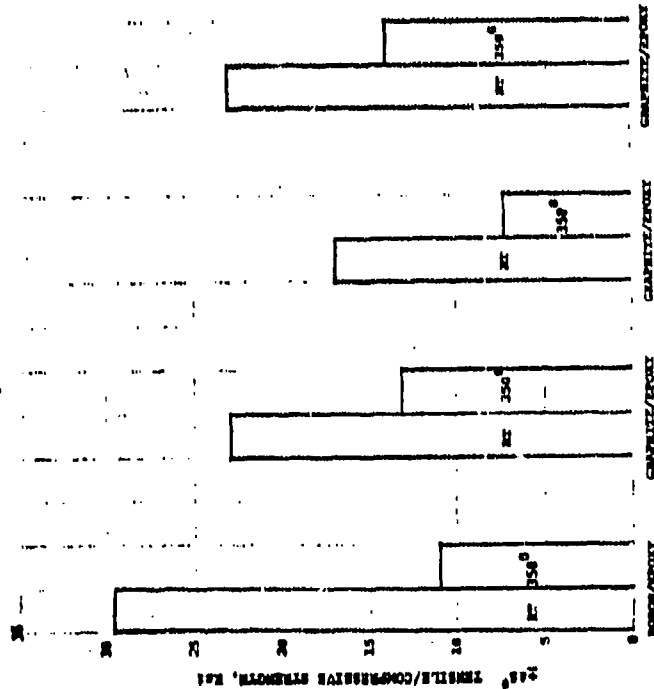


Figure 3.12 Diagonal Tensile/Compressive Strength For Various Single Laminate Composites At Room Temperature (RT) and 350°F (Z-5)

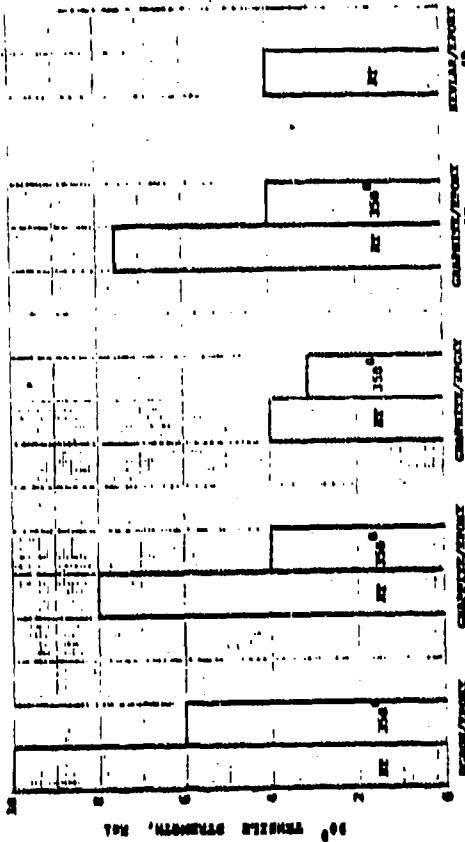


Figure 3.13 Transverse Tensile Strength For Various Single Laminate Composites At Room Temperature (RT) and 350°F (Z-5)

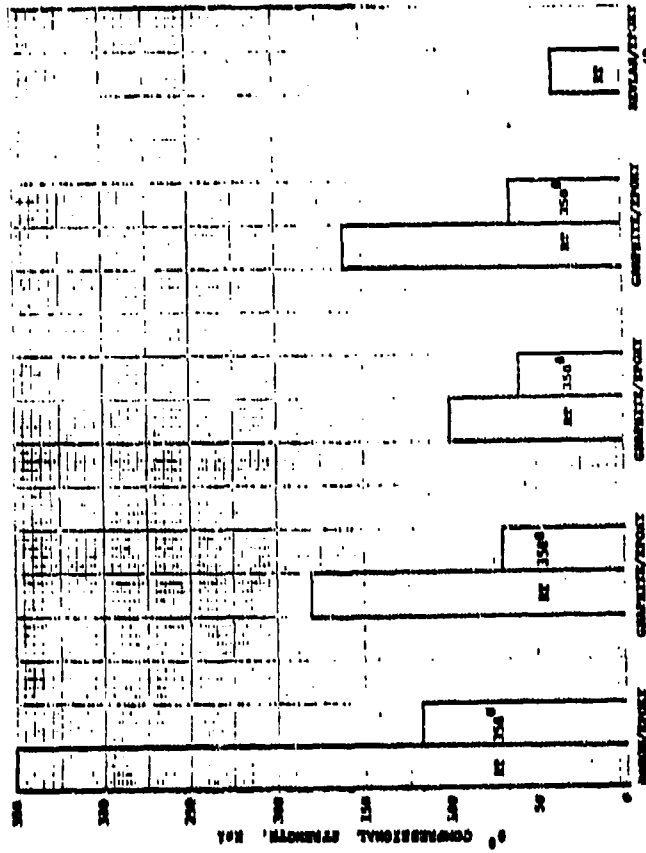


Figure 3.14 Longitudinal Compressive Strength For Various Single Laminate Composites At Room Temperature (RT) and 350°F (Z-5)

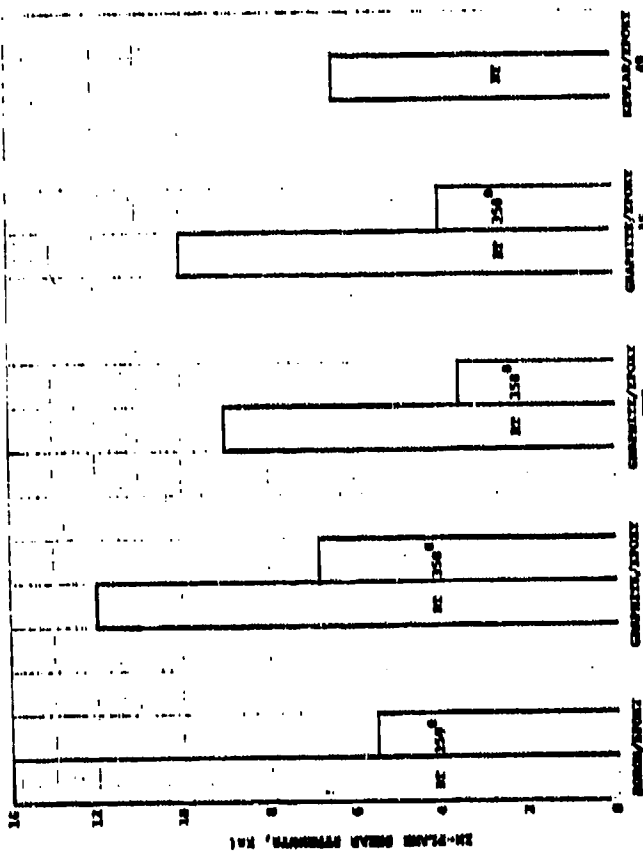


Figure 3.16 In-Plane Shear Strength For Various Single Laminate Composites At Room Temperature (RT) and 350°F (2-5)

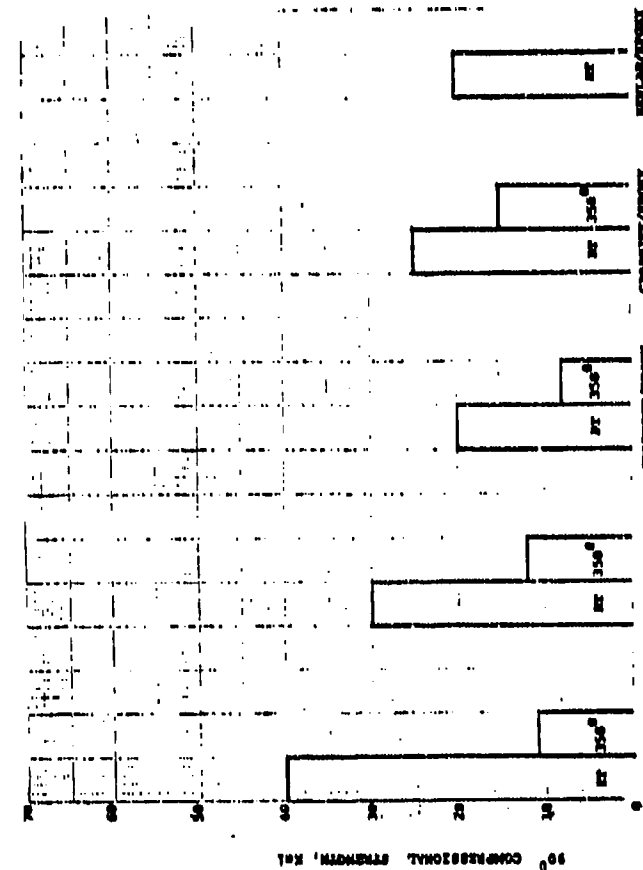


Figure 3.15 Transverse Compressive Strength For Various Single Laminate Composites At Room Temperature (RT) and 350°F (2-5)

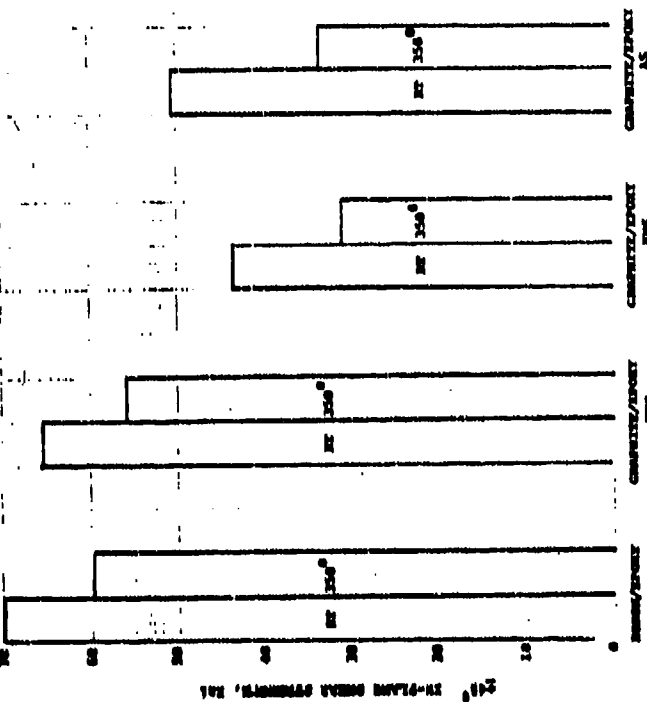


Figure 3.18 In-Plane Shear Strength For Various Single Laminate Composites At Room Temperature (RT) and 350°F (2-5)

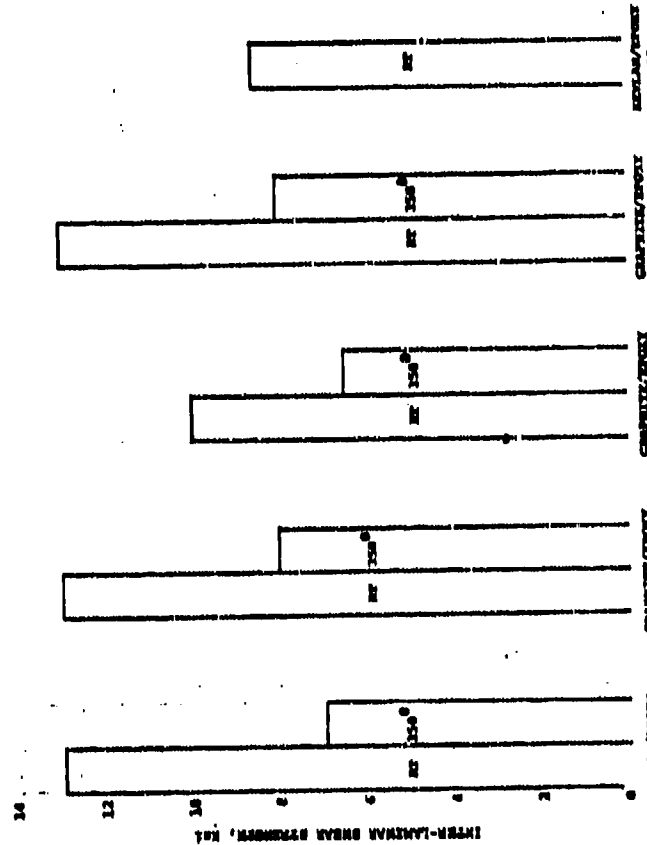


Figure 3.17 Inter-Lamellar Shear Strength For Various Single Laminate Composites At Room Temperature (RT) and 350°F (2-5)

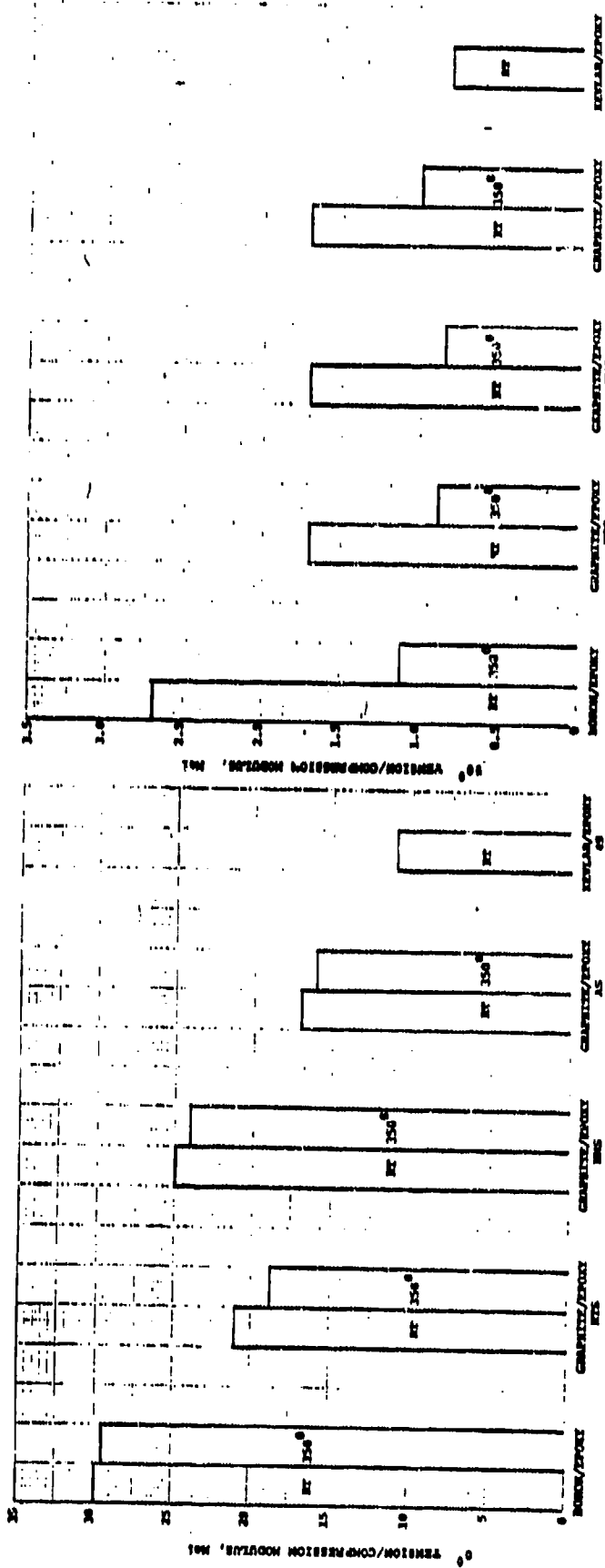


Figure 3.19 Longitudinal Tension/Compression Modulus for Various Single Laminate Composites at Room Temperature (RT) and 350°F(2-5)

Figure 3.20 Transverse Tension/Compression Modulus for Various Single Laminate Composites at Room Temperature (RT) and 350°F(2-5)

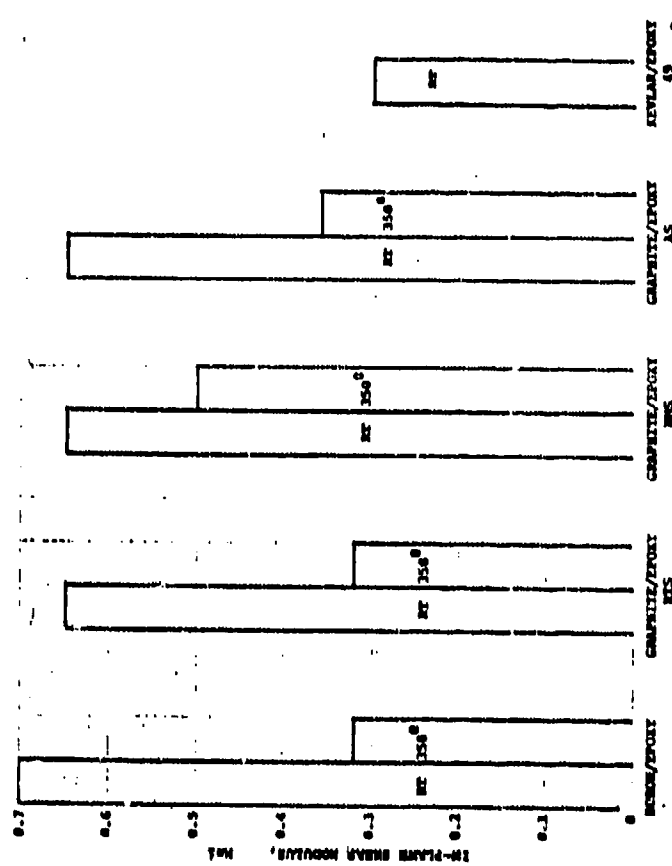


Figure 3.21 In-Plane Shear Modulus for Various Single Laminate Composites at Room Temperature (RT) and 350°F(2-5)

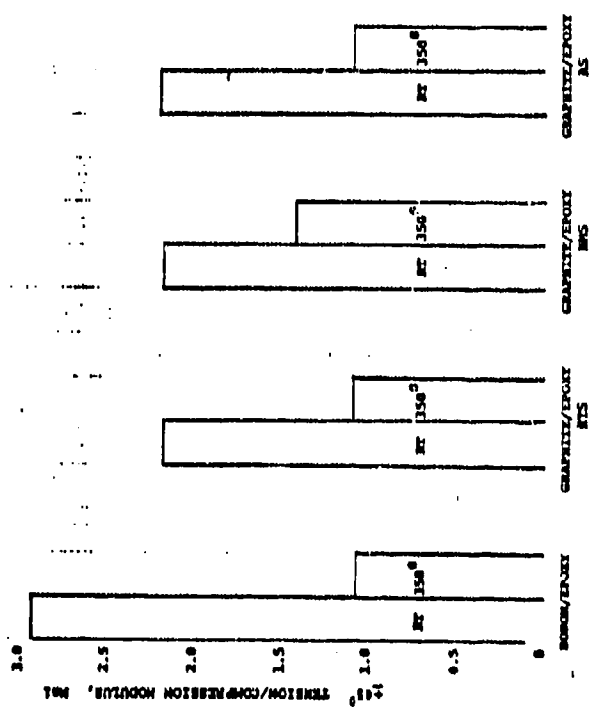


Figure 3.22 Diagonal Tension/Compression Modulus for Various Single Laminate Composites at Room Temperature (RT) and 350°F(2-5)

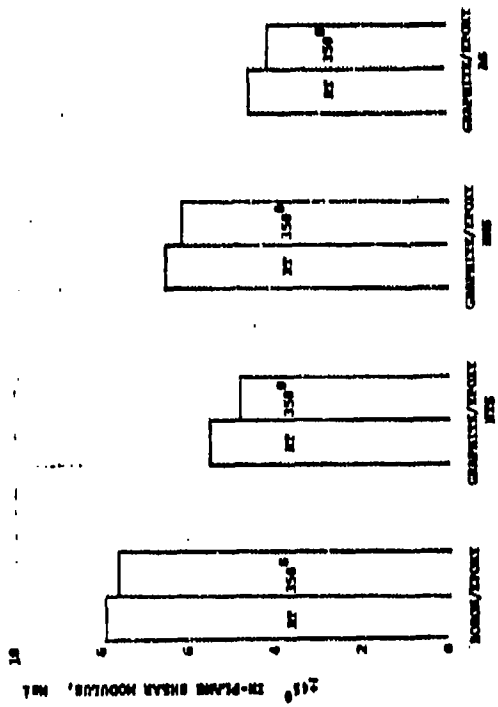


Figure 3.23 In-Plane Shear Modulus for Various Single Laminate Compositions At Room Temperature (RT) and 150°F (2-5)

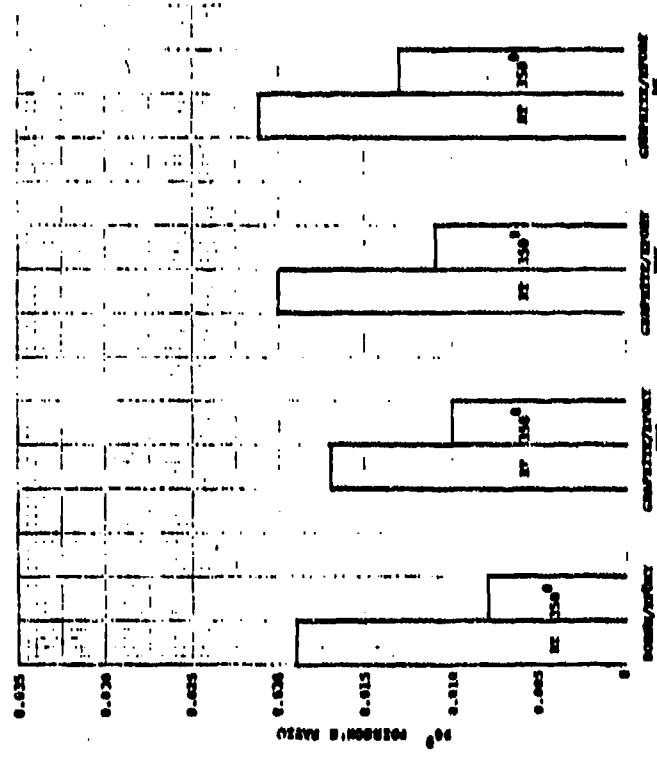


Figure 3.25 Transverse Poisson's Ratio for Various Single Laminate Compositions At Room Temperature (RT) and 150°F (2-5)

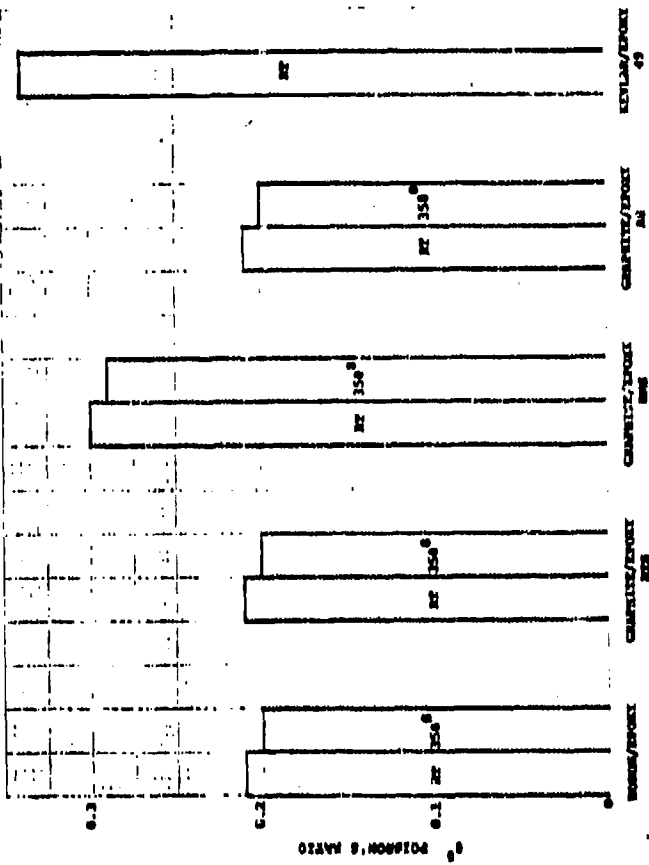


Figure 3.26 Longitudinal Poisson's Ratio for Various Single Laminate Compositions At Room Temperature (RT) and 150°F (2-5)

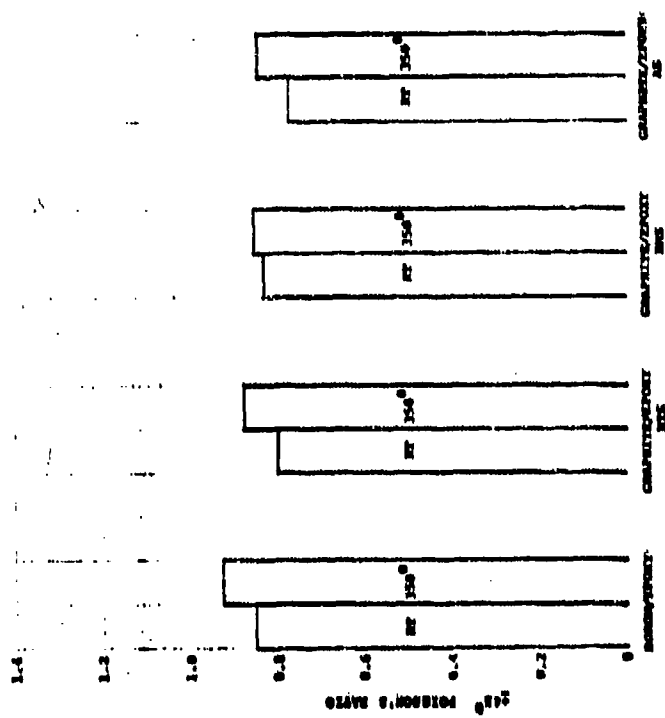


Figure 3.28 Diagonal Poisson's Ratio for Various Single Laminate Compositions At Room Temperature (RT) and 150°F (2-5)

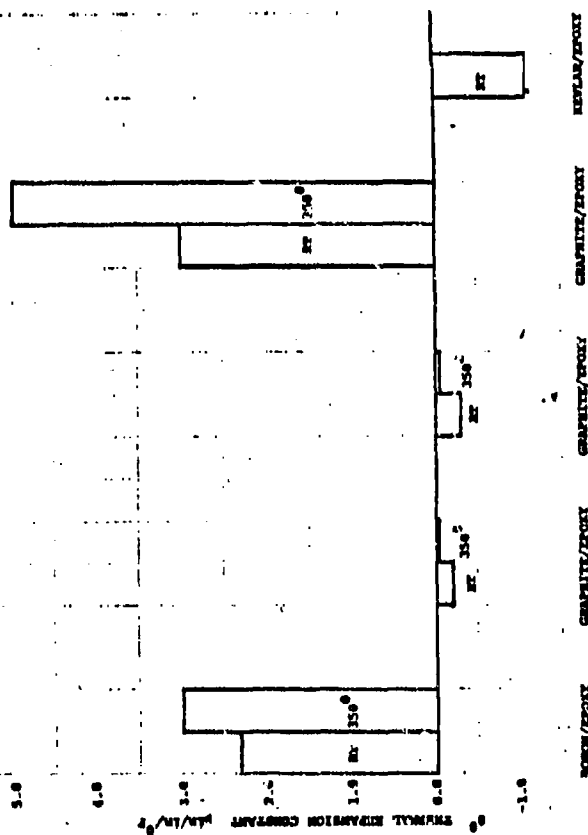


Figure 3.27 Longitudinal Thermal Expansion Constant For Various Single Laminate Composites At Room Temperature (RT) and 350°F (2-3)

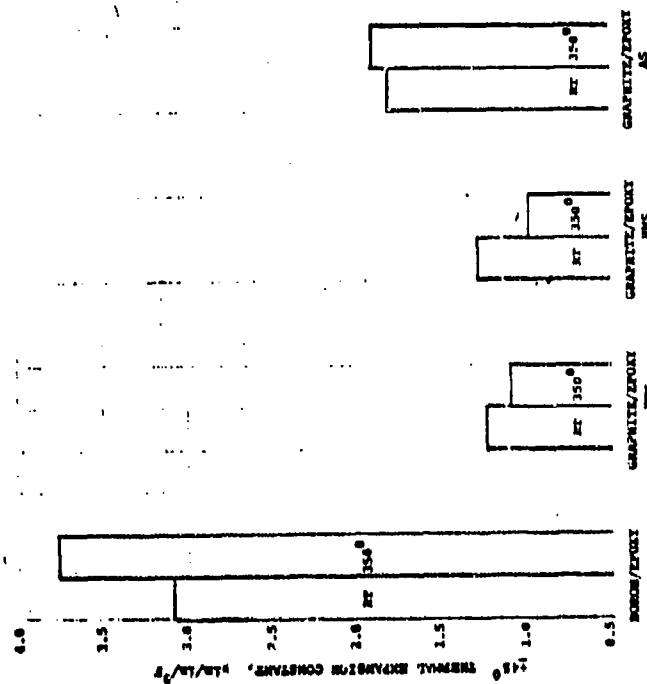


Figure 3.29 Diagonal Thermal Expansion Constant For Various Single Laminate Composites At Room Temperature (RT) and 350°F (2-3)

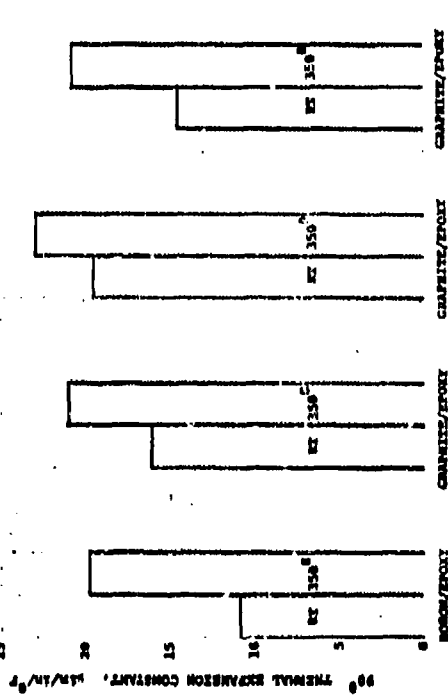


Figure 3.28 Transverse Thermal Expansion Constant For Various Single Laminate Composites At Room Temperature (RT) and 350°F (2-3)



Figure 3.30 Single Laminate Composite Densities At Room Temperature (RT) and 350°F (2-3)

The most notable feature of the numerical data is its strong dependence on the composite orientation. Longitudinal properties are essentially those of the fibers as is shown by the large shear strengths and elastic moduli. Transverse properties are much weaker and reflect the presence of the matrix material. Diagonal properties tend to fall between the transverse and longitudinal properties.

Both mechanical and physical properties tend to degrade somewhat with temperature. The amount of degradation varies with each property but, in general, boron/epoxy appears more temperature-sensitive than either graphite/epoxy or Kevlar/epoxy.

Figures 3.31 - 3.33 show typical tensile stress-strain curves for both graphite and boron composites. Longitudinal, transverse and diagonal stresses are considered at room temperature and 350°F. The transverse and diagonal stress-strain curves are considerably more temperature sensitive than the longitudinal curve.

Figure 3.34 illustrates a bending stress-strain curve for Kevlar, graphite and aluminum. Unidirectional Kevlar 49/epoxy has a linear stress-strain curve when tested in tension to failure. When tested in compression, Kevlar 49 is elastic in low strain, but plastic at high strain⁽⁴⁾ (see Figures 3.11 and 3.14). This unique compressive behavior of Kevlar 49 makes it resemble a metal in its ductility which is illustrated in Figure 3.34

3.3.4 Crossplied Laminate Composite Properties

Crossplied laminate design strengths, elastic properties and physical constants are presented for the boron/epoxy and graphite/epoxy systems. Crossplied laminate property data are difficult to treat in general because of the many structures that are possible. The crossplied laminate systems presented in this section are limited to (0/+60) orientations and the general orientation family ($0_i/+45_j/90_k$) for graphite and boron/epoxy, where the i, j, and k coefficients can be adjusted to any proportion (including none) of the three lamina angles. By proper adjustment, virtually any design requirement can be met for preliminary estimates of crossplied laminate properties.

The properties for the ($0_i/+45_j/90_k$) are given in Figures 3.35 to 3.61 in the form of carpet plots with the percent of 0° and +45° plies treated as independent variables. The remaining percentage of plies are 90° by definition. The carpet plots were generated by computer using standard structural analysis algorithms.⁽³⁾ The unidirectional lamina data (such as given in Figures 3.11 - 3.30) are a basic input for the analysis. The curves given in Figures 3.35 - 3.61 should be construed as a guide to general crossplied composite behavior and not as a set of design curves.

Figures 3.62 - 3.71 present measured mechanical and physical property data for the (0/60) laminate family for boron/epoxy and graphite/epoxy at room temperature (RT) and 350°F.⁽³⁾ The properties are measured with stresses longitudinal (0° with respect to fiber axis) and transverse (90° with respect to fiber axis) to the fibers. Where no direction to the fiber is given, the property is isotropic. As in the case of a single laminate, the properties of the (0/60) crossplied lamina degrade somewhat with temperature, especially in the case of boron/epoxy.

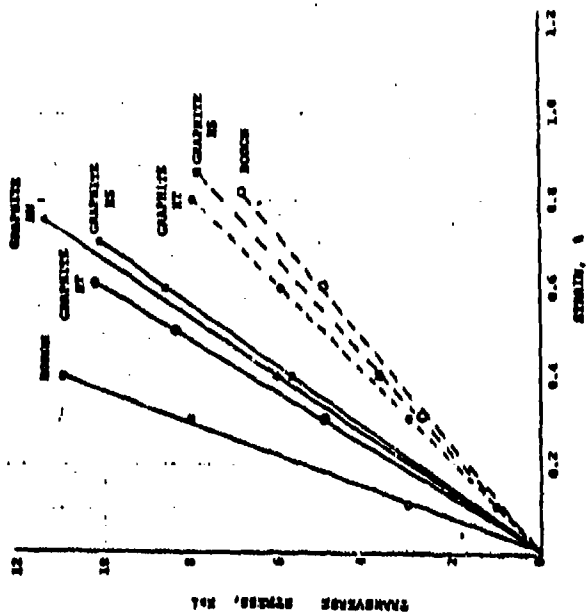


Figure 3.32 Transverse Tension Stress-Strain Curve for Various Single Laminate Composites at Room Temperature (solid lines) and 350°F (dotted lines) (3)

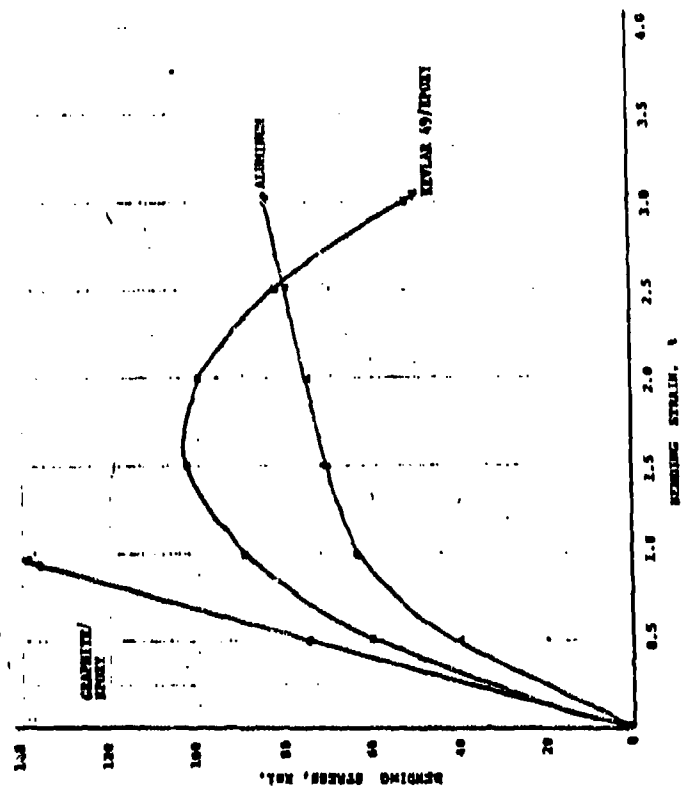


Figure 3.34 Bending Stress-Strain Curve for Kevlar 49/Epoxy Compared to Graphite/Epoxy and Aluminum (4)

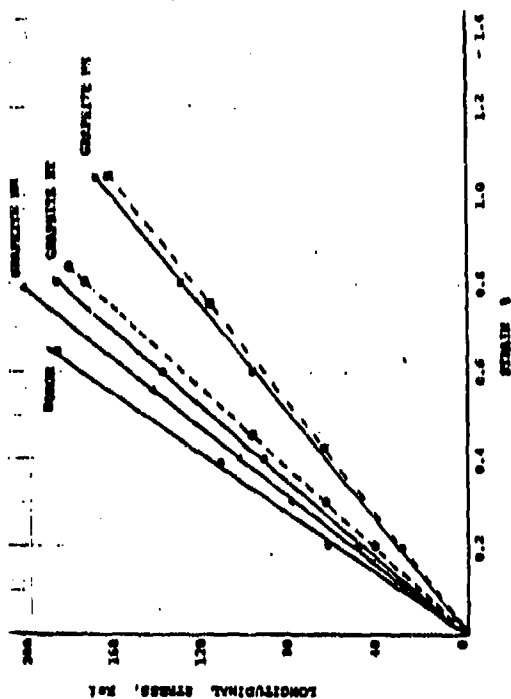


Figure 3.31 Longitudinal Tension Stress-Strain Curve for Various Single Laminate Composites at Room Temperature (solid lines) and 350°F (dotted lines) (3)

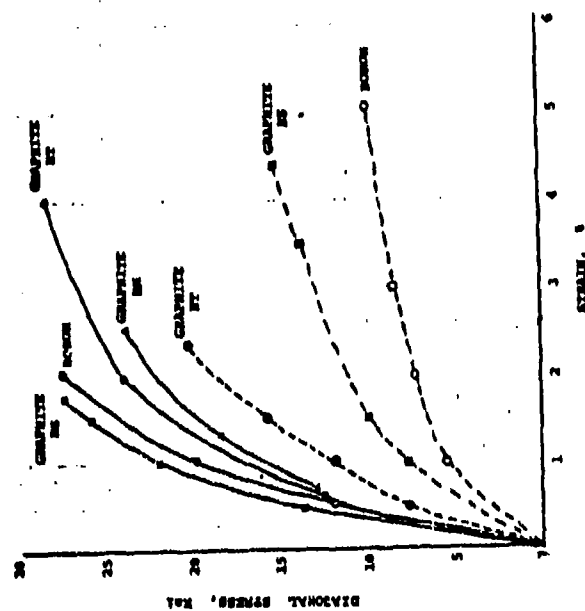


Figure 3.33 Diagonal Tension Stress-Strain Curves for Various Single Laminate Composites at Room Temperature (solid lines) and 350°F (dotted lines) (3)

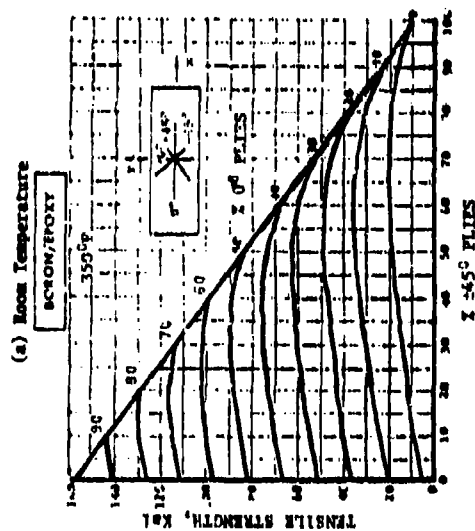
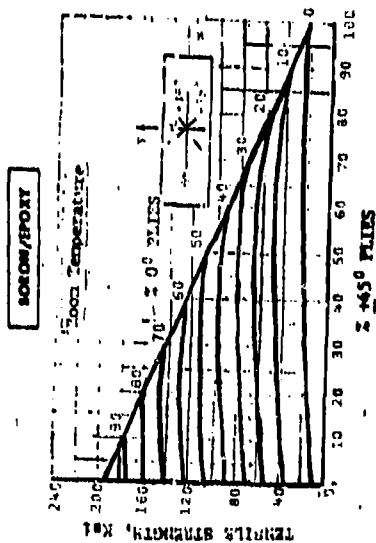


Figure 3.35 Boron/Epoxy Tensile Strength Curves For The $[0_2/45_1/90_1]$ Laminate Family(3)

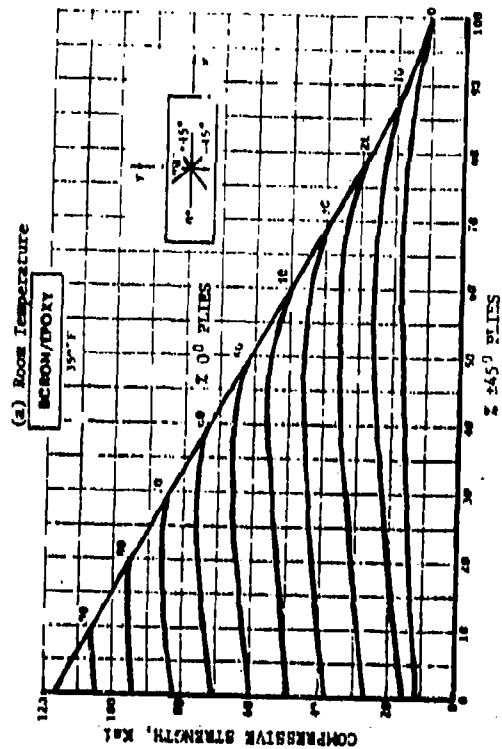
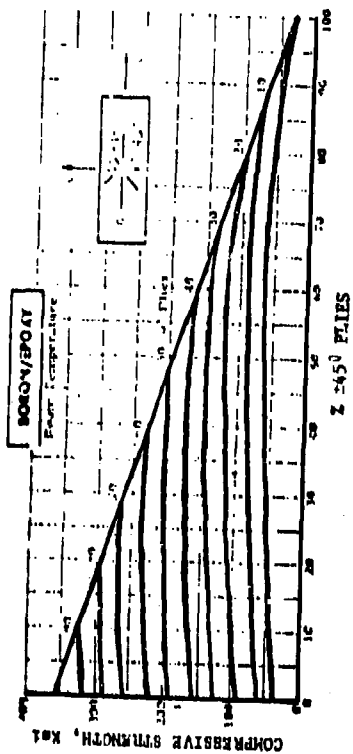
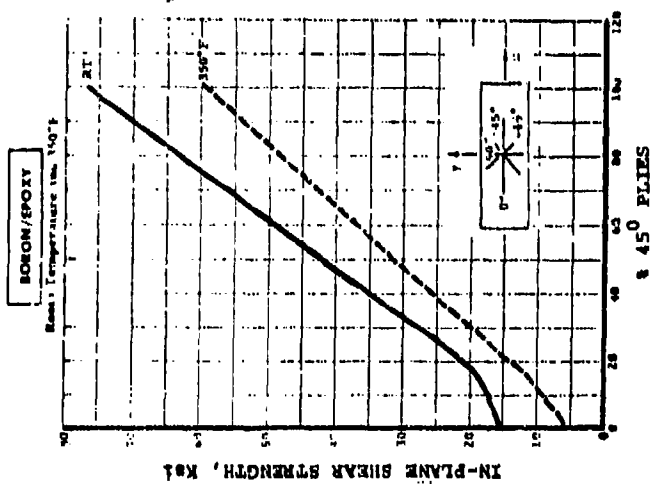
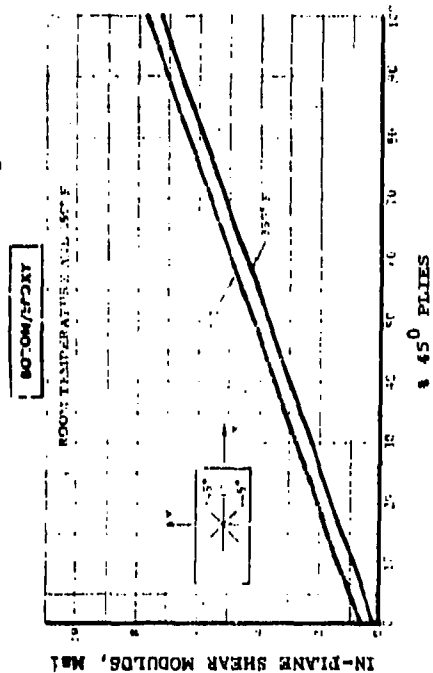


Figure 3.36 Boron/Epoxy Compressive Strength Curves For the $[0_2/45_1/90_1]$ Laminate Family(3)

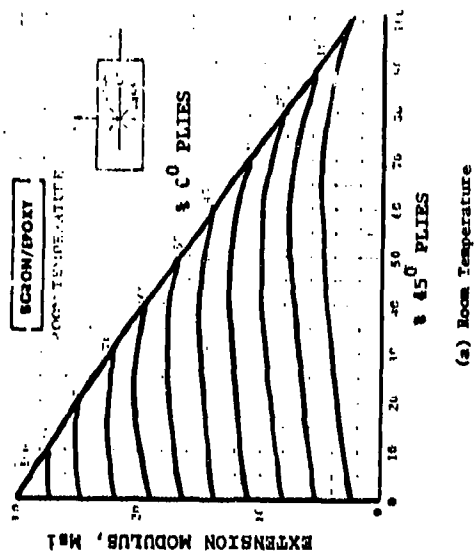


(a) In-Plane Shear Strength

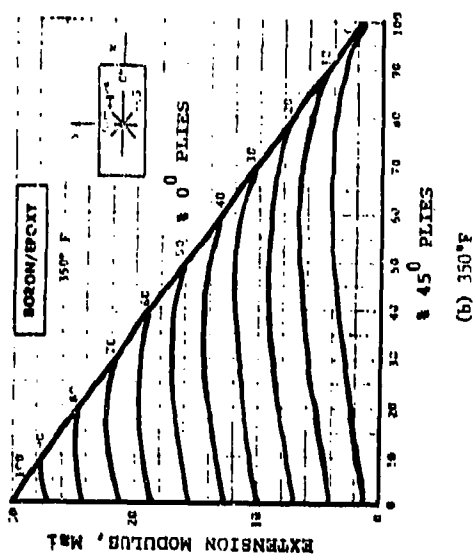


(b) In-Plane Shear Modulus

Figure 3.37 Boron/Epoxy In-Plane Shear Strength and Modulus Curves $[0_1/45_1/90_1]$ Laminate Family (3)

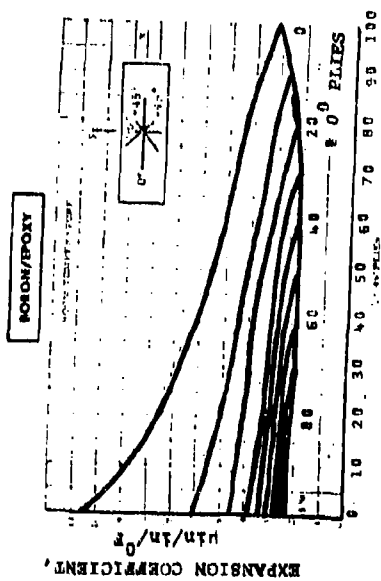


(a) Room Temperature

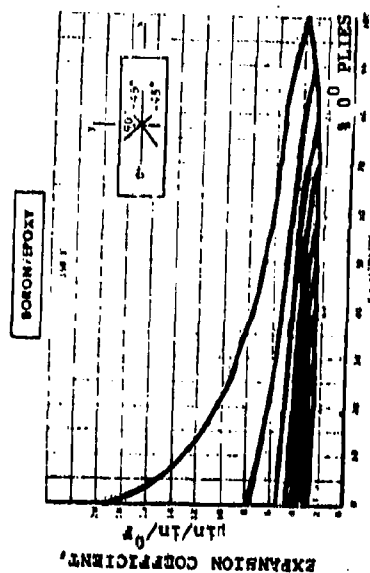


(b) 350°F

Figure 3.38 Boron/Epoxy Extensional Modulus Curves For The $[0_1/45_1/90_1]$ Laminate Family (3)

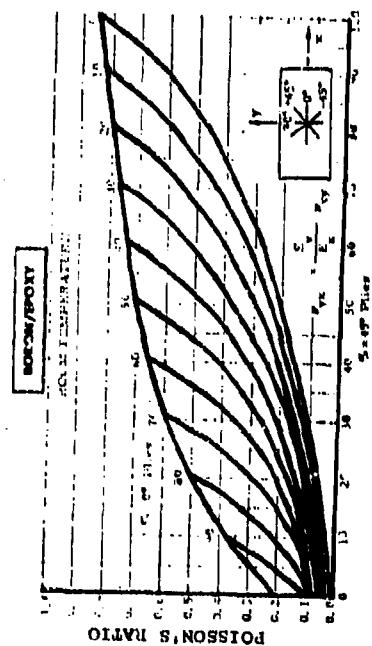


(a) Room Temperature

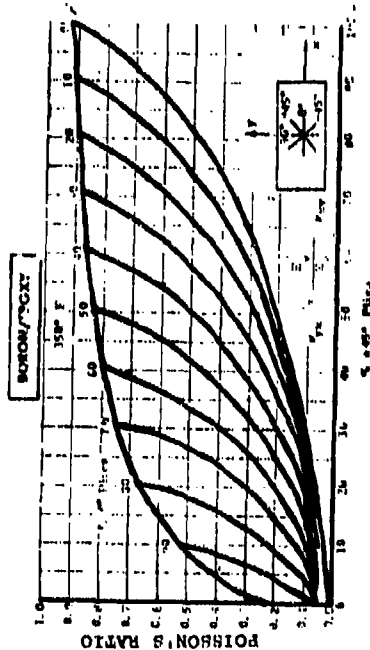


(b) 350°F

Figure 3.40 Boron/Epoxy Thermal Expansion Coefficient Curves For the $[0, \pm 45, 90]_k$ Laminate Family (3)

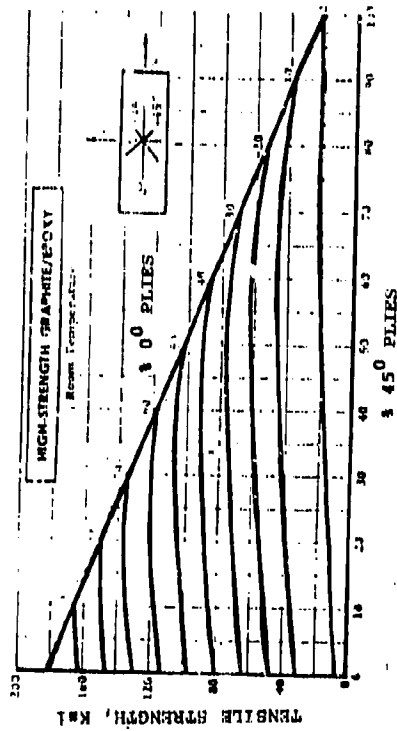


(a) Room Temperature

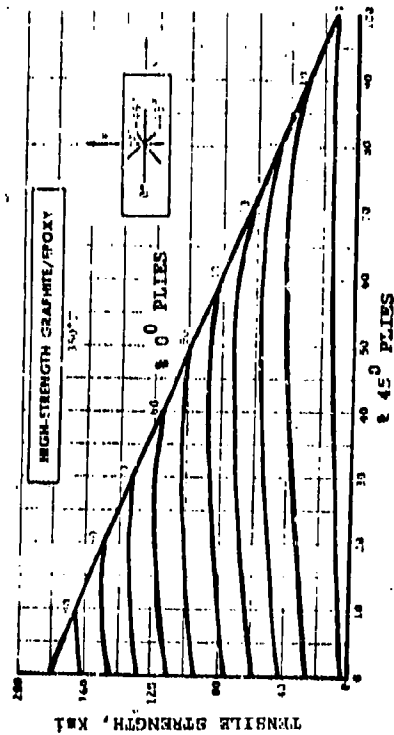


(b) 350°F

Figure 3.39 Boron/Epoxy Poisson's Ratio Curves For The $[0, \pm 45, 90]_k$ Laminate Family (3)

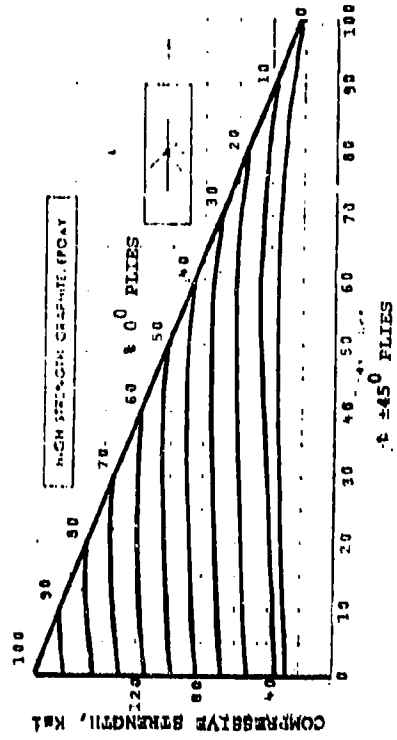


(a) Room Temperature

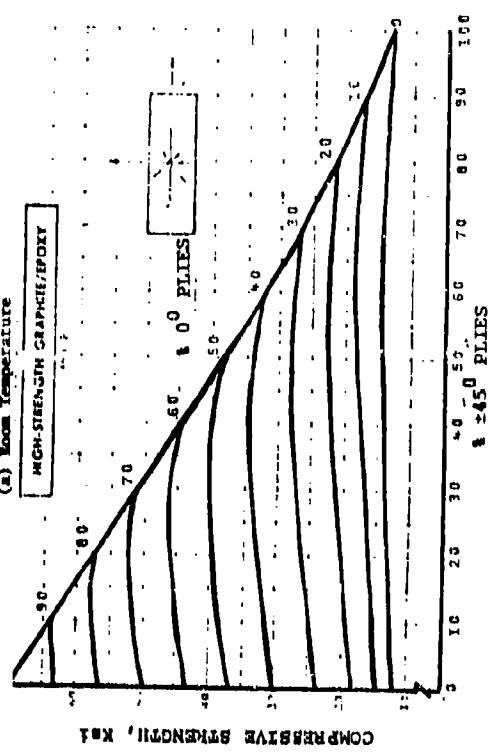


(b) 350°F

Figure 3.41 High-Strength Graphite/Epoxy Tensile Strength Curves For the $[0_1/45_1/90_2]$ Laminate Family (3)



(a) Room Temperature



(b) 350°F

Figure 3.42 High-Strength Graphite/Epoxy Compressive Strength Curves For the $[0_1/45_1/90_2]$ Laminate Family (3)

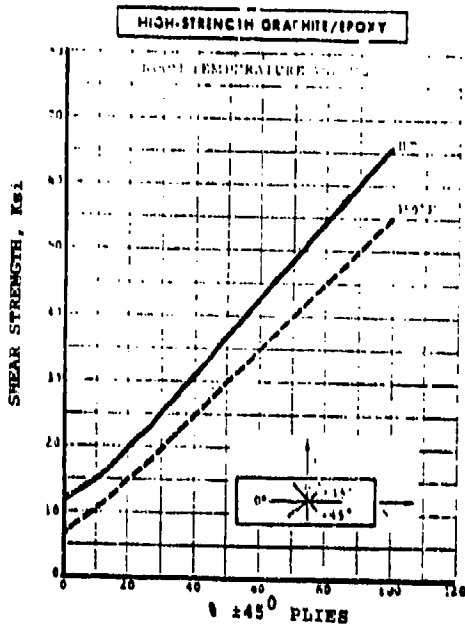


Figure 3.43 Shear Strength Curves for the High-Strength Graphite/Epoxy $[0_1/+45_1/90_1]$ Laminate Family at Room Temperature (RT) and 350°F (3)

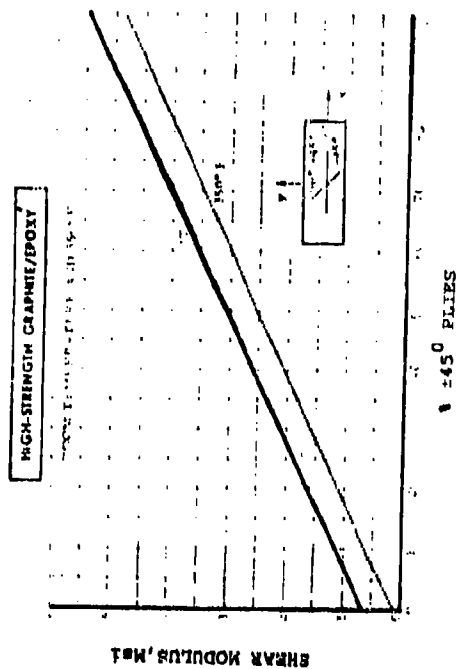
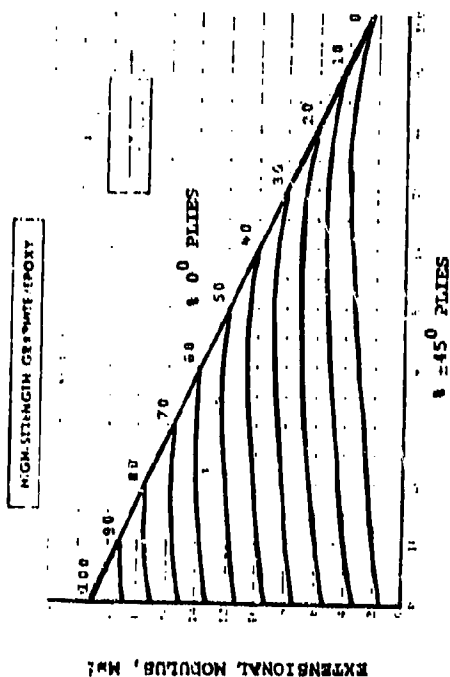
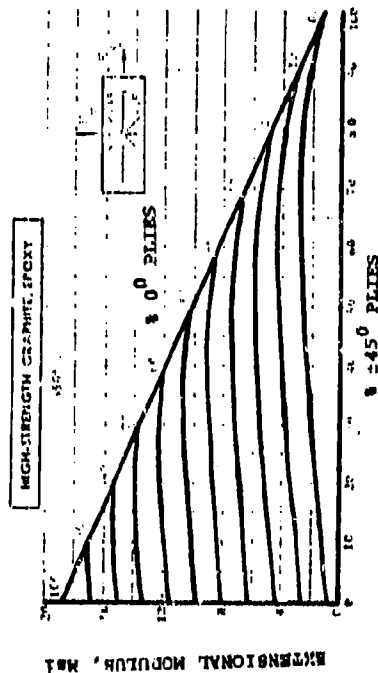


Figure 3.65 Shear Modulus Curves for the High-Strength Graphite/Epoxy $[0_1/+45_1/90_1]$ Laminate Family at Room Temperature (RT) and 350°F (3)

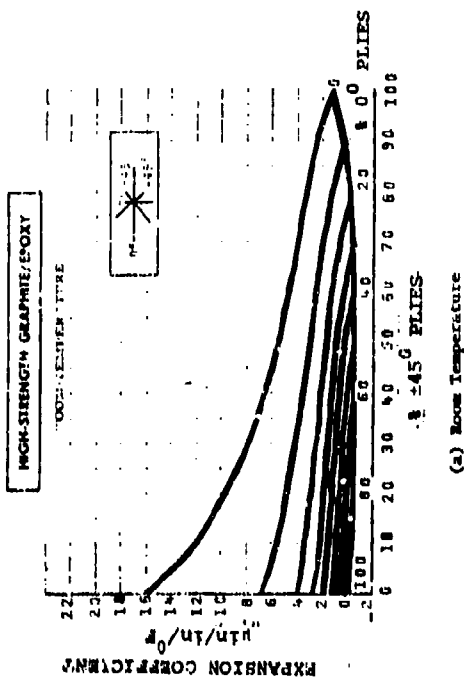


(a) Room Temperature

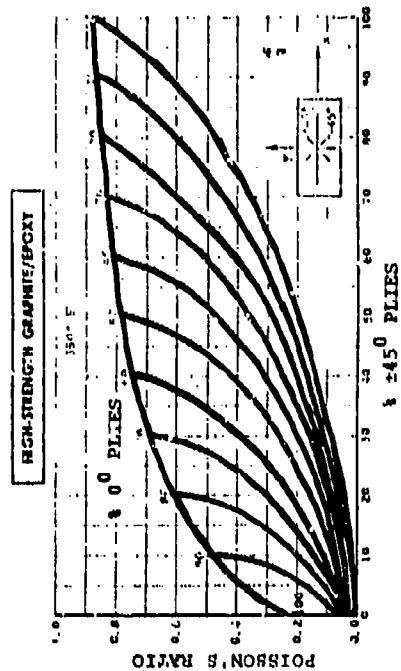


(b) 350°F

Figure 3.44 Extensional Modulus Curves for the High-Strength Graphite/Epoxy $[0_1/+45_1/90_1]$ Laminate Family (3)

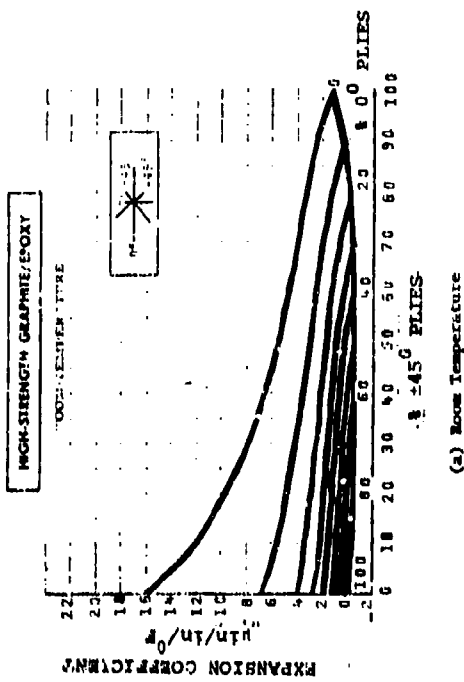


(a) Room Temperature

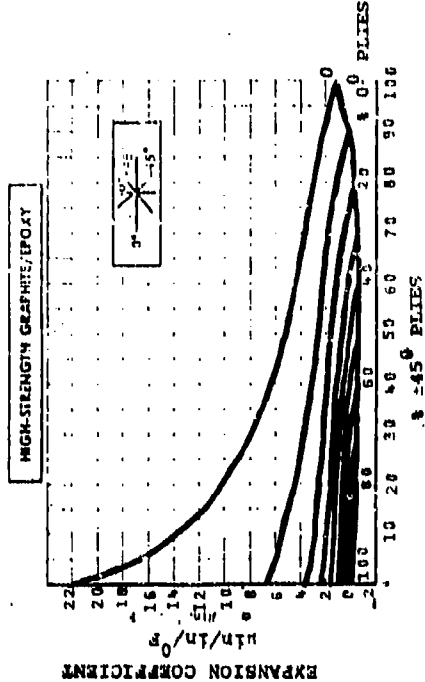


(b) 350°F

Figure 3.46 Poisson's Ratio Curves For The High-Strength Graphite/Epoxy $[0, \pm 45, 90]_k$ Laminate Family (3)

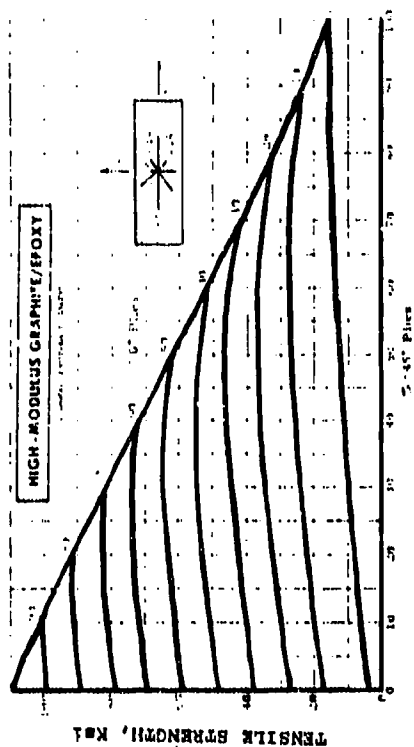


(a) Room Temperature

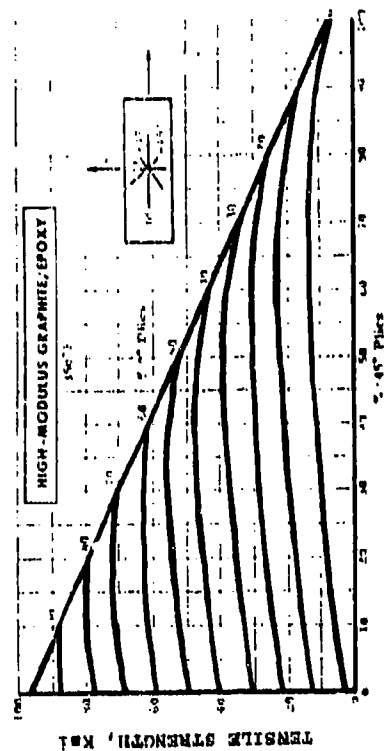


(b) 350°F

Figure 3.47 Thermal Expansion Coefficient Curves For The High-Strength Graphite/Epoxy $[0, \pm 45, 90]_k$ Laminate Family (3)

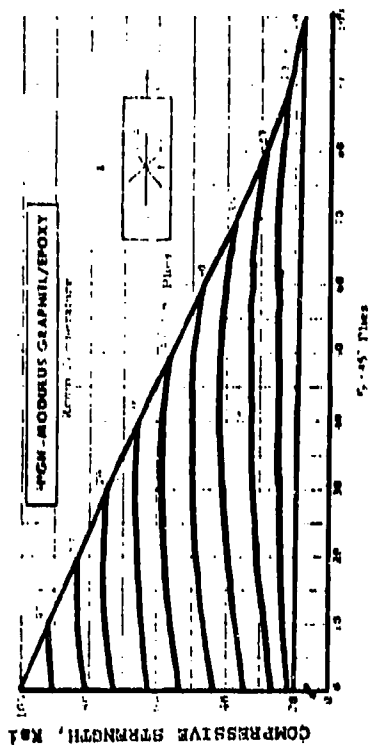


(a) Room Temperature

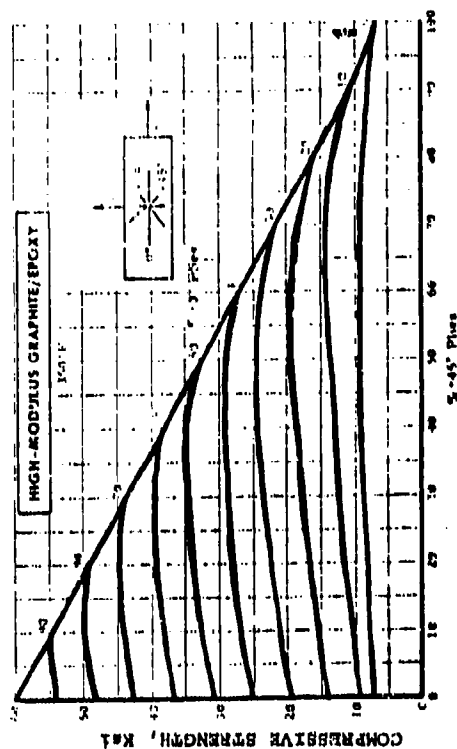


(b) 350°F

Figure 3.48 Tensile Strength Curves For The High-Modulus Graphite/Epoxy $[0_2/+45_2/90_2]$ Laminate Family(3)



(a) Room Temperature



(b) 350°F

Figure 3.49 Compressive Strength Curves For The High-Modulus Graphite/Epoxy $[0_2/+45_2/90_2]$ Laminate Family(3)

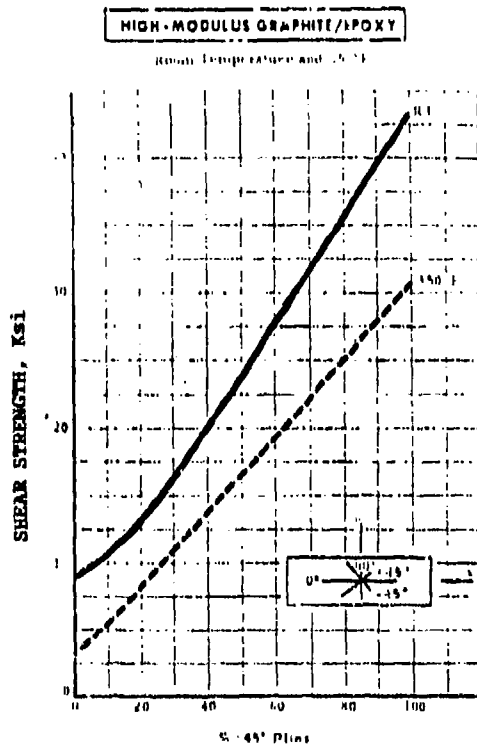


Figure 3.50 Shear Strength Curves For The High-Modulus Graphite/Epoxy $[0_1/\pm 45_1/90_k]$ Laminate Family At Room Temperature (RT) and 350°F(3)

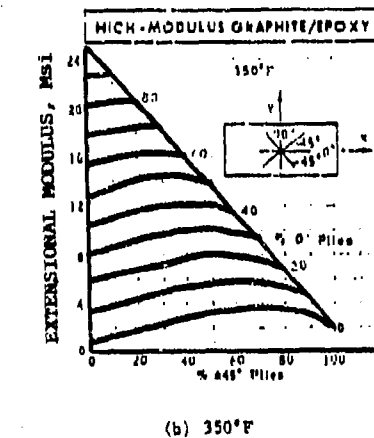
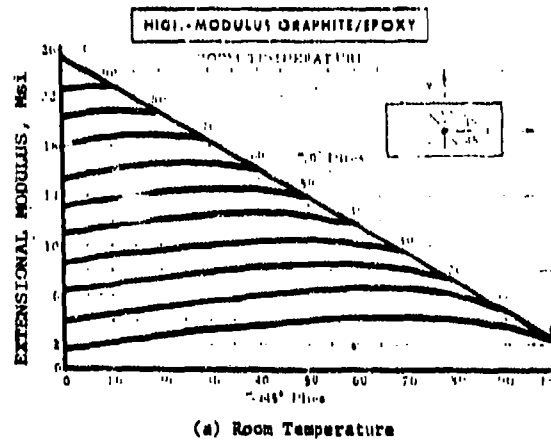


Figure 3.51 Extensional Modulus Curves For The High-Modulus Graphite/Epoxy $[0_1/\pm 45_1/90_k]$ Laminate Family (3)

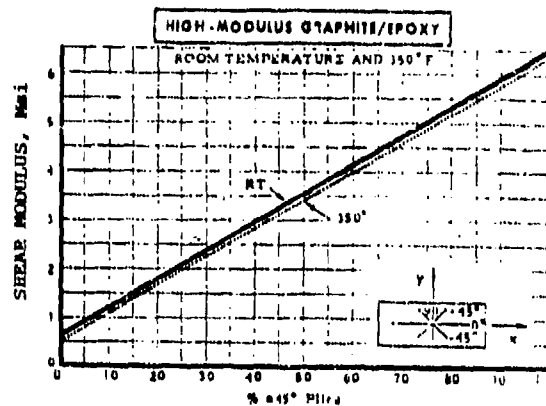
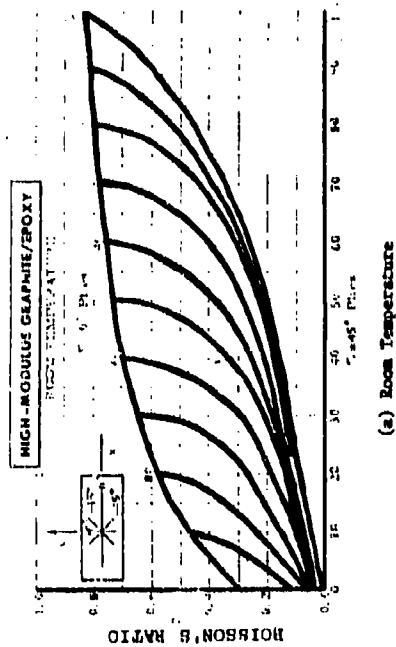
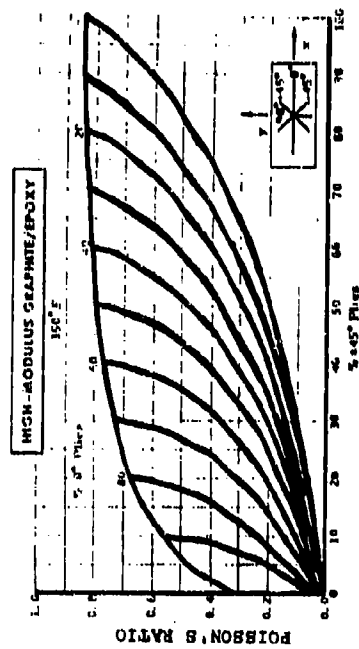


Figure 3.52 Shear Modulus Curves For The High-Modulus Graphite/Epoxy $[0_1/\pm 45_1/90_k]$ Laminate Family At Room Temperature (RT) and 350°F(3)

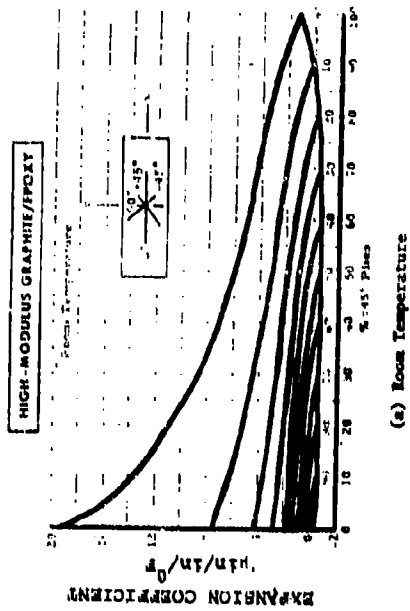


(a) Room Temperature



(b) 350°F

Figure 3.53 Poisson's Ratio Curves For The High-Modulus Graphite/Epoxy [0₁/45₁/90₂] Laminate Family (3)



(a) Room Temperature

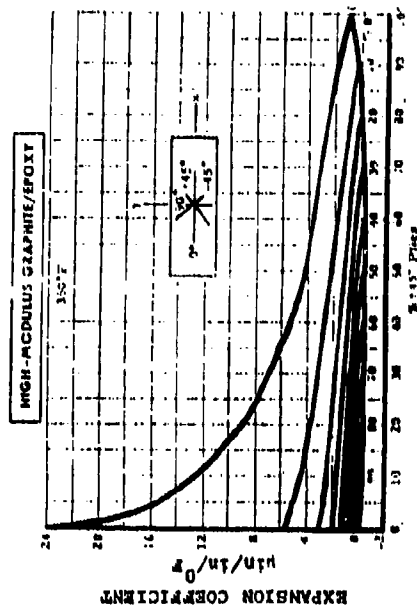


Figure 3.54 Thermal Expansion Coefficient Curves For The High-Modulus Graphite/Epoxy [0₁/45₁/90₂] Laminate Family (3)

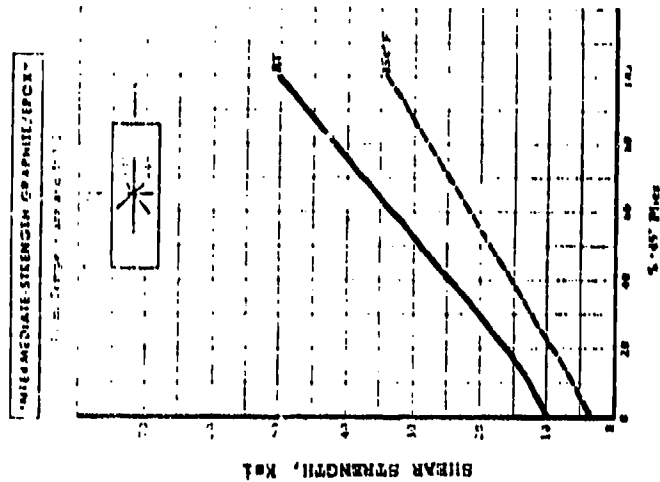


Figure 3.57 Shear Strength Curves For The Intermediate-Strength Graphite/Epoxy $[0_1/+45_1/90_2]$ Laminate Family

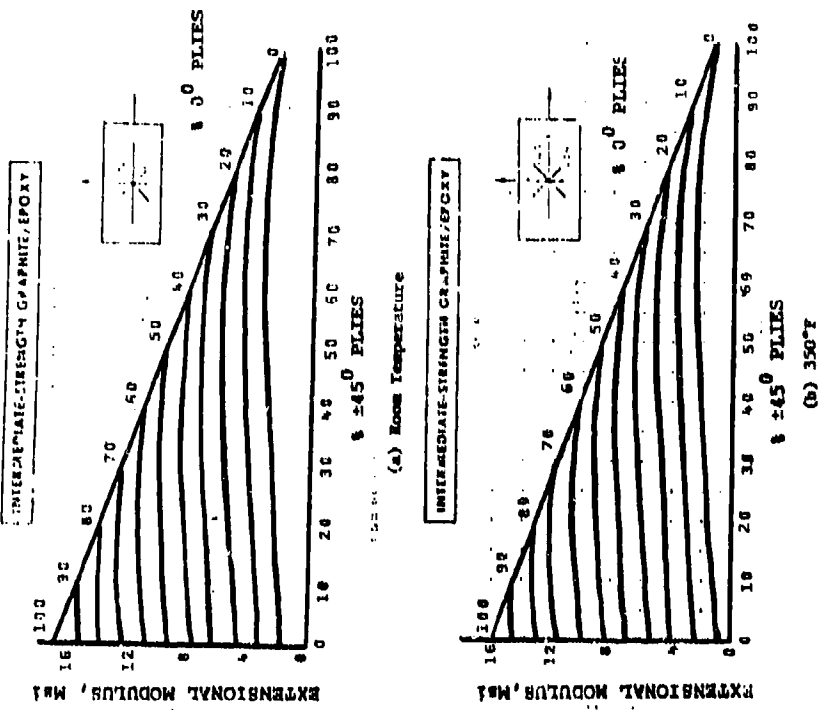


Figure 3.58 Extensional Modulus Curves For The Intermediate Strength Graphite/Epoxy $[0_1/+45_1/90_2]$ Laminate Family

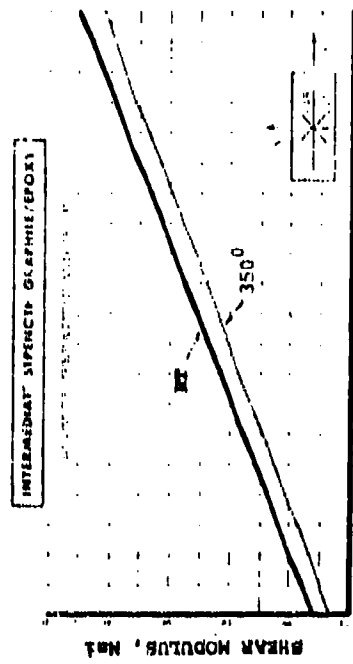


Figure 3.59 Shear Modulus Curves For The Graphite/Epoxy $[0_1/+45_1/90_2]$ Laminate Family at Room Temperature (RT) and 350°F

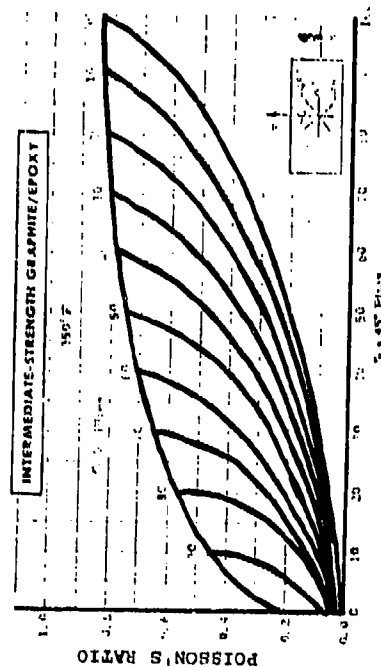
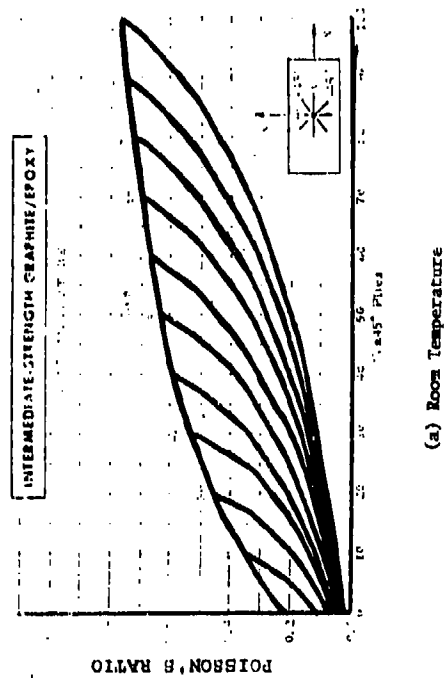


Figure 3.60 Poisson's Ratio Curve For The Intermediate-Strength Graphite/Epoxy $[0_2/45_1/90_k]$ Laminate Family (3)

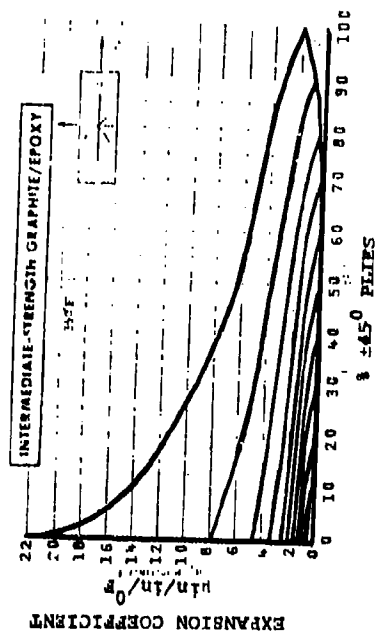
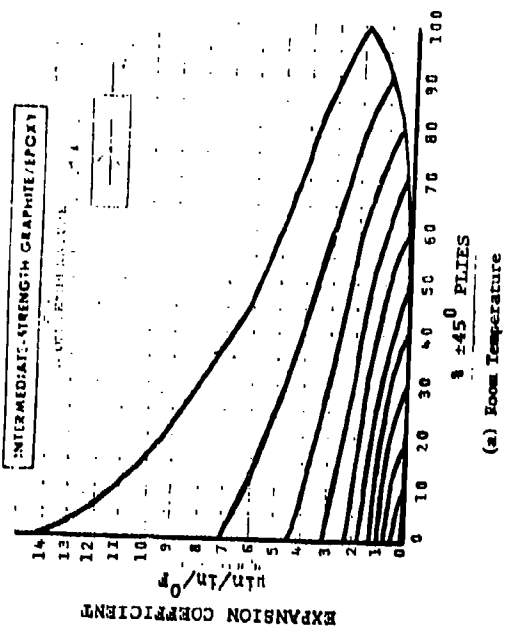


Figure 3.61 Thermal Expansion Coefficient Curves For The Intermediate-Strength Graphite/Epoxy $[0_2/45_1/90_k]$ Laminate Family (3)

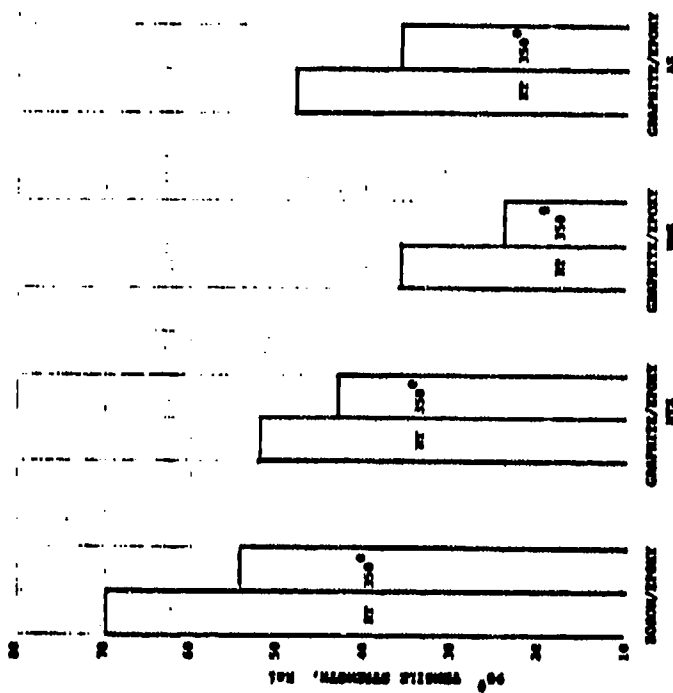


Figure 3.63 Transverse Tensile Strength For The [0/60] Bacon/Epoxy and Graphite/Epoxy Cured/Laminates At Room Temperature (RT) and 350°F(3)

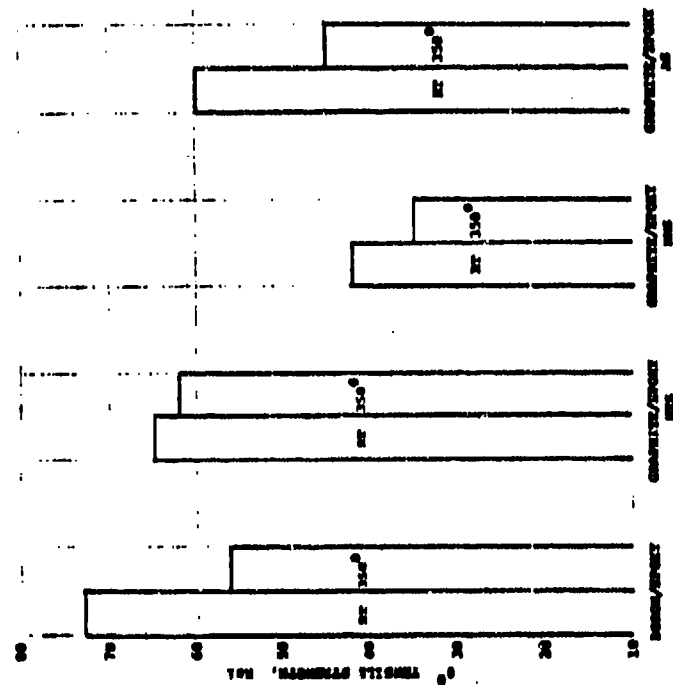
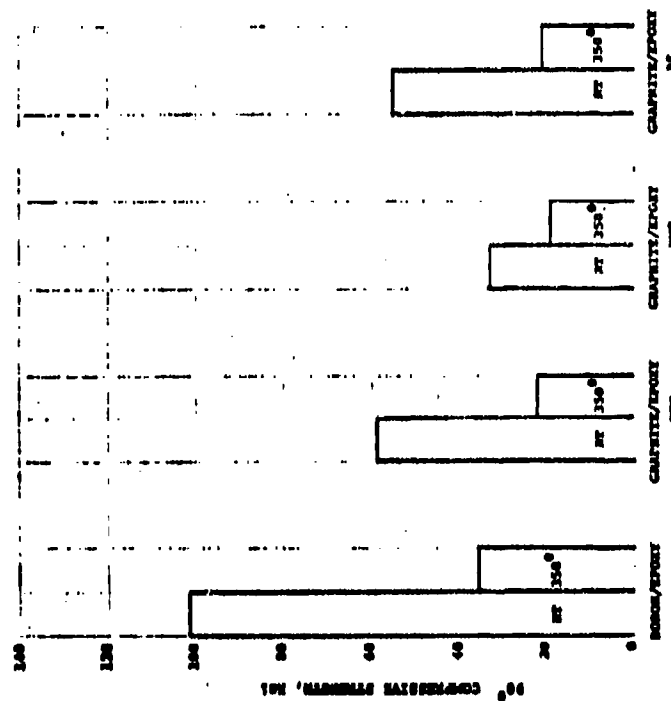
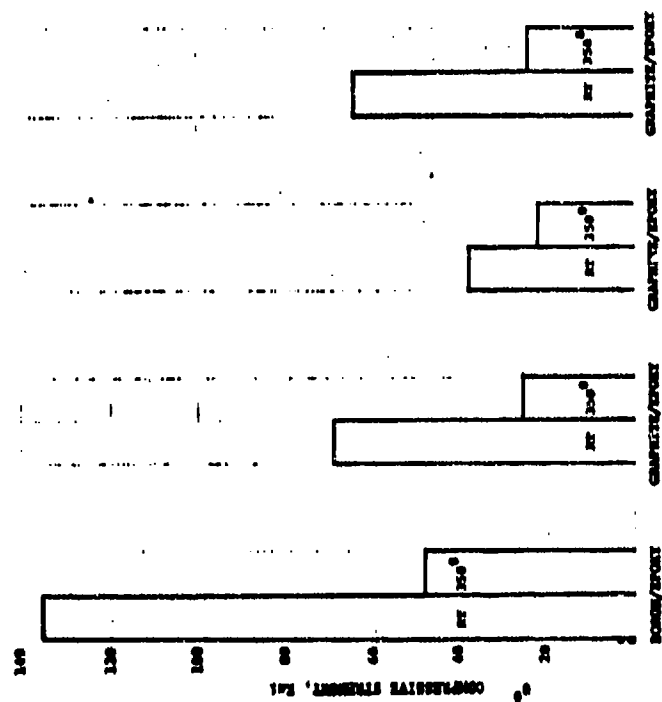


Figure 3.62 Longitudinal Tensile Strength For The [0/60] Bacon/Epoxy and Graphite/Epoxy Laminates At Room Temperature (RT) and 350°F(3)



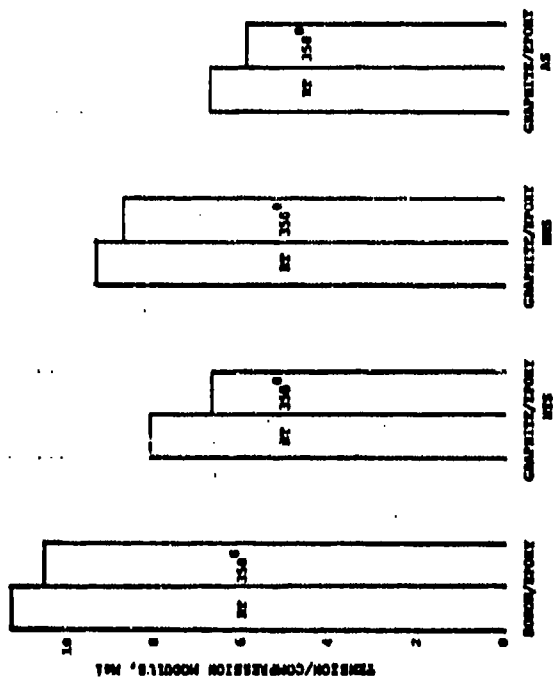


Figure 3.67

Tension/Compression Modulus For The [0/60] Bismal/Epoxy and Graphite/Epoxy Crossplied Laminates At Room Temperature (RT) and 350°F(3)

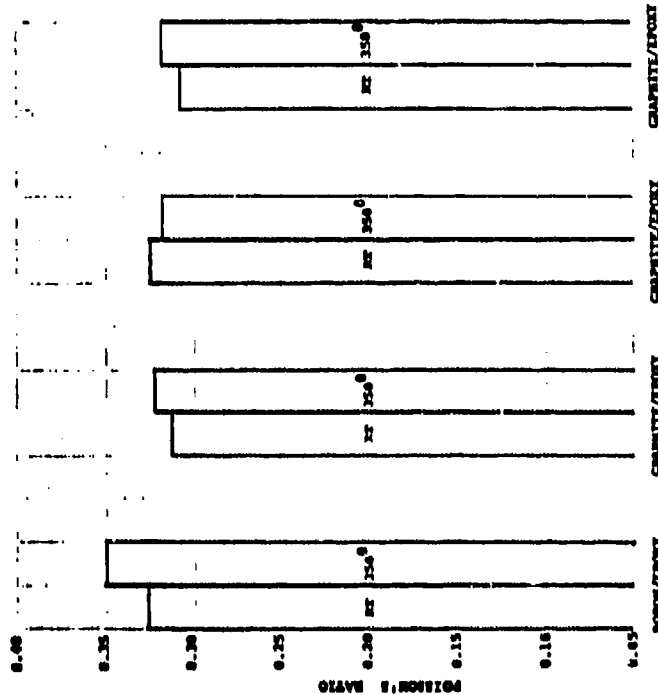


Figure 3.69 Poisson's Ratio For The [0/60] Bismal/Epoxy and Graphite/Epoxy Crossplied Laminates At Room Temperature (RT) and 350°F(3)

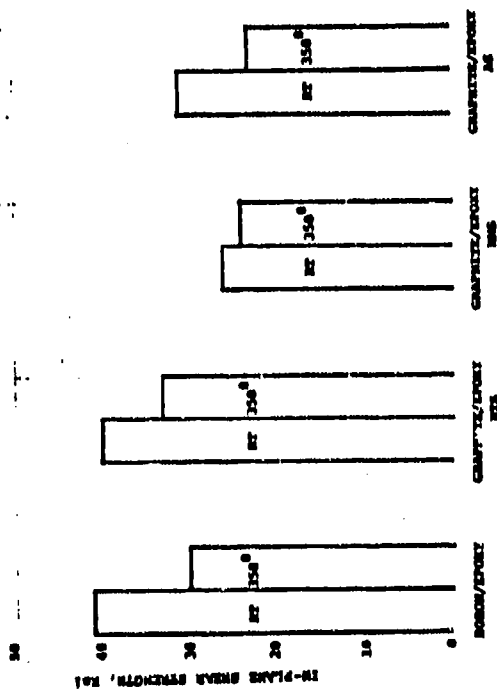


Figure 3.66

In-Plane Shear Strength For The [0/60] Bismal/Epoxy and Graphite/Epoxy Crossplied Laminates At Room Temperature (RT) and 350°F(3)

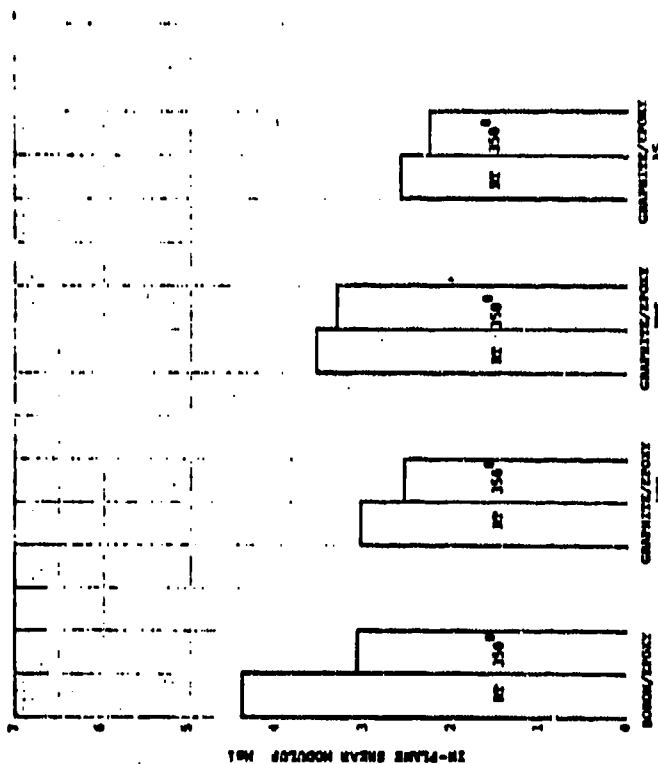


Figure 3.68 In-Plane Shear Modulus For The [0/60] Bismal/Epoxy and Graphite/Epoxy Crossplied Laminates At Room Temperature (RT) and 350°F(3)

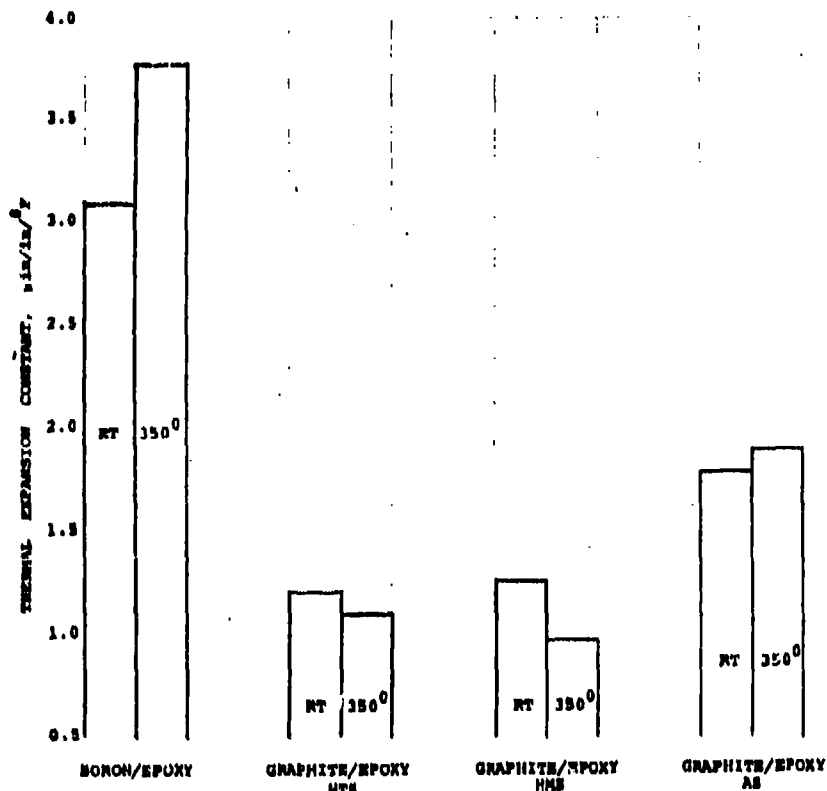


Figure 3.70 Thermal Expansion Constants For The [0/60] Boron/Epoxy and Graphite/Epoxy Crossplied Laminates At Room Temperature (RT) and 350°F(3)

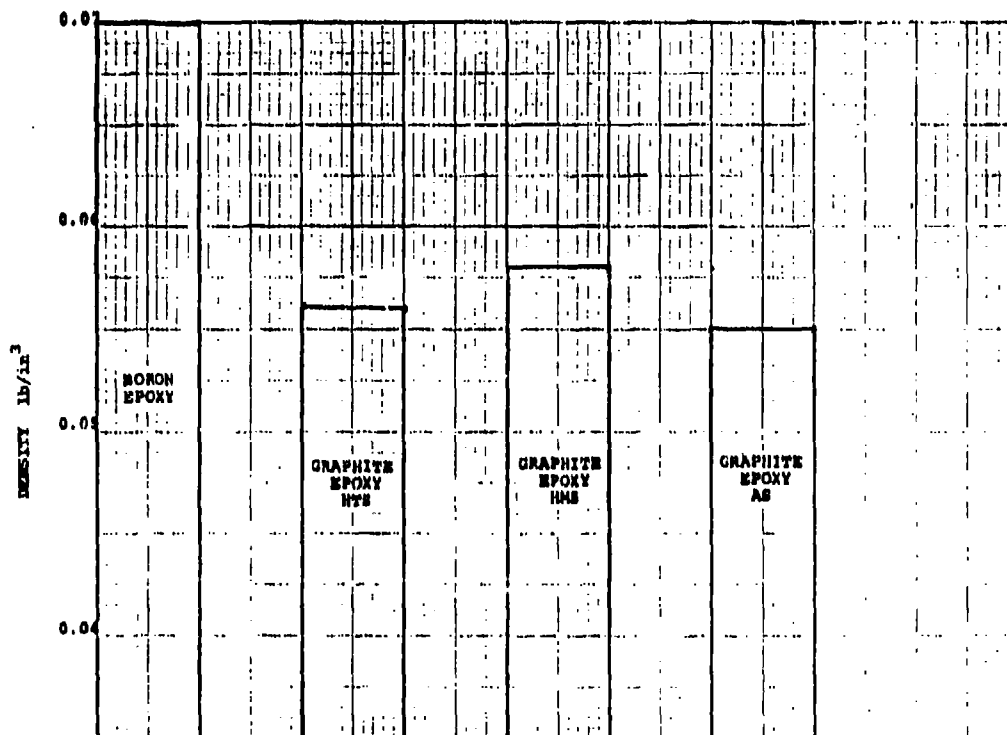


Figure 3.71 Density For [2/60] Boron/Epoxy and Graphite/Epoxy Crossplied Laminates (3)

3.3.5 Hybrid Composite Properties

Hybrid composite structures consist of a combination of two or more different composite fiber types in a matrix material. Since a myriad of hybrid structures is possible, three common structures (boron: graphite/epoxy, S-glass: graphite/epoxy and Kevlar: graphite/epoxy), will be considered.

The boron: graphite/epoxy system is $(0_B/+45_{GE}/90_{GE})_8$ with key properties listed in Table 3.3. Values are given for longitudinal (0°) and transverse (90°) orientations with respect to the laminate and for room temperature and 350°F .

The S-glass: graphite/epoxy and Kevlar: graphite/epoxy hybrid systems have been recently evaluated by Boeing as possible approaches to low cost composite structures.⁽⁶⁾ The basic idea is to place low-cost fibers, such as S-glass or Kevlar, in secondary load directions and place high cost fibers, such as boron or graphite, in the primary load direction. Cost savings for the hybrid laminate over regular laminates range from 10% to 40%.

The S-glass: graphite/epoxy system is (S-glass/T-300 graphite/S-glass) and the measured mechanical properties are given in Table 3.4 for several test orientations and temperatures. The Kevlar: graphite/epoxy hybrid system has the configuration (T-300 graphite/Kevlar-49/T-300 graphite). The mechanical properties are given in Table 3.5 for several orientations and temperatures.⁽⁶⁾

Boeing⁽⁶⁾ has generated a set of design curves in carpet plot format for use in constructing hybrid composites composed of S-glass: graphite/epoxy and Kevlar: graphite/epoxy. The curves for the S-glass: graphite/epoxy hybrid are given in Figures 3.72 - 3.76 while those for Kevlar: graphite/epoxy are given in Figures 3.77 - 3.81.

3.4 Environmental Effects on Composite Materials

The information in this section is a summary of data available on the various environmental effects on the mechanical properties of graphite/epoxy, boron/epoxy and Kevlar/epoxy composite materials. All data is presented in Table 3.6 and the impact of each environmental effect is measured as a percent degradation of the unperturbed properties. The results should be regarded as general trends applicable to a whole class of materials.

3.5 Composite Fatigue

A limited set of fatigue data is presented for boron/epoxy, graphite/epoxy and Kevlar/epoxy in the form of stress-failure curves under constant amplitude cyclic loading conditions. The data are meant to give a general feel for the fatigue behavior of composites and not to be used in detailed design curves. The data is displayed in Figures 3.82 - 3.85. In general, the unidirectional laminates give the best fatigue results with a general lessening of values for crossplied laminates. Fatigue characteristics also tend to degrade somewhat with temperature as is shown for boron/epoxy in Figures 3.82 - 3.85.

Table 3.3 Mechanical Properties For The Boron:graphite/epoxy Hybrid Laminate System [0/+45/90_{GE}]

PROPERTY	ORIENTATION	PROPERTY VALUE	
		ROOM TEMPERATURE	350°
TENSILE STRENGTH, ksi	0°	54	40
	90°	54	40
COMPRESSIVE STRENGTH, ksi	0°	177	96
	90°	38	22
IN-PLANE SHEAR STRENGTH, ksi	0°	20	27
TENSION MODULUS, msi	0°	11.5	10.5
	90°	6	5
COMPRESSION MODULUS, msi	0°	11.5	10.5
	90°	6	5
THERMAL EXPANSION CONSTANT min/in/°F	0°	-	2.5
	90°	-	3.0
DENSITY lb/in ³	-	0.061	0.061

Table 3.4 Mechanical Properties of The [S-glass/T-300 graphite/S-glass] Hybrid System⁽⁶⁾

(S-GL/T300/S-GL)

PROPERTY	TEST ORIENTATION	AVERAGE PROPERTY AT:			
		-65F	75F	250F	350F
TENSION STRENGTH, ksi	0°	159.4	166.2	160.6	135.1
	45°	28.0	33.7	34.7	28.8
	90°	25.5	25.3	28.5	27.4
TENSION MODULUS, 10 ⁶ , psi	0°	6.1	5.7	5.9	6.1
	45°	4.2	4.4	3.9	4.0
	90°	4.6	3.6	3.4	2.9
COMPRESSIVE STRENGTH, ksi	0°	102.2	101.0	58.4	43.8
	45°	66.2	63.8	56.2	43.1
	90°	51.3	51.3	41.2	33.8
COMPRESSIVE MODULUS, 10 ⁶ psi	0°	8.7	9.2	8.5	8.6
	45°	4.1	4.7	4.1	3.5
	90°	3.7	3.8	3.4	3.1
IN-PLANE SHEAR STRENGTH, ksi	0°	6.7	27.6	26.4	22.1
IN-PLANE SHEAR MODULUS, 10 ⁶ psi	0°	1.9	1.8	1.6	2.6
INTERLAMINAR SHEAR, ksi	0°	9.0	8.7	8.2	4.9

Table 3.3 Mechanical Properties of the [T-300 graphite/Kevlar 49/
T-300 graphite] Hybrid System For Several Test
Orientation and Temperatures⁽⁶⁾

(T300/K-49/T300)

PROPERTY	TEST ORIEN- TATION	AVERAGE PROPERTY AT:			
		-65F	75F	250F	350F
TENSION STRENGTH, ksi	0°	93.6	109.6	110.1	89.7
	45°	42.3	41.0	41.9	30.7
	90°	32.3	32.9	33.6	33.1
TENSION MODULUS, 10 ⁶ psi	0°	10.6	11.3	11.1	10.5
	45°	4.0	3.8	3.0	2.6
	90°	3.9	3.7	3.4	3.6
COMPRESSIVE STRENGTH, ksi	0°	91.8	112.5	113.7	102.7
	45°	41.4	37.3	23.1	14.8
	90°	40.1	53.5	44.3	20.9
COMPRESSIVE MODULUS, 10 ⁶ psi	0°	6.6	6.7	6.6	6.1
	45°	4.4	3.5	2.6	2.0
	90°	7.8	3.8	3.5	3.5
IN-PLANE SHEAR STRENGTH, ksi	0°	23.9	27.2	23.2	16.2
IN-PLANE SHEAR MODULUS, 10 ⁶ psi	0°	1.4	1.6	1.1	.9
INTERLAMINAR SHEAR, ksi	0°	9.3	8.7	4.8	3.2

Table 3.6 Data Summary of Environmental Effects on Composite Mechanical Properties (3,4)

COMPOSITE	BORON/EPOXY	GRAPHITE/EPOXY	KEVLAR/EPOXY
ENVIRONMENT			
Humidity	Ambient humidity has little effect at 95% relative humidity for 500 hours at 355°F, 50% reduction in interlaminar shear strength and 20% reduction in flexure strength	Ambient humidity has little effect at 95% relative humidity and 120°F for 33 days little change in flexure strength is shown. At 270°F and 35°F longitudinal flexural strength reduced by 60% and 70%. Transverse flexure strength and interlaminar shear strength were reduced 10% to 22%	
Salt Spray Exposure	The 350°F flexure strengths were reduced 20%. Interlaminar strengths unaffected. Stressed panels showed 25% decrease in 350°F flexure strength	A 12% reduction in room temperature compressional strength after 35 day exposure. Flexure strength (Long.) reduced 13% at 250°F and 53% at 350°F. Transverse flexure strength reduced by 34%. Interlaminar shear strength reduced by 14% at room temperature, 33% at 270°F and 40% at 350°F.	For 5% salt water solution, tensile strength reduced by 0.5%
Fresh Water Immersion	The 350°F flexure and interlaminar shear strengths reduced 30%-35% after 30 days immersion at room temperature	6% reduction in room temperature tensile and compressive strength after 30 day immersion	-
Ambient Room Temperature Aging	None up to 180 days at room temperature. Tests to 350°F showed losses in strength up to 50%	350°F strengths drop by up to 50%	-
Elevated Temperature Aging	None below 350°F and less than 100 hours exposure. Compressive strength reduced 13% for 300 hours at 400°F and 17% reduced for 200 hours at 375°F.	At 270°F A5 type graphite unaffected by 900 hours exposure. Transverse properties reduced by 18%	-
Fuel Immersion	The 350°F flexure and interlaminar shear strength reduced by 17% after 500 hours exposure at room temperature.	Immersion of M4 graphite in JP-4 for seven days gave little effect. M7 graphite gave 6% reduction in flexure strength at room temperature.	No change in tensile strength when immersed in gasoline
Chemical and Solvent Immersion		No effect upon immersion in hydraulic fluid. Reduction of 5%-6% after immersion in methanol	Strength reduced 50% by hydrofluoric acid and 40% by nitric acid. Lye reduces properties by 50%
Boiling Fresh Water Immersion		Room temperature flexural and interlaminar shear strengths reduced 8-32% after 24 hour boil. The 350°F properties reduced by 61%	Strength reduced by 2% after 100 hours boil.
Thermal Cycling	350°F flexural strength unaffected by 50-500 cycles from -67°F to 350°F. Compressive strength reduced by 47% for 200 cycles.	Room temperature and 270°F flexure properties unaffected by up to 500 cycles. Transverse properties reduced 22%	-
Thermal Pulse	About 30% reduction in tensile strength if preloaded in 50% or less of ultimate tensile strength	20% reduction in tensile and compression strengths	-
Radiation Exposure	Tensile strength reduced 1-2% upon radiation with neutron flux. Compression and interlaminar shear reduced 10-24%	No effect on properties from nuclear radiation	Fabric exposed to Florida sun 5 weeks had 40% reduction in strength. Kevlar rope in sun 6-24 months lost 10-12% of strength.

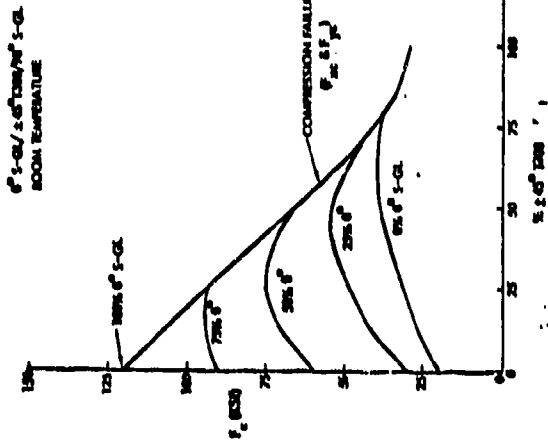


Figure 3.71 : LAMINATE ULTIMATE COMPRESSION STRENGTH
VERSUS PERCENT OF LAMINATE, 5-GL/1200/5-GL
FAMILY (6)

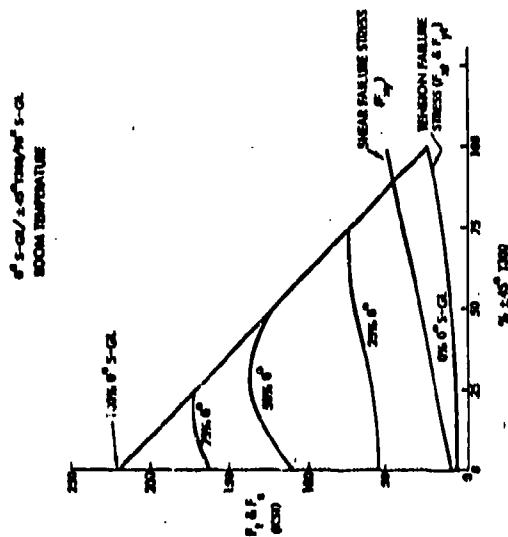


Figure 3.72 : LAMINATE ULTIMATE TENSILE AND SHEAR STRENGTH
VERSUS PERCENT OF LAMINATE, 5-GL/1200/5-GL
FAMILY (6)

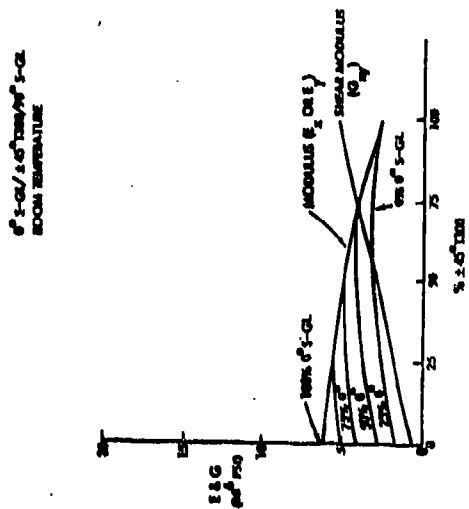


Figure 3.73 : LAMINATE E & G, VERSUS PERCENT
LAMINATE 5-GL/1200/5-GL F&G/2.05/1200 FAMILY (6)

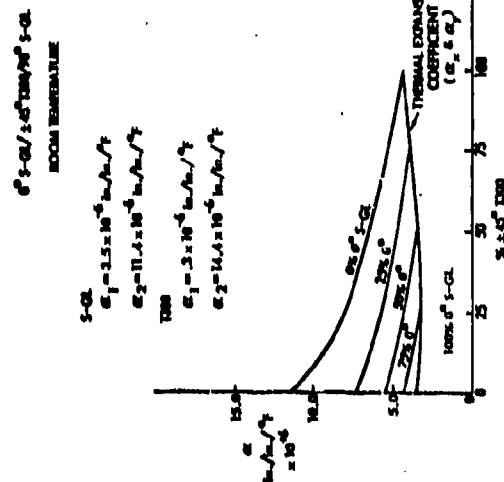


Figure 3.74 : LONGITUDINAL COEFFICIENT OF THERMAL EXPANSION
5-GL/1200/5-GL F&G/2.05/1200 FAMILY (6)

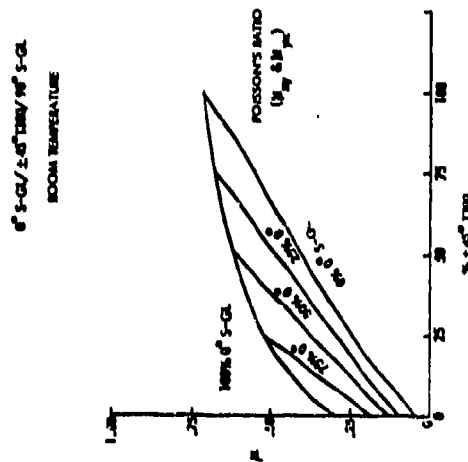


Figure 3.75 : POISSON'S RATIO, 5-GL/1200/5-GL
F&G/2.05/1200 FAMILY (6)

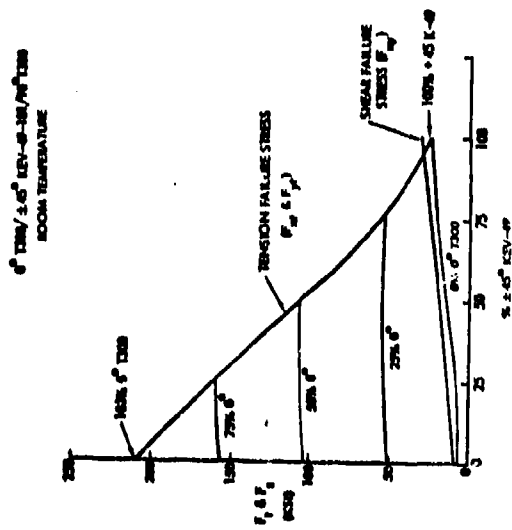


Figure 3.77 : LAMINATE ULTIMATE TENSILE AND SHEAR STRENGTH
VERSUS PERCENT OF LAMINATE, 1200/2.05/1200
F&G/2.05/1200 FAMILY (6)

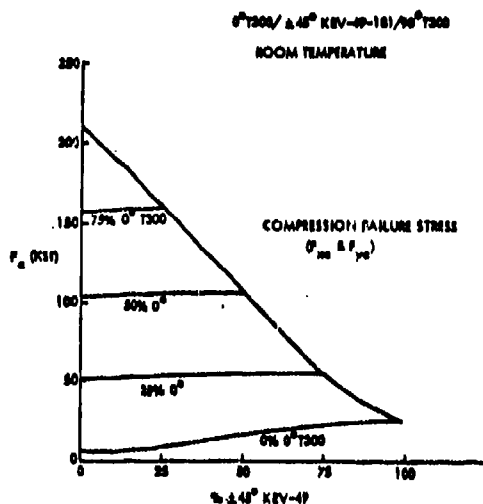


Figure 3.74 : LAMINATE ULTIMATE COMPRESSIVE STRENGTH
VERSUS PERCENT OF LAMINATE T300/K-49/T300
($0^\circ/\pm 45^\circ/90^\circ$) FAMILY (4)

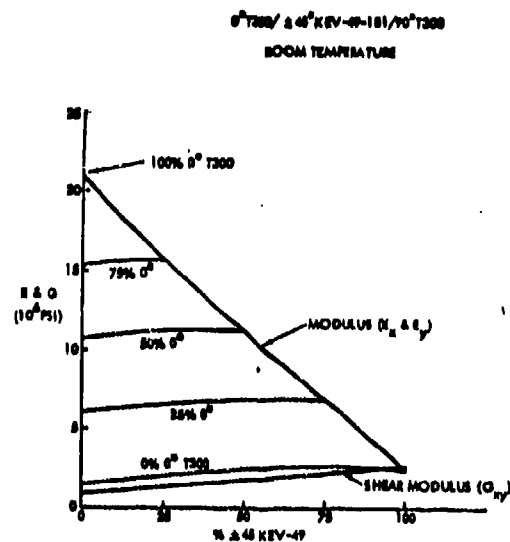


Figure 3.75 : LAMINATE E_x & G_{xy} VERSUS PERCENT
OF LAMINATE T300/K-49/T300
($0^\circ/\pm 45^\circ/90^\circ$) FAMILY (4)

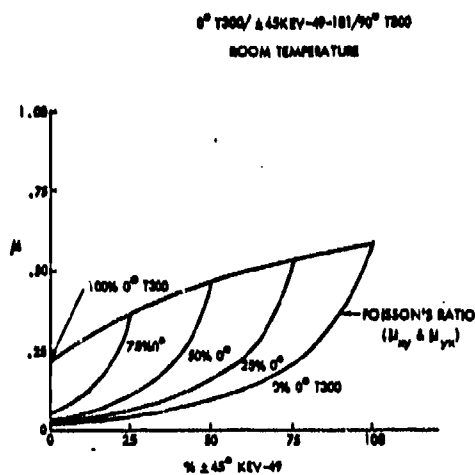


Figure 3.80 : POISSON'S RATIO μ_{xy} T300/KEV-49-181/T300
($0^\circ/\pm 45^\circ/90^\circ$) FAMILY (4)

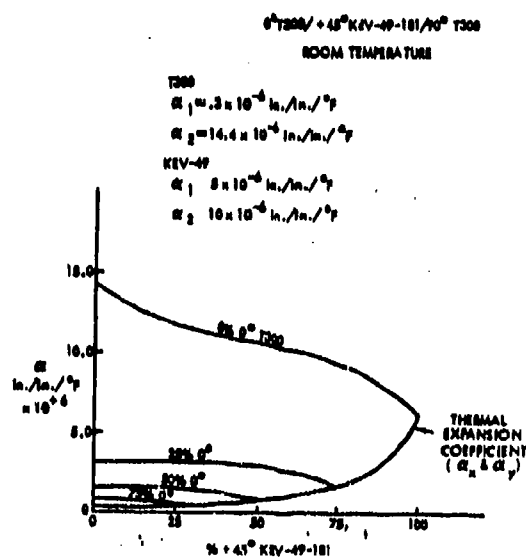


Figure 3.81 : LONGITUDINAL COEFFICIENT OF THERMAL EXPANSION
T300/KEV-49-181/T300 ($0^\circ/\pm 45^\circ/90^\circ$) FAMILY (4)

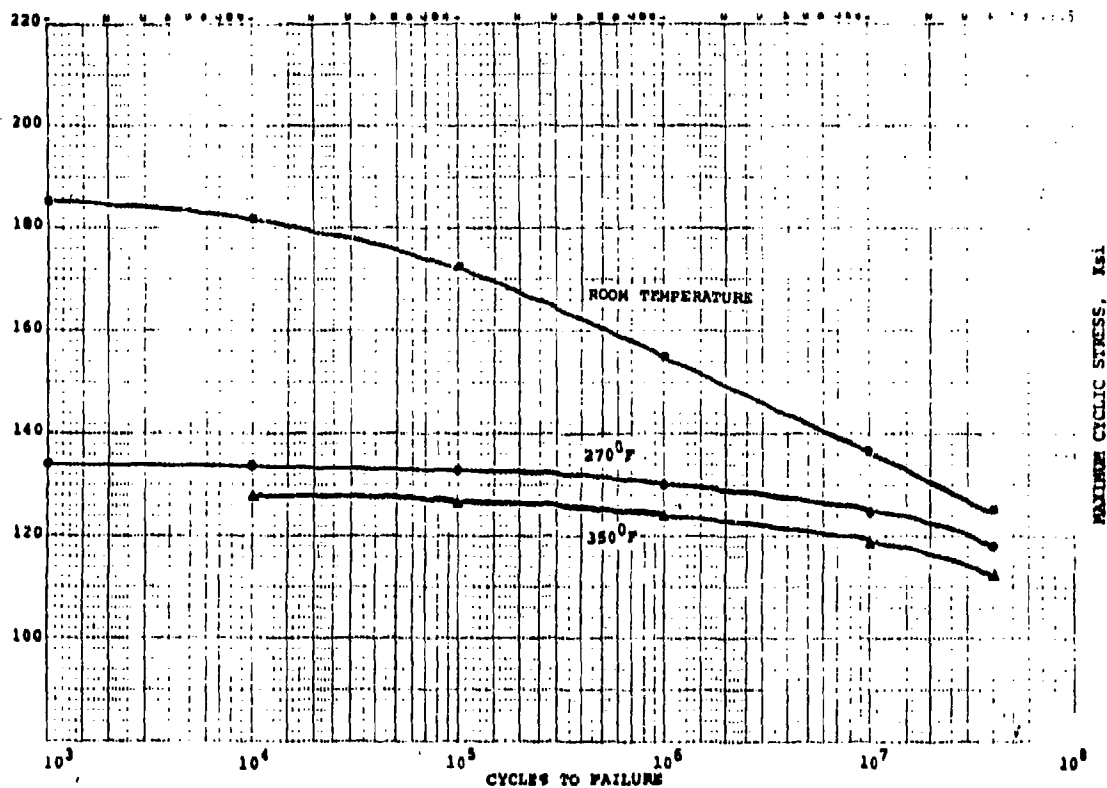


Figure 3.82 Constant Amplitude Fatigue Data For Unidirectional Boron/Epoxy For $R=0.1$ At Various Temperatures (3)

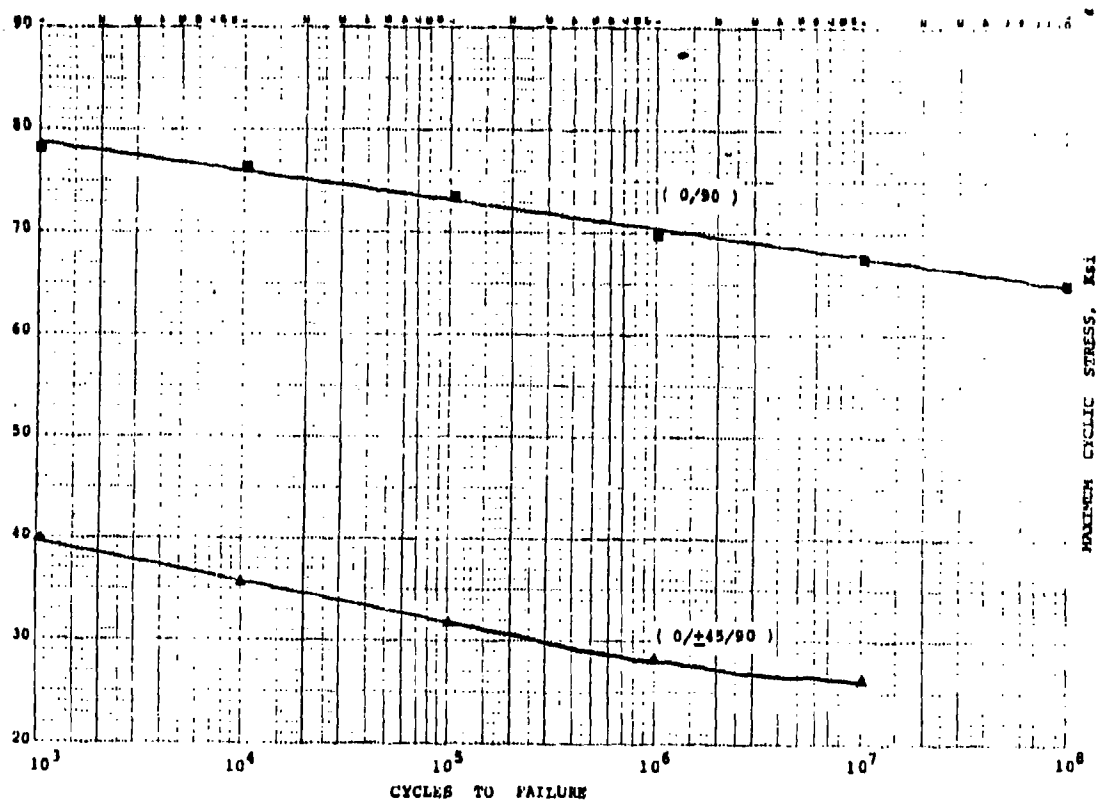


Figure 3.83 Constant Amplitude Fatigue Data For [0/90] and [0/±45/90] Crossplied Boron/Epoxy Laminates At Room Temperature at $R=0.1$ (3)

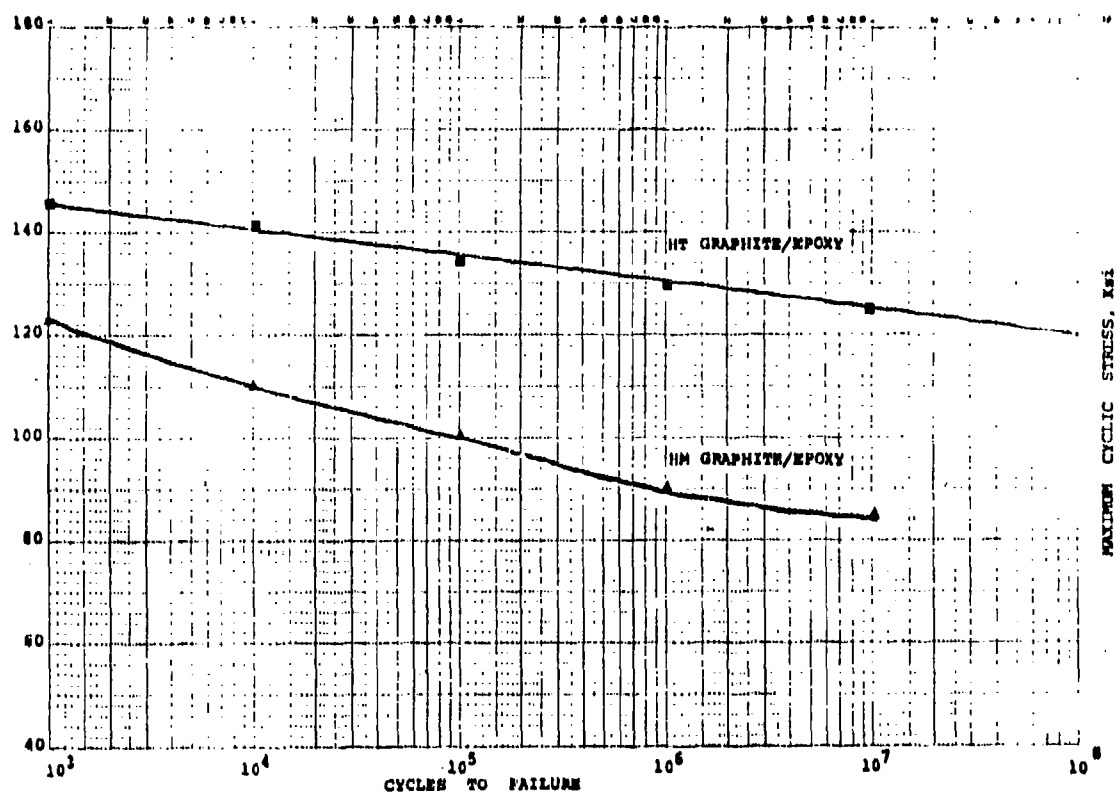


Figure 3.84 Constant Amplitude Fatigue Data For Unidirectional High-Strength (HT) and High-Modulus (HM) Graphite/Epoxy Laminates At Room Temperature and $R=0.1$ (3)

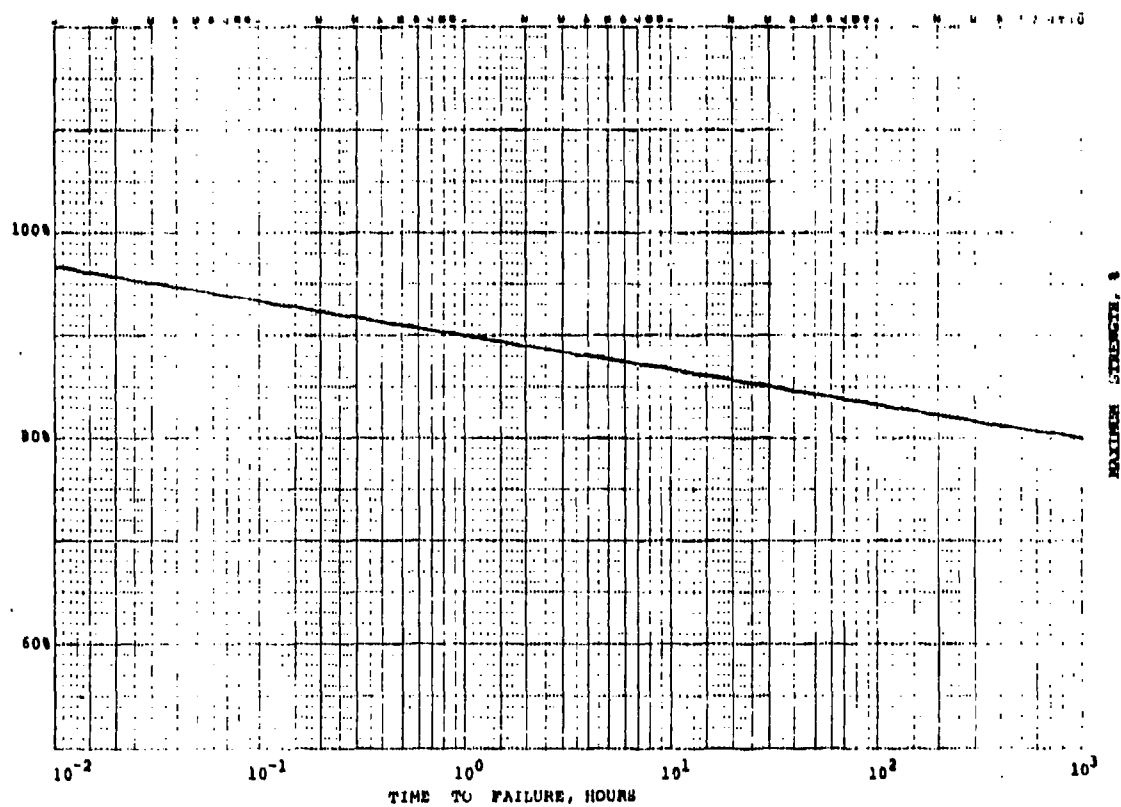


Figure 3.85 Constant Amplitude Fatigue Data For Unidirectional Kevlar/Epoxy At Room Temperature and $R=0.1$ (4)

3.6

References

1. DOD/NASA Structural Composites Fabrication Guide, 2nd Edition, Vol. I May 1979.
2. P. Beardmore, et.al, Fiber-Reinforced Composites: Engineered Structural Materials, Science, Vol. 208, 23 May 1980, p. 833.
3. Advanced Composites Design Guide, Third Edition, Air Force Materials Laboratory, Wright-Patterson Air Force Base, Ohio, Vol. I, 1973.
4. DuPont Technical Information, Characteristics and Uses of Kevlar 49 Aramid High Modulus Organic Fiber, Bulletin K-2, February 1978.
5. Graphite Materials, Hercules Inc., 1976.
6. J. T. Hoggatt and A. L. Dobyns, Evaluation of Hybrid Composites, AFML-TR-76-53, May 1976.

4.0 APPLICATIONS OF COMPOSITE MATERIALS

Composite materials have been in extensive use in the aerospace industry and other commercial sections of the economy for a number of years. The first two sections of this chapter profile the past and present applications of composites to various commercial and military aircraft systems with some space applications. No attempt is made to be complete but a good representative survey of such applications is given. The third section deals with certain specific problems in using composites on aircraft. The last section projects future trends in composite use for both the aerospace and automobile industries.

4.1 Early (pre-1973) Aerospace Composite Materials Applications

Composite materials have been used on aircraft and spacecraft for a number of years. Although much interest in using these materials has been voiced, past applications have been limited to small secondary structures and have involved principally boron and glass-fiber composites. A representative history of pre-1973 composite applications is given in Table 4.1. The history is not meant to be inclusive but rather to illustrate the types of composite structures that have been fabricated, the variety of composites that have been used, the aerospace companies involved, and the weight savings obtained from composite structures over the counterpart metallic structures.

4.2 Recent (post-1973) and Current Aerospace Composite Material Applications

Numerous applications of composites to aerospace systems have been made since 1973 and will continue to be made in the present and near future. The principal materials are graphite/epoxy and Kevlar, both individually and as hybrid composites. This section presents a representative sample of recent composite applications to aircraft, propulsion, spacecraft and helicopter systems. Two very interesting applications, composite mechanical fasteners and aircraft seats and galleys, are included. Each application is described and the actual or projected weight or cost savings obtained using composites is given. All recent composite applications are summarized in Table 4.2.

4.2.1 Aircraft Systems

Twelve uses of composites on various aircraft are presented in this section. Both military and civilian aircraft are included.

4.2.1.1 McDonnell Douglas DC-10

the DC-10 uses composites on both a secondary structure and a small primary structure. The primary structure is the vertical stabilizer (2) which is fabricated from graphite/epoxy. The composite stabilizer has a projected weight savings of 20-22%⁽³⁾ and is scheduled for completion in 1982.⁽²⁾

Table 4.1 Composite Application History (before 1973) (1)

Component	Manufacturer	Composite	Percent weight Savings
<u>Aircraft Systems</u>			
F-111 Horizontal Stabilizer	General Dynamics	Boron/Epoxy	27%
F-4 Rudder	McDonnell Douglas	Boron/Epoxy	36%
F-14A Horizontal Stabilizer	Grumman	Boron/Epoxy	19%
F-15 Horizontal Stabilizer	McDonnell Douglas	Boron/Epoxy	
A-4 Horizontal Stabilizer	McDonnell Douglas	Graphite/Epoxy	20%
F-100 Wing Skin	Rockwell	Boron/Epoxy	25.6%
F-111B Wing Box Extrusion	Grumman	Boron/Epoxy	
C-5A Leading Edge Slat	Lockheed	Boron/Epoxy	
F-111 Aft Fuselage	General Dynamics	Boron/Epoxy	19%
F-5 Aft Fuselage		Graphite/Epoxy	
F-5 Landing Gear Door	Northrop	Boron/Aluminum	
		Boron/Epoxy	22%
<u>Engine Systems</u>			
JFT22 First-Stage Fan Blade	Pratt & Whitney	Boron/Platinum	44%
Fan Blade	General Motors	Boron/Titanium	50%
JFT22 Third-Stage Fan Blade	Pratt & Whitney	Boron/Aluminum	36%
T56-A-18 Gearbox Case	General Motors	Boron-Glass/Epoxy	13%
<u>Space Systems</u>			
Reentry Frustrum	General Electric	Boron/Epoxy	
Missile Interstage	Boeing	Graphite/Epoxy	27%
Missile Payload Adapter	General Dynamics	Boron/Aluminum	40%
Tubular Struts	Rockwell	Boron/Epoxy	30%
Tubular Struts	Northrop	Graphite/Epoxy	46%
		Glass/Epoxy	
<u>Helicopter Systems</u>			
CH-47 Rotor Blade	Boeing-Vertol	Boron/Epoxy	
		Glass/Epoxy	
S-61 Tail Rotor	Sikorsky	Boron/Epoxy	5%
		Glass/Epoxy	
CH-54B Tail Cone	Sikorsky	Boron/Epoxy	

Table 4.2 Present (post 1973) and Near Future Aerospace Composite Applications

Component	Manufacturer	Composite	Comments
Aircraft Systems			
DC-10 Vertical Stabilizer (2,3)	McDonnell Douglas	Graphite/Epoxy	Ready in 1982; 20-22% weight savings
DC-10 Upper Aft Rudder (2,3)	McDonnell Douglas	Graphite/Epoxy	27% weight savings
727 Elevator (2)	Boeing	Graphite/Epoxy	26% weight savings
737 Horizontal Stabilizer (2)	Boeing	Graphite/Epoxy	Ready in 1980-81; 23% weight savings
L-1011 Inboard Aileron (3)	Lockheed	Graphite/Epoxy	Ready in 1980; 20% weight savings
L-1011 Vertical Fin (3,4)	Lockheed	Graphite/Epoxy	Ready in 1982; 30% weight savings
Lear Fan 2100 (3)	Lear Avia	Graphite/Epoxy	All-composite air-frame and wings
757/767 Control Surfaces (2,3)	Boeing	Graphite/Epoxy Graphite/Kevlar	Ready in mid-1980's
747 Outboard Ailerons (3) and Cowling Panels	Boeing	Graphite/Epoxy	26% weight savings on ailerons and 38% on cowling panels
AV-8B Wing Skin and Frames (3)	McDonnell Douglas	Graphite/Epoxy	20% weight savings
F-16 Tail Structure (7)	General Dynamics	Graphite/Epoxy	
F/A-18 Wing Skin	McDonnell Douglas/ Northrop	Graphite/Epoxy	50% of aircraft surface is composite
C-141 Wing Section (10)	Lockheed	Graphite-Glass/ Epoxy	75% lower maintenance and repair costs
THK-90 Landing Gear Doors (11) and Fairings	Messerschmidt-Boelkow-Blohm	Fiberglass/Epoxy Graphite/Epoxy	
Dornier Light Transport (12)	Dornier	Glass/Kevlar Graphite/Epoxy	Ready in 1980's; large composite surface area
Propulsion Systems			
RB.211-535 Engine Thrust Reverser and Fan Case Access Doors (2,10)	Rolls-Royce	Graphite/Epoxy	To be used on Boeing 757; reduction of 15-20% in engine weight
Composite Propeller (14,15)	Hartzell T.M. Development Dowty-Rotol	Kevlar	
Pressure Jet Rotor Blade (15)	T.M. Development	Kevlar	
Space Systems			
Intelsat V Truss and Dish (6) Antennas	Ford Aerospace	Graphite/Epoxy	
Space Beam Builder (16)	Grumman	Thermal Plastics	Ready in 1985
Helicopter Systems			
206L LongRanger Vertical Fin and Horizontal Stabilizer (17)	Bell Textron	Graphite/Epoxy	Vertical fin saves 27.5% by weight. Horizontal stabilizer saves 15% by weight
206L LongRanger Fairing, Litter Door and Baggage Door (18)	Bell Textron	Kevlar	Fairing saves 21% by weight. Litter door saves 37% and baggage door saves 12.5% by weight.
Other Applications			
Mechanical Fasteners (19)	Vought	Glass/Epoxy	Competitive with Titanium
Aircraft Seats and Galleys (12)	Weber Aircraft Aerospace Div., UOP	Graphite/Epoxy	

4.2.1.2 Boeing 727/737

One secondary graphite/epoxy application to both the 727 and 737, an elevator, is scheduled to be completed in 1980.⁽²⁾ This composite structure produces a 26% weight reduction.

The Boeing 737 is being modified with a composite horizontal stabilizer⁽²⁾ box and is scheduled to be completed in the 1980-1981 time frame. This component represents a medium size primary structure. The projected weight savings is 23%.⁽²⁾

4.2.1.3 Lockheed L-1011

There are two graphite/epoxy applications on the L-1011. The first application, finished in 1980, was the composite inboard aileron. The weight savings on this secondary structure was 20%. The second application, to be finished in 1982, is to the vertical fin.^(3,4) The projected weight savings is 30%.⁽³⁾

4.2.1.4 Lear Fan 2100

The Lear Fan 2100, a business aircraft, represents the first aircraft with a nearly all-composite airframe.⁽³⁾ The aircraft uses graphite/epoxy, Kevlar and graphite/Nomex honeycomb as shown in Figure 4.1. The Lear Fan 2100 is scheduled for test flight in October 1980 and certification by 1982. An estimated 11-18% is saved in fabrication costs.⁽⁵⁾

4.2.1.5 Boeing 757/767 Transports

The Boeing 757 and 767 wide body transport aircraft represent the Boeing entry for the next generation of air transports. Both aircraft will make extensive use of composite materials on such secondary structures as⁽³⁾ movable surfaces, seat doors, fixed trailing edges, fairings and cowl doors. Graphite/epoxy is to be used on control surfaces such as ailerons, elevators, rudders and spoilers because of its stiffness and light weight.⁽²⁾ A graphite-Kevlar hybrid composite will replace glass fiber in the wing/body fairings.⁽²⁾ Great care is being taken in the aircraft design to avoid graphite/aluminum interfaces and the resulting galvanic corrosion which has been the chief complaint of airlines about graphite composites in the past.⁽²⁾ The location of composites on the Boeing 767 is shown in Figure 4.2.

4.2.1.6 Boeing 747 Transport

Boeing aircraft has undertaken an in-house effort to retrofit the 747 with graphite/epoxy outboard ailerons and engine inlet outer cowl panels.⁽³⁾ The effort is expected to save 26% by weight on the ailerons and 38% on the cowl panels.⁽³⁾

4.2.1.7 Navy/McDonnell Douglas AV-8B Advance Harrier

The AV-8B Advance Harrier represents the most ambitious use to date of composites on military systems.⁽³⁾ Graphite/epoxy composites are used for the first time on cover skins and sub-structure frames on an



Figure 4.1

Lear Fan 2100, All-Composite Business Aircraft⁽³⁾

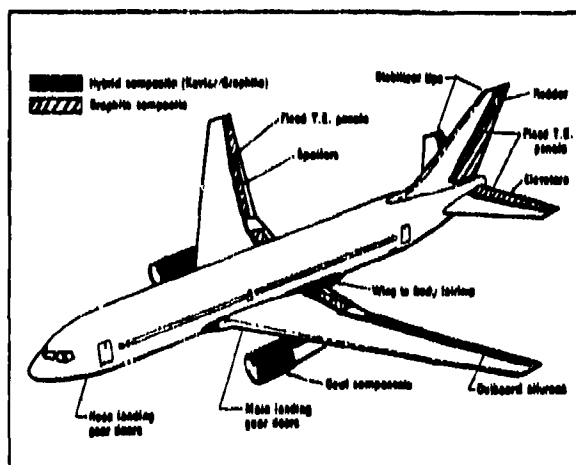


Figure 4.2

Advanced Composites on the Boeing 767 Transport⁽⁶⁾

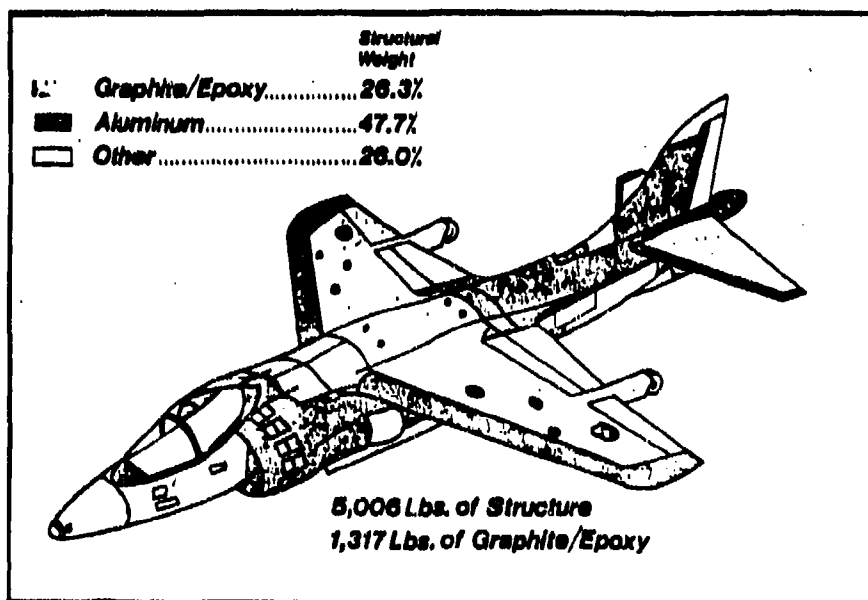


Figure 4.3

Navy/McDonnell Douglas AV-8B Advance Harrier Composite Aircraft⁽³⁾

aircraft wing.⁽³⁾ Approximately 75% of wing weight is composite which results in a 20% savings over an aluminum/titanium wing design.⁽³⁾ The overall aircraft weight savings is 26%.⁽³⁾ The use of composites on the AV-8B Harrier is illustrated in Figure 4.3.

4.2.1.8 USAF/General Dynamics F-16

The General Dynamics F-16 in the original version has a tail structure made of graphite/epoxy skin bonded to full-depth aluminum honeycomb.⁽⁷⁾ Modifications of the F-16 tail structure are currently underway which will permit better handling characteristics with the wider variety of missile loads the F-16 will be required to carry.⁽⁷⁾ Primary components of the new tail will be graphite/epoxy top and bottom skins connected to a corrugated aluminum sheet substructure tapered in span and chord.⁽⁷⁾ The new tail will have 30% greater area.

4.2.1.9 Navy/McDonnell Douglas/Northrop F/A-18

The F/A-18 is the second Navy aircraft (after the AV-8B Harrier) to make major use of composite materials.⁽³⁾ More than 50% of the aircraft surface area is covered by graphite/epoxy accounting for 10% of structural weight.⁽³⁾ The use of composites on the F/A-18 is illustrated in Figure 4.4.

4.2.1.10 USAF/Lockheed/C-141 Composite Wing Section

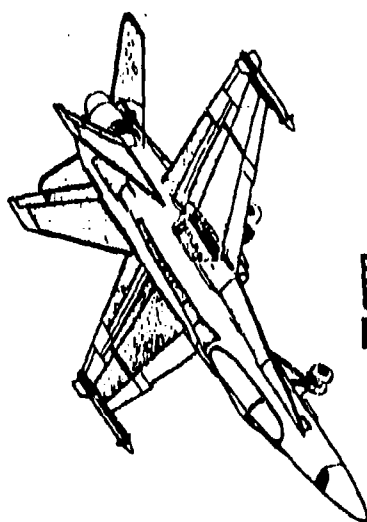
The inboard leading edge sections on the C-141 aircraft are composed of aluminum honeycomb. This material suffers from core corrosion resulting in high repairs and maintenance costs.⁽¹⁰⁾ A graphite-glass/epoxy leading edge has been substituted for the metal edge. The skin of the leading edge consists of 10 plies of glass fiber and 8 plies of graphite/epoxy tape.⁽¹⁰⁾ The ribs are fabricated with glass fiber and the rib cap has 11 plies of graphite tape.⁽¹⁰⁾ One layer of aluminum flame spray gives lightning protection. Maintenance and repair costs are estimated to be 75% lower.⁽¹⁰⁾

4.2.1.11 Panavia Tornado Multirole Combat Aircraft: THK-90 and THK-190

The THK-90 is a West German fighter made by Messerschmidt-Boelkew-blohm with Britain and France as coproduction partners.⁽¹¹⁾ The aircraft has landing gear doors and spine hood fairings made of glass fiber composite and a graphite/epoxy taileron.⁽¹¹⁾ An advanced model, the THK-190, will have graphite/epoxy wings, control surfaces and parts of the fuselage.⁽¹¹⁾

4.2.1.12 Dornier Light Transport

The Dornier light transport aircraft (shown in Figure 4.5) will be produced in France in the 1980 time frame and will use graphite/epoxy and glass/Kevlar composite over large areas of the aircraft surface.⁽¹²⁾ The glass/Kevlar composite will be used on the fuselage and wing surfaces and the graphite/epoxy on wing and tail control surfaces.⁽¹²⁾



■ STEEL
 □ GRAPHITE/EPoxy
 □ OTHER

Figure 4.4
Use of Composites on the Navy F/A-18 (9)

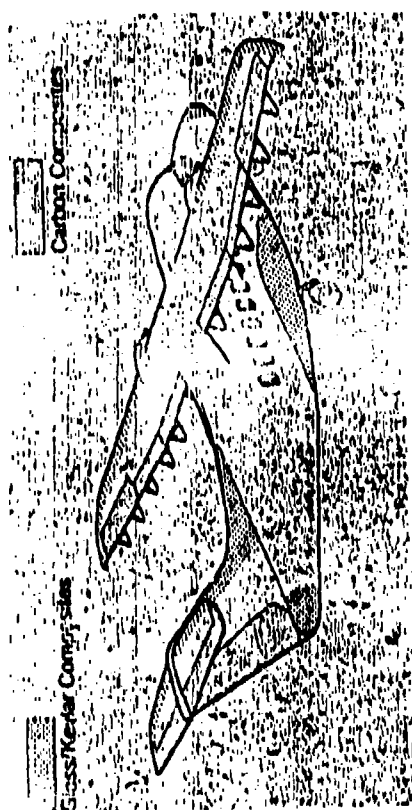


Figure 4.5
Composite Applications on the Dornier Light Transport Aircraft (12)

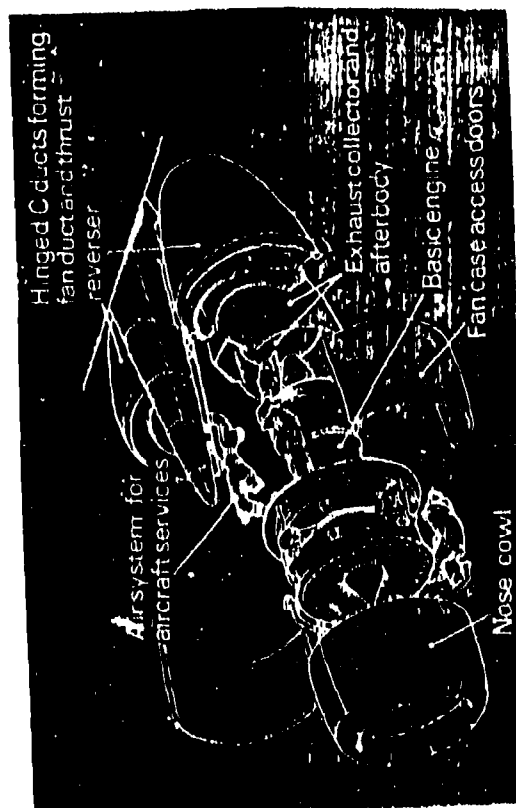


Figure 4.6
Rolls-Royce RB.211-535 Aircraft Engine (12)

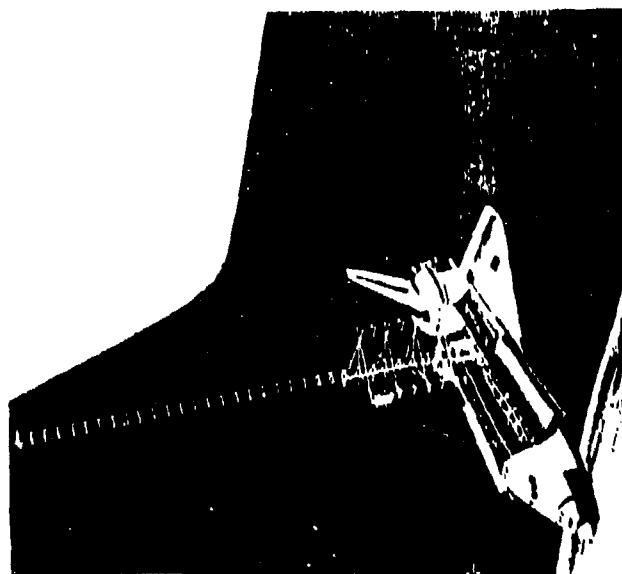


Figure 4.7
Simple Beam Builder Concept for Space Shuttle Applications Using the Space Shuttle (16)

4.2.2 Propulsion Systems

In this section, one example is given of composite application in the construction of a jet engine. Two examples are presented of all-composite propeller blades and one example is given of an all-composite helicopter rotor blade.

4.2.2.1 Rolls-Royce RB.211-535 Aircraft Jet Engine

Rolls-Royce is currently committed to a major use of composites on the RB-211-535 engine which will be used on the Boeing 757 transport aircraft. Plans call for use of graphite/epoxy and aluminum honeycomb for a reduction in engine weight by 15-20%.⁽¹²⁾ Composites will be used on the fan thrust reverser and fan case access doors,⁽¹⁰⁾ and are being considered for lightly loaded parts of the engine cowl and hearing spokes.⁽²⁾ A diagram of the engine is given in Figure 4.6.

4.2.2.2 Composite Propeller and Pressure-Jet Helicopter Rotor Blade

An all-composite Kevlar/epoxy has been developed by Hartzell Propeller, Inc. and T.M. Development, Inc. for the CASA C.212 feederline transport aircraft.⁽¹⁵⁾ Certification of the blade by the Federal Aviation Administration (FAA) was achieved in September, 1978.⁽¹⁵⁾ T. M. Development, Inc. has also recently produced the first all-composite pressure-jet helicopter rotor blade.

A second all-composite blade will soon be produced by Dowty-Rotol in England. The blade will be used on the Saab-Fairchild commuter transport.⁽¹⁴⁾

4.2.3 Space Systems

One example is given of a communications satellite constructed with composites. A further example involves a composite beam builder using the space shuttle.

4.2.3.1 Intelsat V

The Intelsat V series of advanced communication satellites by Ford Aerospace is one example of present satellite systems that make extensive use of composite materials.⁽⁶⁾ Graphite/epoxy is used for the truss structure and large dish antennas of the satellite.⁽⁶⁾ It is scheduled to be launched by NASA in 1980 and carry telephone calls, television, telex and telegrams.⁽⁶⁾

4.2.3.2 Structural Beam Builder Assembly in Space

Marshall Space Flight Center and Grumman are studying deployable structures for use on platforms deployed by single space shuttle missions⁽¹⁶⁾

One current configuration is a simple beam builder designed by Grumman using composite materials and plastics. These materials are attractive because of their light weight, strength and insensitivity to thermal variations. The beam builder is targeted for 1985 and could double as a space applications platform. The beam builder concept is illustrated in Figure 4.7.

4.2.4 Helicopter Systems

Two helicopter composite programs are discussed. The first one is the Bell 206L Long Ranger and the second is a Bell/Grumman study of an all-composite helicopter airframe.

4.2.4.1 Bell Helicopter Textron/206L Long Ranger Helicopter

Bell Helicopter Textron has a NASA/Army research contract for the flight testing and servicing of the composite 206L Long Ranger helicopter. (17)

Two helicopter primary components, the vertical fin and the horizontal stabilizer, involve graphite/epoxy composites. (17) Three secondary components, the upper forward rotor mast fairing, litter door and a baggage compartment door, are constructed from Kevlar/epoxy. (17) Weight savings estimates for the graphite/epoxy components are 27.5% (vertical fin), and 15% (horizontal stabilizer), for the Kevlar components, the figures are 21% (fairing), 37% (litter door) and 12.5% (baggage door). (17)

4.2.4.2 Bell/Grumman All-Composite Helicopter Airframe

Bell Helicopter and Grumman Aerospace Corporation are working on U.S. Army studies on the application of composites to helicopters. (18)

One study involves the investigation of crash characteristics of helicopter composite structures. (18) The second study is of an all-composite airframe having a goal of reductions of 17% in cost and 22% in weight over a metal airframe. Structural and radar cross-section characteristics are to be optimized. (18)

4.2.5 Other Aerospace Applications

Three additional aerospace composite applications, mechanical fasteners and aircraft seats and galleys are discussed in this section.

4.2.5.1 Composite Mechanical Fasteners

Two types of glass-fiber composite fasteners have been developed by Vought Corporation for use in joining composite materials containing graphite. (19) Use of conventional mechanical fasteners with graphite/epoxy composite may cause serious galvanic corrosion unless expensive titanium or special stainless steel alloy fasteners are used. (19) Conventional fasteners and installation methods also may cause composite fiber damage and delamination of the joined pieces. (19)

One fastener type consists of two pieces (the pin and the sleeve) fabricated from thermoset epoxy resin reinforced with glass fiber. (19) Both pieces are bonded together during installation using an epoxy adhesive that is applied under heat and pressure. (19)

The second fastener type consists of a single piece designed like that of a conventional fastener (a pin with a head) and fabricated from thermoplastic polysulfone resin reinforced with glass fiber. (19) The fastener is installed under heat and pressure using a machine that produces a second head on the fastener opposite the permanent head. (19)

Both fastener types have shear properties similar to conventional aluminum fasteners.⁽¹⁹⁾ They are competitive in cost, weight and strength to the titanium fasteners presently used to join composite structures.⁽¹⁹⁾

Fasteners made from graphite/polyimide composite have also been produced by Vought Corporation for NASA.⁽¹⁹⁾ These composite fasteners are usable at higher temperatures than is possible with glass-fiber composite fasteners.⁽¹⁹⁾

4.2.5.2 Composite Aircraft Seats and Galleys

Considerable interest currently exists for producing a lighter, more durable aircraft seat for use in the coming generation of wide-body transports. These transports will emphasize more passengers, greater seating comfort and economy of operations.

Weber Aircraft, a division of Walter Kidde & Co. - an aircraft seat manufacturer -- is studying the use of composites in seats and galleys. Aerospace Division of UOP, Inc. is testing a graphite/epoxy material for seats using a molding rather than a lay-up technique. A 40% weight reduction in seats is considered possible using this technique.⁽²⁾

4.3 Problems in Composite Material Applications

Three important problems involved with the use of composites are discussed in this section. The first problem, graphite fiber release, has been studied intensely for the past 3 years and has been resolved only recently. A second problem, galvanic corrosion, has been a major complaint from aircraft companies about graphite composites. The third problem concerns the high production costs of composite fabrication. Attempts to improve the manufacturing process are discussed.

4.3.1 Graphite Fiber Release

Graphite/epoxy composite material has been used extensively on many recent aircraft, spacecraft and helicopter systems (see Table 4.2 for a representative list of composite applications) and plans currently exist that involve fabrication by the major aerospace firms of primary airframes and possible whole aircraft using this composite.⁽²³⁾ A major obstacle to the continuing advances in composite development has been the concern over possible graphite fiber release into the atmosphere due to crashes, fire and/or explosion of graphite composite commercial transport aircraft.^(2,3,20)

A government-wide graphite fiber hazard study was initiated in July 1977 which included a NASA risk-analysis study directed by the Executive Branch's Office of Science and Technology.⁽²⁹⁾ The major initial impact of the study effort was an immediate freeze upon all new graphite/epoxy composite component development work funded through the NASA Aircraft Energy Efficiency Program at Langley Research Center until the magnitude of the threat could be evaluated.⁽²⁰⁾ The study did not address fiber release from military aircraft but only from commercial transports.^(2,3,20)

The concern that motivated the study was that the fine, conducting graphite fibers, released by fire or explosion of a composite aircraft and blown possibly tens of kilometers by wind, could possibly penetrate buildings and electrical equipment enclosures to short out or disrupt electronic equipment for which the airline would be financially liable.(2,3,20) Related concerns were effects upon human health from inhaling the fibers (3) and effects arising from deliberate fiber release by terrorists.(2)

After extensive testing, which included large scale fires and large test rigs, the threat of fiber release was judged to be very small.(3,21) Tests with consumer appliances, industrial electronic systems and avionics revealed them to be very nonsusceptible to damage by graphite fibers.(3,21) No adverse effects on human health were found because of the inconsequential amount of fiber released.(3)

The final report on the NASA graphite fiber hazard was due in December 1980. A recommendation is expected that will rejuvenate the large NASA composite program.

4.3.2 Galvanic Corrosion

The chief complaint of the aerospace companies regarding the use of graphite/epoxy composite material is the very severe corrosion that results from galvanic action between graphite and other aircraft material (chiefly aluminum). Galvanic corrosion weakens the metal and makes a fastened joint subject to poor electromagnetic shielding and even to catastrophic failure.(19) Consequently, direct aluminum-to-graphite composite joints are avoided. Titanium alloy fasteners are the best metals to use to bond graphite composite joints. Some recent work on all-composite fasteners has been done and is promising as a solution to the graphite/epoxy composite joint problem.(19)

4.3.3 Fabrication Techniques

A major problem using composite materials is the large tooling and fabrication costs involved. Many composite parts are very labor intensive because lay-up procedures are usually used during the fabrication process. Some steps have been taken, chiefly by automobile companies and makers of certain composite aircraft parts to use molding and mass production techniques to make composite parts more cost-effective.

4.4 Future Uses of Composite Materials

A small survey is given of several future efforts involving extensive use of composite materials. Examples are discussed in the aerospace industry and other commercial sections.

4.4.1 Future Composite Uses in Aerospace Systems

A common factor runs through all future approaches to civilian and many military aircraft designs: fuel efficiency.(2) This factor is especially critical for future transport aircraft to be competitive internationally.(2) A major determinant of fuel efficiency is aircraft weight. Small secondary composite structures have already been used on past aircraft

systems with weight savings typically 10-30% over the equivalent metallic structures. Secondary structures, however, represent a small part of total system weight (3% for Boeing 757 and 767⁽²⁾). In order to meet future aircraft fuel efficiency requirements, a commitment must be made by the big airframe manufacturers and the government towards large composite primary structures such as the wings and wing box, stabilizer box and fuselage sections.^(2,3) Efforts are underway in both government and industry to determine the most cost-effective ways of making this commitment.

The composites that will be used to fabricate the large primary structures are graphite/epoxy with advanced resins and hybrid composites consisting of alternating graphite and Kevlar.^(2,3) Increased resin toughness is being emphasized as a major means of improving composite performance, particularly for graphite/epoxy.⁽²⁾ Future aircraft fabricated from these composites will be more than 50-55% composite by weight.^(3,9) The weight and cost savings realized on transports using the composite primary structures are shown in Figure 4.8.

After composites are used to remove large amounts of weight from the primary structures, a second determinant of fuel efficiency can come into play: new aircraft aerodynamic shapes. Such shapes, impossible or impractical with metal structures, could allow a given aircraft performance to be achieved using smaller, more efficient engines, or allow better performance with the present engines.⁽²⁾

The main factor that gives the major airframe companies pause before making a massive commitment to composites is the tremendous cost of new facilities required in converting from aluminum to composites.⁽³⁾ In order to lower costs, such facilities must be based on rapid and automated mass-production of composite structures that are of high quality, reliability, and low unit cost. Such an automated factory would greatly reduce the current labor-intensive character of present composite processing techniques. Northrop currently is operating a prototype automated composite manufacturing plant, referred to as the Integrated Flexible Automation Center, in Los Angeles, California.⁽¹⁸⁾ It will evaluate robotics and computerized curing temperature and cycle control for use in automated composite manufacturing.

A further strategy to lower composite costs is increased commercial applications. Although graphite/epoxy golf clubs, tennis rackets and fishing rods are expanding in sales volume,⁽⁶⁾ the main hope is for greatly expanded use of composites in the automobile industry.^(6,9) This topic will be discussed in section 4.4.2.

The first primary structures, as currently envisioned by NASA, would be a graphite/epoxy wing box and fuselage segment. One design for the wing box is shown in Figure 4.9. Both structures would be available about 1985 if funding begins in 1981.

Future efforts by Boeing are to attain the capability of building an all-composite advanced transport with the major primary structures, wings and fuselage sections, fabricated from graphite and Kevlar composites.⁽²⁾ A \$200 million in-house investment has been proposed to prepare the necessary facilities.⁽²⁾

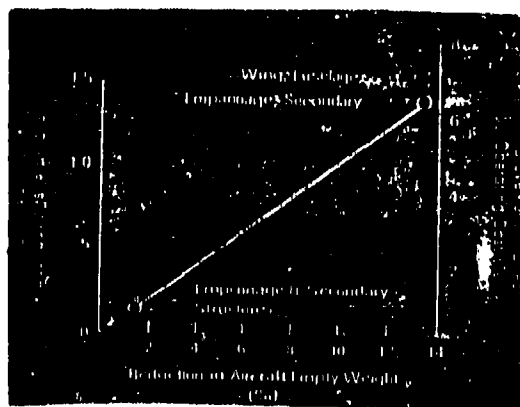


Figure 4.8
Weight and Cost Savings Possible by Use of
Composites for Primary Structures in Transport
Aircraft. Chart prepared by NASA.⁽³⁾

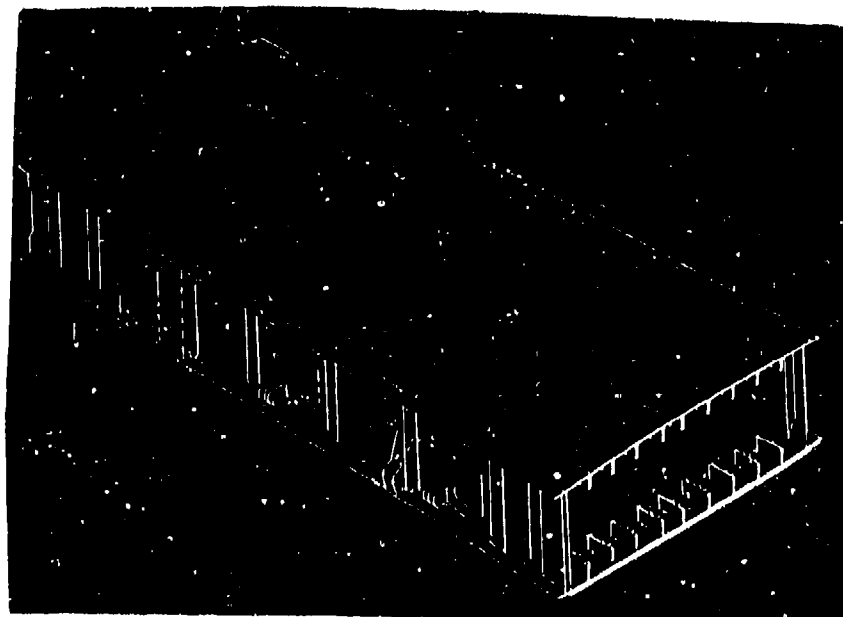


Figure 4.9
Graphite/Epoxy Wing Box⁽²⁾

Douglas Aircraft is currently involved with two efforts for large composite aircraft. Under study is an Advanced Technology Medium Range (ATMR) transport designed to compete with the Boeing 757.⁽²⁾ The second effort is a DC-9 super 80 using Kevlar nacelles and graphite/epoxy rudder controls and possibly a graphite/epoxy wing box.⁽²²⁾

An ongoing study has been performed by Grumman on the Advanced Design Composite Aircraft (ADCA)⁽²³⁾ concept. Such a design, a fighter, would have 60-70% composites, have a deep strike and penetration capability and be available in the 1990 time frame.⁽²³⁹⁾

4.5 References

1. Advanced Composites Design Guide, U of I, Air Force Materials Laboratory, Wright-Patterson AFB, Ohio, January 1973.
2. Aviation Week and Space Technology, Nov. 12, 1979.
3. Aviation Week and Space Technology, Sept. 15, 1980.
4. Aviation Week and Space Technology, June 9, 1980.
5. Aviation Week and Space Technology, Dec. 4, 1978.
6. P. Beardmore, et al, Fiber Reinforced Composites: Engineered Structural Materials, Science, Vol. 208, 23 May 1980.
7. Aviation Week and Space Technology, Sept. 1, 1980.
8. Aviation Week and Space Technology, July 21, 1980.
9. Aviation Week and Space Technology, Oct. 8, 1979.
10. Aviation Week and Space Technology, Dec. 10, 1979.
11. Aviation Week and Space Technology, April 2, 1979.
12. Aviation Week and Space Technology, Sept. 4, 1978.
13. Aviation Week and Space Technology, Sept. 10, 1979.
14. Aviation Week and Space Technology, Sept. 1, 1980, p. 281.
15. Aviation Week and Space Technology, Oct. 13, 1980, p. 88.
16. Aviation Week and Space Technology, April 14, 1980, p. 50.
17. Aviation Week and Space Technology, Feb. 26, 1979, p. 42.
18. Aviation Week and Space Technology, Oct. 8, 1979, p. 18.
19. Aviation Week and Space Technology, Feb. 16, 1980, pp. 38-45.
20. Aviation Week and Space Technology, March 5, 1979, p. 47.
21. Aviation Week and Space Technology, Dec. 17, 1979, p. 74.
22. Aviation Week and Space Technology, Oct. 23, 1980.
23. Aviation Week and Space Technology April 19, 1976.

5.0 INTRINSIC MATERIAL PROPERTIES

The electromagnetic behavior⁽¹⁾ of composite materials is ultimately determined by their intrinsic material properties. The key properties considered in this section are the composite material permeability, permittivity, and conductivity as functions of frequency and field strength. A brief analysis of composite material resistivity is presented separately. Property modification is discussed and includes property improvement through doping and intercalation, and property changes due to thermal and environmental effects. Nonlinear properties of composites are also briefly considered.

5.1 Material EM Parameters

The measured relative values of permeability and permittivity and the measured values of conductivity as functions of frequency and field strength, for boron/epoxy, Kevlar/epoxy and graphite/epoxy composites are tabulated in this section. Some data is presented on the resistivity of composites. Separate data is given on the conductivity of boron/epoxy and graphite/epoxy for individual fibers, the epoxy and bulk composite material.

5.1.1 Permeability

The basic macroscopic parameter used to characterize the magnetic state of a material is the permeability. This parameter (designated by μ) is defined in terms of the magnetic induction (B) and the magnetic field intensity (H) by the equation

$$B = \mu H \quad (5-1)$$

In view of the fact that the composites boron/epoxy, graphite/epoxy and Kevlar/epoxy are presently fabricated using nonmagnetic materials, it may be anticipated that their magnetic permeability will be essentially that of free space.

Permeability measurements for the composites boron/epoxy, graphite/epoxy and Kevlar/epoxy have been performed^(3,4) using the standard testing procedures specified by the American Society for Testing and Materials (ASTM). The permeabilities of representative samples of each composite were determined at D.C. and 60 Hz using the sample weighing technique and at 100 Hz using the most sensitive vibrating sample magnetometer. All results indicated that these materials were weakly diamagnetic with a measured magnetic susceptibility $\chi_m \times 10^{-7}$. The permeability is given in terms of the magnetic susceptibility by the equation

$$\mu = \mu_0 (1 + \chi_m) \quad (5-2)$$

where μ_0 is the permeability of free space. The results are tabulated in Table 5.1 in terms of the relative permeability μ/μ_0 . These results indicate that boron/epoxy, graphite/epoxy and Kevlar/epoxy all have the permeability of free space to the accuracy measured and the frequencies checked. Due to the apparent lack of sensitivity of the measured permeabilities to frequency, no higher frequency measurements have been undertaken. Further details on the measurement process may be found in Section 9.0 on Measurement, Test and Evaluation or in the references.^(3,4,6)

5.1.2 Permittivity

The electrical parameter analogous to the magnetic permeability is the electric permittivity (designated by ϵ) and is defined in terms of the applied electric field (E) and electric displacement (D) by the equation

$$D = \epsilon E \quad (5-3)$$

Because composite materials are heterogeneous substances by virtue of their process of manufacture, the permittivity of these materials can be expected to be anisotropic and to be frequency dependent. A further complicating factor in the measurement of the permittivity is the existence of conducting charge in the composite materials. As a consequence, the conduction current (as measured by the conductivity σ) and the displacement current (as measured by the permittivity ϵ) are mixed together as shown in the equation

$$\nabla \times H = (\sigma + j\omega\epsilon) E \quad (5-4)$$

where ω is the angular frequency. The measureability of the permittivity then depends on the magnitude of the material conductivity.

The standard ASTM method used to measure permittivity involves the measurement of the capacitance of a composite filled capacitor. Details of the measurement process are given in Section 9.0 on measurement, test and evaluation and in the references.(3,4,6)

The relative permittivity ϵ/ϵ_0 (also called the dielectric constant where ϵ_0 is the permittivity of free space) of Kevlar/epoxy, graphite/epoxy and boron/epoxy have been measured from D.C. to 50 MHz.(3,4) The results are tabulated in Table 5.2. These results show that Kevlar/epoxy is a very good insulator with the permittivity essentially a constant independent of direction and frequency. The range of values reported for the Kelvar/epoxy permittivity are attributed to variations in epoxy chemistry.

The permittivity of graphite/epoxy was found to be essentially unmeasurable at any test frequency due to the high value ($10^2 - 10^4$ mhos/m) of the conductivity in any direction in the composite.(3,4) It has been estimated that the permittivity of graphite/epoxy will not be measurable until frequencies are of the order of 10^{12} Hz.(4)

The permittivity of boron/epoxy falls between the two extreme cases of Kevlar/epoxy and graphite/epoxy. This permittivity was found to be measurable only when the existing fields were normal to the direction of the composite fibers. In this case the permittivity was constant and frequency independent from D.C. to 50 MHz. The permittivity in the direction parallel to the composite fibers proved to be unmeasurable due to high fiber conductivity.(4) Finally the permittivity of the epoxy resins which hold the fibers was measured from D.C. to 50 MHz with the result listed in Table 5.2 for 1 MHz. The permittivity of the epoxy resin was found to be independent of direction and frequency in the range considered.(3,4)

5.1.3 Conductivity

In this section, the conductivity of Kevlar/epoxy, boron/epoxy and graphite/epoxy composite materials is discussed in detail. Measured

conductivities are given for Kevlar/epoxy at two frequencies. Conductivities for boron/epoxy and graphite/epoxy are reported for the bulk composite in several ply orientations as well as for the constituent fibers and epoxy.

5.1.3.1 Kevlar/Epoxy

The conductivity of several samples of Kevlar/epoxy have been investigated⁽³⁾ to a limited extent as a function of frequency and electric field strength.⁽³⁾ The experimental method used was the standard two-point probe method specified by the American Society for Testing and Materials (ASTM). Details on this method and related methods can be found in Section 9.0 on Measurement, Test and Evaluation and in the references.⁽⁴⁾ These investigations show that Kevlar/epoxy conductivity has a slight dependence on frequency and field strength. The conductivity decreases slightly with increasing frequency and increases slightly with increasing field strength. The results are also independent of direction. The conductivity results for frequency are tabulated in Table 5.3 and the results for field strength are graphed in Figure 5.1. Because of the apparent insensitivity of the conductivity to low frequency, high frequency conductivities have not been investigated to date.

5.1.3.2 Boron/Epoxy

Conductivity studies on boron/epoxy have dealt with the conductivity of the individual boron fibers, of the epoxy resin matrix holding the fibers, and of the total boron/epoxy composite. These results are presented and discussed in the three separate sections that follow.

5.1.3.2.1 Boron Epoxy Resins

Samples of the uncured epoxy resins were obtained from AVCO, a maker of boron/epoxy composite, and heated as is done during the manufacture of the composite. The conductivity was then measured at a frequency of 1 MHz⁽⁴⁾. The result is listed in Table 5.4. This result was found to be frequency and direction independent in the range D.C. - 50 MHz.

5.1.3.2.2 Boron Fibers⁽²⁾

Boron fibers used in boron/epoxy composite materials are typically 10^{-2} cm in diameter. Although considerably larger than graphite fibers, boron fibers prove hard to characterize electrically because of the difficulty in fabricating reliable, low resistance ohmic contacts to the fibers. The reasons for these difficulties lie in the process used to make the fibers. Boron is deposited on hot tungsten wire (of diameter 1.8×10^{-3} cm) in an atmosphere of hydrogen (H_2) and boron chloride (BCl_3). The boron reacts with the tungsten to form an inner core of boron-tungsten compounds (such as WB_4 , W_2B_5 with possibly some free tungsten) surrounded by an outer sheath of pure boron. The details of the process are proprietary.

Great care is necessary in fabricating the electrical contacts. Mounting the fiber using conducting points or ink gives very nonlinear, even memory-displaying V-I characteristics. One successful approach is to plate nickel contacts onto the sheath and the core separately. Linear V-I characteristics result and it is possible to characterize the sheath and core by

Table 5.1 Composite Material Relative Permeability. (3,4)

RELATIVE PERMEABILITY μ/μ_0 at D.C., 60 Hz and 100 Hz	BORON/EPOXY		
	BORON/EPOXY	KEVLAR/EPOXY	GRAPHITE/EPOXY
	1.0	1.0	1.0

Table 5.2 Relative Permittivity (Dielectric Constant of Kevlar/Epoxy, Boron/Epoxy, Epoxy Resin, and Graphite/Epoxy in the Frequency Range D.C. - 50 MHz. (3,4)

RELATIVE PERMITTIVITY ϵ/ϵ_0	KEVLAR/EPOXY	GRAPHITE/EPOXY	BORON/EPOXY	
			PARALLEL TO COMPOSITE FIBERS	SERIAL TO COMPOSITE FIBERS
	3.6-5.85	Unmeasurable	Unmeasurable	5.6
				3.4

Table 5.3 The Conductivity σ (mho/m) of Kevlar/Epoxy as a Function of Frequency. (3)

	D.C.	100 kHz
σ	2.2×10^{-8}	5×10^{-9}

Table 5.4 Conductivities of Boron/Epoxy Fibers and Resin in Frequency Range D.C. - 50 MHz. (2,4)

CONDUCTIVITY (mho/m)	BORON FIBER (2)			EPOXY RESIN
	CORE	SHEATH	FIBER	
	3×10^5	0.25	2.3×10^3	6×10^{-8}

Table 5.5 Effective Conductivity of Boron/Epoxy as a Function of number of plies and ply orientation. These results are calculated by Stoney using electromagnetic shielding results. (1)

PLIES	PLY ORIENTATION	σ (mho/m)	
		50 kHz-70 MHz	100 MHz - 18 GHz
1	σ^0		
2	$0^\circ, 90^\circ$		
4	$0^\circ, 45^\circ, 90^\circ$	≈ 10	≈ 100
8	$0^\circ, 45^\circ, 90^\circ$		

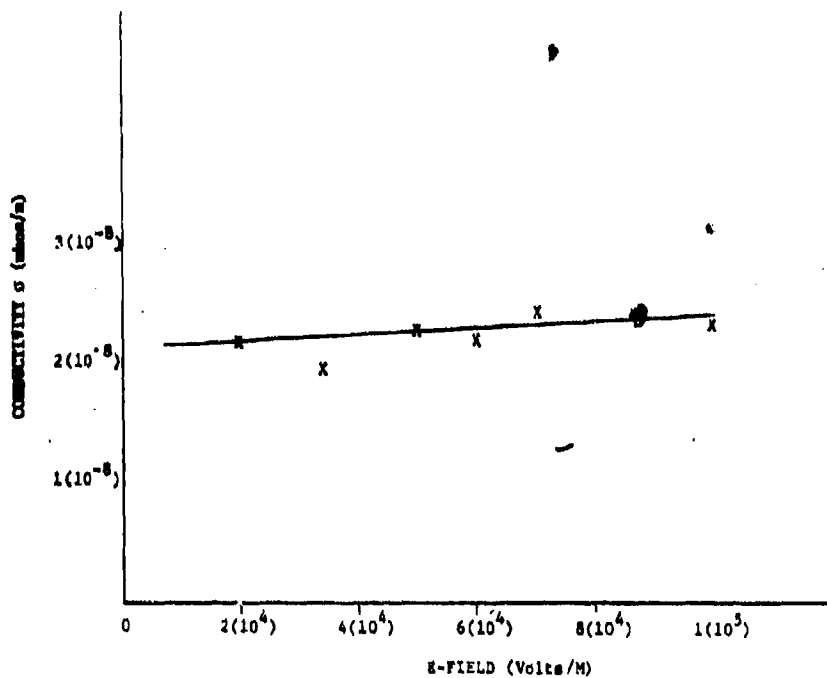


Figure 5.1. Conductivity σ (mhos/m) of Kevlar/Epoxy as a Function of E-Field.⁽³⁾

conductivities together with an effective fiber conductivity. These conductivities are given in Table 5.4. Boron fibers conductivities are seen to be very anisotropic with most of the current confined to the inner core of the fiber.

5.1.3.2.3 Boron/Epoxy Composite

There have been several investigations on the conductivity of boron/epoxy with varying results. One set of effective conductivities was obtained during an investigation of the shielding effectiveness of advanced composites. The shielding data becomes consistent with shielding theory provided the effective conductivity of boron/epoxy is taken as 10 mhos/m at low frequencies (50 kHz-70 MHz) and 100 mhos/m at high frequencies (100 MHz-18 GHz). These boron/epoxy test specimens range from 1-ply to 8-ply and involve several ply orientations as listed in Table 5.5. Preliminary investigation reported by Allen et.al.⁽⁴⁾ on samples of AVCO Rigidite 5505 Boron/epoxy over a frequency range from D.C. to 50 MHz (given in Table 5.6) tend to confirm these results. More recent work involving great care in forming ohmic contacts using thin nickel-plated films onto abraded edges of boron/epoxy has resulted in revised figures for the longitudinal conductivities of multiply unidirectional samples.⁽³⁾ These results are given in Table 5.7. They show conductivities much higher than previously reported with an average of about 1000 mhos/m. Included for comparison in Table 5.7 is a unidirectional conductivity value (σ_{wh}) obtained by Walker and Heintz⁽⁵⁾ using a standing wave pattern on a slotted stripline at a frequency of 2 GHz. This conductivity value is significantly higher than values obtained by other methods and does not depend on ohmic contacts made to the composite. The basic conclusion reached by Gajda⁽³⁾ was that the longitudinal conductivity of boron/epoxy is about 1000 mhos/m while the transverse conductivity is about 2×10^{-8} mhos/m. The large anisotropy in conductivity is explained by the lack of fiber-to-fiber contact (confirmed by optical micrographs) in boron/epoxy. Little dependence on frequency was observed for low frequency conductivities, however the high conductivity value obtained by Walker and Heintz at 2 GHz raises the possibility of significantly higher conductivities at frequencies higher than 50 MHz.

5.1.3.3 Graphite/Epoxy

Conductivity measurements have been performed on the epoxy resins and graphite fibers used in making graphite/epoxy as well as on the composite material itself. These results are presented in 5.1.3.3.1 - 5.1.3.3.3.

5.1.3.3.1 Graphite/Epoxy Fibers

The electrical characteristics of individual graphite fibers have been studied for one fiber type - Thornel T300 which is found in Narmco 5208 pre-preg tapes.^(2,4) Some variation in conductivities is to be expected in fibers produced by different companies.

The fiber tows were unwound and cleaned with solvent and mounted on glass slides. Ohmic contact was made with conductive ink. All fiber displayed linear V-I characteristics up to fields of 4000 volts/m. Non-

Table 5.6. Preliminary Conductivities for Multiply Boron/epoxy Composites from Allen. (6) (DC to 50 MHz)

PLIES	PLY ORIENTATION	CONDUCTIVITY (mbars/m)
7	0°, 0°, 0°, 90°	$\sigma_a = 25(a)$ $\sigma_{90} = 3.8(b)$
1-8	Unidirectional	$\sigma_L = 23(c)$ $\sigma_T = 2 \times 10^{-8}(d)$

- Corresponds to currents parallel to 0° fibers.
- Corresponds to currents parallel to 90° fibers.
- Corresponds to current longitudinal to fibers.
- Corresponds to currents transverse to fibers.

Table 5.7. Final Boron/epoxy Conductivities of Multiply Unidirectional Samples Together With An Average Conductivity From Gajda. (3)

PLIES	TRANSVERSE CONDUCTIVITY σ_T (mbars/m)
2	3300
5	1400
17	1400
20	1100

- This is the average conductivity found for unidirectional multi-ply samples.
- Value of conductivity for unidirectional samples at 2 GHz using standing wave techniques from Walker, McIntz. (5)

Table 5.9 Edge-to-Edge Resistivity of Graphite/epoxy as a Function of Ply Thickness at 1 kHz. (7)

PLY THICKNESS	EDGE-TO-EDGE RESISTIVITY ρ (ohms/m)
16	64.3×10^{-6}
32	55.7×10^{-6}

Table 5.8 Maximum, Minimum and Average Conductivities Found in a 60 Fiber Sample of Thermal T300 Fiber-type Taken From Maruco 5209 Pre-ply Types of Graphite/epoxy. (2,4)

	CONDUCTIVITY OF GRAPHITE FIBERS (mbars/m)
MINIMUM FOUND	1.4×10^{-4}
MAXIMUM FOUND	3×10^{-4}
AVERAGE	2×10^{-4}

Table 5.10 Volume Resistivity of Graphite/epoxy as a Function of Ply Thickness at 1 kHz. (7)

PLY THICKNESS	VOLUME RESISTIVITY ρ (ohm/m)
4	82×10^{-3}
16	51.2×10^{-3}
32	45.9×10^{-3}

linear characteristics were also observed and these results are given in Section 5.5 on nonlinear properties of composites. Conductivities of a 60 fiber sample are listed in Table 5.8. These results indicate that graphite fibers may be classed as reasonably good conductors with an average conductivity of 2×10^4 mhos/m. Fibers with conductivities of 2×10^5 mhos/m have also been reported.⁽⁹⁾ Because of their high conductivity, the permittivity of the graphite fibers could not be measured in the frequency range D.C. - 50 MHz. All measurements were done at D.C. but it was verified that the conductivities of graphite fibers are independent of frequency in the range D.C. - 50 MHz.

5.1.3.3.2 Epoxy Resins

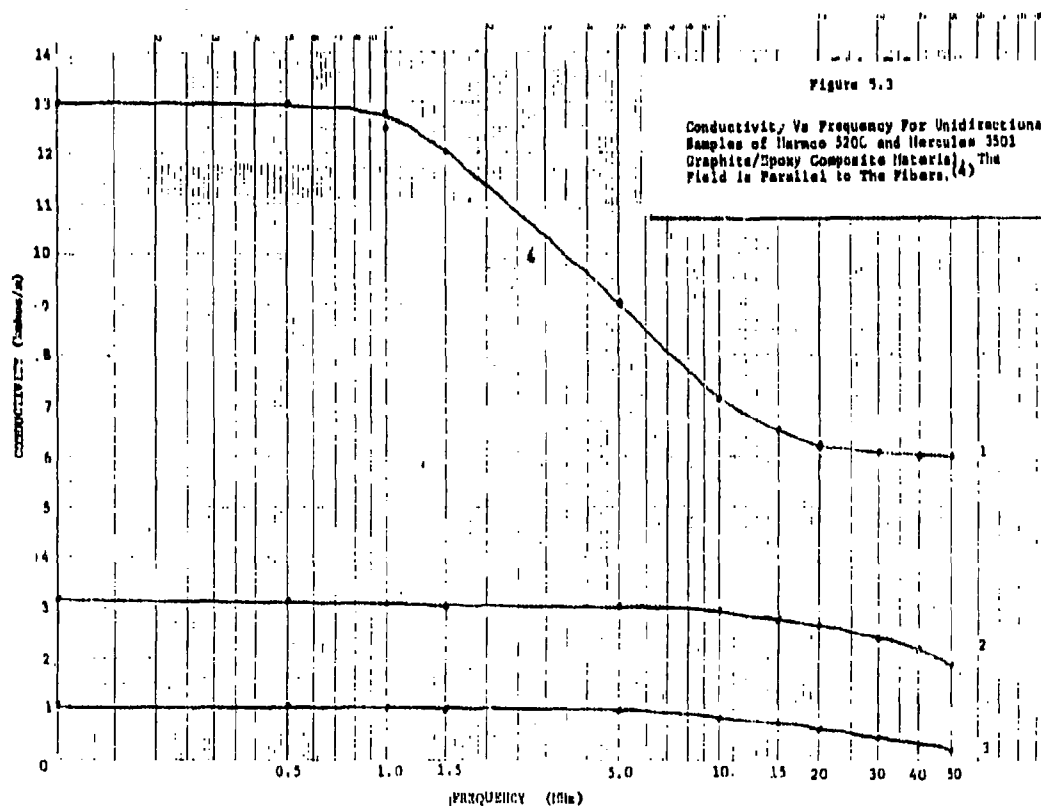
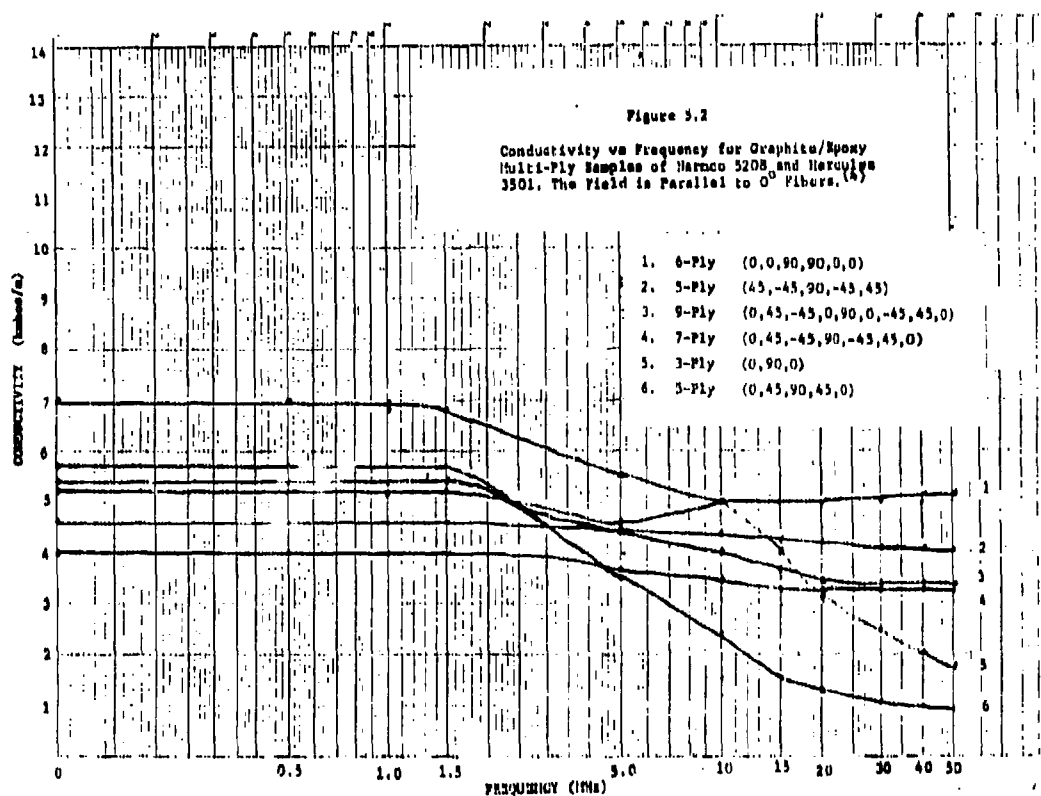
The resins used in graphite/epoxy had similar electrical permittivity and conductivity as was given for boron/epoxy resins. The permittivity is listed in Table 5.2 and the conductivity in Table 5.4.

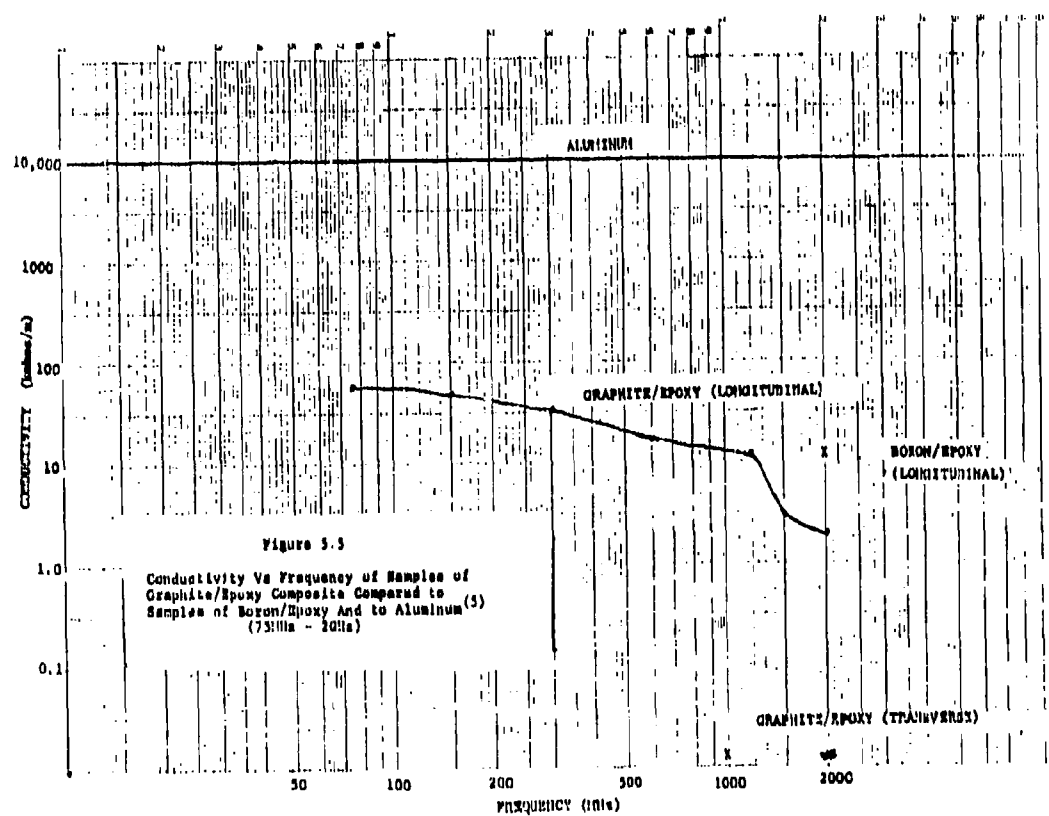
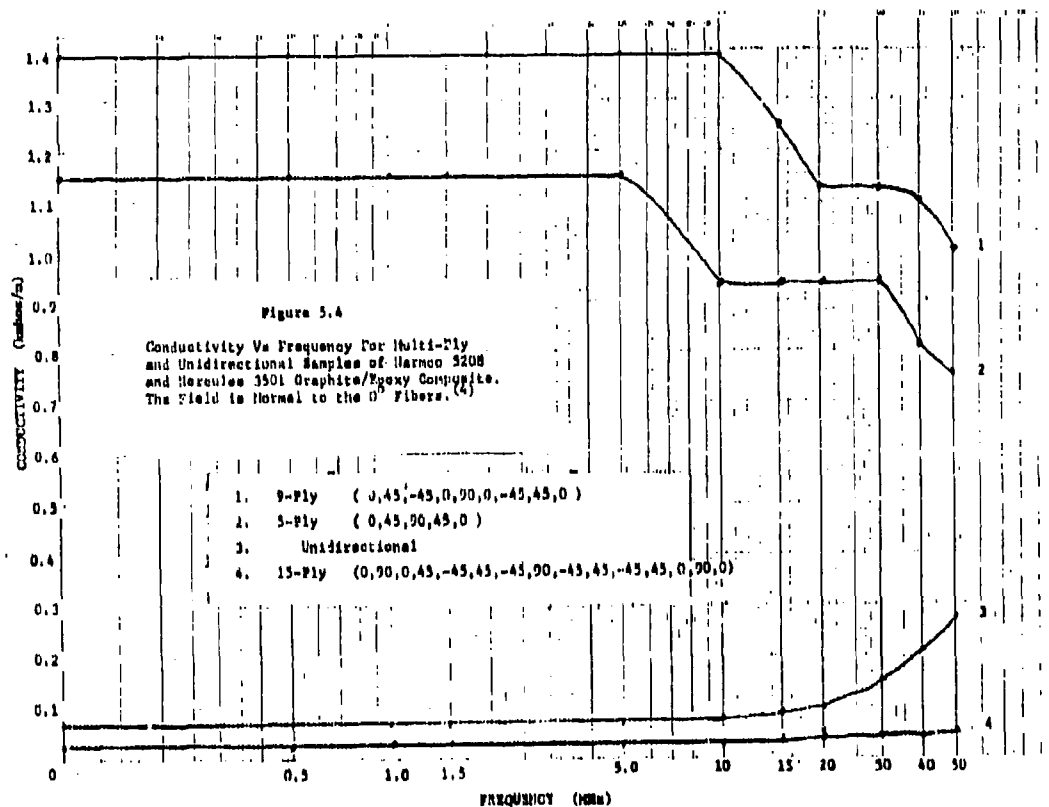
5.1.3.3.3 Graphite/Epoxy Composites

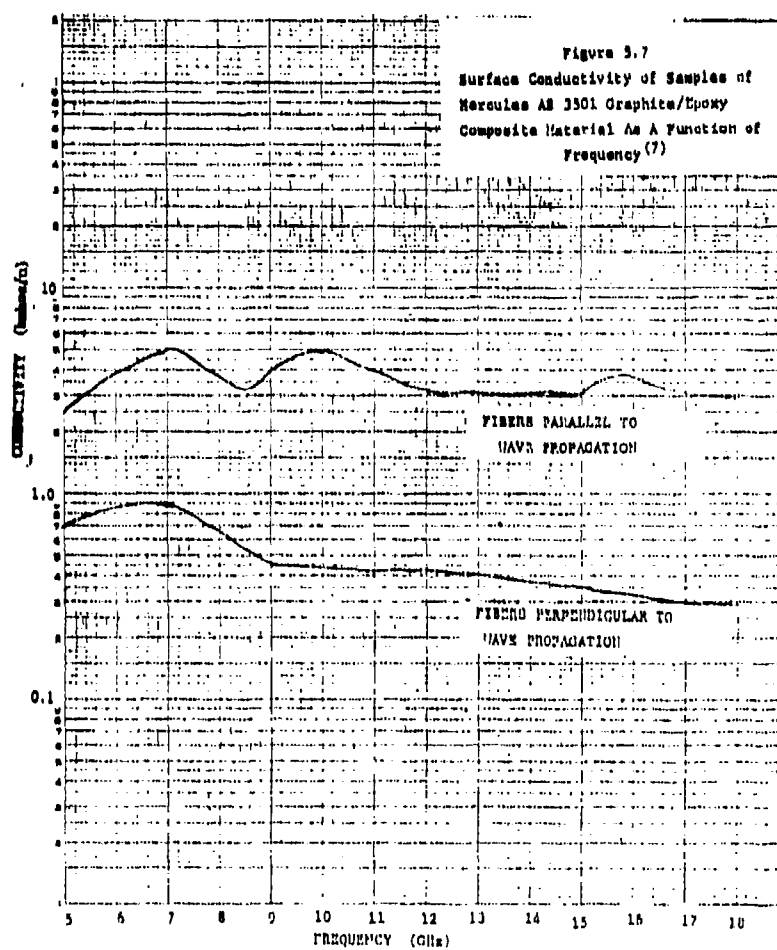
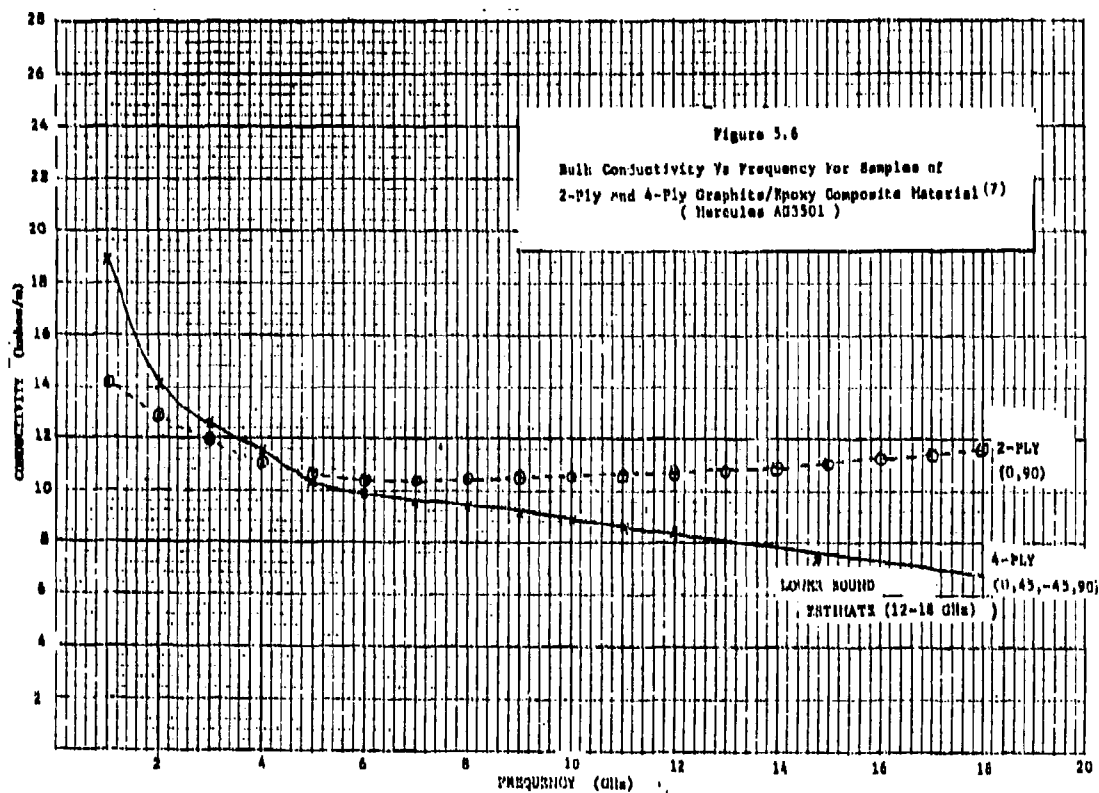
There have been several investigations into the conductivity of graphite/epoxy as a function of frequency. One set of measurements was done by Gajda⁽⁴⁾ in the frequency range D.C. - 50 MHz. The details of the measurement process are described in Section 9.0 Measurement, Test and Evaluation and in the references.^(4,6) The results are illustrated in Figures 5.2 - 5.4. Figure 5.2 is a plot of conductivity vs frequency for multiply laminates for the case of the existing field parallel to the 0° fibers. Figure 5.3 is a plot of conductivity vs frequency for unidirectional graphite/epoxy samples with the existing field parallel to the fibers. Figure 5.4 is a plot of conductivity vs frequency for multiply samples with the field normal to the 0° fibers. The conductivity for all samples is essentially constant below 5 MHz after which it may increase or decrease slightly. A combination of skin effect and inductive and capacitive coupling between fibers has been used to explain and model this effect.

Higher frequency conductivity data has been reported by Walker and Heintz⁽⁵⁾ for unidirectional samples of graphite/epoxy with the field parallel to the fibers. The measurement apparatus used was a slotted strip line with the conductivity being extracted from the standing wave data. Details are given in Section 9.0 on Measurement, Test and Evaluation and in the references.⁽⁵⁾ The results are plotted in Figure 5.5. Included for comparison are conductivities of aluminum, boron/epoxy and transverse conductivity of the graphite/epoxy at selected frequencies. All conductivities were computed by the same stripline method. These results are particularly important because these measurements are essentially free of the electrical contact ambiguities present in other measurements.

A further investigation of the conductivity of graphite/epoxy was undertaken by Boeing Corp.⁽⁷⁾ Boeing measured the free space transmission coefficients of 2-ply (0,90) and 4-ply (0,145,90) samples made from Hercules AS 3501-6B material over the frequency range 1.0 - 18 GHz. Measurements were taken using an anechoic chamber test system described in detail elsewhere.⁽⁷⁾ The transmission data was smoothed using least squares method and the conductivity extracted from the data using standard theory. The results are shown in Figure 5.6 for bulk conductivity (fields penetrating the material) and Figure 5.7 for surface conductivity (fields propagating parallel to the surface). Surface conductivity data was taken using waveguide methods.







All existing conductivity data indicates that graphite/epoxy is a good conductor even in the direction transverse to the fibers. The conductivity is nearly constant for low frequencies and generally decreases as the frequency increases. The relatively large value of the conductivity perpendicular to the fiber direction is a direct result of the high fiber-to-fiber contact (observable by optical micrograph) in graphite/epoxy composite. This contact is a consequence of the manufacturing process in which large numbers of individual fibers are wound together to make a tow which is then implanted in the composite.

5.1.4 Resistivity

A few limited measurements of the resistance of graphite/epoxy laminates have been reported by Boeing.⁽⁷⁾ All measurements were made at a frequency of 1 kHz.

The edge-to-edge resistivity of 16-ply and 32-ply laminates was measured with the results listed in Table 5.9. The epoxy surface coating was removed from the edges and copper contacts deposited by plating.

The volume resistivity of 4-ply, 16-ply and 32-ply laminates was also measured using a pressure contact method. The resistance was measured as a function of pressure until linear slope was obtained. Such a slope was presumed to indicate a good electrical contact. The resistance at zero pressure was then determined by extrapolation. The resulting resistivities are given in Table 5.10.

It proved impossible to uniquely define a surface resistivity at 1 kHz for the laminates used. At this frequency the skin depth or penetration of the radiation is far larger than the laminate thickness. All "surface" resistances are then actually volume resistances and show the expected increase in resistance with laminate thickness.

5.2 Improvement of Intrinsic Parameters

This section describes the methods currently in use to improve the EM performance of composite materials by changing the intrinsic properties of the composite. All methods fall under the general headings of doping of the composite fibers and intercalation of the composite layers. Most efforts to date have concentrated on increasing the composite conductivity in order to better approximate the properties of a metal. The basic constraint that must be observed in any method of changing the intrinsic EM properties of a composite is that the mechanical properties should not be degraded in the process. This immediately rules out increasing fiber-to-fiber contact in a composite to increase the conductivity because microbuckling in the composite will greatly increase and the mechanical strength will correspondingly decrease.⁽⁴⁾ Coating the fibers with metallic sheaths to increase conductivity and/or permeability is ruled out for similar reasons and for adding an unacceptable weight penalty. Other methods are required and are discussed in the following sections.

5.2.1 Doping

In semiconductor physics, doping is the process of adding carefully controlled amounts of impurities to certain semiconductor crystals in

order to increase electron and hole densities and/or mobilities. The conductivity will then be increased, possibly by many orders of magnitude. In the cases of graphite (crystallized carbon) and boron, their positions in the periodic chart of the elements makes them fairly good candidates for semiconductors. Some supporting evidence is available to support this statement.^(2,3)

However, most semiconductor activity depends on a high degree of crystalline order. While most details of the manufacturing process of composite fibers are not available, most fibers are not ordered crystals and consequently conductivity improvements by doping techniques can be expected to be less than for crystalline semiconductors. More attention could be given to the fiber manufacturing process in order to optimize the efficiency of the doping process.

A thermal diffusion process was investigated by Gajda⁽²⁾ to assess in a preliminary manner the effects of doping on graphite and boron fibers. The details of the diffusion process are described in Section 9.0 on Measurements, Testing and Evaluation and in the references.⁽²⁾

One set of experiments involved using borosilicate compounds and boron nitride (BN) as the impurity for graphite fibers. The semiconductor process is the doping of graphite with boron. The experiments were carried out at temperatures up to 1200°C and for as long as 20 hours. A second set of experiments using improved equipment was performed at a temperature of 2800°C. The results are shown in Figure 5.8.

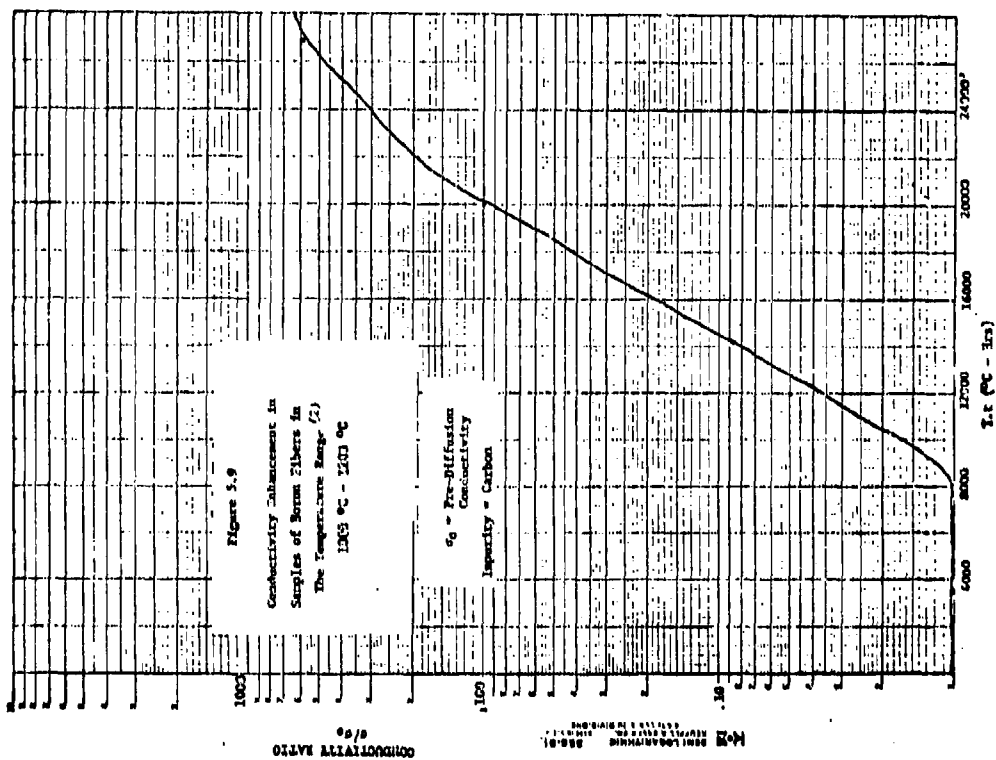
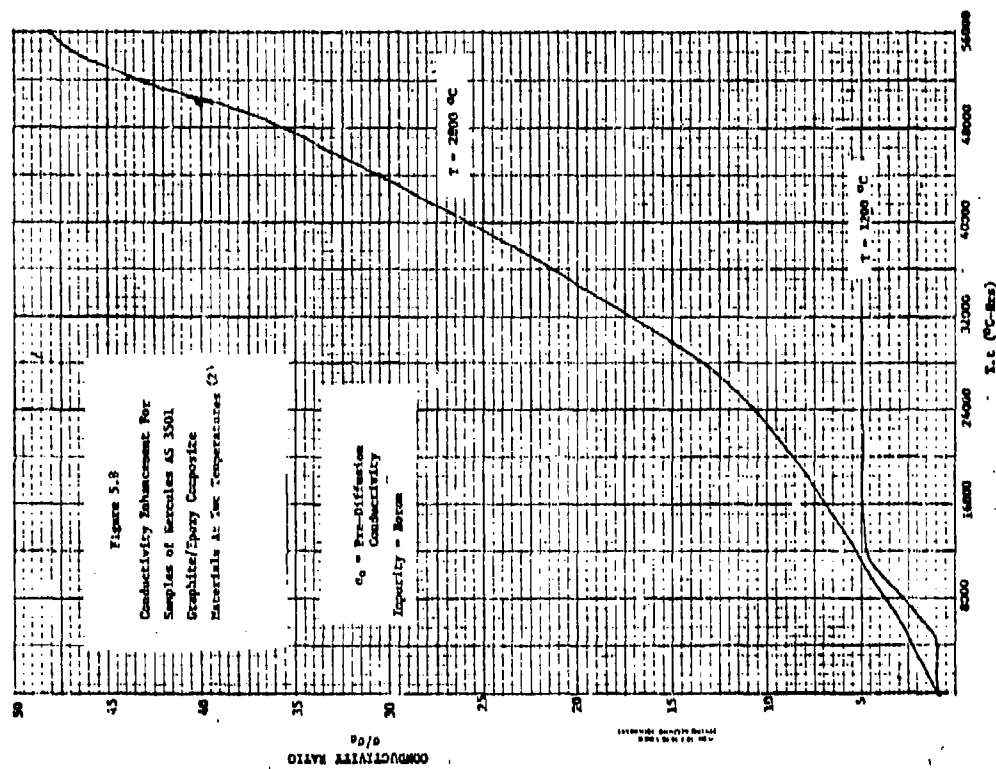
For the lower temperature case, conductivities were not increased more than a factor of five even after 20 hours of baking in the diffusion oven. At the higher temperature conductivity increased by a factor of 50 with some fiber conductivities reading 10^6 mhos/m.

Only a few experiments were done with boron doped with carbon due to the difficulties with proper ohmic contacts. The first experiments were run at 1000° - 1200°C for up to 20 hours. The results are given in Figure 5.9 and show significant increases in conductivity.

5.2.2 Intercalation⁽⁸⁻¹⁰⁾

One procedure that holds great promise for increasing the conductivity of graphite/epoxy composite is the intercalation of graphite fibers with various metallic or nonmetallic molecular species. The intercalation process is very much dependent for its success upon the physical and chemical properties of graphite.

Pure graphite is a crystallized form of carbon whose crystal structure is shown in Figure 5.10. All the carbon atoms are hexagonally packed into individual planar layers. The intraplane chemical bonds holding the carbon atoms in a given plane are sp^2 hybridized σ -type bonds and are quite strong. These bonds give the planar layer a high degree of stability and order. The various carbon planes are then stacked on top of each other in an ABAB...sequence as shown in Figure 5.10. The interplane chemical bonds holding the carbon planes together are π -type bonds and are weak compared to the intraplane σ -bonds. Because the interplane bonds are weak, it is possible to insert various chemical species between the carbon layers



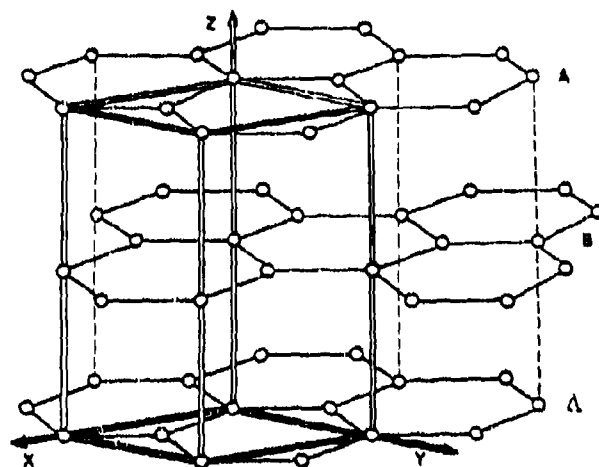


Figure 5.10 Graphite Crystal Structure⁽⁸⁾

to form what are called intercalation compounds. The composition of these compounds is described by stage, the definition of which is portrayed in Figure 5.11.

The molecular species used in the intercalation process are characterized as electron donors or acceptors. Donors are typically metals usually from Group I in the periodic table (the alkali metals). Common choices are potassium, cesium, rubidium and lithium. In addition, many additional compounds that also act as donors can be formed from these metals together with hydrogen and aromatic molecules such as benzene and toluene. Acceptors are usually nonmetallic compounds such as bromine, sulphuric acid, nitric acid and halide and oxide compounds. The intercalation of the graphite fibers is easily accomplished by simple exposure of the fibers to the liquid or vapor of the intercalant.

A list of conductivities for selected acceptor and donor intercalated graphite compounds is given in Table 5.11 together with the conductivities of pur graphite and various metal conductors. Compared to graphite, donor intercalated graphite increased the interplane conductivity by a factor of six to eight while for acceptor intercalated graphite, the increase was a factor of fifteen or more. Intraplane conductivities are increased for donor compounds and decreased for acceptor compounds. Conductivities of acceptor intercalated graphite are comparable and even superior to conductivities of copper, aluminum and silver.

Less dramatic results are obtained when commercially available graphite fiber is intercalated because the conductivity of such fibers is one to two orders of magnitude below the intraplane conductivity of pure graphite (see Table 5.8). The fiber may be viewed as a highly defective graphite crystal having lower electron mobility and hence lower conductivity. Conductivities of typical 3-ply graphite/epoxy laminates with and without intercalated fibers are shown in Figure 5.12 as a function of fiber content. For a given fiber filling factor, the intercalated composite is about a factor of twenty to forty times higher than the regular composite. These results suggest that more attention should be given to the manufacturing process of graphite fibers to attain as high a conducting fiber as possible.

An important tradeoff to be considered is the effect of intercalation on the graphite/epoxy mechanical properties. Reports of no decrease and significant decrease in tensile strength and elastic modulus have been made in the literature (9) depending on the intercalation process used. It is also possible to enhance certain mechanical properties. Table 5.12 shows the results of intercalating Thornel 75 graphite/fibers with red, fuming nitric acid (HNO_3). There was a 17% average decrease in tensile strength and a 69% average increase in elastic modulus. The tensile strength is sensitive to micro defects in the fibers which act as concentrators of stress. Fuming, red nitric acid etches out surface impurities leaving voids in the fiber which act as defects. The elastic modulus is sensitive to the crystal perfection. Intercalation serves to reorder the ABAB...graphite crystal pattern to AAA...on either side of the intercalated layer. The result is a greater crystal perfection and a higher modulus.

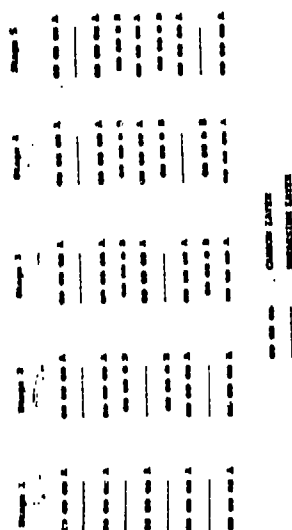
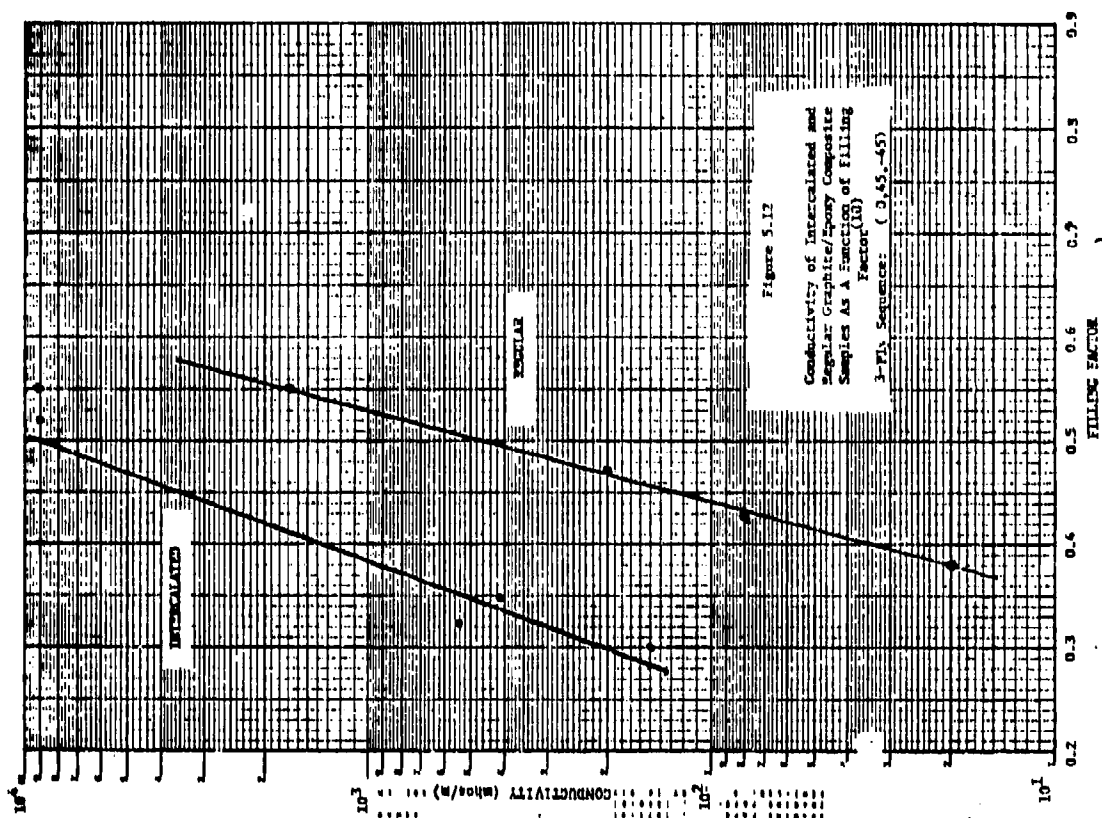


Table 3.11 Conductivities of Selected Donor and Acceptor Intercalated Graphite Compounds Compared to Pure Graphite and Common Metals⁽⁸⁾

Compound and Stage	Interplane Conductivity σ_p (mhos/m)	Intraplane Conductivity σ_a (mhos/m)
Donor Intercalated Compounds		
K-1	1.1×10^7	
2	1.7×10^7	
3	2.1×10^7	
Rb-1	1.0×10^7	Range of Values for Donor Compounds is 10^3 - 10^4
2	1.3×10^7	
Cs-1	1.0×10^7	
3	1.2×10^7	
Li-1	1.0×10^7	
Acceptor Intercalated Compounds		
HNO_3 -1	1.7×10^7	200
2	3.3×10^7	-
3	2.9×10^7	-
4	2.4×10^7	-
AsF_5 -1	3.0×10^7	23
2	6.3×10^7	24
3	5.8×10^7	26
SbF_5 -1	3.5×10^7	-
2	4.0×10^7	-
3	1.0×10^7	-
6	5.8×10^7	-
FeCl_3 -1	1.1×10^7	1000
2	2.3×10^7	-
Common Conductors		
Copper	5.9×10^7	-
Aluminum	3.8×10^7	-
Silver	6.3×10^7	-
Pure Graphite	2.6×10^6	10-1000

Table 3.12 Changes in Mechanical Properties of Thermal 75 Graphite Fibers after Intercalation with HNO_3 ⁽⁹⁾

Sample	Conductivity (mhos/m)		Tensile Strength (psi)		Modulus (psi)	
	Initial	Final	Initial	Final	Initial	Final
1.	1.3×10^5	1.4×10^6	4.3×10^5	2.3×10^5	82×10^6	99×10^6
2.	1.7×10^5	1.3×10^6	4.0×10^5	3.8×10^5	65×10^6	108×10^6
3.	1.5×10^5	1.1×10^6	2.6×10^5	2.3×10^5	42×10^6	92×10^6

5.3 Thermal Modification of EM Intrinsic Parameters

A preliminary investigation on the temperature dependence of conductivity has been done by Gajda.⁽²⁾ No work on the temperature dependence of the permittivity or permeability has been found.

5.3.1 Conductivity

Since graphite and boron display semiconductor behavior to some extent, it is useful to display a conductivity vs. temperature curve for a typical semiconductor. Such a curve is shown in Figure 5.13 and is composed of three regions: intrinsic, extrinsic and freeze out. In the intrinsic region, the thermally generated charge carriers are large in number compared to the carriers of the impurity. There is an exponential dependence on the reciprocal of the absolute temperature. The extrinsic region is characterized by the thermal charge carriers being few compared to the impurity charge carriers. The freeze-out region begins typically at 100° and is not considered significant.

Preliminary studies were made with boron fibers whose resistance was measured as a function of temperature. In terms of resistance R, the conductivity σ is given by

$$R = \frac{V}{\sigma} \quad (5.4)$$

where V depends on the fiber geometry and is essentially constant (neglecting thermal expansion effects). The results are shown in Figure 5.14 and show boron to be in the intrinsic range.

5.4 Environmental Modification of EM Intrinsic Parameters

A limited investigation⁽²⁾ of the effects of moisture on the EM properties of composite materials is given in this section.

5.4.1 Moisture

Because of the anticipated exposure of composites to high temperatures and high humidities (e.g., in tropical environments), it is important that the effects of moisture on composites be studied. Most moisture studies have been concerned with its effect on the mechanical properties. One study of the effects of moisture on conductivity of composites has been done by Gajda.⁽²⁾

Samples of Kevlar/epoxy, boron/epoxy and graphite/epoxy were immersed in distilled, deionized water for up to 40 days (to simulate a "worst case" humidity) and their conductivities measured. No changes in Kevlar/epoxy or boron/epoxy were found for any direction of the current. For unidirectional samples of graphite/epoxy (the only samples measured) changes in conductivity were found to occur only in the transverse direction. There was a fairly large decrease in conductivity found and the results are shown in Figure 5.15. One possible explanation for this behavior is that the major mechanical effect of the absorbed water is expansion of the epoxy and a reduction in fiber-to-fiber contact. The transverse conductivity thus decreases.

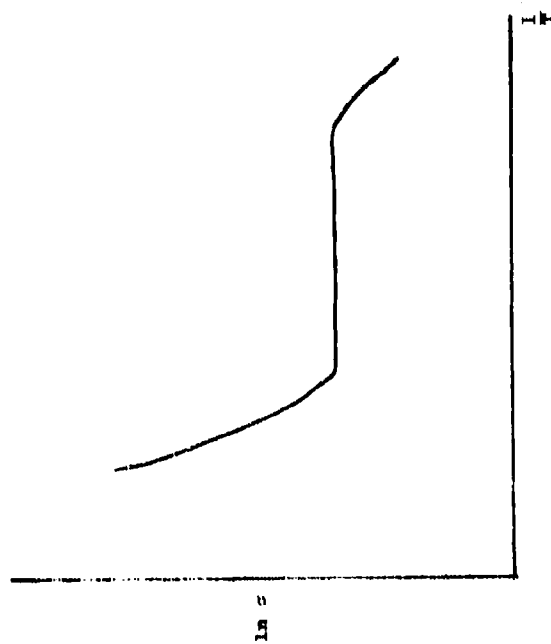


Figure 5.15 Typical Conductivity-Temperature Profile for a Semiconductor(2)

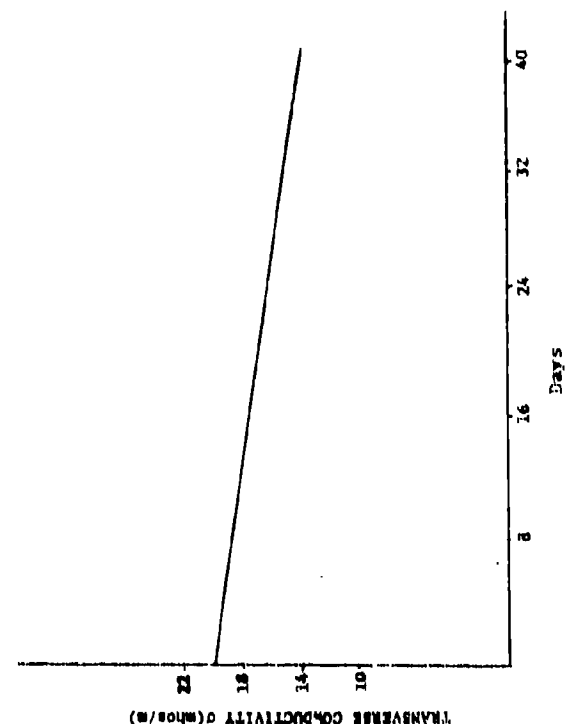


Figure 5.16 Transverse Conductivity of Graphite/epoxy (Unidirectional) as a Function of Immersion Time in Water at 73°C.

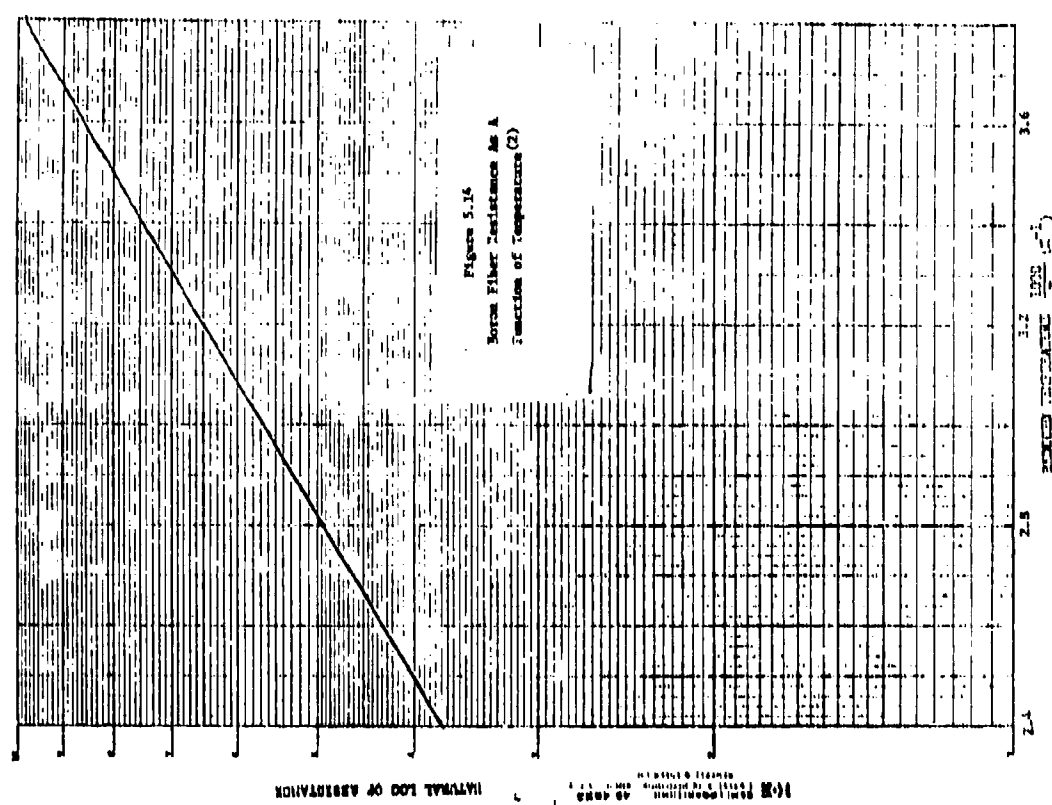


Figure 5.16 Boron Fiber Resistance As A Function of Temperature (2)

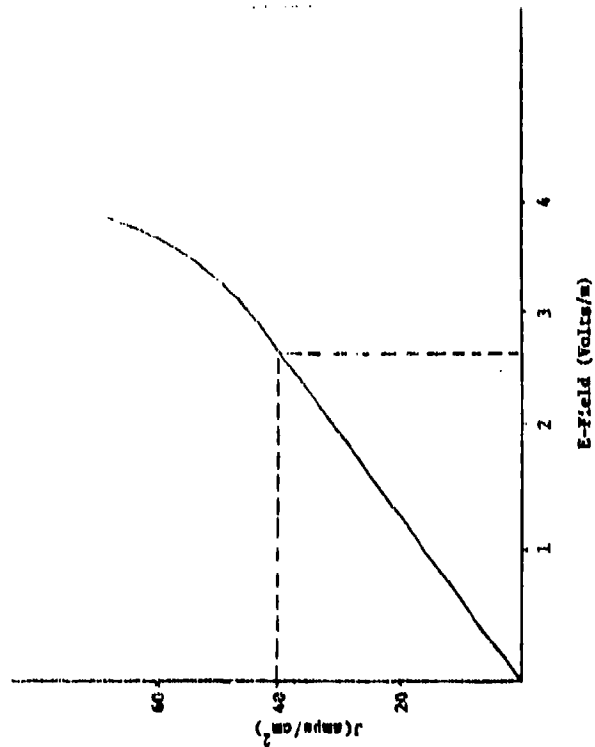


Figure 5.16 Current-field Characteristics for Unidirectional Unidirectional Graphite/epoxy in Longitudinal Direction (2.4)

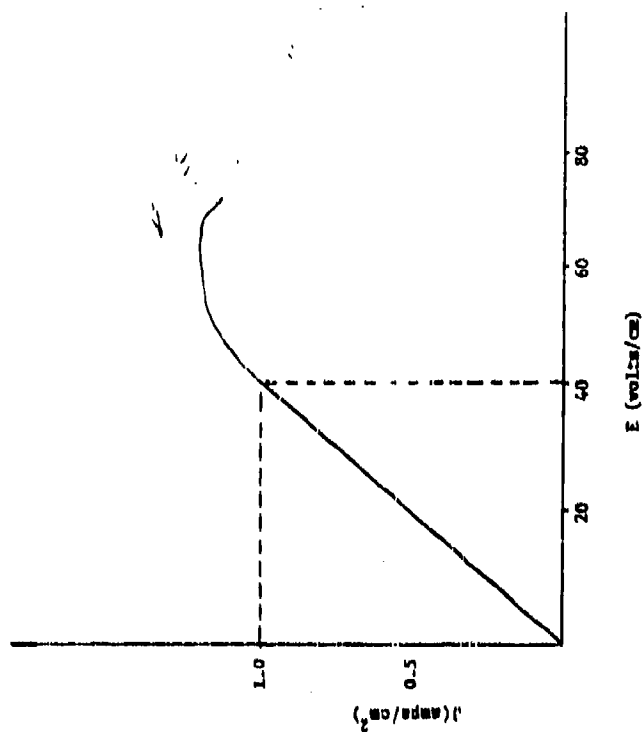


Figure 5.17 Current-field Characteristics for unidirectional unidirectional graphite/epoxy in transverse direction (2.4)

Table 5.13 Nonlinear Thresholds for Unidirectional Unidirectional Graphite/epoxy (2)

CURRENT DIRECTION	E-FIELD (VOLTS/m)	J (AMPS/m²) CURRENT DENSITY
LONGITUDINAL	250	4×10^5
TRANSVERSE	4000	1×10^4

5.5 Nonlinear Effects

A limited investigation on high field conductivities of graphite/epoxy is given in this section.

5.5.1 High-Field Effects

Nonlinear thresholds for unidirectional samples of Narmco 5213 single ply laminates have been determined at D.C. The voltage-current characteristics were determined in the longitudinal and transverse directions. All current was confined to the surface. The voltage-current characteristics are given in Figures 5.16 and 5.17 while the nonlinear thresholds are listed in Table 5.13. In the longitudinal case, the current is linear up to the threshold at which time the current is greater than a linear response. In the transverse case the current is less than a linear response after the threshold is passed. The transverse nonlinearity is explained as local ohmic heating causing a decrease in fiber-to-fiber contact and a subsequent drop in conductance. No explanation is available for the longitudinal nonlinearity.

5.6 References

1. G. Dike et.al., Electromagnetic Relationships Between Shielding Effectiveness and Transfer Impedance, IEEE EMC Symposium, October 1979.
2. W. J. Gajda, A Fundamental Study of the Electromagnetic Properties of Advanced Composite Materials, RADC-TR-78-158.
3. W. J. Gajda, Measurement of the Electrical Properties of Composite Materials in the Frequency Range of D.C. to 30 MHz.
4. J. L. Allen et.al., Electromagnetic Properties and Effects of Advanced Composite Materials: Measurement and Modeling, RADC-TR-78-156, June 1978.
5. W. F. Walker and Roger E. Heintz, Measurement of Electrical Conductivity in Carbon/Epoxy Composite Material Over the Frequency Range >5 to 2.0 GHz, RADC-TR-79-255, October 1979.
6. A Technology Plan for Electromagnetic Characteristics of Advanced Composites, RADC-TR-76-206, July 1976.
7. R. Force, P. Green et.al., Investigation of Effects of Electromagnetic Energy on Advanced Composite Aircraft Structures and Their Associated Avionic/Electrical Equipment, Phase II, Vol. I Boeing Aircraft Corp. (D180-20186-4), September 1977.
8. Vogel, F. L., Intercalation Compounds of Graphite, Molecular Metals, Plenum Publishing Co., 1979.
9. Vogel, F. L., Carbon, 14, 175 (1976).
10. Vogel, F. L., Some Potential Applications for Intercalation Compounds of Graphite with High Electric Conductivity (to be published).

6.0 EXTERNAL-TO-INTERNAL COUPLING

In this chapter, electromagnetic shielding by advanced composite materials is presented in detail from both a theoretical and measurement point of view. The shielding data is presented for both low and high frequency situations.

A brief theoretical discussion of joint and aperture coupling is also presented along with measured joint admittance for three common composite joints.

6.1 Airframe Shielding Effectiveness

In this section, the shielding effectiveness to be expected from composite airframes is presented both in theory and with measured values from composite structures. A general theory of shielding is given in Section 6.1.1 for very general composite structures. Section 6.1.2 then presents measured values for shielding effectiveness. Finally a brief discussion is given on composite and metallic weight-shielding tradeoffs.

6.1.1 Shielding Effectiveness - Theoretical Considerations

Composite airframes, equipment boxes, etc., generally afford less EM shielding than do their metal counterparts. The shielding effectiveness of composite enclosures is generally a function of enclosure shape and internal complexity (e.g., devices, tables, support structures) as well as the composite thickness, and constitutive parameters, and frequency and direction of excitation and source location and type. In this section a general discussion of shielding effectiveness for composite airframes is presented.

Shielding effectiveness, for plane wave penetration of an infinite flat, isotropic, homogeneous material with identical media on either side, has been defined by Schelkunoff as (1,2)

$$S = -20 \log|T| \quad (6-1)$$

where T is the normal incidence transmission coefficient derived by Schelkunoff from analogy with transmission line theory as

$$T = \frac{4\bar{n}}{(\bar{n}+1)^2} \left(1 - \frac{(\bar{n}-1)^2}{(\bar{n}+1)^2} e^{-2\gamma d}\right)^{-1} e^{-\gamma d} \quad (6-2)$$

where

$$\bar{n} = n/\eta_0 \text{ or } \eta_0/n$$

η = wave impedance in shield

η_0 = free space wave impedance either side of shield

γ = complex propagation constant of shield ($\gamma = jk$ where k is the complex wavenumber of shield)

d = shield thickness

Schelkunoff also considered shields composed of n cascaded homogeneous layers of differing material.(2)

Equation (6-1) with T given by (6-2) has been shown by Moser⁽¹⁾ and Bannister⁽³⁾ to yield good agreement with both experiment and an approximate vector wave equation solution for the low frequency shielding effectiveness of a highly conducting shield excited and observed by uniform current source loops as shown in Figure 6.1. For this agreement, $\eta_0 = j\omega\mu_0 z/3$ where ω is the radian frequency and μ_0 is the free space permeability, $z \ll d$, $z \gg a$, $z \ll \lambda_{\text{air}}$, d , must exceed two shield skin depths, and z must exceed 10 times the shields skin depth divided by its relative permeability.

At higher frequencies a source field often can be decomposed into a relatively few significant plane waves, and transmission analysis performed on each component wave in assessing shielding effectiveness.

Relations predicting plane wave transmission through planar composite shields, therefore, are highly useful. It is desirable that these relations apply to oblique incidence excitation and shields composed of layers of homogeneous anisotropic material. These relations are derived in the following section in a general transmission parameter framework. The transmission parameters are defined below in Section 6.1.1.2 (Equation 6-11) and provide the transmission coefficient T , as defined above, immediately as

$$T = T_1^{21} - \frac{T_1^{21} T_1^{12}}{T_1^{22}}$$

Since $T_1^{12} = -T_1^{21}$ and it can be shown that $T_1^{11} T_1^{22} + (T_1^{12})^2 = 1$

it follows that

$$T = \frac{1}{T_1^{22}}$$

and, from (6-1)

$$S = +20 \log |T_1^{22}|$$

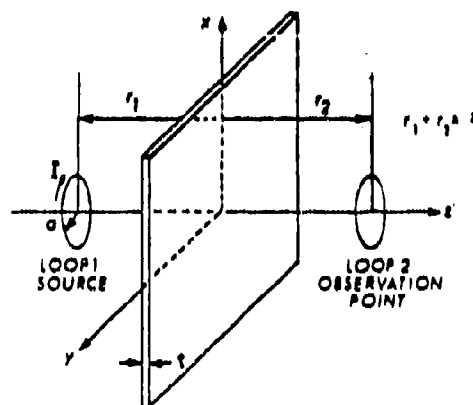


Fig. 6.1 Coaxial loops separated by an infinite plate.

Fig. 6.1. Coaxial Loops Separated By An Infinite Plate.

6.1.1.1 Plane Wave Excitation of Cascaded Composite Layers

Plane wave penetration through and reflection from homogeneous layers of composite material will be analyzed in this section. The layers are of varying thickness in the cascaded dimension. Each layer is homogeneous; however, the constitutive parameters and thicknesses may differ between layers. Expressions are derived for anisotropic layers as well as for isotropic layers and for oblique incidence excitation as well as for normal incidence excitation.

The transmission parameters (4) are employed because they lead naturally to a cascading of any number of layers and because they deal directly with incident and scattered E-fields rather than total E- and H-fields. Allen, et.al., (5) derived equivalent expressions in a less direct manner using the ABCD chain parameters for the cascading property and transforming the overall ABCD parameters, relating total E- and H-fields on either side of the multilayer composite, to scattering parameters. The isotropic case and anisotropic/normal incidence case are considered in Reference (5); the anisotropic/oblique incidence case will be treated in a later report (6). The transmission parameter treatment reported here is similar to that of Collin. (7)

6.1.1.2 Isotropic Layers/Normal Incidence

A homogeneous, isotropic composite layer of infinite extent in the x and y directions and width d in the z direction is shown in Figure 6.2. The medium conductivity σ , permittivity ϵ , and permeability μ are related to the medium complex wave number k_1 and complex wave impedance η_1 by

$$k_1 = \sqrt{-(j\omega\mu)(\sigma + j\omega\epsilon)} \quad (6-3)$$

$$\eta_1 = \sqrt{\frac{j\omega\mu}{\sigma + j\omega\epsilon}} \quad (6-4)$$

where ω is the radian frequency.

The field quantity superscripts i or r denote "incident" or "reflected" respectively. The field quantity subscripts a, b, or l denote that the field medium is free space to the "left" of the composite ($z < 0$), is free space to the "right" of the composite ($z > d$), or the composite ($0 < z < d$) respectively. The subscript 0 or 1 on media quantities ($k, \eta, \epsilon, \mu, \sigma$) denote "free space" or "composite" respectively. The E-fields are given by

$$\left. \begin{aligned} \vec{H}_a^i &= A_a^i e^{-jk_0 z} \hat{x} \\ \vec{H}_a^r &= A_a^r e^{jk_0 z} \hat{x} \end{aligned} \right\} \text{Region a} \quad (6-5)$$

$$\left. \begin{aligned} \vec{H}_b^r &= A_b^r e^{-jk_0(z-d)} \hat{x} \\ \vec{H}_b^i &= A_b^i e^{jk_0(z-d)} \hat{x} \end{aligned} \right\} \text{Region b} \quad (6-6)$$

$$\left. \begin{aligned} \vec{H}_1^i &= A_1^i e^{-jk_1 z} \hat{x} \\ \vec{H}_1^r &= A_1^r e^{jk_1 z} \hat{x} \end{aligned} \right\} \begin{array}{l} \text{Composite} \\ \text{(Region 1)} \end{array} \quad (6-7)$$

where " $\hat{}$ " indicates "unit vector." The corresponding H-fields that satisfy the source free Maxwell equations are

$$\left. \begin{aligned} \vec{H}_a^i &= \frac{1}{\eta_0} A_a^i e^{-jk_0 z} \hat{y} \\ \vec{H}_a^r &= \frac{-1}{\eta_0} A_a^r e^{jk_0 z} \hat{y} \end{aligned} \right\} \text{Region a} \quad (6-8)$$

$$\left. \begin{aligned} \vec{H}_b^r &= \frac{1}{\eta_0} A_b^r e^{-jk_0(z-d)} \hat{y} \\ \vec{H}_b^i &= \frac{-1}{\eta_0} A_b^i e^{jk_0(z-d)} \hat{y} \end{aligned} \right\} \text{Region b} \quad (6-9)$$

$$\left. \begin{aligned} \vec{H}_1^i &= \frac{1}{\eta_1} A_1^i e^{-jk_1 z} \hat{y} \\ \vec{H}_1^r &= \frac{-1}{\eta_1} A_1^r e^{jk_1 z} \hat{y} \end{aligned} \right\} \begin{array}{l} \text{Composite} \\ \text{(Region 1)} \end{array} \quad (6-10)$$

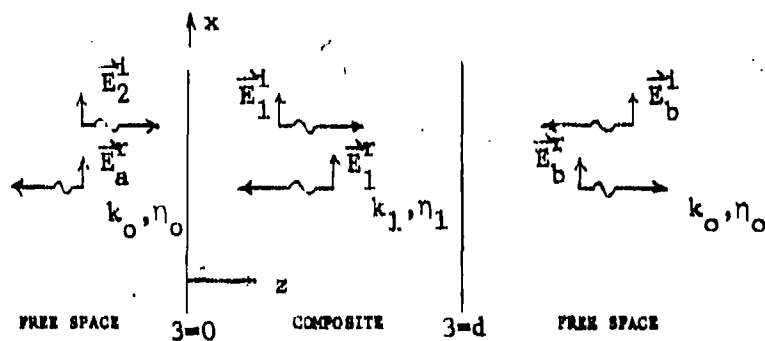


Figure 6.2 Normal Incidence of a Single Isotropic Composite Layer

where the y coordinate direction is given, as usual, by $\hat{y} = \hat{z} \times \hat{x}$ ("out of the page" in Figure 6.2).

The boundary conditions at $z = 0$ and $z = d$ are continuity of total tangential E- and H-fields. In combination with (6-5) - (6-10) these conditions yield the matrix equation

$$\begin{bmatrix} A_b^r \\ A_b^i \end{bmatrix} = \begin{bmatrix} T_1^{11} & T_1^{12} \\ T_1^{21} & T_1^{22} \end{bmatrix} \begin{bmatrix} A_a^i \\ A_a^r \end{bmatrix} \quad (6-11)$$

relating A_b and A_a coefficients. In (6-11), the "transmission coefficients" T_1 are given by

$$\begin{aligned} T_1^{11} &= \frac{(1+\bar{n}_1)^2}{4\bar{n}_1} [e^{-jk_1d} - \frac{(1-\bar{n}_1)^2}{(1+\bar{n}_1)^2} e^{jk_1d}] \\ T_1^{12} &= \frac{(1-\bar{n}_1)^2}{4\bar{n}_1} (e^{-jk_1d} - e^{jk_1d}) \\ T_1^{21} &= -T_1^{12} \\ T_1^{22} &= \frac{(1+\bar{n}_1)^2}{4\bar{n}_1} [e^{jk_1d} - \frac{(1-\bar{n}_1)^2}{(1+\bar{n}_1)^2} e^{-jk_1d}] \end{aligned} \quad (6-12)$$

with

$$\bar{n}_1 = n_1/n_0$$

Consider a second composite layer located in the $z > d$ region. The field incident on this second layer is \bar{E}_b^i and the field reflected is \bar{E}_b^r . This natural "cascading" trait is why A_b^r is ordered ahead of A_b^i in (6-11). From (6-5), (6-6), and (6-11), it is immediately apparent that for the cascading of n isotropic composite layers between $z=0$ and $z=d$ (Figure 6.3) the Region a and Region b fields are given by (6-5), (6-6), (6-8) and (6-9) where

$$\begin{bmatrix} A_b^r \\ A_b^i \end{bmatrix} = \left(\prod_{i=1}^n \begin{bmatrix} T_i^{11} & T_i^{12} \\ T_i^{21} & T_i^{22} \end{bmatrix} \right) \begin{bmatrix} A_a^i \\ A_a^r \end{bmatrix} \quad (6-13)$$

The i^{th} layer transmission parameters T_i in (6-13) are given by

$$T_i^{11} = \frac{(1+\bar{n}_i)^2}{4\bar{n}_i} [e^{-jk_i d_i} - \frac{(1-\bar{n}_i)^2}{(1+\bar{n}_i)^2} e^{jk_i d_i}] \quad (6-14)$$

$$T_i^{12} = \frac{(1-\bar{n}_i^2)}{4\bar{n}_i} [e^{-jk_i d_i} - e^{jk_i d_i}]$$

$$T_i^{21} = -T_i^{12}$$

$$T_i^{22} = \frac{(1+\bar{n}_i)^2}{4\bar{n}_i} [e^{jk_i d_i} - \frac{(1-\bar{n}_i)^2}{(1+\bar{n}_i)^2} e^{-jk_i d_i}]$$

where $\bar{n}_i = n_i/n_0$.

where

6.1.1.3 Isotropic Layers/Oblique Incidence

The transmitted and reflected fields excited by plane waves obliquely incident on a planar, isotropic medium are analyzed by decomposing all fields into two decoupled "modal" fields. Let the normal to the medium and the propagation direction of the incident wave form the "incidence plane" (plane of the paper in Figure 6-4). One mode is characterized as having an H-field normal to the incidence plane and the other as having an E-field normal to the incidence plane. All obliquely incident fields can be analyzed by decomposition into these two modes. Each modal component can be analyzed separately (they "decouple") only for isotropic media in general.

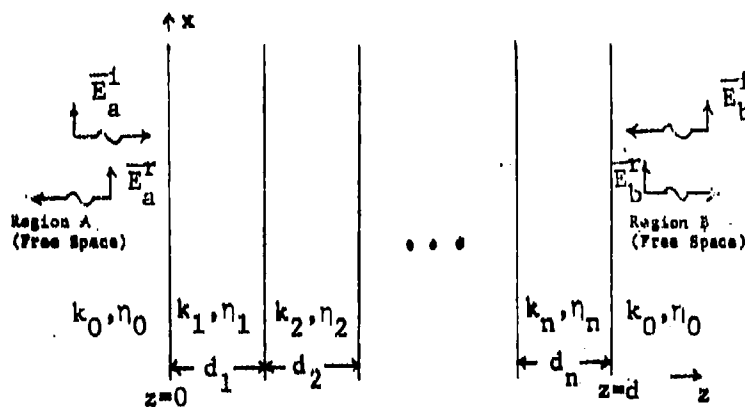


Figure 6.3 Normal Incidence Excitation of n Isotropic Composite Layers.

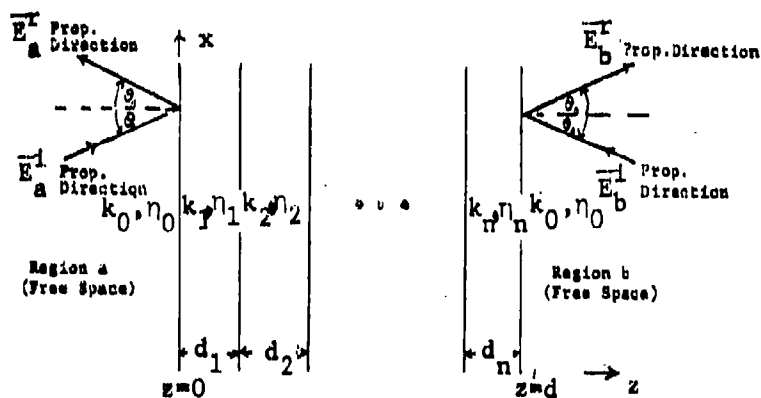


Figure 6.4 Oblique Incidence Excitation of n Isotropic Composite Layers.

6.1.1.3.1 H-Field Normal

The E-fields incident and reflected on the layered composite of Figure 6-4 are, for the H-field normal to incidence plane mode, given by

$$\vec{E}_a^i = A_a^i e^{-jk_0 z \cos \theta_0} e^{-jk_0 x \sin \theta_0} (\cos \theta_0 \hat{x} - \sin \theta_0 \hat{z}) \quad (6-15)$$

$$\vec{E}_a^r = A_a^r e^{jk_0 z \cos \theta_0} e^{-jk_0 x \sin \theta_0} (\cos \theta_0 \hat{x} + \sin \theta_0 \hat{z})$$

for $z < 0$ (Region a) and by

$$\vec{E}_b^r = A_b^r e^{-jk_0(z-d) \cos \theta_0} e^{-jk_0 x \sin \theta_0} (\cos \theta_0 \hat{x} - \sin \theta_0 \hat{z}) \quad (6-16)$$

$$\vec{E}_b^i = A_b^i e^{jk_0(z-d) \cos \theta_0} e^{-jk_0 x \sin \theta_0} (\cos \theta_0 \hat{x} + \sin \theta_0 \hat{z})$$

for $z > d$ (Region b). The fields in each composite layer are constrained to having the same x variation. Then, the boundary condition of continuity of tangential components of total E-field and total H-field across each interface boundary, and the cascading property of the transmission parameters yields (6-13) with the i th layer transmission parameters T_i now given by

$$\begin{aligned} T_{i11} &= \frac{(1 + \bar{n}_i v_i)^2}{4 \bar{n}_i v_i} (e^{-jk_i d_i \cos \theta_i} - \frac{(1 - \bar{n}_i v_i)^2}{(1 + \bar{n}_i v_i)^2} e^{jk_i d_i \cos \theta_i}) \\ T_{i12} &= \frac{1 - (\bar{n}_i v_i)^2}{4 \bar{n}_i v_i} (e^{-jk_i d_i \cos \theta_i} - e^{jk_i d_i \cos \theta_i}) \\ T_{i21} &= -T_{i12} \\ T_{i22} &= \frac{(1 + \bar{n}_i v_i)^2}{4 \bar{n}_i v_i} (e^{jk_i d_i \cos \theta_i} - \frac{(1 - \bar{n}_i v_i)^2}{(1 + \bar{n}_i v_i)^2} e^{-jk_i d_i \cos \theta_i}) \end{aligned} \quad (6-17)$$

In (6-17)

$$\theta_i = \sin^{-1} \left(\frac{k_0}{k_i} \sin \theta_0 \right)$$

$$\bar{n}_i = n_i / n_0$$

$$v_i = \frac{\cos \theta_i}{\cos \theta_0}$$

6.1.1.3.2 E-Field Normal

The Region a and Region b incident and reflected E-fields for the E-field normal to the incidence plane mode take the form

$$\vec{E}_a^i = A_a^i e^{-jk_0 z \cos \theta_0} e^{-jk_0 x \sin \theta_0} \hat{y} \quad (6-18)$$

$$\vec{E}_a^r = A_a^r e^{jk_0 z \cos \theta_0} e^{-jk_0 x \sin \theta_0} \hat{y}$$

for $z < 0$ and

$$\begin{aligned} \vec{E}_b^r &= A_b^r e^{-jk_0(z-d) \cos \theta_0} e^{-jk_0 x \sin \theta_0} \hat{y} \\ \vec{E}_b^i &= A_b^i e^{jk_0(z-d) \cos \theta_0} e^{-jk_0 x \sin \theta_0} \hat{y} \end{aligned} \quad (6-19)$$

for $z > d$. The A coefficients are related again by (6-13) with the T_1 now given by

$$\begin{aligned} T_1^{11} &= \frac{(\bar{n}_1 + v_1)^2}{4\bar{n}_1 v_1} (e^{-jk_1 d_1 \cos \theta_1} - \frac{(\bar{n}_1 - v_1)^2}{(\bar{n}_1 + v_1)^2} e^{jk_1 d_1 \cos \theta_1}) \\ T_1^{12} &= \frac{(\bar{n}_1^2 - v_1^2)}{4\bar{n}_1 v_1} (e^{jk_1 d_1 \cos \theta_1} - e^{-jk_1 d_1 \cos \theta_1}) \\ T_1^{21} &= -T_1^{12} \\ T_1^{22} &= \frac{(\bar{n}_1 + v_1)^2}{4\bar{n}_1 v_1} (e^{jk_1 d_1 \cos \theta_1} - \frac{(\bar{n}_1 - v_1)^2}{(\bar{n}_1 + v_1)^2} e^{-jk_1 d_1 \cos \theta_1}) \end{aligned} \quad (6-20)$$

Note that (6-17) with v_1 replaced by $1/v_1$ yields (6-20).

6.1.1.4 Anisotropic Layers/Normal Incidence

Consider a homogeneous composite layer with anisotropic conductivity σ and permittivity ϵ , and isotropic permeability μ . The composite fiber directions determine the principal constitutive coordinates (x' , y' , z). These coordinates are assumed to diagonalize both the and tensors, and the z axis is normal to the fiber directions and also the composite plane as in Figure 6.2.

The x' and y' coordinates are related to the x and y coordinates of Figure 6.2 (y is directed out of the page) by the rotation angle ϕ shown in Figure 6.5. The principal components of complex wave number and relative complex impedance are given respectively by

$$k_p = \sqrt{-j\omega\mu(\sigma_p + j\omega\epsilon_p)}$$

$$\bar{n}_p = \frac{1}{n_0} \sqrt{j\omega\mu/(\sigma_p + j\omega\epsilon_p)}$$

where $p = x'$ or y' .

The anisotropy generally results in coupling between x polarized normally incident fields and y polarized reflected and transmitted fields. However, x' polarized normally incident fields yield only x' polarized reflected and transmitted fields. Also, y' polarized normally incident fields yield only y' polarized reflected and transmitted fields. The approach taken here for obtaining the normal incidence transmission parameters, therefore, is similar to that employed by Allen (5) whereby the transmission parameters of normally incident and reflected fields are expressed as linear combinations of the transmission parameters of the two fields:

1. E-field polarized parallel to principal coordinate x'
2. E-field polarized parallel to principal coordinate y' .

This approach is described below.

Consider a single anisotropic composite layer of thickness d normally excited as in Figure 6.2. The Region a and Region b incident and reflected E-fields are given by

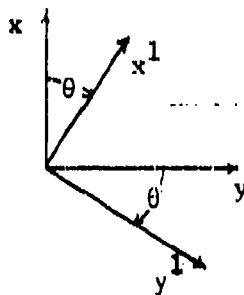


Figure 6.5 Anisotropic Composite Layer Principal Coordinates (Primed) as Related to Global Coordinates (Unprimed)

$$\vec{E}_a^i = A_{ax}^i e^{-jk_0 z} \hat{x} + A_{ay}^i e^{-jk_0 z} \hat{y}$$

$$\vec{E}_a^r = A_{ax}^r e^{jk_0 z} \hat{x} + A_{ay}^r e^{jk_0 z} \hat{y} \quad (6-21)$$

$$\vec{E}_b^r = A_{bx}^r e^{-jk_0(z-d)} \hat{x} + A_{by}^r e^{-jk_0(z-d)} \hat{y}$$

$$\vec{E}_b^i = A_{bx}^i e^{jk_0(z-d)} \hat{x} + A_{by}^i e^{jk_0(z-d)} \hat{y} \quad (6-22)$$

in terms of the "global" coordinates (x,y,z) and by

$$\vec{E}_a^i = A_{ax'}^i e^{-jk_0 z} \hat{x}' + A_{ay'}^i e^{-jk_0 z} \hat{y}' \quad (6-23)$$

$$\vec{E}_a^r = A_{ax'}^r e^{jk_0 z} \hat{x}' + A_{ay'}^r e^{jk_0 z} \hat{y}'$$

$$\vec{E}_b^r = A_{bx'}^r e^{-jk_0(z-d)} \hat{x}' + A_{by'}^r e^{-jk_0(z-d)} \hat{y}'$$

$$\vec{E}_b^i = A_{bx'}^i e^{jk_0(z-d)} \hat{x}' + A_{by'}^i e^{jk_0(z-d)} \hat{y}' \quad (6-24)$$

in terms of the composites principal coordinates (\hat{x}' , \hat{y}' , \hat{z}). Equations (6-21) and (6-22) equated respectively with (6-23) and (6-24) and the relations $\hat{x} = \hat{x}' \cos \phi - \hat{y}' \sin \phi$ and $\hat{y} = \hat{x}' \sin \phi + \hat{y}' \cos \phi$ yield

$$\begin{bmatrix} A_{ax'}^i \\ A_{ax'}^r \\ A_{ay'}^i \\ A_{ay'}^r \end{bmatrix} = [\Phi] \begin{bmatrix} A_{ax}^i \\ A_{ax}^r \\ A_{ay}^i \\ A_{ay}^r \end{bmatrix} \quad (6-25)$$

$$\begin{bmatrix} A_{bx'}^r \\ A_{bx'}^i \\ A_{by'}^r \\ A_{by'}^i \end{bmatrix} = [\phi] \begin{bmatrix} A_{bx}^r \\ A_{bx}^i \\ A_{by}^r \\ A_{by}^i \end{bmatrix} \quad (6-26)$$

where

$$[\phi] = \begin{bmatrix} \cos\phi & 0 & \sin\phi & 0 \\ 0 & \cos\phi & 0 & \sin\phi \\ -\sin\phi & 0 & \cos\phi & 0 \\ 0 & -\sin\phi & 0 & \cos\phi \end{bmatrix} \quad (6-27)$$

Equations (6-21) - (6-27) relate the incident and reflected fields in terms of the global coordinates to these fields in terms of the principal coordinates. The x' polarized fields are decoupled from the y' polarized fields and, therefore, may be analyzed separately.

6.1.1.4.1 E-Field Polarized Parallel to x'

Here, the incident and reflected fields are given by

$$\begin{aligned} \vec{E}_b^r &= A_{bx'}^r e^{-jk_0(z-d)} \hat{x}' \\ \vec{E}_b^i &= A_{bx'}^i e^{jk_0(z-d)} \hat{x}' \end{aligned} \quad (6-28)$$

for $z < 0$ (Region a in Figure 6.2) and

$$\begin{aligned} \vec{E}_a^i &= A_{ax'}^i e^{-jk_0 z} \hat{x}' \\ \vec{E}_a^r &= A_{ax'}^r e^{jk_0 z} \hat{x}' \end{aligned} \quad (6-29)$$

for $z > d$ (Region b in Figure 6.2). A solution to the anisotropic Maxwell's equations in the composite ($0 < z < d$) and continuity conditions on total tangential E- and H-fields yields

$$\begin{bmatrix} \Lambda_{bx'}^r \\ \Lambda_{bx'}^i \end{bmatrix} = \begin{bmatrix} p_{x'}^{11} & p_{x'}^{12} \\ p_{x'}^{21} & p_{x'}^{22} \end{bmatrix} \begin{bmatrix} \Lambda_{ax'}^i \\ \Lambda_{ax'}^r \end{bmatrix} \quad (6-30)$$

where

$$\begin{aligned} p_{x'}^{11} &= \frac{(1 + \bar{n}_{x'})^2}{4\bar{n}_{x'}} (e^{-jk_{x'}d} + \frac{(1 - \bar{n}_{x'})^2}{(1 + \bar{n}_{x'})^2} e^{jk_{x'}d}) \\ p_{x'}^{12} &= \frac{1 - (\bar{n}_{x'})^2}{4\bar{n}_{x'}} (e^{-jk_{x'}d} - e^{jk_{x'}d}) \\ p_{x'}^{21} &= -p_{x'}^{12} \\ p_{x'}^{22} &= \frac{(1 + \bar{n}_{x'})^2}{4\bar{n}_{x'}} (e^{jk_{x'}d} - \frac{(1 - \bar{n}_{x'})^2}{(1 + \bar{n}_{x'})^2} e^{-jk_{x'}d}) \end{aligned} \quad (6-31)$$

6.1.1.4.2 E-Field Polarized Parallel y'

Here, the incident and reflected fields are given by

$$\begin{aligned} \vec{E}_a^i &= \Lambda_{ay}^i e^{-jk_0 z} \hat{y} \\ \vec{E}_a^r &= \Lambda_{ay}^r e^{jk_0 z} \hat{y} \end{aligned} \quad (6-32)$$

for $z < 0$ and

$$\begin{aligned} \vec{E}_b^r &= \Lambda_{by}^r e^{-jk_0(z-d)} \hat{y}, \\ \vec{E}_b^i &= \Lambda_{by}^i e^{jk_0(z-d)} \hat{y}, \end{aligned} \quad (6-33)$$

for $z > d$. As with the x' polarized case, the A coefficients here are related by

$$\begin{bmatrix} \Lambda_{by}^r \\ \Lambda_{by}^i \end{bmatrix} = \begin{bmatrix} p_{y'}^{11} & p_{y'}^{12} \\ p_{y'}^{21} & p_{y'}^{22} \end{bmatrix} \begin{bmatrix} \Lambda_{ay}^i \\ \Lambda_{ay}^r \end{bmatrix} \quad (6-34)$$

where the $P_{y'}$ are given by (6-31) with x' replaced by y' .
Let

$$[P_{x'}] = \begin{bmatrix} p_{x'}^{11} & p_{x'}^{12} \\ p_{x'}^{21} & p_{x'}^{22} \end{bmatrix}$$

and

$$[P_{y'}] = \begin{bmatrix} p_{y'}^{11} & p_{y'}^{12} \\ p_{y'}^{21} & p_{y'}^{22} \end{bmatrix}$$

Equations (6-30) and (6-34) then combine to form

$$\begin{bmatrix} \Lambda_{bx'}^r \\ \Lambda_{bx'}^i \\ \Lambda_{by'}^r \\ \Lambda_{by'}^i \end{bmatrix} = \begin{bmatrix} [p_{x'}] & [0] \\ [0] & [p_{y'}] \end{bmatrix} \begin{bmatrix} \Lambda_{ax'}^i \\ \Lambda_{ax'}^r \\ \Lambda_{ay'}^i \\ \Lambda_{ay'}^r \end{bmatrix} \quad (6-35)$$

where (0) is the 2x2 null matrix. Also, (6-25), (6-26) and (6-35) combine to form

$$\begin{bmatrix} \Lambda_{bx}^r \\ \Lambda_{bx}^i \\ \Lambda_{by}^r \\ \Lambda_{by}^i \end{bmatrix} = [\Phi]^{-1} \begin{bmatrix} [p_{x'}] & [0] \\ [0] & [p_{y'}] \end{bmatrix} [\Phi] \begin{bmatrix} \Lambda_{ax}^i \\ \Lambda_{ax}^r \\ \Lambda_{ay}^i \\ \Lambda_{ay}^r \end{bmatrix} \quad (6-36)$$

The generalization of (6-36) to n layers between the a and b regions is obtained directly from the cascading property of the transmission coefficients as

$$\begin{bmatrix} \Lambda_{bx}^r \\ \Lambda_{bx}^i \\ \Lambda_{by}^r \\ \Lambda_{by}^i \end{bmatrix} = \left(\prod_{i=1}^n \left([\Phi_i]^{-1} \begin{bmatrix} [p_{ix_i}] & [0] \\ [0] & [p_{iy_i}] \end{bmatrix} [\Phi_i] \right) \right) \begin{bmatrix} \Lambda_{ax}^i \\ \Lambda_{ax}^r \\ \Lambda_{ay}^i \\ \Lambda_{ay}^r \end{bmatrix} \quad (6-37)$$

where a subscript i denotes parameters peculiar to the i^{th} layer. Note that in using (6-27) and (6-31) to obtain (6-37), η_x' , and k_x' are functions of the i^{th} layer and d is the i^{th} layer thickness. Also, the A coefficients in (6-37) relate the fields on either side of the layered composite via (6-21) and (6-22) where d in (6-22) is now the thickness of the entire layered composite as in Figure 6.3.

6.1.1.5 Anisotropic Layers/Oblique Incidence

The transmission parameters for oblique incidence plane wave excitation of cascaded anisotropic composite layers are derived in this section. A composite layer is defined, as in the previous section, with homogeneous, isotropic impedance

$$\hat{Z} = j\omega\mu \quad (6-38)$$

and anisotropic admittivity defined by the tensor

$$\hat{Y}' = \begin{bmatrix} \hat{Y}_x' & 0 & 0 \\ 0 & \hat{Y}_y' & 0 \\ 0 & 0 & \hat{Y}_z' \end{bmatrix} \quad (6-39)$$

with respect to the composite's principal coordinates (x', y', z) where

$$\hat{Y}_p = \sigma_p + j\omega\epsilon_p \quad (6-40)$$

for $p = x', y',$ or z . As before, the x', y' plane is parallel to the global x, y plane and the z coordinates in both systems are coincident and normal to the plane of the composite layers.

Since composite layers with differing principal axis directions are to be cascaded, the transmission parameters for a single layer must relate the global x and y components of incident and reflected fields on either side of the composite. As before, Region a and Region b sandwich the composite with the coordinate system as in Figure 6.2. The fields now are obliquely incident, however, as in Figure 6.4 with incidence angle θ_0 measured in the plane of incidence (defined in Section 6.1.1.3). The Region's a and b incident and reflected fields can be decomposed into H-normal-to-the-plane-of-incidence and E-normal-to-the-plane-of-incidence modes. For Region a the H-normal incident and reflected E-fields are respectively

$$\vec{E}_a^{hi} = \Lambda_a^{hi} e^{-jk_0(x \sin\theta_0 + z \cos\theta_0)} (\cos\theta_0 \hat{x} - \sin\theta_0 \hat{z}) \quad (6-41)$$

$$\vec{E}_a^{hr} = \Lambda_a^{hr} e^{-jk_0(x \sin\theta_0 - z \cos\theta_0)} (\cos\theta_0 \hat{x} + \sin\theta_0 \hat{z})$$

The E-normal E-fields are

$$\vec{E}_a^{ei} = A_a^{ei} e^{-jk_0(x \sin \theta_0 + z \cos \theta_0)} \hat{y} \quad (6-42)$$

$$\vec{E}_a^{er} = A_a^{er} e^{-jk_0(x \sin \theta_0 - z \cos \theta_0)} \hat{y}$$

For Region b the H-normal reflected and incident E-fields are respectively

$$\vec{E}_b^{hr} = A_b^{hr} e^{-jk_0(x \sin \theta_0 + (z-d) \cos \theta_0)} (\cos \theta_0 \hat{x} - \sin \theta_0 \hat{z}) \quad (6-43)$$

$$\vec{E}_b^{hi} = A_b^{hi} e^{-jk_0(x \sin \theta_0 - (z-d) \cos \theta_0)} (\cos \theta_0 \hat{x} + \sin \theta_0 \hat{z})$$

The E-normal E-fields are

$$\vec{E}_b^{er} = A_b^{er} e^{-jk_0(x \sin \theta_0 + (z-d) \cos \theta_0)} \hat{y}$$

$$\vec{E}_b^{ei} = A_b^{ei} e^{-jk_0(x \sin \theta_0 - (z-d) \cos \theta_0)} \hat{y} \quad (6-44)$$

The transmission parameters relate

A_b^{hr} , A_b^{hi} , A_b^{er} , and A_b^{ei} of (6-43) and (6-44) to

A_a^{hi} , A_a^{hr} , A_a^{ei} , and A_a^{er} of (6-41) and (6-42)

This relation is obtained by constructing solutions to the anisotropic Maxwell's equations for the composite medium and satisfying the boundary conditions at the layer interfaces.

A decomposition of the composite medium field into two decoupled modes with respect to the composite's principal coordinates is not obvious here as it was for normal incidence excitation (Section 6.1.1.4). The global components of the composite field, therefore, are found by satisfying Maxwell's equations with respect to the global coordinates (x,y,z). The admittivity tensor \vec{Y} is then (from Figure 6.5 and Maxwell's equations)

$$\vec{Y} = \begin{bmatrix} (\hat{Y}_x, \cos^2 \phi + \hat{Y}_y, \sin^2 \phi) & (\hat{Y}_x, -\hat{Y}_y) \cos \phi \sin \phi & 0 \\ (\hat{Y}_x, -\hat{Y}_y) \cos \phi \sin \phi & (\hat{Y}_x, \sin^2 \phi + \hat{Y}_y, \cos^2 \phi) & 0 \\ 0 & 0 & \hat{Y}_z \end{bmatrix}$$

A solution to the homogeneous Maxwell's equations that exhibits the x variation of (6-41) - (6-44) then has x any y components of E and H given by

$$\begin{aligned} E_x &= e^{-j(k_0 x \sin \theta_0 + \alpha_z z)} \\ E_y &= f e^{-j(k_0 x \sin \theta_0 + \alpha_z z)} \\ H_x &= -\frac{f}{\bar{n}_z n_0} e^{-j(k_0 x \sin \theta_0 + \alpha_z z)} \\ H_y &= \left(\frac{1}{\bar{n}_x n_0} + \frac{f}{\bar{n}_{xy} n_0} \right) e^{-j(k_0 x \sin \theta_0 + \alpha_z z)} \end{aligned} \quad (6-45)$$

where

$$\begin{aligned} \bar{n}_x &= j\alpha_z / (n_0 (\hat{Y}_x, \cos^2 \phi + \hat{Y}_y, \sin^2 \phi)) \\ \bar{n}_{xy} &= j\alpha_z / (n_0 \cos \phi \sin \phi (\hat{Y}_x, -\hat{Y}_y)) \\ \bar{n}_z &= \hat{z} / (j\alpha_z n_0) \\ f &= \frac{-\hat{z} \cos \phi \sin \phi (\hat{Y}_x, -\hat{Y}_y)}{k_0^2 \sin^2 \theta_0 + \alpha_z^2 + \hat{z} (\hat{Y}_x, \sin^2 \phi + \hat{Y}_y, \cos^2 \phi)} \end{aligned} \quad (6-46)$$

and α_z , the complex z component of wave number, satisfies

$$\alpha_z^2 = -\frac{b}{2} \pm \sqrt{\left(\frac{b}{2}\right)^2 - c} \quad (6-47)$$

where

$$b = \hat{z}(\hat{Y}_x + \hat{Y}_y) + (1+\psi)k_0^2 \sin^2 \theta_0$$

$$c = \frac{\hat{z}}{\hat{Y}_z} (\hat{Y}_x \hat{Y}_y + \psi \hat{Y}_z^2) k_0^2 \sin^2 \theta_0 + \psi k_0^4 \sin^4 \theta_0 + \hat{Y}_x \hat{Y}_y \hat{z}^2$$

$$\psi = \frac{1}{\hat{Y}_z} (\hat{Y}_x \cos^2 \phi + \hat{Y}_y \sin^2 \phi)$$

There are four solutions for α_z :

$$\alpha_z = \begin{cases} \pm \alpha_z' \\ \pm \alpha_z'' \end{cases}$$

The positive sign is for positive z traveling waves and the negative sign for negative z traveling waves. For normal incidence, $\sin \theta_0 = 0$ and (6-47) reduces to

$$\alpha_z' = \sqrt{-2\hat{Y}_x}, \quad \text{and} \quad \alpha_z'' = \sqrt{-2\hat{Y}_y}$$

as expected for agreement with the analysis of Section 6.1.1.4. For an isotropic composite with oblique incidence excitation, $\hat{Y}_x = \hat{Y}_y = \hat{Y}_z = \hat{Y}$ and (6-47) reduces to $\alpha_z' = \alpha_z'' = k_1 \cos \theta_1$ where $k_1 = \sqrt{-2\hat{Y}}$ and θ_1 is defined following (6-17) thus agreeing with the analysis of Section 6.1.1.3.

Decomposition of the composite medium field into the four component fields corresponding to the solutions to (6-47), and satisfaction of the boundary conditions at the composite interface with Regions a and b (tangential continuity with E-fields of (6-41) - (6-44) and their H-field counterparts) yields

$$\begin{bmatrix} A_b^{hr} \\ A_b^{hi} \\ A_b^{er} \\ A_b^{ci} \end{bmatrix} = [G]^{-1} [F] [D] [F]^{-1} [0] \begin{bmatrix} A_a^{hi} \\ A_a^{hr} \\ A_a^{ci} \\ A_a^{er} \end{bmatrix} \quad (6-48)$$

where

$$\begin{aligned}
 [0] &= \begin{bmatrix} \cos \theta_0 & \cos \theta_0 & 0 & 0 \\ 1 & -1 & 0 & 0 \\ 0 & 0 & 1 & 1 \\ 0 & 0 & -\cos \theta_0 & \cos \theta_0 \end{bmatrix} \\
 [D] &= \begin{bmatrix} -j\alpha_z' d & 0 & 0 & 0 \\ 0 & -j\alpha_z' d & 0 & 0 \\ 0 & 0 & -j\alpha_z'' d & 0 \\ 0 & 0 & 0 & -j\alpha_z'' d \end{bmatrix} \\
 [F] &= \begin{bmatrix} 1 & 1 & 1 & 1 \\ g' & -g' & g'' & -g'' \\ f' & -f' & f'' & -f'' \\ -h' & h' & -h'' & h'' \end{bmatrix}
 \end{aligned}$$

$$g = \frac{1}{\bar{n}_x} + \frac{f}{\bar{n}_{xy}}$$

$$h = f/\bar{n}_z$$

and a primed f, g , or h indicates evaluation at $\alpha_z = \alpha_z'$ and double primed f, g , or h indicates evaluation at $\alpha_z = \alpha_z''$.

Equation (6-48) defines the transmission parameter matrix $[T]$ as

$$[T] = [0]^{-1} [F] [D] [F]^{-1} [0]$$

for a single anisotropic composite layer for oblique incidence excitation. The cascading property of the transmission parameters generalizes (6-48) immediately to n layers as

$$\begin{bmatrix} \Lambda_b^{hr} \\ \Lambda_b^{hi} \\ \Lambda_b^{er} \\ \Lambda_b^{ci} \end{bmatrix} = [0]^{-1} \left(\prod_{i=1}^n ([F_i] [D_i] [F_i]^{-1}) \right) [0] \begin{bmatrix} \Lambda_a^{hi} \\ \Lambda_a^{hr} \\ \Lambda_a^{ci} \\ \Lambda_a^{er} \end{bmatrix} \quad (6-49)$$

where a subscript i denotes parameters peculiar to the ith layer. The discussion following (6-37) regarding d applies here as well.

6.1.1.6 Shielding Effectiveness For a Uniform Magnetic Field

The magnetic shielding effectiveness is commonly defined by the expression

$$MSE = 20 \log_{10} |MSR^{-1}|$$

where the inverse magnetic shielding ration, MSR^{-1} , is given by

$$MSR^{-1} = \frac{H_{INCIDENT}}{H_{INTERIOR}}$$

and $H_{INCIDENT}$ and $H_{INTERIOR}$ are the H-fields incident on the shield and interior to the shield respectively. A general problem with this definition is that it is very dependent on shield geometry and is not unique to the material and the incident radiation. For uniform magnetic fields and certain geometric shapes, the magnetic shielding effectiveness can be characterized uniquely.

6.1.1.6.1 Flat Plate Geometry

The exact expression for the magnetic shielding effectiveness is

$$MSE = 20 \log_{10} |\cosh(\gamma d) + \frac{377}{\eta} \sinh \gamma d| \quad (6-50)$$

where

$$\gamma = [j\omega\mu\sigma]^{1/2}$$

$$\eta = [j\omega\mu/\sigma]^{1/2}$$

d = shield thickness

For low frequencies, the magnetic shielding effectiveness in (6-50) can be well-approximated by

$$MSE \approx 20 \log_{10} |1 + 377\sigma d|$$

where the frequency f satisfies

$$f < \frac{0.1}{2\pi\mu\sigma d^2}$$

The low frequency shielding effectiveness is determined by the shield thickness and conductivity, i.e., material parameters only.

For $f < \frac{0.1}{2\pi\mu\sigma d^2}$ the shielding effectiveness increases sharply with frequency as in (6-50).

6.1.1.6.2 Enclosure Geometries

For enclosure geometries such as parallel plates, cylindrical shells and spherical shells, the magnetic shielding effectiveness can be written as

$$MSE = 20 \log_{10} \left| \cosh(\gamma d) + \frac{V}{S} \gamma \sinh(\gamma d) \right| \quad (6-51)$$

where $\frac{V}{S}$ is the volume-to-surface ration in MSK units of the enclosure.

For low frequencies satisfying $f < \frac{0.1}{2\pi\mu\sigma d^2}$

the magnetic shielding effectiveness in (6-51) can be written as

$$MSE = 20 \log_{10} \left| 1 + \left(\frac{V}{S}\right) \gamma^2 d \right| \quad (6-52)$$

For the enclosure geometries, the magnetic shielding effectiveness depends on the incident magnetic field frequency and the enclosure geometry (expressed as $\frac{V}{S}$) as well as the material parameters (σ and d) of the shield. At a frequency given by

$$f_b = \frac{1}{2\pi\left(\frac{V}{S}\right)\mu\sigma d}$$

the magnetic shielding effectiveness in (6-52) has a "break point" below which the shielding effectiveness is essentially zero above this frequency. The shielding effectiveness increases as

$$20 \log_{10} \left(\frac{f}{f_b} \right)$$

for high frequencies satisfying

$$f > \frac{0.1}{2\pi\mu\sigma d^2} \quad (6-53)$$

For frequencies less than (6-53), the magnetic shielding effectiveness is given by

$$MSE = 20 \log_{10} \left| \cosh(\gamma d) + \frac{1}{3} \left[\frac{j\omega\mu R}{n} + \frac{2n}{j\omega\mu R} \right] \sinh(\gamma d) \right| \quad (6-54)$$

The variable R is a geometry dimension equal to one-half the plate separation for parallel plates or to the radius of a sphere or cylinder.

6.1.1.7 Shielding Effectiveness For a Uniform Electric Field

Analogously to magnetic shielding effectiveness, electric shielding effectiveness can be defined as

$$ESE = 20 \log_{10} |ESR^{-1}| \quad (6-55)$$

where the inverse electric shielding ratio is

$$ESR^{-1} = \frac{E_{\text{INCIDENT}}}{E_{\text{INTERIOR}}}$$

The same problems infect this definition of electric shielding as for magnetic shielding. Following Schelkunoff, (6-55) can be written as

$$ESE = A + R + B$$

where A is absorption loss, R is reflection loss and B accounts for loss due to multiple reflections in thin shields.

For a planar interface, the absorption loss is given by

$$A = 8.686 \frac{d}{\delta} \quad (6-56)$$

where d is the shield thickness and δ is the skin depth. Since

$$\delta = \sqrt{\frac{2}{\omega \mu \sigma}} \quad (6-56) \text{ becomes}$$

$$A = 8.686 d \sqrt{\frac{\omega \mu \sigma}{2}} \quad (6-57)$$

Reflective losses occur primarily as a characteristic impedance difference between different media. The reflection loss can then be written as

$$B = 20 \log_{10} \frac{4 |Z_1|}{|Z_2|} \quad (6-58)$$

where Z_1 is the wave impedance of the media multiple reflection loss (B) is small for incident electric fields due to the large impedance mismatch present.

The inverse electric shielding ratio for enclosures (cylinder, parallel plates and spheres) is

$$ESR^{-1} = \frac{Y \sinh(\gamma d)}{(4\pi/\lambda) \frac{V}{S}} \quad (6-59)$$

For frequencies sufficiently low that the skin depth is greater than $\sqrt{20d}$, (d is shield thickness) and

$$\omega < \frac{0.1}{\mu_0 d^2}$$

(6-60)

$$RSE = 20 \log_{10} \left[\frac{\omega d}{8 \pi c} \sqrt{\frac{\mu}{\epsilon}} \right] - 20 \log_{10} f$$

and is primarily reflective loss at frequencies where the skin depth is close to $\sqrt{20d}$ absorption losses become large and grow exponentially. The result is a minimum in the electric shielding effectiveness at a frequency where the skin depth is approximately one-third the shield thickness.

6.1.1.8 Transfer Impedance as a Measure of Shielding Effectiveness

The main difficulty with the usual methods of measuring the EM shielding effectiveness of materials is that the shielding effectiveness so measured depends upon the material geometry as well as the material physical properties. The measured values of shielding effectiveness are then valid only for the geometry of the measurement and cannot be extended to more complex geometries.⁽⁸⁾

One comment, valid for shields that are thin compared to their radii or curvature and for which the wavelength of the incident EM field within the shield is much smaller than that external to the shield, is that of transfer impedance.⁽⁸⁾ The surface transfer impedance of a homogeneous conducting shield (also applicable to mixed-orientation graphite/epoxy composites) is given by the ratio of the interior tangential electric field to the exterior current induced by the external field.⁽⁸⁾

(6-61)

$$Z_{st} = \frac{E_t}{J} = \eta \cosh(rd)$$

where

$$\eta = [j\omega\mu/\sigma]^{1/2}$$

$$r = [j\omega\mu\sigma]^{1/2}$$

d = shield thickness

The low frequency limit for the surface transfer impedance is

$$Z_{st} \approx \frac{1}{\sigma d} \quad (\omega \text{ small}) \quad (6-62)$$

which depends only on material thickness and conductivity.

The surface transfer impedance can be related to the magnetic shielding effectiveness for the case of a uniform magnetic field by the relation⁽⁸⁾

$$MSE = 20 \log_{10} \left| \frac{Z}{Z_{st}} \right| \quad (6-63)$$

where

$$Z = \left(\frac{\mu}{\epsilon} \right)^{1/2} \text{ for flat plate}$$

$$Z_{st} = \left(\frac{V}{S} \right) j\omega\mu \text{ for a cylindrical, spherical or parallel plate enclosure with volume-to-surface ratio } \frac{V}{S}$$

For a homogeneous conducting enclosure (parallel plates, cylinder or sphere) the surface transfer impedance is related to the electric shielding effectiveness by⁽⁸⁾

$$ESE = 20 \log_{10} \left| \frac{Z}{Z_{st}} \right| \quad (6-64)$$

where

$$Z = \frac{j}{8\pi\epsilon f \left(\frac{V}{S} \right)}$$

Both (6-63) and (6-64) are valid over a frequency interval dependent on shield geometry, conductivity and thickness.

The dependence of surface transfer impedance function on frequency is shown in Figure 6-6. Measured surface transfer impedance of 24-ply T-300 graphite/epoxy is shown in Figure 6.7.

6.1.2 Measured and Predicted Composite Shielding Effectiveness

In this section, the shielding effectiveness of graphite and boron composite materials is presented in graphical form as a function of frequency. A comparison is made to titanium where data is available. Several different composite laminates are considered in several geometrical shapes to show the dependence of shielding effectiveness on the enclosure geometry.

The shielding effectiveness data will be presented in two parts, low frequency data (frequency less than 1 GHz) and high frequency data (frequency greater than 1 GHz), because of the different shielding behavior of the composites in each frequency range.

6.1.2.1 Low Frequency Shielding

The low frequency shielding data presented in this section is divided into magnetic shielding, electric shielding and plane wave shielding because of their fundamentally different behavior.

MATERIAL THICKNESS CORRESPONDS TO 8 PLY COMPOSITE
MATERIAL AT 0.00525 IN/PLY

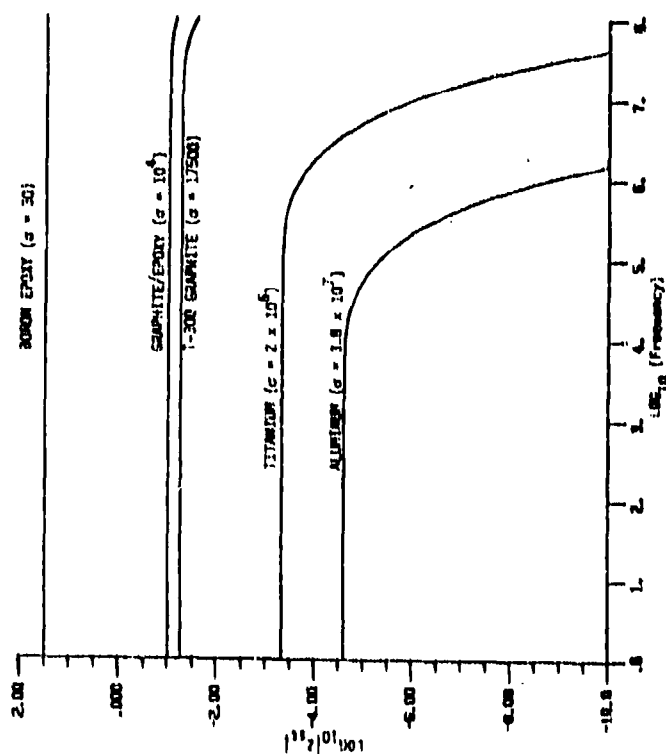


Figure 6.6 Surface Transfer Impedance as a Function of Frequency (5)

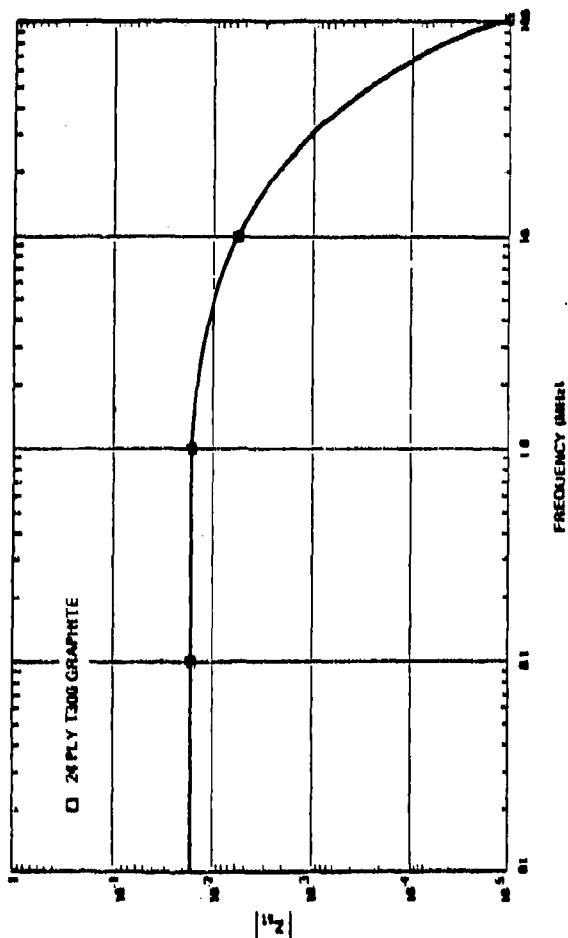


Figure 6.7 Measured Surface Transfer Impedance of 24 Ply T-300 Graphite/Epoxy (8.9)

6.1.2.1.1 Magnetic Shielding Effectiveness

The penetration of magnetic fields through aircraft enclosures is most serious at low frequency. Figure 6.8 shows the magnetic shielding effectiveness of composites and metals shaped into flat plates and illuminated by a uniform magnetic field. The shielding in the low frequency limit is determined by the conductivity and shield thickness alone. The metals have highest conductivity and shield most; the composites, having less conductivity, shield correspondingly less.

For an enclosure geometry (parallel plates, cylinder or sphere) the magnetic shielding decreases with frequency sharply to a breakpoint where there is essentially no shielding at all. In figure 6.9 the magnetic shielding effectiveness of an enclosure is compared to that of a flat plate. Only at about 100 MHz is enclosure shielding as good as that of the plate. The shielding effectiveness also depends upon the shield geometry through the volume-to-surface ratio $\frac{V}{S}$. Figure 6.10 illustrates the shielding effectiveness of an enclosed geometry as a function of $\frac{V}{S}$ a higher $\frac{V}{S}$ yields a bet-

ter shielding effectiveness for uniform magnetic fields. The breakpoint where magnetic shielding drops to a very small value is shown in Figure 6.11 for a uniform magnetic field. The breakpoint is lower in frequency for higher conducting materials. Consequently metals, such as aluminum and titanium, have the breakeven point lowest in frequency followed by composites.

The magnetic shielding effectiveness can be improved by using a metallic coating to protect against lightning and surface charging hazards. Figures 6.12 and 6.13 show the measured magnetic shielding effectiveness of 12- and 24-ply graphite/epoxy both bare and protected using various lightning protection schemes. Considerable improvement in magnetic shielding is possible with proper lightning protection.

The magnetic shielding effectiveness is also sharply dependent on the external field. In Figure 6.14 the shielding for an infinite flat plate is shown for both a uniform and nonuniform magnetic field. The nonuniform field shielding drops with frequency to zero very fast while a uniform field levels out at a high value.

Figure 6.15 illustrates measurements of shielding effectiveness made with a nonuniform magnetic field produced by a loop antenna for several flat graphite/epoxy composite laminate structures. The results indicate essentially no shielding below 1 MHz. Figure 6.16 shows magnetic shielding effectiveness for a nonuniform magnetic field for various metal and composite (8-, 12- and 24-ply) flat plates. The metals (aluminum and titanium) shield best and are followed by graphite. Boron has essentially no shielding in nonuniform fields up to 100 MHz.

Figure 6.17 illustrates the use of surface transfer impedance to calculate magnetic shielding effectiveness for a flat plate under both a uniform and nonuniform field, and for a volume in a uniform field. Transfer impedance offers the advantage that it is a characteristic of the material only, not of its shape or of the external field incident on it.

PLATE THICKNESS CORRESPONDS TO 8 PLY COMPOSITE MATERIAL AT 0.00525 IN/PLY

SHIELD CONDUCTIVITY, σ , IN UNITS OF mbos/m

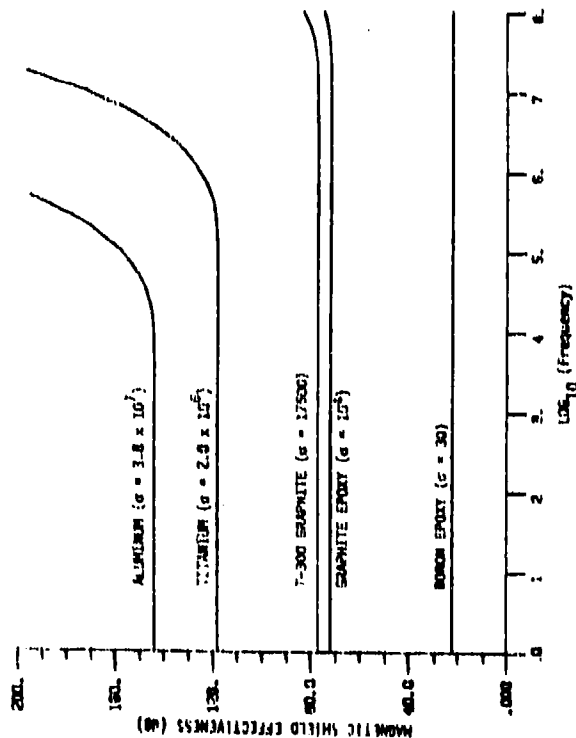


Figure 6.3 Magnetic Shielding Effectiveness of a Flat Plate under a Uniform Magnetic Field (8)

SHIELD THICKNESS CORRESPONDS TO 8 PLY COMPOSITE MATERIAL AT 0.00525 IN/PLY

SHIELD CONDUCTIVITY = 10^4 mbos/m

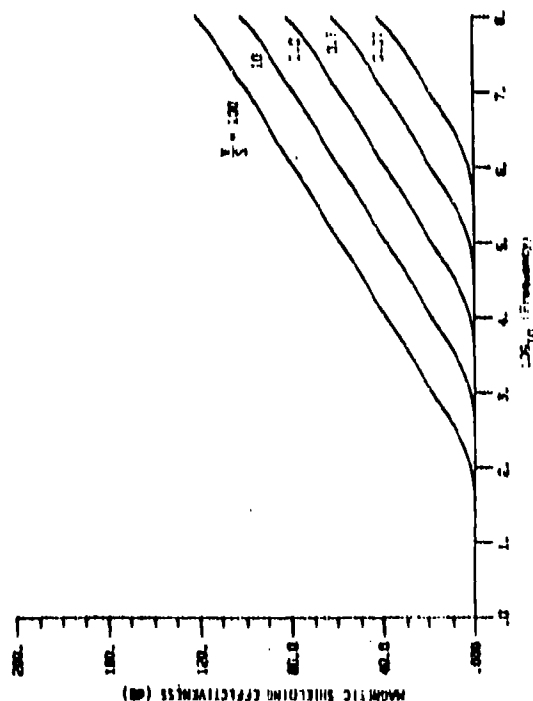


Figure 6.10 Magnetic Shielding Effectiveness of an Enclosure under a Uniform Magnetic Field as a Function of Volume-to-Surface Ratio (9)

SHIELD THICKNESS CORRESPONDS TO 8 PLY COMPOSITE MATERIAL AT 0.00525 IN/PLY

SHIELD CONDUCTIVITY = 10^4 mbos/m

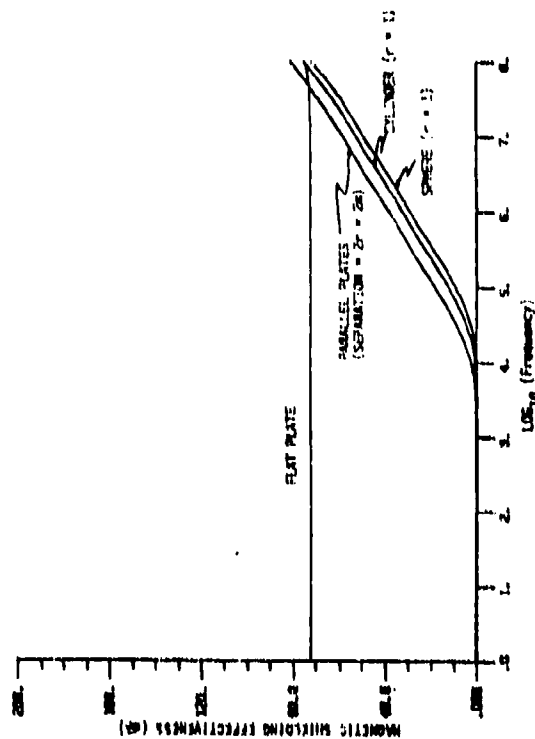


Figure 6.9 Magnetic Shielding Effectiveness With a Uniform Incident Magnetic Field (8)

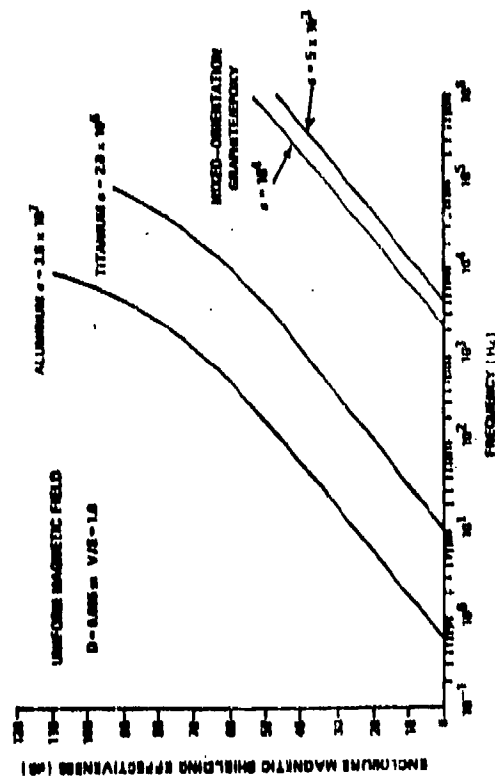


Figure 6.11 Magnetic Shielding Effectiveness Breakpoint Behavior for Enclosures

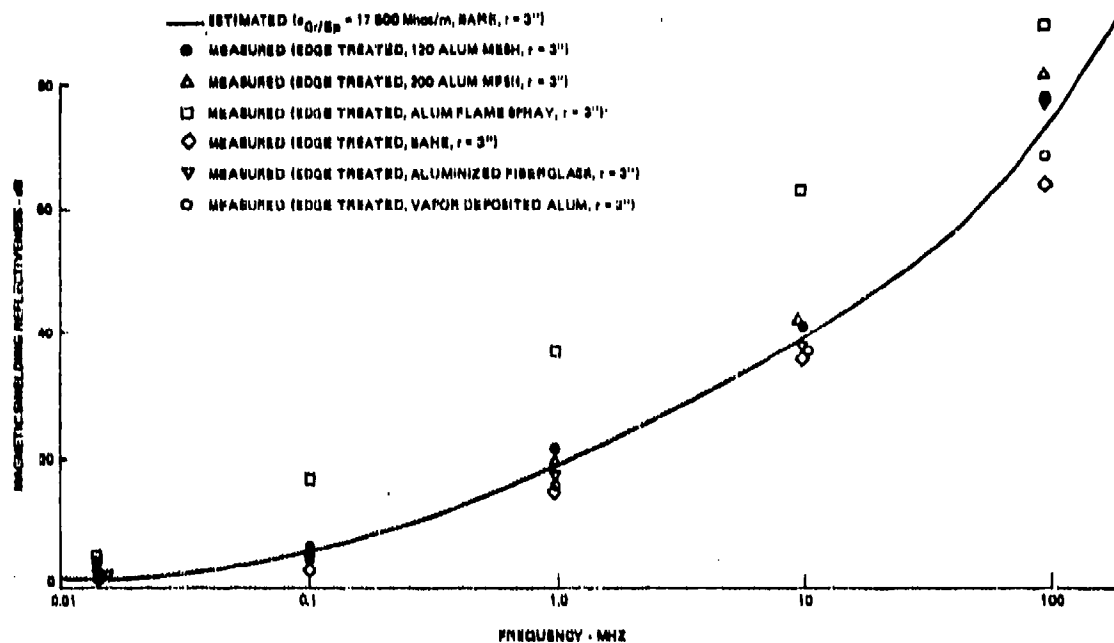


Figure 6.12 Magnetic Shielding of 12 ply ($0^\circ, \pm 45^\circ, 90^\circ$) Graphite/Epoxy Bare and With Protection⁽¹¹⁾

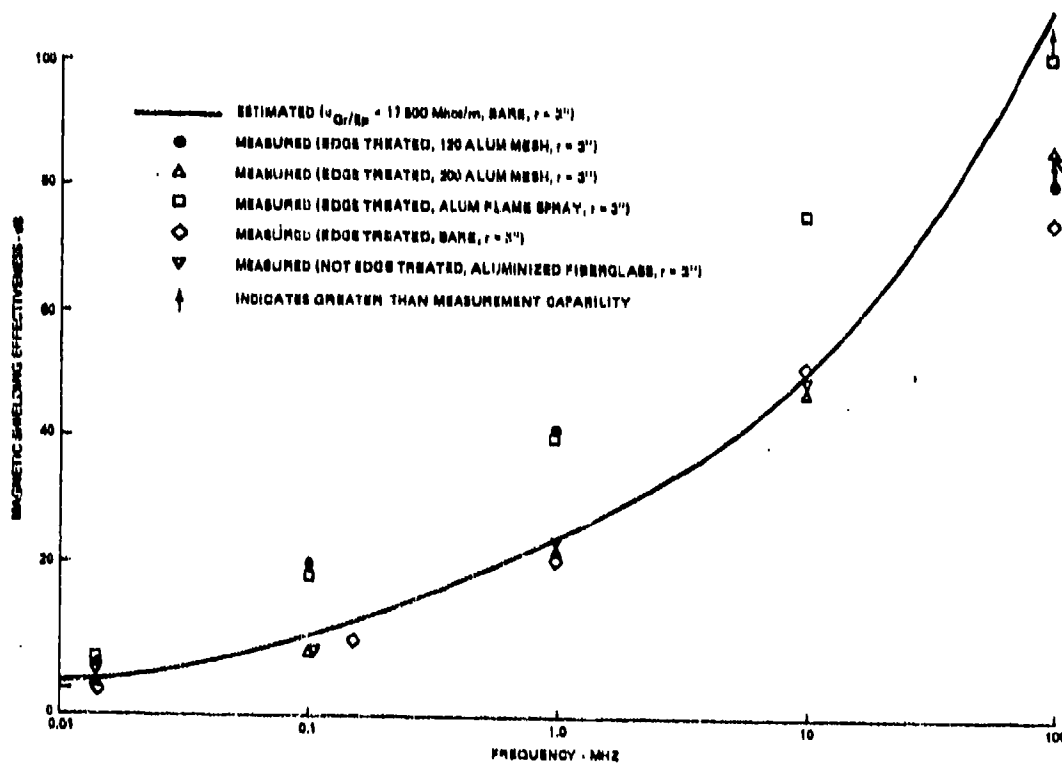


Figure 6.13 Magnetic Shielding For 24-Ply ($0^\circ, \pm 45^\circ, 90^\circ$) Graphite/Epoxy Bare and With Protection⁽¹¹⁾

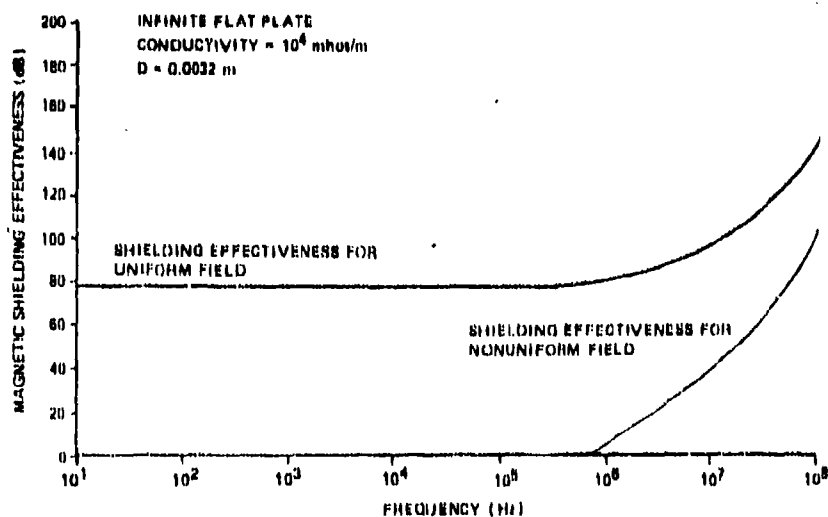
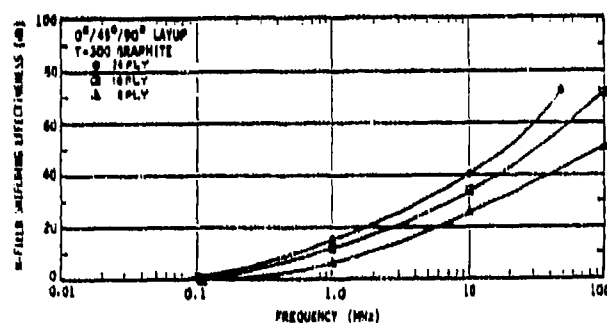
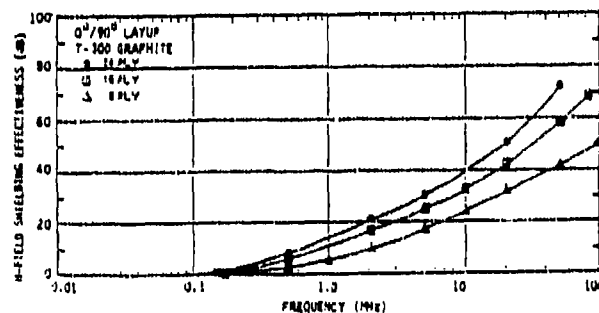


Figure 6.14 Magnetic Shielding Effectiveness for a Mixed-Orientation Graphite/Epoxy Composite Enclosure under a Uniform Field as a Function of Volume-to-Surface, Conductivity = 10^4 , Shield Thickness = 0.003 m (8)



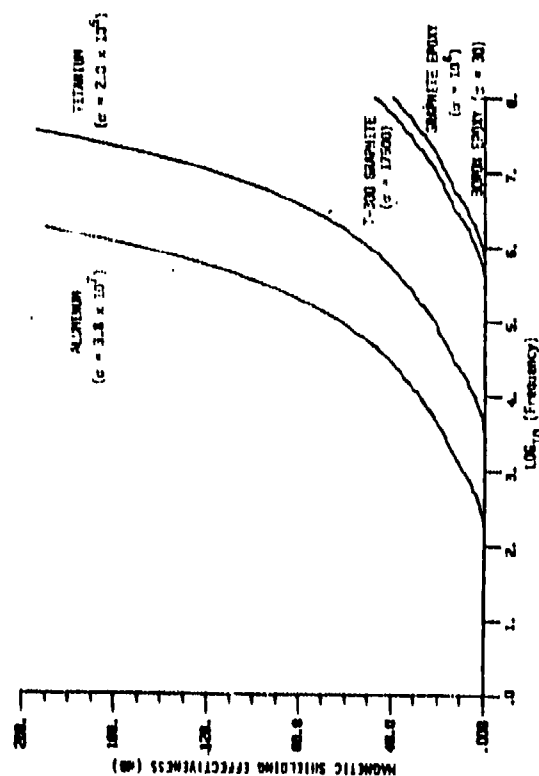
(a) 0°/45°/90° Layup



(b) 0°/90° Layup

Figure 6.15 Infinite Flat Plate with a Nonuniform Incident Magnetic Field Test Results (8)

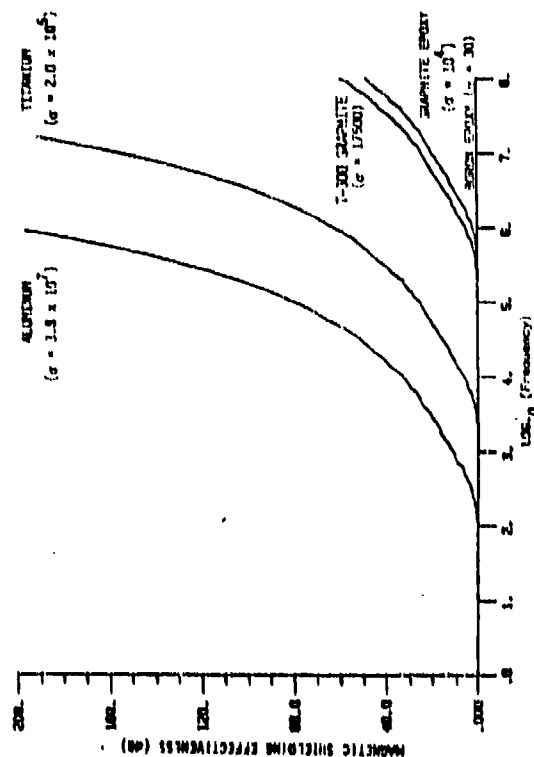
LOOP DIAMETER
= 1 in.
ANTENNA-PLATE SEPARATION = 1 in.
PLATE THICKNESS CORRESPONDS TO 8 PLY COMPOSITE
MATERIAL AT 0.00525 IN/PLY



(a) Plate Thickness = 0.0032 in

Figure 6.16 Magnetic Shielding Effectiveness of a Flat Plate under a Non-uniform Magnetic Field generated by a Loop Antenna Parallel to the Plate (Sheet 1 of 3)(8)

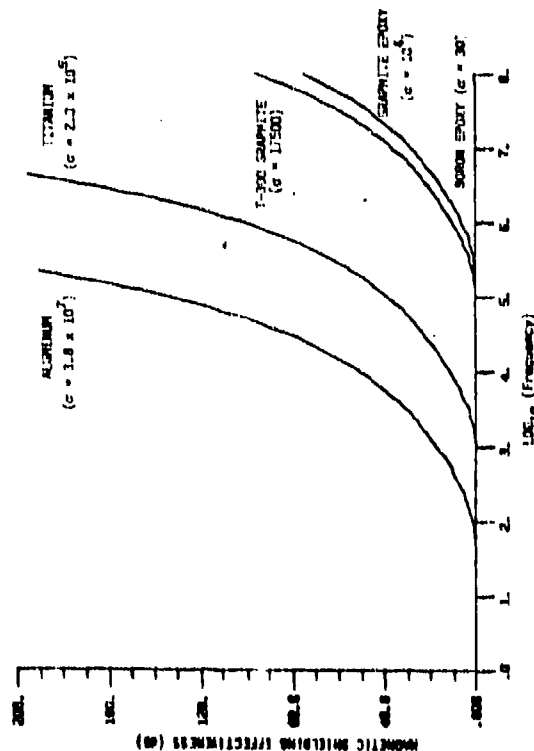
LOOP DIAMETER
= 1 in.
ANTENNA-PLATE SEPARATION = 1 in.
PLATE THICKNESS CORRESPONDS TO 12 PLY COMPOSITE
MATERIAL AT 0.00525 IN/PLY



(b) Plate Thickness = 0.00214 in

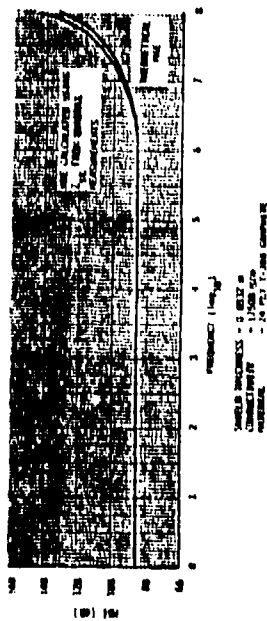
Figure 6.16 Magnetic Shielding Effectiveness of a Flat Plate under a Non-uniform Magnetic Field generated by a Loop Antenna Parallel to the Plate (Sheet 2 of 3)(8)

LOOP DIAMETER
= 1 in.
ANTENNA-PLATE SEPARATION = 1 in.
PLATE THICKNESS CORRESPONDS TO 24 PLY COMPOSITE
MATERIAL AT 0.00525 IN/PLY

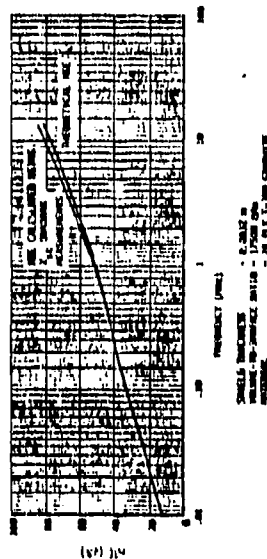


(c) Plate Thickness = 0.00107 m

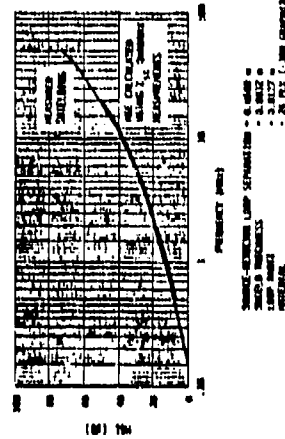
Figure 6.16 Magnetic Shielding Effectiveness of a Flat Plate under a Non-uniform Magnetic Field Generated by a Loop Antenna Parallel to the Plate (Sheet 3 of 3)(8)



(a) Flat Plate under a Uniform Magnetic Field



(b) Volume under a Uniform Magnetic Field



(c) Flat Plate under a Nonuniform Magnetic Field

Figure 6.17 Shielding Effectiveness using Surface Transfer Impedance(8)

6.1.2.1.2 Electric Shielding Effectiveness

Figure 6.18 illustrates electric shielding effectiveness for an 8-ply graphite/epoxy enclosed shield compared to an aluminum structure. Because the low frequency shielding is primarily reflective loss, the electric shielding effectiveness decreases with frequency at high frequency until absorption (which increases with frequency) becomes more important. In between, the electric shielding effectiveness goes through a minimum as shown in Figure 6.18 for aluminum.

Electric shielding effectiveness also depends on the volume-to-surface ratio, $\frac{V}{S}$, of the enclosure. The higher the ratio, the less

electric shielding. This behavior is shown in Figure 6.19 for 8-ply graphite/epoxy for several volume to surface ratios.

E-field shielding for 12- and 24-ply graphite/epoxy panels which are bare and protected is shown in Figures 6.20 and 6.21. The frequency range is from 10 kHz to 1 GHz.

6.1.2.1.3 Plane Wave Shielding Effectiveness

Some limited data on low frequency plane wave shielding effectiveness is given in Figures 6.22 and 6.23 for 12-ply and 24-ply graphite/epoxy composite panels.

6.1.2.2 High Frequency Shielding

Most measurements to date appear to confirm the opinion that graphite/epoxy composites tend to behave like metals at frequencies above 200 GHz. The best data to date on high frequency composite shielding were taken by Boeing (10) using anechoic chamber techniques. The frequency range was from 1 GHz to 18 GHz and the composite panels were 2-ply and 4-ply graphite/epoxy laminates. The data are given in Figure 6.24 as a set of points with a range of uncertainty. A least-squares fit was then performed and is represented in Figure 6.24 by the smooth curves. The trend is clearly towards higher shielding as frequency increases. These curves should represent good lower bounds for multiply graphite composite laminates.

Boron/epoxy and especially Kevlar/epoxy require higher frequencies before much shielding is apparent.

6.1.3 Metallic/Composite Aircraft Weight-Shielding Tradeoffs

This section presents some preliminary work (8) that has done in formulating the weight-shielding tradeoffs necessary in evaluating various materials and protective coatings for use in modern aircraft. An appropriate measure of EM shielding is combined with physical data from various materials (metals, graphite/epoxy, boron/epoxy and Kevlar/epoxy) to make the tradeoffs.

The data used in formulating the tradeoffs is given in Table 6.1. The data assumes a frequency less than 100 kHz so the tradeoffs should be considered valid only in the low frequency situation (where poor shielding may be a problem).

VOLUME-TO-SURFACE RATIO = 1
SHIELD THICKNESS CORRESPONDS TO 8 PLY COMPOSITE
MATERIAL OF 0.00525 IN/PLY

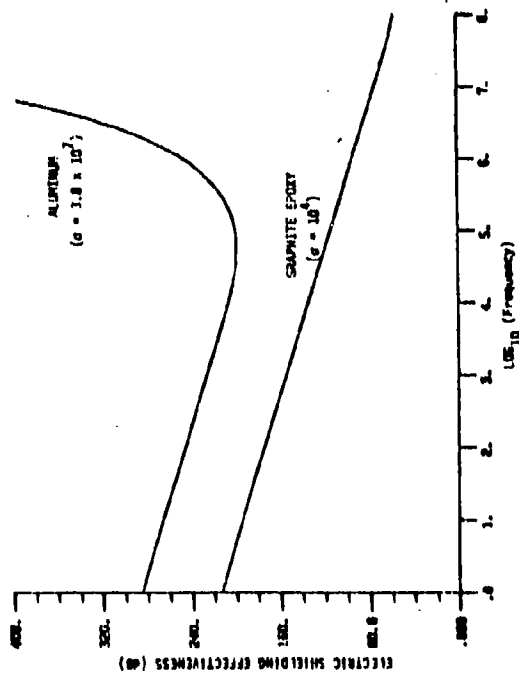
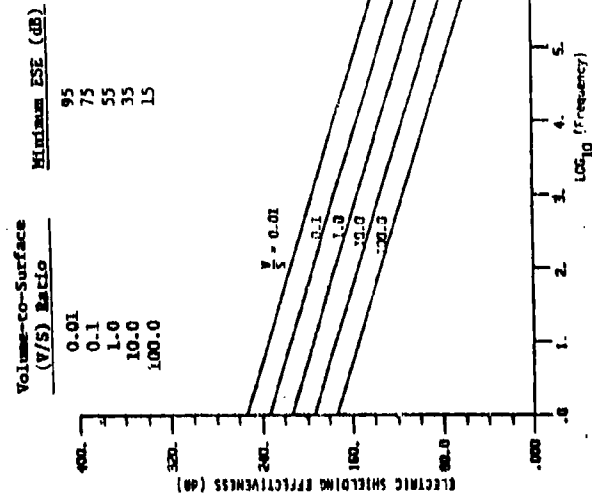


Figure 6.18 Electric Shielding Effectiveness of an Enclosure under a Uniform Electric Field (8)

Shield Conductivity = 10^4 mhos/m
Shield Thickness corresponds to 8-ply
composite material at 0.00525 in/ply



Volume-to-Surface (V/S) Ratio	Minimum ESE (dB)
0.01	95
0.1	75
1.0	55
10.0	35
100.0	15

Figure 6.19 Electric Shielding Effectiveness of an Enclosure under a Uniform Electric Field as a Function of Enclosure Volume-to-Surface Ratio (8)

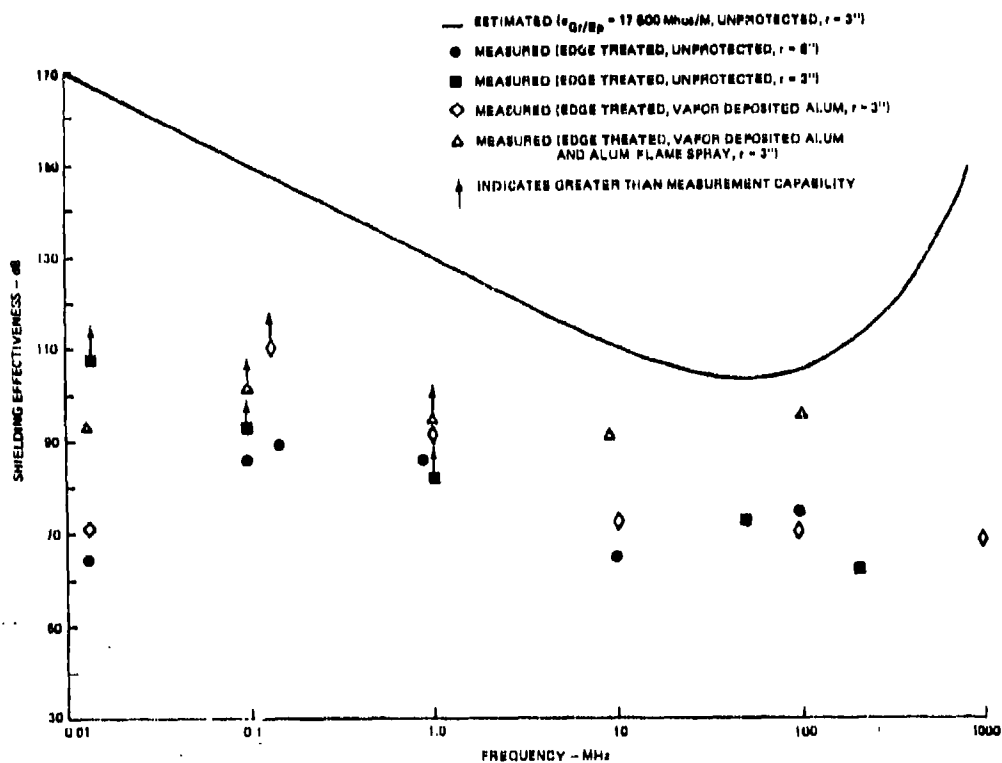


Figure 6.20 E-Field Shielding for 12-ply Graphite/Epoxy Composite Panel⁽¹¹⁾

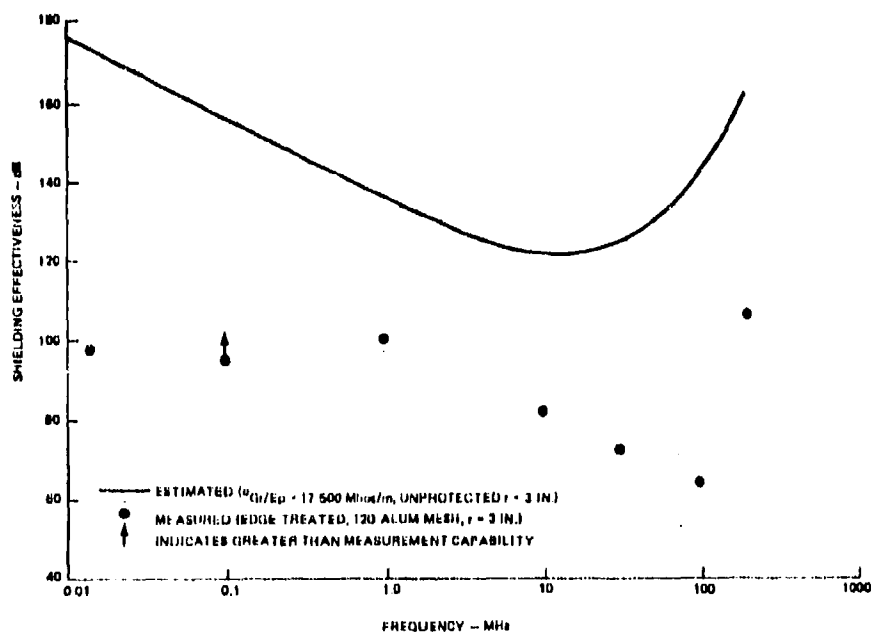


Figure 6.21 E-Field Shielding for 24-ply Graphite/Epoxy Composite Panel⁽¹¹⁾

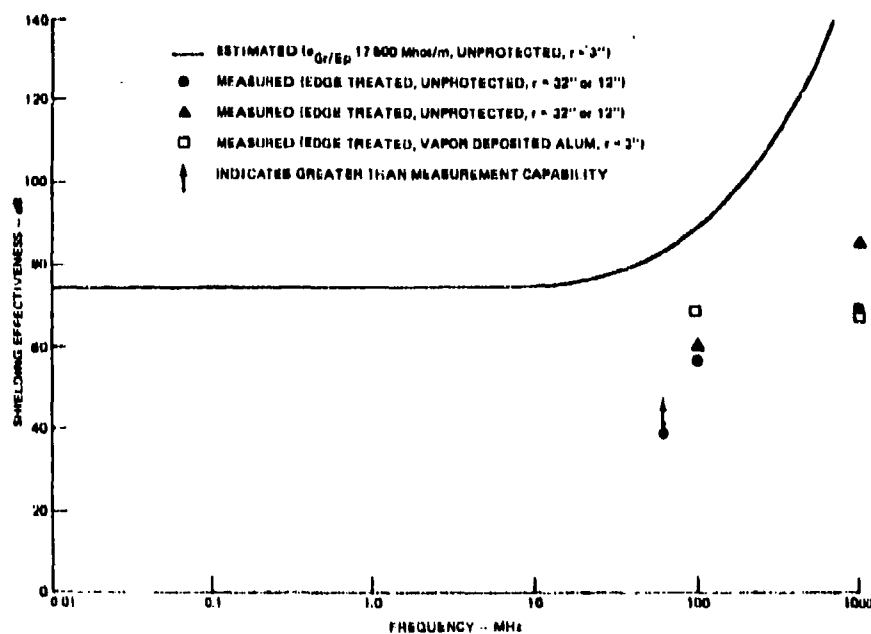


Figure 6.22 Plane-Wave Shielding Effectiveness For 12-ply Graphite/Epoxy Composite Panel⁽¹¹⁾

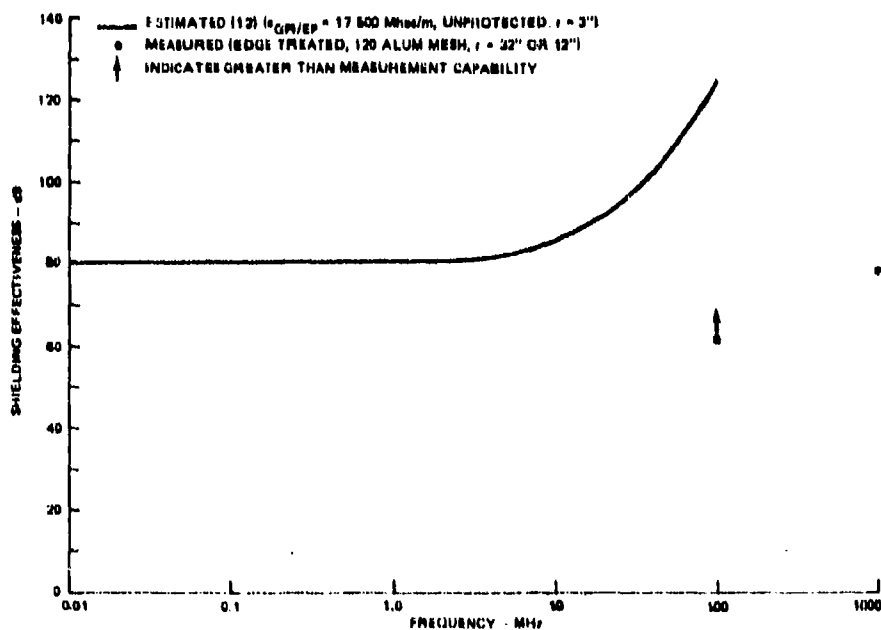


Figure 6.23 Plane-Wave Shielding Effectiveness for 24-ply Graphite/Epoxy Panel⁽¹¹⁾

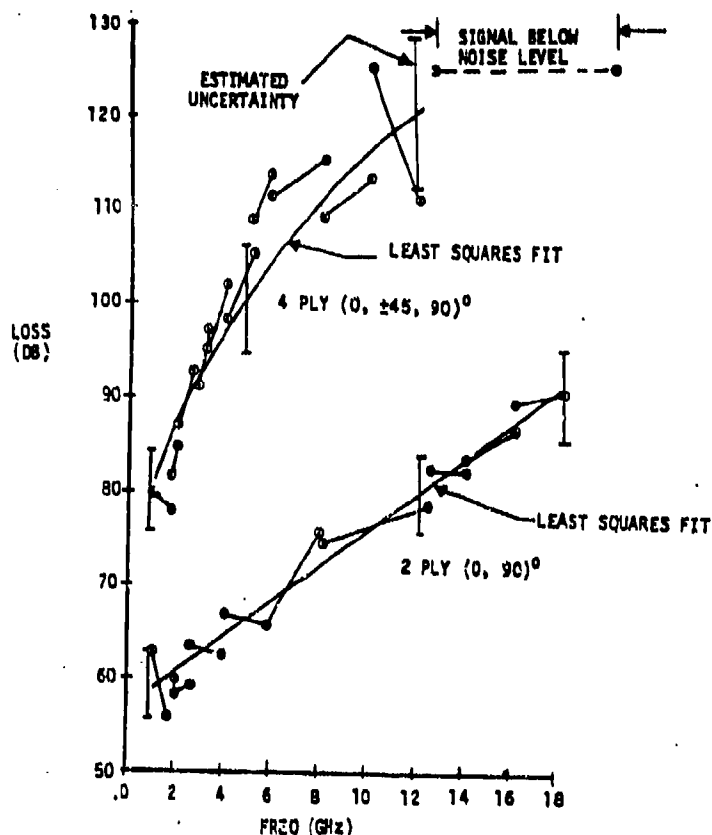


Figure 6.24 High Frequency Graphite/Epoxy Shielding Effectiveness Data ⁽¹⁰⁾

Table 6.1 Material Parameters Used in EM/Weight Tradeoffs
(Valid for Frequencies below 10⁵ Hz) ⁽⁸⁾

MATERIAL	CONDUCTIVITY (Ω^{-1}/m)	DENSITY (lb/ft ³) ρ_s	20 LOG Z_{ST} AT 10 ⁵ Hz (dB)	ΔZ_{ST} WRT G/E (dB)	$\left \frac{Z_{ST}}{Z_{ST}^{mat}} \right $ G/E	WEIGHT PENALTY (lb) AREA = 98.6 sq ft	SHIELDING MERIT
8-ply Aluminum	3.12×10^7	-	-102.32	-	-	-	-
Aluminum Foil (4 mil)	3.12×10^7	0.056	- 70.04	43	141.3	5.52	2523.2
Cu foil (4 mil)	7.29×10^7	0.1866	- 77.0	50	327.3	18.4	1754.0
120 Mesh Aluminum (4 mil)	-	0.045	- 50.0	23	14.1	4.44	313.3
Titanium Foil (4 mil)	2.1×10^6	0.0965	- 46.6	19.6	9.55	9.5	98.9
Aluminum Flame Spray (4 mil)	-	0.00971	- 47.98	20.98	11.2	0.96	1153.0
Nickel Foil (4 mil)	1.28×10^7	0.162	- 62.3	35.3	58.2	15.97	369.3
Tin Foil (4 mil)	8.78×10^6	0.146	- 59.0	32.0	39.8	14.4	272.6
8-Ply T-300 Graphite Epoxy	2×10^4	-	- 27.0	-	-	-	-
Boron Epoxy	-	-	30.0	-	-	-	-
Kelvar	-	-	224.0	-	-	-	-

The measure of EM shielding adopted in this tradeoff study is the surface transfer impedance. For all materials considered and for a frequency less than 100 kHz, the transfer impedance is independent of frequency and is given by

$$Z_{st} \approx \frac{1}{\sigma d} \quad (6-65)$$

This impedance depends only on the conductivity (σ) and the shield thickness (d) of the material.

The transfer impedance is given in Figure 6.25 for various aircraft materials and protective coatings including metals and composites. All transfer impedance data is listed in Table 6.1 and all samples are 4 mils thick. The results list the metals as having the best shielding characteristics as measured by the transfer impedance. The composites follow with graphite/epoxy the best in shielding. At frequencies less than 100 kHz boron/epoxy and Kevlar/epoxy have no shielding characteristics. Figure 6.25 shows the improvement in shielding provided by various protective coatings relative to 8-ply graphite/epoxy. It has been shown by Boeing⁽⁹⁾ that the transfer impedance of a coated material at low frequency is due almost entirely to the coating and the shielding improvement is just the ratio of the transfer impedances

$$\text{Improvement} = \frac{Z_{st}(\text{graphite/epoxy})}{Z_{st}(\text{coating})} \quad (6-66)$$

The data is listed in Table 6.1 and the results shown in Figure 6.26. Copper coatings give the best improvement in shielding while titanium foil gives the least improvement.

Any protective coating extracts a weight penalty. The weight penalties for 100 ft² (about the forward fuselage surface area of the AV-8B) of the coatings given in Figure 6.26 are shown in Figure 6.27. Besides giving the best shielding improvement, copper also extracts the highest weight penalty. The least penalty is paid by using aluminum flame spray.

Both the shielding and weight penalty produced by a given coating can be combined in an overall figure of merit defined as⁽⁸⁾

$$\text{Figure of merit} = \frac{\text{Improvement}}{\text{surface density of coating}} \quad (6-67)$$

The results are given in Figure 6.28 and show aluminum foil the best followed by copper foil and aluminum flame spray.

Figure 6.29(a) and 6.29(b) illustrate the gain in shielding effectiveness of a 24-ply and 8-ply graphite/epoxy respectively after application of various protective coatings. The tradeoff made determines the resulting shielding. A second set of tradeoffs involves the thickness of various coatings required to produce a given amount of shielding.⁽⁸⁾ All data for

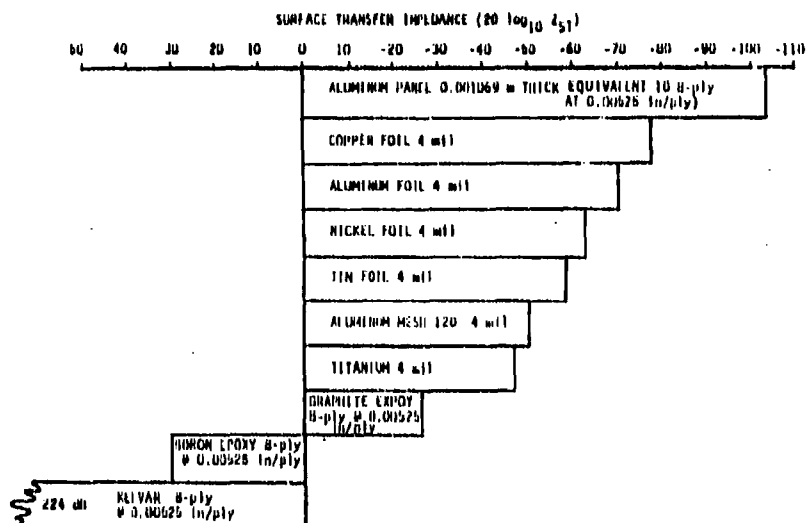


Figure 5.25 Transfer Impedance Shielding of Structural Materials and Protective EM Coatings (Valid for Frequencies below 10^5 Hz) (H)

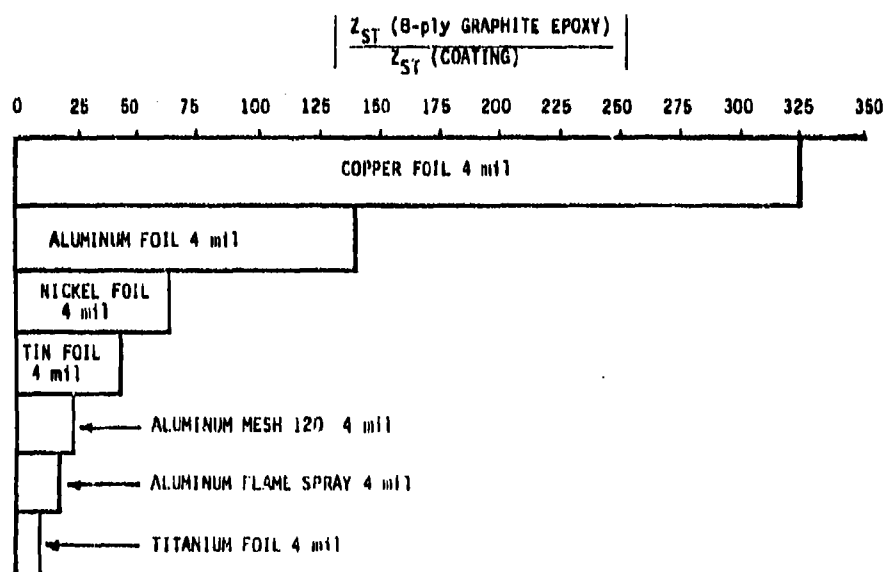


Figure 5.26 Improvement Protective Coatings Provide Relative to 8-Ply Graphite/Epoxy (Valid for Frequencies below 10^5 Hz) (B)

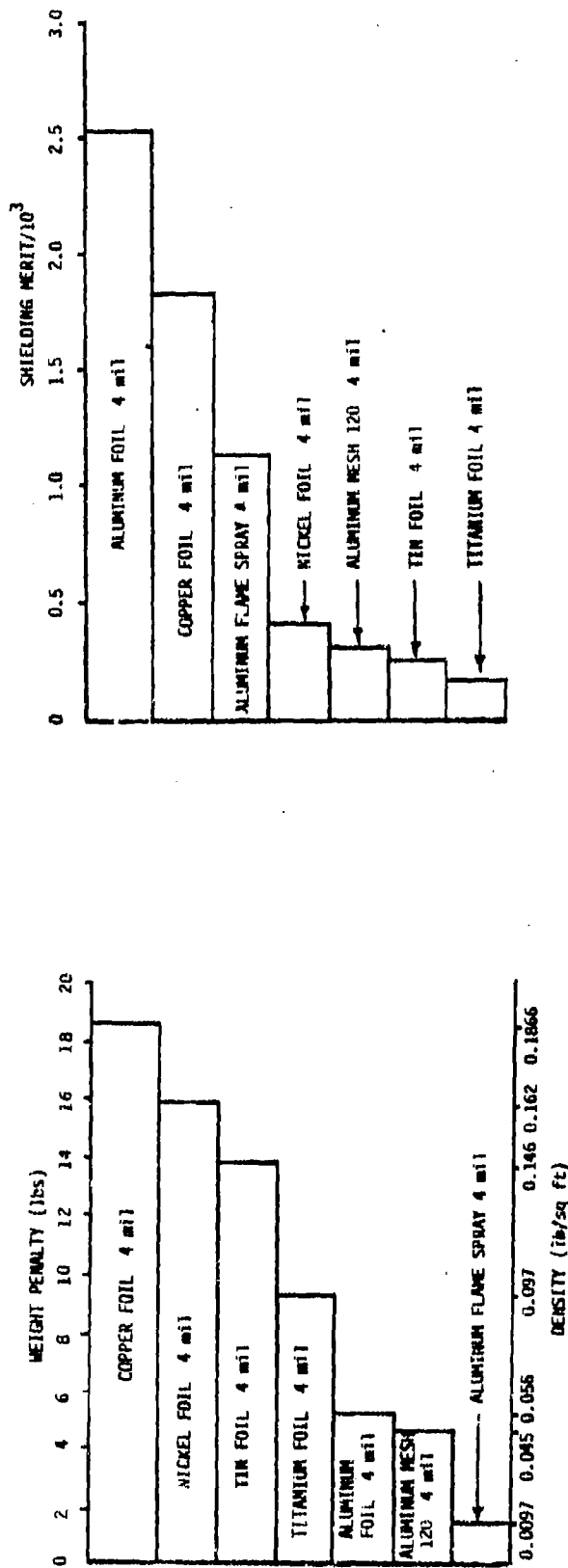


Figure 6.27 Forward Fuselage (Area = 100 ft²) Weight Penalty (lbs) Imposed by EM Protective Coatings

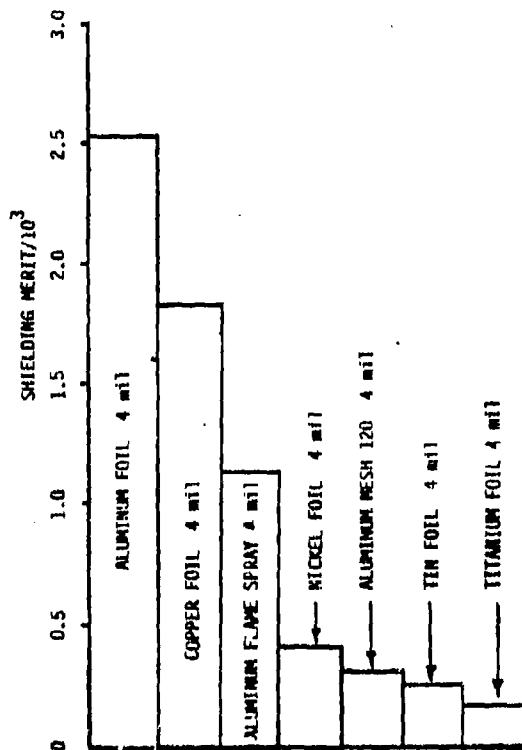


Figure 6.28 Weight Shielding Figure of Merit (Shielding Beyond 8-Ply Graphite/Epo of EM Protective Coatings)

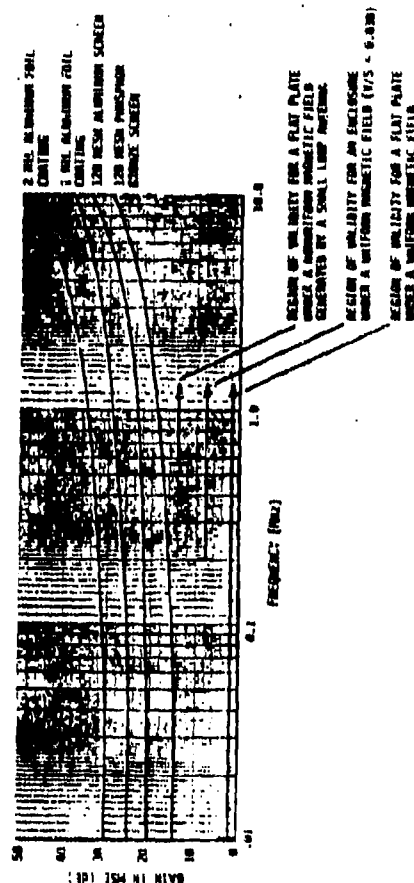
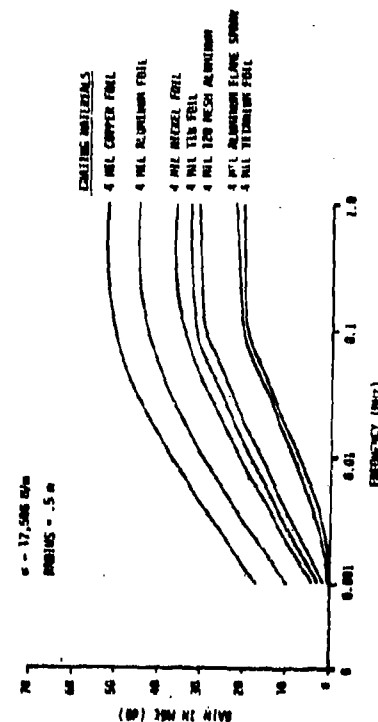


Figure 6.29 a Gain in the Magnetic Shielding Effectiveness of 24-Ply T-300 Graphite Composite Through Applications of Aluminum Foil, Aluminum Screens, and Phosphor Bronze Screens to 24-Ply T-300 Graphite (8)



this set of tradeoff studies is listed in Table 6.2. Again the surface transfer impedance is used as the measure of shielding effectiveness. Table 6.2 lists thicknesses of various composite coatings to achieve 40 dB, 60 dB and 72 dB shielding effectiveness along with the weight penalties involved. The results are given in Figures 6.30, 6.31 and 6.32 respectively. Copper foil requires the thinnest coating for a given improvement in shielding effectiveness and is closely followed by aluminum foil. Titanium foil requires the thickest coat with aluminum flame spray somewhat thinner. Aluminum foil extracts the least weight penalty with copper a close second and aluminum flame spray third. Titanium extracts the largest weight penalty by far with tin foil the next worst.

6.2 Composite Joints

In this section a theoretical overview is given of joints in air-frame skins together with some measured joint admittance data. Measured changes in shielding effectiveness are given for composite panels with joints.

6.2.1 Theory

External EM fields will induce currents on the surface of both metal and composite aircraft. The existence of a joint in the aircraft skin results in a voltage drop across the joint as shown in Figure 6.32. The external field induces a surface current J_s on the skin which produces a field E_j across the joint. The joint voltage drop V_j is then

$$V_j = \int_{-a}^b E_j \cdot dl = \frac{J_s}{Y_j} \quad (6-68)$$

where Y_j is the joint admittance per unit joint width.

Three common types of joint construction are shown in Figure 6.34. The measured joint admittances for these joints are given in Figure 6.35. These joint admittances range from a few mhos/m to a few hundred mhos/m depending on the joint type. Joint 2 with Y_k 15 mhos/m is typical of the joints currently used in aircraft. The joint admittance is rather insensitive to frequency over a large frequency range.

A theoretical model can be developed for the simple infinite butt joint shown in Figure 6.36a modeled as a uniform slot of width W . An equivalent transmission line circuit for the butt joint is shown in Figure 6.36b which results in the following expression for Y_j :

$$Y_j = (Y^a + Y^c) \cosh(\gamma_b d) + \left(Y_o + \frac{Y^a Y^c}{Y_o} \right) \sinh(\gamma_b d) \quad (6-69)$$

Table 6.2 Coating Thickness and Weight Penalty
for Fixed Shielding (8)

Shielding	σ	Coating Thickness in mils		
		$20 \log_{10} Z_{at}$		
		40 dB	60 dB	72 dB
Aluminum Foil	3.12×10^7	0.1259	1.259	5.0121
Copper Foil	7.29×10^7	0.034	0.34	2.1451
Titanium Foil	2.1×10^6	1.87	18.7	74.46
Nickel Foil	1.28×10^7	0.31	3.1	12.217
Tin Foil	8.78×10^6	0.45	4.47	17.81
Aluminum Flame Spray	2.46×10^6	1.6	16.0	63.6
Graphite/Epoxy	10^4	392.8	3928.0	15638.0

Shielding	Density (lb/ft ³) for 1 mil coating (lb)	Weight Penalty/ft ² Applied Coating (lb)		
		$20 \log_{10} Z_{at}$		
		40 dB	60 dB	72 dB
Aluminum Foil	0.014	0.00177	0.0177	0.0702
Copper Foil	0.04665	0.00232	0.0232	0.100
Titanium Foil	0.024125	0.45	0.45	0.797
Nickel Foil	0.0403	0.0126	0.126	0.495
Tin Foil	0.0365	0.016	0.16	0.65
Aluminum Flame Spray	0.00243	0.004	0.04	0.155

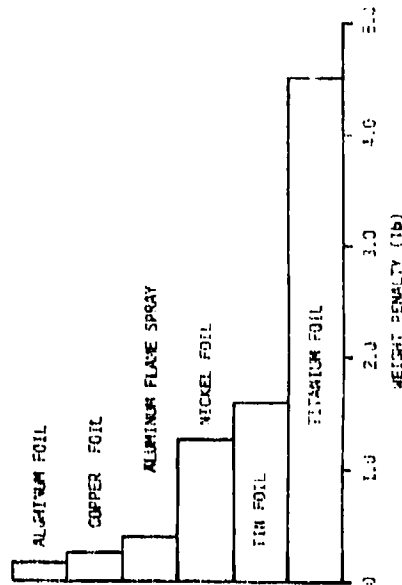
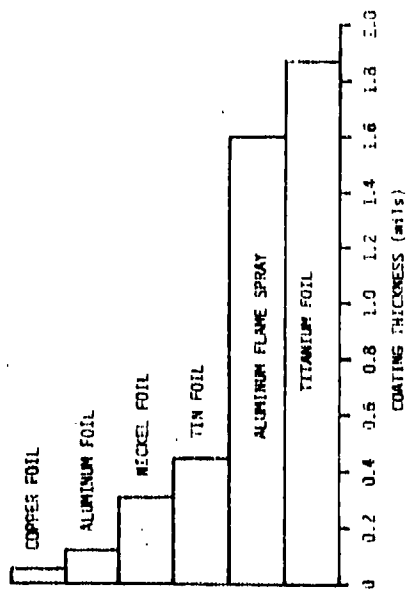


Figure 6.30 Coating Thickness and Weight Penalty for $Z_{sc} = -40 \text{ dB}$ at Low Frequency (8)

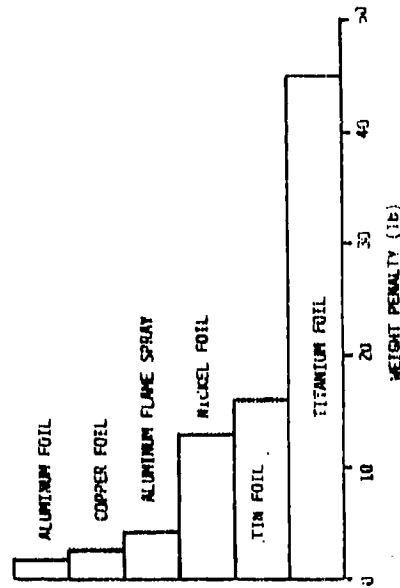
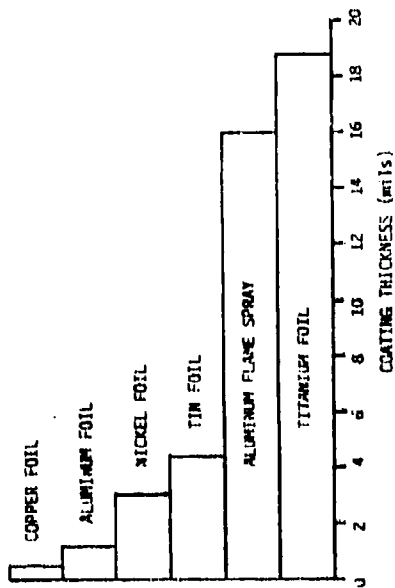


Figure 6.31 Coating Thickness and Weight Penalty for $Z_{sc} = -60 \text{ dB}$ at Low Frequency (8)

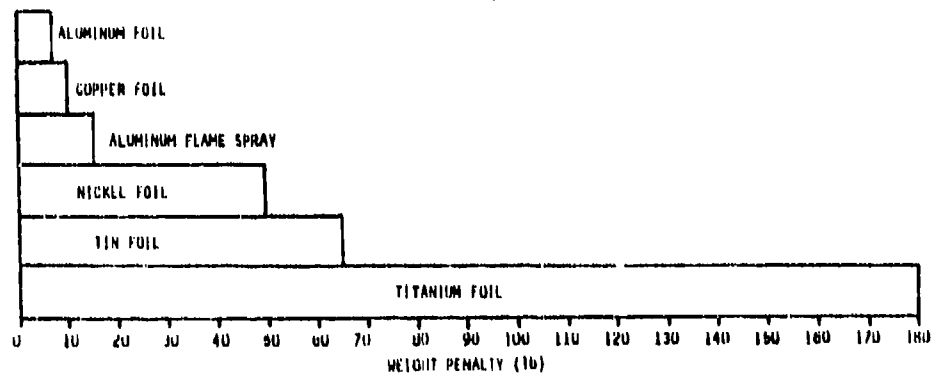
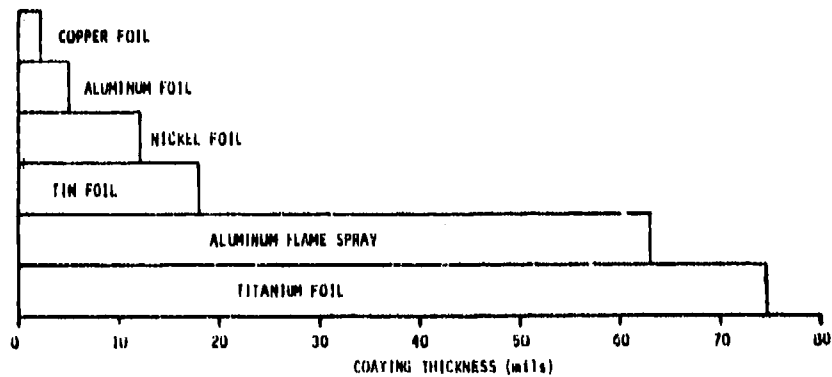


Figure 6.32 Coating Thickness and Weight Penalty for $Z_{at} = -72$ dB at Low Frequency⁽⁸⁾

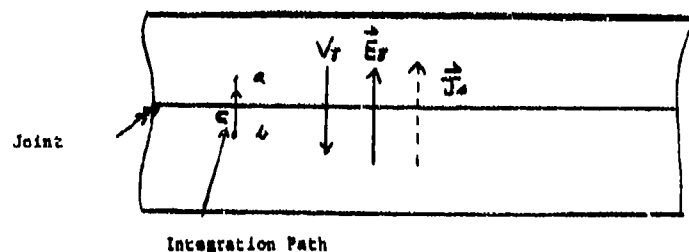
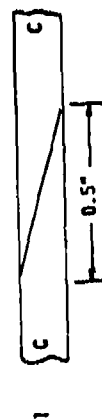
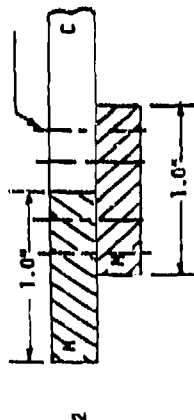


Figure 6.33 Joint Coupling⁽⁸⁾

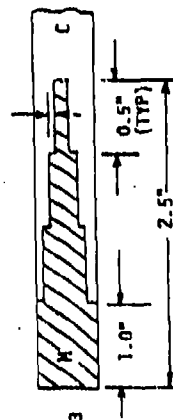


CYLINDER WAS FABRICATED EXTRA LONG, CUT, MACHINED AND SECONDARILY BONDED WITH EA-934 ADHESIVE.



1/8 DIA RD. HO. RIVET C TO M
1/8 DIA BOLT M TO M.

CYLINDER CENTER TOWARDS BOTTOM OF PAGE. METAL RINGS FABRICATED FROM ALUMINUM SHEET, CUT, FOLDED AND WELDED. THE RIVETS OR BOLTS WERE PLACED IN A CIRCUMFERENTIAL ROW APPROXIMATELY ONE INCH APART AND ALTERNATING 1/8 INCH TO EITHER SIDE OF THE CIRC. CTR LINE.



FIRST THREE STEPS (4 PLY PER STEP) WERE PRECURED (COMPACTED). EA-934 APPLIED TO SANDED COMPOSITE STEPS, AND THEN LONGITUDINALLY SLIT METAL RING MANEUVERED INTO PLACE. REMAINING COMPOSITE STEPS WERE APPLIED TO EA-934 COATED METAL RING IN PLACE. METAL RING WAS FABRICATED FROM 2024 ALUMINUM.

Figure 6-34 Structural Joints (6,10)

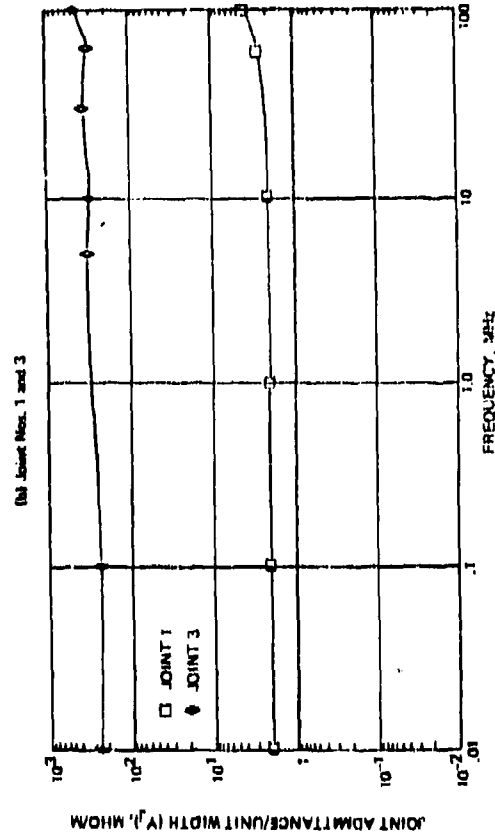
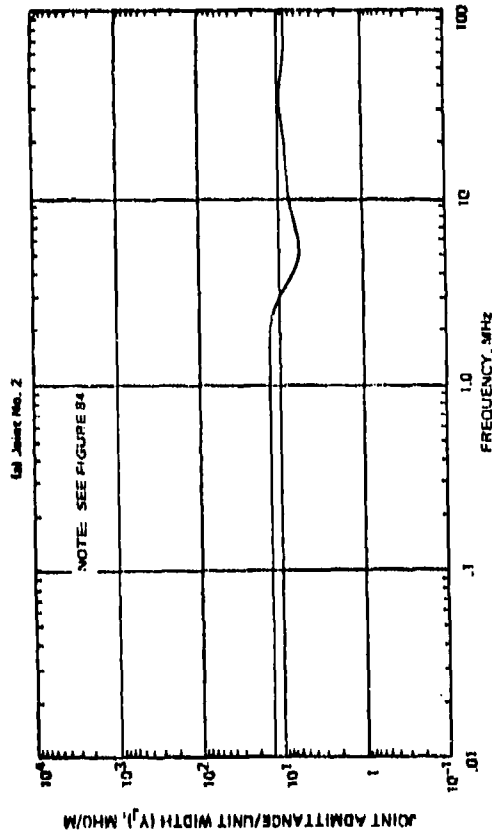


Figure 6-35 Measured Joint Admittance (6,10)

Here Y^a and Y^c are the admittances of a thin slot looking into Region a and Region c as in Figure 6.36a and Y_o is given in 6.36b. The aperture admittance is given by

$$Y^a = \frac{W}{\eta_a \lambda_a} [\pi - 2j \ln(C k_a W)] \quad (6-70)$$

where η_a , λ_a and k_a are the impedance, wavelength and wave number for Region A. The constant C depends on how the tangential electric field varies in the slot. For a quasi-static field in a slot of zero thickness⁽⁸⁾ $C \approx 0.2226$.

For a highly lossy slot, equation (6-69) reduces to:

$$Y_J \approx \frac{\sigma_b d}{W} \quad (6-71)$$

independent of frequency. This is the behavior shown by the measured joint admittances in Figure 6.35.

6.2.2 Effect on Shielding Effectiveness

As part of its Protection Optimization Program, Grumman⁽¹¹⁾ has performed measurements on graphite/epoxy panels with various types of doublers and fasteners. Tests were made under various conditions, such as tight joints, loose joints or no joints, to verify that degrading the quality of the joint reduces the shielding effectiveness of the composite panels.

The tightly jointed panel shielding effectiveness is shown in Figures 6.37 - 6.39 for magnetic, electric and plane wave shielding as a function of frequency. The results indicate that little difference in shielding resulted from use of different fasteners to join the panels. Two joined aluminum plates were also tested for shielding effectiveness as a standard and performed better than the joined composite panels.

Figure 6.40 shows the magnetic shielding behavior of two joined composite panels; one 12 ply the other a 24 ply. As the joint quality is degraded the magnetic shielding decreases dramatically for high frequencies. The same general trend, although less dramatic, held for electric and plane wave shielding effectiveness as shown in Figures 6-41 and 6-42.

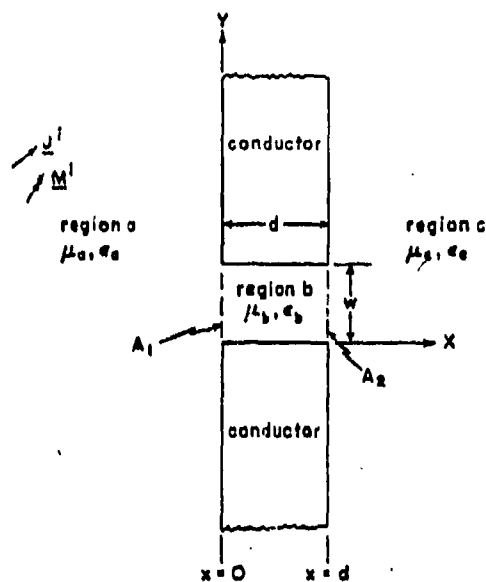


Figure 6.36a Uniform Slot of Width w in a Perfectly Conducting Screen of Thickness d (8)

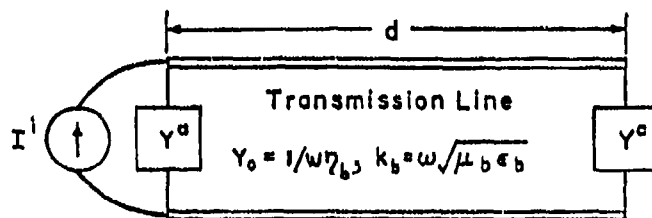


Figure 6.36b Equivalent Circuit for a Narrow Slot in a Thick Conducting Screen (8)

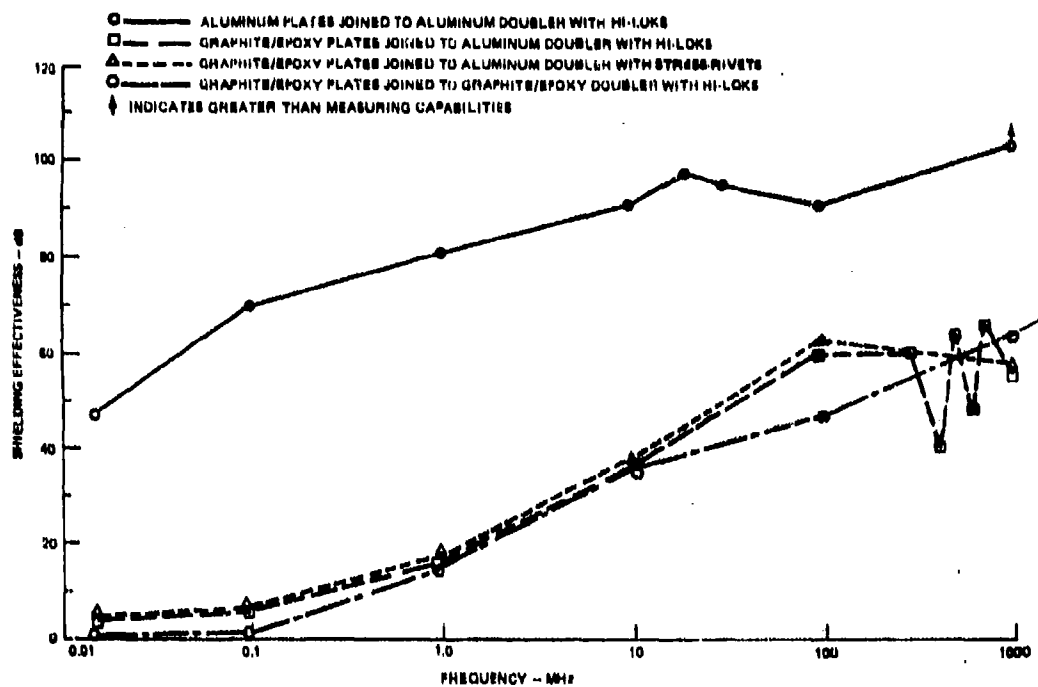


Figure 6.37 Magnetic Shielding Effectiveness For Tightly Joined Panels (11)

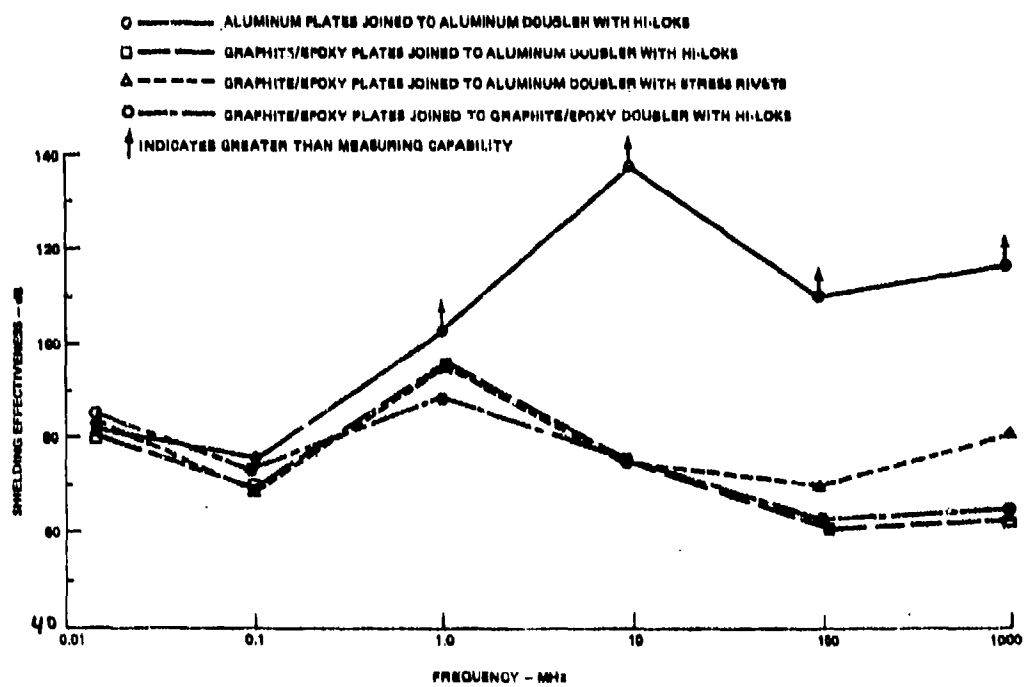


Figure 6.38 Electric Shielding Effectiveness of Tightly Joined Panels (11)

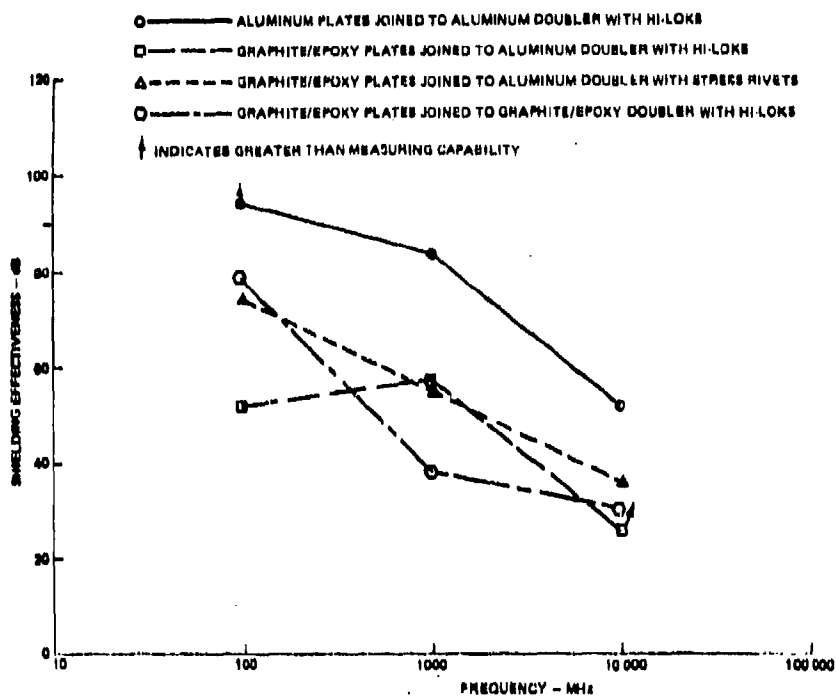


Figure 6.39 Plane-Wave Shielding Effectiveness of Tightly Joined Panels (11)

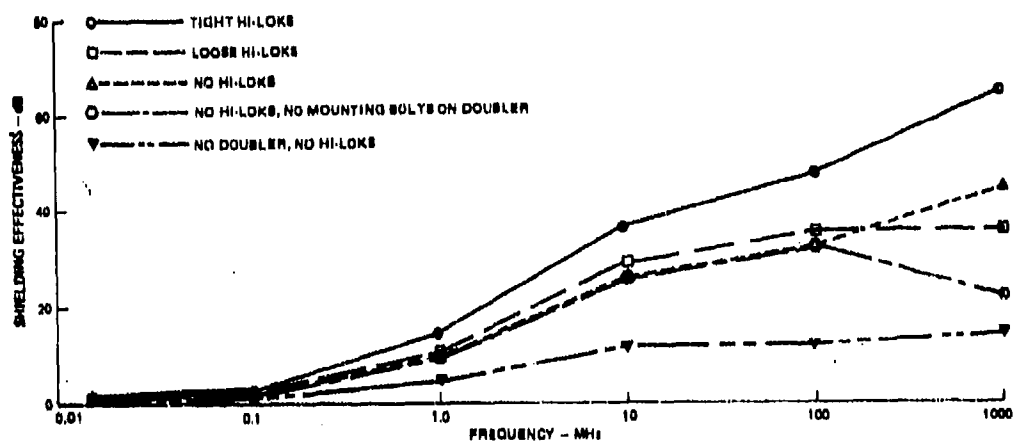


Figure 6.40 Variation of Magnetic Shielding Effectiveness of 12-ply Graphite/Epoxy Panels Joined to 24 Ply Graphite/Epoxy Doubler With Hi-Loks (11)

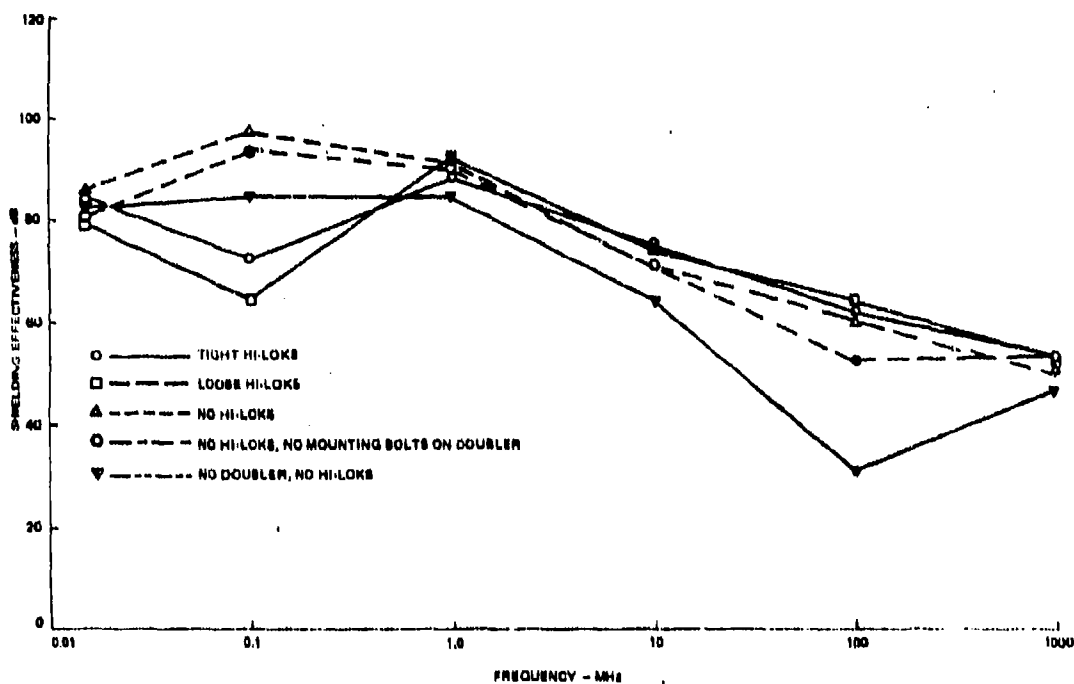


Figure 6.41 Variation of E-Field Shielding Effectiveness of 12-ply Graphite Epoxy Joined to 24 Ply Graphite/Epoxy Doubler With Hi-Loks (11)

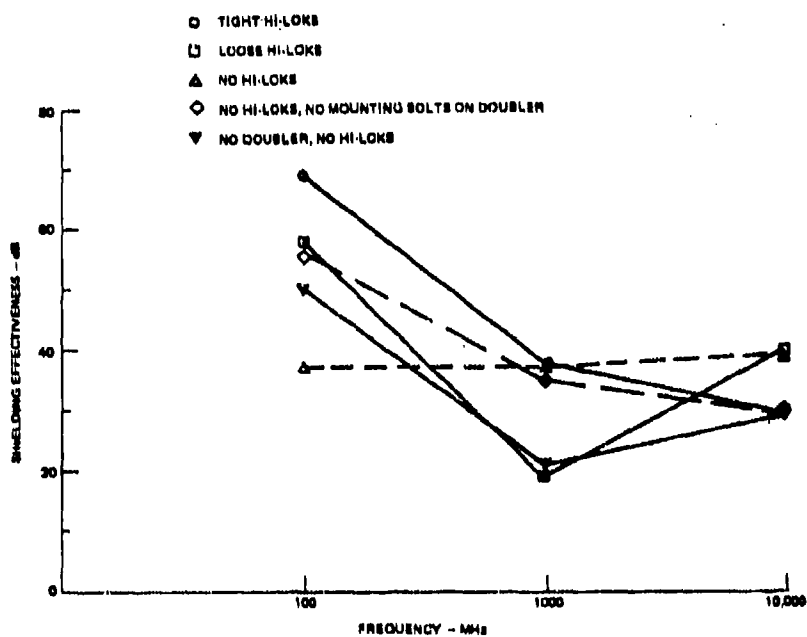


Figure 6.42 Variation of Plane-Wave Shielding Effectiveness for 12-ply Graphite/Epoxy Panels Joined to 24 Ply Graphite/Epoxy Doubler With Hi-Loks (11)

6.3 References

1. J. R. Moser, "Low Frequency Shielding of a Circular Loop Electromagnetic Field Source, " IEEE Trans. Elec. Comp., Vol EMC-9, No. 1, pp 6-18, March 1967.
2. S. A. Schelkunoff, Electromagnetic Waves, Van Nostrand, 1943.
3. P. R. Bannister, "New Theoretical Expressions for Predicting Shielding Effectiveness for the Plane Shield Case," IEEE Trans. Elec. Comp., Vol EMC-10, No. 1, pp 2-7, March 1968.
4. R. F. Harrington, Time Harmonic Electromagnetic Fields, McGraw Hill, Section 8-5, 1961.
5. J. L. Allen, et. al., "Electromagnetic Properties and Effects of Advanced Composite Materials: Measurement and Modeling," USAF Rome Air Development Center, TR-78-156, Phase Report, June 1978.
6. R. F. Stratton, USAF Rome Air Development Center, Private Communication, December 1980.
7. R. E. Collin, Field Theory of Guided Waves, McGraw-Hill, Section 3.4, 1960.
8. R. Wallenberg, et. al., "Advanced Composite Aircraft Electromagnetic Design and Syntheses," Interim Report, SRC-TR-79-490, April 1980.
9. D. Strawe, L. Piszher, Interaction of Advanced Composites With Electromagnetic Pulse (EMP) Environment, The Boeing Co.
10. F. Force, et. al., Investigation of Effects of Electromagnetic Energy on Advanced Composite Aircraft Structure and Their Associated Avionic Electrical Equipment Phase D, Vol 1, The Boeing Co., Final Report, September 1977.
11. Protection Optimization For Advanced Composite Structures, Fourth Quarter Report, Grumman Aerospace Corp. 15 June 1978.
12. "Engineering Design Handbook, Electromagnetic Compatibility," DARCOM-P-706-410, Hq USA Material Development and Readiness Command, March 1977.

This chapter will discuss the susceptibility of various electronic components and subsystems that may be expected to be found aboard composite aircraft. The origin of the component or subsystem susceptibility is treated and susceptibility curves presented for those components and subsystems for which models that are available and able to predict system degradation due to RF interference are also discussed. The components treated are analog and digital circuits, diodes, transistors, integrated circuits, microwave devices and electro-explosive detonators. Subsystems include communication and navigation equipments, control equipment, weapons, and radar.

7.1

Component and Circuit Susceptibility

In this section the susceptibility of a number of electronic components and circuits to interference and damage from various RF energy levels is examined. General analog and digital circuits are discussed and representative susceptibility curves presented. A more detailed examination is given to semi-conductor devices and integrated circuits with numerous performance curves and some device models described. Finally a description is given of the susceptibility of electro-explosive detonators and microwave devices.

7.1.1

Analog Circuits

Analog (or linear) circuits are characterized by electronic operations over a continuous parameter range or by having a continuous output. Interference in such a circuit will exist when an unwanted signal is superimposed upon a desired signal. The amount of degradation caused by this interference may be either proportional to the amount of interference present or depend on the existence of an interference threshold level. Below the threshold, almost no degradation may result but above it there may be almost total degradation of circuit performance. Analog circuits operate over a very wide range or levels from a few nanovolts to several kilovolts. The low level circuits can be expected to be the most sensitive to interference.

The most susceptible part of an analog circuit is usually the input because of its lower signal level. The circuit susceptibility can be controlled by the use of balanced circuits at low frequency and coaxial shields at high frequency.

Other parts of the system may exhibit significant susceptibility levels. Power lines and control cables, especially near high field regions such as cathode ray tubes, can be sources of susceptibility unless properly shielded.

One analog device that operates at high voltage but is still quite susceptible to interference is the synchro. This device, which is used to transmit position or control information, operates on a null principle using a reference circuit. Consequently, even a small coupling of undesired signals onto the reference circuit can cause significant errors in the nulling process.

A susceptibility curve for a typical amplifier is shown in Figure 7.1. The linear susceptibility is defined as the field level producing a voltage equal to the internal circuit noise.⁽¹⁾

7.1.2 Digital Circuits

Digital circuits are characterized by electronic operations in one of two levels designated as high or low.^(1,4) Such circuits require that signal levels must surpass a certain threshold level before the device will respond. Consequently, digital devices tend to be insensitive to interference below the threshold level, but a full-level bit error is likely if the interference exceeds the threshold level.⁽¹⁾

Digital circuits generate interfering signals primarily through the operation of numerous internal switching circuits with rapid rise times.⁽¹⁾ The circuits are synchronized by clock-timing logic. For this type of interference the interference spectrum frequencies will be the clock frequency and its harmonics.⁽¹⁾

Other potential sources of interference are the basic oscillator, time pulse distributors, register counters, drums, discs and magnetic tape devices. An emission spectrum for a digital computer is shown in Figure 7.2 as an example of interference frequencies and voltage levels that could be encountered in nearby equipment.

There are several coupling mechanisms responsible for the susceptibility of digital equipment. One mechanism is induction coupling,⁽¹⁾ either externally from cables and connectors or internally within the device itself. Both forms of inductive coupling result from parasitic mutual capacitance and inductance present in the neighborhood of the digital device. The result is either internal crosstalk between device gates or extraneous external signals induced in a given gate. In particular, magnetic material in tapes, discs drums, shift registers, decoders, buffer storage and memory are all sensitive to external magnetic fields which may arbitrarily shift bit positions and destroy stored data. A second mechanism is conduction coupling.⁽¹⁾ The high speed switching circuits that are characteristic of digital devices may produce large switching transients in the power and ground circuits which can couple into sensitive digital circuits. A third coupling mechanism is radiation coupling.⁽¹⁾ Strong RF sources such as high powered radar, lightning, and even precipitation static may penetrate and couple to digital circuits. Significant interference may result if the radiation is close to the clock frequency. A typical set of susceptibility curves for digital circuits is shown in Figure 7.3.

7.1.3 Semiconductor Devices

Individual solid state devices such as diodes and transistors are susceptible to interference and damage from external RF sources. In this section, the mechanisms for interference and damage of semiconductor devices by RF signals is discussed in detail. Models for transistors and diodes are presented that are capable of assessing the effect of RF interference on device operating characteristics. Damage characteristics of semiconductors are discussed using the Wunach model.

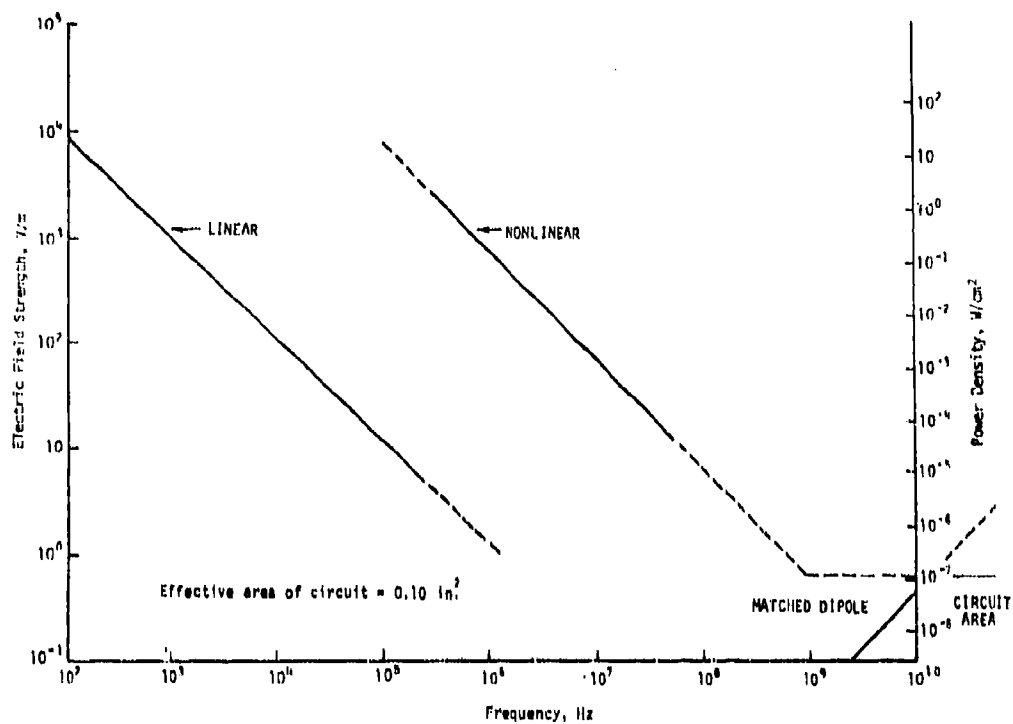


Figure 7.1 Amplifier Susceptibility⁽¹⁾

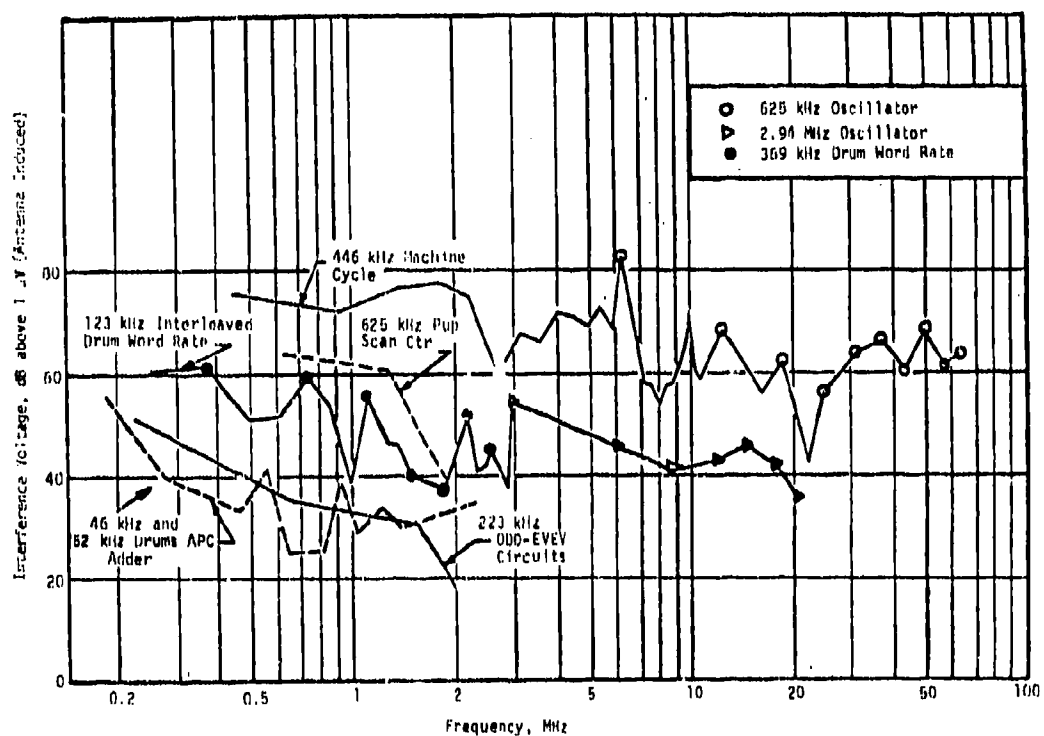


Figure 7.2 Digital Computer Emission Spectrum⁽¹⁾

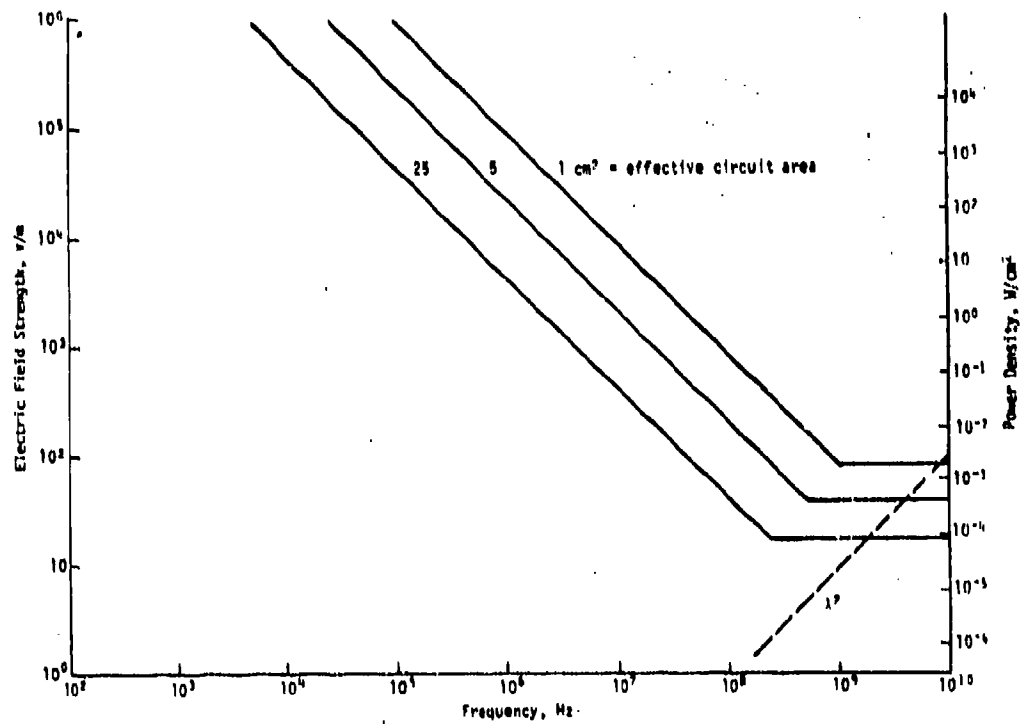


Figure 7.3 Typical Digital Circuit Susceptibility Curves⁽¹⁾

7.1.3.1 Device Interference

In electronic systems, undesired electromagnetic signals can be picked up on circuit wiring and conducted into individual semiconductor devices such as diodes and transistors. These devices are constructed out of PN junctions which have non-linear DC voltage-current characteristics.⁽⁵⁾ When an RF signal is induced on the device, rectification of the RF by the semiconductor junction results.^(4,5) The effect of the rectified RF on the device is to change the device operating point by modifying the DC voltage-current characteristics. The RF-modified diode characteristics are shown in Figure 7.4a for several different induced RF power levels. The shift is towards increased current and decreased voltage.⁽⁵⁾

Figure 7.4b shows a circuit constructed to model⁽⁵⁾ the diode DC voltage-current characteristics given in Figure 7.4a. The device voltage and current are v_d and i_d , respectively. Diode D1 with current i_{D1} is assumed not to be under the influence of an RF signal. The diode D2 (assumed for simplicity to have characteristics identical to diode D1 and current i_{D2} , the current source i_x , and shunt resistor R_x model the RF induced offset voltage and current and depend on the RF power level frequency and source impedance. A given choice of R_x and i_x simulates the diode interference for a given frequency and source impedance.

Transistors, like diodes, will exhibit interference characteristics when coupled to RF signals. Again like diodes, the transistor operating point is modified by RF rectification at the transistor junctions. This modification can be seen in the transistor DC voltage-current characteristics.^(4,5) Figures 7.5 and 7.6 show the voltage-current characteristic curves for two different NPN transistors with and without interference RF on the collector lead. The shift in voltage and current is readily apparent in the figures.

When an NPN transistor has RF induced on the base or emitter leads, beta reduction usually takes place.⁽⁵⁾ This effect is illustrated in Figure 7.7 for several transistors stimulated on the base by RF at 220 MHz.⁽⁵⁾

The properties of NPN transistors, including nonlinear effects at junctions, can be accurately modeled by the standard Ebers-Moll NPN transistor representation.⁽⁵⁾ This representation is shown in Figure 7.8a as an equivalent circuit. In order to take RF interference effects into account each diode in the Ebers-Moll transistor model is replaced by the diode interference model shown in Figure 7.4b. The result is the modified Ebers-Moll transistor model shown in Figure 7.8b that is capable of modeling RF interference effects.⁽⁵⁾ The RF-modified DC voltage-current characteristics of two NPN transistors calculated with the model are shown in Figure 7.9. The results compare favorably with the measured RF-modified characteristic shown in Figures 7.5 and 7.6.

The semiconductor models described in this section have been used⁽⁶⁾ to develop models for IC devices to predict IC susceptibilities. A discussion of this approach together with some results are given in Section 7.1.4.

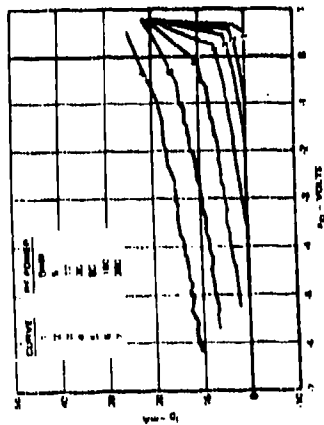


Figure 7.4a RF induced diode characteristics for 1N914 diode at 220 MHz (15)

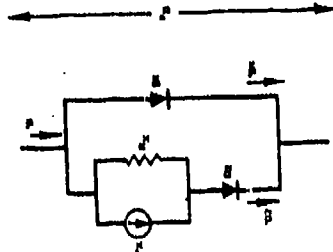


Figure 7.4b Circuit model of diode under RF influence (5)

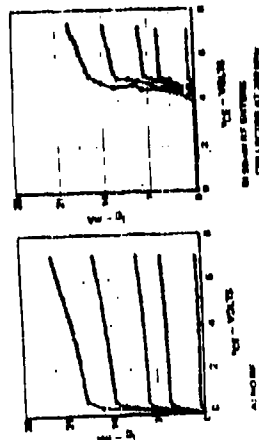


Figure 7.5 Characteristics of a 2N2369A transistor with and without RF interference on the collector lead (5)

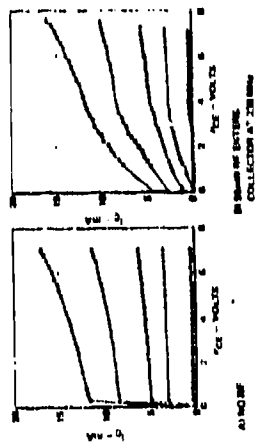


Figure 7.6 Characteristics of a 2N2222A transistor with and without RF interference on the collector lead (5)

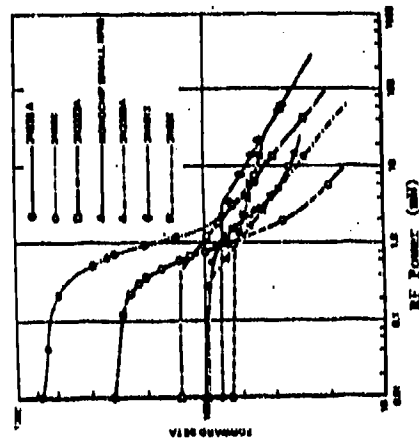


Figure 7.7 RF induced beta reduction at 220 MHz. RF stimulates the base lead (5)

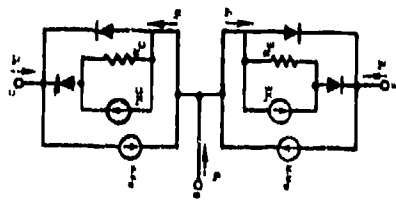


Figure 7.8b Modified Ebers-Moll MPN transistor model including RF interference effects (5)

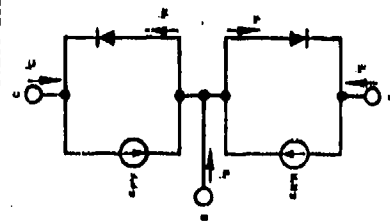


Figure 7.8a Standard Ebers-Moll MPN transistor model (5)

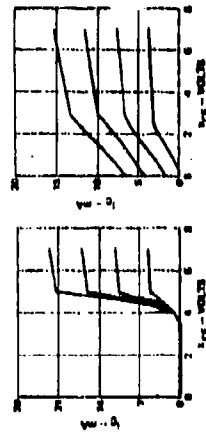


Figure 7.9 Transistor characteristics calculated using modified Ebers-Moll model for the 2N2369A and 2N2222A transistors (5)

7.1.3.2 Device Damage and Failure

If the absorbed RF interference level exceeds the susceptibility level of a semiconductor by a sufficiently large amount, device damage and/or catastrophic failure will result. The burnout characteristics of a semiconductor are commonly described by the Wunsch model ⁽⁴⁾ given by

$$P = kt^{1/2} \quad (7.1)$$

where P is the power to fail the device (in watts), k is the damage (Wunsch) constant (in watt-sec ^{1/2}) determined by device junction properties and geometry, and t is the RF pulse time (in seconds).

A range of values for the Wunsch constant is given in Figure 7.10a for selected diodes ⁽⁴⁾ and in Figure 7.10b for selected transistors. ⁽⁴⁾

Three computational procedures exist for the calculation of the Wunsch constant K. The most accurate method ⁽⁴⁾ of determining K is from the device junction area. The appropriate relations ⁽⁴⁾ are

$$\text{for diodes:} \quad K = 550A \quad (7.2)$$

$$\text{for transistors:} \quad K = 470A \quad (7.3)$$

where A is the junction area in cm². Device junction areas are not readily obtainable from manufacturer's data sheets so the method is usually not used in practice.

A second method depends on the thermal resistance of the device. ⁽⁴⁾ The equations for K define three categories of semiconductor device: ⁽⁴⁾

Category 1 - Germanium diodes and transistors

Category 2 - Silicon diodes and transistors
except planar and mesa

Category 3 - Silicon planar and mesa transistors

The relations for K are then ⁽⁴⁾

$$\text{Category 1 - Insufficient data} \quad (7.4)$$

$$\text{Category 2 - } K = 31.5 \theta_{jc}^{-1.11} \quad (7.5)$$

$$K = 972.2 \theta_{jc}^{-1.24} \quad (7.6)$$

$$\text{Category 3 - } K = 338.3 \theta_{jc}^{-1.73} \quad (7.7)$$

$$K = 4.625 \times 10^6 \theta_{ja}^{-3.08} \quad (7.8)$$

where

$$\theta_{jc} = \frac{T_j(\text{max}) - T_c}{P_d} \quad (7.9)$$

$$\theta_{ja} = \frac{T_j(\text{max}) - T_{\text{amb}}}{P_d} \quad (7.10)$$

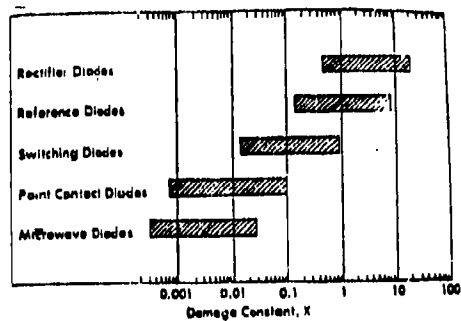


Figure 7.10a Wunsch Constant Range for Representative Diodes⁽⁴⁾

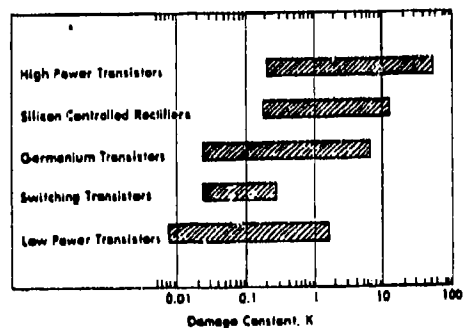


Figure 7.10b Wunsch Constant Range for Representative Transistors⁽⁴⁾

and $T_j(\text{max})$ is the maximum operating junction temperature, T_c is the case temperature, T_{amb} is the ambient temperature, and P_d is the power dissipated. Usually either θ_{jc} or θ_{ja} can be calculated from manufacturer's data sheets.⁽⁴⁾

The third, and most reliable method, calculating K utilizes the junction capacitance C_j and breakdown voltages V_{bd} . The equations for K are⁽⁴⁾

$$\text{Category 1} - K = 2.2 \times 10^{-3} C_j V_{bd}^{(0.20)} \quad (7.11)$$

$$\text{Category 2} - K = 1.1 \times 10^{-3} C_j V_{bd}^{(0.81)} \quad (7.12)$$

$$\text{Category 3} - K = 0.008 \times 10^{-3} C_j V_{bd}^{(1.63)} \quad (7.13)$$

The junction capacitance and breakdown voltage are usually available on data sheets, making this method quite practical.

Typical upset and burnout energies for various semiconductor devices are given in Figure 7.25 in Section 7.1.4.2.

7.1.4 Integrated Circuits

Integrated circuits (ICs), like individual circuit components, are susceptible to interference effects and catastrophic failure from RF radiation. The IC susceptibility and failure data presented in this section are based in large part on the IC susceptibility handbook developed by McDonnell-Douglas.^(2,4)

7.1.4.1 IC Interference

The basic cause of interference in an IC device is rectification of the interfering signal in the nonlinear pn or np transistor or diode junction in the IC.^(2,4) The rectified signal shifts the current or voltage operating point of the IC device. The practical effect in the circuit is that the IC may be driven from a "low" state to a "high" state or vice versa.⁽⁴⁾

The susceptibility curves for a number of IC devices tested by McDonnell-Douglas⁽¹⁾ are given in Figures 7.11 to 7.16 inclusive. The IC devices types are transistor-transistor logic devices (TTL's), CMOS devices, line dividers and receivers, operational amplifiers (op amps), voltage regulators and comparators. Each IC device figure consists of a part describing the varieties of each device tested (part a) and a part giving the device susceptibility curve (part b). The susceptibility curves for all devices represent the "worst-case" situation of power absorbed by the device through leads that are half-wave dipoles.⁽⁴⁾ The general trend of the susceptibility curves is for a decreasing device susceptibility as frequency increases over the range from 0.1 GHz to 10 GHz. Operational amplifiers were found to be the most susceptible to RF interference, and 3-pin regulators were the least susceptible. The susceptibility curves for all devices are shown in Figure 7.17 for comparison.

A power density curve for each device can be constructed using the Figure 7.17 power curves. If the worst case aperture of a half-wave dipole

DEVICE NO.	DEVICE TYPE
7400	QUAD 2 INPUT NAND GATE
7402	QUAD 2 INPUT NOR GATE
7404	HEX INVERTER
7405	HEX INVERTER (OPEN COLLECTOR)
7406	QUAD 2 INPUT AND GATE
7408	QUAD 2 INPUT OR GATE
7432	EXPANDABLE DUAL 2 WIDE, 2 INPUT AND-OR-INVERT GATE
7456	DUAL J-K FLIP-FLOP
7473	DUAL D FLIP-FLOP
7479	DUAL D FLIP-FLOP

Figure 7.11a TTL Devices Tested (4)

Minimum Specification Value for Low V_{OUT} = 0.4 Volt and
Minimum Specification Value for High V_{OUT} = 2.4 Volts

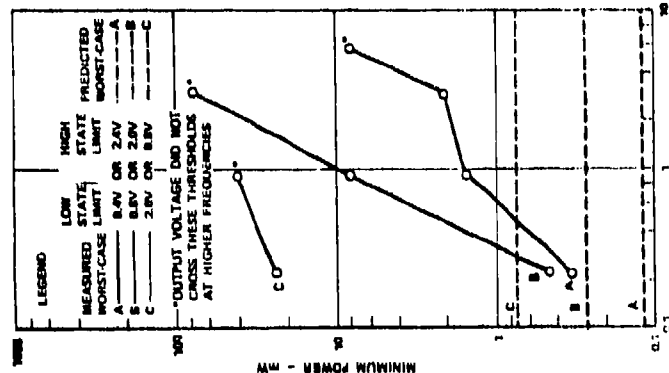


Figure 7.11b Worst Case Susceptibility Values for TTL Devices (4)

DEVICE NO.	DEVICE TYPE
4011A	QUAD 2 INPUT NAND GATE
4012B	QUAD 2 INPUT NOR GATE
4027A	DUAL COMPLEMENTARY PAIR PLUS INVERTER
4049B	DUAL COMPLEMENTARY PAIR PLUS INVERTER
4070A	QUAD 2 INPUT NOR GATE
4071A	QUAD 2 INPUT NOR GATE
4013A	DUAL "D" - TYPE FLIP-FLOP

Figure 7.12a CMOS Devices Tested (4)

Minimum Specification Value for Low V_{OUT} = 0.05 Volt and Minimum
Specification Value for High V_{OUT} = 4.55 Volts

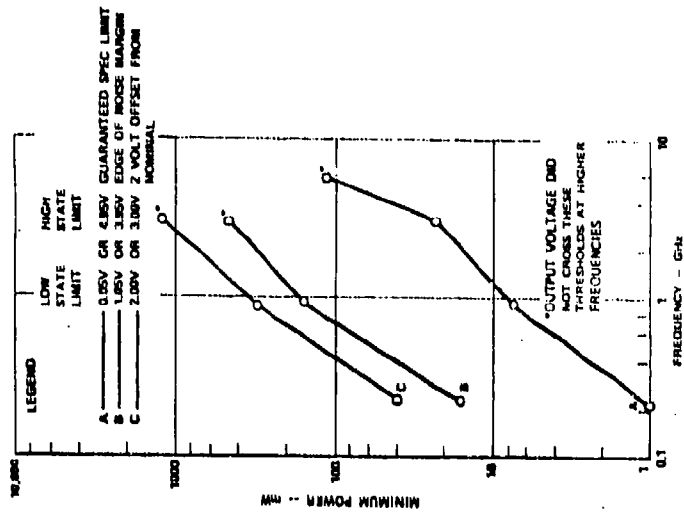


Figure 7.12b Worst Case Susceptibility Values for CMOS Devices (4)

1-PIN IS VOLT

300
305
306
70000
8-PIN
300
305

Figure 7.15a Voltage Regulators Tested (4)

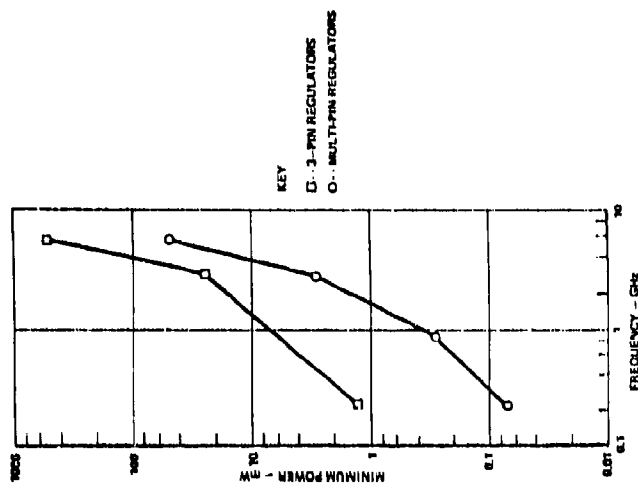


Figure 7.15b Worst Case Susceptibility Values for Voltage Regulators (4)

701
7061
201A
207
0000C
511

Figure 7.13a 0 Amp Devices Tested (4)

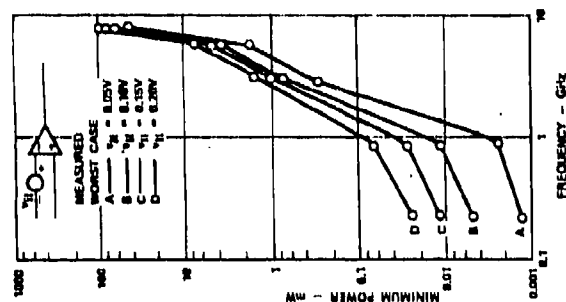


Figure 7.14b Worst Case Susceptibility Values for 0 Amps (4)

LINE DRIVERS	LINE RECEIVERS
8020	8020
8014	8015
55109	55107A
55110	

Figure 7.13a Line Drivers and Receivers Tested (4)

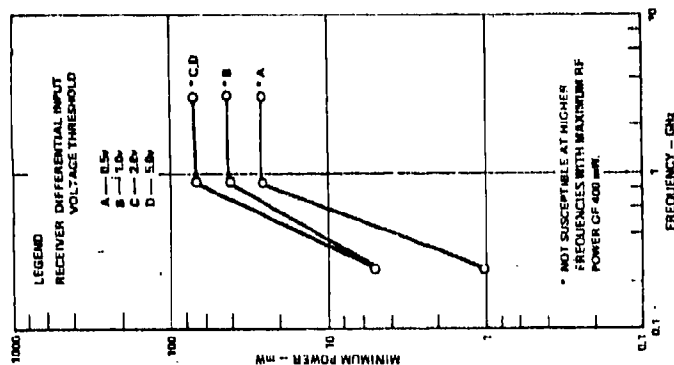


Figure 7.13b Worst Case Susceptibility Values for Line Drivers and Receivers (4)

306
311
328
360
710
760

Figure 8.16a Comparators Tested⁽⁶⁾

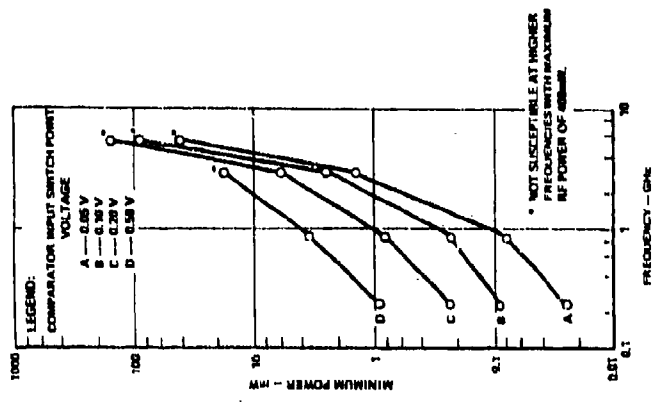


Figure 7.16b Worst Case Susceptibility Values for Comparators⁽⁷⁾

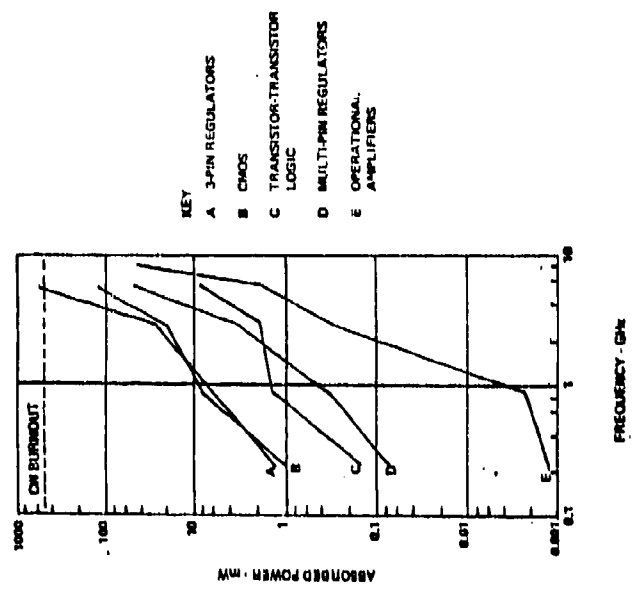


Figure 7.17 Worst-Case Susceptibility Curves for all IC Devices⁽⁴⁾

is assumed for the circuit, the IC power density susceptibility, P_d , is related to the IC power susceptibility P given in Figure 7.17 by

$$P = 0.13 \lambda^2 P_d \quad (7.14)$$

where λ is the radiation wavelength. The superimposed power density susceptibility curves for all IC devices are shown in Figure 7.18. Using these curves, it would be possible to assess the EM shielding required to protect IC devices against a given RF threat level (such as described in Section 2.0).

Besides experimental susceptibility curves, IC device models have been developed which allow IC susceptibilities to be predicted theoretically.⁽⁶⁾ The IC models consist of a collection of models of the individual semiconductor components that comprise the IC. The semiconductor models are described in Section 7.1.3 of this handbook.

The modified Ebers-Moll transistor model⁽⁵⁾ described in Section 7.1.3 has been used to construct a model of a 7400 NAND gate IC that is useful in describing interference in the device.⁽⁶⁾ A schematic circuit diagram of a 7400 NAND gate IC device is shown in Figure 7.19a and the modified Ebers-Moll circuit model of the IC is in Figure 7.19b. Both circuits are configured for use in the IC circuit analysis program SPICE (Simulation Program with Integrated Circuit Emphasis).^(6,9) The results of the simulation are given in Figure 7.20 for three 7400 NAND gate types (74, 74H and 74L). The simulations show device output voltages vs. the incident RF power. Two susceptibility levels, one for a low state (0.8V) and one for a high state (2.0V) are also shown. Figure 7.21 gives the values of RF power predicted by SPICE which cause the susceptibility levels in the three 7400 NAND gate types to be exceeded. The results compare favorably to the experimental data that is available.^(2,4)

7.1.4.2 Device Damage and Failure

Integrated circuits can be subjected to excessively high levels of RF energy just like individual semiconductor devices. Damage results at some level above the device susceptibility. The result will then be impaired IC operation or catastrophic failure of the whole device. Device failure results from excessive RF heating of the silicon junctions or wires which causes thermal destruction of the IC. The peak power absorbed by an IC is a function of pulse width and is illustrated in Figure 7.22. This figure shows a zone of definite IC operation, a zone of definite IC failure and a zone of uncertainty where the IC may or may not fail.

Integrated circuit device failure caused by electromagnetic pulse (EMP) can be modeled by the equation

$$P = At^{-B} \quad (7.15)$$

where P is the average failure power (in watts), t is pulse duration (sec), and A , B are experimental constants. This model is analogous to the Wunsch model used for semiconductor failure. The empirical values of the constant A are given in Figure 7.23 for a number of IC devices and semiconductors. The constant B has yet to be evaluated in the same manner, however the data in Figure 7.22 corresponds to a choice of A of 3.5×10^{-3} and B of 0.5.

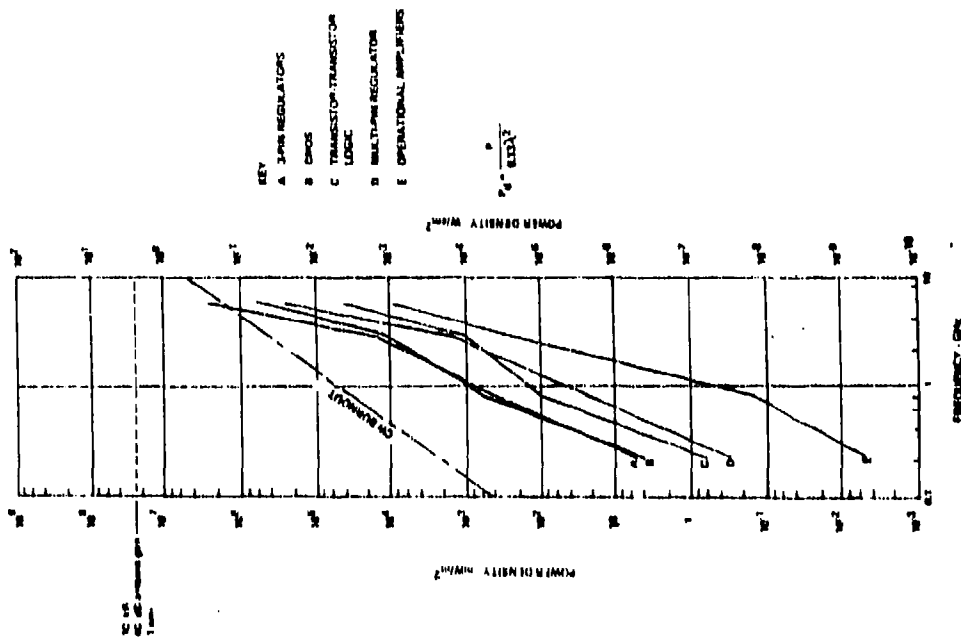


Figure 7.16 Integrated Circuit Power Density Susceptibility Curves (4)

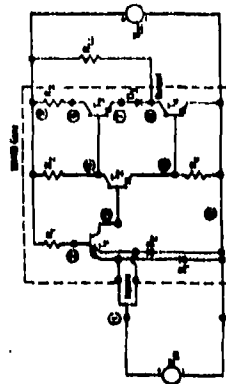


Figure 7.19a Schematic circuit of 7400 NAND gate with external connections. Node numbers are used in computer circuit program SPICE(5)

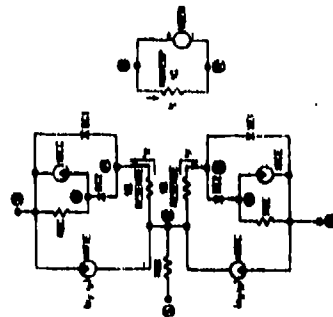


Figure 7.19b Modified Ebers-Moll model of 7400 NAND gate with external model configuration used with computer circuit program SPICE(5)

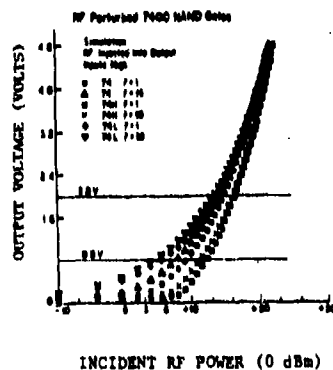


Figure 7.20 Output voltage for three 7400 NAND gate types vs incident RF power as simulated by SPICE. Susceptibility levels of 0.8V for low state and 2.0V for high state are shown (6)

Type of Gate	VOUT = 0.8V		VOUT = 2.0V	
	SPICE ^a P ₁ (dBm)	Eq 1 ^b P ₂ (dBm)	SPICE ^a P ₃ (dBm)	Eq 1 ^b P ₄ (dBm)
7400L (P = 10)	4.4		13.4	
7400L (P = 1)	5.4		14.0	
7400 (P = 10)	7.6	6.0	16.6	14.5
7400 (P = 1)	9.0		16.6	
7400H (P = 10)	11.2		16.0	
7400H (P = 1)	12.2		16.5	

^a Values of simulated RF power.
^b Values of simulated RF power.
 Values of simulated RF power would be higher.

Figure 7.21 Values of RF Power Which Cause EM Susceptibility Criteria To Be Exceeded for Three 7400 NAND Gate Types (6)

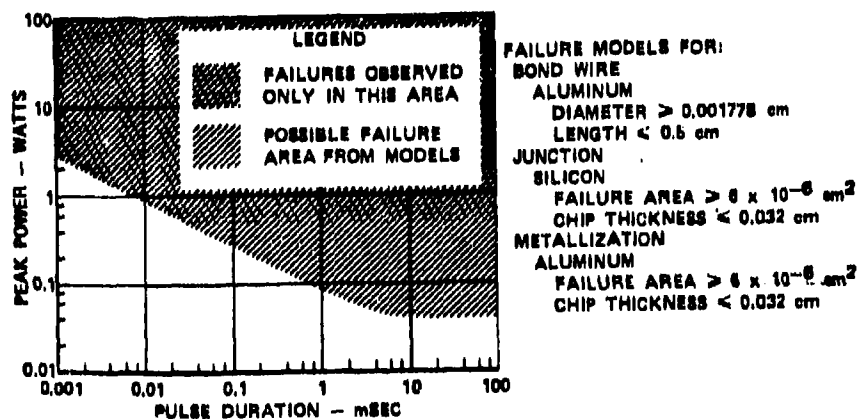


Figure 7.22 Worst Case IC Failure Levels (4)

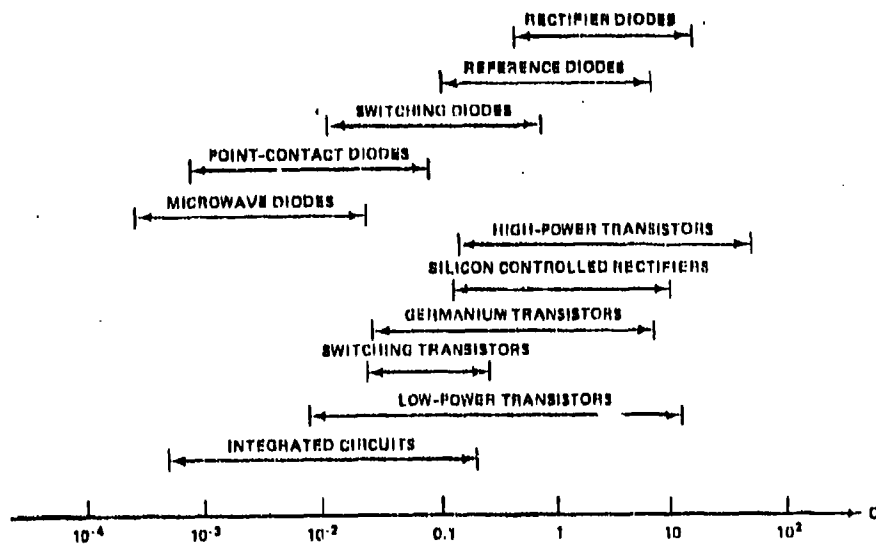


Figure 7.23 Range of A for Various Devices (4)

Some distinction can be drawn between linear and digital IC devices in terms of damage caused by EMP. Usually linear IC devices are less susceptible than digital devices. The general trend in both device types is illustrated in Figure 7.24 for IC damage power as a function of pulse width.

A general ranking of circuit elements (both solid state and IC) is given in Figure 7.25 on the basis of susceptibility to upset and burnout. Integrated circuits are clearly the most susceptible devices.

7.1.5 Electro-Explosive Detonators

The criteria for the proper design of electro-explosive detonators (EED's) and their integration into systems such that the electromagnetic radiation hazards to EED's are minimal are contained in MIL-STD-833 and MIL-STD-1385. The maximum allowable field strength levels of exposure of EED's to electromagnetic radiation⁽³⁾ are given in Figure 7.26.

7.2 Subsystem Susceptibility

A number of subsystems commonly found on aerospace vehicles are examined in this section for their susceptibility to RF interference. The subsystems include communication equipment (voice, digital, and picture), navigation equipment, flight control equipment, weapons, and radar. The discussion is general and describes how susceptibility to interference is measured. Some susceptibility and performance curves are presented for subsystems.

7.2.1 Communication and Navigation

Interference in and susceptibility of communication subsystems is usually treated by first dividing the systems into two types; those which are voice and those which are teletype or digital.^(7,8)

7.2.1.1 Voice Communication

The problems encountered in specifying the susceptibility or other performance criteria for voice communication systems revolves around the random nature of the received voice signal, and differences in hearing and understanding abilities of one receiver operator as compared to another.^(7,8) Two general approaches have been formulated to treat this problem.

One approach uses trained talkers and listeners to determine the levels of intelligibility in various communication receivers. The figure of merit in this procedure is the articulation score for the receivers under test. The articulation score can be related to a signal-to-interference ratio as shown in Figure 7.27 for different receivers.

Another method of evaluating voice communications is the articulation index of the receiver.⁽⁷⁾ To determine this index, the audio spectrum is first divided into weighted bands in such a way that they contribute equally to voice intelligibility. The signal-to-interference-plus-noise ratio $S/(I+N)$ is then specified for each band. The percentage contribution of each band to the articulation index will then depend on the signal-to-in-

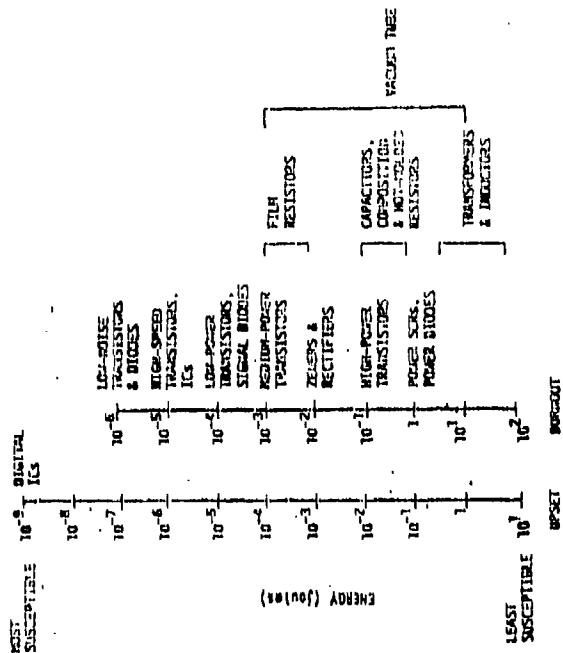


Figure 7.25 Upset and Burnout Energy of Various Circuit Elements (4)

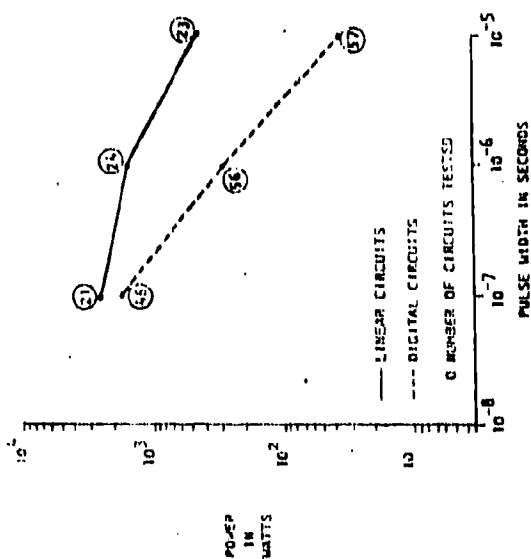


Figure 7.24 Damage Levels for Linear and Digital IC Devices (4)

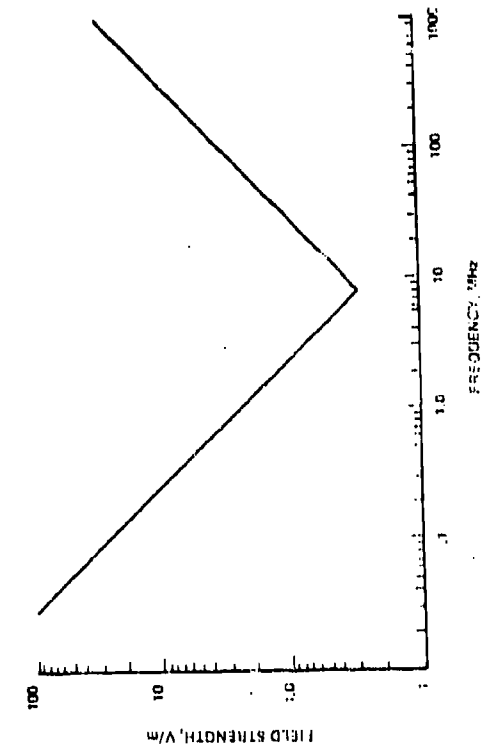


Figure 7.26 Maximum Field Strength Limits for EIR-6

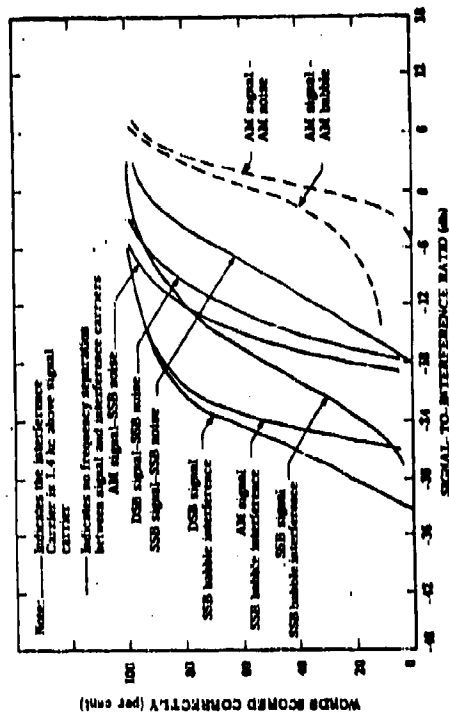


Figure 7.27 Signal-to-Interference Ratio Versus Articulation Score (7-6)

terference ratio S/I in the band. The band is said to contribute in a maximum sense if the $S/(I+N)$ is greater than or equal to +18 dB, and in a minimum sense if $S/(I+N)$ is less than or equal to -12 dB. In between, the contribution is defined by linear extrapolation between the extreme values.

7.2.1.2 Teletype of Digital Communication

Digital or teletype communication subsystems can be evaluated by finding their probability of error.⁽⁷⁾ Two types of error are mistaking interference for the signal (false acceptance), and not recognizing the presence of the signal (false dismissal). From a knowledge of the statistical nature of the particular digital communication subsystem under test, it is possible to relate the error rate to the signal-to-noise ratio of the system^(7,8) to determine the susceptibility.

7.2.1.3 Picture Communication

Picture communications in the form of television and facsimile subsystems have become increasingly important. Interference takes the form of dots, lines and bars in the picture or may cause the picture to be blurred, lose sync or roll.⁽⁷⁾ Susceptibility and interference levels are difficult to define because of the variable perceptions of the images by different observers. Digital images can be improved in quality using modern digital signal processing and image enhancement techniques.

7.2.1.4 Navigation Systems

Radio navigation systems are widely used in marine and aerospace applications.⁽⁷⁾ The characteristics of some of the more common radio navigation systems are given in Table 7.1. For proper use, the station must be correctly identified and the information in the signal correctly determined. Interference can cause incorrect identification of station and message information resulting in navigational errors.^(7,8)

Modern aircraft depend on sophisticated inertial navigation subsystems for the proper fulfillment of mission requirements. A typical navigation subsystem consists of a stable platform consisting of a set of gyro-stabilized accelerometers whose outputs are fed to a computer.⁽¹⁾ The computer calculates aircraft position and velocity as well as gyro precession signals which maintain platform stability. Other equipment includes a display and control panel, power supplies and a backup battery for the computer.⁽¹⁾ A block diagram of an inertial navigation system is shown in Figure 7.28.⁽¹⁾

Because the inertial navigation subsystem is a precision instrument, care must be taken to reduce transients and variations in current and isolate sources of such transients and variations from the instrument.⁽¹⁾ Cables carrying digital and analog data to and from synchros may be susceptible because of the precision required in the data.⁽¹⁾

7.2.2 Flight Control Equipment

Flight control equipment is concerned with the adjustment of aircraft surfaces for purposes of maneuvering the aircraft.⁽¹⁾ A block diagram of flight control operation is shown in Figure 7.29.⁽¹⁾ Sensors

Table 7-1 Radio Navigation Systems (7)

System	Frequency	Range (Nautical miles)	Propagation	Error ± degrees or ± feet			Comments
				Site	Instrument	System	
Direction finder	Many	200	Negligible	1°	1°	2°	Earliest radio navigation system; still in use as a backup system.
Ground VHF/OMF			Up to 25°	3°	2°	Variable	
Airborne MF							
Four-course low-frequency range	200 to 400 kHz	200	Up to 25°	1°	2°	Variable	Obsolete and being replaced by VHF omni range.
Non-directional beacon	200 to 1700 kHz	200					Worldwide use with airborne LF/MF direction finders.
Marker beacons	75 MHz	200	Negligible	None	300 ft	300 ft	Used throughout U.S. as check points along airways and distance markers in instrument-landing systems.
VHF omnidirectional range (VOR)	108 to 118 MHz	200	Negligible	3°	1°	3.5°	Successor to low-frequency range; accepted international standard.
Decca	70 to 130 kHz	200	Up to 10,000 ft	None	20 ft	30 to 10,000 ft	Continuous-wave hyperbolic system used extensively in Europe by ships and fishing fleets.
Ground-based radar	1250 to 10,000 MHz	200	Negligible	None	1°/1000 ft	1°/1000 ft	Widely used.
Loran-A	2 MHz	600	100 ft	None	1500 ft	1500 ft	Long range.
Tacan Range	960 to 1215 MHz	200	Negligible	None	260/2000 ft	2000 ft	Military short range omnibearing and distance measuring system.
Distance-measuring equipment (DME)	960 to 1215 MHz	200	Negligible	None	2°	2°	International standard often co-located with VOR to form a single site area-converge system.
Vortac					200 ft to 2°/1/2	3000 ft or 3°/1/2	Co-location of VOR and Tacan to provide en-route navigation.
Loran-C	100 kHz	1200	300 ft	None	100 ft	100 to 1200 ft	Expected successor to Loran-A; longer range and improved accuracy obtained by cycle-matching techniques.
Loran-D	100 kHz						Short-range tactical system compatible with Loran-C.
Omega	10 to 14 kHz	8000	5000 ft	None	500 ft	5000 ft	Hyperbolic system with longer range and less accuracy than Loran-C.

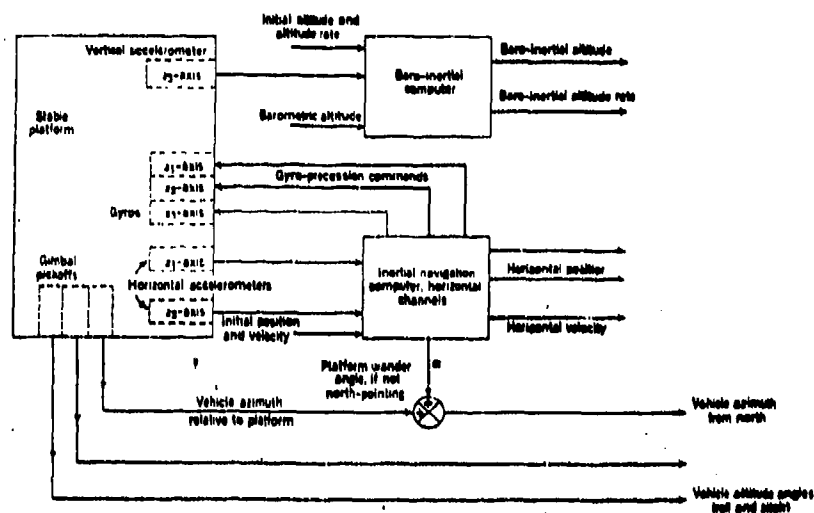


Figure 7.28 Inertial Navigation System⁽¹⁾

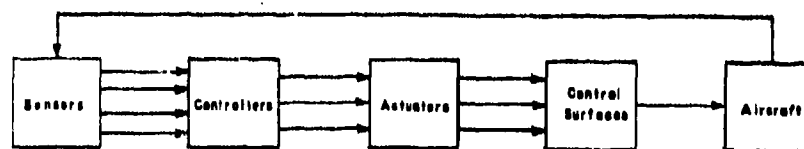


Figure 7.29 Flight Control System Block Diagram⁽¹⁾

detect one or more airframe motions and a control signal. The signal activates the activator to produce the required surface motion. The controller is in general a computer system.⁽¹⁾ Sensors required include gyroscopes, accelerometers, angle of attack sensors and sensors to measure temperature and pressure.⁽¹⁾

The activators are not directly susceptible due to the high voltages commonly used. The sensors are much more susceptible, especially those that use a null principle to produce accurate readings⁽¹⁾ (e.g., potentiometers). Transients can also be propagated into the subsystem and interpreted as a signal.

7.2.3 Weapons

Boeing Aircraft Corporation⁽³⁾ has compiled a list of unclassified data on EM threshold levels for various weapon systems that is useful as a weapons system susceptibility guide. The list is given in Figure 7.30. An unclassified EM radiation limit for nuclear weapons is given in Figure 7.31.

7.2.4 Radar

Because a radar subsystem can be quite extensive, it is useful to divide it into several cascaded stages when determining radar susceptibility to interference. A useful representation of this type is given in Figure 7.32. It allows radar performance to be determined by determining the performance of each stage.⁽⁷⁾ The major sources of interference for each stage are shown in Table 7.2 and the flow chart shown in Figure 7.33 outlines the overall radar interference prediction process.⁽⁷⁾

Because radars are very complicated subsystems, they may be subjected to many possible interference situations. Most pulse radars use a single antenna for both transmitter and receiver. Consequently, the radar transmitter itself can be an interference source.⁽¹⁾ Other sources include ⁽¹⁾ undesired echoes from ground, sea, clouds, rain or birds, extraneous environmental fields from machinery, natural sources such as stars or the sun (sunspots), communication and navigation equipment, and most importantly, other radars and ECM devices that have frequencies close to the radar operating frequency.

For surveillance radars with pulse interference the main interference effect is distorted receiver output at the radar scope. The factor of merit for the scope output is termed the scope condition. To determine the scope condition, a set of parameters N_i are first calculated, one for each combination of antenna mainbeam orientation and unintentional region orientation. The parameters are determined by the equation⁽⁷⁾

$$N_i = 20 Q_{20} + \sum_{P_i} Q_i (P_r - P_{mds}) \quad (7.16)$$

where Q_{20} = number of pulses/scan with level greater than $(P_{mds} + 20)$ dBm
 P_{mds} = minimum discernible signal in dBm
 Q_i = number of pulses/scan at level P_i where $P_{mds} \leq P_i \leq P_{mds} + 20$

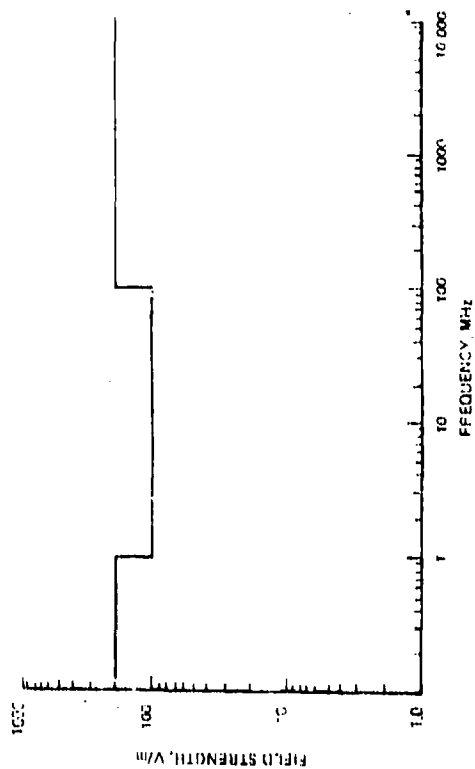


Figure 7.31 EM Threshold Limits for Nuclear Weapons(3)

Weapon Systems	Allowable induced levels											
	Control		Status		Monitoring		Power		EED		Nuclear	
SRW	Volt	Amp	Volt	Amp	Volt	Amp	Volt	Amp	Volt	Amp	Volt	Amp
	100 A surface current 10 A common mode current connector								1 A 1 watt 8,100 watts in average power density which is (greater)		See figure 7.31	
ALCM	Designations of SRW/ALCM ALCMs to be compared with same						5500 V peak amplitude		See figure 133		NA	
F 57												
SRW/T												
ALCM/T												
Harpoon												
GBU 15	DNA						DNA		DNA		DNA	
GBU 16	DNA						DNA		DNA		DNA	
GBU 17	DNA						DNA		DNA		DNA	
GBU 18	DNA						DNA		DNA		DNA	
GBU 19	DNA						DNA		DNA		DNA	
GBU 20	DNA						DNA		DNA		DNA	
GBU 21	DNA						DNA		DNA		DNA	
GBU 22	DNA						DNA		DNA		DNA	
GBU 23	DNA						DNA		DNA		DNA	
GBU 24	DNA						DNA		DNA		DNA	
GBU 25	DNA						DNA		DNA		DNA	
GBU 26	DNA						DNA		DNA		DNA	
GBU 27	DNA						DNA		DNA		DNA	
GBU 28	DNA						DNA		DNA		DNA	
GBU 29	DNA						DNA		DNA		DNA	
GBU 30	DNA						DNA		DNA		DNA	
GBU 31	DNA						DNA		DNA		DNA	
GBU 32	DNA						DNA		DNA		DNA	
GBU 33	DNA						DNA		DNA		DNA	
GBU 34	DNA						DNA		DNA		DNA	
GBU 35	DNA						DNA		DNA		DNA	
GBU 36	DNA						DNA		DNA		DNA	
GBU 37	DNA						DNA		DNA		DNA	
GBU 38	DNA						DNA		DNA		DNA	
GBU 39	DNA						DNA		DNA		DNA	
GBU 40	DNA						DNA		DNA		DNA	
GBU 41	DNA						DNA		DNA		DNA	
GBU 42	DNA						DNA		DNA		DNA	
GBU 43	DNA						DNA		DNA		DNA	
GBU 44	DNA						DNA		DNA		DNA	
GBU 45	DNA						DNA		DNA		DNA	
GBU 46	DNA						DNA		DNA		DNA	
GBU 47	DNA						DNA		DNA		DNA	
GBU 48	DNA						DNA		DNA		DNA	
GBU 49	DNA						DNA		DNA		DNA	
GBU 50	DNA						DNA		DNA		DNA	
GBU 51	DNA						DNA		DNA		DNA	
GBU 52	DNA						DNA		DNA		DNA	
GBU 53	DNA						DNA		DNA		DNA	
GBU 54	DNA						DNA		DNA		DNA	
GBU 55	DNA						DNA		DNA		DNA	
GBU 56	DNA						DNA		DNA		DNA	
GBU 57	DNA						DNA		DNA		DNA	
GBU 58	DNA						DNA		DNA		DNA	
GBU 59	DNA						DNA		DNA		DNA	
GBU 60	DNA						DNA		DNA		DNA	
GBU 61	DNA						DNA		DNA		DNA	
GBU 62	DNA						DNA		DNA		DNA	
GBU 63	DNA						DNA		DNA		DNA	
GBU 64	DNA						DNA		DNA		DNA	
GBU 65	DNA						DNA		DNA		DNA	
GBU 66	DNA						DNA		DNA		DNA	
GBU 67	DNA						DNA		DNA		DNA	
GBU 68	DNA						DNA		DNA		DNA	
GBU 69	DNA						DNA		DNA		DNA	
GBU 70	DNA						DNA		DNA		DNA	
GBU 71	DNA						DNA		DNA		DNA	
GBU 72	DNA						DNA		DNA		DNA	
GBU 73	DNA						DNA		DNA		DNA	
GBU 74	DNA						DNA		DNA		DNA	
GBU 75	DNA						DNA		DNA		DNA	
GBU 76	DNA						DNA		DNA		DNA	
GBU 77	DNA						DNA		DNA		DNA	
GBU 78	DNA						DNA		DNA		DNA	
GBU 79	DNA						DNA		DNA		DNA	
GBU 80	DNA						DNA		DNA		DNA	
GBU 81	DNA						DNA		DNA		DNA	
GBU 82	DNA						DNA		DNA		DNA	
GBU 83	DNA						DNA		DNA		DNA	
GBU 84	DNA						DNA		DNA		DNA	
GBU 85	DNA						DNA		DNA		DNA	
GBU 86	DNA						DNA		DNA		DNA	
GBU 87	DNA						DNA		DNA		DNA	
GBU 88	DNA						DNA		DNA		DNA	
GBU 89	DNA						DNA		DNA		DNA	
GBU 90	DNA						DNA		DNA		DNA	
GBU 91	DNA						DNA		DNA		DNA	
GBU 92	DNA						DNA		DNA		DNA	
GBU 93	DNA						DNA		DNA		DNA	
GBU 94	DNA						DNA		DNA		DNA	
GBU 95	DNA						DNA		DNA		DNA	
GBU 96	DNA						DNA		DNA		DNA	
GBU 97	DNA						DNA		DNA		DNA	
GBU 98	DNA						DNA		DNA		DNA	
GBU 99	DNA						DNA		DNA		DNA	
GBU 100	DNA						DNA		DNA		DNA	
GBU 101	DNA						DNA		DNA		DNA	
GBU 102	DNA						DNA		DNA		DNA	
GBU 103	DNA						DNA		DNA		DNA	
GBU 104	DNA						DNA		DNA		DNA	
GBU 105	DNA						DNA		DNA		DNA	
GBU 106	DNA						DNA		DNA		DNA	
GBU 107	DNA						DNA		DNA		DNA	
GBU 108	DNA						DNA		DNA		DNA	
GBU 109	DNA						DNA		DNA		DNA	
GBU 110	DNA						DNA		DNA		DNA	
GBU 111	DNA						DNA		DNA		DNA	
GBU 112	DNA						DNA		DNA		DNA	

Table 7.2 Interference Effects on Radar Receiver Stages Shown in Figure 7.32⁽⁷⁾

Receiver Stage	Interference Effect	Result on Operational Performance	Important Factors
Output	Scope Clutter Error Voltages	May mask desired signal; Increase Acquisition Time; Lose Track	Type of Output Characteristics of Interference at Output
Post-Detector Processing	May Reduce Certain Interference Effects	May improve in presence of interference but may be reduced otherwise	Type of Processing; Interfering Pulse Level, Width, and Rate out of Detector
Detector	Production of Interference at Detector Output	Interference appears on scope and may tend to obscure or mask desired signal	Desired Signal Pulse Level, Width and Rate; Interfering Signal Level, Width, and Rate at IF
Pre-detector Processing	May Reduce Certain Interference Effects AGC	May improve in the presence of interference but may be reduced otherwise Decrease Range and/or Probability of Detection	Type of Processing; Interfering Pulse Level, Width, Rate and Frequency at IF AGC Level and Time Constant Interfering Pulse Level, Width, Rate and Frequency at IF
IF	Saturation	Decrease Range and/or Probability of Detection	IF Saturation Level and Bandwidth; Interfering Pulse Level, Width, Rate and Frequency at IF
RF	Saturation	Decrease Range and/or Probability of Detection	RF Saturation Level and Interfering Pulse Level, Width & Rate and Frequency at RF

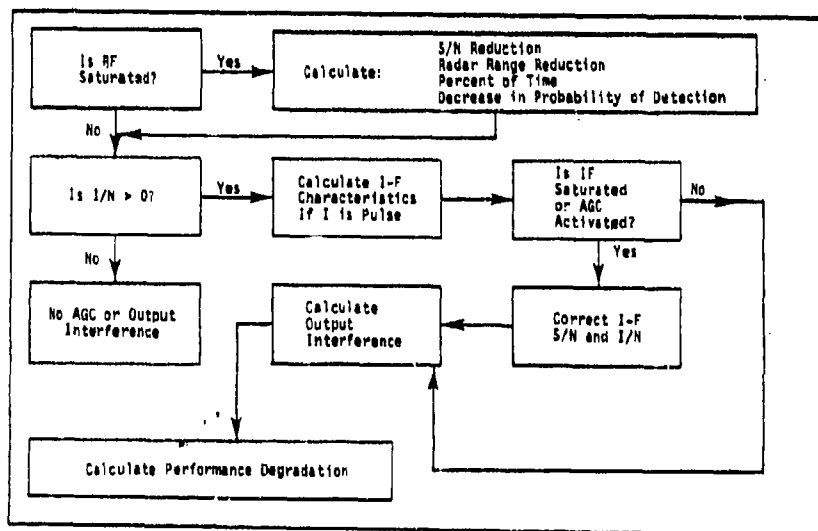


Figure 7.33 Radar Performance Prediction Flow Chart⁽⁷⁾

After N_1 is calculated, if those antenna orientations involving the antenna main beams make $N_1 > 0$ then the scope condition is unity.⁽⁷⁾ If antenna orientations involving unintentional regions make $N_1 > 0$, then a parameter N^* is calculated as follows⁽⁷⁾

$$N^* = 10^{-4} \sum_{i=1}^4 N_1 \quad (7.17)$$

The scope condition is then determined by the following conditions.⁽⁷⁾

if $0 < N^* < 3.7$	scope condition 1
if $3.8 < N^* < 9.4$	scope condition 2
if $9.5 < N^* < 14.7$	scope condition 3
if $14.8 < N^* < 25.2$	scope condition 4
if $N^* \geq 25.3$	scope condition 5

An increasing scope condition corresponds to an increasing degradation of scope image.

The effect of CW interference on a surveillance radar is to desensitize the RF and IF stages making the receiver less sensitive to the desired signal. This desensitization translates into a fractional decrease in maximum antenna range as expressed by the equation⁽⁷⁾

$$\text{Fractional range} = 10^{210^{-1} \left(\frac{\text{sensitivity reduction in dB}}{40} \right)} \quad (7.18)$$

The fractional range reduction is illustrated in Figure 7.34.

Tracking radars experience problems similar to the surveillance radars. System degradation for tracking radars is usually expressed in terms of an increase in target acquisition time. This increase in time can be expressed by the equation⁽⁷⁾

$$\Delta t_s = \frac{MT\Theta}{Ws} \quad (7.19)$$

where

Δt_s	= increase in target acquisition time (sec)
Θ	= angle searched (deg)
Ws	= angular scan rate (deg/sec)
M	= average number of interference pulses/sec
T	= antenna dwell time upon detection

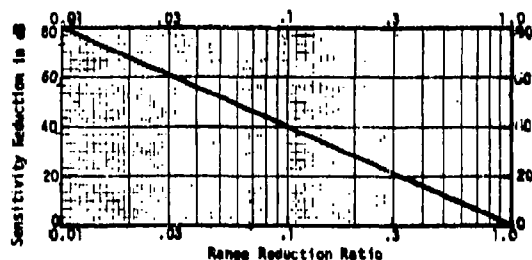


Figure 7.34 Radar Range Reduction Due to Radar Desensitization⁽⁷⁾

References

1. Engineering Design Handbook, Electromagnetic Compatability, USA Material Development and Readiness Command, DARCOM-P-706-410, March 1977.
2. IC Susceptibility Handbook, McDonnell-Douglas Company, Report No. MDC E1929, August 1978.
3. R. Force, P Green et. al., Investigation of Effects of Electromagnetic Energy on Advanced Composite Aircraft Structures and Their Associated Avionic/Electrical Equipment, Phase II, Vol. I Boeing Aircraft Corp. (D180-20186-4), September 1977.
4. Wallenberg, et. al., Advanced Composite Aircraft Electromagnetic Design and Synthesis, Interim Report, Syracuse Research Corp., April 1980.
5. C. E. Larson and J. M. Roe, A Modified Ebers-Moll Transition Model for RF Interference Analysis, 1978 IEEE Electromagnetic Compatibility Symposium Record, Atlanta Georgia, June 20-22, 1978.
6. J. J. Wilen, J. Tront, C. E. Larson, J. M. Roe, Computer-Aided Analysis of RFI Effects in Integrated Circuits, 1978 IEEE Electromagnetic Compatibility Symposium Record, Atlanta Georgia, June 20-22, 1978.
7. W. G. Duff and D. R. J. White, EMI Prediction and Analysis Techniques, Vol. 5, Don White Consultants, Inc., 1972.
8. Interference Notebook, Vol. I, RADC-TR-66-1, 1966.
9. L. W. Nagel and D. O. Pederson, "SPICE: Simulation Program with Integrated Circuit Emphasis," Technical Memorandum No. ERL-M382, Electronics Research Laboratory, University of California, Berkeley, California 94720, 12 April 1973.

8.0 GENERAL ANALYSIS AND TRADEOFF PHILOSOPHY

A prime goal in the conception, development and deployment of new or modified communication and electronic (C-E) systems is the achievement of satisfactory system performance at acceptable cost under all anticipated operating conditions. Such a goal is not easily met in the modern electronics world, and all indications suggest that the problem will worsen in the more complicated electronics world of the future. To meet this goal, a well organized, comprehensive analysis is required of all variables affecting system performance beginning with system conception and ending with system deployment.

Total system performance is described by a number of general factors such as reliability, maintainability, vulnerability, and electromagnetic compatibility (EMC). Ideally, each factor should be studied both separately and in conjunction with all other factors in determining total impact on system performance. By performing the analysis at every stage in the system life cycle, performance problems will tend to be caught or predicted early in the system design stage or pinpointed if they develop later. Tradeoff studies are performed as a part of the analysis to resolve incompatibilities between system performance variables in such a way as to produce a satisfactory cost-effective system.

Such an analysis requires a judicious use of various theoretical analysis tools, pertinent standards and specifications and actual system measurements. The analysis and standards are particularly useful early in the conception and design phases when measurements may not be available. In later system phases, measurements can augment and validate analysis efforts and serve as an overall check on system performance.

In keeping with the emphasis of the report, this chapter will focus on the analysis and tradeoffs required to achieve system EMC. To be sure, the EMC analysis and tradeoffs program must interface a more comprehensive system performance program, yet the EMC program is comprehensive and important enough in itself to merit individual discussion.

8.1 Standards and Specifications

For a number of years, the triservices have required that certain standards and specifications be met on all procured electrical and electronic equipments for the general purpose of interference suppression. Three standards, MIL-STD-461, -462, and -463 provide overall coordination for emission and susceptibility control. In MIL-STD-461, acceptable limits of emission and susceptibility are given for various equipments. MIL-STD-462 describes test procedures for determining actual equipment emission and susceptibility. MIL-STD-463 defines terms and specifies units. A list of standards and specifications is given in the references.

The limits set by the standards and specifications regulate the contribution of electronic emissions and susceptibilities to the system electromagnetic environment. This environment is taken to be a "typical" or "normal" equipment and operating environment, and the system designer is to use the standards to insure that this environment is not degraded.

The standards and specifications will control EMC problems for many equipments in many situations. It is nevertheless important to realize that compliance to the standards does not imply system EMC; conversely, noncompliance does not imply system incompatibility. The reason is that each system operating environment is unique and often requires unique EMC specifications to ensure system compatibility. The standards serve as general guidelines to EMC but may not completely solve a specific EMC problem.

8.2 The System Approach

To achieve EMC in modern electronics systems, EMC specifications for very many equipments often must be tailored to the system operating environment. Such a tailoring may require an evaluation of all interactions between system emitters and susceptors on a pair by pair basis. Such an evaluation should begin during system conception and continue through each acquisition phase to system deployment and modification in order that costly and time consuming EMC fixes caused by unforeseen interference problems be avoided or at least minimized.

Evaluation of EMC in any phase of the system life cycle is done by theoretical analysis, measurements or a combination of both. Interference analysis requires the existence of adequate models for all emitters, susceptors and the coupling between them. Such an analysis performed during system conception using simple models and general system data is relatively inexpensive, straight-forward to perform and is a valuable tool in engineering EMC into the system. In later system phases, an accurate analysis using complex models and detailed system data can be costly and time consuming. Unfortunately, any analysis will be only as accurate as the interference models being used in the interference prediction process. Measurement, on the other hand, deal with real equipments and subsystems but require costly test equipment, facilities and prototype systems. Such measured data (if it exists) is usually available only in later system phases, however, it does serve both as a guide to analysis and as an overall check on system EMC.

Once the EMC status of a system has been determined, information on interference reduction techniques and their costs must be used to perform appropriate system tradeoffs to ensure system EMC in a cost-effective manner. Such a tailoring of EMC specifications either by analysis or by measurements is designed to produce satisfactory system performance at least cost.

8.2.1 Electromagnetic Compatibility (EMC) Program

The Department of Defense (DOD) has established an integrated EMC program to ensure the compatibility of all procured electronic equipments and subsystems during all phases of the system life cycle.⁽¹¹⁾ Goals of the EMC program include the following.

- A. Achievement of EMC for all equipments.
- B. Initial design of EMC into the system rather than later EMC fixes.

- C. Traceability of EMC requirements and modifications throughout the system lifecycle to allow the impact of design changes and tradeoffs to be assessed.
- D. Redefinition of EMC requirements to reflect system changes.
- E. Tailoring of EMC specifications to each unique system.
- F. Smooth integration of the EMC program with all other programs that impact system performance.

The EMC program for a particular Communications - Electronics (C-E) system should be directed by an authority able to designate specific responsibilities for preparation of EMC control plans, test plans, reports and documentation, as well as EMC testing at all levels. The authority should coordinate all EMC activities with all other system engineering requirements and provide overall guidance to the EMC program.⁽¹⁾

8.2.2 Electromagnetic Compatibility (EMC) Plans

The complete system EMC plan typically consists of the following three plans.⁽¹⁾

- A. EMC program plan.
- B. EMC control plan.
- C. EMC test plans.

Additionally, or in conjunction with the EMC control plan, provision is usually made for theoretical interference analysis efforts, equipment frequency assignments and cost-effective tradeoff studies. These topics will be discussed separately from the control plan.

8.2.2.1 EMC Program Plan

The EMC program plan describes the overall EMC program for the C-E system in question and is usually a separate part of a proposal or statement of work.⁽¹⁾ The program plan clearly defines tasks to be accomplished and milestones to be met. Particular attention is given to establishing an interface with other system engineering programs. An outline of such a program plan is given in Table 8.1.

8.2.2.2 EMC Control Plan

The control plan is the major EMC document to be produced by the system program as required by MIL-STD-461 and MIL-E-6051. It is the source of all system EMC information and defines all requirements, lines of responsibility and authority and directives such as organization, design criteria, analysis, frequency allocation assignments and test plans.⁽¹⁾ Many of these directives may exist as separate documents which together comprise the control plan. An outline for an EMC control plan is illustrated in Table 8.2.

Table 8.1

OUTLINE OF CONTENT OF EMC PROGRAM PLAN (1)

- 1 INTRODUCTION
 - 1.1 Purpose of plan
 - 1.2 Scope of program
 - 1.3 Description of system, subsystem, or equipment
- 2 ORGANIZATION AND RESPONSIBILITIES
 - 2.1 Contractor responsibilities
 - 2.1.1 Interface with procuring activity
 - 2.1.2 Key personnel
 - 2.1.3 Line and functional organization
 - 2.1.4 EMC advisory board (EMCAB)
 - 2.1.5 Facilities
 - 2.2 Subcontractor responsibilities
 - 2.2.1 Interface with prime contractor
 - 2.2.2 Coordination between prime contractor and subcontractors (how, when, and with whom?)
 - 2.2.3 Reporting of problems to procuring activity and how such problems are to be handled within company.
- 3 EMC MILESTONES
- 4 APPLICABLE EMC DOCUMENTS AND REQUIREMENTS
 - 4.1 Military
 - 4.2 Company
 - 4.3 Other
- 5 EMC ENGINEERING ACTIVITIES
 - 5.1 Application of applicable documents
 - 5.2 Design review and schedules
 - 5.3 Degradation criteria
 - 5.4 Safety margins
- 6 EMC DESIGN CRITERIA
 - 6.1 Design techniques to preclude EMI (shielding, grounding, shielding, cable separation, etc.)
 - 6.2 Precautions to preclude spurious emissions, responses and unwanted resonances
 - 6.2.1 Precautions to conserve frequency spectrum
 - 6.2.2 Consideration of operational electromagnetic environment
 - 6.3 Utilization of suppression techniques
- 7 PREDICTION OF PROBLEM AREAS
 - 7.1 Description of prediction and analysis techniques to be employed
 - 7.2 Identification of operational problems anticipated
 - 7.3 Proposed solutions for problems
- 8 EMC TESTING FOR SYSTEMS, SUBSYSTEMS, AND EQUIPMENT
 - 8.1 Engineering development
 - 8.2 First article
 - 8.3 Acceptance
 - 8.4 Integration
 - 8.5 Spectrum signature
- 9 DOCUMENTATION AND SCHEDULE
 - 9.1 Control plan
 - 9.2 Test plan
 - 9.3 Test report
 - 9.4 Charter for EMCAB

Table 8.2
Outline of Content of EMC CONTROL PLAN (1)

1. MANAGEMENT
 - 1.1 Organizational responsibilities
 - 1.2 Lines of authority
 - 1.3 Milestones and schedules
 - 1.4 Complete list of EMC requirements
2. SPECTRUM CONSERVATION
 - 2.1 Minimize emissions and susceptibilities
 - 2.2 Specific design parameters used to control emissions and susceptibilities of equipments
3. EMC MECHANICAL DESIGN
 - 3.1 Describe material and construction procedure to attenuate emissions and susceptibilities of equipments
 - 3.2 Describe types of metal, composites used in design
4. ELECTRICAL AND ELECTRONIC WIRING DESIGN
 - 4.1 All wiring and cable design required to minimize emission and susceptibility will be described
 - 4.2 Grounding, bonding and shielding of cables is described
5. ELECTRICAL AND ELECTRONIC CIRCUIT DESIGN
 - 5.1 Describe signal suppression techniques that will be used in all circuit parts
 - 5.2 Describe bonding and grounding, filter characteristics, parts location and critical circuit isolation
6. ANALYSIS
 - 6.1 Verification of adequacy of mechanical construction and shielding technique
 - 6.2 Complete frequency matrix of all emitter and receptor operating frequencies and spurious frequencies
 - 6.3 Analysis of vibrators, switches, logic and clock circuits
 - 6.4 Analysis of circuits, equipments and subsystems to pinpoint system interference problem
7. PROBLEMS
 - 7.1 Real and potential interference problems will be presented
 - 7.2 Procedures for analysis and solution of interference problems will be reported
8. UPDATING
 - 8.1 A method of updating the control plan will be indicated

8.2.2.3 EMC Test Plans

Test plans include all facilities and instrumentation required, all test procedures used on equipments, subsystems or systems and all test documents needed to perform the measurements. The tests may be conducted at the equipment or subsystem level (as per MIL-STD-461), the system level (as per MIL-E-6051), or at the intersystem level to show the system is compatible with itself and with other deployed systems in the operating environment. An outline for EMC test plans is illustrated in Table 8.3.

8.2.2.4 Theoretical EMC Analysis

In order that EMC be designed into the system, serious interference problems must be foreseen as early in the system life cycle as possible. Interference analysis is particularly appropriate for this purpose since detailed system measurements usually do not exist during early system phases while sufficient emitter, receptor and coupling models may exist to allow an initial EMC analysis to be performed.

As the system life cycle proceeds and more detailed system data becomes available, sophisticated EMC analysis (supplemented possibly by measurements) can be performed. This analysis can evaluate possible trouble spots that were predicted early in the system life cycle using simpler analysis, and predict or pinpoint interference problems in later life cycle phases. This is particularly important for situations in which measurements are not possible or not feasible.

If system interference occurs after deployment or modification, the test and analytical data base accumulated during system design can be used to quickly pinpoint a problem and propose a solution. The overall result of the analysis program will be a more effective, reliable system with more internally engineered EMC and fewer costly EMC fixes.

8.2.2.5 Frequency Allocations

One of the most important parts of the EMC control plan is the requesting and obtaining of equipment frequency allocations for a system.⁽¹⁾ Such an allocation begins during system conception with an application for an experimental RF spectrum allocation. As the system proceeds to the validation phase, it is necessary to apply for a developmental RF spectrum allocation. Finally, during full-scale development, the actual operating frequency allocations are made.⁽¹⁾ The details of the allocation process follow guidelines set down by the Department of Defense and related government agencies.

8.2.2.6 Cost-Effectiveness Tradeoff

Cost-effectiveness considerations enter into system performance evaluation at every stage in the system life cycle. Because of the expenses involved in both time and money to develop and deploy an electronics system, it is necessary that a tradeoff be made between system performance and system cost.⁽¹⁾

Table 8.3
Outline of Content of EMC Test Plans (1)

1. SCOPE
 - 1.1 Statement of purpose of plan and its relation to the total EMC problem
 - 1.2 List of all tests to be conducted
2. APPLICABLE DOCUMENTS
 - 2.1 Military
 - 2.2 Company
 - 2.3 Other
3. TEST SITE
 - 3.1 Description of test facility
 - 3.2 Ground plane description along with grounding and bonding.
 - 3.3 Ambient electromagnetic environment
4. TEST INSTRUMENTATION
 - 4.1 Equipment list
 - 4.2 Instrumentation bandwidths
 - 4.3 Transformer and filter characteristics
5. SAMPLE Test SETUP
 - 5.1 Physical layout of equipment under test
 - 5.2 Layout of measurement systems
6. TEST SAMPLE OPERATION
 - 6.1 Operation modes for each test
 - 6.2 Control setting list
 - 6.3 Test frequencies
 - 6.4 Performance checks
 - 6.5 Outputs to be monitored
 - 6.6 Test malfunction criteria
7. TEST PROCEDURE
 - 7.1 Test setup block diagram
 - 7.2 Test equipment used together with grounding, bonding, and shielding
 - 7.3 Procedures for probing test sample
8. SUBSYSTEM TESTS
 - 8.1 Receiver to receiver interactions
 - 8.2 Transmitter to receiver interactions
 - 8.3 Transmitter to active and passive devices
9. DATA TO BE RECORDED
 - 9.1 Sample data sheet
 - 9.2 Sample test log
 - 9.3 Sample graphs

To achieve system EMC requires a judicious choice between interference analysis and measurements at each stage in the system life cycle. Analysis allows a tailoring of EMC specification to be performed to prevent incompatibilities yet not require too stringent specifications to be made. Measurements validate the analysis and supply data for situations analysis cannot treat. The final result, ideally, is satisfactory system performance at least cost. A typical cost-effectiveness model for selecting a compatible system configuration is shown in Figure 8.1.

8.2.3 EMC Program Implementation

The successful design of EMC into the system at each system phase requires that certain EMC decisions be made and certain milestones met. A review of the system acquisition life cycle is given in Table 8.4, along with tasks to be performed at each phase.

Besides the tasks listed in Table 8.4, a set of decisions must be made during the system life cycle in order that EMC be incorporated into the system. A list of these decisions is given in Table 8.5, along with the system phase in which they must be made.

In order that EMC decisions be made correctly, a set of guidance categories has been assembled to guide the EMC program manager and are listed in Table 8.6. Each EMC decision is reached through consideration of one or more of these categories. A matrix of EMC decisions and relevant categories is illustrated in Table 8.7. The EMC decisions and guidance categories provide for a systematic evaluation of system EMC design.

8.3 EMC Systems Analysis Procedure Synthesis⁽³⁾

In this section a set of guidelines is presented for constructing an analysis tool (or procedure) to perform an EMC interference analysis of an electronics system.⁽³⁾ Such a tool is, in general, quite complicated to assemble owing to the large number and variety of electronic components to be modeled, irregular system geometrics that are required, and complicated electronic component coupling that is present and limited time and funds that are available. Depending on the system life cycle phase, the system data available may be limited, incomplete or overwhelming. A systematic method for EMC systems analysis procedure synthesis is clearly desirable.⁽³⁾

8.3.1 Drivers in Procedure Synthesis

There is a logical sequence of steps or flow in constructing an EMC procedure to perform an EMC systems analysis. The driving elements are shown schematically in the flow chart in Figure 8.2. The procedure consists of available data, possible tasks, problem constraints, electromagnetic emitter, receptor and coupling models all interfaced by appropriate expressions (systems equations) that relate electromagnetic source characteristics to receptor responses.⁽³⁾ This procedure is usually realized in terms of one or more computer codes. The individual driving elements comprising the procedure will now be discussed.

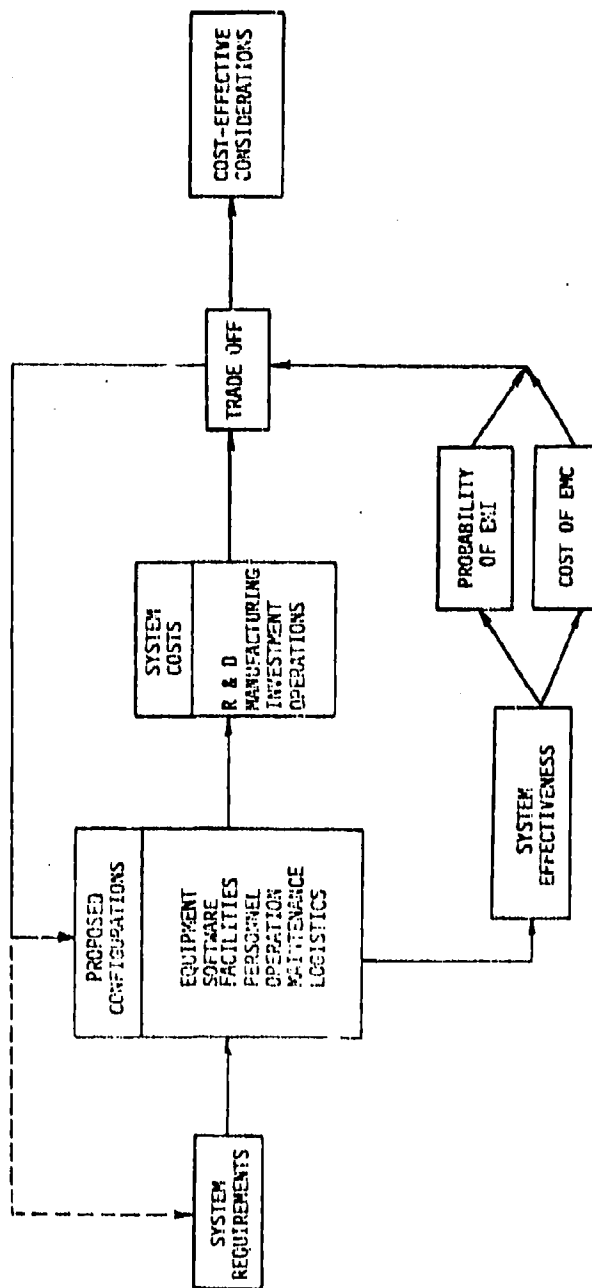


Figure 8.1 EMC - Cost Effectiveness Tradeoff Model for a System Configuration. (1)

Table 8.4

Phases of the System Acquisition Life Cycle (3)

Conceptual Phase

- Required Operational Capability (ROC)
- Mission Analysis
- Tradeoff Studies
- Alternative Concepts
- Feasibility Studies
- Experimental Hardware Development and Evaluation
- Risk Assessments
- System Functional Baseline

Validation Phase

- Define Technical Objective
- Define Operational Deployment Concepts
- Pinpoint and Resolve High Risk Areas
- Establish Performance Specifications
- Evaluate Tradeoffs
- Hardware Development and Evaluation
- Prototype Demonstration
- System Definition
- Category 1 Tests - Subsystem/System Level
- Prepare RFP

Full-Scale Development

- System and Equipment Design
- System and Equipment Fabrication
- System and Equipment Test and Evaluation
- Define Total System Configurations
- Output: Production System

Documentation
Test Results

Production Phase

- Production and Development of All Principal and Support Equipment

Deployment Phase

- First Unit to Phase Out
- Overlaps Production Phase
- Evaluation of Hardware Performance and Operational Procedures

Table 8.5

EMC DECISIONS WITHIN SYSTEM LIFE CYCLE (1)

CONCEPTUAL PHASE:

1. Select preliminary equipment characteristics and ascertain frequency supportability
2. Apply for experimental RF spectrum allocation

VALIDATION PHASE:

3. Determine prototype equipment specification
4. Verify prototype equipment performance
5. Apply for developmental RF spectrum allocation

FULL SCALE DEVELOPMENT PHASE:

6. Determine developmental equipment specifications
7. Verify development equipment performance
8. Apply for operational RF spectrum allocation
9. Determine initial production equipment specifications
10. Approve table of organization and equipment and training material
11. Verify initial production equipment performance

12. Apply for frequency assignments

PRODUCTION AND DEPLOYMENT PHASES:

13. Determine production specifications
14. Verify operational equipment performance

Table 8.6
EMC GUIDANCE CATEGORIES (1)

1. System feasibility and performance requirements
2. Command and organizational principles
3. System operational factors
4. Economic assessments
5. Electromagnetic environment evaluation
6. Natural environment evaluation
7. Hazard evaluation
8. Equipment and performance characteristics
9. Conformance to waivers of EMC standards or specifications
10. Spectrum signatures
11. Measures of system effectiveness
12. Site survey and election
13. EMC training data
14. Electronic warfare evaluation

Table 8.7
GUIDANCE FOR EMC DECISIONS (1)

EMC DECISIONS WITHIN SYSTEM LIFE CYCLE*	EMC GUIDANCE CATEGORIES ^b													
	1	2	3	4	5	6	7	8	9	10	11	12	13	14
CONCEPTUAL PHASE														
1.	X	X	X	X	X	X	X	X			X			
2.	X		X		X	X			X			X		
VALIDATION PHASE														
3.			X				X	X	X					
4.					X	X	X	X	X	X	X			
5.	X		X		X	X	X	X		X				
FULL SCALE DEVELOPMENT														
6.				X			X	X	X					
7.					X	X	X	X	X	X				
8.					X	X	X	X	X	X				
9.						X	X	X	X	X	X			
10.												X		
11.					X	X	X	X	X	X	X	X		
12.								X				X		X
PRODUCTION AND DEPLOYMENT														
13.							X	X	X	X	X	X		
14.					X	X	X	X	X	X	X	X		X

a. See Table 5.5 for decisions

b. See Table 8.6 for guidance categories

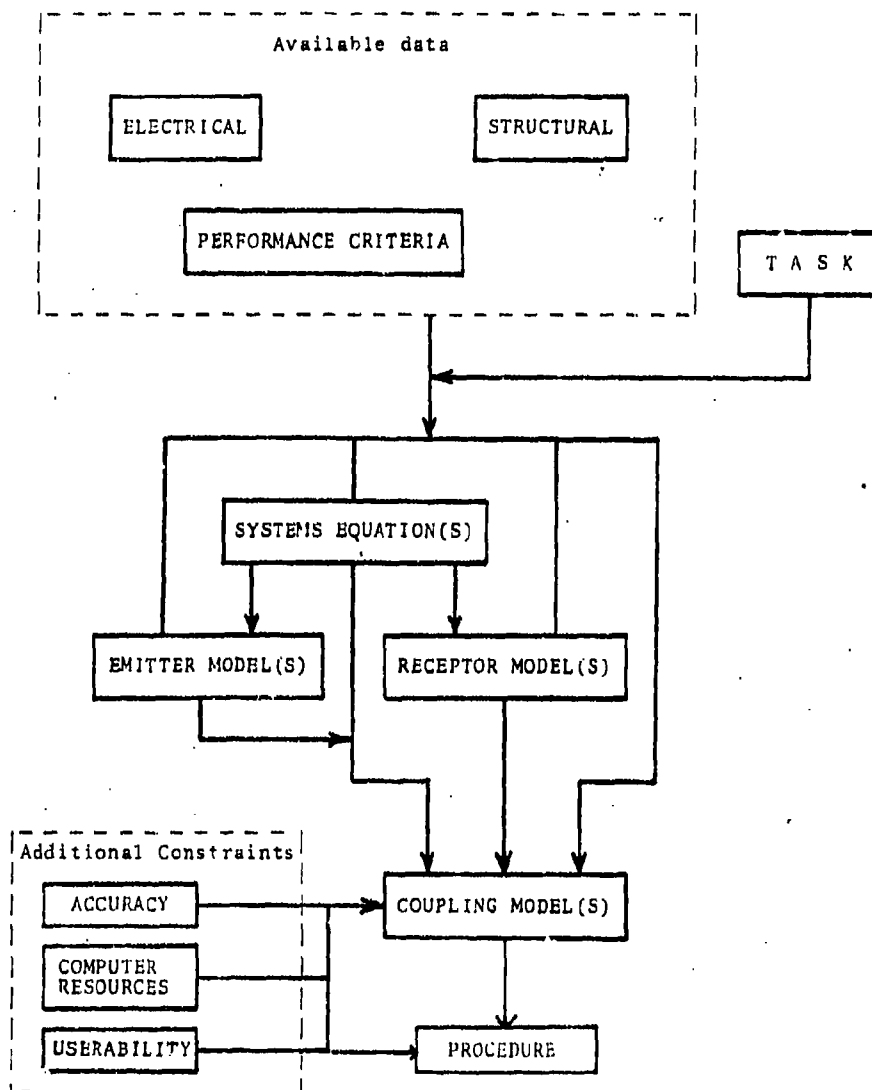


Figure 8.2 Driving Elements in EMC Procedure Synthesis.⁽³⁾

8.3.1.1 Tasks

Each procedure is guided by the particular purpose or task to be performed. The analyst is responsible for identifying the task which may be to survey a receptor for interference when in the field of one or more emitters. Other tasks may involve waiver analysis or tradeoff studies such as the frequency assignment of many receivers among many emitters.

8.3.1.2 Available Data

The data available for analysis is a prime determinant of any EMC procedure. Clearly detailed analysis is impossible if only general data is available. The complexity of data available is primarily a function of the system life cycle. Table 8.8 illustrates the system data as a function of life cycle.

Structural data includes the physical size and shape of the system. Detailed analysis such as method of moments requires structure geometry accurate to fractions of a wavelength, while for more general analysis generic shapes may suffice.

The electrical data needed by various procedures may be as detailed as time waveforms or as general as frequency bands of operation. Many coupling models require waveform source descriptions in terms of amplitude versus frequency while other more detailed models may require phase information.

Performance criteria in the form of performance degradation curves, or thresholds are also viewed as data because they are necessary for determining parameters (such as receptor susceptibility) necessary for any EMC analysis.

8.3.1.3 Additional Constraints

Any analytical tool must operate within certain physical constraints. The previously discussed available data is an example of one such constraint powerful enough to drive the analysis. Examples of other constraints are computer resources, accuracy, and usability.

8.3.1.3.1 Computer Resources

The majority of analytical tools used for EMC analysis are computer programs. As such, the analysis is limited by the resources of the computer, primarily processing time and main memory storage size. Computer limitations restrict the accuracy of EMC analysis because of the necessity of using simpler models and procedures to tailor the analysis capability to the computer. Computer technology continues to progress at a rapid rate allowing for more accurate EMC analysis on future systems.

8.3.1.3.2 Accuracy

Any EMC analysis is at least approximate. The approximations that enter into an analysis generally arise from two sources: problem idealization and model analysis.

Table 8.3

Data Available Versus Phases of Life Cycle⁽³⁾

Conceptual

- System Component Function Definitions
- Organizations Responsible for Each System Component
- Generic System Component

Power Circuits

Communication Circuits

Telemetry Circuits

Data Processing Circuits

- Expected Geometry

Size

Weight

Generic Shape

Validation

- Characteristics of Individual Component Power Requirements

Power Requirements

Time Waveforms

Spectrum

Susceptibility

- Prototype Specifications

Geometric Data

Schematics and Diagrams

Material Characteristics

- Support Equipment Characteristics

Full Scale Development

- Geometric Data

Shape and Surface Information

Wire Routing

Component Locations

- Test Results

Production

- Measure Data Production Sample
- Refined Data on Geometry and Electrical Characteristics
- Description of Equipment Down to Brand Names

Deployment

- Maintenance Statistics
- Modification Specifications

In problem idealization, the actual problem is replaced by a simpler, more treatable problem. The simpler problem should include all important factors of the actual problem in order that the solution of the simple problem should resemble the solution of the actual problem in all important respects. The quality of the simpler solutions is judged by comparison with experiment or other analysis or by increasing the complexity of the simpler problem until the problem parameters show little change.

In model analysis, a model or method of solution is applied to the simple or idealized problem. Different models or methods of solution will result in different solutions to the same problem. Accurate model analysis depends on the accuracy with which an analytical tool predicts important system parameters.

8.3.1.3.3 Userability

Userability refers to the level of competence assumed for the EMC analyst in search of an analytical procedure or tool. There are two aspects of userability: understanding of the implementation and execution of associated computer codes, and understanding of the applicabilities and limitations of the tool or procedure.

The first aspect depends on the ease of use of the computer code. This aspect impacts the learning curve for a procedure but not the resulting analysis.

The second aspect pertains to the level of understanding necessary to correctly apply the analysis and interpret the results. Many analysis models require years of experience to adequately use and understand. If a user has a choice between a complicated but accurate analysis tool that is poorly understood and a simplified, less accurate tool that is well understood, the user should choose the latter procedure.

8.3.1.4 Emitter, Receptor, and Coupling Models

Due to the large number of sources of electromagnetic emissions, the variety of emission models is very large, ranging from lightning and nuclear electromagnetic pulse models on the one hand to solid state device models on the other. The number of possible coupling paths between emitters and a given receptor can be very large in a sophisticated electronics equipment and are becoming increasingly important to accurately assess due to modern digital devices which are sensitive to low power interference. Similar comments apply to receptors. The result is that a large number of such models in either the time domain or the frequency domain are usually required for any general systems analysis procedure. The emitter, receptor and coupling models are chosen to simulate system equipment operation and as such are strongly dependent on available data, computer power, accuracy and userability discussed earlier.

8.3.1.5 Systems Equations

Systems equations relate electromagnetic source characteristics to receptor responses. Such equations form the basis for the interference

prediction process. The emitter, receptors and coupling model characteristics are used to form a mathematical expression for assessing the interference present at a receptor due to a set of emitters. The assessment is often in the form of a figure of merit. The form taken by the system equations depends on the system models used. If waveforms, such as a time varying voltage, are used then waveform system equations are required and take the form of voltage and/or current margin calculations. If waveform parameters, such as average power or peak power, are used then parameter type system equations are required. For average power sensitive receptors the systems equations may be power margin calculations in terms of signal bandwidth.

8.3.2 Guide to EMC Procedure Synthesis⁽³⁾

As an aid to the analyst, a logical sequence of steps that act as a guide to constructing an EMC analysis procedure is now presented. The sequence of steps is based on the flow chart illustrated in Figure 8.2. By following the steps the analyst can choose emitter and receptor models, coupling models, and system equations that make best use of the available system data yet fit the constraints of the problem.

Step 1. The task to be performed is clearly defined. It may be to survey a system for interference, conduct tradeoff analysis or generate tailored EMC specifications.

Step 2. The performance criteria for all receptors are examined. The receptors may, for example, be "peak" power or average power sensitive. Based upon the task to be performed and the receptor performance criteria, a choice of systems equations can be made.

Step 3. All emitter and receptor models are now selected on the basis of available data and chosen systems equations. Performance criteria are also used in selecting the receptors. For example, if emitter data available is average power spectral density, then the emitter model is power versus frequency and an emitter time waveform model would be inappropriate.

Step 4. A choice of coupling models is now made based upon available data, systems equations and emitter and receptor models chosen. At this point, a complete list of coupling models is assembled that fits with the above emitter and receptor models.

Step 5. A choice is now made among the coupling models, emitter models and receptor models to form the analysis procedure with the systems equations. The choice is constrained in accordance with tradeoffs defined by the task and the further constraints of computer resources, usability and accuracy.

The procedure synthesis is now complete when all models have been identified, interface specifications defined, limitations and inaccuracies documented and computer codes assembled.

8.4 Description of Programs and Facilities

This section presents an overview of various analysis programs and

facilities supported by the Department of Defense that are available to the analyst as tools to perform a systems analysis of a complex electronics system.

Two facilities, the Electromagnetic Compatibility Analysis Center (ECAC) and the Air Force Intrasystem Analysis Program (IAP) support center are discussed in detail regarding both their EMC data bases and analysis capabilities. A brief discussion is also given of the IAP data base management system.

8.4.1 Electromagnetic Compatibility Analysis Center (ECAC)

The Electromagnetic Compatibility Analysis Center (ECAC) is an organization under the direction of the Department of Defense (DOD) whose mission is to provide data and expertise to the DOD on matters pertaining to intersystem and intrasystem electromagnetic compatibility. Other government agencies and government contractors are served on a limited basis.^(1,2)

ECAC maintains a data base which consists of environmental information on deployed C-E equipment, detailed technical information about such equipment, and various kinds of topographic information. Portions of the data are stored on magnetic tape or random access devices; other portions exist in technical reports and documents.^(1,2)

ECAC provides EMC engineering and consulting services through its collection of mathematical models and computer programs that are designed to predict potential electromagnetic interference (EMI) problems.

The data base and services provided by ECAC are discussed in some detail in the following sections.

8.4.1.1 Data Base

The following nine files and subfiles are maintained by ECAC as a primary EMC resource.^(1,2) Information stored on computer files may be retrieved using data base management programs maintained by ECAC.

8.4.1.1.1 Environmental File^(1,2)

The environmental file is a set of subfiles which describe the location and operating characteristics of communications and electronic equipment. The principal use of the data is to identify equipments located in a particular environment which may pose an interference threat to a proposed receiver, or which may be susceptible to interference from a proposed transmitter. The data is divided into files that are either frequency oriented or equipment oriented (E-file). A list of environmental parameters collected in the environmental file is given in Table 8.9. Table 8.10 is a description of the individual environmental subfiles.

8.4.1.1.2 Nominal Characteristics File (NCF)^(1,2)

The Nominal Characteristics File (NCF) is a set of technical data on various characteristics of both civilian and military communications and electronic equipment used in the United States and certain foreign coun-

Table 8.9 Major Parameter Fields Contained
In Environmental File (E-File)⁽²⁾

Identity number	Operating cycle
Security classification	Modulation types
Date of Report	Emission bandwidth
Cognizant military service or agency	Pulse Width Values
Organizational Unit name	Pulse repetition rate values
City/Base	Power levels used
State/Country	Frequency and/or frequency range
Mobility class	Equipment function
Number of equipments	Deactivation date
Latitude	Call Sign/linkage identifier
Longitude	Antenna vertical beamwidth
Site elevation	Antenna horizontal beamwidth
Terrain type	Mainbeam gain
Equipment nomenclature	Area of Operation
Antenna nomenclature	Activation date
Antenna height	Image Rejection level
Antenna elevation angle	Harmonic Output Level
Antenna azimuth or scan rate	IF selectivity
	Preselector bandwidth
	Output device type

Table 8.10(Continued)

Table 8.10
DESCRIPTION OF ENVIRONMENTAL DATA SUBFILES (1)

SUBFILE	DESCRIPTION	UPDATE SCHEDULE	FREQUENCY BANDS, MHz	COVERAGE AREA	AGENCIES	FORMAT
1374 Data	Contains data on transmission and reception at fixed locations and transient locations. Data are obtained from reports made on DD-1374 form. The instructions on the form include reporting of location, equipment and equipment in operation, time of day, date, and time of day. The Army is the major provider of 1374 data.	New data received on DD-1374 form	Primarily Continental US, Europe, and AF-Europe	USARP AF-Europe	DDO FAA	84 word E-File
NAVAIDS	Contains data on TACAN, ILS, VOR, GCR, and other navigation aids. Data are obtained from 1374 forms from the IFR Handbook, from FCC Licensee, and from other available sources. Although this file is often considered part of the "E-File", it is not strictly a file of 1374 report data.	Monthly	0.2-6.015 100-130 215-600 900-1215	USARP (FOR- TACAN Worldwide)	DDO FAA FCC	84 word E-File
IFF	Contains data on IFF ground interrogators obtained from DD 1374 file and interrogated with data every 3 seconds. IFF systems from the TRAC file and systems under development by industry from the FCC file. Additional data fields have been added which are used to describe IFF systems. The file is maintained apart from the E-File but reports are included in the E-File corresponding to each in the 1374 file.	Update from DD 1374 file every 3 seconds	800-900 1000-1500 2100-2200 2400-2600 3700-4300 5025-6025 6525-6875 8700-11700 12200-12700	USARP AF-Europe	DDO FAA FCC	84 word E-File
Common- and Micro- wave	Contains data which are extracted from the FCC license for microwave communication stations. This includes data on primary and secondary microwave stations and on the frequency, power, and other characteristics of the stations. Data are for the largest common carrier, the AT&T Corp., the microwave stations in the AT&T file. This is a condensed part of E-File.	Weekly		USARP	Non-Govt	84 word E-File
AT&T	The data in this file are obtained from AT&T. It contains high quality location and equipment data. It does not contain specific operating frequency but does have the range of frequencies used on each file.	Semi-annually	3000-4300 5025-6025 11200-11700	USARP	AT&T	84 word E-File

tries. Individual electronic components are cross-indexed to the equipments of which they are a part. The computer stored data originates mostly from technical manuals and manufacturer's data sheets. The data fields included in the NCF file are given in Table 8.11.

8.4.1.1.3 Organization and Platform Allowance File (OPAF)⁽¹⁾

All equipment data contained in the E-file and NCF file are fixed-site oriented. The Organization and Platform Allowance File (OPAF) contains information on computers, by subfile, which when merged with the E-file and NCF file information, describes C-E equipments on mobile systems such as ships, aircraft, missiles, satellites and tactical ground units. If the mobile system is known, the OPAF gives a list of equipments that are on it. The OPAF subfiles are listed in Table 8.12.

8.4.1.1.4 Spectrum Allocation and Use File (SAUF)⁽¹⁾

The SAUF contains information on agreements, regulations and laws concerning the use of the various allocated bands in the frequency spectrum. The information has been extracted from available source documents and is computer stored. All information concerning a frequency band of interest can be obtained upon request, within appropriate security requirements. The documents in SAUF are listed in Tables 8.13 - 8.15.

8.4.1.1.5 Topographic File^(1,2)

The Topographic File consists of computer stored terrain elevation data extracted from topographic maps obtained from the Army Topographic Command. The data are used to construct topographic profiles (elevations and obstructions) between any two points in the Continental United States (CONUS) as well as parts of Vietnam, Korea, Alaska, Hawaii and Germany.⁽²⁾ Grid point separation is variable but is nominally 30 seconds of arc (about 1/2 mile).⁽¹⁾

8.4.1.1.6 Frequency Allocations Application File (FAAF)^(1,2)

The FAAF comprises information pertaining to the frequency allocation status of present and future military C-E systems. Detailed data is kept of the operational and functional features of the systems. The file may be interrogated by application number, frequency, operational data, geographic area, operational environment and equipment function. A partial list of data fields in the FAAF is given in Table 8.16.

8.4.1.1.7 Spectrum Signature File^(1,2)

The Spectrum Signature File contains spectrum signature hard copy reports that characterize the emission and reception characteristics of selected C-E equipments. The spectrum signature measurements are made in accordance with MIL-STD-449⁽²⁾ (Radio Spectrum Measurement Characteristics). A list of parameters contained in the Spectrum Signature File is given in Table 8.17.

Table 8.11 Major Parameter Fields in the Nominal
Characteristics Field (NCF) (2)

Output Tube Type	Vertical beamwidth
Average power output	Electrical tilt angle range
Peak power output	Number of mainbeams
Frequency range	Reflector dimensions
Pulse width capability	Vertical antenna scan rate
PRF capability frequency	Sector scan limits
PM-CW deviation ratio	Horizontal scan rate
Emission bandwidth	Elevation angle range
Rise time	Master scan - number of bars
Decay time	Angle tracking bandwidth
First IF	Angle tracking open loop gain
First IF selectivity	Range tracking bandwidth
Second IF	Range tracking open loop gain
Second IF selectivity	Velocity tracking bandwidth
Third IF	Velocity tracking open loop gain
Third IF selectivity	Frequency generation scheme
Sensitivity	Base bandwidth
Noise Figure	Harmonic output level
Antenna type	Preselector selectivity
Antenna lead type	Image rejection level
Antenna feed type	Antenna lead cutoff frequency
Reflector shape	Polarization
Fundamental antenna gain	Detector type
Horizontal beamwidth	Special circuitry remark

Table 8.12

ORGANIZATION AND PLATFORM ALLOWANCE FILES (OPAF) (1)

SUBFILES	DESCRIPTION	UPDATE SCHEDULE
WATER	Contains data on the C-E equipment complement on Navy and Coast Guard ships by type, class, hull number, and ship name. The C-E complements are listed by systems nomenclatures and do not include components of systems unless the component is operating independently from the system. The US Army watercraft are entered as typical C-E configurations by basic design number for each type of vessel. The file also contains actual C-E configurations for Commercial Dry Cargo and Tanker Maritime ships operating under the US Flag.	<ul style="list-style-type: none"> Navy - Quarterly Coast Guard - Semiannually Army - Semiannually Commercial Maritime - As required
AIR	Contains Air Force, Army, Navy, and Marine Corps Aircraft by Type/Model/Series of aircraft together with their complete C-E configurations. Information as to what equipments may be installed on specific tail numbers within a type/model/series of aircraft is not available. The file also contains the quantities of the type/model/series of aircraft in the present inventory for each Service. The file contains the Typical C-E Configuration of Commercial Air Carrier Type Aircraft by type, model, and manufacturer. It does not contain information on Air Carrier Aircraft manufactured by Lockheed Corporation.	<ul style="list-style-type: none"> Air Force - Annually Navy - Semiannually Army - Depends on availability of publications Commercial Air Carrier - Annually
LAND	Contains the complement of equipment in US Army, US Marine Corps, and US Air Force Land Tactical units including mobile tactical units. The C-E configuration for the US Army units is entered as typical configuration for TO&E Company/Battery Level of Tactical Ground Units. The C-E configuration for the US Marine Corps and US Air Force Tactical Units is based on the actual on hand C-E equipment.	<ul style="list-style-type: none"> Army - No fixed schedule (Update source being investigated) US Marine Corps - Quarterly US Air Force - Annually

Atlantic Research Corporation
N00019-79-C-0634
AIR-518-5
Jan 1981

THIS PAGE HAS BEEN DELETED

Atlantic Research Corporation
N00019-79-C-0634
AIR-518-5
Jan 1981

THIS PAGE HAS BEEN DELETED

Table 8.16

Major Data Fields in the Frequency Allocation Application File (FAAF)⁽²⁾

Date
 Title
 Agency
 Status
 Application numbers (include supporting references)
 Security classification
 Function
 Operational environment
 Geographic area of use
 Nomenclature
 Physical installation or platform
 Number of equipments
 Operation date
 Spectrum signature requirement
 Frequency range
 Frequency control method
 Modulation type
 Power
 Pulse width and pulse repetition frequency
 Receiver IF bandwidth
 Antenna beamwidth
 Antenna polarization

Table 8.17

Data Fields in the Spectrum Signature File⁽²⁾

Power output	Standard response
Emission spectrum characteristics	Receiver intermodulation
Modulation characteristics	Pulse and CW desensitization
Transmitter intermodulation	Adjacent signal interference
Modulator bandwidth	Dynamic range
Carrier frequency stability	Oscillator radiation
Sensitivity	Audio selectivity
Selectivity	Discriminator bandwidth
Spurious response	Antenna measurements
Overall susceptibility	Antenna patterns
Receiver modulation	

8.4.1.1.8 Tactical File⁽²⁾

The Tactical File contains information that pertains to various military tactical deployments, simple and complex. The file also contains routine C-E environments present in various regions as well as the Equipment Allowance File (EAF), an inventory of equipments used by various categories (ships, aircraft operation centers, etc.) of the military.⁽²⁾

8.4.1.1.9 Future File⁽¹⁾

This file contains equipment characteristics data concerning future communications and electronic systems.

8.4.1.2 Analytical Models⁽¹⁾

ECAC maintains a collection of analytical models that operate either as a part of EMC systems analysis computer codes or in a stand-alone mode. These models and codes provide users with solutions to various electromagnetic interference (EMI) problems as well as an EMI prediction capability. A list of analytical models maintained by ECAC is given in Table 8.18.

8.4.1.3 Engineering Services⁽²⁾

Based on the analytical techniques and data available, the following services are available from ECAC.

- assistance to C-E equipment developers on all aspects of frequency selection and equipment design.
- guidance in analysis of potential site locations for new equipment.
- power density analysis as a function of distance and topography.
- prediction of EMC loss for various tactical operations.
- prediction of EMC effects by incorporating new electronic systems into existing and future environments.

The outputs supplied by ECAC are not in a standard format but are tailored to the particular task. They range from narrative discussions to tabulations of data in numerical or graphical form.

8.4.2 Intrasystem Analysis Program

The Intrasystem Analysis Program (IAP) is a set of computer codes used in analyzing electromagnetic compatibility (EMC) problems for aircraft, space/satellite, and ground based systems.⁽³⁾ The emphasis of the IAP is on intrasystem compatibility, i.e., the compatibility of numerous electri-

Table 8.18
LISTING OF ECAC MODELS (1)

<p>1. SUBSYSTEM MODELS</p> <p>Transmitter Emission Spectrum Synthesis Transmitter Emission Spectrum Models Fourier Transform of FM Trapezoidal Pulses (HTRANS)</p> <p>Receiver Waveform Simulation Model (RWS) Frequency Analysis Subroutine (FAS) Receiver Response to a Family of Pulses Butterworth and Chebyshev Digital Filters Pulse Compression Matched Filter Impedance Computation and Analysis Program (ZCAP)</p> <p>Multiple Level Antenna Model (MLS) Antenna Data Analysis Program (ANDATA) Pattern Analysis Subroutine (PATAS) Transmitter/Receiver Antenna Coupler (TRACE)</p> <p>Intermodulation Analysis Model Spurious Response Identification Model Mixer Response Model Adjacent Channel Interference Summary</p>	<p>4. COSITE MODELS</p> <p>Cosite Analysis Model (COSAM) Airframe Communications Analysis (AVPAK) Aircraft Ordinance RF Analysis (AVPAK 2)</p>
<p>2. PROPAGATION MODELS</p> <p>MASTER PROPAGATION SYSTEM Terrain Integrated Rough Earth Model (TIREM) Integrated Propagation System (IPS) Smooth Curve Smooth Earth (SCSE) Distance Free Space Spherical Reflection Field (SFSRF) Simplified Theoretical Ground Wave (STGW) Modified YEH Troposcatter (MYEH) NLAMBDA (NL) Ground Wave Model SKYWAVE HF PROPAGATION MODEL COSITE COUPLING MODEL PROPAGATION STATISTICS GENERATOR</p>	<p>5. SPECTRUM MANAGEMENT ANALYSIS MODELS (FREQUENCY ASSIGNMENT)</p> <p>Multiple Channel Assignment Systems (MCAS) LOS Angle Data Channel Assignment Mutual Interference Table Frequency Assignment Support Subroutine (GRAFAS) FAA-ATC-VIIIF Frequency Model Tactical Landing Force EMC Evaluation Off-Frequency Rejection-Distance Calculation (OFRCAL)</p>
<p>3. ENVIRONMENT ANALYSIS SYSTEMS</p> <p>Demand Analysis Programs Model B Pulse Density Model Site Analysis Model (SAM) Target Acquisition Model (TAM) Power Density Display Program (PDDP) IFF MARK X (SIF) Model (AIMS-PPM) IFF MARK XII Model (AIMS-PPM) Rapid Cull Model Equipment Density Program</p>	<p>6. DEGRADATION ANALYSIS MODEL</p> <p>Degradation Analysis</p> <p>7. STATISTICAL AND NUMERICAL ANALYSIS</p> <p>Auto-Cross Correlation Analysis Model (ACCAM) List Processing Routines for Digital Simulations Generalized File Statistics Analyzer (Q63) MATH-PACK STAT-PACK Random E-File Generator (REG) E-File Equipment Statistics (X08K36) Antenna Data Analysis System (ADAS2) Topographic Data Scatter Diagram (SCATER) Experimental Calculation-INR Distribution</p>

cally connected equipments and subsystems residing in a relatively small volume and regarded as a single system. The IAP effort is directed by the Reliability Branch, Rome Air Development Center (RADC/RBCT), Air Force Systems Command, at Griffiss Air Force Base, New York.

The principal component of the IAP is the Intrasystem Electromagnetic Compatibility Analysis Program (IEMCAP). The IEMCAP code provides the basic EMC computer analysis at the system level for all phases of the system lifecycle. The IEMCAP can survey a system for interference, provide tradeoff and waiver analysis and generate specification limits. Aircraft, spacecraft and ground installations can be analyzed with the IEMCAP code. IEMCAP contains models for sources of electromagnetic signals, receptors of such signals and transfer coupling of electromagnetic energy between source and receptor.

A set of supplemental computer codes are included with IEMCAP in the IAP. One code, The General Electromagnetic Model for the Analysis of Complex Systems (GEMACS), is a user-oriented general purpose program for solving electromagnetic radiation and scattering problems using thin-wire, method of moment (MOM) techniques. GEMACS provides a near-field analysis capability for the IAP and a more detailed backup analysis to supplement IEMCAP.

A nonlinear circuit analysis capability is provided by the Nonlinear Circuit Analysis Program (NCAP). Analysis of transmission lines is supported by the IAP codes XTALK, XTALK2, FLATPAK and FLATPAK2 while precipitation static charging is handled by the IAP code PSTAT. The IAP codes are discussed in more detail in the following sections.

8.4.2.1 Intrasystem Electromagnetic Compatibility Analysis Program (IEMCAP)

The Intrasystem Electromagnetic Compatibility Analysis Program (IEMCAP) is an IAP computer code designed to perform an EMC analysis on a complete electronic system level at any or all stages of the system life cycle, from conceptual design of the new system to retrofit and/or modification of the old system.⁽¹⁾ In accomplishing the system's analysis, any or all of the following tasks may be performed.^(1,4)

- provide a data base that can be continuously maintained and updated to follow system design changes.
- generate EMC specification limits tailored to the system.
- survey a system for interference.
- evaluate the impact of granting waivers to the tailored specifications.
- assess the effect of design changes on system EMC.
- provide comparative analysis results on which to base EMC tradeoff decisions.

8.4.2.1.1 Emitter and Receptor Models⁽⁴⁾

Each IEMCAP emitter and receptor is modeled as a part characterized by an emission or susceptibility spectrum. Each spectrum consists of a broadband component, which represents continuous spectra in units of power spectral density, and a narrowband component, which represents discrete spectra in units of power. Each spectrum is also divided into a required spectrum deemed necessary for system operation, and a nonrequired spectrum, not required for system operation but present as a spurious emission or susceptibility. The required spectrum may be specified by the user or calculated by IEMCAP using a model in the code. The emitter models present in IEMCAP are:⁽⁴⁾

- binary frequency-shift keying.
- amplitude modulation with stochastic process.
- angle modulation with stochastic process.
- single sideband amplitude, phase and frequency modulation with a stochastic process.
- chirp radar.
- pulse code modulation/amplitude modulation - nonreturn to zero.
- pulse position modulation.
- pulse code modulation/amplitude - biphase.
- pulse amplitude modulation/frequency modulation.
- pulse duration modulation.
- single pulse.
- pulse train (rectangular, trapezoidal, triangular, sawtooth, high frequency exponential, damped sinusoidal).

The susceptibility model in IEMCAP equates an RF receptor port susceptibility to the receiver sensitivity that is provided in the input data, over the entire receptor spectrum, as defined by the user-specified bandwidth. For a signal, or control port, the susceptibility is the operating level less 20 dB. The nonrequired spectra are set to the levels specified by MIL-STD-461A or MIL-I-6181D unless a change is specified by the user.

8.4.2.1.2 Transfer Models⁽⁴⁾

The coupling and transfer of electromagnetic energy from emitter port to receptor port in IEMCAP is accomplished by the transfer models discussed in the following sections.

8.4.2.1.2.1 Antenna-Coupled Models⁽⁴⁾

Included in this model are antenna-to-antenna and antenna-to-wire coupling on an aircraft, spacecraft or ground system at all common emitter and receptor frequencies. In computing the coupling path, propagation through free space, around the fuselage, and diffraction from wing edges are taken into account. Two groups of antennas are considered in this model. The first group is a set of low gain antennas including the dipole, slot loop and monopole antennas. They are modeled by trigonometric expressions, or as specified by the user. The second type is a set of high gain antennas such as arrays or reflectors, and is modeled by a three section representation of the gain pattern. The gain of each sector currently is frequency independent and is a user input. For antenna-to-wire coupling to occur, the wire must have at least one segment behind an aperture.

8.4.2.1.2.2 Wire-To-Wire Model⁽⁴⁾

Wire-to-wire coupling occurs if a wire connected to an emitter and a wire connected to a receptor are in the same wire bundle segment. The wire-to-wire routine calculates the voltage induced in the receptor wire due to the presence of the emitter wire at each common emitter-receptor frequency. Models for open wires, shielded wires and double shielded wires in a balanced or unbalanced configuration are used as required.

8.4.2.1.2.3 Case-to-Case Model⁽⁴⁾

This model computes coupling between equipment cases. These cases are modeled as dipoles.

8.4.2.1.2.4 Environmental Field Models⁽⁴⁾

These models compute the coupling of external and internal EM fields to a receptor port. The port may be an antenna, wire, or equipment case. Induced current is calculated for wire or antenna receptor ports, while the impressed field is determined for an equipment case port.

8.4.2.1.2.5 Filter Models⁽⁴⁾

The filter models available in IEMCAP are: single tuned, low pass, high pass, band pass and band reject. The models calculate the insertion loss in dB provided by the filter at a given frequency.

The filters are represented as ideal lossless networks made up only of capacitors and inductors. Dissipation is considered in the models by providing for a minimum insertion loss at the tuned frequency or in the pass band. A maximum insertion loss is provided in the rejection band. These minimum and maximum insertion losses bound the filter transfer function.

8.4.2.1.3 Spectrum Representation^(1,4)

Each emitter and receptor port is characterized by an emission or susceptibility spectrum. A table of up to 90 frequencies ranging from 30 Hz to 18 GHz is assigned to each equipment in the system. This is used to establish the characteristics of all port spectra within the equipment. The

frequencies are specified in two ways. (1) The user may specify the upper and lower frequency limits, the maximum number of frequencies, and number of frequencies per octave. The IEMCAP code then generates a set of geometrically spaced frequencies within the set limits. (2) Alternatively, the user may specify the upper and lower frequency limits, the maximum number of frequencies, and a set of specific frequencies to be included (up to the maximum number). The code then generates geometrically spaced frequencies to fill in the frequencies not specified.

At the port level, the required frequency range is specified within the overall equipment frequency range. In order not to miss peaks or valleys between sample frequencies, the spectrum is sampled in the half-interval between a given frequency and each of its neighboring frequencies. The maximum frequency is picked for emission spectra, and the minimum, for susceptibility spectra. This process quantizes the port spectra relative to the sample frequencies.

8.4.2.1.4 Basic Systems Analysis Approach⁽⁴⁾

All system ports are considered to be emitters and/or receptors of electromagnetic energy. Each port is characterized by both a required and a nonrequired spectrum. An EMC problem is said to exist when sufficient electromagnetic energy is unintentionally coupled into a receptor port to exceed its susceptibility threshold. If no threshold is exceeded for any receptor, the system is said to be compatible.

The required spectrum for each port is nonadjustable in the code. The nonrequired spectrum can be adjusted, to make the system compatible. An adjustment limit is usually included to prevent too stringent a spectrum adjustment.

To determine if interference is present at a given receptor port, the level of power coupled into the receptor at its terminals must be calculated. This task is accomplished by a set of linear systems equations that relate receptor models, transfer models and emitter models to each other. The systems equations in IEMCAP characterize the power coupled into a receptor in terms of power spectral density. This adequately characterizes devices sensitive to average power, but may not be sufficient to treat peak power devices. Electromagnetic interference (EMI) is assessed by computation of an EMI margin that serves as a figure of merit.⁽⁶⁾ The EMI margin is first calculated for a given receptor by computing the ratio (in dB) of power from a given emitter incident at the receptor's input to the given receptor power susceptibility level at each frequency common to a given emitter-receptor port pair. The ratio is called the EMI point margin for the port pair at the given frequency. The integrated EMI margin is then calculated over all frequencies common to the port pair. The calculations are repeated for every emitter-receptor port pair. Total EMI margins are next calculated for each receptor by summing the contributions to the receptor from each coupled emitter, at each frequency (total point margins), and over all frequencies (total integrated margin). The total integrated EMI margin represents the overall figure of merit for the receptor.⁽⁶⁾

8.4.2.1.5 Program Flow and Task Analysis⁽⁴⁾

The IEMCAP work is divided into two sections. The first section,

called the Input Decode and Initial Processing Routine (IDIPR), reads and checks data for correct format, builds working files, interfaces with spectrum models, analyzes wire bundles and wire connections to ports, and constructs the initial port spectra. The second section called the Task Analysis Routine (TART), performs the requested EMC systems analysis. A functional flow chart of IEMCAP is given in Figure 8.3.

Two permanent files of major importance are constructed during execution of IEMCAP. The first file, called the Intrasystem Signature File (ISF), is initially built in IDIPR and is a data base containing all input data defining the system and the port spectra. The ISF file can be updated in IDIPR or TART as the system design is modified. The second file is the Post Processor File (PPF) and contains all of the IEMCAP output from IDIPR and TART. The file is either in printed form or in a computer file. Data base management tools are being developed to manage both the ISF and PPF files.

The TART section of IEMCAP can perform four different EMC analysis tasks.

One task is a Baseline System EMC Survey that simply scans the system for interference. If the integrated EMI margin for an emitter-receptor port pair exceeds a user-supplied limit, a summary of the port pair interference is printed as well as total signal received by the receptor.

A second IEMCAP task is Specification Generation. The nonrequired emitter and receptor port spectra are adjusted until the system is compatible to within a user-specified limit. Any incompatibilities that still exist are reported as unresolved interference. The adjusted spectra represent the maximum emission and minimum susceptibility specifications.

A third task is a tradeoff analysis. The IEMCAP code compares the interference of a modified system to that from a previous baseline or specification generation run. The effects on interference of antenna changes, filter changes, spectrum parameter changes, and wire changes can be assessed. No ports, equipments or subsystems may be deleted or spectra frequencies changed in this analysis.

The fourth task is Specification Waiver Analysis. Portions of specific port spectra are shifted and the resulting interference compared to a previous baseline or specification generation run. The effects of granting waivers for specific ports can then be assessed.

8.4.2.2 Electromagnetic Model for the Analysis of Complex Systems (GEMACS)^(7,8)

The GEMACS program is a general user-oriented code designed to solve radiation and scattering problems using thin-wire method of moment (MOM) techniques.

A high level functional flow chart of GEMACS is shown in Figure 8.4. The executive routines control file manipulation, take checkpoints in the analysis and handle restart from the checkpoints. The input language processor handles the command language and sends the data; the task

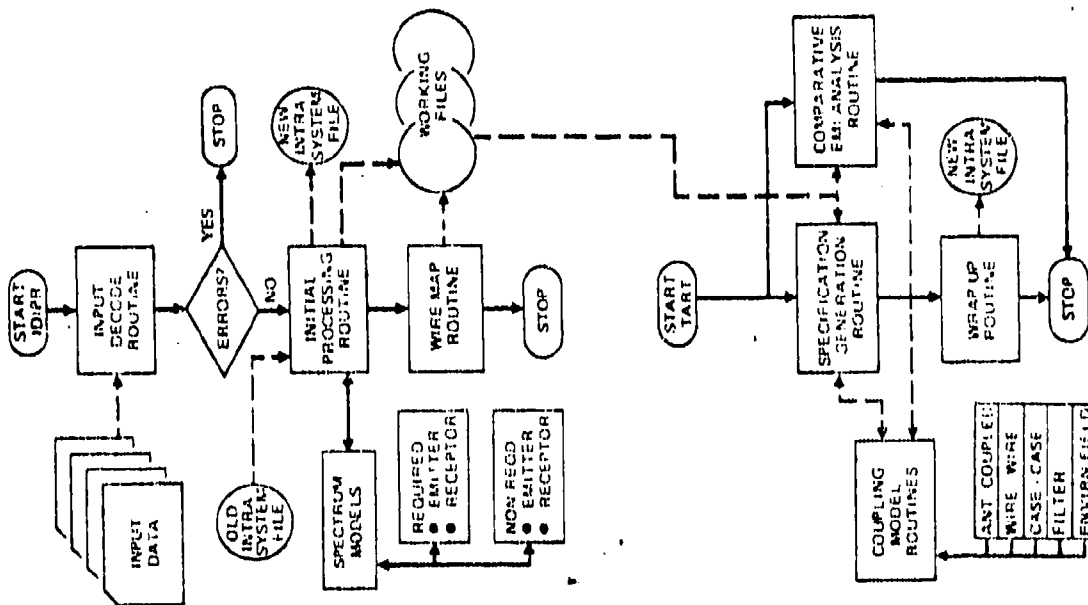


Figure 8.3 IDMAP Functional Flow (4)

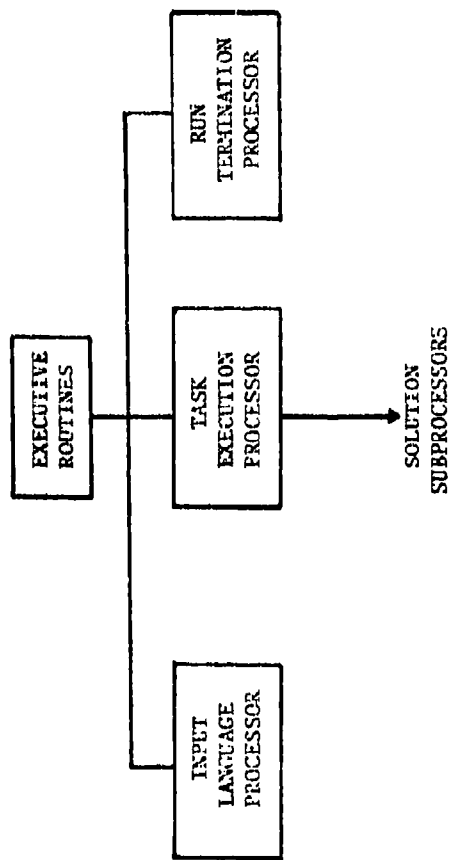


Figure 8.4 GENACS Structure (7)

execution processor calls the appropriate subprocessor to perform the analysis; and the run termination processor ends the analysis. The processor and executive routine constitute a data management system.

The subprocessors solve a radiation or scattering problem formulated using an electric field, integral equation. The system geometry is modeled in GEMACS as a thin-wire grid structure. The integral equation is then reduced by standard MOM techniques⁽¹⁰⁾ to a matrix equation with the following general form

$$\underline{Z} \underline{I} = \underline{E} \quad (8-1)$$

where \underline{Z} is the interaction matrix that represents field coupling between the various currents on the wire grid, \underline{I} is the current matrix, and \underline{E} is the excitation matrix.

In order to calculate \underline{I} , the \underline{Z} matrix must be inverted and GEMACS contains a matrix inversion routine. In the case of a large \underline{Z} matrix, full inversion is impractical and GEMACS employs an approximate solution procedure called the Banded Matrix Iteration (BMI) technique.⁽⁸⁾ In this technique, the \underline{Z} matrix is divided into a banded matrix \underline{B} , a lower triangular matrix \underline{L} , and an upper triangular matrix \underline{U} as shown in (8-2), where M is the bandwidth.

$$\begin{bmatrix} \diagdown \underline{Z} \diagup \end{bmatrix} = \begin{bmatrix} \diagdown \underline{L} \diagup \end{bmatrix} + \begin{bmatrix} \overset{M}{\diagup} \underline{B} \diagdown \end{bmatrix} + \begin{bmatrix} \diagup \underline{U} \diagdown \end{bmatrix} \quad (8-2)$$

$$= \underline{L} \cdot \underline{B} \cdot \underline{U}$$

Equations (8-1) and (8-2) lead to the following iterative equation for the current \underline{I} :

$$\underline{B} \underline{I}_{j+1} = \underline{E} - (\underline{L} + \underline{U}) \underline{I}_j \quad (8-3)$$

The first step in the solution process is to decompose the banded matrix \underline{B} into upper and lower triangular matrices \underline{B}_U and \underline{B}_L respectively. Equation 8-3) is written in the form

$$\underline{B}_L \underline{Y}_j = \underline{E} - (\underline{L} + \underline{U}) \underline{I}_j \quad (8-4)$$

The matrix \underline{Y}_j is solved by forward elimination, using \underline{I}_j , the currents at the j^{th} iterative step. The matrix \underline{Y}_j is just the product of \underline{B}_U with \underline{I}_{j+1} .

$$\underline{B}_U \underline{I}_{j+1} = \underline{Y}_j \quad (8-5)$$

The current matrix \underline{I}_{j+1} is then solved by backward substitution. The process is repeated until convergence is obtained. The convergence rate is sharply dependent on M , the bandwidth of \underline{B} . Many field problems have been treated with success using GEMACS.

The GEMACS code belongs to the Air Force Intrasytem Analysis Program (IAP). It provides a near-field analysis capability and serves as a complement to IEMCAP, the IAP system level EMC program. GEMACS has a checkpoint/restart capability allowing long analyses to be stopped and restarted at will, both as a protection against computer failures and as an aid in changing the command language stream. An extensive debugging and error-checking capability is built into the code to aid analysis and future upgrading of the software.

8.4.2.3 Nonlinear Circuit Analysis Program (NCAP)⁽⁹⁾

The Nonlinear Circuit Analysis Program (NCAP) calculates the nonlinear transfer functions of an electronic circuit. Standard circuit elements are used in interconnecting networks containing up to 500 nodes. The following circuit element models are included in NCAP:

- Independent Voltage Source
- Linear Dependent Sources
- Nonlinear Dependent Sources
- Linear Components
- Nonlinear Components
- Vacuum Diode
- Vacuum Triode
- Vacuum Pentode
- Semiconductor Diode
- Bipolar Junction Transistor
- Field Effect Transistor

NCAP has a free-field format for input data, a user-oriented command language, a capability to build device models, in addition to the stored models and a frequency sweep feature that allows an analysis of the circuit to be done over a range of frequencies in one run.

NCAP solves the nonlinear network problems by forming the model admittance matrix for the entire network, and first order generator (current source) excitation vector for all linear sources in the network. The first order model voltage vector, which contains the first order transfer functions at the given frequency, is then calculated. Higher order transfer functions are then solved interactively.

8.4.2.4 Precipitation Charging, Noise Generation and Coupling (PSTAT)⁽¹¹⁾

The program Precipitation Charging, Noise Generation and Coupling (PSTAT) predicts the effect of precipitation static noise upon a wide variety of aircraft under many different flight situations. The code is based upon the results of both theory and experiment. The accuracy of PSTAT varies from a few percent to tens of percent depending on the aircraft design. It cannot be applied to helicopters or missiles because their geometrics are radically different from aircraft.

8.4.2.5 Transmission Line Codes

Four transmission line codes are supported in the IAP.⁽¹²⁾ The first code, XTALK, analyzes N+1 bare wires; N bare wires above an infinite ground plane, and N wires within a cylindrical shield containing a homogeneous dielectric. All wires are considered in equivalent XTALK except the

wires may be imperfect conductors. The code FLATPAK analyzes N+1 wire ribbon cables for perfectly conducting wires. The code FLATPAK2 considers the N+1 wire ribbon cable problem for imperfectly conducting wires. All codes assume a steady state sinusoidal excitation and a lossless medium around the conductors.

8.4.3 Interference Prediction Process - Number 1 (IPP-1)

The Interference Prediction Process - Number 1 (IPP-1) is a computer code developed by the Rome Air Development Center (RADC), Griffiss Air Force Base, New York to analyze and predict possible interference situations for any proposed or existing deployment of transmitters and receivers.^(1,2,5) The IPP-1 code can be used for:⁽²⁰⁾

- A. the preliminary development of system or equipment requirements and specifications.
- B. the preparation of specification compliance test plans.
- C. the evaluation of test results.
- D. the revision of specifications or equipments for conditions of noncompliance.
- E. the evaluation of systems in a specific operational environment.

Specific problems that IPP-1 may analyze include the following:⁽²⁾

- A. Examine the EMC situation for a complex of equipments and identify problem areas.
- B. Examine the impact of changing the operating frequency of one or more equipments in the complex.
- C. Examine the impact of adding a transmitter to an existing complex of equipments.
- D. Examine the interference produced in a receiver when added to an existing complex.
- E. Determine which one of several possible locations for a receiver provides the least probable interference.
- F. Determine the source and cause of a known interference problem.
- G. Determine the amount of suppression required to correct a specified interference situation.
- H. Obtain site survey or EMC environment type of information for a given location.

- I. Obtain site survey or EMC environment type of information for a given receiver or group of receivers.
- J. Determine propagation loss over a specified path.
- K. Obtain specific interference characteristic data on transmitters, receivers or antennas contained on the equipment characteristic tape

In addition, several basic types of analysis may be requested which include: (2,13)

- A. Data base management.
- B. Rapid cull EMC analysis.
- C. Frequency cull EMC analysis.
- D. Detailed EMC analysis.
- E. Propagation loss.
- F. Power density and field strength analysis.
- G. Internodulation analysis.
- H. Frequency band analysis.
- I. Adjacent signal analysis.
- J. Frequency/signal analysis.

The IPP-1 code is controlled by an executive routine that processes data, builds files and oversees the type of analysis to be performed.

The remaining routines carry out the analysis. (1,13) The interference analysis is divided into two parts: (1) a rapid cull used for eliminating the obviously noninterfering parts of the problem by means of simple criteria, and (2) a frequency cull which involves a frequency dependent analysis of possibly interfering situations.

The frequency cull uses detailed emitter, receptor and propagation models to predict a figure of merit (interference margin) for each receiver. Included in the analysis is a statistical description of emitter output signal propagation, and receiver response. The figures of merit are then tabulated for each receiver.

8.4.4 The Cosite Analysis Model (COSAM)

The Cosite Analysis Model (COSAM) is a computer code designed to evaluate the electromagnetic compatibility of a single site in the neighborhood of a large number (50) of communication transmitting and receiving equipments. (1,14) A cosite EMC problem implies close proximity of transmitting and receiving receiver input.

In performing the interference analysis, up to five interactions are considered by COSAM: (1) adjacent signal, (2) spurious emissions, (3) spurious responses, (4) receiver intermodulation, and (5) transmitter intermodulation. The results from each required interaction are combined in COSAM to produce an output signal-to-noise (S/N) and signal-to-interference plus noise (S/I+N) ration that serve as performance scores.

8.4.5 Specification and Electromagnetic Compatibility Analysis Program (SEMCAP)

Specification and Electromagnetic Compatibility Analysis Program (SEMCAP) is a computer code developed by TRW Systems, Redondo Beach, California for the NASA Manned Spacecraft Center, Houston, Texas. (1,15-17) The code is designed to:

- A. analyze a system for electromagnetic compatibility;
- B. develop EMC specification generation and susceptibility limits consistent with desired signals;
- C. perform a waiver analysis on the system.

SEMCAP is a systems level EMC code and is very similar in design to the IEMCAP code discussed in Section 8.2.2.1.

8.4.5.1 Analysis Models

The analysis models used in SEMCAP include models for emitters, receptors and coupling paths between an emitter-receptor pair.

Emitters and receptors are each given a spectrum representation divided into a priority 1 functional port (similar to the IEMCAP code required spectrum) and a priority 2 extraneous port (similar to the IEMCAP code nonrequired spectrum).

Coupling paths are modeled by the following electromagnetic transfer functions: (1) antenna-to-antenna, (2) antenna-to-wire, (3) wire-to-wire and (4) field-to-wire. All transfer function models are similar to the models found in the IEMCAP code (Section 8.2.2.1).

8.4.5.2 Compatibility Analysis

The first step in the analysis is the calculation of the required spectrum (priority) interference of emitters upon receptors. Unless the spectra are incompatible with the priority 1 receptors spectra, a margin between interference and malfunction will exist for the receptor. Priority 2 (nonrequired) emission spectra are then not allowed to exceed this margin.

The voltage V_{ij} included by generator i at receptor j is calculated by

$$V_{ij} = \int_{b_1}^{b_2} G_i(b) T_{ij}(b) P_j(b) db \quad (8-6)$$

where $G_i(f)$ is the amplitude at frequency f of the source i ; voltage spectrum; P_j is the amplitude at frequency f of the receptor j voltage spectrum, and $T_{ij}(f)$ is the amplitude at frequency f of the voltage transfer function between generator i and receptor j . Equation (8-6) gives the peak response of a receptor model due to source and coupling models characterized by an amplitude density. The SEMCAP compatibility analysis is then best suited for treating transient or impulsive signals and devices characterized by peak power.⁽³⁾ This is in contrast to the IEMCAP code which uses a power spectral density model for emitters, receptors and transfer functions and characterizes devices sensitive to average power.

8.4.5.3 Specification Generation and Waiver Analysis

Besides surveying the system for interference, SEMCAP generates tailored specifications by modifying the extraneous emitter and receptor spectra to produce a compatible system, and assesses the effect on the system of granting waivers to the specifications. The general procedure is similar to the specification generation and waiver analysis capability in the IEMCAP code (Section 8.2.2.1).

8.4.6 Shipboard Electromagnetic Compatibility Analysis (SEMCA)

The Shipboard Electromagnetic Compatibility Analysis model (SEMCA) is a set of computer codes designed by General Electric Company, Dayton Beach, Florida (1,18,19) to perform an EMC analysis of the radiating and receiving equipments located on a ship. The SEMCA code is tailored to shipboard design in that intraship coupling is tied to ship topside modeling. SEMCA is used primarily in the VLF/LF/HF and VHF/WHF frequency ranges, but has been extended to microwaves in the SEMCAM (Shipboard Electromagnetic Compatibility Analysis Microwave) code. This code has been used⁽¹⁾ in topside design of new ships, to assess EMC impact of alternate equipment and antenna site, for frequency assignment, and for generation of EMC specifications for new equipment design. The code has been expanded from a cosite model which considers only intraship problems to include off-ship signals sources.

8.5 Data Base Management

In Section 8.2 of this chapter, a number of facilities and programs were described that are necessary and useful in performing an EMC analysis. In performing such an analysis, the systematic manipulation of large amounts of data may be required, both as program input and output. Such data handling is best performed by proper data base management software tools.

8.5.1 ECAC Data Base Management

The Electromagnetic Compatibility Analysis Center (ECAC) has a set of programs that are designed to primarily retrieve specific information from its collection of EMC data files. These files have been described in Section 8.2.1 of this report. A list of ECAC data base query programs is given in Table 8.19.

8.5.2 IAP Data Base Management

The Intrasytem Analysis Program (IAP), under the direction of the Rome Air Development Center, Griffis Air Force Base, New York, is being currently expanded to include a number of data base management tools. A brief description of existing and currently planned programs is given in the following sections.

8.5.2.1 System File Handler

The System File Handler (SFH) is a FORTRAN software code capable of building and editing sequential files on magnetic tape or random devices.⁽²⁰⁾ The primary function of the SFH is to access the IAP files in the Electromagnetic Compatibility Analysis Program (IEMCAP) called the Intrasytem Signature File (ISF) and the Post Processor File (PPF), as well as to access the IAP System Data File (SDF) which is described in the next section. The SFH provides a variety of services and is designed so that additional services can be easily incorporated as they become available.

The basic services offered by the SFH are: ACCESS, LOAD and UPDATE. The ACCESS function allows a user to query a file to obtain specific attributes about the data, display requested information, or create a subset copy of the original file. The LOAD function allows a user to generate a data file from scratch. The UPDATE functions allow for file modification and maintenance.

The SFH is designed to be used on a general purpose digital computer and to be essentially free of any particular machine or operating system. The command language is designed to be as user oriented as possible. The SFH will allow the user to access the wealth of data that exists either as input data for the various IAP codes, or output data from an IAP analysis of a system.

8.5.2.2 System Data File

The System Data File (SDF) is a data base that digitally stores in a standard format all of the electrical and physical characteristics of a system necessary to perform an EMC analysis using any code in the IAP.⁽²¹⁾ A SDF will exist for each system analyzed using the IAP codes.

Access to the SDF will be by means of the System File Handler (SFH) described in Section 8.3.2.1. The SFH will be used in conjunction with an IEMCAP translator (currently under development at RADC) to access the SDF and automatically prepare most of the input data required to perform an IEMCAP analysis on a given system. This will relieve the user of the burden of preparing the data manually. All codes will be available in the near future.

Table 8.19 ECAC Data Base Management Program⁽¹⁾

DATA BASE SELECT CAPABILITIES

On-Line E-File General Format and Print Program
On-Line E-File General Select Capability
On-Line E-File (SPACE)
The C&E Deployment System
Topographic Data File Select and Print Program
(TOPSEL)
Profile Print Program
Operational Platform Allowance File (OPAF)
General Format and Print Program
Nominal Characteristics File (NCF) Equipment
Selection Programs
Propagation Measurement Retrieval System (PMRS)

8.6 References

1. Engineering Design Handbook Electromagnetic Compatibility, prepared by Headquarter US Army Material Development and Readiness Command, DARCOM-P706-410, March 1977.
2. William G. Duff, Electromagnetic Interference and Compatibility, Vol.5, Don White Consultants Inc., 1972.
3. Intrasystem Analysis Program (IAP) Structural Design Study, Atlantic Research Corporation, ARC No. 53-6111, April 1980.
4. J. L. Bogdanor, R. A. Pearlman, and M. D. Siegel, Intrasystem Electromagnetic Compatibility Analysis Program, Volume II: "User's Manual Usage Section," Final Report prepared by McDonnell Aircraft Company for Rome Air Development Center under Contract F30602-72-C-0277, RADC-tr-74-342, December 1974.
5. Interference Notebook, RADC-TR-66-1, Rome Air Development Center, Griffiss Air Force Base, NY, June 1966.
6. R. A. Pearlman, "Physical Interpretation of the IEMCAP Integrated EMI Margin," IEEE 1978 Symposium on Electromagnetic Compatibility, June, 1978.
7. Kenneth R. Siarkiewicz, "General Electromagnetic Model for the Analysis of Complex Systems," IEEE 1978 Symposium on Electromagnetic Compatibility, June 1978.
8. General Electromagnetic Model for the Analysis of Complex Systems, Vol. I, II, the BDM Corporation, RADC-TR-77-137, April 1977.
9. J. Spina, et.al., "Nonlinear Circuit Analysis Program (NCAP) Documentation," RADC-TR-79-245, Vol. 1 - Engineering Manual; Vol. 2 - User's Manual; Vol 3 - Programmer's Manual, Rome Air Development Center, Griffiss Air Force Base, NY, 1979.
10. R. F. Harrington Field Computation by Moment Methods, The MacMillian Co., 1968.
11. J. E. Nanevich and D. G. Douglas, "Static Electricity Analysis Program, Vols. I and II, SAMSO-TR-75-44, Standord Research Institute, Oct. 1974.
12. C. R. Paul, "Applications of Multiconductor Transmission Line Theory to the Prediction of Cable Coupling," RADC-TR-76-101, Volume VII, Rome Air Development Center, Griffiss AFB, NY, July 1977.
13. W. G. Duff, et.al., "IPP-1 User's Manual, RADC-TR-71-300, Rome Air Development Center, Griffiss AFB, NY, January 1972. (See also "IPP-1 Program Improvements," Atlantic Research Corp., Alexandria, VA, 1972.

14. M. N. Lustgarten, "COMSAM (co-Site Analysis Model)," 1970 IEEE Electromagnetic Compatibility Symposium Record, 394-406, July 14, 15, 16, 1970.
15. W. R. Johnson, B. D. Cooperstein, and A. K. Thomas, "Development of a Space Vehicle Electromagnetic Interference/Compatibility Specification," TRW Document No. 08900-6001-T000, TRW Systems, One Space Park, Redondo Beach, CA 90878, 28 June 1968.
16. W. R. Johnson, J. A. Spagon, and A. K. Thomas, "Application of Computer Technology to the Implementation of EMC Programs" 1969 IEEE Electromagnetic Compatibility Symposium Record, pp. 155-166, June 17-19, 1969.
17. A. K. Thomas, "Math Modeling Techniques for a Computerized EMC Analysis," SEMCAP Selected Technical Papers, TRW Systems Group, Redondo Beach, CA, 1969 IEEE EMC Symposium Record.
18. Shipboard Electromagnetic Compatibility Analysis, SEMCA III, Vol. VIIA, User's Reference Manual, General Electric Company Apollo Systems, Daytona Beach, FL, January 1970.
19. SEMCA V, Volumes C, XA and XB, General Electric Co. Daytona Beach, FL.
20. IEMCAP PRE/POST Processor System File Handler, Atlantic Research Corp., Report prepared for RADC/RBCT, February 1980.
21. System Data File (SDF) for the Intrasystem Analysis Program (IAP), RADC-TR-79-213 Vols 1 and 2, Dec. 1979.

9.0 MEASUREMENT TEST AND EVALUATION

This chapter addresses the alternative methods by which the various parameters of composite materials are experimentally measured. Section 9.1 outlines the various experimental techniques used to measure various composite intrinsic properties such as permeability, permittivity, resistivity and conductivity. Several mathematical models of conductivity have been developed and they are included for comparison. Section 9.2 addresses electric and magnetic shielding effectiveness measurement techniques using several different approaches of what constitutes shielding. The advantages and limitations of all techniques are reviewed.

9.1 Techniques for Measuring Intrinsic Parameters

In this section the methods used to measure the permeability, permittivity, conductivity and resistivity of composite materials are discussed in detail. In addition, certain mathematical models for the conductivity of composites are presented.

9.1.1 Permeability

Because the present fabrication of Kevlar/epoxy, boron/epoxy and graphite/epoxy does not involve magnetic materials, permeability measurements have been somewhat limited in scope. Low frequency permeability measurements have been made using the sample weighing ASTM method⁽¹⁾ which is illustrated schematically in Figure 9.1. In this method, a strip of composite sample of known dimensions is suspended in an air gap between two magnetic poles. The sample is attached to an analytic balance and the weight of the sample is recorded with the magnetic field on and off. The permeability is then given by the formula⁽³⁾

$$\mu = \mu_0 \left(1 + \frac{24.6F}{AH^2} \right) \quad (9-1)$$

where F is the magnetic force (in mg), H is the magnetic field strength (in oersteds) and A is the area of the magnetic poles (in cm²). The strip dimensions are a function of the formula (9-1). The accuracy of the method is limited primarily by the sensitivity of the analytic balance and the accuracy of the strip dimensions.

At 100 Hz the permeability of the composites was determined using a vibrating sample magnetometer.⁽³⁾ For the frequency range 100 Hz - 1000 Hz, Epstein frames^(1,2) consisting of alternating strips of composite and ferromagnetic material in a solenoid core can be used to determine the permeability. Higher frequency techniques have not been developed since the high frequency permeability of present day boron/epoxy, Kevlar/epoxy and graphite/epoxy is not expected to differ much from the permeability of free space (μ_0).

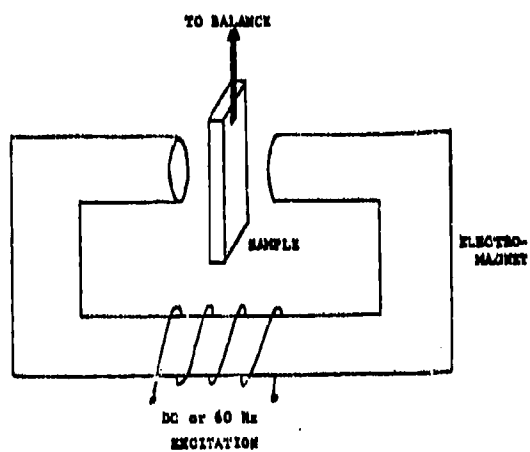


Figure 9.1. Permeability measurement apparatus⁽³⁾

9.1.2 Permittivity

Two methods of measuring the permittivity are reviewed in this section.

9.1.2.1 ASTM Standard Method

The ASTM standard procedure⁽⁴⁾ for measuring the permittivity of composite materials consists of constructing a capacitor containing a composite sample between two flat, parallel metal electrodes. The capacitance is then measured using a standard capacitance bridge. The permittivity is then calculated using the formula

$$\epsilon = \frac{CL}{A} \quad (9-2)$$

where C is the capacitance, L is the sample length between the electrodes, and A is the sample cross-section between the electrodes.^(2,3) Equation (9-2) assumes the flat parallel plate geometry illustrated in Figure 9.2. This is the best geometry to use since the capacitance can be accurately calculated and the composite samples are easy to prepare.

Sample preparation is extremely important in order for this method to give reliable results. Proper sample and electrode cleaning procedures are required since an impure surface will give poor capacitance data. Good electrical contact is required to give low contact resistance. To accomplish this goal, a vacuum deposition technique is usually necessary.

The principal limitation of the method is the fringing of the electric field at the electrodes. This effect can be greatly reduced by using guarded electrodes which are illustrated in Figure 9.3 for a dielectric sample holder. The top electrode consists of a center piece and each edge piece. For gaps small compared to sample thickness and if all top electrode potentials are assumed the same, the center electrode will not fringe. The method is valid from D.C. to about 30 MHz.

9.1.2.2 Effective Permittivity

An effective or average permittivity can be calculated using plane wave EM shielding measurements. Plane wave shielding is discussed in Sections 6.1 and 9.2 of this report so only a summary of the relevant formulas will be given here.

The plane wave transmission coefficient through a composite barrier is

$$T = \frac{(1-\rho^2)e^{-rt}}{1-\rho^2e^{-2rt}} \quad (9-3)$$

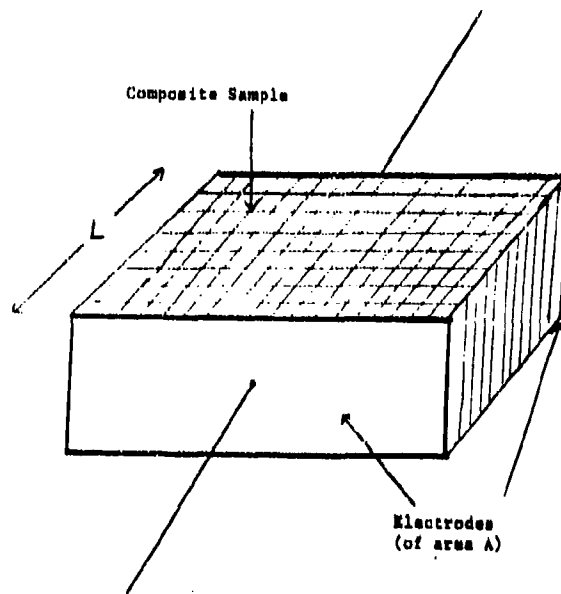


Figure 9.2. Permittivity measurement apparatus

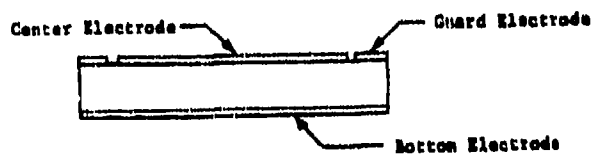


Figure 9.3. Use of a guarded electrode in composite sample capacitors (2)

where ρ is the reflection coefficient, r is the propagation constant, and t is the composite sample thickness. Shielding measurements that yield amplitude and phase information on T allow ρ to be determined.^(2,9) Knowledge of ρ allows the effective complex permittivity ϵ^* to be determined.

$$\epsilon^* = \epsilon(1 - j \tan \delta) \quad (9-4)$$

where ϵ is the real part of the effective permittivity and $\tan \delta$ is the loss tangent.⁽²⁾

9.1.3 Resistivity

The two ASTM standard methods for measuring the low frequency resistivity of composite materials are the two-point and four-point probe methods,^(2,3,5) described in this section.

9.1.3.1 Two-Point Method

Ohmic contacts are made to the ends of a rectangular cross section of material. A known current is passed through the sample and the voltage is measured. The resistance of the sample is taken to be

$$R = \frac{V}{I} \quad (9-5)$$

where V is the measured sample voltage and I is the known test current. The resistivity is then given by

$$\rho = \frac{RWL}{I} \quad (9-6)$$

where W is the sample width; L , the sample length between the drive contacts, and t the sample thickness. The two-point method is illustrated in Figure 9.4. Results are valid to about 30 - 50 MHz.⁽²⁾

The two-point method assumes a uniform current across the sample face and a homogeneous material.⁽²⁾ The most reliable resistivity measurements in practice are done on single material crystals. For materials of mixed orientation such as composites the two-point method works best.⁽³⁾ It is necessary that low resistance ohmic contacts be made to the sample, preferably by vacuum deposition of aluminum or indium. Sample preparation is critical for reliable results to be obtained. At high excitation levels, the two-point method can be used by just increasing the voltage. Because of possible nonlinear response, equations (9-3)-(9-4) are replaced by

$$\rho = \frac{Wt}{L} \frac{dV}{dI} \quad (9-7)$$

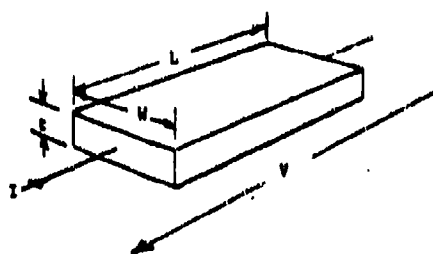


Figure 9.4. The two-point method for measurement of resistivity or conductivity(2)

9.1.3.2 Four-Point Method

In this technique, four probes are aligned equidistant on a material sample as illustrated in Figure 9.5. The outer two probes inject and extract a known current. A voltage (both DC and AC) is then measured at the surface across the inner two probes. The resistivity is then given by one of the following two formulas⁽²⁾

$$\rho = 2\pi s \frac{V}{I} \quad (9-8)$$

if $s \ll t$

$$\rho = 4.5t \frac{V}{I} \quad (9-9)$$

if $t \ll s$

This method has the advantage that no ohmic contacts need be made to the composite surface. A disadvantage to the method is that it is sensitive to the composite surface state and geometry.⁽³⁾ In addition, localized point contacts on composites are unreliable because of the presence of broken fibers (especially in graphite/epoxy)⁽²⁾

9.1.4 Conductivity

Three methods for measuring the conductivity of composite materials will be discussed in the first section. One method is the standard ASTM test procedure which applies for relatively low frequencies. The second method uses a slotted stripline and applies for higher frequency. The third method extracts "effective" conductivity from EM shielding measurements. In the second section, various mathematical models for the conductivity of composite materials will be discussed.

9.1.4.1 Measurements

Individual methods for measuring conductivity in composite materials are now discussed in detail.

9.1.4.2 ASTM Method

The ASTM method for measuring the conductivity for composites^(2,3,5) consists of measuring the resistance of a rectangular sample of composite using the 2-point and 4-point probe technique as described in Section 9.1.3. The expression for the conductivity is then

$$\sigma = \frac{L}{RWt} \quad (9-10)$$

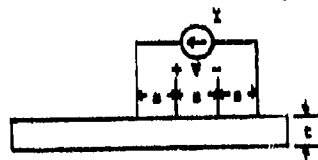


Figure 9.5. Four-point method for measurement of resistivity or conductivity⁽²⁾

9.1.3.2 Four-Point Method

In this technique, four probes are aligned equidistant on a material sample as illustrated in Figure 9.5. The outer two probes inject and extract a known current. A voltage (both DC and AC) is then measured at the surface across the inner two probes. The resistivity is then given by one of the following two formulas⁽²⁾

$$\rho = 2\pi s \frac{V}{I} \quad (9-8)$$

if $s \ll t$

$$\rho = 4.5t \frac{V}{I} \quad (9-9)$$

if $t \ll s$

This method has the advantage that no ohmic contacts need be made to the composite surface. A disadvantage to the method is that it is sensitive to the composite surface state and geometry.⁽³⁾ In addition, localized point contacts on composites are unreliable because of the presence of broken fibers (especially in graphite/epoxy)⁽²⁾

9.1.4 Conductivity

Three methods for measuring the conductivity of composite materials will be discussed in the first section. One method is the standard ASTM test procedure which applies for relatively low frequencies. The second method uses a slotted stripline and applies for higher frequency. The third method extracts "effective" conductivity from EM shielding measurements. In the second section, various mathematical models for the conductivity of composite materials will be discussed.

9.1.4.1 Measurements

Individual methods for measuring conductivity in composite materials are now discussed in detail.

9.1.4.2 ASTM Method

The ASTM method for measuring the conductivity for composites^(2,3,5) consists of measuring the resistance of a rectangular sample of composite using the 2-point and 4-point probe technique as described in Section 9.1.3. The expression for the conductivity is then

$$\sigma = \frac{L}{RWt} \quad (9-10)$$

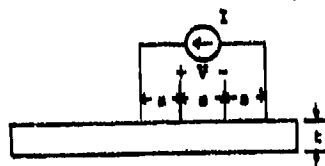


Figure 9.5. Four-point method for measurement of resistivity or conductivity⁽²⁾

where L is the sample length; R is the resistance; W, the sample width, and t, the sample thickness (see Figure 9.4). Equation (9-10) assumes a uniform current across the slab and a homogeneous slab of material. Composites are not homogeneous so the conductivity of (9-10) represents an "average" conductivity which need not correspond to the "local" conductivity in the composite. Other limitations on the method mentioned in Section 9.1.3 for resistivity apply equally well for the conductivity. The frequency range for the model is typically from D.C. to 30 - 50 MHz.

9.1.4.1.2 Slotted Stripline

In this method a slotted stripline⁽⁶⁾ using unidirectional composite materials is used for conductivity measurements from 50 MHz to a few GHz. The geometry of the stripline is shown in Figure 9.6 and consists of a center conductor of composite separated from an outer metallic conductor by a dielectric strip (Teflon). A movable probe measures the electric field (or voltage) at any point on the line. The slotted line is driven by RF at one end and terminated at the other end in an "open circuit." The line constitutes a lossy transmission line and the probe measures a lossy VSWR pattern.

From analysis^(3,6) of the line, the magnitude of the square of the electric field (or voltage) is given by

$$|E^2| = K[\cosh(2\alpha x + 2\mu) + \cos(2\beta x + 2\phi)] \quad (9-11)$$

where K is a gain factor depending on the source (volts/m); x is the distance (in meters) from the line termination; α is the real part of the propagation constant (nepers/m); ρ is the imaginary part of the propagation constant (radians/m), and μ and ϕ are termination factors for the line (zero for a pure open circuit). If the skin depth is small compared to the thickness of the composite strip and the composite fibers are parallel to the line (high conductivity case) the conductivity in mhos/m is^(3,6)

$$\sigma = \frac{\omega \epsilon_d \beta_o^2}{t^2 ([\alpha^2 - \beta^2 + \beta_o^2]^2 + 4\alpha^2 \beta^2)} \quad (9-12)$$

where ϵ_d is the permittivity of the dielectric space, the quantity β^2 is equal to $\omega^2 \mu_o \epsilon_d$ where ω is the angular frequency and μ_o is the permeability of free space ($4 \cdot 10^{-7}$ henries/m), and t is the dielectric spacer thickness.

For the case of the conductivity being sufficiently low so that the skin depth is large compared to sample thickness (as in transverse conductivity of graphite/epoxy), a uniform current over the sample may be assumed resulting in a simple transmission line model⁽⁶⁾ used for calculating the conductivity. The approximate value for the conductivity is

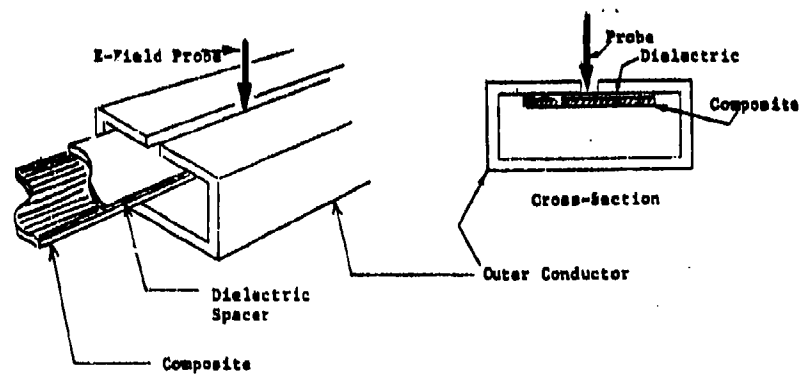


Figure 9.6. The Slotted Stripline⁽⁶⁾

$$\sigma = \frac{\omega \epsilon_d}{2\alpha^2 t_a} \quad (9-13)$$

where "a" is the sample thickness.

The justification of (9.13) is given elsewhere.⁽⁶⁾ This model for low conductivity is shown in Figure 9.7.

The advantages of the slotted stripline method include the lack of ohmic contacts and a broad band of experimental frequencies. The lower frequency limit is set by the requirement to obtain at least one cycle of standing wave data. The upper limit is determined by the line cross section as shown in Figure 9.6. One disadvantage is that the method is applicable to unidirectional samples and not to multi-ply crossed samples.

9.1.4.1.3 Conductivity From EM Shielding Measurements

It is very common and convenient to use EM shielding measurements to calculate an "effective" conductivity for composite material test panels. A summary of the necessary equations are given here with details reserved for Section 6.1 of this handbook and the references at the end of this chapter.^(2,3,9) A coaxial transmission line or waveguide structures filled with a planar composite test panel can be used to calculate the RF transmission through the panel. Details on these experimental methods are discussed in Section 9.2.2 of this handbook. The transmission coefficient across the composite panel is given by

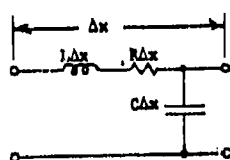
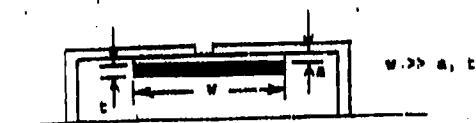
$$T = \frac{(1-\rho^2)e^{-rt}}{1-\rho^2e^{-2rt}} \quad (9-14)$$

where ρ is the reflection coefficient for the panel, r is the panel propagation constant, and t is the panel thickness. Measurements of the panel shielding effectiveness enable the reflection coefficient (ρ) and the complex permittivity $\epsilon = \epsilon_0(\epsilon' + j\epsilon'')$ to be determined. The "effective" conductivity σ_{eff} of the panel is then given by

$$\sigma_{eff} = \omega \epsilon_0 \epsilon'' \quad (9-15)$$

where ω is the angular frequency of the radiation, ϵ_0 the free space permittivity, and ϵ'' the relative loss factor.

A second method of calculating an effective conductivity utilizes the concept of transfer impedance. The theory of transfer impedance is discussed in Section 6.1 while the measurement process is summarized in Section 9.2.3.1. Further details may be found in the references.^(2,3,10) The effective conductivity σ_{eff} in terms of transfer impedance Z_s is



L = inductance/meter
 C = capacitance/meter
 R = series resistance/meter
 Δx = small length of stripline (meter)

Figure 9.7. Low Conductivity Stripline together with Transmission Line Model⁽⁶⁾

$$\sigma_{\text{eff}} = \frac{1}{tZs}$$

(9-16)

where t is the panel thickness.

9.1.4.2 Analytical Models

In this section, several composite conductivity models that have been recently developed are presented and discussed.

9.1.4.2.1 Single Ply Longitudinal Conductivity Model

In this model, the longitudinal conductance of a sample of composite material is taken to be the sum of the conductances of the individual fibers plus the conductance of the epoxy material. The sample is shown in Figure 9.8 and is modeled as a set of identical conductances in parallel.^(3,7) For a single fiber the conductance is

$$G_1 = \frac{\sigma_1 A_1}{L} \quad (9-17)$$

where σ_1 is the fiber conductivity, A_1 is the fiber cross section, and L is the fiber length. The conductance of the epoxy is

$$G_2 = \frac{\sigma_2 A_2}{L} \quad (9-18)$$

where σ_2 is the conductivity of the epoxy and A_2 is the epoxy cross section. For an N fiber composite as in Figure 9.8, the total conductance is given by

$$G = \frac{\sigma_1 A_1 N}{L} + \frac{\sigma_2 (A - N A_1)}{L} \quad (9-19)$$

where the total epoxy cross section A_2 is written as $(A - N A_1)$; A is the total composite cross section and N is the number of fibers.

The composite conductivity σ_L in the longitudinal direction is now defined as^(3,7)

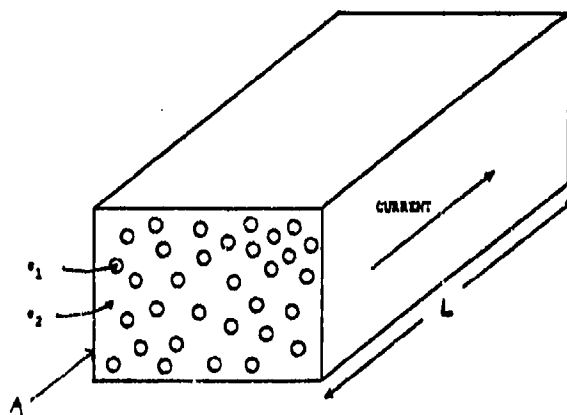


Figure 9.6 Longitudinal Conductivity Model^(3,7)

$$G = \frac{\sigma_L A}{L} \quad (9-20)$$

where A and L are the sample dimensions and G is the total conductance given in (9.19). The conductivity σ_L becomes

$$\sigma_L = \frac{\sigma_1 A_1 N_1}{A} + \frac{\sigma_2 (A - N_1 A_1)}{A} \quad (9-21)$$

or more conveniently

$$\sigma_L = \sigma_1 f + \sigma_2 (1-f) \quad (9-22)$$

where $f = \frac{N_1 A_1}{L}$ is the volume fraction of fiber in the composite. If the composite fibers are orders of magnitude more conducting than the epoxy, σ_L can be well approximated as

$$\sigma_L \approx \sigma_1 f \quad (9-23)$$

This model works well for graphite/epoxy or Kevlar/epoxy. A more general model is required for boron/epoxy.⁽⁸⁾ For this composite the fibers consist of a sheath of boron surrounding a conducting inner core. The longitudinal conductance G is then the sum of the conductances of all fiber sheaths, fiber cores and epoxy. For N fibers the conductance is⁽⁸⁾

$$G = \frac{\sigma_e A_e}{L} + \frac{\sigma_b N A_b}{L} + \frac{\sigma_c N A_c}{L} \quad (9-24)$$

where σ_e , σ_b , σ_c are the conductivities of epoxy, sheath and core respectively; A_e , A_b , A_c are the cross sections of epoxy, sheath and core respectively; and L is the sample length. The model is shown in Figure 9.9.

The effective longitudinal conductance is

$$G = \frac{\sigma_L A}{L} \quad (9-25)$$

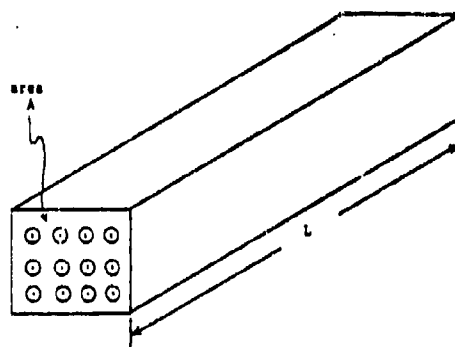
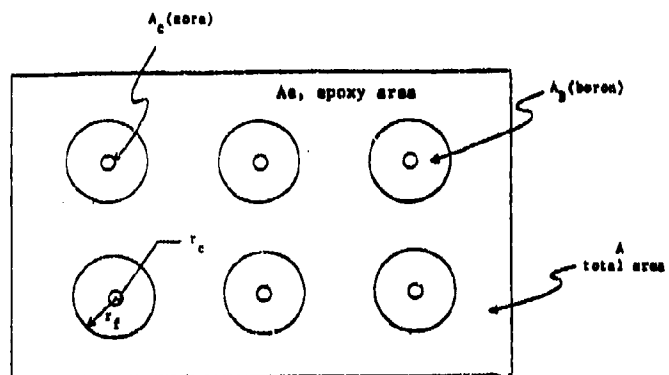


Figure 9.9. Longitudinal Conductivity Model for Boron/epoxy (8)

and σ_L becomes(8)

$$\sigma_L = \sigma_e(1-f) + \sigma_b \frac{\eta-1}{\eta} f + \sigma_c \frac{f}{\eta} \quad (9.26a)$$

where

$$\eta = \frac{A_b}{A_c} \quad (9.26b)$$

and A_b is the cross section of a fiber in boron/epoxy composite. This ratio depends on the core size in the boron/epoxy fiber. Since the fiber core is the most conductive part of the boron/epoxy fiber,(8) the longitudinal conductivity σ_L can be approximated by

$$\sigma_L \approx \sigma_c \frac{f}{\eta} \quad (9.27)$$

The core size of a boron/epoxy fiber (as measured by η) is a critical parameter in this boron/epoxy longitudinal conductivity model. Because the core size depends on the extent of reaction of boron with tungsten during the fiber manufacturing process, this parameter may be difficult to determine for general samples of boron/epoxy.

9.1.4.2.2 Single Ply Transverse Conductivity Model

The transverse conductivity model to be discussed applies only to graphite/epoxy composite. Both Kevlar/epoxy and boron/epoxy have negligible transverse conductivity, but this conductivity is significant for graphite/epoxy because of the large number of fibers that touch.

In this model, called the random fiber model,(3,7) the sample is divided into a set of parallel planes. The fibers are then distributed randomly in each plane in accordance with the fiber volume fraction f . The model is shown in Figure 9.10 for two planes. At any lateral point, the measured conductivity depends on whether the probe contacts are fiber-fiber, fiber-epoxy, epoxy-fiber, or epoxy-epoxy. The transverse conductivity can be shown(3) to be

$$\sigma_T = \sigma_1 f^2 + 4 \frac{\sigma_1 \sigma_2}{\sigma_1 + \sigma_2} f(1-f) + \sigma_2 (1-f)^2 \quad (9.28)$$

where σ_1 is the fiber conductivity, σ_2 is the epoxy conductivity, and f , the volume fraction of fibers. A basic assumption made is that the electric field is uniform through both layers. For graphite/epoxy where $\sigma_1 > \sigma_2$, σ_T can be written as

$$\sigma_T \approx \sigma_1 f^2 + 4\sigma_2 f(1-f) + \sigma_2(1-f) \quad (9.29)$$

If f does not approach zero, the expression for σ_T simplifies to

$$\sigma_T \approx \sigma_1 f^2 \quad (9.30)$$

For N layers in the model, T becomes

$$\sigma_T \approx \sigma_1 f^N \quad (9.31)$$

This value for the conductivity is strongly dependent on the number of planes used in the random fiber model. Results to date with this model are fair.^(3,7)

9.1.4.2.3 Multi-Ply Conductivity Model

The simplest model for multi-ply structures treats the individual plies as conductances in parallel.^(3,8) For the i_{th} ply, the conductance is of the form^(3,8)

$$G_i = \frac{\sigma_i W t}{L} \quad (9.32)$$

where W is the sample width; L , the sample length; t , the ply thickness (assumed identical for all plies) and σ_i , the i_{th} ply conductivity. The total conductance of the sample (composed of N plies) is

$$G = \sum_{i=1}^N \frac{\sigma_i W t}{L} \quad (9.33)$$

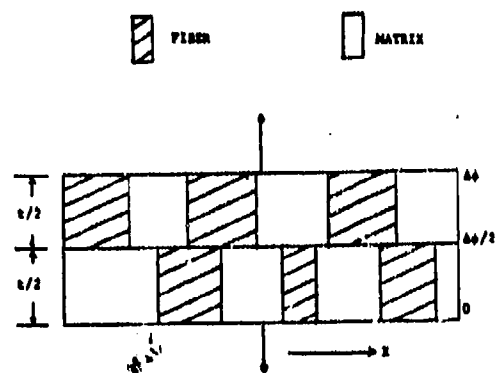
An effective conductivity, σ_e , of the multi-ply sample is defined^(3,8) as

$$G = \frac{\sigma_e A}{L} \quad (9.34)$$

where A is the total sample cross section and L , the sample length. The sample cross section is given by

$$A = N W t \quad (9.35)$$

where N is the number of plies; W , the sample width; and t , the common ply thickness. The effective conductivity is then



$\Delta\phi$ = voltage drop across planes
 t = thickness of layer consisting
of two planes

Figure 9.10. Random Fiber Model^(2,7)

$$\sigma_0 = \frac{1}{N} \sum_{i=1}^N \sigma_i$$

(9-36)

The basic assumptions in the model are uniform ply thickness, uniform excitation of the sample and electrical independence of the plies.^(3,8) The results of the model are mixed⁽⁸⁾ with indications that the electrically independent ply assumption is somewhat poor even under low frequency excitations.⁽⁸⁾

9.2 EM Shielding Effectiveness Measurement Techniques

In this section, the various methods of measuring the electromagnetic shielding of composite materials are discussed in detail. The first three parts of this section treat shielding as measured by coupled loops or probes, plane wave transmission and reflection, and surface impedance parameters. The advantages and disadvantages of each method are reviewed. Shielding measurements when joints are present as discussed as well as the special situations of composite structures under high current and high voltage conditions.

9.2.1 Coupling Between Loops and Probes

In this section the coupling between two loop antennas, two dipole antennas, and two monopole antennas is examined as a measure of shielding effectiveness for an infinite homogeneous (or multi-ply composite) planar shield and for one or more parts of the test system in an enclosure.

9.2.1.1 Infinite, Planar Shield

The shielding effectiveness is defined as the insertion loss caused by the introduction of an infinite, planar shield of composite material between a source and detector antenna system. The antennas are coaxial with a line perpendicular to the shield. The coupled antenna systems discussed are two loops, two dipoles and two monopoles.

9.2.1.1.1 Two Loop Method

The two loop method^(2,3,10) is illustrated in Figure 9.11a. The source loop is driven by a current I , and a voltage E_2 is measured at the terminals of the detector loop. The source loop has radius a_1 and is a distance r_1 away from the shield. The detector loop has radius a_2 and is a distance r_2 away from the shield. A voltage E_{2a} is measured first with air between the antennas and a voltage E_{2m} is measured with the composite shield between the antennas. The magnetic shielding effectiveness is given by ⁽²⁾

$$S_m = 20 \log_{10} \left| \frac{E_{2a}}{E_{2m}} \right| \quad (9-37)$$

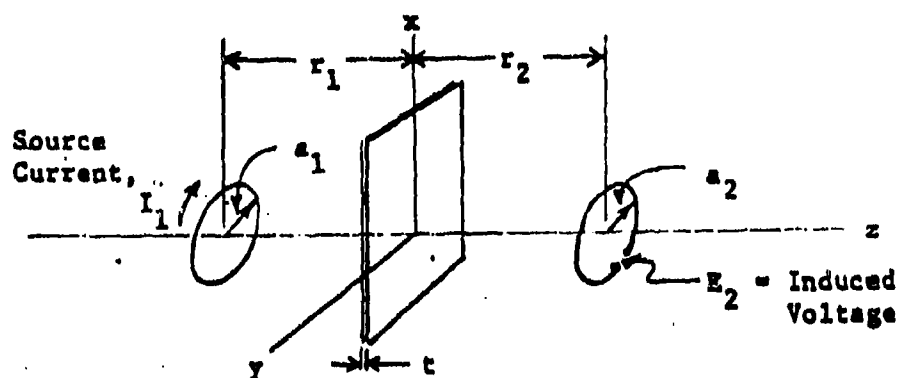


Figure 9.11a. Two Loop Method⁽²⁾

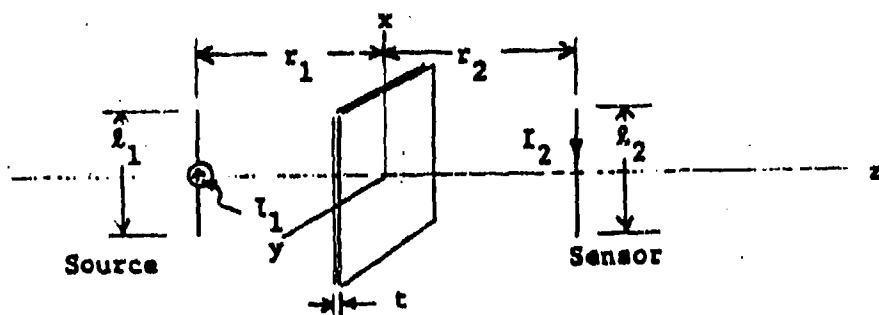


Figure 9.11b. Two Dipole Method⁽²⁾

The voltages E_{2m} and E_{2a} are complicated functions of a_1 , a_2 , r_1 , r_2 and the shield thickness t .^(2,10)

9.2.1.1.2 Two Dipole Method

The two dipole method^(2,3) is illustrated in Figure 9.11b. The dipoles are of length l_1 , l_2 and are located at distances r_1 , r_2 from the shield. The source dipole is driven by a current I_1 and a current I_2 is measured in the detector dipole. The shielding effectiveness is then given by⁽²⁾

$$S_E = 20 \log_{10} \left| \frac{I_{2a}}{I_{2m}} \right| \quad (9-38)$$

where I_{2a} is the dipole detector current without the shield and I_{2m} , the current with composite shield present. The currents I_{2a} and I_{2m} are complicated functions of l_1 , l_2 , r_1 , r_2 and the shielded thickness t .

9.2.1.1.3 Two Monopole Method

This method⁽²⁾ is similar to the two dipole method illustrated in Figure 9.11b except the two dipoles are replaced by two monopoles over a ground plane. If the monopoles used each have a length $\frac{\lambda}{4}$ then the monopole coupling is the same as coupling between dipoles of length $\frac{\lambda}{2}$, where λ is the radiation wavelength.⁽²⁾

9.2.1.1.4 Limitations

One basic limitation of these measurement methods is the extent to which data obtained from a finite composite shield can replicate the data obtained using an infinite shield to which these methods strictly apply. Some leakage around the edges will always occur and the amount of leakage is frequency dependent. This limitation is critical for good shields where leakage may be comparable to the penetrating field.^(2,3)

A second limitation is that the shielding effectiveness pertains only to the antenna pair and composite shield geometry. It cannot easily be related to other methods or other geometries.^(2,3,10)

9.2.1.2 Enclosed Shield

When actually making a measurement of shielding effectiveness, it is usually more practical to enclose one or more parts of the measurement system. Figure 9.12a shows the use of a metal enclosure around the source loop of a two loop system. The purpose of this enclosure is to eliminate the edge leakage which occurs in the infinite plane methods when using a finite plane, as discussed in Section 9.2.1. This permits use of a finite composite shield. The disadvantage of this approach is that the shielding

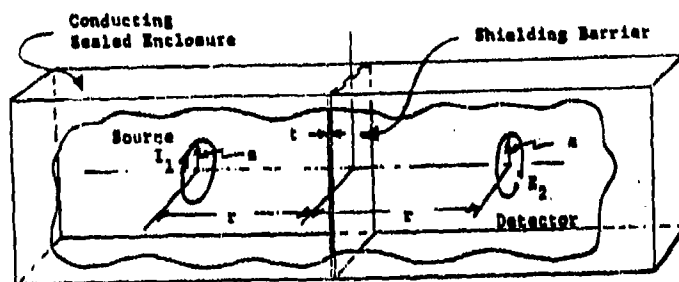


Figure 9.12a. Partially Enclosed System For Measuring Shielding(2)

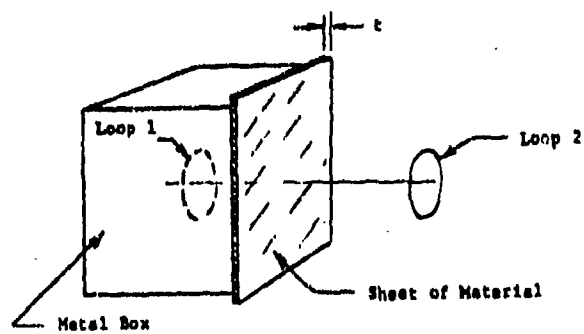


Figure 9.12b. Fully Enclosed System For Measuring Shielding(2)

effectiveness now depends on the box geometry since the box charges the field of the source because of reflections and resonances from the enclosure walls. These problems could be reduced if the box were an anechoic chamber with the composite shielding barrier being one side of the chamber and the other sides covered with absorbing material.

A second method involves enclosing the entire measurement apparatus (including composite shielding barrier) in a large anechoic chamber. This method is illustrated in Figure 9.12b for a two loop system. It allows the use of a finite piece of material and assures minimum interference from reflections and resonances. However the shielding effectiveness still depends on the chamber geometry to some extent and may be hard to relate to other methods of measurement. For certain test frequencies the size of the chamber required would be too big to be practical.

9.2.2 Plane Wave Transmission/Reflection Methods

A very simple definition^(2,3,10) of shielding effectiveness arises from the case of a uniform plane wave incident on an infinite homogeneous, or multi-ply composite. This situation is shown in Figure 9.13. For shields of nonzero thickness, the overall effect is composed of reflections from the incident wave striking the shield surface and the internal material boundaries, plus transmission loss through the shield. Several experimental methods for measuring the shielding effectiveness for incident plane waves on shields will be discussed.

9.2.2.1 Sample Experimental Methods

In this section several different methods for mounting and illuminating the test sample with a uniform EM plane wave are described.

9.2.2.1.1 Coaxial System

The coaxial system^(2,3) is illustrated in Figure 9.14. This system gives rise to a radial electric field and propagates a transverse electric and magnetic (TEM) wave. The radial nature of the electric field is a significant departure from the required linearly polarized uniform plane wave. Unambiguous results are obtained only for homogeneous materials or multi-ply composites. This system is not useful for unidirectional composites or other highly anisotropic materials.

9.2.2.1.2 Rectangular Waveguide System

This system is shown in Figure 9.15. These guiding structures can give rise to a transverse electric (TE) or transverse magnetic (TM) propagating wave in the fundamental mode,^(2,3) and are useful because of the unidirectional nature of the electric or magnetic fields produced. This transverse field can be aligned with the composite fibers or at least aligned with a principal symmetry axis of an anisotropic material. The other field, then, is then not aligned with the axis. The waveguide fields can be resolved into two obliquely incident plane waves. The incident angles of these waves depend on the ratio of operating frequency to cutoff frequency.⁽²⁾ Thus the incident wave from the waveguide cannot be considered a uniform plane wave with a different wave impedance.

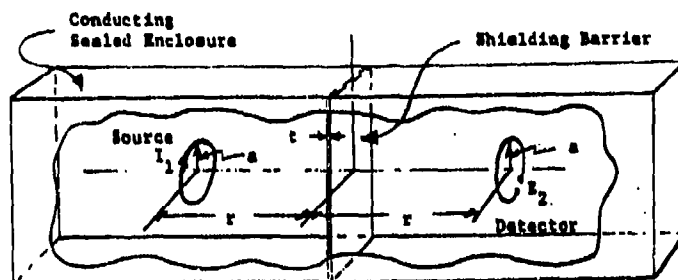


Figure 9.12a. Partially Enclosed System For Measuring Shielding⁽²⁾

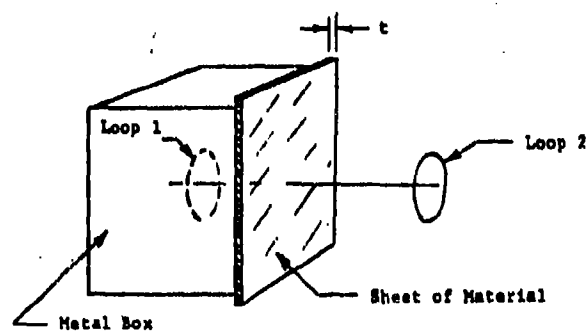


Figure 9.12b. Fully Enclosed System For Measuring Shielding⁽²⁾

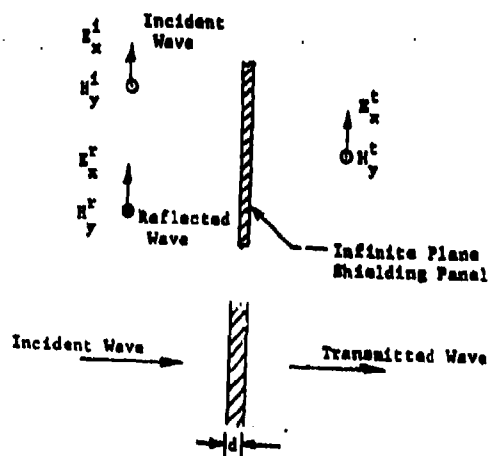


Figure 9.13. Uniform Plane Wave Shielding Concepts⁽²⁾

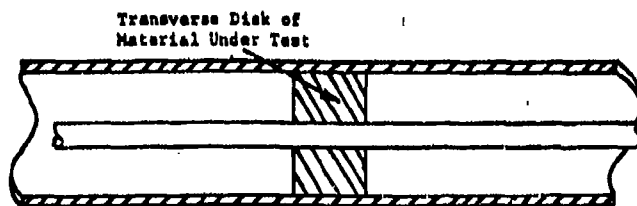


Figure 9.14. Coaxial System⁽³⁾

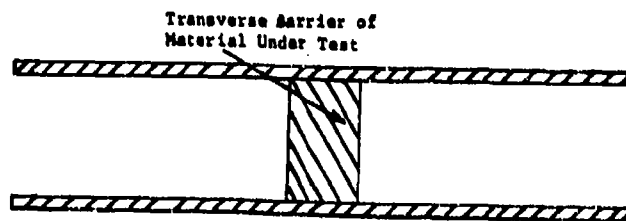


Figure 9.15. Rectangular Waveguide System⁽³⁾

9.2.2.1.3 Far Field Anechoic Chamber System

A typical chamber setup is shown in Figure 9.16. The use of a chamber avoids many of the problems of sample preparation inherent in the coaxial and waveguide systems. Chamber measurements should very closely approximate the results of uniform plane wave illumination for a proper choice of test antennas.⁽²⁾ The main limitation of this system is the lower frequency limit imposed by the chamber size (typically 500 MHz).⁽²⁾

9.2.2.1.4 TEM Cell

This method avoids the difficulties of coaxial or waveguide systems in producing linearly polarized uniform plane electric and magnetic fields over the composite material barrier.⁽²⁾ The TEM cell is illustrated in Figure 9.17 and resembles a distorted coaxial transmission line⁽²⁾ having an inner conductor and an outer conductor with extended edges. The design allows the existence of a TEM wave over a large section of the test barrier. The orientation of the electric and magnetic fields with respect to principal axes of symmetry in anisotropic materials can then be controlled.⁽²⁾ Proper design of the extended edges minimizes the fringing effects.

There are two main limitations on TEM cells.⁽²⁾ The probability of higher modes propagating on the line increases if too wide a line is used to reduce fringing and improve the TEM wave illumination. This limits the frequency of operation of the device. Also, a TEM cell designed to minimize fringing and optimize TEM wave propagation may have a characteristic impedance considerably different from the impedance of the feed lines for the cell (typically 50 ohm lines). This results in a mismatch in the TEM cell test system.⁽²⁾ This problem places a further restriction on the operating frequency of the cell. The mismatch can be controlled, however, by use of proper interface devices between feed lines and cell.

9.2.2.1.5 Near Field Method

The near field⁽²⁾ antenna measurement test setup is shown in Figure 9.18. A source antenna illuminates a test barrier of composite material and an antenna in the near field of the source makes field measurements in a plane parallel to the barrier. Field measurements are made both with and without the barriers. These field values are then Fast Fourier Transformed to far field values. The theory is described in Section 6.1 of this handbook and in the references.^(2,11) The plane wave shielding effectiveness (S_e) is then given by⁽²⁾

$$S_e = -20 \log_{10} T \quad (9-39)$$

where

T is the transmission coefficient

$$T = \frac{E}{E_0} \quad (9-40)$$

E is the field at the barrier and E_0 is the field in the absence of the barrier.

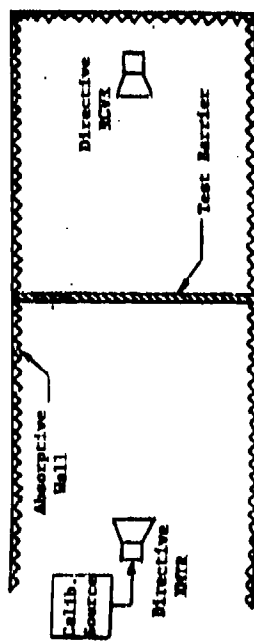


Figure 9.16. Anechoic Chamber System (2)

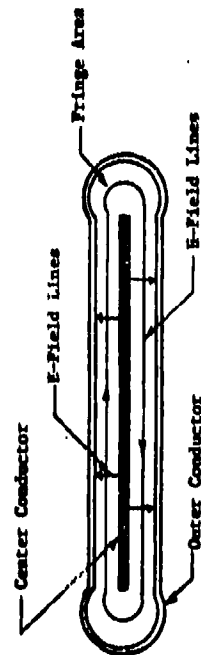
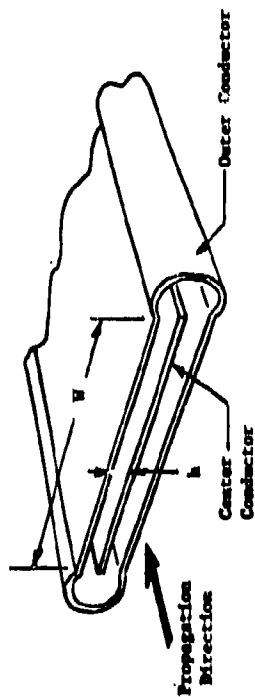


Figure 9.17. TEM Cell System (2)

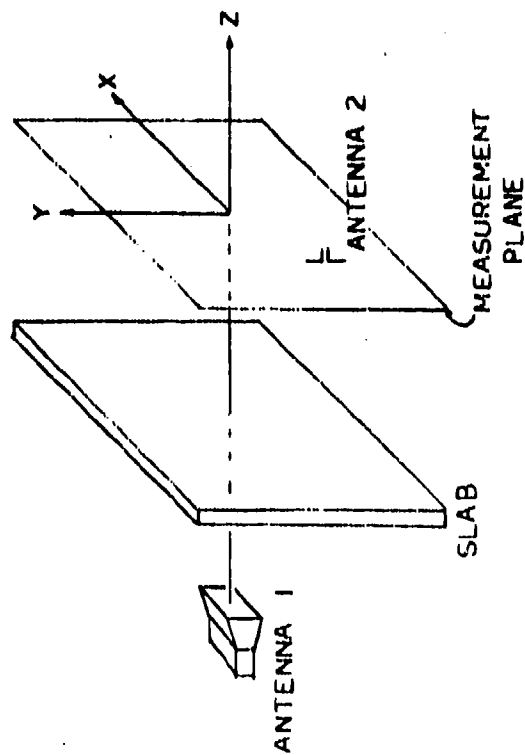


Figure 9.18. Near Field Antenna Measurement System (2)

The basic limitation to this method is a limitation on the frequency range where large enough barriers are available to minimize fringing. Also the theory applies strictly to homogeneous, isotropic and possibly to multi-ply composites.

9.2.2.2 Instrumentation Configurations

In this section, two common instrumentation configurations used for measuring plane wave shielding effectiveness using transmission/reflection methods are discussed along with limitations in the configurations.

9.2.2.2.1 Substitution

This configuration⁽²⁾ is shown schematically in Figure 9.19a. Any of the methods (coaxial line, waveguide, TEM cell) discussed in Section 9.2.2.1 for mounting and illuminating the composite sample may be used in this configuration provided the necessary isolation techniques are available. The shielding effectiveness is then the difference in attenuator readings when the sample and lossless line are excited separately.⁽²⁾

9.2.2.2.2 Bridge

In this configuration⁽²⁾ a suitably isolated sample mounted and illuminated by any method (coaxial line, waveguide TEM cell) in Section 9.2.2.1 is connected in parallel with an attenuator and phase shifter with suitable isolation. The configuration is shown in Figure 9.19b. The proper amplitude and phase adjustment to produce a null in the detector constitutes the shielding measurement. In this approach both amplitude and phase shielding information is obtained.

9.2.2.2.3 Limitations

Great care is required in preparing and mounting the test material in the material holder to properly interface it to the rest of the test configuration. An idealized interface is shown by a network in Figure 9.20a and is represented as three cascaded transmission lines with the sample represented by a transmission line of modified impedance and propagation constants. Poor interfacing and mounting of the sample will introduce coupling between the sample input/output ports and between gaps in the material sample and holder walls. This situation is illustrated in Figure 9.20b by a network. Elements Y_5 and Y_6 represent leakage through sample gaps.

9.2.3 Surface Impedance Parameters

Surface impedance parameters offer a very useful way to characterize the shielding effectiveness of shield that are thin with respect to their radii of curvature, and for which the wavelength of the field in the shield is much smaller than the wavelength of the field external to the shield. Such a shield is said to be locally planar.^(3,10)

For shields involving closed surfaces, the surface transfer impedance is defined as^(2,3,9,10)

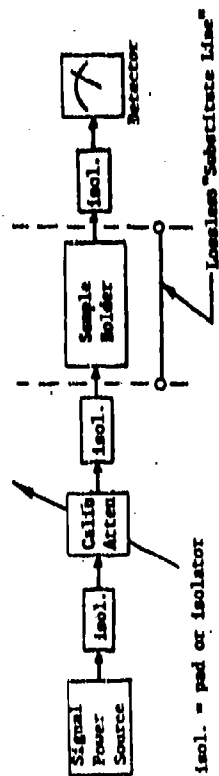


Figure 9.19a. Substitution Configuration (2)

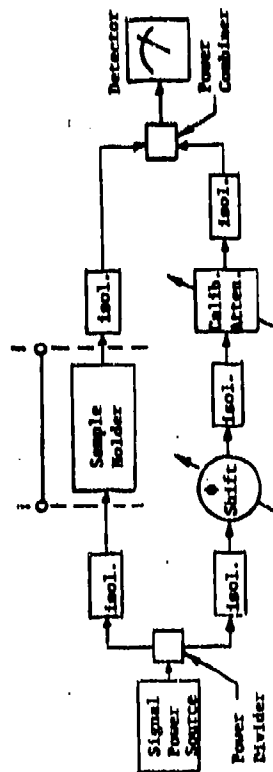


Figure 9.19b. Bridge Configuration (2)

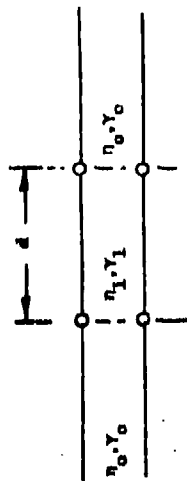


Figure 9.20a. Equivalent Circuit of Ideal Partition (2)

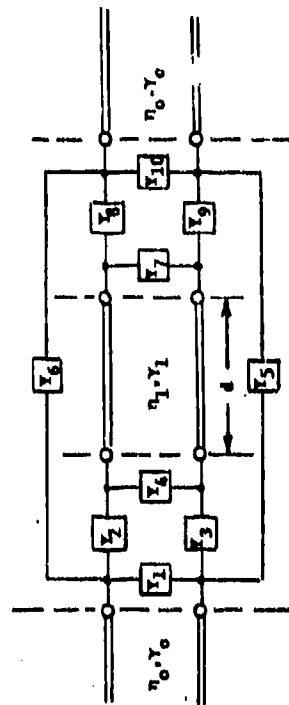


Figure 9.20b. Equivalent Circuit of Non Ideal Partition (2)

$$Z_{st} = \frac{E_t}{J_s} \quad (9-41)$$

where E_t is the inner shield surface tangential electric field, and J_s is the outer shield surface current density. The theoretical treatment of transfer impedance and its relation to EM shielding may be found in Section 6.1 of this report and the references. (2,3,9,10)

For locally planar shields the surface transfer impedance has the form (2,3,10)

$$Z_{st} = \eta \operatorname{csch}(rd) \quad (9-42)$$

where

$$\eta = \left[\frac{j\omega\mu}{(\sigma + j\omega\epsilon)} \right]^{1/2} \quad (9-43)$$

$$r = [j\omega\mu (\sigma + j\omega\epsilon)]^{1/2} \quad (9-44)$$

and d is the shield thickness.

The transfer impedance in (9.42) can be shown (2,3,10) to be equal to the "two-port" surface impedance parameters (2) used to characterize the shielding of an infinite planar plate, thus justifying the term "locally planar" to describe the shield.

9.2.3.1 Measurement Techniques

This section will treat two methods for measuring the surface transfer impedance: triaxial and quadraxial cable techniques.

9.2.3.1.1 Triaxial Method

This method is a modification of a technique used to measure the shielding effectiveness of shielded cables. (2,12) The composite under test is first fabricated into a cylinder which takes the place of the cable shield. This shield and an enclosed sensing wire conductor become the inner conductor of a coaxial transmission line driven by RF at one end and terminated in an "open" circuit at the other end. The situation is depicted schematically in Figure 9.21a. The composite shield is driven with a current I , and a voltage V_{oc} is measured at the termination. The surface transfer impedance is then (2)

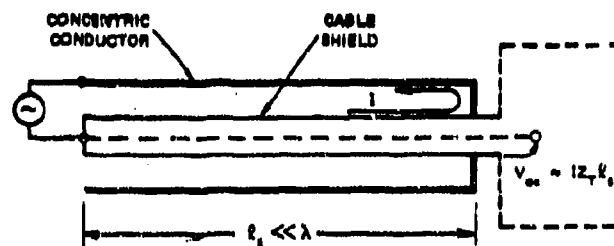


Figure 9.21a. Surface Transfer Impedance Measurement With Open Circuit Termination(2)

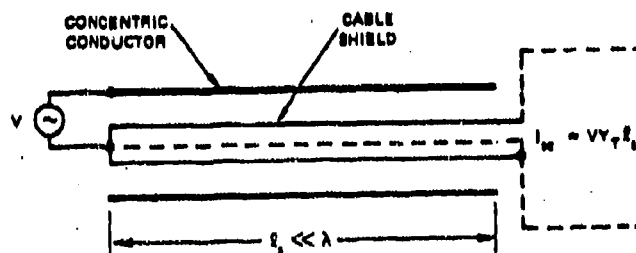


Figure 9.21b. Surface Transfer Admittance Measurement With Short Circuit Termination(2)

$$Z_{st} = \frac{V_{oc}}{I_{ls}}$$

(9-45)

where l_s is the length of the coaxial line and $l_s \ll \lambda$, where λ is the radiation wavelength. This same device can be used to measure the surface transfer admittance. The coaxial line is now driven with a voltage source and terminated in a short circuit (Figure 9.21b). The short circuit current I_{sc} is measured and the surface transfer admittance Y_T is (2)

$$Y_T = \frac{I_{sc}}{V_{ls}}$$

(9-46)

One limitation on this method is the fact that the coaxial line must satisfy $l_s \ll \lambda$ in order that the open circuit termination can be used and line resonances avoided. This places a constraint on the frequency range of operation (2). A further limitation involves the radii on the outer two cylinders. They must be chosen so as to avoid cavity resonance which places a further restriction on the frequency of operation. (2) Detectors used in the measurement should be well isolated from the line itself. It is essential to have proper sample preparation and good electrical contact between sample and measuring apparatus.

9.2.3.1.2 Quadraxial Method

This method is a modification of the triaxial structure to minimize resonances and external perturbations in the measured data. (2,12)

A sensing conductor (wire) is placed inside a cylinder made of the composite to be tested and the coaxial line terminated in its characteristic impedance. This coaxial structure then becomes the inner conductor of a coaxial line with an outer conducting cylinder. This outer coaxial line is also terminated in its characteristic impedance. This is similar to Figures 9.21a and 9.21b except that the terminal contains a finite nonzero impedance. This triaxial structure is shown in Figure (9.22a). The signal line serves as a reference line but the reference is different at points A and B. The quadraxial structure in Figure 9.22b uses the signal line as the source line while a balance line goes from the composite inner cylinder to the outer cylinder and serves both as a reference and as a method of maintaining uniform current on the composite cylinder. (2,12) Measurements of transfer impedance or admittance are then carried out as in the triaxial method described in 9.3.2.1.1.

One realization of this quadraxial method is the Boeing quadrax test configuration (2,12) pictured schematically in Figure 9.23.

9.2.4 Joint Measurement Techniques

A very important determinant of the overall shielding effectiveness of aircraft structures fabricated from composite and/or metallic materials is the existence of joints in the structure. Skin currents

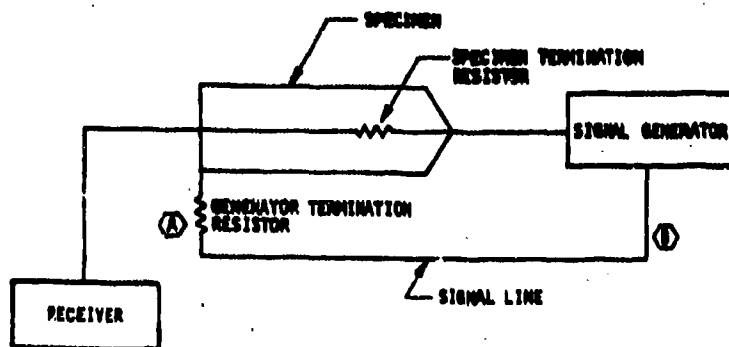


Figure 9.22a. Triaxial Schematic (2)

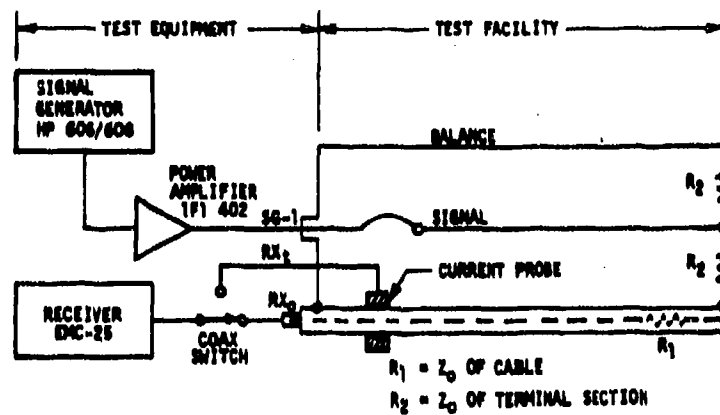


Figure 9.22b. Quadaxial Schematic (2)

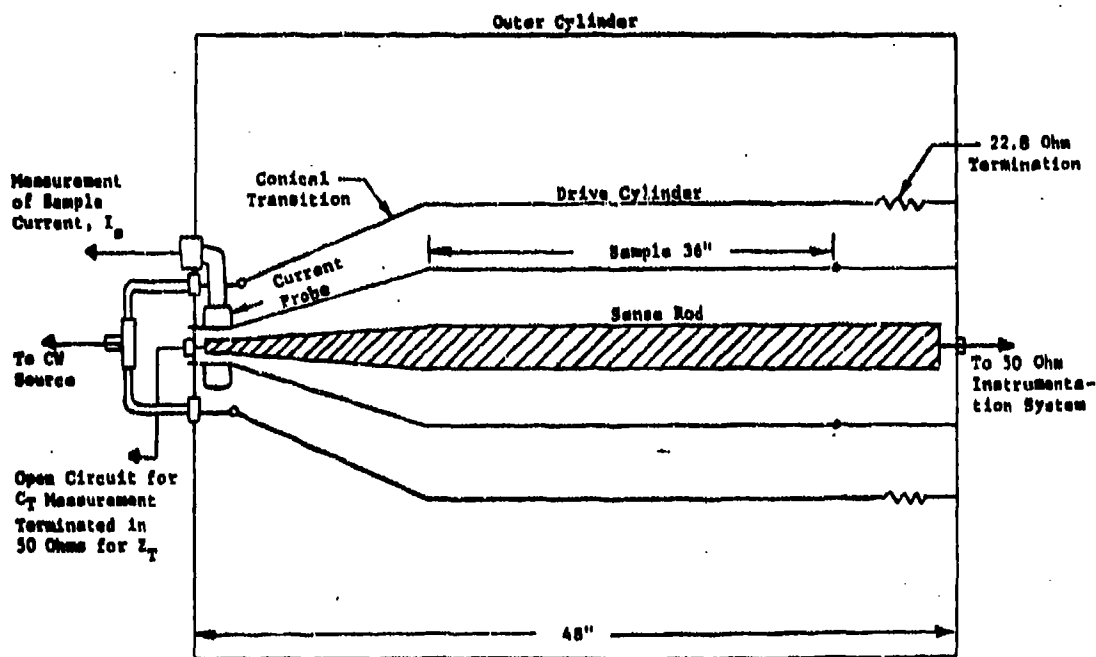


Figure 9.23. Schematic of Quadaxial Test Fixture (2,12)

flowing on the surface of the material create electric fields that are coupled onto aircraft avionic systems through the joint. The appropriate parameter for measuring this joint coupling is the joint admittance per unit length of joint (Y_J). The theory of joint admittance and its contribution to composite shielding effectiveness is described in Section 6.1 of this handbook.

One set of measurements for Y_J uses basically the same measurement techniques that are used in measuring the surface transfer admittance of composite panels described in 9.2.3.1. The Boeing Quadrax Test Configuration⁽¹²⁾ (see Figure 9.23) has been used to measure joint admittances and the procedure is summarized in Figure 9.24a. The cylinder consists of two identical materials jointed together and is assumed to have a surface transfer impedance Z_T . The circumferential joint has a joint admittance per unit length, Y_J . The cylinder is driven by a known current I_s (current density is J_s) and the open circuited voltage V_{oc} measured. Then V_{oc} is ⁽⁹⁾

$$V_{oc} = L I_s Z_T + \frac{I_s}{Y_J 2\pi a} \quad (9-47)$$

where L is the cylinder length and a , the cylinder radius. The joint admittance is then

$$Y_J = \frac{1}{2\pi a} \frac{I_s}{V_{oc} - Z_T L I_s} \quad (9-48)$$

The surface transfer impedance Z_T is assumed known from measurements on a cylinder with the same material but no joint.

This procedure can be generalized to joints between two dissimilar materials (different composites, different metals or metal and composite) and is shown in Figure 9.24b. The dissimilar materials have surface transfer impedances Z_{T1} and Z_{T2} and the joint has an admittance Y_J . The open-circuited voltage at the line termination is

$$V_{oc} = L_1 I_s Z_{T1} + L_2 I_s Z_{T2} + \frac{I_s}{Y_J 2\pi a} \quad (9-49)$$

where L_1 and L_2 are the lengths of the two dissimilar cylinder sections and a is the cylinder radius. The joint admittance is then

$$Y_J = \frac{1}{2\pi a} \left[\frac{I_s}{V_{oc} - Z_{T1} L_1 I_s - Z_{T2} L_2 I_s} \right] \quad (9-50)$$

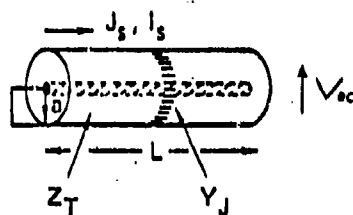


Figure 9.24a. Joint Admittance (identical materials joined) (9)

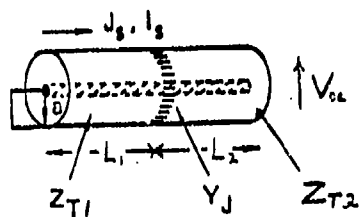


Figure 9.24b. Joint Admittance (different materials joined)

9.2.5 High Current Injection

In this section the effects of high current injection onto composite structures are discussed. The high current is assumed to result from a lightning strike or near miss. Methods of simulating lightning strokes on aircraft are treated and the various effects of lightning on aircraft are reviewed.

9.2.5.1 Standard Current Waveforms

In order to ascertain the effects of high current on composite structures, a standard waveform for the test current must be chosen. Since almost all high current phenomena involving composite aircraft are due to lightning, the standard high current waveform is chosen to be as close as possible to the current waveform of natural lightning. Numerous experimental studies of natural lightning flashes have assigned nominal values to a number of different lightning parameters such as peak current, rise time, amplitude and charge transfer. A general list of these parameter values is given in Table 2.1.1 of this report.

The effects on composite aircraft due to high currents are conveniently divided into two groups.⁽¹⁴⁾

Group 1 includes effects such as burning, eroding, blasting, structural deformation, high pressure shock wave and magnetic forces. These effects are associated with the high currents and charge transfer caused by a direct lightning strike.⁽¹⁴⁾

Group 2 effects arise from the electromagnetic field produced by the lightning and include induced voltages on interior avionic systems and sparking across bonded structures. These effects are associated with high peak currents and large rates of change of current caused by a direct lightning strike or a near miss. A list of important lightning effects together with the lightning parameters that significantly influence these effects is given in Table 9.1.

The reason for dividing the lightning effects and parameters into two groups is because it is experimentally difficult to adequately simulate all significant lightning parameters in one standard current waveform.⁽¹⁴⁾ Different lightning parameters, and hence different lightning effects, are usually sensitive to different parts of the lightning waveform. Consequently, when investigating various lightning effects only portions of the total current waveform need to be simulated.

To meet these requirements, a standard lightning current waveform has been proposed.^(13,15) The waveform for investigating Group 1 lightning effects is shown in Figure 9.25 and consists of four basic components. The values of the parameters that describe the components are given in Table 9.2.

The waveform for investigating Group 2 lightning effects is the same as that for Group 1 except that component D is modified. This modification is given in Figure 9.26 and the lightning parameters describing the component are listed in Table 9.3.

Table 9-1 Lightning Parameters and Lightning Effects⁽¹⁴⁾

Basic Effect	Important Parameter
<u>Group 1</u> metal skin puncture hot spot formation mechanical damage magnetic forces damage to composite structures fuel ignition damage to lightning arresters sparking	coulombs I^2 $\int I^2 dt$
<u>Group 2</u> induced voltages voltage flashover sparking fuel ignition	n I dI/dt d^2I/dt^2

n is the number of restrikes in a flash

I is the peak value of the current

i is the instantaneous value of the current

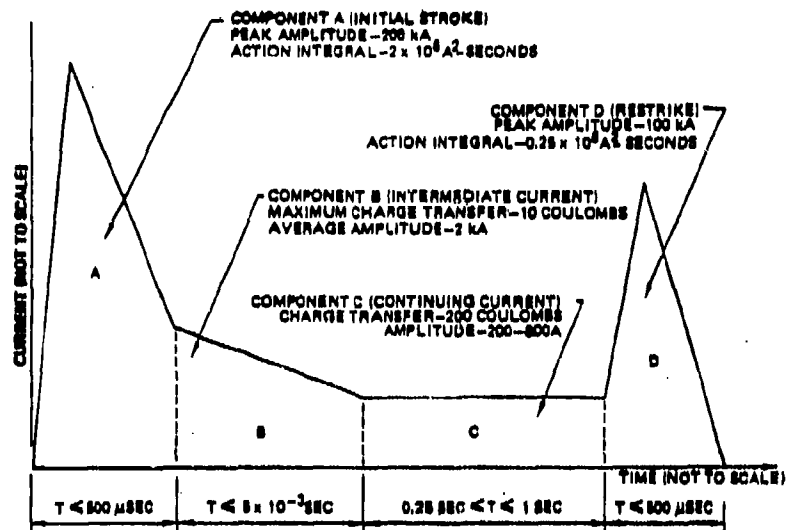


Figure 9.25 Group 1 Standard Lightning Waveform (13-15)

Table 9-2 Group 1 Lightning Waveform Parameters (14,15)

Component	Parameter	Value	Tolerance
high current component A	peak current	200kA	$\pm 10\%$
	action integral	$2 \times 10^6 \text{ A}^2\text{s}$	$\pm 10\%$
	pulse length	$< 500\mu\text{s}$	
	rise time	$< 25\mu\text{s}$	
intermediate current component B	average amplitude	2kA	$\pm 10\%$
	charge transfer	10C	$\pm 10\%$
continuing current component C	amplitude	200-800A	
	charge transfer	200C	$\pm 20\%$
restrike (group 1 effects) component D	peak amplitude	100kA	$\pm 10\%$
	action integral	$0.25 \times 10^6 \text{ A}^2\text{s}$	$\pm 10\%$
	pulse length	$< 500\mu\text{s}$	

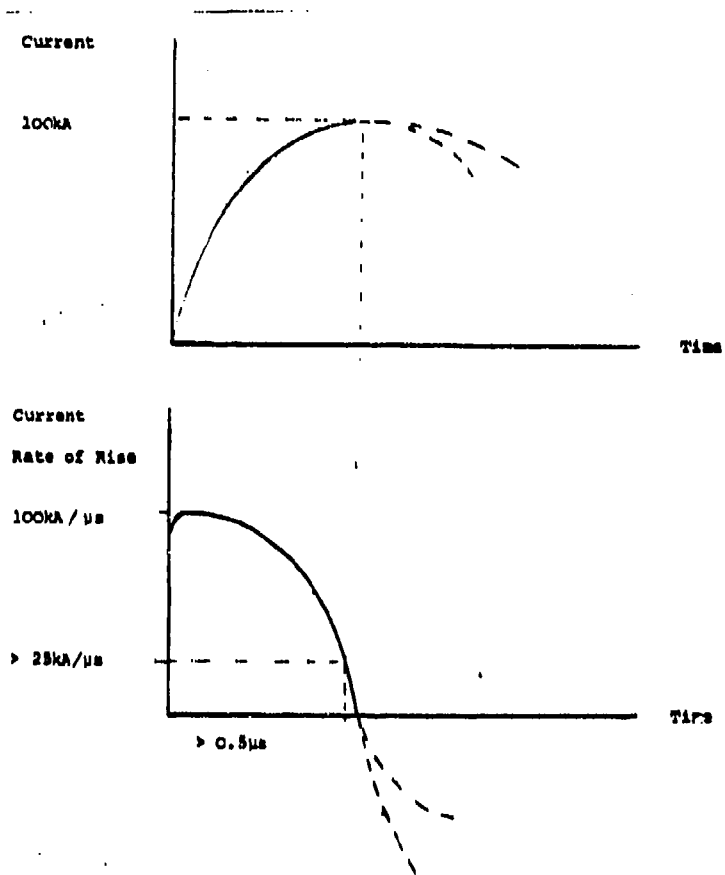


Figure 9.26 Group 2 Component D Standard Lightning Waveform⁽¹⁴⁾

Table 9-3 Group 2 Component D Parameters⁽¹⁴⁾

Component	Parameter	Value	Tolerance
restrike (group 2 effects)* component D	peak current	100kA	± 10%
	peak initial rate of rise of current	100kA/μs	± 10%
	time for which di/dt should exceed 25kA/μs	0.5μs	± 10%

In determining the different effects of lightning on a test specimen, the components of the waveform can be used separately or in combination with other components as needed.

9.2.5.2 High Current Waveform Generation

The basic circuit used for producing the various test current waveforms is illustrated in Figure 9.27. The energy used to produce the lightning waveforms is initially stored in the circuit capacitor which represents a large capacitor bank. The waveform is generated⁽¹⁴⁾ by first closing the starting switch to discharge the capacitor bank into an inductive, underdamped circuit. When the current I , is maximum, the switch in the clamp or short circuit is closed. Because of the low impedance of the clamp, the inductor will discharge through the clamp. The advantage of this system is that the current is effectively coming from a constant current source without limitations on the voltage. The sample to be tested is placed in the AB or CD position depending on which current components are to be simulated. A set of circuit parameters necessary to produce the standard current waveform is given in Table 9.4. More recent developments in generating lightning waveforms have been reported by Hanson.

9.2.5.3 High Current Methods and Techniques

Test techniques involving the use of high currents on test specimens will now be described.

9.2.5.3.1 Stationary Arc Testing⁽¹⁴⁻¹⁶⁾

A very common test technique consists of a stationary electrode suspended a measured distance above a test specimen. An electric arc then discharges into the test specimen. The arc current, waveform and voltage are recorded. In addition, each discharge is photographed to determine the arc root location and quality of the arc.

Careful placement of the current return conductor is required since the magnetic field produced by the conductor can interact with the arc significantly.

9.2.5.3.2 Swept Stroke Testing

The basic items needed to measure swept lightning strokes are a test specimen, a discharge electrode and apparatus to move the discharge electrode at the aircraft relative air velocity. Several detailed methods for measuring swept lightning strokes experimentally have been described in the literature.⁽¹⁴⁻¹⁶⁾

A primary use of swept stroke testing is to determine the aircraft strike zones. In order to determine these zones, a proper combination of standard current waveform components must be used. The standard combinations used are given in Table 9.5 for both groups of lightning effects.

Other important quantities to be measured during a swept stroke test are a number of attachment points, arc dwell time, dielectric or coating material breakdown, and puncture points. These can be determined by high speed photographs of the arc.

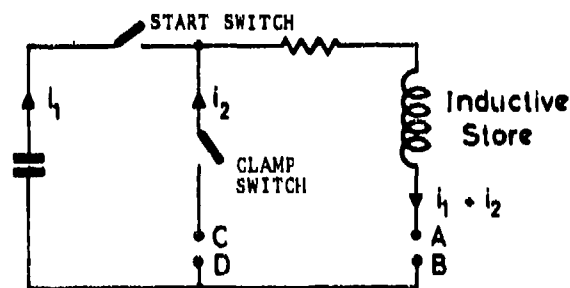


Figure 9.27 Basic Circuit For Generating Standard Test Current Waveforms⁽¹⁴⁾

Table 9.4 Current Generator Specifications to Produce Standard Lightning Waveforms⁽¹⁴⁾

Circuit Configuration	Current Components	Stored Energy kJ	Capacitance μF	Voltage kV	Circuit Inductance H	Rise Time s	Peak Current kA	Charge Transfer C	Action Integral $10^6 \text{ A}^2 \text{ s}$	Exponential Time to 1/e s	Linear Decay Time to Zero Current s
clamped	fast	130	42.1	76	$6 \cdot 10^{-6}$	$25 \cdot 10^{-6}$	200	20	2	$100 \cdot 10^{-6}$	$150 \cdot 10^{-6}$
clamped	fast	130	42.1	76	$6 \cdot 10^{-6}$	$25 \cdot 10^{-6}$	200	15	2		
critically damped	fast	892	104	131	$6 \cdot 10^{-6}$	$25 \cdot 10^{-6}$	200	13.6	1.9	$100 \cdot 10^{-6}$	
clamped	intermediate	60	533	15	$7.8 \cdot 10^{-3}$	$3.1 \cdot 10^{-3}$	4.0	10	0.03		$3 \cdot 10^{-3}$
critically damped	intermediate	75	667	15	$1.8 \cdot 10^{-3}$	$1 \cdot 10^{-3}$	3.7	10	0.03	$3 \cdot 10^{-3}$	
clamped	continuing	100	889	15	0.31	$25 \cdot 10^{-3}$	0.8	200			0.5
clamped	restrike group 1 effects	30	6.8	94	$6 \cdot 10^{-6}$	$10 \cdot 10^{-6}$	100		0.25	$50 \cdot 10^{-6}$	
clamped or oscillatory	restrike group 1 effects	30	0.15	630	$6 \cdot 10^{-6}$	$1.5 \cdot 10^{-6}$	100				

Table 9-3 Waveform Requirements for Component Testing of Aircraft Zones⁽¹⁴⁾

(a) Group 1 Composite Tests

Test Zone	Current Component			
	A	B	C	D
1A	x	x	x (note 1)	
1B	x	x	x	x (note 2)
2A		x	x (note 1)	x (note 2)
2B		x	x	x (note 2)
3	x (note 3)		x (note 3)	

(b) Group 2 Component Tests

Test Zone	Current Component	
	A	D
1A	x	
1B	x	x (note 4)
2		x (note 4)
3	x (note 3)	x (notes 3 & 4)

Note 1 Assume a current duration of 43ms for continuing current components unless swept stroke testing shows otherwise.

Note 2 The continuing current should drop to near zero before the restrike commences.

Note 3 Current to be applied through a solid connection not an arc.

Note 4 Component D to have a rate of rise of 100kA/μs ± 10%

Swept stroke phenomena are important because they cause sections of the aircraft not normally involved in the lightning process to become vulnerable because of the sweeping action.

9.2.5.3.3 Induced Voltage Testing and Sparking

Induced voltage and sparking is primarily a function of high peak current and high rate of change of current which correspond to Group 2 lightning parameters. The physical layout is very important for the test setup. In particular, the return lines should be arranged to yield a minimal magnetic field at the test specimen, and the monitoring equipment placed so it will not influence the results.

9.2.6 High Voltage Charging-Discharging Phenomena

The principal high voltage charging-discharging phenomenon involving composite aircraft is the precipitation static threat discussed in Section 2.0 of this handbook.

9.2.6.1 Test Techniques

One commonly used test method involves the direct connection of the specimen to the source of charge. This method is not a very realistic simulation of the precipitation static charging process.

Another method involves blowing "wondra" flour particles across a test specimen. This method simulates the actual charging process more closely than direct connection but results in a low charging rate. This procedure is discussed in Chapter 2 in connection with precipitation static charging of aircraft.⁽⁹⁾

A precipitation static test technique has been developed by Boeing⁽⁹⁾ which combines high charging rates with carefully controlled conditions. The apparatus is shown schematically in Figure 9.28. A discharge probe is connected to a high voltage source and is used to spray electric charge directly onto a test specimen. The height of the probe above the specimen controls the charging rate. All charge leakage away from the specimen is carefully monitored by current test probes. This apparatus has been used successfully in measuring the charging process of various graphite/apoxy panels.

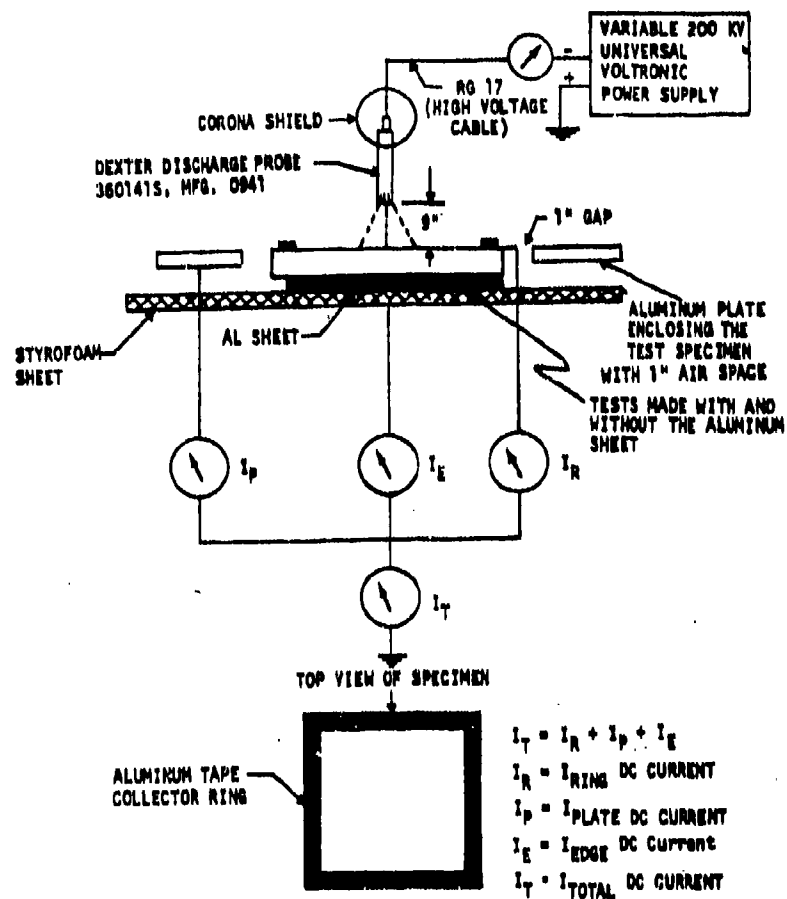


Figure 9.28 Precipitation Static Test Technique (8)

9.3 References

1. 1974 Annual Book of ASTM Standards, Part 44, p. 39, 1974.
2. Allen, et. al., A Technology Plan for Electromagnetic Characteristics of Advanced Composites, RADC-TR-76-206, July 1976.
3. Allen, et. al., Electromagnetic Properties and Effects of Advanced Composite Materials: Measurement and Modeling, RADC-TR-78-156, June 1978.
4. 1974 Annual Book of ASTM Standard Part 39, p. 23, 1974.
5. 1974 Annual Book of ASTM Standard Part 43, p. 206, 1974.
6. W. F. Walker and Roger E. Heintz, Measurement of Electrical Conductivity in Carbon/Epoxy Composite Material over the Frequency Range 75 MHz to 2.0 GHz, RADC-TR-79-233, October 1979.
7. W. J. Gayda, A Fundamental Study of the Electromagnetic Properties of Advanced Composite Materials, RADC-TR-78-158, July 1978.
8. W. J. Gayda, Measurement of the Electrical Properties of Composite Materials in the Frequency Range of D.C. to 30 MHz, RADC-TR-79-203, August 1979.
9. Strawe, et. al., Investigation of Effects of Electromagnetic Energy on Advanced Composite Aircraft Structures and their Associated Avionic/Electrical Equipment, Phase II, Volume 1, The Boeing Company, 1977.
10. Wallenberg, et. al., Advanced Composite Aircraft Electromagnetic Design and Synthesis, Interim Report, Syracuse Research Corp., April 1980.
11. E. B. Joy, D. T. Paris, "Spatial Sampling and Filtering in Near-field Measurement," IEEE Trans. on Ant. & Prop., Vol. AP-20, No. 3, May, 1972.
12. D. Strawe, L. Piszker, "Electromagnetic Shielding of Advanced Composites in the 10 kHz to 100 MHz Frequency Range," (AFML) Final Report, July 1975 Contract F33515-74-C-5158, Boeing Aerospace Co.
13. Lightning Test Waveforms and Techniques for Aerospace Vehicles and Hardware, Report SAE Committee AE4, Special Task F, (1976).
14. J. Phillpott, Recommended Practice for Lightning Simulation and Testing Techniques for Aircraft, Culham Laboratory Report CLM-RH3, Abington Oxfordshire England, (1977).
15. Schneider, Kendrichs and Olson, Vulnerability/Survivability of Composite Structures - Lightning Strike, AFFDL-TR-77-127 Vol. 1 (1978).
16. Protection Optimizatin for Advanced Composite Structures, Fourth Quarterly Progress Report prepared by Gruman Aerospace Corporation for Air Force Systems Command, Wright-Patterson Air Force Base under Contract F33615-77-C-5169, June 1978.

10.0 PROTECTION METHODS AND TECHNIQUES

Structures involving composites such as graphite/epoxy, boron/epoxy and Kevlar/epoxy are a common feature on present day commercial and military high-performance aircraft. The high strength and stiffness of these materials together with their low densities make them excellent for constructing the high-performance and fuel efficient aircraft required for the future.

Composite materials, however, are not without their problems. Because of their lower conductivities compared to most metals (such as aluminum), composites are more susceptible to lightning strikes, static charge buildup and possess poorer electromagnetic shielding properties. Possible consequences include structural damage, EM interference in sensitive digital electronic equipment, and possible catastrophic failure of the aircraft. Protection systems are needed that will protect composite aircraft adequately, yet not extract a severe weight or cost penalty nor degrade mechanical properties unacceptably. Such systems also must be compatible with the thermal, fatigue and moisture environments the composite aircraft may experience. Finally, adequate repair techniques should exist for the protection system.

In this section, a number of different aircraft protection systems will be examined. The main emphasis is on lightning protection but other systems for protection against precipitation static, EM field penetration of the aircraft structure, moisture and chemical action will also be considered.

10.1 Present Aircraft Protection Systems

In this section a brief survey is given of protection systems currently being used on modern aircraft. The main protection afforded by these systems is against lightning and precipitation static, although some of the coatings applied to composites increase their shielding effectiveness and protect against moisture and chemicals.

Both lightning and precipitation static threats have been described in detail in Chapter 2.0 (electromagnetic threats) and only a brief synopsis will be given here. Lightning damage to composite aircraft is caused by thermal effects and high current densities. Thermal effects occur at the lightning arc attachment point where temperatures as high as 27,000°C are possible.⁽¹⁾ The usual result is burning or charring of the composite. Damage from high current densities tends to occur away from the attachment point and results in vaporization and rupture of the composite fibers due to their lower conductivities compared to metals.⁽¹⁾ Lightning damage is proportional to the arc attachment time which, in turn, depends on the aircraft strike zone involved. Typical strike zones are shown in Figures 2.16 and 2.17.

Precipitation static is caused by triboelectric charging of an aircraft region due to particle or precipitation bombardment. The resulting corona discharge causes RF interference. Composites (especially Kevlar) are more prone to charge buildup due to their lowered conductivities. Both lightning and precipitation static can be controlled by use of proper protection devices which will now be described.

10.1.1 Static Dischargers

Static dischargers are commonly positioned at points of high static charge buildup on aircraft to quietly discharge the aircraft.⁽⁵⁾ The oldest type of discharge is the "discharge wick". The wick is usually made from graphite-impregnated cotton sealed in a plastic tube. Mounting is usually done by bolts, rivets or resin. A discharge wick is shown in Figure 10.1(a).

Ortho-coupled dischargers⁽⁵⁾ consist of a high impedance rod with a tungsten pin through the rod angled to minimize coupling of corona discharge RF noise to antennas. These devices are used mainly on high performance aircraft. An example is shown in Figure 10.1(b).

10.1.2 Lightning Arresters

Lightning arresters were developed to prevent the direct coupling of lightning to sensitive electronic equipment via an aircraft antenna.⁽⁵⁾ Arresters usually include a spark gap between antenna and aircraft structure, a blocking capacitor and leak resistor as shown in Figure 10.1(c). The gap provides a path for the lightning to jump from the antenna to the airframe before the electronic equipment is reached. Arresters are commonly used in conjunction with static dischargers.

10.1.3 Radome Strips

Because radomes are made from dielectric material to provide transparent protection for radar systems, they are very susceptible to lightning strike. A common protection device consists of metallic foil strips placed on the radome which act as lightning diverters. Douglas Aircraft^(6,7) has developed a protection method based on segmented diverters connected together by high resistance material. The diverter provides a controlled conductive channel to the airframe by flashover from segment to segment. Radome diverters are illustrated in Figure 10.2.

10.1.4 Composite Coating Protection Systems

A variety of protection systems presently exist that rely on coatings or coverings to protect the composite structure. Such systems range from screens and foils to metallic coatings, paints and sprays. These systems are principally protectors against lightning and static charging but often increase the electromagnetic shielding of the aircraft as well. Each system, of course, has advantages and disadvantages which usually requires that a tradeoff study be done to pick a best system.

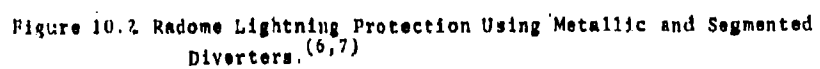
Both Boeing and Grumman Aircraft have done such studies of protection under a variety of test conditions. The results of these studies are given in the following sections.

10.1.4.1 Boeing Composite Protection System Evaluation⁽¹⁾

A study of composite protection systems was performed recently by Boeing⁽¹⁾ to determine those systems which would be optimum choices under various cost and weight constraints. The results of the study are presented in this section.



Figure 10.1 Aircraft Protection Devices ⁽⁵⁾



10.1.4.1.1 Standard Laminates

All candidate protection systems studied by Boeing are listed in Table 10.1 together with aircraft zones where applied, installation methods, advantages and disadvantages of each system and certain weight information. All candidate system screening and subsequent evaluation were performed on flat laminates and sandwich specimens of graphite, boron, glass and Kevlar composites. A very limited study was performed using nickel foil, nickel plate and titanium foil protection systems, however, these systems will not be discussed further since all information on them is very preliminary.

A subset of the original candidate systems was chosen for final evaluation. Table 10.2 ranks these protection systems in terms of manufacturability which includes material availability, cost, weight and ease of application and repairability. Each factor is rated on a numerical scale; the higher the scale, the more favorable the factor.

Lightning tests were conducted on each protection system as applied to 10-ply composite laminates. The relative merits of each protection system as a function of aircraft lightning strike zone are summarized in Figure 10.3. Relative damage to both substrate and protective coating is summarized in Figure 10.4. Each system offered some protection.

Tension tests were conducted before and after lightning strikes on the laminates with and without protection systems.⁽¹⁾ The unprotected graphite/epoxy laminates lost about 50% tensile strength and 40% tensile strain when struck in the 1A or 1B lightning zone. Graphite-glass/epoxy hybrids lost about 50% tensile strain while graphite-boron/epoxy lost 60% in tensile strength and 50% in tensile strain. The panels with protection showed various levels of improvement depending on the system used. The results are shown in Figure 10.5 - 10.8.

The damage done to composite laminates by Zone 2A or 2B lightning strikes was considerably less than that done by Zone 1A or 1B strikes.

10.1.4.1.2 Protection System Evaluation

The lightning protection systems were evaluated from several points of view. The primary consideration, of course, was system effectiveness but other considerations played a major role. One such consideration was material availability. The materials required for the system must be commercially available. Other considerations were material cost, manufacturability and repairability. All systems were ranked according to merit for each consideration and the results are listed in Table 10.2.

10.1.4.1.3 Joints and Panels With Substructure

Any lightning protection system development must evaluate the effects of joints and panels with substructure on the protection system.

Composite joints are of two types: bolted or bonded. In bolted joints, the required electrical continuity across the joint is maintained by the fasteners that join the surface panels to the substructure. Such a bolted joint panel is shown in Figure 10.9. Currents are transmitted from

Table 10.1 Possible Lightning Protection Systems⁽¹⁾

PROTECTION SYSTEM	APPLICATION	WEIGHT, lb/ft ²	INSTALLATION METHOD	ADVANTAGES	DISADVANTAGES
Aluminum flame spray	Zones 1 and 2	0.08 (estimated)	Cocured or secondary application	1. Independent of surface shape 2. Partial environmental seal of advanced com- posite surface	1. Coating weight and quality operator-dependent
Kapton dielectric coating	Zone 2 (see note)	0.07 (estimated)	Adhesive bonded	1. Provides good dielectric strength for stroke diver- sion	1. Difficult to apply on com- plex shapes 2. Low peel resistance
MIL-C-83286 Polyurethane paint, Dielectric coating	Zone 2 (see note)	0.08 (estimated)	Spray	1. Independent of surface shape 2. Ease of application 3. Simple repair	1. Potential weather degra- dation 2. Coating weight is operator- dependent
Kapton dielectric coating in combination with metallic diverters	Zone 2 (see note)	0.08 (estimated)	Bond-cure	1. Provides good path for stroke stepping	1. Difficult to apply on com- plex shapes 2. Low peel resistance
Aluminum foil (6 mil)	Zone 1	0.070-0.080	Adhesive bonded- cocured	1. Environmental seal of advanced composite surface 2. Uniform surface conductivity 3. Surface material com- pletely replaceable	1. Relatively heavy 2. Difficult to install on com- plex shapes 3. Poor reparability 4. Poor part handling charac- teristics
Aluminum foil (1-3 mil)	All zones	0.020-0.030	Adhesive bonded- cocured	1. Environmental seal of advanced composite surface 2. Uniform surface com- pletely replaceable 3. Surface material com- pletely replaceable	1. Foil stock width limitations 2. Difficult to install on com- pound contours 3. Poor reparability charac- teristics 4. Poor part handling charac- teristics
PROTECTION SYSTEM	APPLICATION	WEIGHT, lb/ft ²	INSTALLATION METHOD	ADVANTAGES	DISADVANTAGES
Aluminum wire fabric (woven) screen (200 x 200)	All zones	0.030-0.036	Cocured	1. Minimum shape constraints 2. Lightweight system 3. Repairable 4. Low maintenance	1. Difficult to install in complex shapes
Aluminum wire fabric (knitted) screen (200 x 200)	All zones	0.040 (estimated)	Cocured	1. Minimum shape constraints 2. Lightweight system 3. Repairable 4. Low maintenance 5. Lowest cost	1. Screen stock width limitations 2. Difficult to install in complex shapes
Aluminized glass	Zone 2	0.10 (estimated)	Bond-cure	1. Potential limited appli- cation to Zone 2	1. Relatively heavy 2. Relatively expensive 3. Difficult to repair
Kapton dielectric with thin reinforced plastic covering	Zone 2 (see note)	0.07-0.09 (estimated)	Bond-cure	1. Provides good dielectric strength for stroke diversion 2. Kapton dielectric is protected	1. Difficult to apply to com- plex shapes 2. More expensive than other systems

Note: Pinholing or decrease in dielectric strength of dielectric coatings due to environmental effects during the service life of the vehicle may degrade the system beyond an uncoated system. Therefore, the system is not recommended where flight safety is considered (i.e., fuel vapor ignition, etc.).

Table 10.2 Lightning Protection System Ranking⁽¹⁾

SYSTEM	MATERIAL AVAILABILITY ^a	MATERIAL COST ^a	WEIGHT ^a 101 lb/ft ²	APPLICATION & REPAIRABILITY ^a
1. Aluminum Metal Flame Spray 4-6.9 MIL, 100% Coverage	5	4	8	9
2. Aluminum Metal Flame Spray 4-6.9 MIL, 50% Coverage	5	2	12	8
3. 120 x 120 Aluminum Wire Screen 100 % Coverage	2	2	1	6
4. 200 x 200 Aluminum Wire Screen 100 % Coverage	2	2	2	7
5. Aluminum Foil, 2 MIL, 100% Coverage	3	3	4	2
6. Aluminum Foil, 2 MIL, 50% Coverage	3	3	10	3
7. Aluminum Foil, 3 MIL, 100% Coverage	3	3	3	4
8. Aluminum Foil, 3 MIL, 50% Coverage	3	3	7	5
9. Aluminum Foil Tape, 2 MIL, Adhesively Backed, 100% Coverage	4	5	9	2
10. Aluminum Foil Tape, 2 MIL, Adhesively Backed, 50% Coverage	4	5	13	3
11. Aluminum Foil Tape, 3 MIL, Adhesively Backed, 100% Coverage	4	5	5	2
12. Aluminum Foil Tape, 3 MIL, Adhesively Backed, 50% Coverage	4	5	11	3
13. Kapton Film, 2 MIL + 2 MIL Aluminum Foil Strips	1	1	6	1

a. The higher the number the more favorable the factor

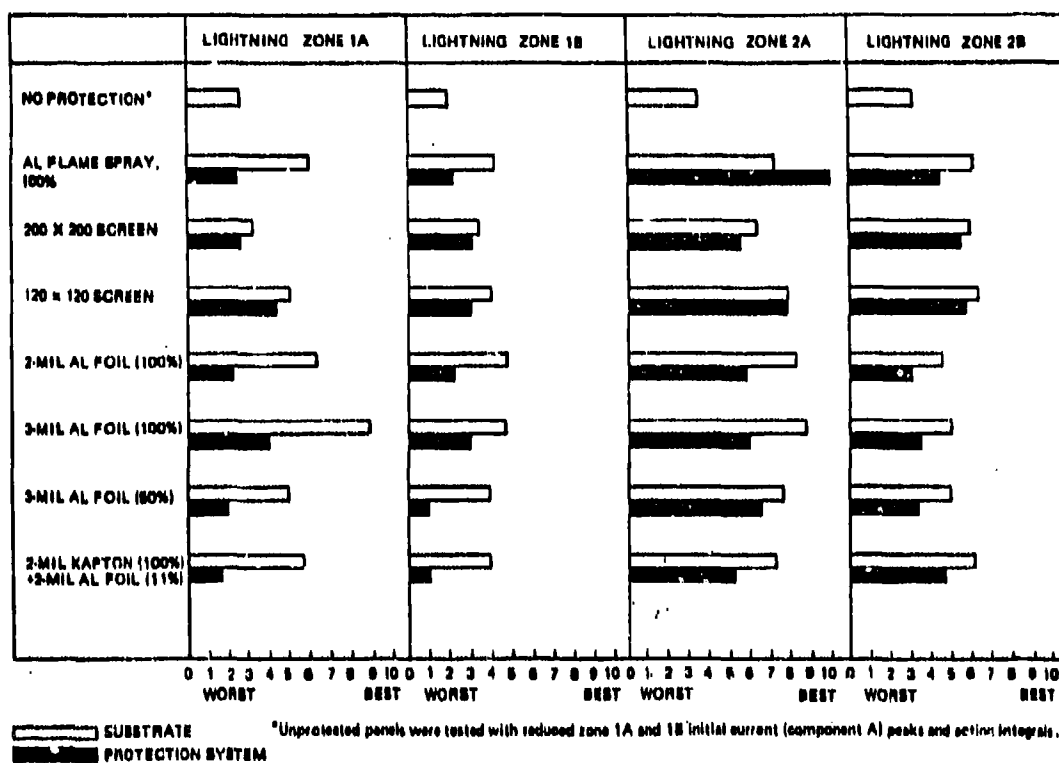


Figure 10.3 Relative Merit of Lightning Protective Systems

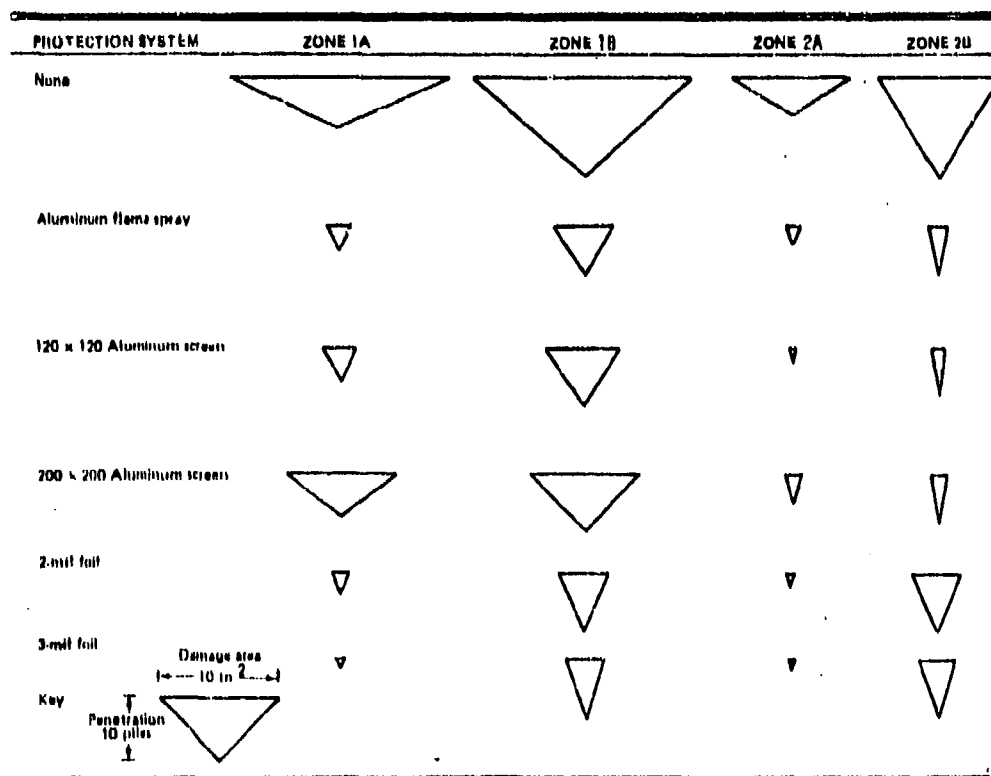


Figure 10.4 Relative Damage Estimates⁽¹⁾

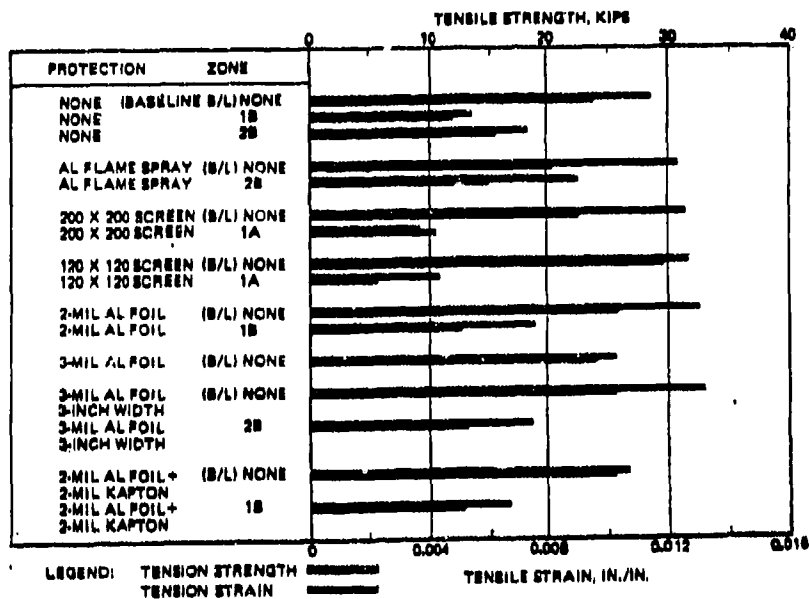


Figure 10.5 Tension Data on Lightning Protected 10-Ply Graphite/Epoxy Laminates⁽¹⁾

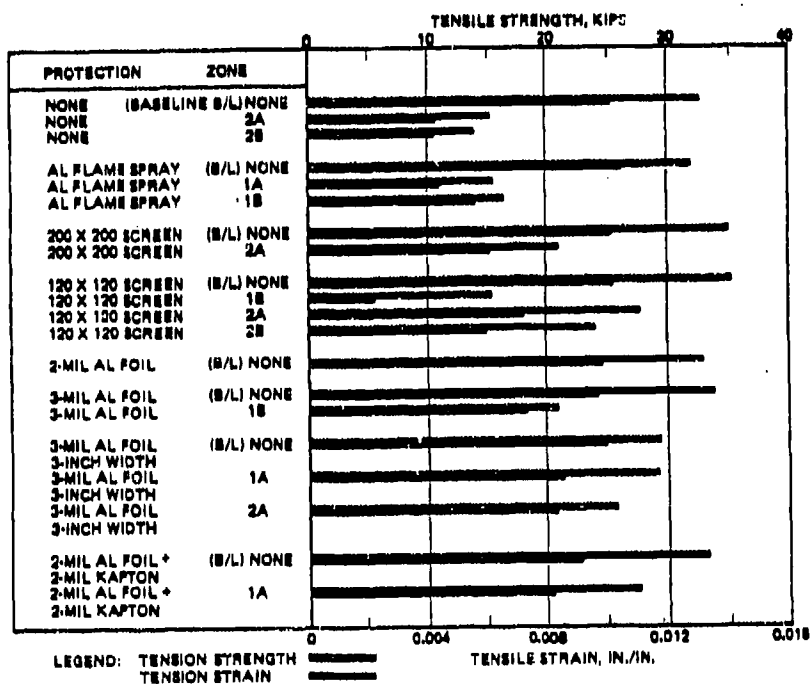


Figure 10.6 Tension Data for Lightning Protected Graphite-Glass/Epoxy 10-Ply Hybrid Laminates⁽¹⁾

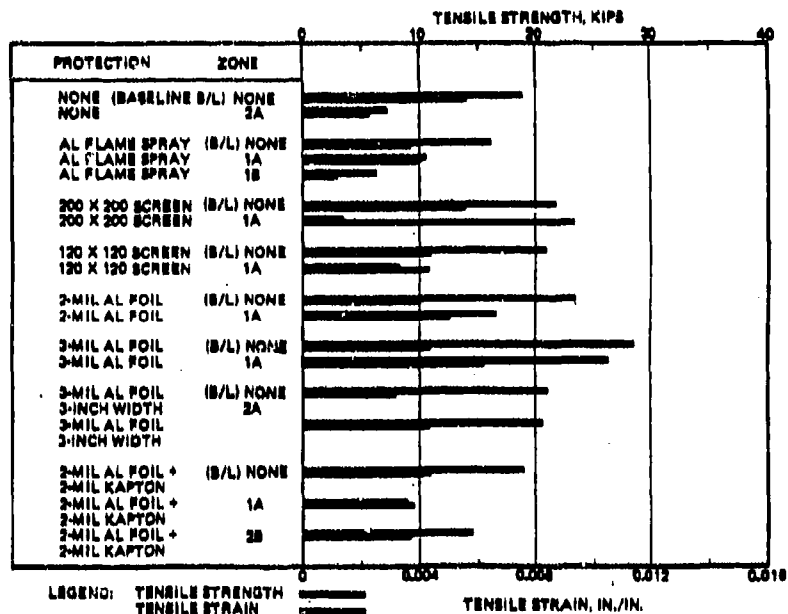


Figure 10.7 Tension Data for Lightning Protected Graphite-Boron/Epoxy 10-Ply Hybrid Laminates⁽¹⁾

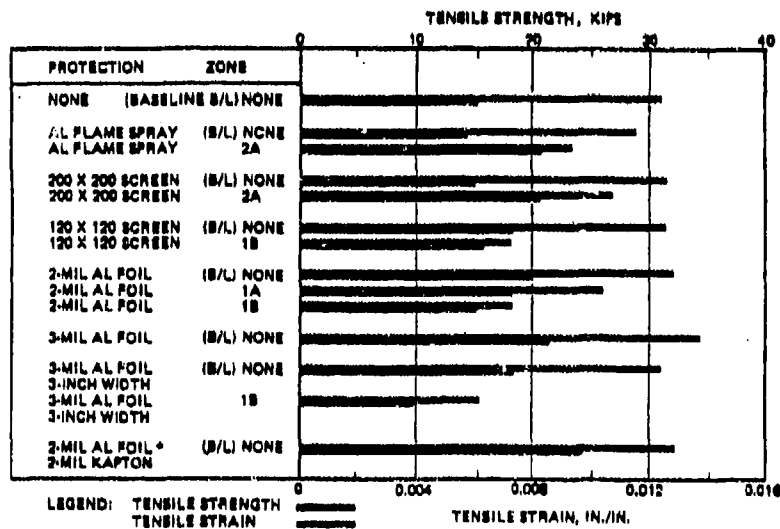


Figure 10.8 Tension Data for Lightning Protected Graphite-Kevlar/Epoxy 10-Ply Hybrid Laminates⁽¹⁾

the composite to the fasteners which in turn transmit it to the substructure. As shown in Figure 10.9, galvanic isolation of titanium splice plate and aluminum lightning protective coating is maintained across the joint to prevent electrochemical action.

A bonded joint is shown in Figure 10.10. In contrast to bolted joints where currents follow the fasteners, bonded joints have discontinuity at the metal-to-composite adhesive bond line. Heating and internal arcing are possible at the interface if the cross-section is too small to carry large current loads that may be produced by lightning. Figures 10.11 and 10.12 illustrate the panels with substructure (laminar and honeycomb) that were also tested.

After lightning tests were conducted, structural damage was found to be most severe for the adhesively bonded joints and least severe for the mechanically bolted joints. Composite structures that utilize an aluminum honeycomb core are particularly susceptible to damage due to the low resistance of the honeycomb compared to the graphite skin. Lightning will puncture the skin and flow through the honeycomb.

10.1.4.1.4 Environmental Exposure

It is necessary that the lightning protection systems be compatible with the expected service environments. Two different exposure conditions were imposed on protected composite panels: 1000 continuous hours at 140°F/100% relative humidity, and simulated flight cycling (1000 cycles) from -65° to 250°F in a Webber chamber. The results are given in Figures 10.13 to 10.15 and show no corrosion to the aluminum and no loss of lightning protection.

10.1.4.1.5 Damage Repair

The effectiveness of the lightning protection systems were evaluated after repair of the system following damage. Two types of damage were considered: minor damage comparable to a tool drop, and major impact damage caused by a heavy or sharp object.

Repair of the damaged laminates consisted in rebuilding the composite structure with reapplication of lightning protection across the repaired area. Heat bond and cold bond repair procedures were used. The hot bond procedure consisted of the following steps:

1. Abrade away damaged material (taper 0.25 in. per ply).
2. Abrade away paint to expose base protection for 0.5 in. minimum in excess of damage area.
3. Place adhesive (AF143, 10 mil) over damaged area.
4. Place tapered prepreg plies in damaged area (mechanically damaged panels) or precured patch (lightning damaged panel) to match panel contour.

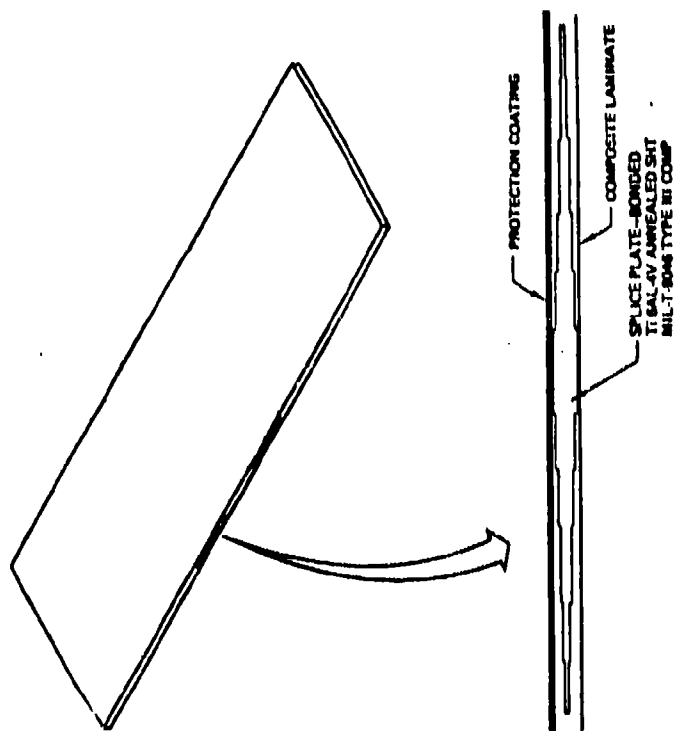
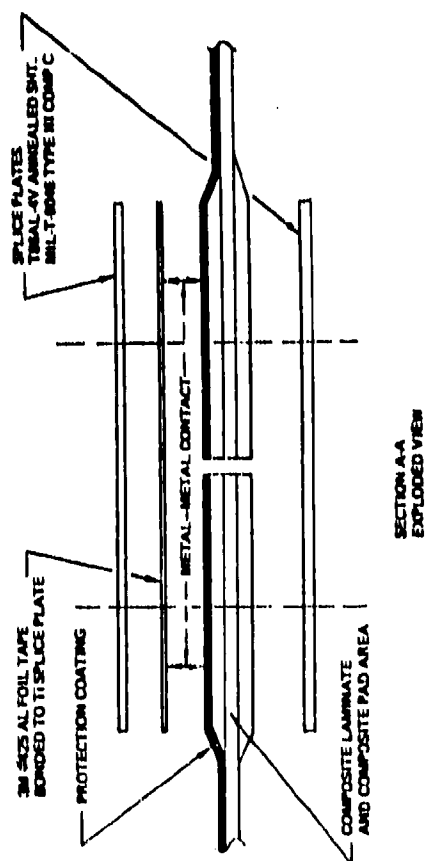
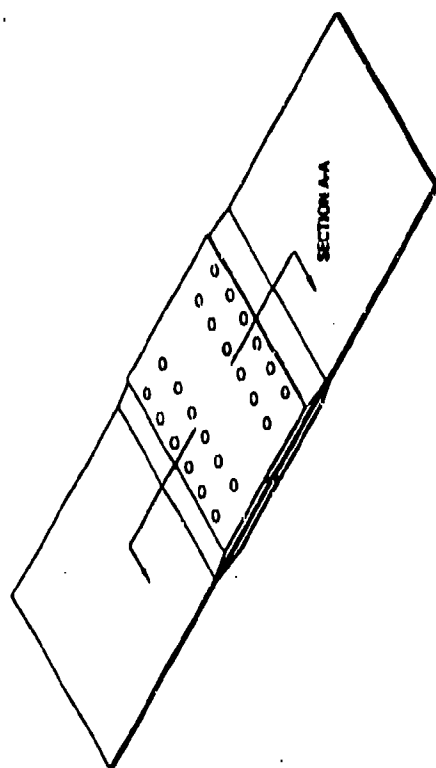


Figure 10.9 Bolted Joint Panel with Protection (i)

Figure 10.10 Bonded Joint Panel with Protection (1)

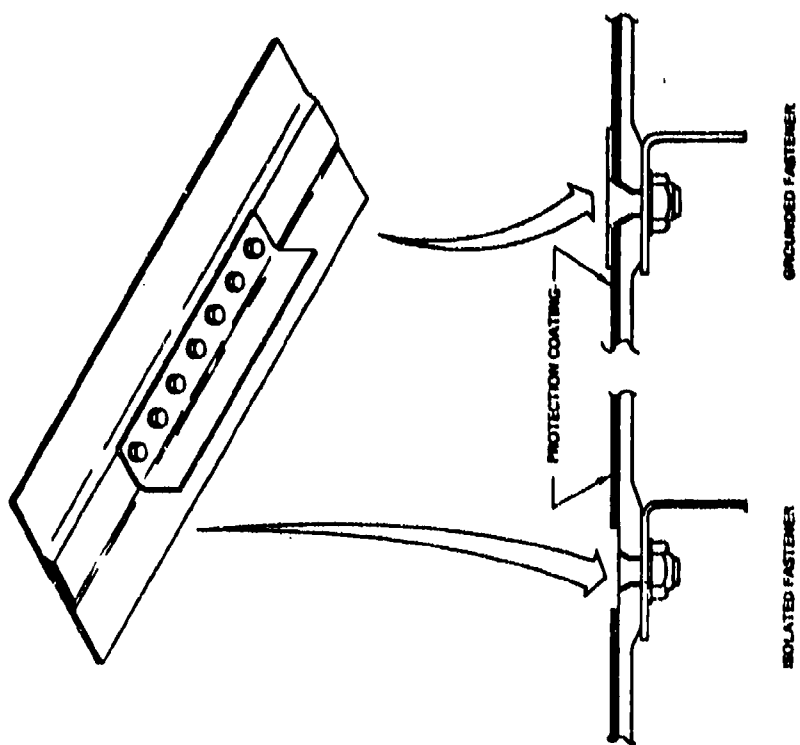


Figure 10.11 Laminate with Substructure with Protection--
Isolated and Grounded Fasteners (1)

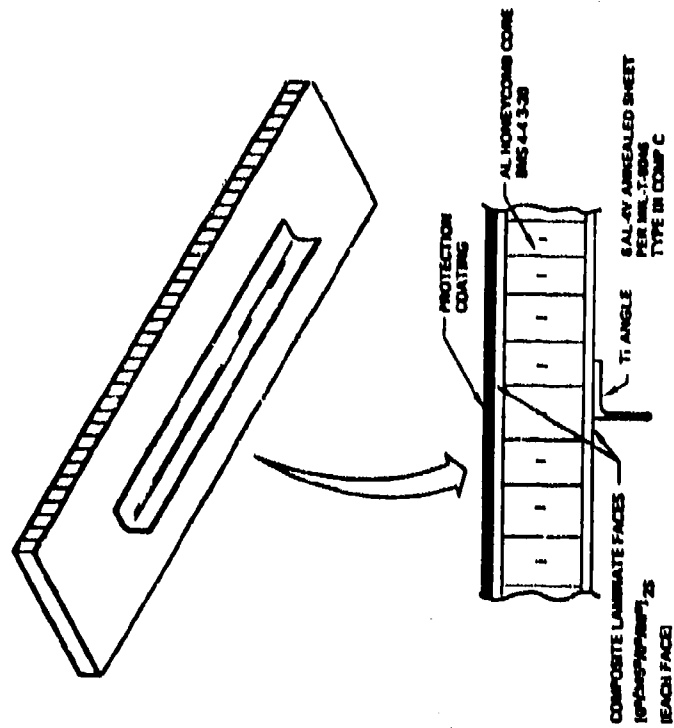


Figure 10.12 Honeycomb Panel with Bonded Titanium
Substructure with Protection (1)

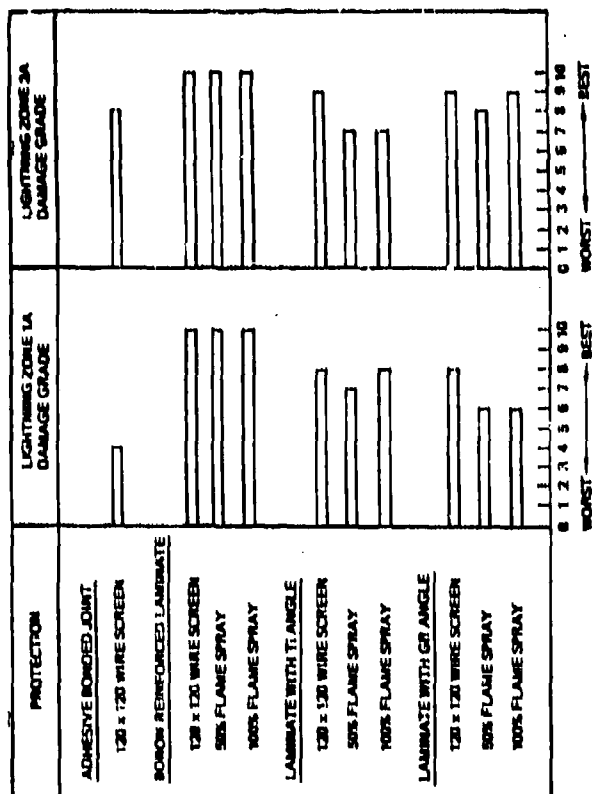


Figure 10.14 Relative Protection Grades of Specimens Exposed to 1,000 cycles in the Webber Chamber (-65°F to +250°F) (1)

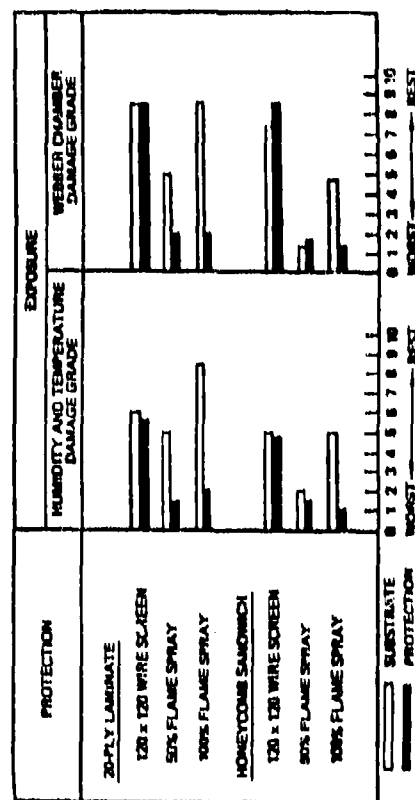


Figure 10.15 Relative Protection Grades of Environmentally Exposed Specimens Zone 1A Lightning Tests (1)

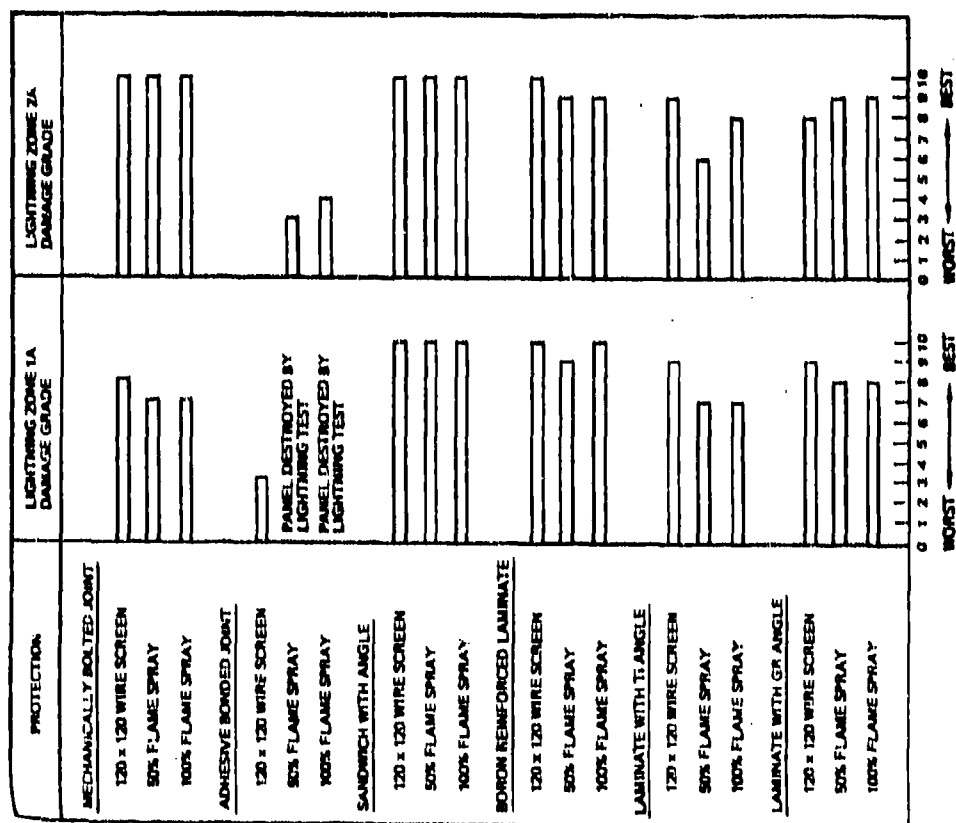


Figure 10.16 Relative Protection Grades of Specimens Exposed to 140°F/100% RH for 1,000 Hours (1)

5. Cure laminated prepreg patch plies to panel using pressure plate and autoclave cure.
6. Mask off undamaged panel area using 3-mil adhesive-backed aluminum tape.
7. Apply aluminum flame spray.
8. Apply MIL-P-23277 yellow primer.
9. Apply MIL-C-23286 Polyurethane enamel.

and the cold bond procedure was:

1. Abrade away damaged material (taper 0.25 in. per ply).
2. Abrade away paint to expose base protection for 0.5 in. minimum in excess of damage area.
3. Fill damaged area with potting compound.
4. Allow potting to cure at room temperature or for 2 hours at 160°F.
5. Fair potting to panel contour.
6. Apply 3-mil adhesive-backed foil to repair area.
7. Mask off undamaged panel area.
8. Apply MIL-P-23277 yellow primer.
9. Apply MIL-C-23286 polyurethane enamel.

After repair, the composite panels were struck with simulated lightning with the results shown in Figure 10.16 - 10.19.

The results indicate that damage to composite protective systems and the composite substrate can be repaired acceptably. The electrical continuity between the repaired area protective coating and that of the base structure is the critical repair. Good temporary repair can be accomplished using aluminum foil tape. The ideal permanent repair is aluminum flame spray but it requires special personnel and facilities not usually available in the field.

10.1.4.1.6 Discussion of Protection Systems

In this section, overall conclusions on the various lightning protection systems are discussed. The first three systems were judged best.

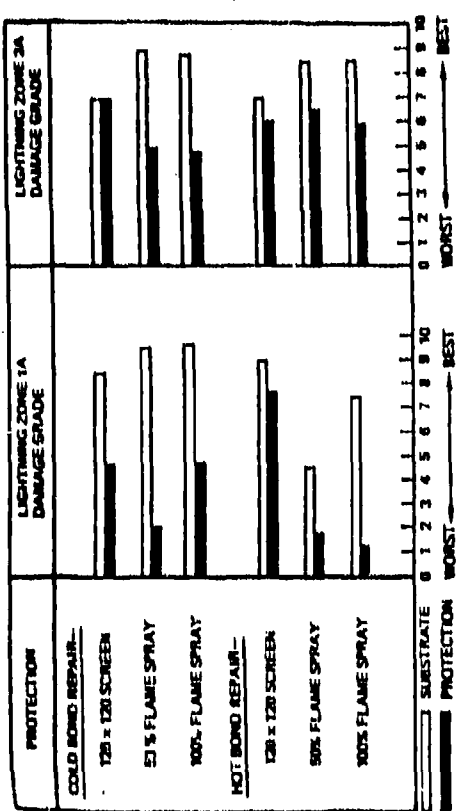


Figure 10.16 Relative Protection Grades of 20-Ply Laminates Mechanically Damaged and Repaired (1)

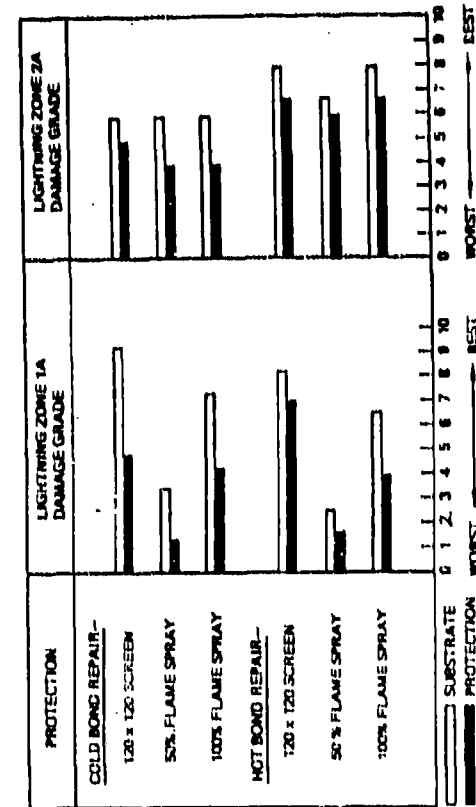


Figure 10.17 Relative Protection Grades of Sandwich Panels Mechanically Damaged and Repaired (1)

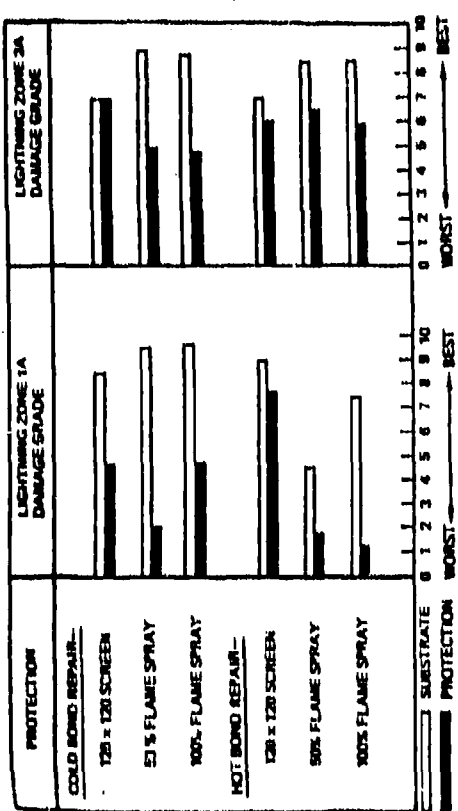


Figure 10.18 Relative Protection Grades of 20-Ply Laminates Lightning Damaged and Repaired (1)

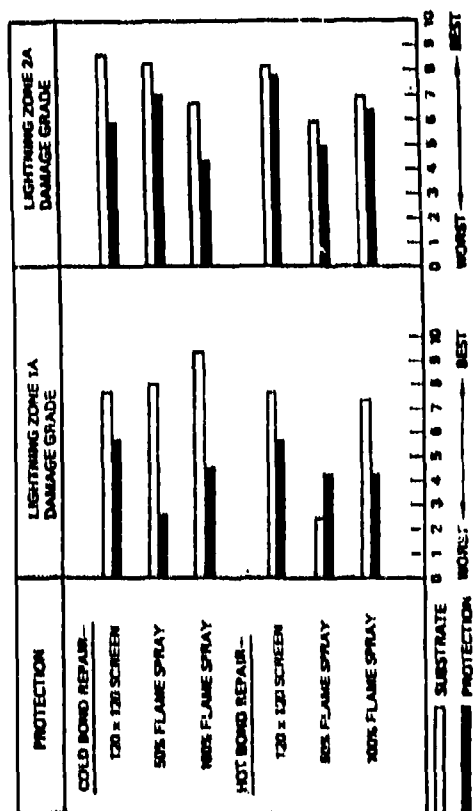


Figure 10.19 Relative Protection Grades of Sandwich Panels Lightning Damaged and Repaired (1)

10.1.4.1.6.1 Aluminum Metal Flame Spray, 4.0 - 6.9 mil
Thickness, 100% Coating

This coating was judged one of three superior lightning protection systems. It can be applied to simple or complex parts, is easily repaired and gives good lightning protection for Zone 1 and Zone 2. It does require special equipment and well trained personnel to obtain good coatings.

10.1.4.1.6.2 Aluminum Metal Flame Spray Strips, 4.0 - 6.9 mil
Thickness (50% coverage)

This system was judged one of three superior lightning protection systems. This provides Zone 2 protection in strips typically 3-inches wide with 3-inch spacing.

10.1.4.1.6.3 Aluminum Wire Screen (120 x 120)

This system was one of three superior protection systems. Good protection is provided in Zone 1 and Zone 2, but is restricted to application on simple shapes. Screen is at most 36 inches wide.

10.1.4.1.6.4 Aluminum Screen (200 x 200)

This system provides limited Zone 2 protection. It is restricted to application on simple shapes and is at most 36 inches wide.

10.1.4.1.6.5 Aluminum Foil (2 mil)

This system offers limited Zone 1 and Zone 2 protection. A good quality surface finish is hard to obtain except for simple, flat surfaces. Width is limited to 36 inches.

10.1.4.1.6.6 Aluminum Foil (3 mil)

This system offers limited Zone 1 and Zone 2 protection. Restrictions mentioned in 10.1.4.1.6.5 apply here.

10.1.4.1.6.7 Aluminum Foil (2 mil, 3 mil adhesively backed)

This system is best applied to cured composite surface. It offers limited Zone 1 and Zone 2 protection. Strip width is limited to 3 inches.

10.1.4.1.6.8 Aluminum Foil Tape Strips (3 mil, adhesively backed)
3-inch Width and 3-inch Spacing

This system is best applied to the composite surface. It is meant for Zone 2 swept-stroke conditions only.

10.1.4.1.6.9 Kapton Film (2 mil) Plus Aluminum Foil Strips
(2 mil, adhesively backed)

This system is the most complex to install (cured) and the most difficult to repair. System is limited to simple contour or flat surfaces.

10.1.4.2 Grumman Composite Metallic Coatings Evaluation⁽²⁾

Grumman⁽²⁾ has made a study of metallic coatings that can be applied to graphite/epoxy used on high performance aircraft. The coatings are designed to prevent moisture absorption, improve shielding effectiveness, reduce lightning strikes and protect against paint strippers during aircraft refinishing.

Three types of protective coatings were applied to test panels of Hercules AS/3501-6 graphite/epoxy preimpregnated tapes:

- solid aluminum foil bonded to graphite/epoxy laminate
- perforated aluminum foil cocured with graphite/epoxy laminates
- spray-and-bake metal-filled organic coatings applied to graphite/epoxy laminates.

Three spray-and-bake coatings, Kerimid 500 with aluminum powder, Alumazite Z with silver and Alumazite Z, were tested initially. Alumazite Z was chosen for further testing because of its lack of moisture pickup compared to the other two as shown in figure 10.20.

10.1.4.2.1 Moisture Resistance

The metallic coating systems were exposed to an environment of 140°F and 98% relative humidity for 90 days. Periodic measurements were taken of the percent moisture pickup. The results are shown in Figure 10.21. The solid foil and cocured foil coatings significantly protect against moisture pickup while the Alumazite Z coating itself absorbed moisture and thus had greater moisture pickup than bare graphite/epoxy.

The moisture resistance was also evaluated under humidity thermal spiking conditions. The cycle was 140°F and 98% relative humidity for 72 hours followed by 260°F for 2 hours to simulate ground storage and supersonic flight. The panels underwent 40 cycles and the results are shown in Figure 10.22. A slight decrease in moisture resistance occurred for the foil coatings while no change was observed for the Alumazite Z coating.

After humidity and thermal spiking exposure the flexural and horizontal shear strengths were measured. The effects of humidity and thermal spiking were found to be severe: a 45-50% reduction in 260°F flexural stress and a 50-50% reduction in 260°F horizontal shear strength. Both solid foil and cocured foil offered significant protection but the Alumazite Z coating offered little protection. The results are given in Figure 10.23 and 10.24.

10.1.4.2.2 Effects of Paint and Paint Remover

Graphite/epoxy laminates were painted with standard Navy paint finish (epoxy polyimide primer (Mil-P-2377) with polyurethane topcoat (MIL-C-81773) and exposed to humidity (140°F and 98% relative humidity)

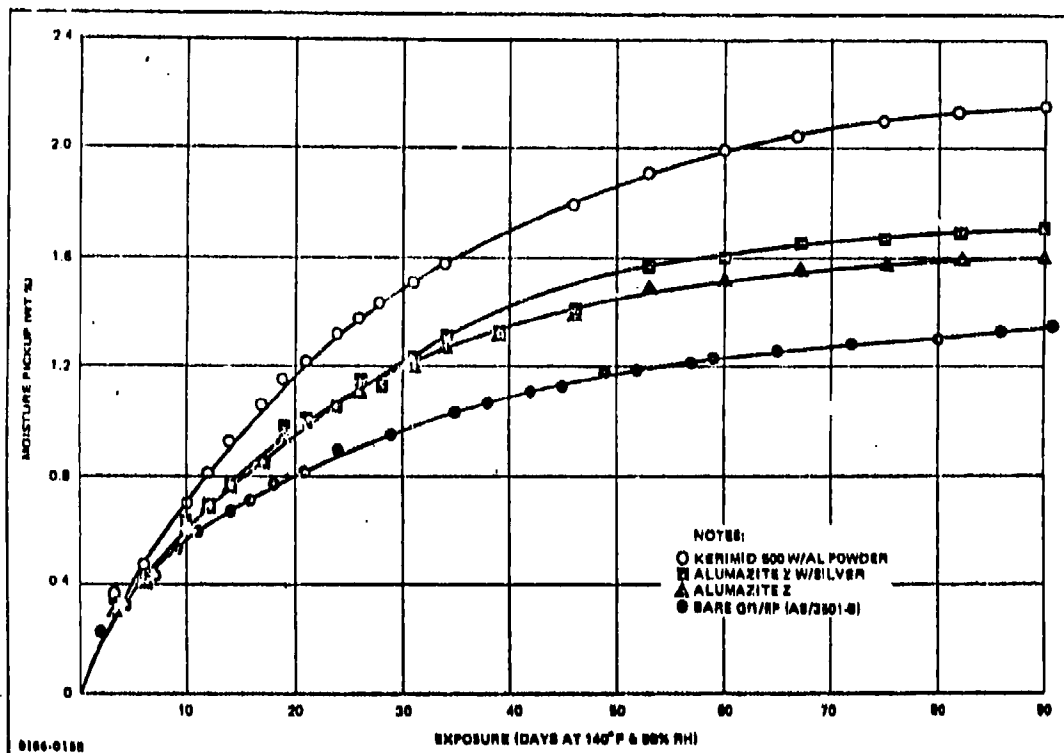


Figure 10.20 Spray-and-Bake Coating Selection - Humidity Tests (2)

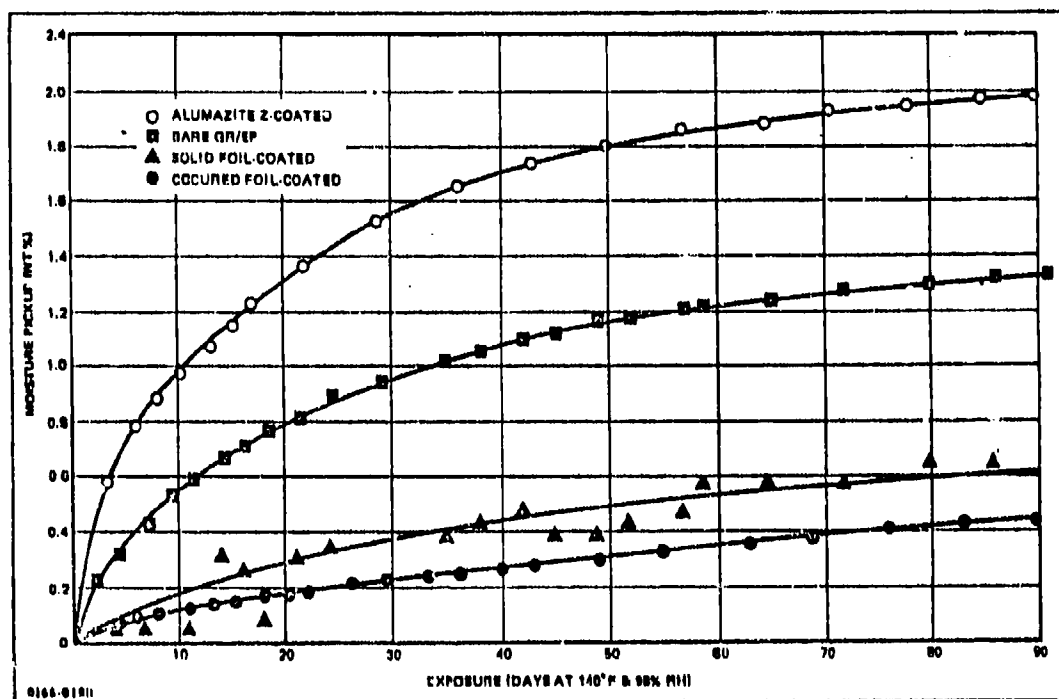


Figure 10.21 Relative Coating Effectiveness in Moisture Penetration Under Humidity Exposure (6 x 6 In. Panels) (2)

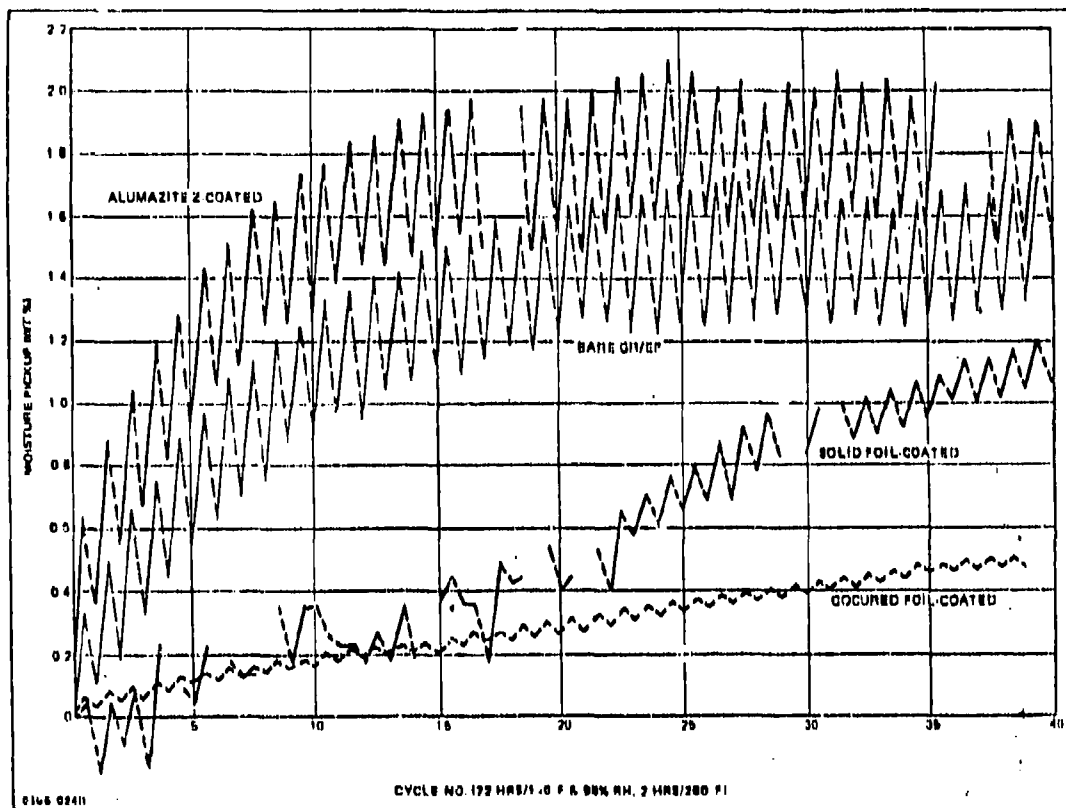


Figure 10.22 Relative Coating Effectiveness in Moisture Penetration Under Thermal Spiking Exposure (6 x 6 In. Panels (2))

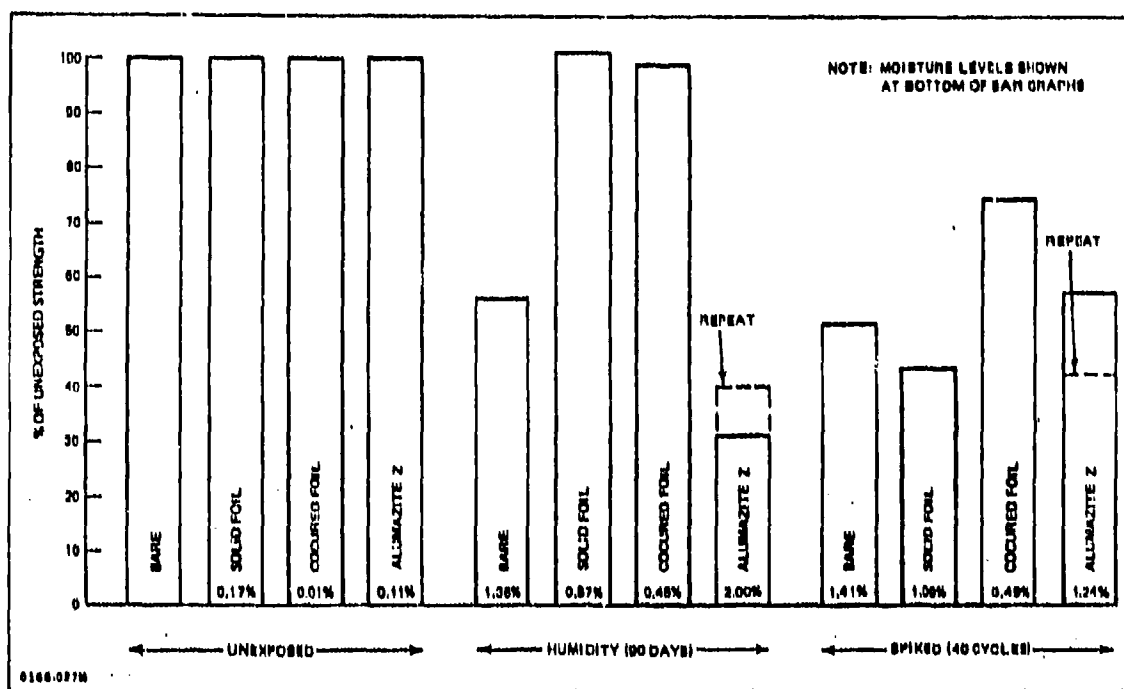


Figure 10.23 Coating Selection -- Flexural Strength (260°F) as Percent of Unexposed Strength⁽²⁾

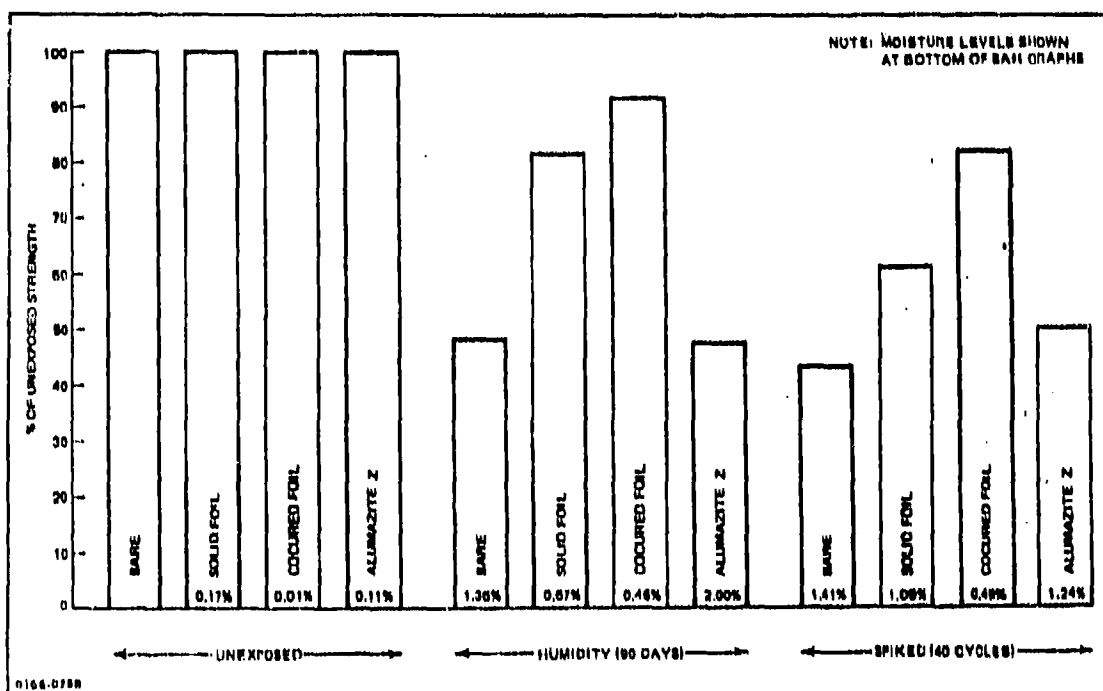


Figure 10.24 Coating Selection -- Horizontal Shear Strength (260°F) as Percent of Unexposed Strength⁽²⁾

and thermal spiking (3 days at 140°F and 98% relative humidity followed by 2 hours at 260°F). The results are given in Figures 10.25 - 10.30. The painted foil protected laminates showed considerable protection from moisture pickup and no loss of flexural or horizontal shear stress.

Paint was removed using Turco T-5469 stripper conforming to MIL-R-81294 and the horizontal shear strength and flexural stress measured. The results are given in Figures 10.29 and 10.30 and show good strength retention by painted foil protected laminates and little change due to humidity or thermal spiking. The Alumazite Z coating protects against paint stripper but not moisture.

10.1.4.2.3 EMI Shielding Effectiveness

The EMI shielding effectiveness of 18-ply graphite/epoxy was measured for both E-field, H-field and plane wave fields. Improvements greater than 30% in E-field, 150% in H-field and 55% in plane wave field shielding was obtained by coating both sides of the laminate with 2 mil solid foil. Humidity and thermal spiking produced a slight decrease in shielding effectiveness. Alumazite Z coating provided no effect on the shielding effectiveness.

10.1.4.3 Shielding Effectiveness of Aircraft Protection Systems

In addition to providing protection to composite aircraft, many of the protection systems may afford a certain improvement in EM shielding effectiveness. A general study of this problem has been done by Grumman as part of its Protection optimization program for composite structures.⁽³⁾

Electric, magnetic and plane wave shielding effectiveness measurements were performed on 12- and 24-ply graphite/epoxy panels treated with the protection systems listed in Table 10.3. All panels were fabricated from Hercules AS/3501-5A graphite/epoxy. The 12-ply panel has the laminates (2/2/8) and the 24-ply panel has the laminates (4/4/16) where the orientations are (0°/90°/+45°) respectively.

The protected panel shielding effectiveness measurement results are shown in Figures 10.31 to 10.36. These results indicate that the aluminum flame spray gave the best overall protection, probably because of the continuous coat.⁽³⁾ The 120 aluminum mesh also did quite well although the 12-ply panel did not perform as well as the 24-ply panel with the same protection. The vapor deposited aluminum and aluminized fiberglass did poorly.

10.2 Future Composite Protection-Doping and Intercalation

Future protection systems for composite aircraft structures tend to stress methods of increasing the composite shielding effectiveness by increasing its conductivity, i.e., making it behave more like a metal. Current efforts stress increasing fiber conductivity since the matrix resin material is a dielectric.

Two methods, doping and intercalation of the graphite fibers, have been described in detail in Chapter 5.0 (Intrinsic Material Properties) and will only be described here in general terms.

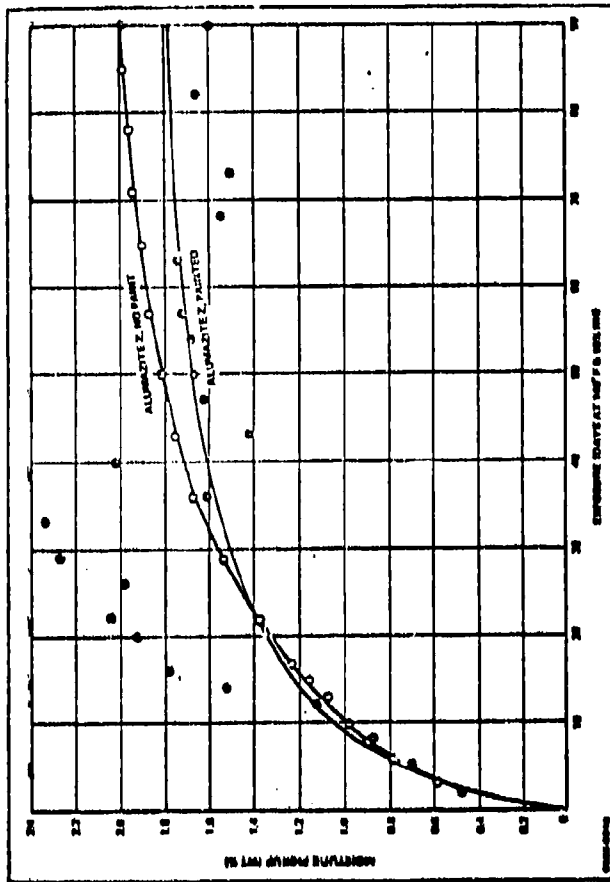


Figure 18.26 Effect of Paint Protection on Moisture Pickup of Alumazite Z-Coated Graphite/Epoxy (2)

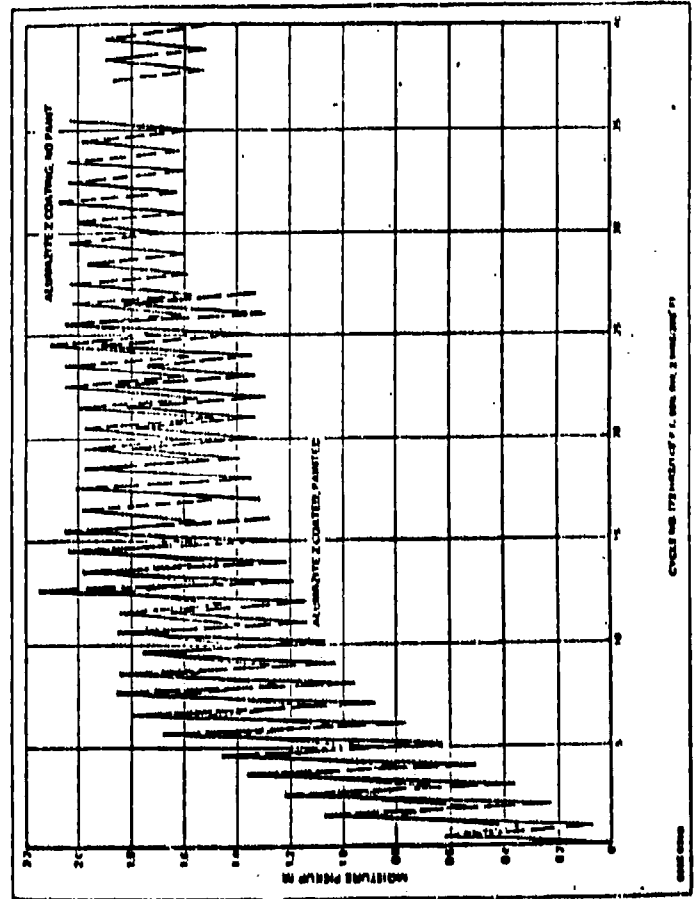


Figure 18.28 Effect of Paint Protection on Moisture Pickup of Thermally

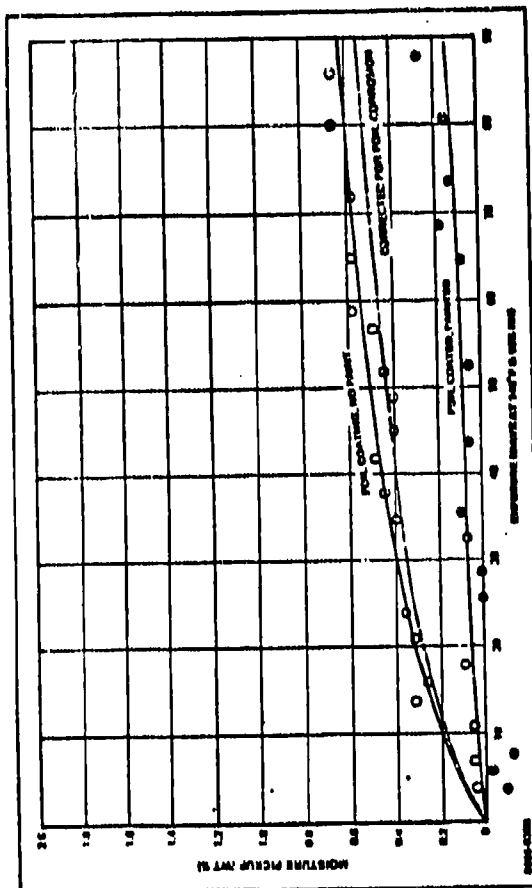


Figure 18.25 Effect of Paint Protection on Moisture Pickup at Solid-Fail-Coated Graphite/Epoxy (2)

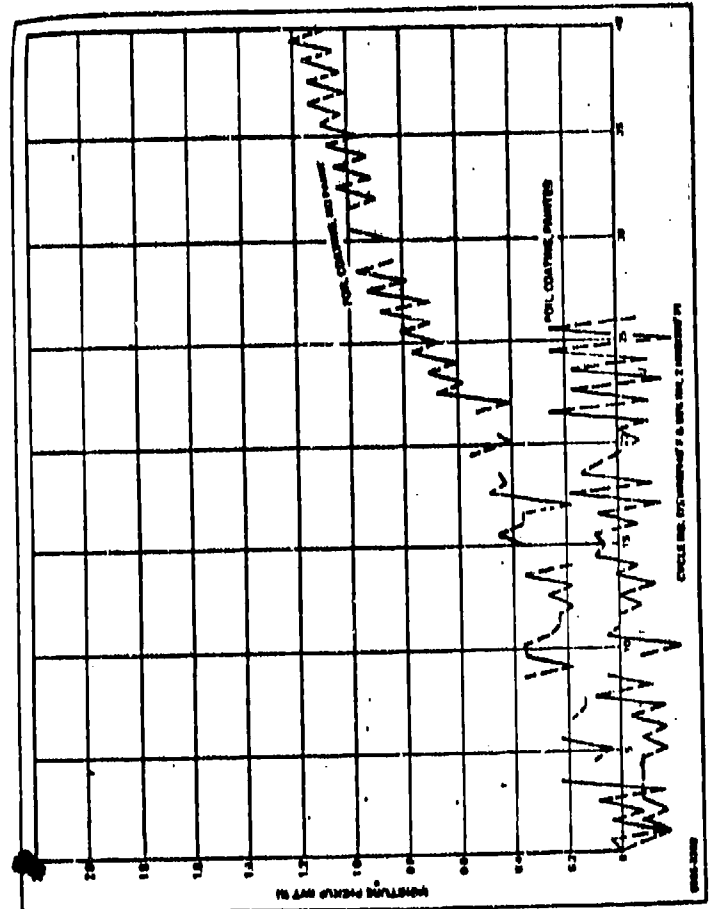
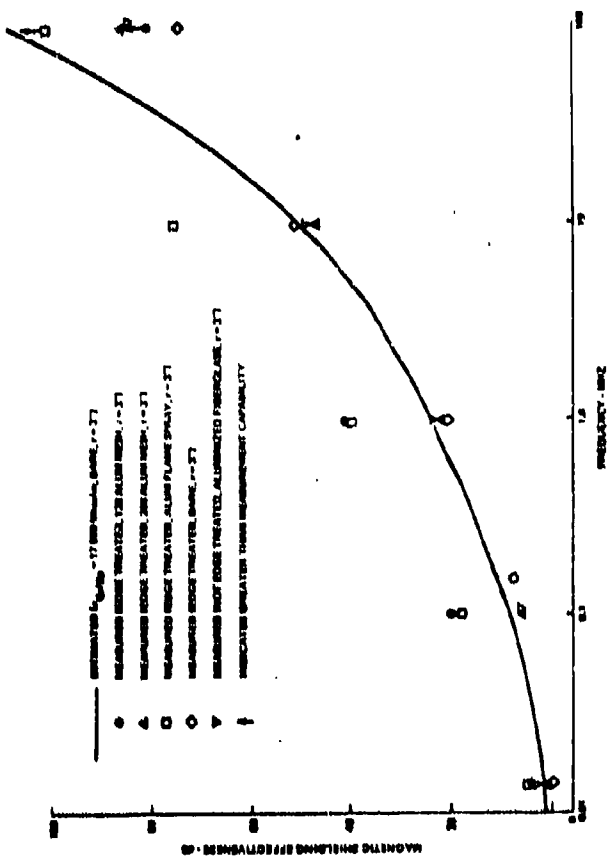
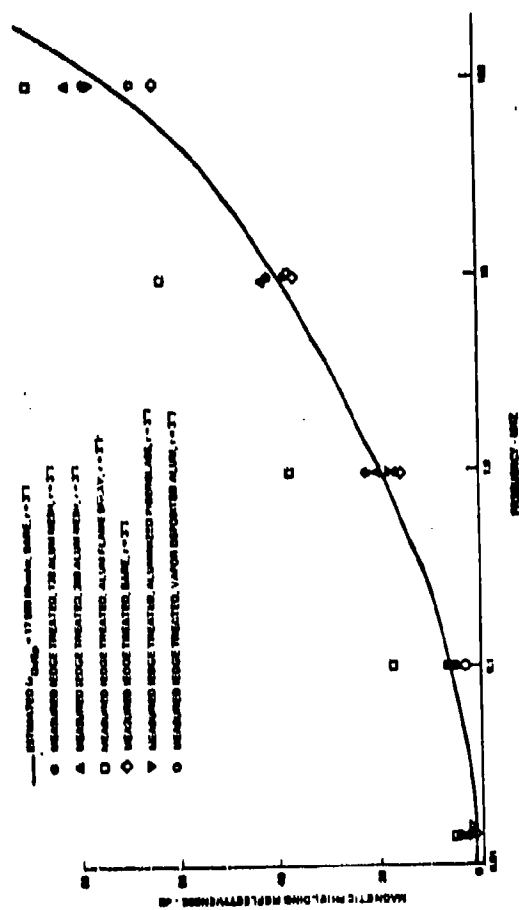
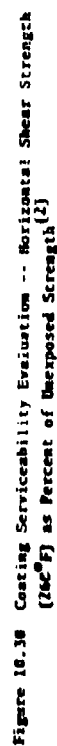
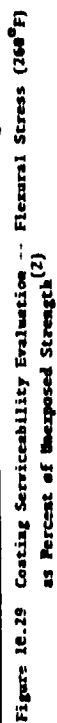
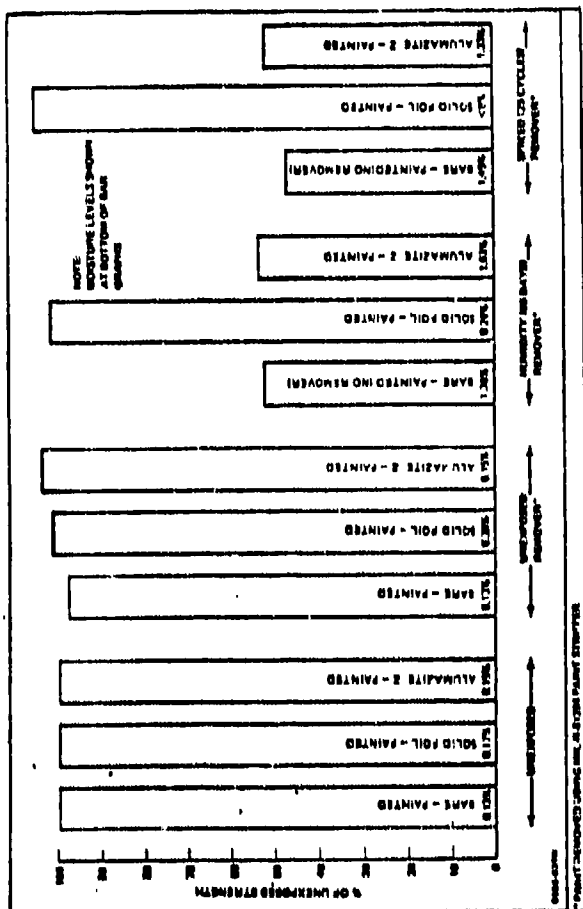
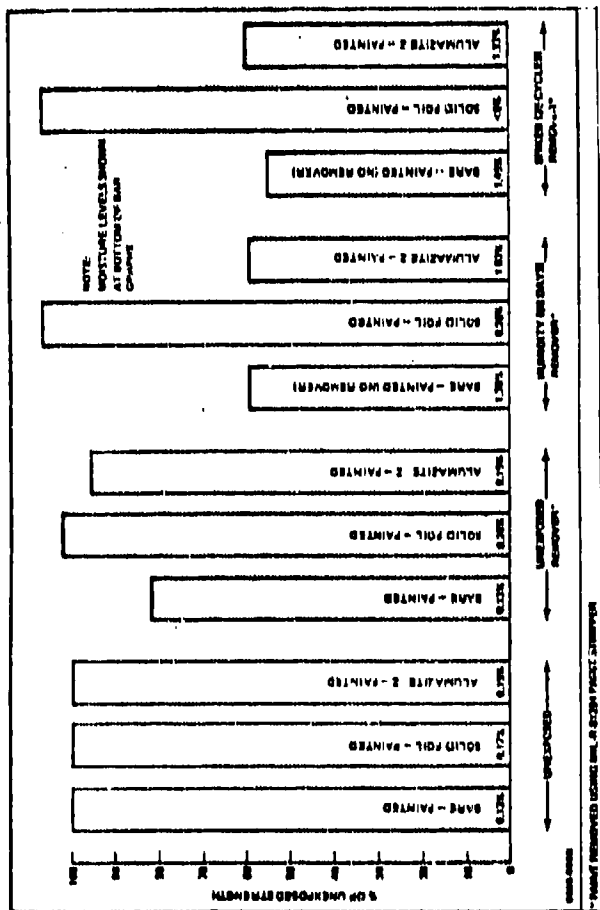


Figure 18.27 Effect of Paint Protection on Moisture Pickup



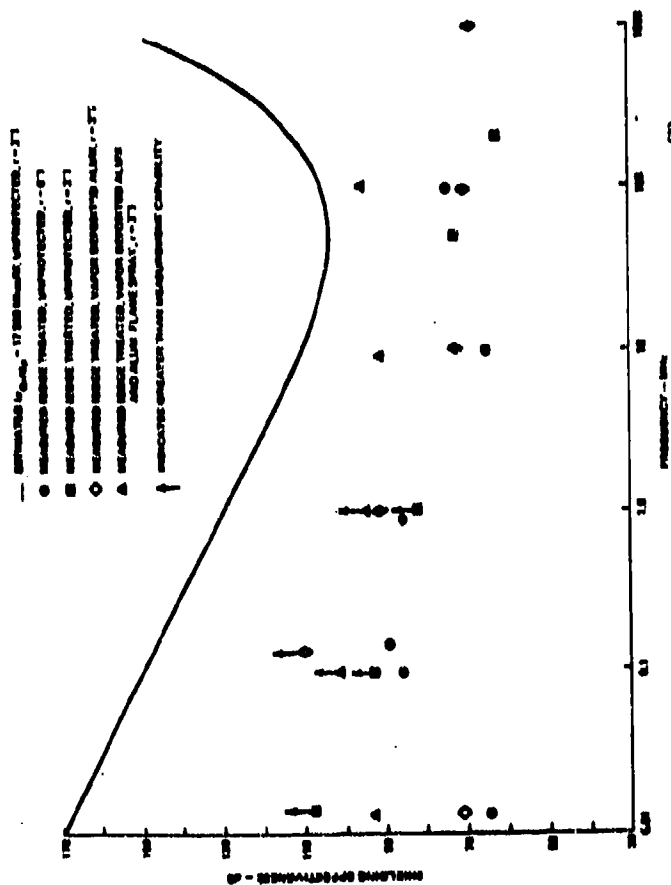


Figure 18.33 Electric Shielding Effectiveness for 12-ply Graphite/Epoxy Panel (3)

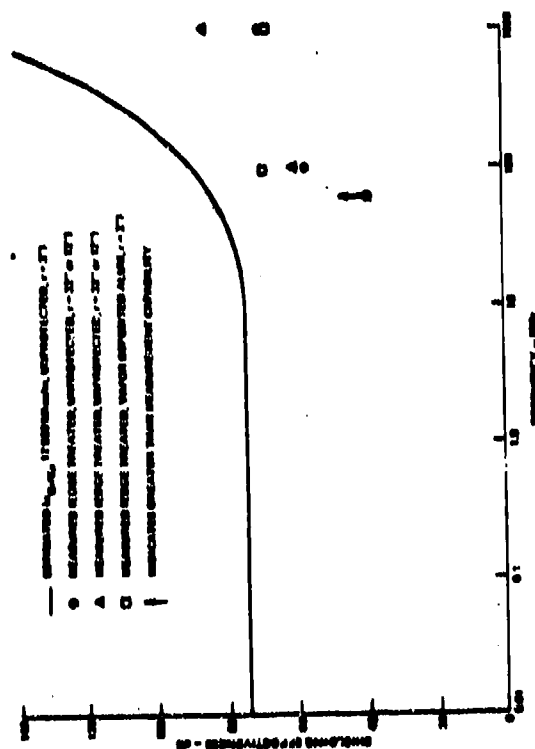


Figure 18.35 Plane Wave Shielding Effectiveness for 12-ply Graphite/Epoxy Panel (3)

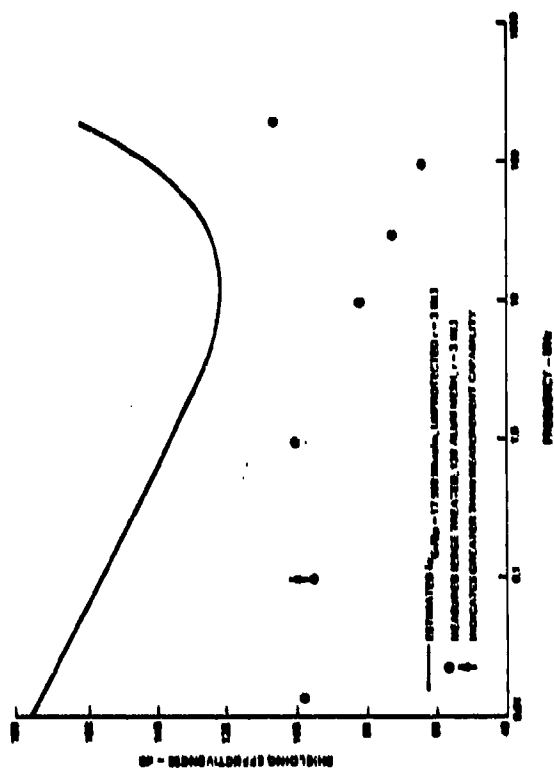


Figure 18.34 Electric Shielding Effectiveness for 24-ply Graphite/Epoxy Panel (3)

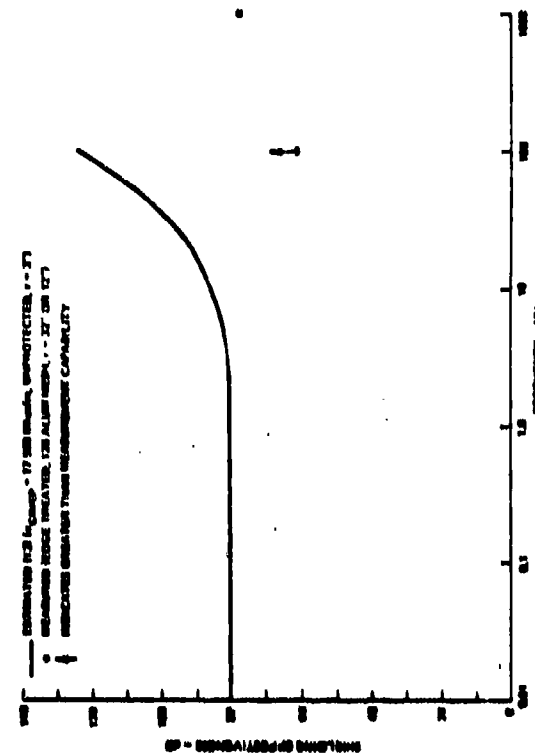


Figure 18.36 Plane Wave Shielding Effectiveness for 24-ply Graphite/Epoxy Panel (3)

Table 10.3 Shielding Effectiveness Measurements⁽³⁾

PROTECTION SYSTEM	NUMBER OF PLYS	SHIELDING MEASUREMENTS		
		H-FIELD	E-FIELD	PLAN WAVE
Bare	12	X	X	X
	24	X		
120 Aluminum Mesh	12	X	X	X
	24	X		
200 Aluminum Mesh	12	X		
	24	X		
Aluminum Flame Spray (4-6 MILs)	12	X		
	24			
Vapor-Deposited Aluminum	12	X	X	X
Aluminum Flame Spray and Vapor-Deposited Aluminum	12	X	X	
Aluminized Fiberglass	12	X		
	24	X		

The doping of graphite fibers is similar to doping a semiconductor by introducing an impurity into the crystal. Results have indicated an increase in fiber conductivity by a factor of 50 in some cases, however the doping process may be hard to control.

Intercalation is the process of inserting metallic or nonmetallic chemical species between graphite crystal layers in graphite fibers. Very dramatic increases have been reported for pure intercalated graphite with conductivities about the same as copper or silver. For commercially available fibers, the resulting intercalated fiber conductivities are about 20 to 40 times that of the regular fiber. These results could probably be improved significantly if more care was taken in the graphite fiber manufacturing process to ensure a more perfect graphite fiber crystal structure.

10.3

References

1. S. D. Schneider, C. L. Kendricks and G. O. Olson, Vulnerability/ Survivability of Composite Structures - Lightning Strike, Vol. 1 (Program Results) and Vol. 2 (Design Guidelines), Boeing Corp. AFFDL-TR-77-127, Feb. 1978.
2. C. J. Staehler and B. F. Simpers, Metallic Coating For Graphite/ Epoxy Composites, Grumman Aerospace Co., prepared for NAVAIR, May 1979.
3. Protection Optimization for Advanced Composite Structures, Grumman Aerospace Co., Fourth Quarterly Progress Report, June 1978.
4. Advanced Composite Aircraft Electromagnetic Designn and Synthesis, SRC-TR-79-490 April, 1980.
5. J. A. Davis, Atmospheric Electricity Protection for Electric and Electronic Systems, Federal Aviation Administration Report No. AAC-213-15 April, 1975.

In this chapter, the information developed and discussed in the previous chapters is condensed into a set of guidelines for designing electromagnetic compatibility into composite aircraft. The approach taken in developing the guidelines is to represent the overall voltage transfer function from external field to internal electronic device feed point as a cascaded set of transfer functions, each one involving only a portion of the whole process. Guidelines are then given for each portion separately.

Section 11.1 describes in general terms the required interaction of a number of separate disciplines to produce a compatible composite aircraft. A description is given of the individual transfer functions that collectively describe the voltage induced at an interior device port as a result of an external electromagnetic field.

Section 11.2 specifically describes each individual transfer function and gives guidelines for its use.

Section 11.3 provides a baseline case, an unprotected composite aircraft, as an example to which the guidelines can be applied. The analysis for this case provides an estimate of the amount of protective shielding that will be required for compatibility.

Section 11.4 provides characteristics on various protective devices used on aircraft to protect against external fields. Simple tradeoff guidelines are estimated to allow required protection to be chosen at minimum weight and least cost.

11.1 Overview

The earlier chapters in the handbook tended to focus on certain individual aspects of composite materials. For example, Chapter 2 treated electromagnetic threats; Chapter 5, intrinsic material properties, and Chapter 7, subsystem susceptibilities. The material typically took the form of formulas and/or diagrams which often had little obvious connection to material found in other chapters. Such analysis, although indispensable for understanding composite material behavior, tends to obscure the fundamental fact that an integrated, interdisciplinary, "total" systems approach is required in all (not just later) phases of aircraft system design when working with composite materials. This procedure is in contrast to procedures used for metallic aircraft of earlier times. Then, the structural, avionic and electromagnetic parts of system design could proceed separately in the early stages. Unification of the parts took place in the later, detailed design phases and usually was accomplished without significant cost or time overruns. For composite aircraft, a number of individual disciplines must be combined (usually on a computer) using mathematical models and/or measurements to produce designs having the required structural, avionic and electromagnetic properties. The situation is illustrated in Figure 11.1. Because such properties are interdependent and rarely optimum, tradeoffs among the system parameters usually are required. The crucial point to be made here is that the use of a few isolated disciplines to determine even preliminary aircraft design, an acceptable strategy for earlier generations

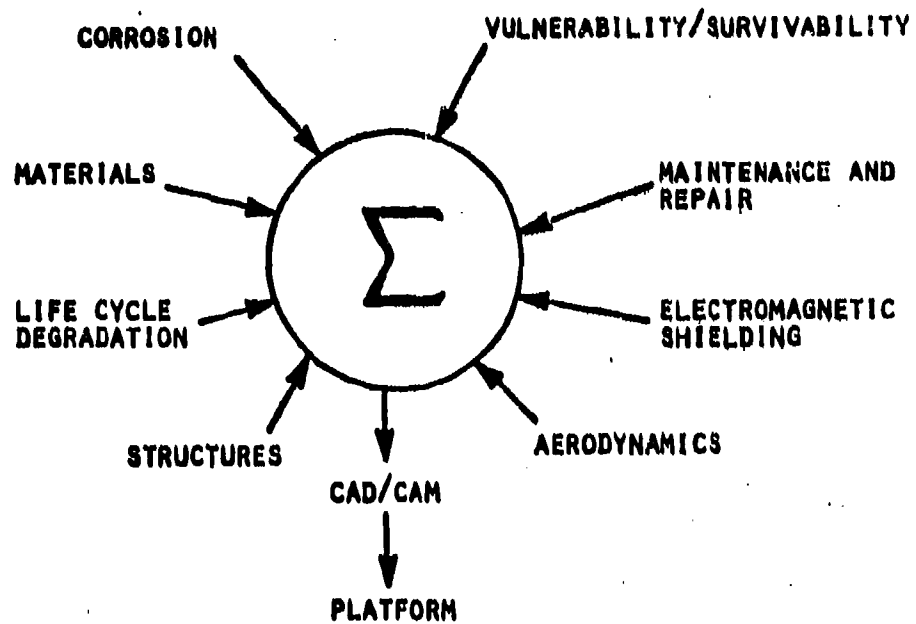


Figure 11.1 Integrated, Multidiscipline Approach
To Composite Aircraft Design

of metallic aircraft and their electronics, is unacceptable for composite aircraft and its electronics. For example, using aluminum foil over a graphite/epoxy panel can solve electromagnetic shielding problems but not corrosion, maintenance or repair problems. A special coating over a composite surface can solve corrosion problems but the weight penalty may be too great and the electromagnetic shielding too poor. Without a "total" systems approach to designing with composites, the final result may be electronically incompatible and require costly and time consuming fixes if, indeed, such fixes can be found. Even if a compatible design is produced the lack of a "total" systems analysis compatibility means the ability is lost to gauge quickly the impact upon composite system performance of rapidly changing technologies and military postures. Such an inability would make the future vulnerability/survivability of a presently sound composite aircraft difficult and/or expensive to determine.

To prevent such shortcomings, a set of design guidelines for the use of composite materials on aircraft is clearly required. This chapter will develop and discuss composite electromagnetic design guidelines only. Such guidelines can be used by design engineers in assessing the electromagnetic performance of composite aircraft at any stage in the system procurement cycle. Although the guidelines focus on the electromagnetic aspects of system performance, the effects of other factors on electromagnetic performance, as illustrated in Figure 11.1, will be taken into account when developing the guidelines.

An overview of the general problems of electromagnetic compatibility for a composite aircraft is given in Figure 11.2. An aircraft, composed in some part of composite materials, is situated in a perturbing electromagnetic environment. One quantity of interest is the frequency dependent open-circuited voltage $V_{ij}(f)$ induced at ports on avionic and other electromagnetic equipment boxes by the external electromagnetic fields. Such voltages must be sufficiently small to prevent avionic or electronic subsystem incompatibility, upset or burnout. They can be estimated by expressing them as a sum of the frequency-dependent transfer functions $D(f)$, $T_1(f)$, $T_2(f)$... $T_6(f)$ as shown in Figure 11.2. $D(f)$ is the intensity of the external electromagnetic fields $T_1(f)$, the material airframe electromagnetic shielding function; $T_2(f)$, the shielding influence of the airframe shape; $T_3(f)$, the joint leakage term; $T_4(f)$, the cable shielding term; $T_5(f)$ the subsystem susceptibility term, and $T_6(f)$, a term that reflects the protection methods used in the system. Each of these terms will be discussed in the following sections. The results will constitute a set of guidelines to be used to design electromagnetic compatibility into a composite aircraft and will form a basis from which tradeoff studies involving weight, cost and protection can be performed.

11.2 Electromagnetic Design Guidelines

In the following section, electromagnetic design guidelines for aircraft using composite materials will be developed and discussed. These guidelines summarize the detailed findings in the earlier chapters of the handbook and present the results in the form of diagrams and tables. The guidelines are organized in such a way that the evaluation of the transfer functions $D(f)$, $T_1(f)$, $T_2(f)$ --- $T_5(f)$ is straightforward. The protection transfer function, $T_6(f)$, is discussed in Section 11.4.

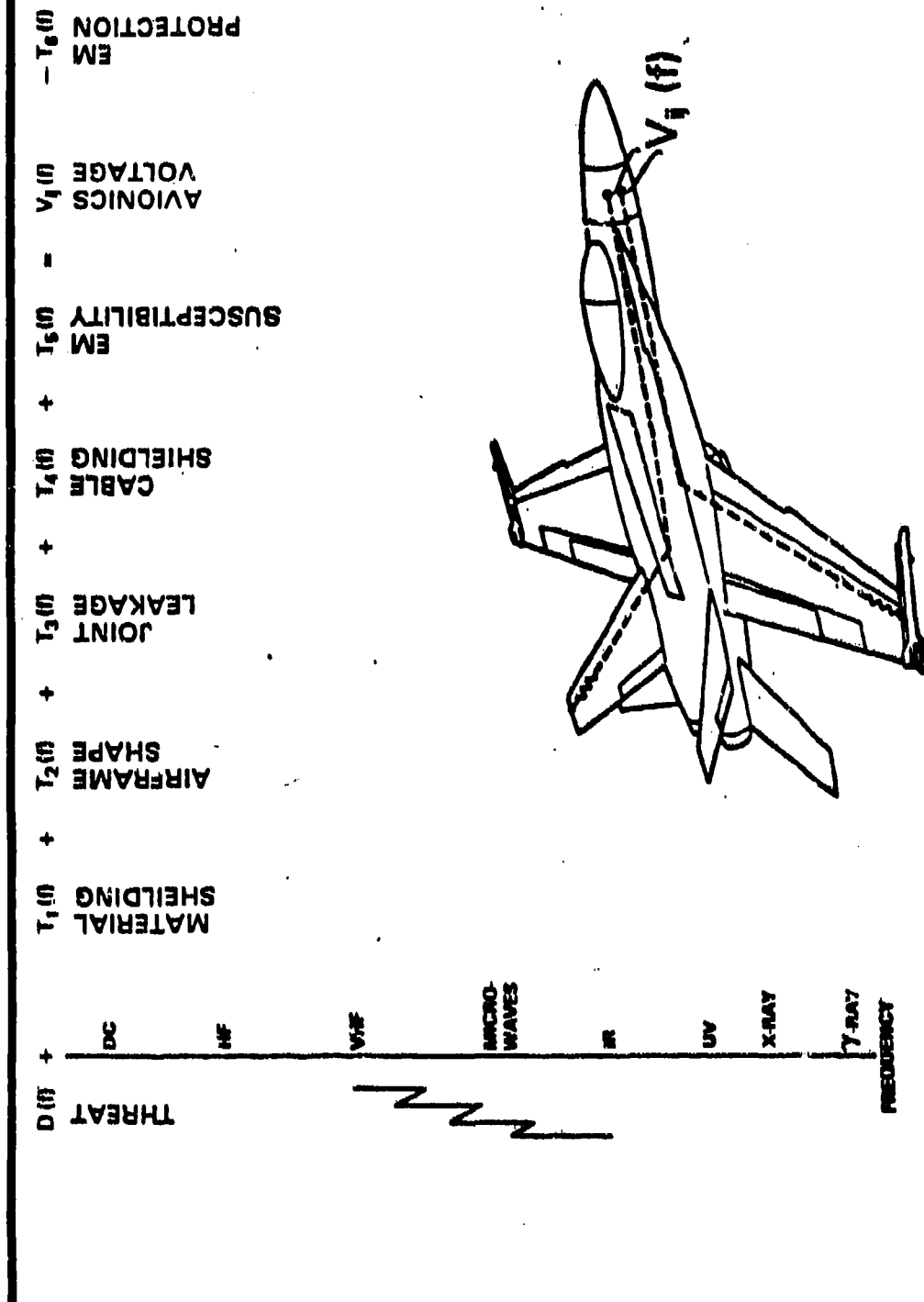


Figure 11.2 Composite Aircraft Electromagnetic System Parameters

11.2.1 External Electromagnetic Fields

The external electromagnetic fields are presumed to arise from lightning, nuclear electromagnetic pulse (NEMP), radio frequency (RF) and high energy laser radiation and precipitation static discharge. A suitable combination of these threats will determine the frequency dependent transfer function $D(f)$.

The lightning, NEMP and laser threats are summarized in Figure 11.3. The threat amplitudes are given as a function of frequency and allow the determination of $D(f)$ in terms of field strength. The precipitation static spectrum is similar to lightning but is many orders of magnitude smaller and is not shown.

The RF threat spectrum is given in Figures 11.4 and 11.5 as a function of frequency. Two cases are considered. Figure 11.4 is a general unclassified RF environment extending from 10 kHz to 100 GHz. The RF fields are made up of a variety of commercial and military transmitters. Figure 11.5 is similar to Figure 11.4 but considers the RF environment in the vicinity of a Navy carrier. In this case, only communication and high powered radars are considered. The information from these figures can be used to estimate the field strengths incident on an aircraft containing composites under a variety of external field conditions.

11.2.2 Electromagnetic Shielding [$T_1(f)$ and $T_2(f)$]

The electromagnetic shielding provided by composite shields differs substantially from that provided by metals. This lack of shielding is due to the different electrical properties of composites, notably poor conductivities, when compared to those of metals. A summary of composite intrinsic electrical properties is given in Figure 11.6 while a comparison of composite and metallic conductivities is shown in Figure 11.7. From these data, graphite/epoxy is seen to have the highest conductivity of the composites surveyed. Even so, it is still about 3800 times less conductive than aluminum and qualifies as only a fair conductor. Boron/epoxy is much less conductive than graphite/epoxy while Kevlar is a nonconducting dielectric. Compared to aluminum, graphite/epoxy will offer reduced shielding; boron/epoxy, poor shielding, and Kevlar no shielding at all in the frequency spectrum of interest (up to 18 GHz).

The standard measures of electromagnetic shielding of a material shield are the magnetic and electric shielding effectiveness, S_H and S_E . These quantities are defined in terms of external and internal electromagnetic fields as:

$$S_H = 20 \log_{10} \frac{H^{EX}}{H^{IN}} \quad (11-1)$$

$$S_E = 20 \log_{10} \frac{E^{EX}}{E^{IN}} \quad (11-2)$$

THREAT (D)

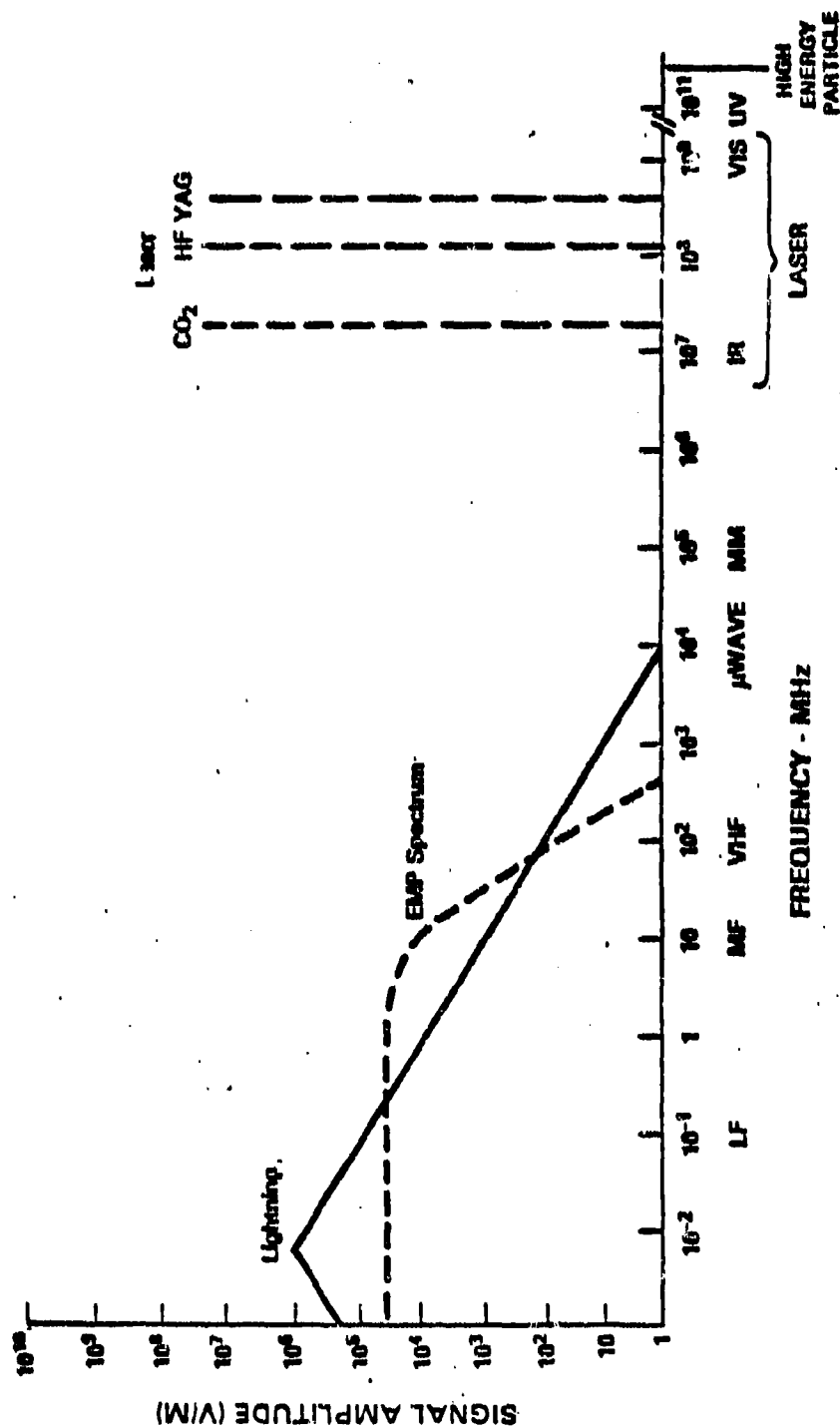


Figure 11.3 Threat Spectrum

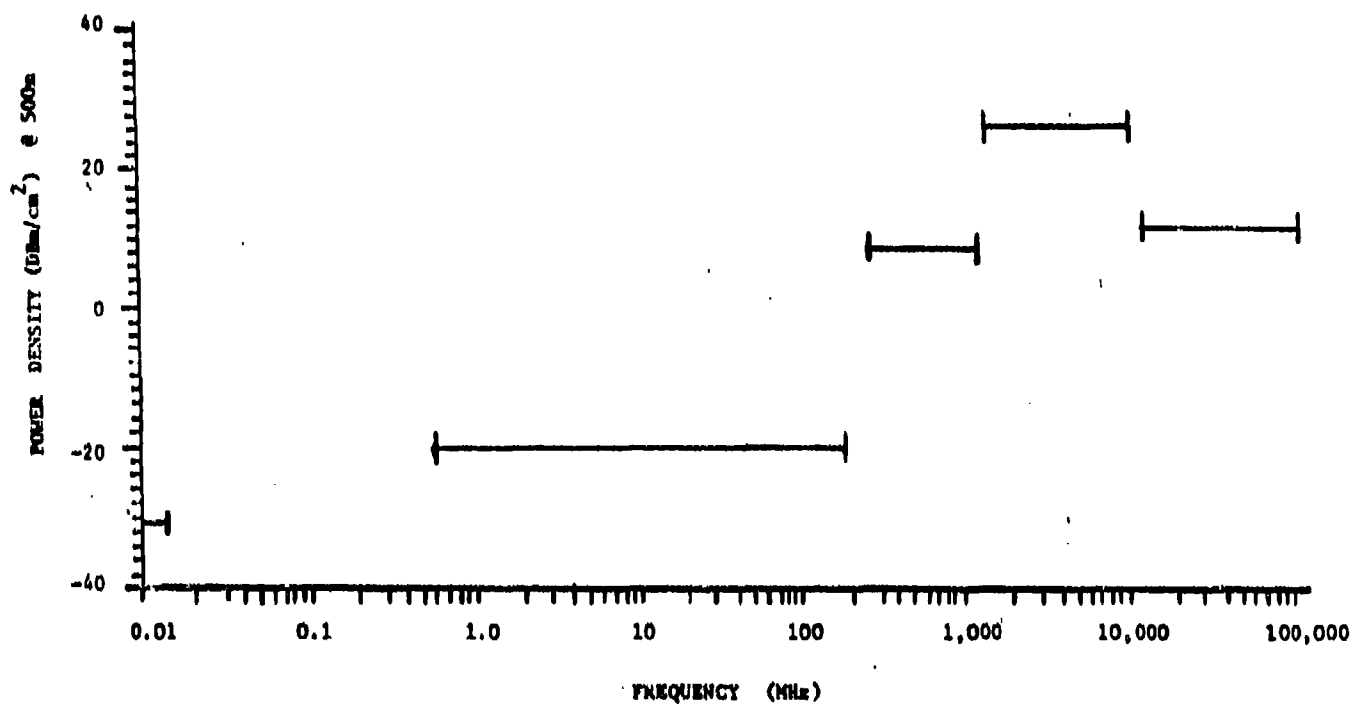


Figure 11.4 RF Signal Threat

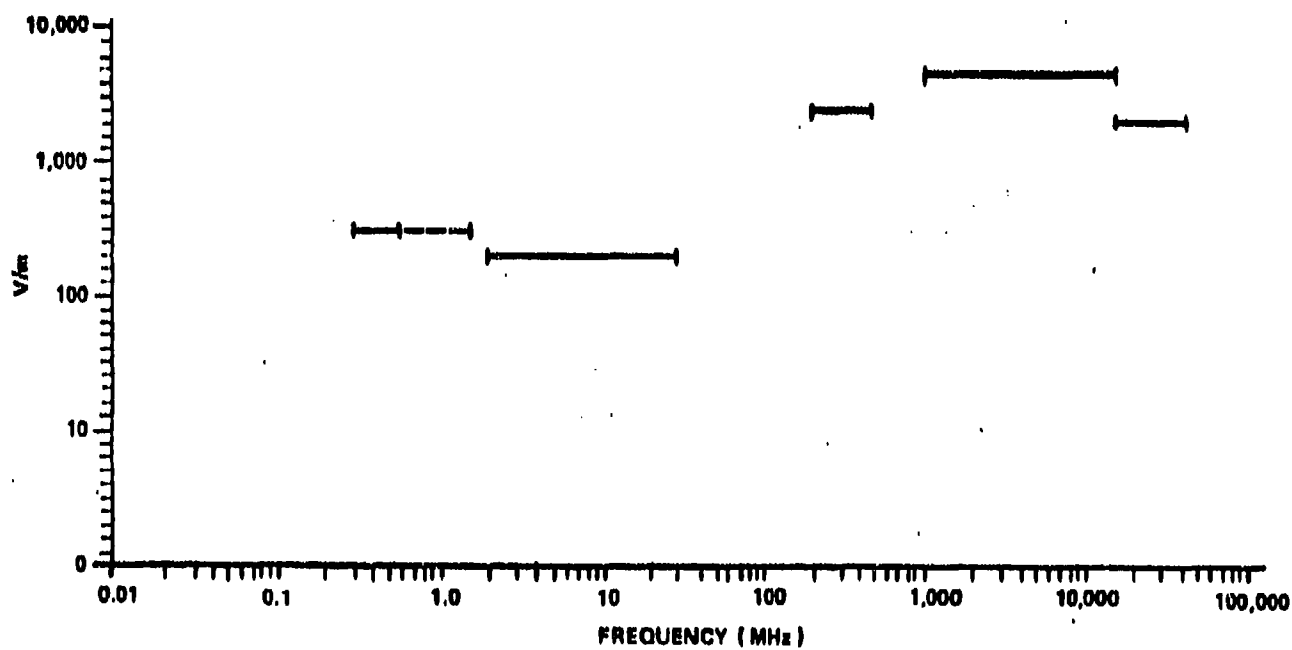


Figure 11.5 Transmitter Strengths on Carrier Flightdeck

	<u>Graphite/Epoxy</u>	<u>Boron/Epoxy</u>	<u>Kevlar</u>
Permeability μ_R	1	1	1
Permittivity ϵ_R	Indeterminant	5.6	3.6
DC Conductivity (mhos/m)			
longitudinal σ_L	$2(10^4)$	30	$6(10^{-9})$
transverse σ_T	100	$2(10^{-8})$	$6(10^{-9})$
Anisotropy Ratios (σ_L/σ_T)	200	$1.5(10^9)$	1
High Field Thresholds			
longitudinal			
E_{NL} (volts/m)	250	not	not
J_{NL} (amps/m ²)	$4(10^3)$	measured	measured
transverse			
E_{NL} (volts/m)	4000	not	not
J_{NL} (amps/m ²)	$1(10^4)$	measured	measured

Figure 11.6 Summary of Composite Material Intrinsic Properties

MATERIAL CONDUCTIVITY

Low Composite Material Electrical Conductivity
Provides Low Electromagnetic Shielding.

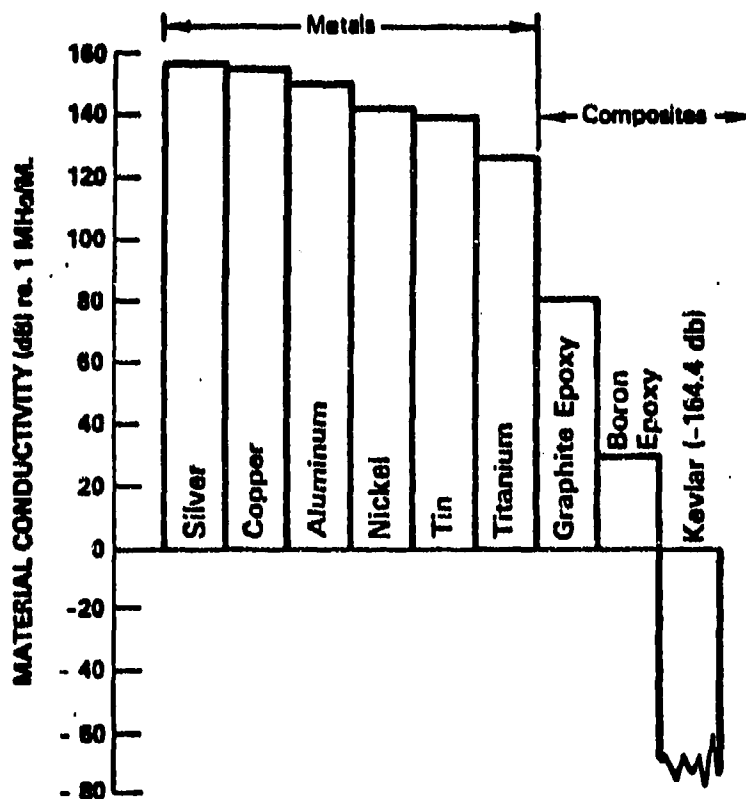


Figure 11.7 Material Conductivities

Considerable published measured data exists for both S_E and S_H for various materials. Published results for graphite/epoxy are given in Figure 11.8 along with theoretical curves. Considerable variation in the measured results is apparent, especially for low frequency S_E . The reasons for this variation are that S_H and S_E not only depend on the shield material but also on the shape of the shield, the nature of the incident field and even the configuration of the test apparatus. The latter fact, in particular, explains why two carefully conducted, but different, shielding experiments may produce very different results. The values for S_H and S_E may be correct for the test apparatus in question, but they cannot be used to characterize accurately the shielding for any other test apparatus or for different material shapes in the same test apparatus.

The electromagnetic shielding for composite materials is illustrated in Figure 11.9 for a small cylindrical test sample and is compared to the shielding of aluminum. Only S_H for aluminum is shown since $S_E > 200$ dB in this frequency range. The electric shielding, S_E , is high at low frequencies and decreases at higher frequencies. The magnetic shielding S_H has the opposite behavior. Both shielding terms are larger for higher conducting materials for a fixed frequency. There exists a frequency (called the cutoff frequency) below which the magnetic shielding is essentially zero. The poorer the material conductivity, the larger this frequency. Figure 11.9 can be used to design $T_1(f)$ for a particular shape and illustration.

If the shape of the material shield changes, the electromagnetic shielding changes. The effect of the shape on magnetic shielding is illustrated in Figure 11.10 for certain generic shapes. High shielding effectiveness is evident for a single flat plate. Such a shape is called an "open" geometry. Aircraft structures, however, are "closed" geometries and are better represented by two parallel plates, a cylinder or a sphere. Such geometries do not provide good uniform shielding across the spectrum but rather have a cutoff frequency below which the shielding is effectively zero. For more general shield geometries illuminated by uniform external fields, the critical shape parameter is the volume-to-surface area ratio. For uniform magnetic fields, the magnetic shielding effectiveness increases for larger $\frac{V}{S}$. Thus, a structure with large $\frac{V}{S}$, like a bomber, has greater magnetic shielding than a structure like a missile with a small $\frac{V}{S}$. Electric shielding effectiveness will tend to behave the opposite way.

To design using S_E and S_H , shielding effectiveness curves analogous to Figures 11.8 - 11.11 must be constructed for the particular composite shield material and for the shape the shield will be. Figures 11.9 - 11.11 assume uniform electromagnetic fields. For nonuniform fields, the shielding will be different. Finally, if attempts are made to measure the shielding to verify design specifications, the experimental test setup can affect the results significantly. Clearly, S_E and S_H are very tricky parameters to use for designing $T_1(f)$ and $T_2(f)$ shielding transfer functions because of their sensitivity to factors other than composite material properties.

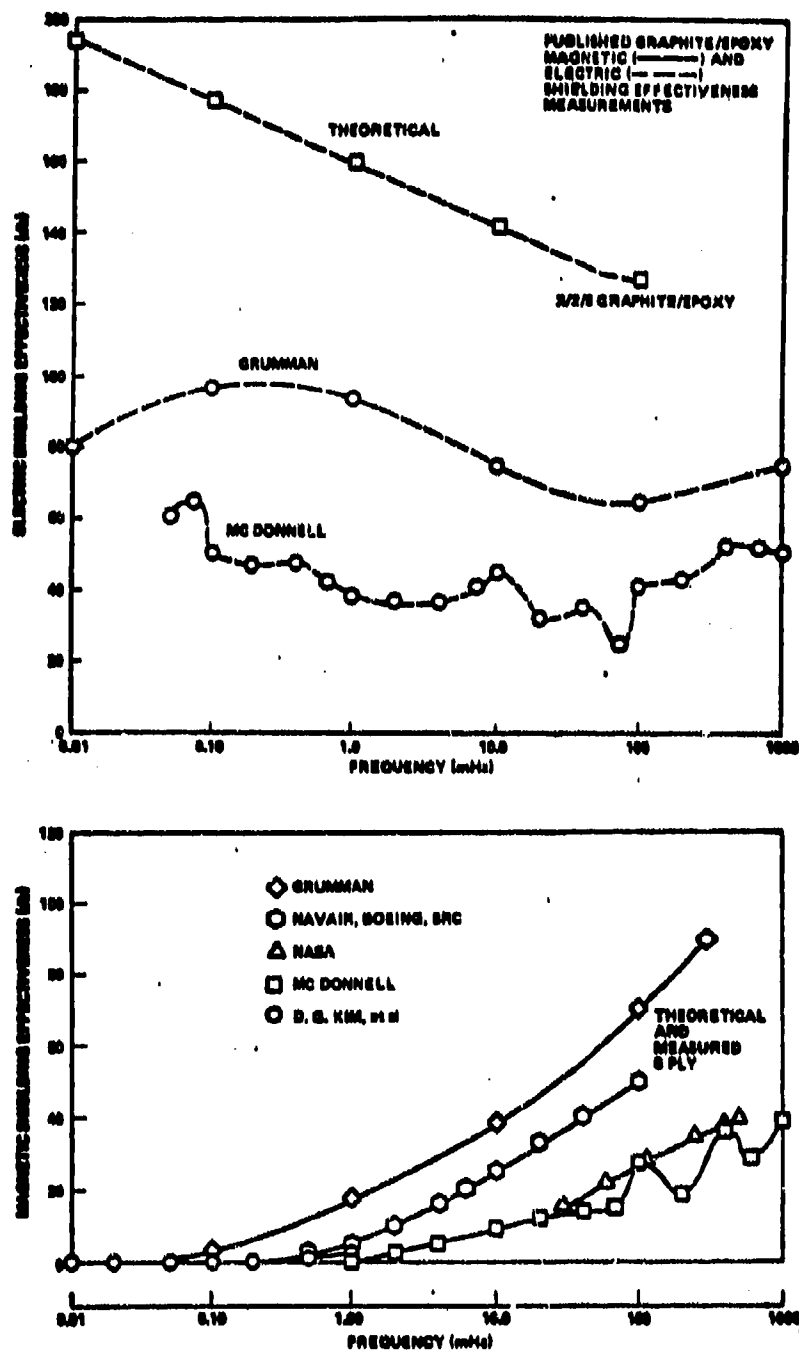


Figure 11.8 Published Graphite/Epoxy Shielding Data

Composite Material Electromagnetic Shielding

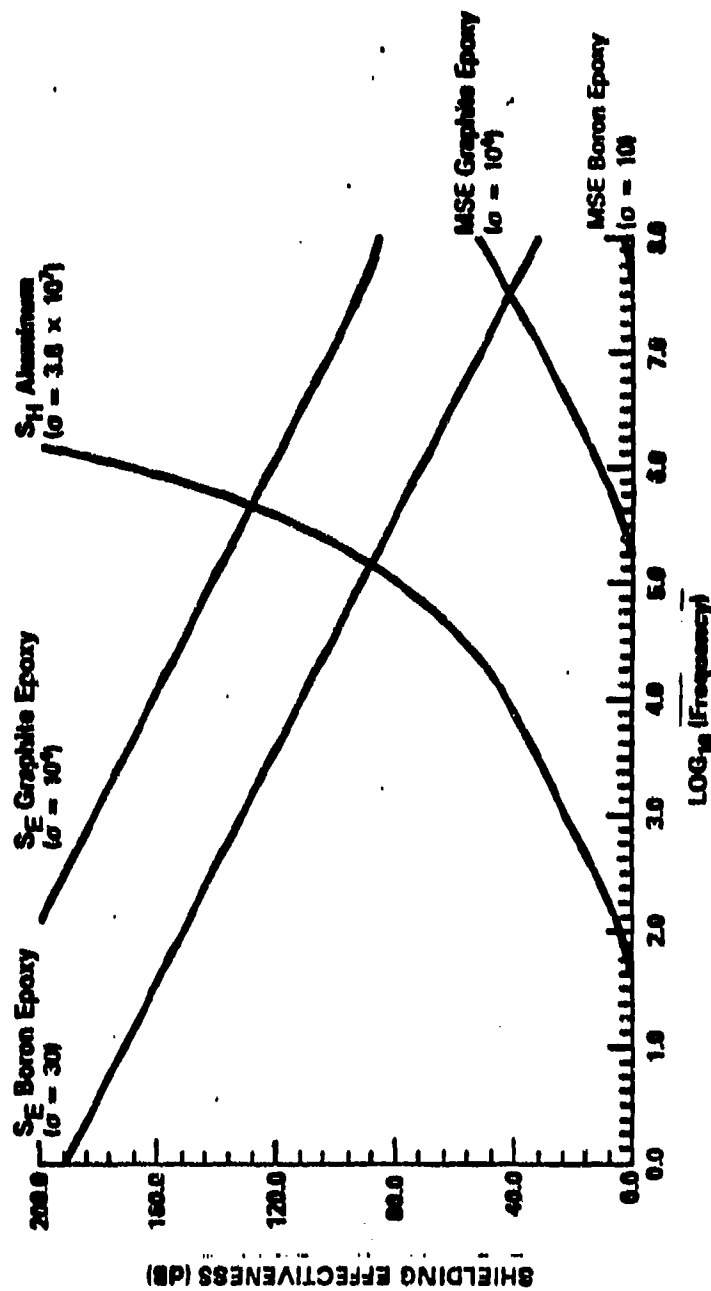


Figure 11.9 Composite Material Electromagnetic Shielding
For 8-Ply Material (0.00107 m) Thickness

AIRFRAME SHAPE (T_2)

The Shape of an Aircraft Influences EM Coupling

MAGNETIC SHIELDING EFFECTIVENESS for a Uniform Incident Magnetic Field. SHIELD CONDUCTIVITY = $10^6 \text{ } \Omega/\text{m}$. Shield Thickness = 0.00107 m (CORRESPONDING TO 8 PLY Composite Material at 0.00525 ln/Phy)

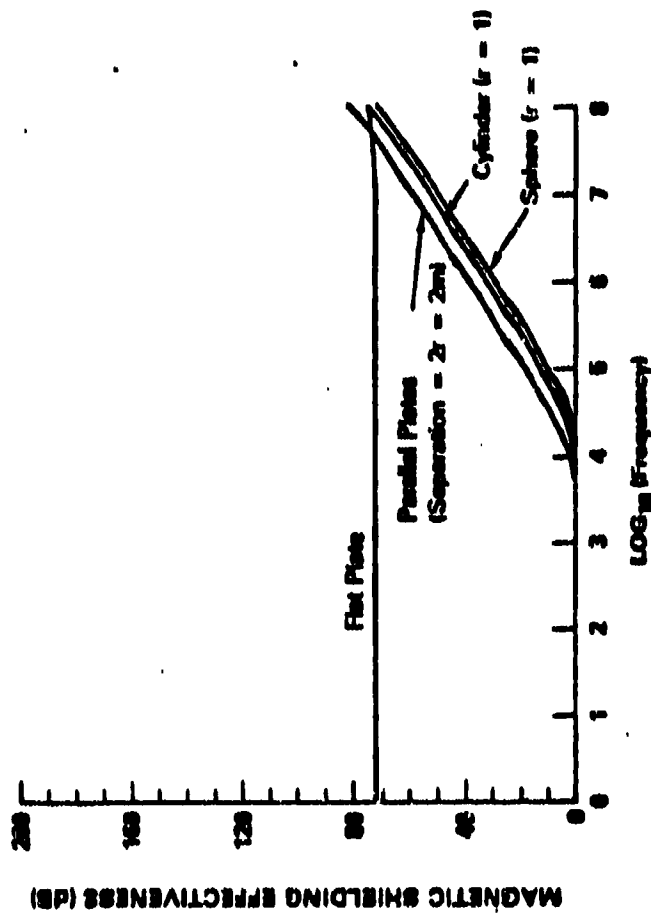


Figure 11.10 Magnetic Shielding Effectiveness for Various Shapes

AIRFRAME SHAPE (T_2)

MAGNETIC SHIELDING EFFECTIVENESS of an Enclosure Under a Uniform Magnetic Field as a Function of Volume-To-Surface Ratio. SHIELD CONDUCTIVITY = $17500 \text{ } \Omega/\text{m}$. Shield Thickness = 0.00107 m (CORRESPONDING TO 8 PLY Composite Material at 0.00525 ln/Phy)

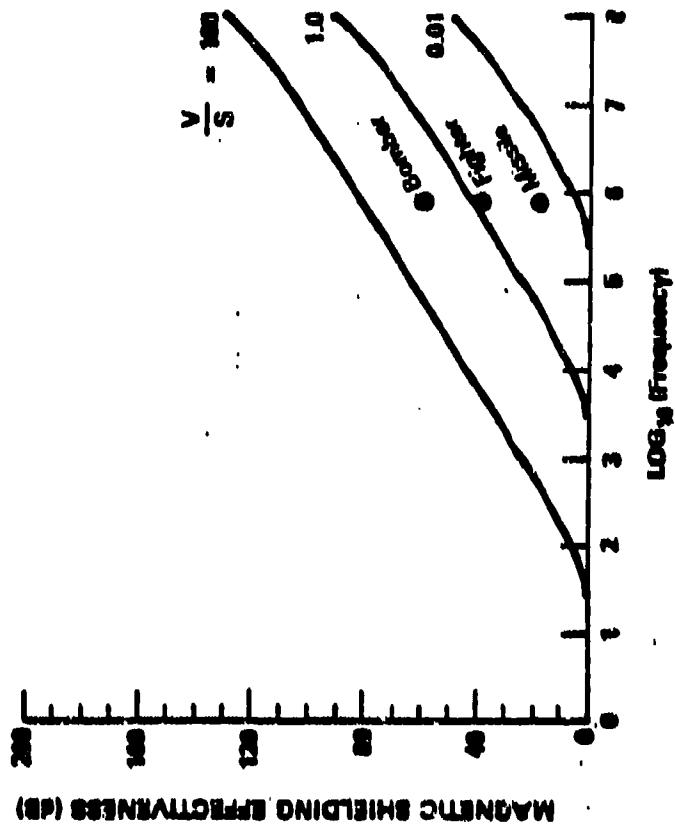


Figure 11.11 Magnetic Shielding Effectiveness for Various Shapes

A more promising shielding design parameter, valid for shields whose local radius of curvature is large with respect to wavelength in the shield, is the surface transfer impedance. This parameter is defined by

$$Z_{ST} = \frac{E_{TAN}^{IN}}{J_s^{EX}} \quad (11-3)$$

where E is the tangential component at the shield surface of the internal electric field, while J_s^{EX} is the external surface current density. An equivalent relation, valid for all frequencies, is

$$Z_{ST} = N \operatorname{csch}(vd) \quad (11-4)$$

where $N = (j\omega\mu/\sigma)$ is the intrinsic impedance of the shield; $v = (j\omega\mu\sigma)$, the propagation factor and d , the shield thickness. These quantities depend only on the composite intrinsic properties (μ, σ) and on the angular frequency (ω). Consequently, the material shape does not influence transfer impedance - material transfer impedances for different shapes and the same. This is the advantage of Z_{ST} over S_E and S_H and makes it a much better shielding design parameter.

The low frequency asymptote of Z_{ST} is given by

$$Z_{ST} = \frac{1}{\sigma d} \quad (11-5)$$

which is a very simple function of material properties and shield thickness. The transfer impedance is shown in Figure 11.12 for composites, aluminum and titanium for thicknesses corresponding to 8-ply composite (0.001069m). These curves can be used to design $T_1(f)$.

The effect of shape on the electromagnetic shielding can be ascertained from the relationship between shielding effectiveness and transfer impedance. For homogeneous, conducting shield

$$S_E = 20 \log_{10} \frac{Z_E}{Z_{ST}} \quad (11-6)$$

$$S_H = 20 \log_{10} \frac{Z_H}{Z_{ST}} \quad (11-7)$$

where $Z_E = (8\pi\epsilon f / (v/5))^{-1}$

and $Z_M = (\mu/\epsilon)^{1/4}$ for a flat plate

$Z_M = j\omega\mu \frac{v}{s}$ for a cylindrical, spherical or parallel plate enclosure.

Here ϵ is the material permittivity; μ , the material permeability; ω , the angular frequency, and $\frac{v}{s}$, the volume-to-surface area ratio. The quantities

MATERIAL THICKNESS CORRESPONDS TO 8 PLY COMPOSITE
MATERIAL AT 0.00525 IN/PLY

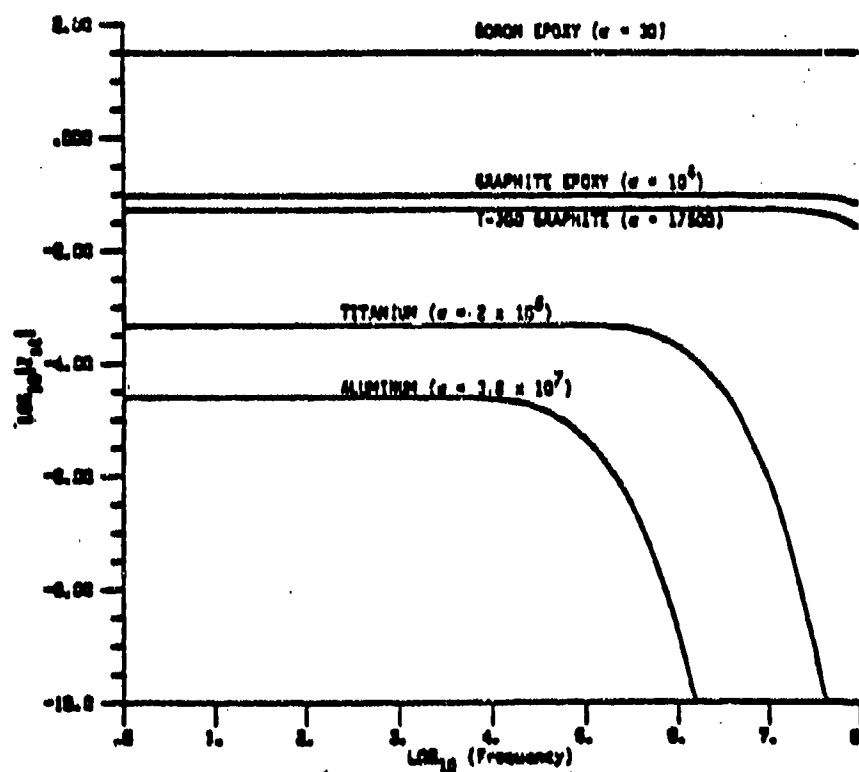


Figure 11.12 Surface Transfer Impedances for Different Materials

Z_E and Z_M will vary with shield geometry and with the nature of the illuminating electromagnetic field.

To design $T_1(f)$ and $T_2(f)$, the transfer impedance (material-dependent only) is combined with an appropriate shape factor to produce the required shielding effectiveness.

11.2.3 Joint Leakage [$T_3(f)$]

The leakage of electromagnetic energy through composite joints, though very important, has been difficult to assess until recently. Part of the reason is that composite joint technology has been viewed largely as a structural and manufacturing problem. In fact, composite joint technology is a prime example of how the manufacturing process together with structural and electromagnetic design considerations must all interact if a joint that has both structural and electromagnetic integrity is to be produced.

Aircraft joints involve connecting two separate components by fasteners or adhesive. Because composite fibers are responsible for most of the material conductivity, most joints involving composites have significantly lower conductivity than that of the components being joined. This general result is due to the lack of fiber continuity across the joint. This problem will be particularly acute if, as has often been the case, a nonconducting adhesive is used thereby allowing electromagnetic energy to leak through the joint. The joint may be structurally sound but will not be electromagnetically "tight".

The most common aircraft joint is one joined with metal fasteners. In contrast to adhesively fastened joints, the use of proper fasteners allows better fiber-to-fiber electrical contact through the fastener. The conductivity is improved but still limited.

Other electromagnetic joint leakage problems can arise from the attempt to prevent galvanic corrosion between aluminum and composite, an acute problem for graphite/epoxy. The common solution, insertion of a dielectric coating between metal and composite panels, prevents corrosion but spoils the electromagnetic integrity of the structure by forming an aperture or slot.

Electromagnetic leakage through joints is described by a joint impedance or admittance. The admittance Y_J is defined by

$$\Delta v = \frac{J_g}{Y_J} \quad (11-8)$$

where Δv is the voltage across the joint and J_g is the current density flowing through the joint. Measured data has recently become available on a few joint types and is given in Figure 11.13. The joint admittance is fairly constant for low frequencies and gradually rises for high frequencies.

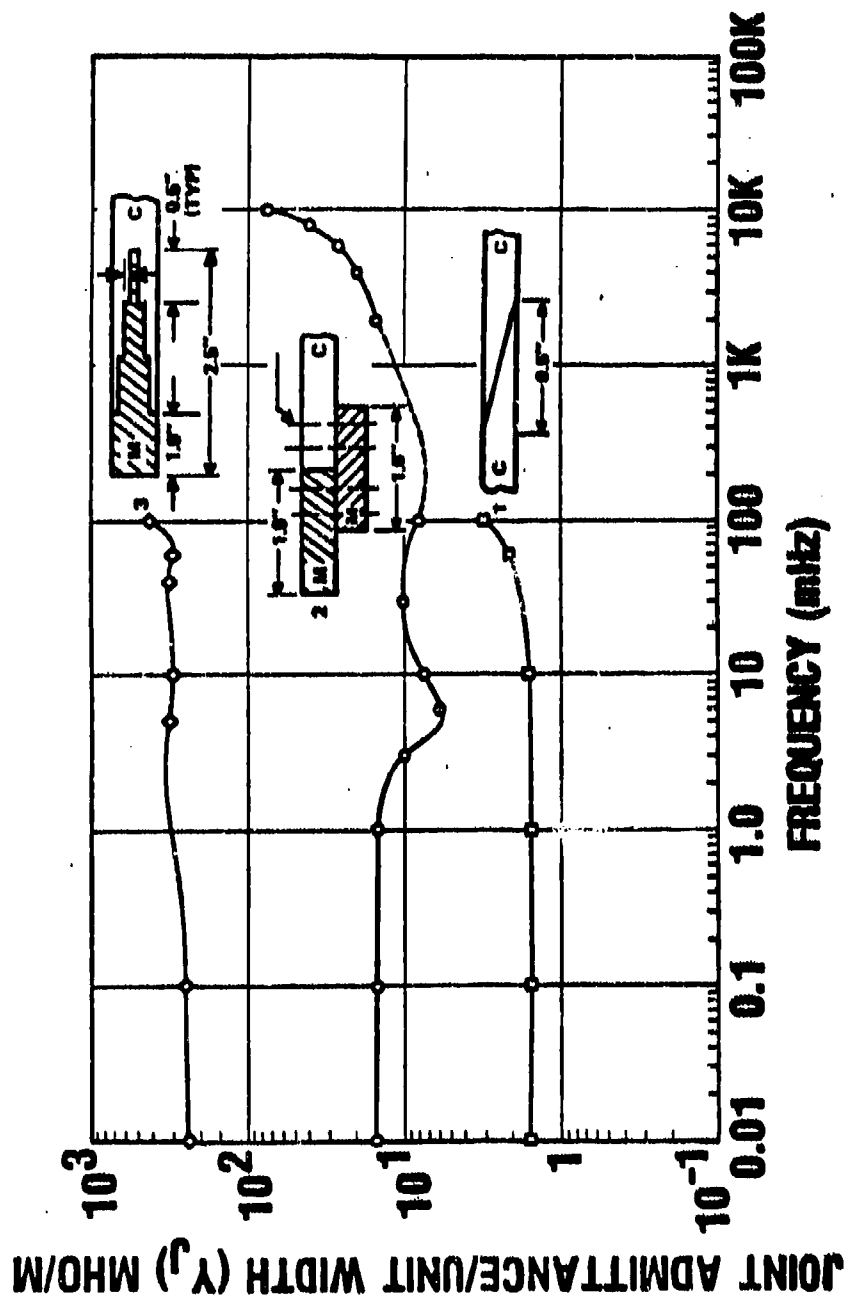


Figure 11.13 Joint Admittance/Unit Width as a Function of Frequency

A limited amount of work has been done to model joint admittances. For a butt joint, the joint admittance has been shown to be approximately

$$Y_j = \frac{\eta_A \eta_C \eta_A \eta_B}{\eta_A \lambda_A + \eta_C \lambda_C} - \frac{2j \ln(Ck_A W)}{\lambda_A \eta_A} - \frac{2j \ln(Ck_C W)}{\lambda_C \eta_C} \quad (11-9)$$

where η_A , λ_A , k_A and η_C , λ_C , k_C are the impedance, wavelength and wavenumber in regions "A" and "C" on either side of the joint of width W. The constant C is 0.2226.

Considerable work remains to be done to characterize and control joint leakage. Data on the effect of mechanical stresses and strains on joint admittances would be very useful. The current standard for joint impedance is 2.5 miliohms/meter which is satisfied only by specially manufactured graphite/epoxy joints.

11.2.4 Cables [$T_A(f)$]

The coupling of electromagnetic fields to internal cables and wiring is an extremely difficult problem for the general multicable, multi-wire bundles found in aircraft. The existence of significant composite structure in the airframe will affect the electromagnetic shielding and the nature of the field incident on the wiring.

This section will consider only the case of a uniform electromagnetic field incident on both a shielded and unshielded transmission line. Although simplified, this case does provide a means for estimating the voltage, current and power levels that occur on real aircraft cable systems.

An isolated two-wire transmission line is shown in Figure 11.14. The uniform E-field is assumed to be polarized parallel to the line and to strike it broadside. The line has characteristic impedance Z_0 , terminating impedances Z_1 and Z_2 , wire diameter a, wire separation b, and line length L. For lossless lines, the open circuit voltage and short circuit current can be shown to be

$$V_{oc}(t) = I_0(t) + \sum_{n=1}^{\infty} \Gamma^n (I_{2n} - I_{2n-1})$$

$$Z_0 I_{sc}(t) = I_0(t) + \sum_{n=1}^{\infty} (-\Gamma)^n (I_{2n} + I_{2n-1}) \quad (11-10)$$

$$I_n(t) = v \int_{nT_0}^{(n+1)T_0} E_0(t - \tau) d\tau$$

where v is the velocity of propagation on the line; $E_0(t)$ is the amplitude of the incident field; $T_0 = \frac{L}{v}$, and Γ , the voltage reflection coefficient

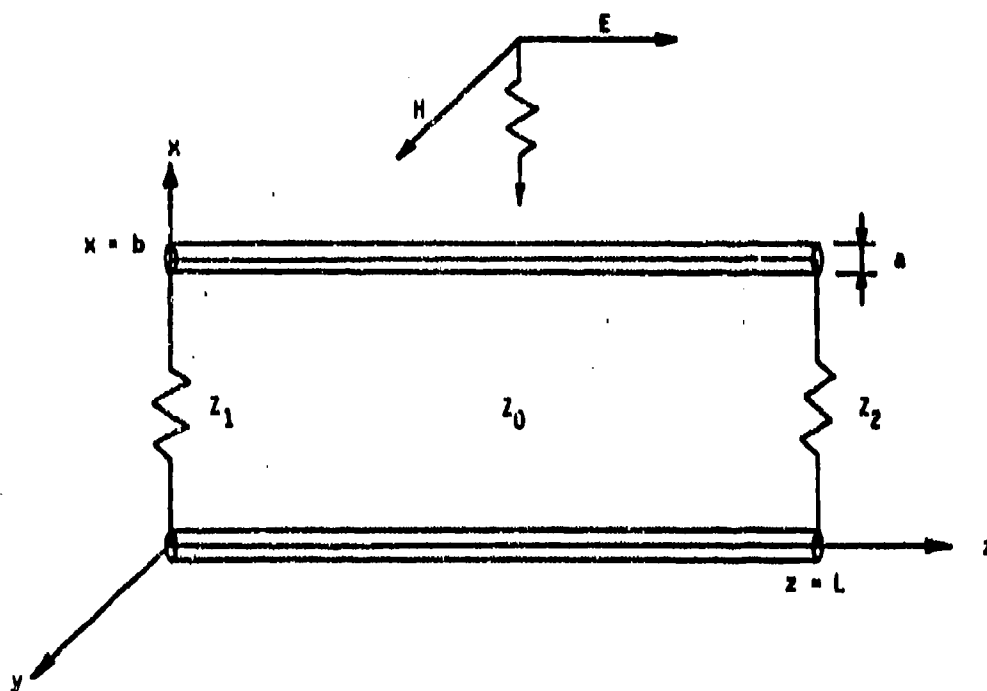


Figure 11.14 Two-Wire Line Illuminated by Uniform EM Field

at the terminated end of the line. is given by:

$$\Gamma = \frac{Z_2 - Z_0}{Z_2 + Z_0} \quad (11-11)$$

minor parameter modifications allow (11-10) to be used when only a portion of the line is exposed to the incident field or if the problem involves a single wire over a ground plane (image theory, see Figure 11.15).

Using (11.10), bounds can be calculated on the peak open-circuited voltage V_{oc}^{PEAK} , peak short-circuited current I_{sc}^{PEAK} , and peak power p^{PEAK} . The quantities V_{oc}^{PEAK} and I_{sc}^{PEAK} are

$$\begin{aligned} |V_{oc}^{peak}| &\leq I_{max} / (1 - |\Gamma|) \\ |Z_0 I_{sc}^{peak}| &\leq I_{max} (1 + |\Gamma|) / (1 - |\Gamma|) \end{aligned} \quad (11-12)$$

where I_{max} can be calculated or estimated as $I_{max} \leq L E_{max}^i$.

These estimates can be modified for fields with a rapid rise time to peak, such as lightning and EMP. Then, only a few terms of (11-10) are non zero and better current and voltage estimates are:

$$\begin{aligned} |V_{oc}^{peak}| &\leq I_{max} (1 + |\Gamma|) \\ |Z_0 I_{sc}^{peak}| &\leq I_{max} (1 + |\Gamma|) \end{aligned} \quad (11-13)$$

The peak power can then be estimated as

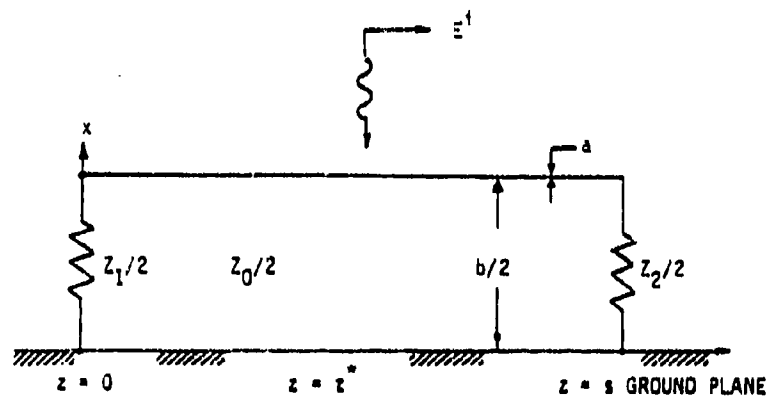
$$p_{peak} \leq V_{oc}^{peak} I_{sc}^{peak} \leq \frac{I_{max}^2 (1 + |\Gamma|)}{Z_0 (1 - |\Gamma|)^2} \quad (11-14)$$

and the delivered energy, by

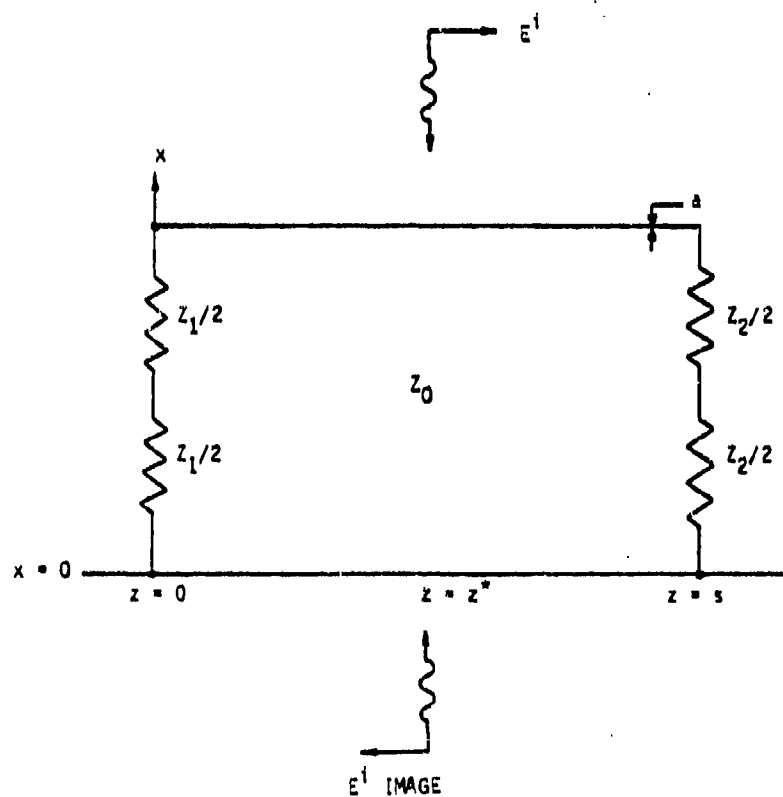
$$E \leq \frac{L^2 ||E^i||^2 (1 + |\Gamma|)}{Z_0 (1 - |\Gamma|)^2} \quad (11-15)$$

where

$$||E^i||^2 = \int_{-\infty}^{\infty} |E^i(t)|^2 dt \quad (11-16)$$



(a) PHYSICAL REPRESENTATION



(b) IMAGE PROBLEM

Figure 11.15 Wire Over a Ground Plane

If the line is electrically short then

$$V_{oc}^{peak} = L E_{max}^1 \quad (11-17)$$

$$I_{sc}^{peak} = \frac{V_{oc}^{peak}}{Z_2} \quad (11-18)$$

A shielded wire above a ground plane is shown in Figure 11.16. Again, with minor modifications of some of the parameters (shown in Figure 11.16), the two-wire transmission line theory can be used to treat shielded wire provided an estimate is available for the effective field illuminating the interior wire.

The effective field, E_{eff} , can be shown, for low frequencies, to be approximately:

$$E_{eff} = \frac{2 Z_t E_o L}{Z_1 + Z_2} \quad (11-19)$$

where E_o is the incident field amplitude; L , the line length; Z_1 and Z_2 , the terminating impedances of the shield, and Z_t , the surface transfer impedance of the shield. Then, for low frequencies:

$$V_{oc} = \frac{2 L^2 Z_t E_o}{Z_1 + Z_2} \quad (11-20)$$

$$I_{sc} = \frac{V_{oc}}{Z_b} \quad (11-21)$$

11.2.5 Subsystem Susceptibility ($T_5(f)$)

Advances in electronic devices has been one of the most rapidly developing technologies in recent times. Vacuum tube and discrete transistor technology have been replaced by integrated circuits and large scale integrated circuit (LSI) technology. These trends are expected to continue with the advent of very large scale integrated circuit (VLSI) technology in the near future.

Figure 11.17 shows changes in electronic device characteristics in parallel with changes in airframe materials and components from pre 1950 to the 1980's. In determining device susceptibility, both the upset voltage across the device and the power for burnout of the device must be considered. As Figure 11.17 shows, the push of technology has lowered device upset voltage and burnout energy dramatically. A key point to note is that

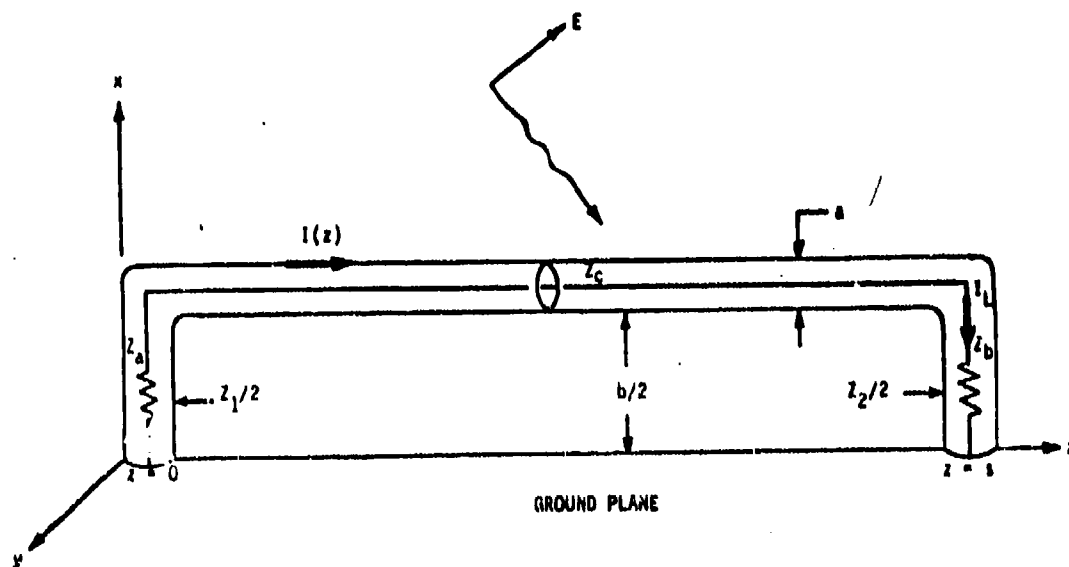


Figure 11.16 Shielded Cable Geometry

TECHNOLOGY TRENDS





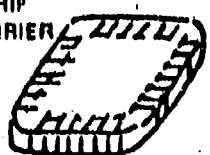
TUBES	DISCRETE TRANSISTORS	INTEGRATED CIRCUITS (IC)	LARGE SCALE INTEGRATED CIRCUITS (LSI)	VERY LARGE SCALE INTEGRATED CIRCUITS (VLSI)
 250V 1 WATT/DEVICE	 TO-8 12V-24V 10-1-10-2 WATTS/DEVICE	FLAT PACK  5V-12V 10-2-10-3 WATTS/TRANS	 DIP 5V-7V 10-3-10-4 WATTS/TRANS	CHIP CARRIER  1.5V-3V 10-5-10-8 WATTS/TRANS
GLASS/ METAL/ CERAMIC	METAL/ CERAMIC	METAL/ CERAMIC/ EPOXY	METAL/ CERAMIC/ EPOXY	CERAMIC/ EPOXY
F-9	F-4	F-14	F-18	VSTOL
ALUMINUM	ALUMINUM	ALUMINUM/TITAN	GRAPHITE-EPOXY ALUMINUM	GRAPHITE-EPOXY ?
PRE-1950's	1950's	1960's	1970's	1980's

Figure 11.17 Aerospace Technology Trends

the development of the most susceptible devices coincides with the increased use of composite materials. Because of the poorer shielding provided by composites compared to aluminum, the vulnerability of modern electronic devices to upset and burnout will be greatly increased unless adequate protection methods are used.

The upset and burnout energies for various circuit components and devices are shown in Figure 11.18. These levels can serve as a general guide to the maximum energy levels a particular device should experience. Key facts are that integrated circuits are most susceptible and burnout energy is 10 times upset. Figures 11.19 and 11.20 present worst case susceptibility data for CMOS and TTL technologies, operational amplifiers and 3-pin and multi-pin regulators as a function of frequency. Device susceptibility becomes much worse below 1 GHz. This trend renders the devices potentially vulnerable to lightning and EMP threats. Protection methods will be discussed in Section 11.4.

11.3 Unprotected Aircraft Performance Guidelines

Section 11.2 discussed the factors that must be considered when designing electromagnetic compatibility into composite aircraft. These factors were characterized as frequency-dependent transfer functions $D(f)$, $T_1(f)$ --- $T_5(f)$. The calculation of these functions for a given incident electromagnetic field (considered a threat) will allow an estimate to be made of the induced voltages, currents, powers and energies that will appear at electronic subsystem entry ports. One important baseline is the performance of an unprotected all-composite aircraft exposed to strong external electromagnetic fields (lightning, RF EMP). The results of such an analysis, of course, will vary with the parameters of the specific problem. In this section, a single example of such an analysis will be given for a set of "typical" conditions. A comparison then will be made between aluminum and graphite/epoxy airframe.

The parameters used in the analysis are: graphite/epoxy conductivity, 10^4 mhos/m; composite thickness, 0.0025 m (19 plies); lightning and EMP threats, worst case double exponential waveforms; the characteristic impedance of the transmission line, 100 ohms, and the reflection coefficient, $| \Gamma | = 0.54$. The integral I_{\max} is approximated as LE_{\max} where L is the exposed line length and E_{\max} , the maximum amplitude of incident field. A shipboard RF threat is given as 400 V/m.

The results are shown in Figures 11.21 and 11.22 as a set of curves. Estimates are given on the open-circuited voltage V_{oc} , the short-circuited current I_{sc} , and the power, $V_{oc} I_{sc}$ delivered to the line termination as functions of line length L and threat type. Estimates are also given on minimum required Wunsch constants for devices that will survive the threat.

The contribution to the upper bounds on V_{oc} , I_{sc} , power and minimum Wunsch constant due to joint coupling is shown in Figure 11.23. Below 100 MHz the joint admittance was taken as a constant 15 mhos/m. Above 2 GHz the joint admittances becomes frequency dependent as shown in Figure 11.13.

EM SUSCEPTABILITY (T_E)

Upset and Burnout Energies for Various Circuit Elements.

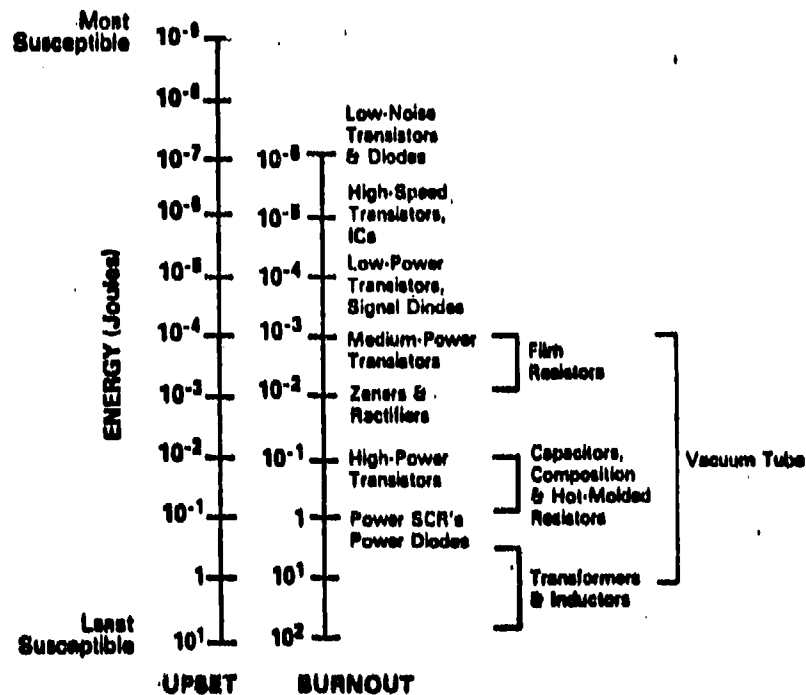


Figure 11.18 Electronic Component Upset and Burnout Energies

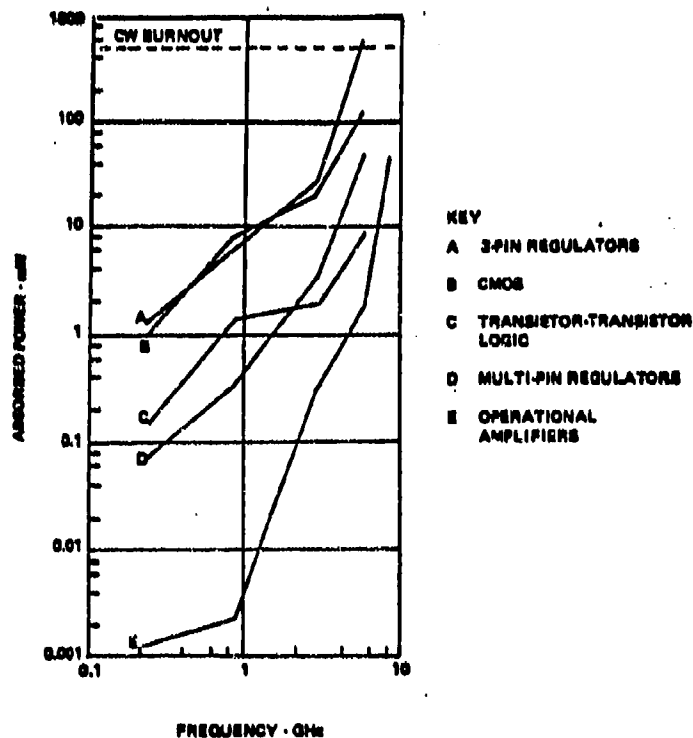


Figure 11.19 Worst Case Absorbed Power Susceptibility

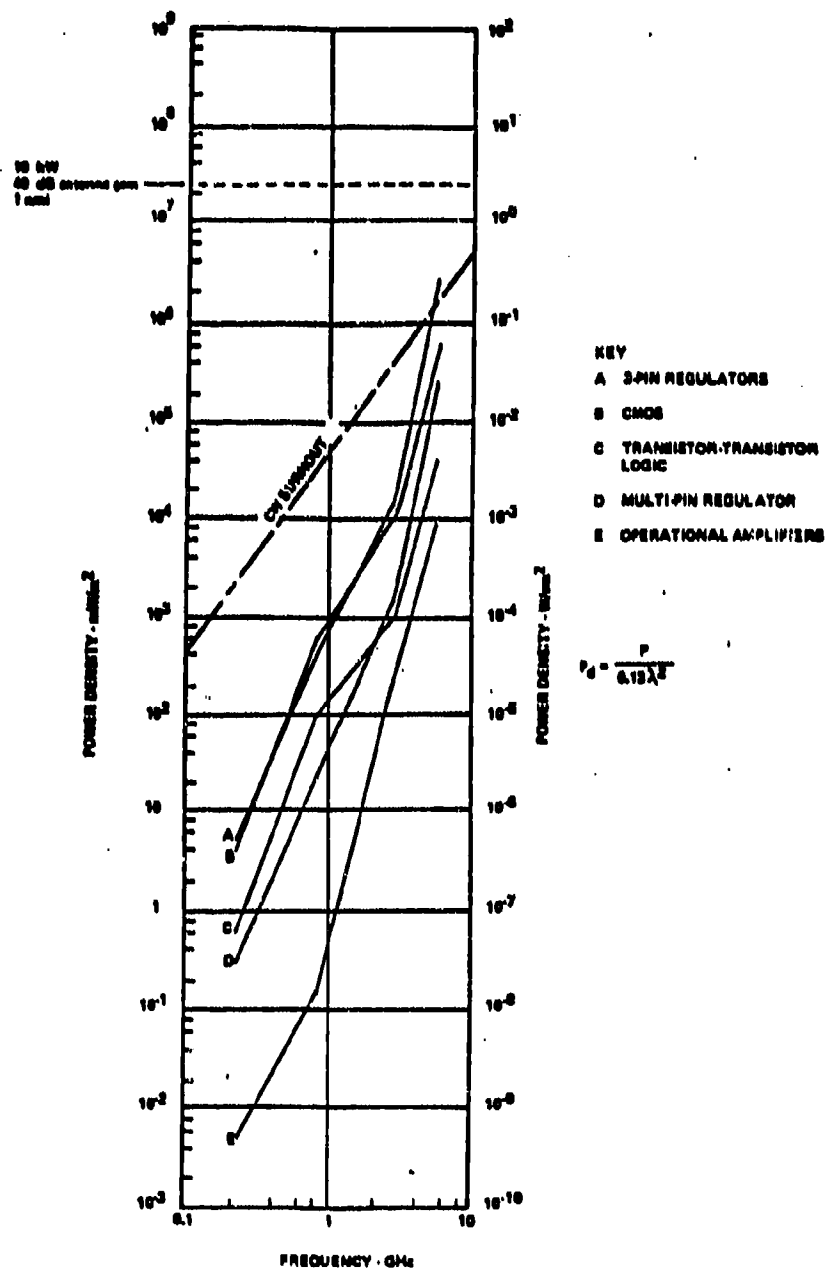


Figure 11.20 Worst-Case Power Density Susceptibility Values
Assuming $\lambda/2$ Aperture

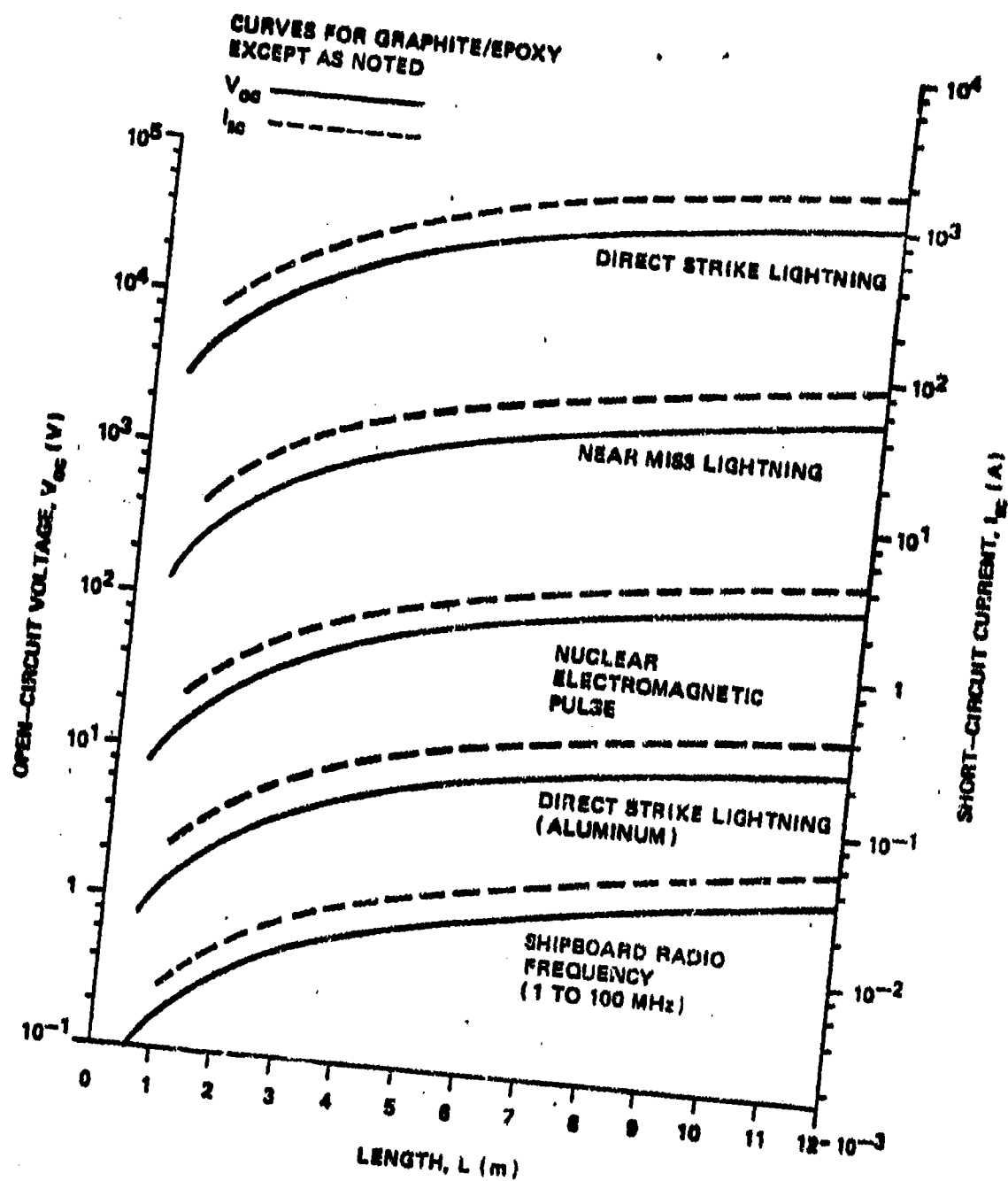


Figure 11.21 Upper Bounds on Open-Circuit Voltage and Short-Circuit Current Due to Diffusion Through Graphite/Epoxy

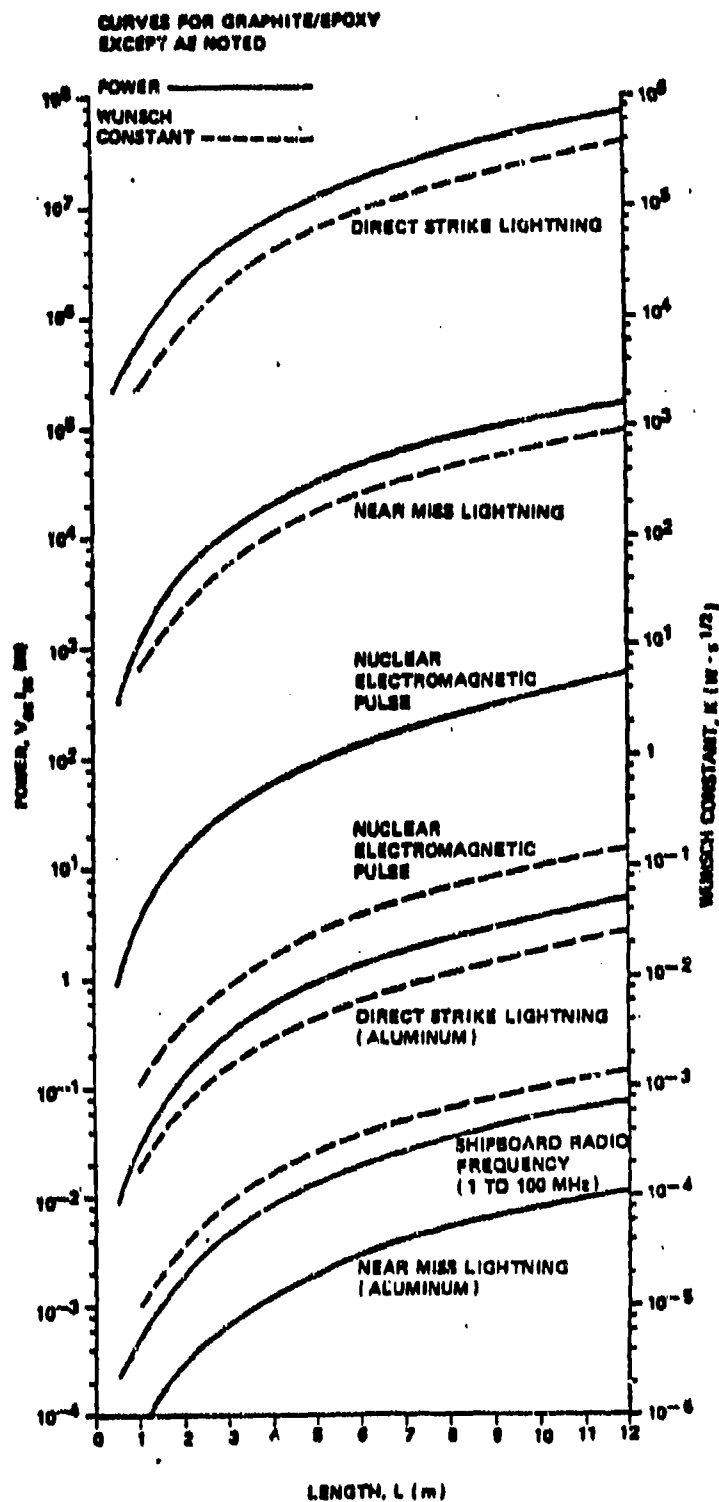
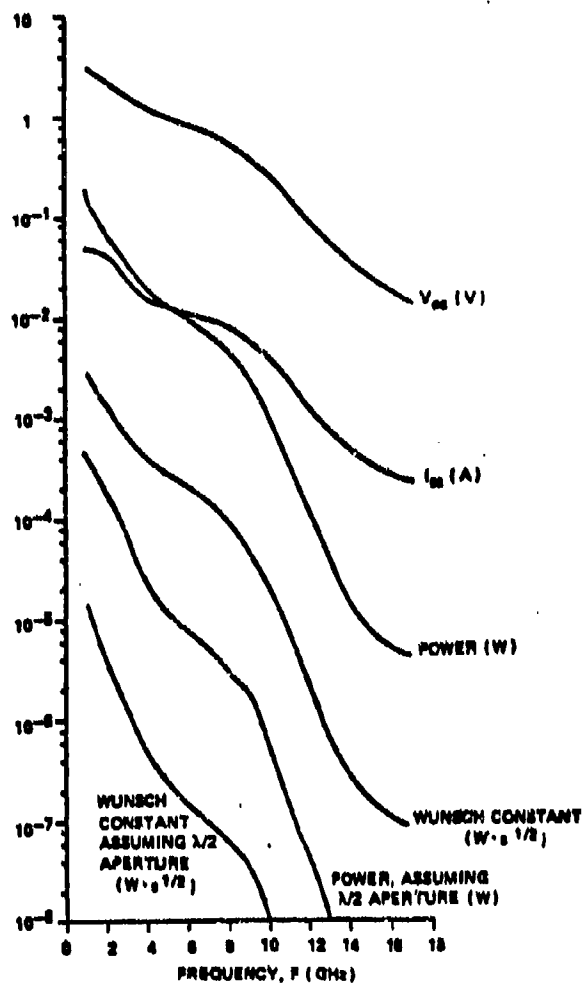


Figure 11.22 Upper Bounds on Power Delivered to Transmission Line Termination; Minimum Wunsch Constant of Devices that Will Survive Threat



(a) above 1 MHz

	V_{oc} (V)	I_{sc} (A)	Power (W)	Wunsch Constant ($W \cdot s^{1/2}$)
Direct Strike Lightning	9.5×10^3	150	1.4×10^6	0.76×10^4
Near by Lightning	460×10^3	7.1	3.2×10^3	18
NEMP	27.7	0.37	10.38	0.0029
Shipboard RP	3.06	0.047	0.144	0.00289

(b) below 1 MHz

Figure 11.23 Upper Bounds, Due to Joint Coupling, on Open-Circuit Voltage, Short-Circuit Current, and Power Delivered to Transmission Line Termination; Minimum Wunsch Constant of Devices that will Survive Threat

This type of analysis can be used to estimate V_{oc} , I_{sc} , power and energy induced on wires running the length of a fighter size aircraft. For an aluminum aircraft $V_{oc} = 10.1$ volts and $I_{sc} = 0.3A$. The results for a composite aircraft are given in Figure 11.24. These estimates have been well confirmed by experiment. Direct lightning strike is seen to be the worst threat.

These estimates on the various parameters can now be compared to device susceptibility curves such as shown in Figures 11.19 and 11.20. This comparison allows an estimate to be made of the amount of protection required for the composite aircraft to insure electromagnetic compatibility. The amount of protection required can be represented by a frequency dependent transfer function $T_6(f)$ which, when added to $D(f)$, $T_1(f) \dots T_5(f)$, will reduce the induced voltage, current and power below device susceptibility levels. For convenience $T_6(f)$ can be represented as a sum of terms

$$T_6(b) = T_{16}^{material} + T_{26}^{shape} + T_{36}^{joints} + T_{46}^{cable} + T_{56}^{box} \quad (11-22)$$

where $T_{16} \dots T_{56}$ represent transfer functions for different kinds of protection. The use of composites directly alters $T_{16}^{MATERIAL}$, T_{36}^{JOINTS} and T_{56}^{BOX} . Changes in T_{26}^{SHAPE} and T_{46}^{CABLE} result from advance in other technologies.

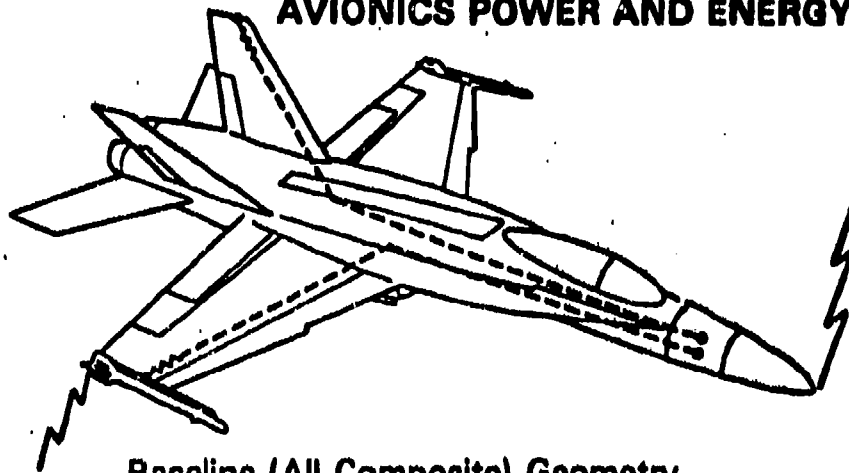
The low frequency electromagnetic hardness of composites and various metals is shown in Figure 11.25 in terms of material surface transfer impedance. Low frequency lightning directly striking an aircraft induces the greatest voltages and current on internal circuits and represents the greatest threat considered here. As Figure 11.25 shows, considerable protection is afforded by various metallic systems. However, weight penalties paid and degradation occurring during the system life cycle must also be considered.

The amount of protection provided by different 4 mil coatings covering graphite/epoxy is shown in Figure 11.26. The improvement in shielding can be expressed as a ratio of material transfer impedances

$$\begin{aligned} \text{SHIELDING IMPROVEMENT} &= \frac{Z_{st}^{composite}}{Z_{st}^{coating}} \\ &= \frac{\sigma_{coating} d_{coating}}{\sigma_{composite} d_{composite}} \end{aligned} \quad (11-23)$$

where σ and d represent conductivity and thickness. Copper reduces the fields by a factor of 325 while an equal thickness of aluminum reduces the fields by a factor of 140. Although nickel and tin reduce the fields only

AVIONICS POWER AND ENERGY



Baseline (All Composite) Geometry

Peak Power and Maximum Energy

Direct Strike	V_i (Volts)	I_i (Amps)	p_i^{peak} (Kilowatts)	E_i (Joules)
Nose/Tail Wire (Nose/Tail Attachment)	32,000	1,100	3,520	1035.2 J
(Nearby Strike)	250	8.2	2	0.050 J
Nose/Wing Tip (Nose/Tail Attachment)	6,600	220	1,430	42.06 J
Wire (Nose/Wing Tip Attachment)	17,000	660	9,350	275.0 J

Figure 11.24 Voltage, Current, Power and Energies
Caused by LEMP, NEMP External Fields
in Aluminum and Graphite/Epoxy

EM PROTECTION OF METALS AND COMPOSITES (IT)

Transfer Impedance Shielding of Structural Materials and Protective Electromagnetic Coatings

(Valid for Frequencies Below 10^5 Hz)

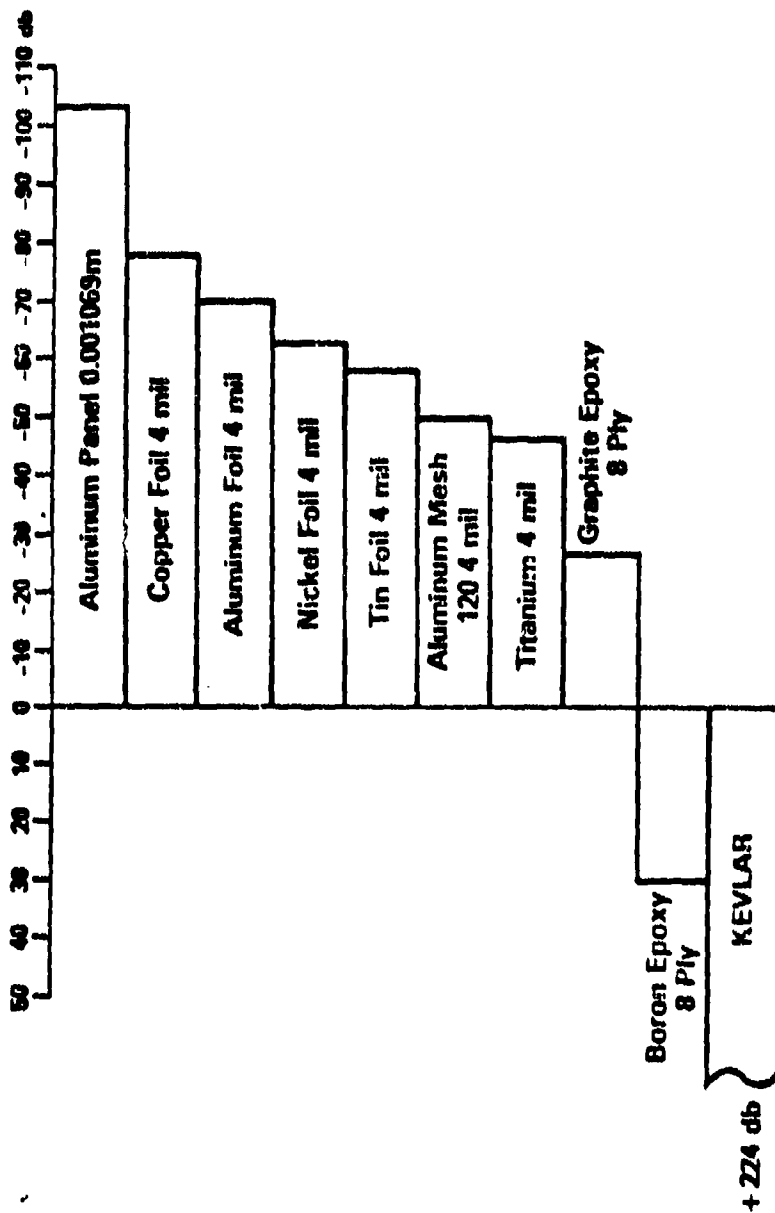


Figure 11.25 Transfer Impedance Shielding of Structural Material and Protective EM Coatings

EM PROTECTION (T_d)

Protective Coatings Improvement Relative to 8-Ply G/E

(Valid for Frequencies Below 10⁵ Hz)

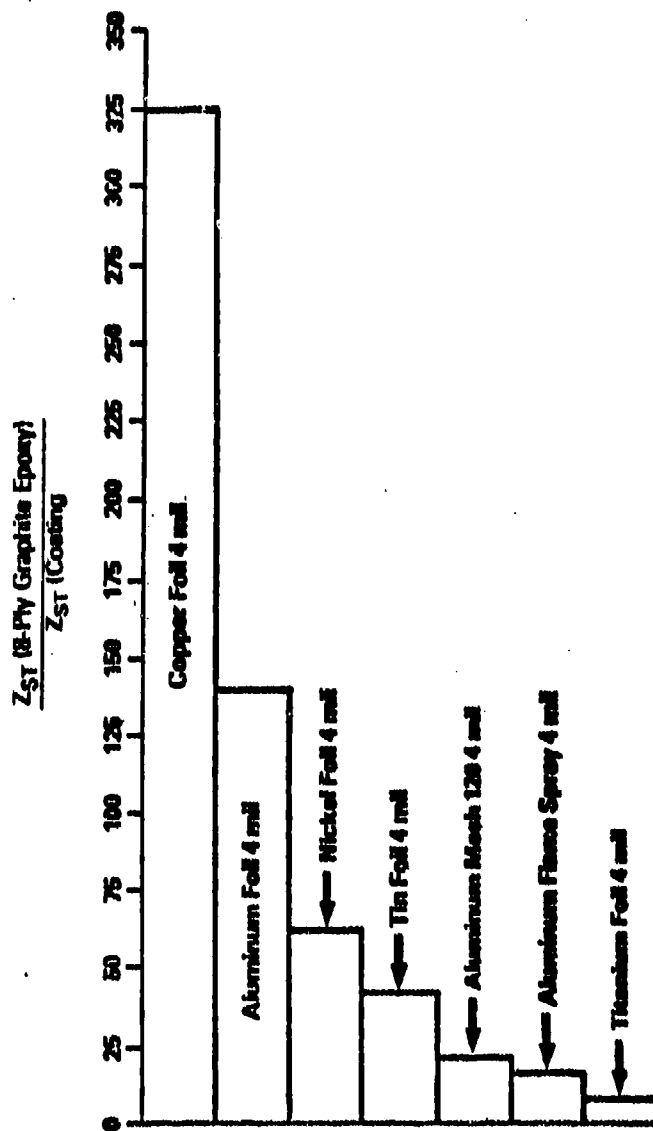


Figure 11.26 Improvement Protective Coatings Provided Relative to 8-Ply Graphite/Epoxy

by a factor of 58 and 40, they are attractive because they are non-corrosive with graphite/epoxy.

Figure 11.27 shows the weight penalty that is incurred by adding 100 ft² of the 4 mil coatings, given in Figure 11.26, to the composite. This area conveniently approximates the area of the AV-8B forward fuselage which is under development. This figure illustrates that copper, besides providing superior shielding, also extracts the worst weight penalty. The least weight penalty is extracted by the various aluminum protection systems.

Both the shielding and the weight penalty can be combined into an overall figure of merit defined as:

$$\text{FIGURE OF MERIT} = \frac{\text{SHIELDING IMPROVEMENT}}{\text{SURFACE DENSITY}} \quad (11-24)$$

The surface densities of the various coatings are given in Figure 11.27.

The tradeoff results are given in Figure 11.28. Aluminum foil is shown to have a superior figure of merit than copper because of its much lower weight. Aluminum flame spray, much considered, ranks third due mainly to its lower conductivity.

A final tradeoff factor, not directly considered here, is cost. Because of the changing price on material commodities, specific price data is not considered. Such a tradeoff, however, must be done during each stage of the system design.

The discussion has considered only the airframe material aspects of electronic system protection. Use of aluminum protection systems on the airframe allows a 100 fold improvement in electromagnetic shielding with only a 5-15% weight penalty. Thicker coatings will provide better protection but extract an increasingly large weight penalty. Consequently, further protective measures should be provided by T₄₆ CABLE, T₅₆ BOX, and T₃₆ JOINTS. A well protected airframe simplifies the hardening of joints, cables and equipment boxes. Cables should be well shielded or, for mission critical systems, provided with fiber optic lines.

EM PROTECTION WEIGHT PENALTIES (T_g)

Forward Fuselage AV-8B (Area - 100 Ft²) Weight Penalty
(Pounds) Imposed by Electromagnetic Protective Coatings

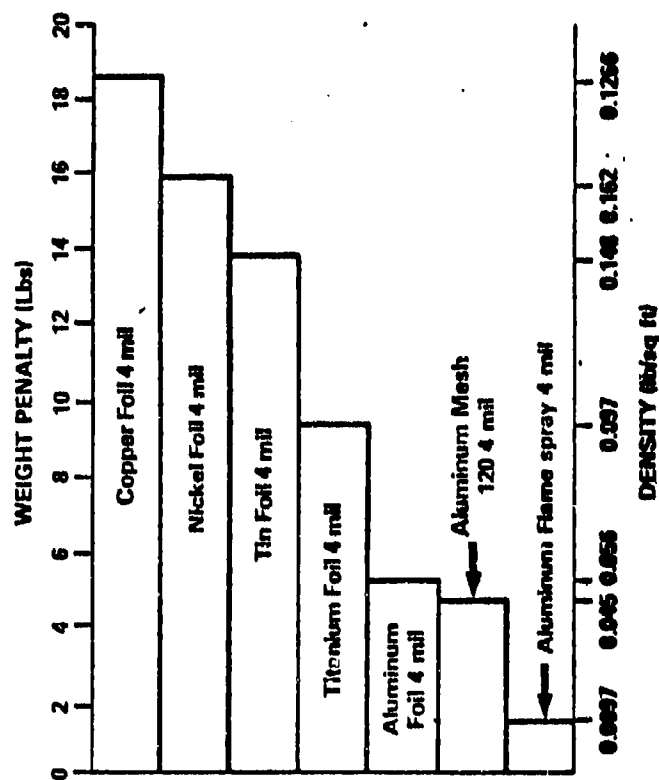


Figure 11.27 Weight Penalty Imposed by Protective Coatings

EM PROTECTION (T_e)

Weight Shielding Figure of Merit

(Protection Beyond 8-Ply G/E Provided by the Weight of 1 Square Foot of Protective Coating)

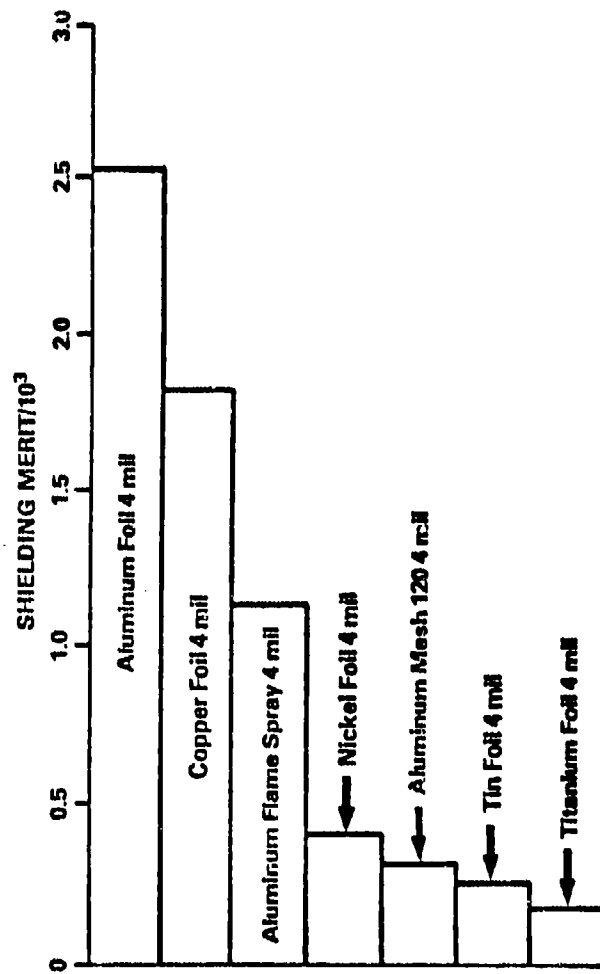


Figure 11.28 Weight/Shielding Figure of Merit of EM Protective Coatings